GEOLOGICAL SURVEY RESEARCH 1967

Chapter D

GEOLOGICAL SURVEY PROFESSIONAL PAPER 575–D

GEOLOGICAL SURVEY RESEARCH 1967

Chapter D

GEOLOGICAL SURVEY PROFESSIONAL PAPER 575–D

Scientific notes and summaries of investigations in geology, hydrology, and related fields

UNITED STATES GOVERNMENT PRINTING OFFICE, WASHINGTON: 1967

UNITED STATES DEPARTMENT OF THE INTERIOR

STEWART L. UDALL, Secretary

GEOLOGICAL SURVEY

William T. Pecora, Director

For sale by the Superintendent of Documents, U.S. Government Printing Office
Washington, D.C. 20402 - Price $2.50

CONTENTS

GEOLOGIC STUDIES

GEOLOGICAL SURVEY RESEARCH 1967

This collection of 48 short papers is the third published chapter of "Geological Survey Research 1967." The papers report on scientific and economic results of current work by members of the Conservation, Geologic, Topographic, and Water Resources Divisions of the U.S. Geological Survey.

Chapter A, to be published later in the year, will present a summary of significant results of work done during fiscal year 1967, together with lists of investigations in progress, reports published, cooperating agencies, and Geological Survey offices.

"Geological Survey Research 1967" is the eighth volume of the annual series Geological Survey Research. The seven volumes already published are listed below, with their series designations.

Geological Survey Research 1960—Prof. Paper 400
Geological Survey Research 1961—Prof. Paper 424
Geological Survey Research 1962—Prof. Paper 450
Geological Survey Research 1963—Prof. Paper 475
Geological Survey Research 1964—Prof. Paper 501
Geological Survey Research 1965—Prof. Paper 525
Geological Survey Research 1966—Prof. Paper 550

NORTHWESTERLY EXTENSION OF THE DARBY THRUST IN THE SNAKE RIVER RANGE, WYOMING AND IDAHO

By HOWARD F. ALBEE, DANIEL A. JOBIN,
and MARVIN L. SCHROEDER, Denver, Colo.

Abstract.—The Darby thrust lies along the eastern edge of the Wyoming Range in western Wyoming and in the Snake River Range, Idaho. Earlier workers thought that the fault terminated in a north-plunging anticline on the east side of Munger Mountain about 2½ miles north of the Snake River, but recent mapping has shown that the Darby thrust extends 27 miles northwest of Munger Mountain and, thus, that the fault is at least 127 miles long. In general, Lower Cretaceous rocks are thrust over Upper Cretaceous rocks along the newly mapped segment of the fault. Near Munger Mountain, however, the only exposed rocks involved in the thrust are the Aspen Formation of Early Cretaceous age.

Recent mapping in southeastern Idaho and western Wyoming by members of the U.S. Geological Survey has revealed that the Darby thrust extends approximately 27 miles northwest of Munger Mountain, where earlier workers thought that the fault ended (fig. 1).

The Darby thrust was first recognized by Peale (1879, p. 630), who described it as a normal fault along the east side of the Wyoming Range. Later, Schultz (1914, p. 84) determined that the fault was a thrust fault and named it for Mount Darby, the highest point along the fault scarp, near the south end of the Wyoming Range. Schultz traced the fault north about 100 miles from near La Barge, Wyo., to the Snake River. Horberg (1938, p. 34–35) mapped the fault north of the Snake River for about 2½ miles to a point on the east side of Munger Mountain where he believed that the fault died out in a north-plunging anticline (fig. 1).

Mansfield (1927, p. 381) estimated a stratigraphic throw of more than 20,000 feet and a horizontal displacement of as much as 15 miles for the fault. Ross and St. John (1960, p. 52) assumed considerably less horizontal displacement and determined a stratigraphic throw of about 9,000 feet at Pow Wow Point about 6 miles south of the intersection of the fault and the Snake River.

In the Munger Mountain quadrangle, the Aspen Formation of Early Cretaceous age was divided into an upper and a lower part on the basis of a prominent porcellanite marker bed (H. F. Albee, unpub. data). Using this stratigraphic refinement, the Darby thrust was extended from where Horberg believed that the thrust ended to the north boundary of the Munger Mountain quadrangle (fig. 1).

The location of the fault in the Jackson and Teton Pass quadrangles is not well defined. The position of the fault trace is inferred largely from small, widely scattered exposures of moderately folded rocks in an area covered mainly by glacial deposits. Across the southwest corner of the Jackson quadrangle the surface rocks involved in the faulting are chiefly of the Aspen Formation. In the Teton Pass quadrangle, M. L. Schroeder found rocks of both Early and Late Cretaceous ages thrust over rocks of the Frontier Formation. Further support is given to the location of the Darby thrust in the Jackson and Teton Pass quadrangles by the large difference in the thickness of the Aspen Formation. North of the inferred location of the thrust the Aspen is about 1,500 feet thick, and south of the inferred location the Aspen is about 3,000 feet thick.

Recently, Jobin (1965) and Pampeyan and others (1967) mapped a thrust fault on strike with the Darby thrust to the northwest in the Palisades Peak and Driggs quadrangles. Tightly folded to overturned rocks of Early Cretaceous age are thrust onto overturned rocks of the Frontier Formation of Late Cretaceous age. In the Palisades Peak quadrangle exposures along the fault trace are scarce, but the fault (fig. 1) can be mapped with certainty owing to its

U.S. GEOL. SURVEY PROF. PAPER 575-D, PAGES D1-D3

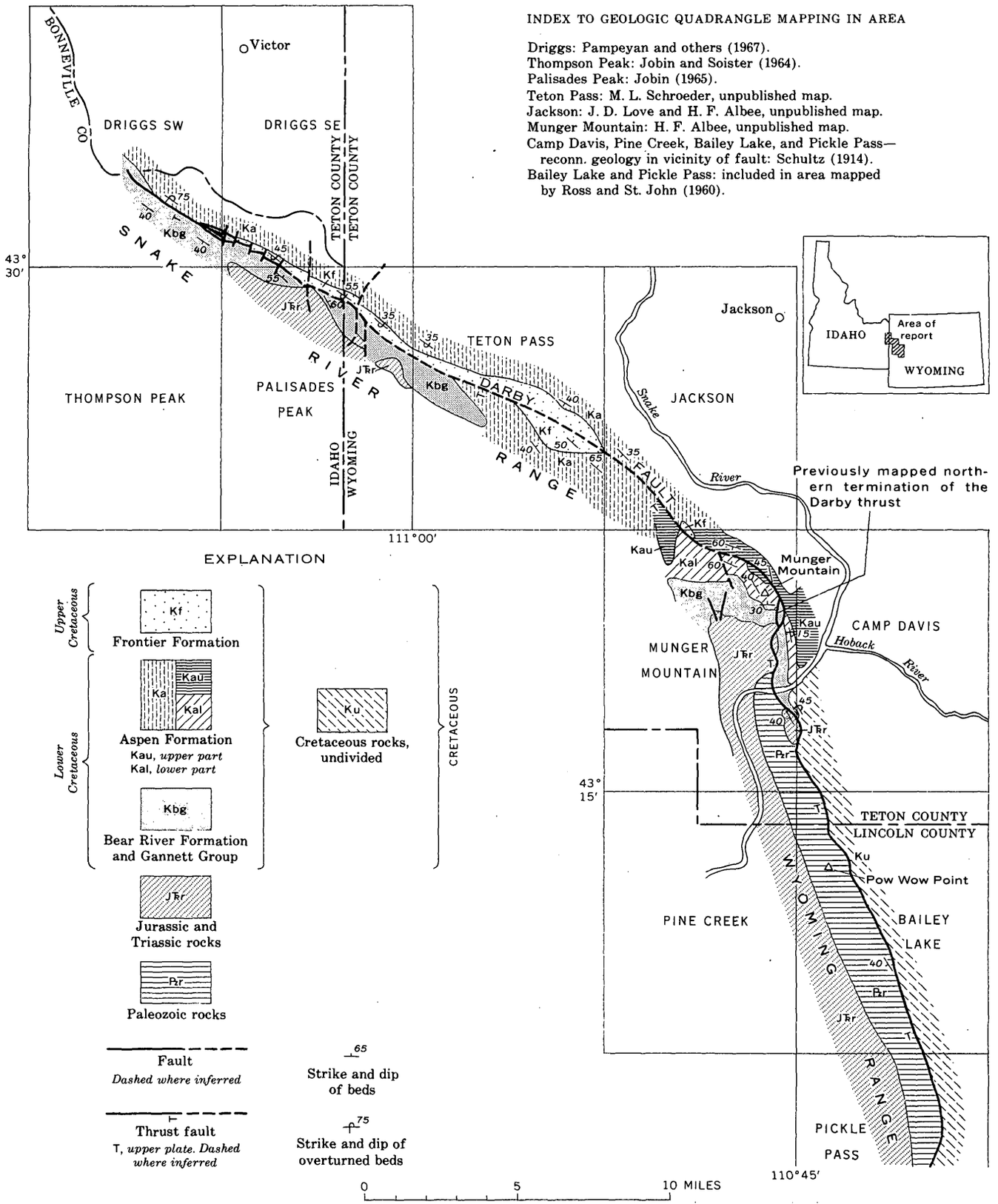

FIGURE 1.—Geologic map showing northwesterly extension of the Darby thrust in southeastern Idaho and western Wyoming.

topographic expression as a linear fault valley. The fault seemingly dies out in the upper part of the Bear River Formation in the Driggs SW quadrangle.

REFERENCES

Hörberg, Leland, 1938, The structural geology and physiography of the Teton Pass area, Wyoming: Augustana Library Pub. 16, 86 p.

Jobin, D. A., 1965, Preliminary geologic map of the Palisades Peak quadrangle, Bonneville County, Idaho, and Teton County, Wyoming: U.S. Geol. Survey open-file map.

Jobin, D. A., and Soister, P. E., 1964, Geologic map of the Thompson Peak quadrangle, Bonneville County, Idaho: U.S. Geol. Survey Mineral Inv. Field Studies Map MF–284.

Mansfield, G. R., 1927, Geography, geology, and mineral resources of part of southeastern Idaho: U.S. Geol. Survey Prof. Paper 152, 409 p.

Pampeyan, E. H., Schroeder, M. L., Schell, E. M., and Cressman, E. R., 1967, Geologic map of the Driggs quadrangle, Bonneville and Teton Counties, Idaho, and Teton County, Wyoming: U.S. Geol. Survey Mineral Inv. Field Studies Map MF–300.

Peale, A. C., 1879, Report on the geology of the Green River district [Wyo.]: U.S. Geol. and Geog. Survey Terr. (Hayden), 11th Ann. Rept., p. 509–646.

Ross, A. R., and St. John, J. W., 1960, Geology of the northern Wyoming Range, Wyoming, *in* Wyoming Geol. Assoc. Guidebook, 15th Ann. Field Conf., Overthrust belt of Southwestern Wyoming and adjacent areas, 1960: p. 44–56.

Schultz, A. R., 1914, Geology and geography of a portion of Lincoln County, Wyoming: U. S. Geol. Survey Bull. 543, 141 p.

STRATIGRAPHIC EVIDENCE FOR THE LATE DEVONIAN AGE OF THE NATION RIVER FORMATION, EAST-CENTRAL ALASKA

By EARL E. BRABB and MICHAEL CHURKIN, JR.,
Menlo Park, Calif.

Abstract.—The stratigraphic position and age of the Nation River Formation have long been controversial problems, primarily because previous workers failed to recognize an unconformity at the base of the overlying Tahkandit Limestone of Permian age at the type locality of these formations near the mouth of the Nation River. In the vicinity of McCann Hill and the Tatonduk River, the Nation River Formation is stratigraphically above shale and chert of the McCann Hill Chert of Early, Middle(?), and Late Devonian age and below similar rocks of Late Devonian to Mississippian age, and thus by superposition is no older than Middle Devonian and no younger than Late Mississippian. Spores collected from the Nation River Formation at 18 localities throughout its type area and elsewhere corroborate the stratigraphic evidence and indicate that the formation is almost certainly Late Devonian.

A recent report by Laudon and others (1966) on the Paleozoic stratigraphy of east-central Alaska has focused attention on the problem of the stratigraphic position and age of the Nation River Formation. The stratigraphic position of this thick sequence of conglomerate, sandstone, and shale, considered since 1930 to be of Pennsylvanian(?) age, is important in reconstructing the tectonic history of eastern Alaska. A Late Devonian age assignment and a revision in the stratigraphic position of this formation were first formally reported briefly by Churkin and Brabb (1965). Subsequently, Laudon and his colleagues offered alternate explanations for its stratigraphic position and its assignment to the Devonian. The purpose here is to document more fully the stratigraphic evidence for the Devonian age of the formation. The palynological evidence for the age of the Nation River Formation has been described by Scott and Doher (1967).

All the basic stratigraphic conclusions of the present report were shown on the preliminary maps of the Charley River (1:250,000) and Eagle D–1 (1:63,360) quadrangles by Brabb (1962) and Brabb and Churkin (1964, 1965) released in open files of the U.S. Geological Survey.

The Nation River Formation crops out in the vicinity of the Yukon River and its tributaries (fig. 1) near the town of Eagle and the Alaska-Yukon Territory boundary. Rocks in this area range in age from late Precambrian to Quaternary, with nearly every geologic system being represented. All the pre-Tertiary rocks have been extensively folded and faulted.

The writers were ably assisted in the field by R. N. Passero and H. J. Roepke, in 1960; J. C. Melik and R. L. Taylor, in 1961; and A. J. Aadland, in 1962.

PREVIOUS WORK

The first map to show the distribution of conglomerate, sandstone, shale, and coal now referred to the Nation River Formation was made by Collier (1903, fig. 2). He thought that these rocks might be Carboniferous or Permian inasmuch as they seemed to lie beneath an unnamed limestone of Permian age, but he also thought that they could be infolded rocks of Eocene age. Collier's stratigraphic interpretation is shown on figure 2, column 1.

Brooks and Kindle (1908, p. 294, 295) named these rocks the Nation River Formation, stating,

> The Nation River series included about 3,700 feet of gray clay shales, with some clay slates interpolated with heavy beds of conglomerate and some sandstone. It is typically exposed along Nation River, where it includes some small seams of bituminous coal. The limits of this formation are well defined. The base is believed to be marked by an unconformity which separates it from the shales and limestone of the Calico Bluff formation. At the top it is limited by the heavy limestone which previously formed the topmost member of the Carboniferous . . .

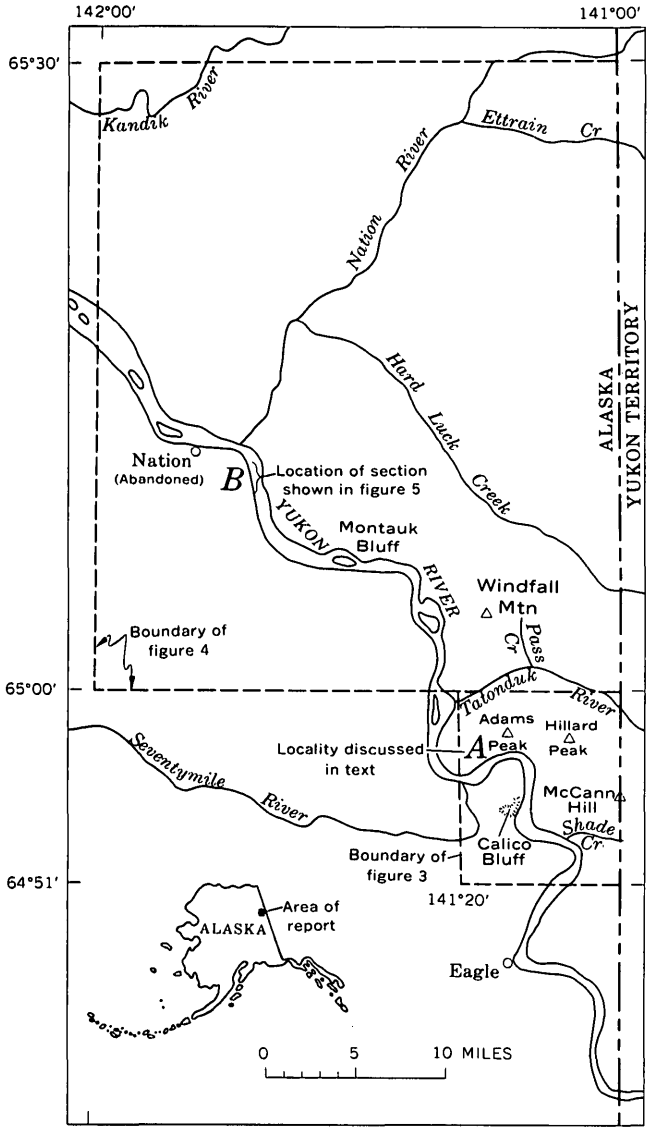

FIGURE 1.—Index map showing location of Nation River area, Alaska.

The stratigraphic succession envisioned by Brooks and Kindle is also shown in figure 2, column 2, but the basal unconformity they observed is near Adams Peak (locality *A*, fig. 1), 20 miles southeast of the Nation River area (locality *B*, fig. 1), and apparently is between the Calico Bluff Formation of Late Mississippian age and unnamed rocks of Late Cretaceous age (Mertie, 1930, p. 146, Kindle collection 11h note).

Cairnes (1914) included in the Nation River Formation the overlying "heavy" limestone mentioned by Brooks and Kindle and extended the age of the Nation River to possibly include Permian, mainly because he worked along the Alaska-Yukon Territory border where the Permian is represented largely by conglomerate and sandstone (fig. 2, column 3). He also included a "peculiar" conglomerate which he thought might represent a till formed during a Permo-Carboniferous glacial period. Subsequent mapping by Mertie (1933, p. 27) and Brabb and Churkin (1964) has shown that this conglomerate is part of the Tindir Group of Precambrian age. Cairnes recognized that still another conglomerate on McCann Hill (fig. 1) might represent the base of the Nation River Formation, but he found no diagnostic fossils to date these beds.

J. B. Mertie's (1930, 1933, 1937) stratigraphic concepts (fig. 2, columns 4 and 5) were based on the first detailed geologic mapping and on a synthesis of earlier work. Mertie designated the Nation River Formation as Pennsylvanian(?) because he believed it graded upwards into the Tahkandit Limestone of Permian age. Fossil plant fragments collected by Mertie and earlier geologists, however, were referred with some uncertainty to the Mississippian or Late Devonian by David White, of the U. S. Geological Survey. Mertie clearly recognized (1937, p. 145) that the age of the Nation River Formation was an unsettled problem.

Nelson (1961) in discussing the Carboniferous and Permian stratigraphy in the adjacent part of the Yukon Territory has shown that the rocks he recognizes as the Calico Bluff and Tahkandit Formations are separated by a limestone and shale unit, not the Nation River Formation.

Churkin and Brabb (1965, p. 182) reported that spores collected throughout the Nation River Formation at several localities, including its type area, are all probably Upper Devonian, according to Richard A. Scott. We also stated that stratigraphic relations show that the formation cannot be younger than the Late Mississippian Calico Bluff Formation.

Laudon and others (1966) questioned this Late Devonian age assignment, stating (p. 1869), "Assignment of a Devonian age to the Nation River Formation introduces complicated and as yet unresolved stratigraphic and structural problems." They, like Mertie, could not see how the Nation River Formation could be overlain by shale and chert of Mississippian age in the vicinity of McCann Hill and Calico Bluff (fig. 1) and by the Tahkandit Limestone of Permian age in the vicinity of the Nation River (fig. 1). They did not consider the possibility of an unconformity at the base of the Tahkandit Limestone, which we believe explains all the stratigraphic and structural relationships observed.

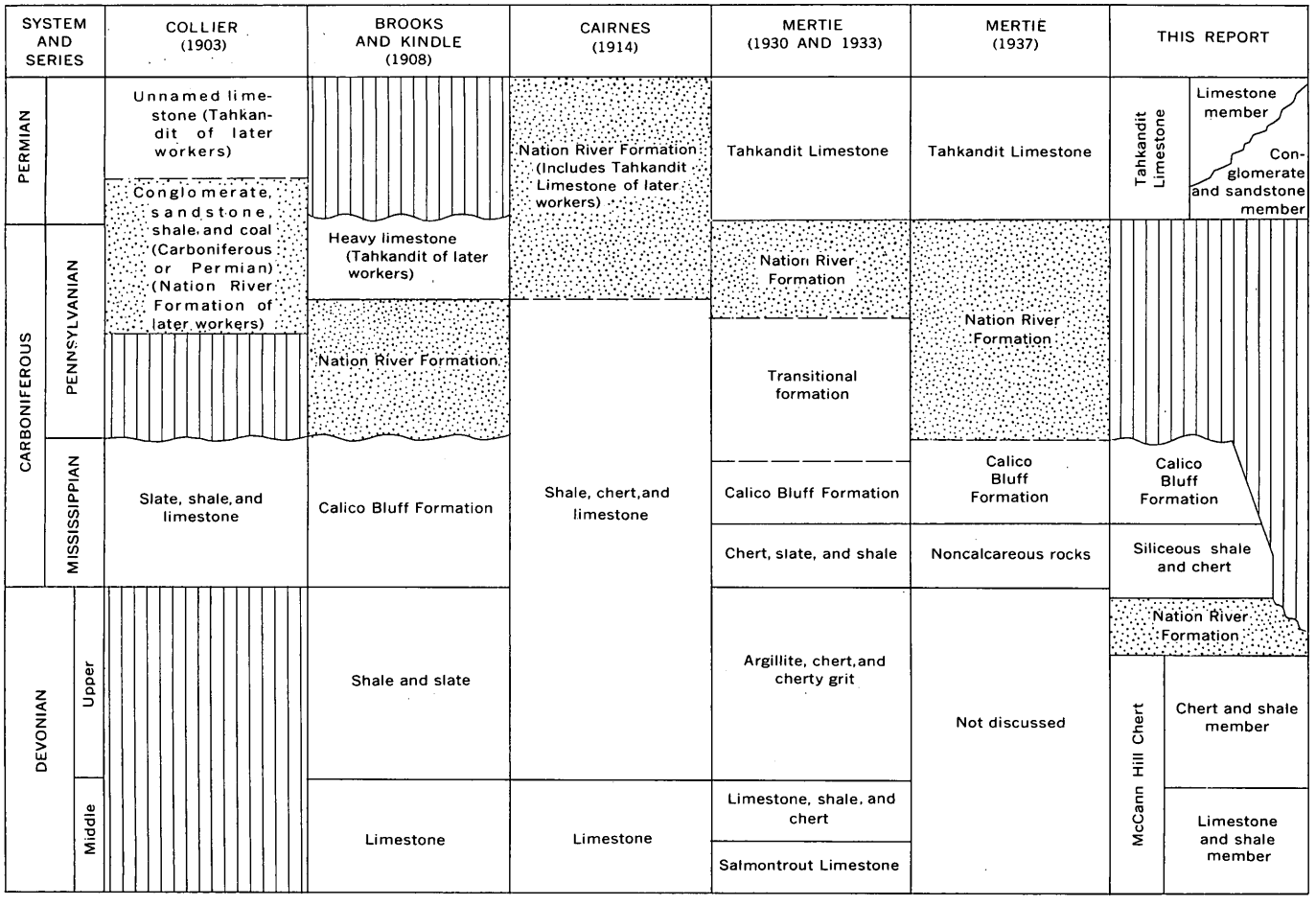

FIGURE 2.—Stratigraphic position and age of the Nation River Formation according to various authors.

Laudon and others (1966, p. 1871) proposed three possible explanations for the problems they presented, as paraphrased in smaller type below:

1. Rocks mapped by Churkin and Brabb (1965) as the Nation River Formation in the Calico Bluff area may be of Devonian age, and a second sequence of clastic rocks, now without a formation name and presumably of Pennsylvanian age, may underlie the Tahkandit Limestone in the Nation River area.

This explanation by Laudon and others is not valid because the second "unnamed" sequence of clastic rocks they refer to is the Nation River Formation at its type locality. If the type Nation River Formation is Pennsylvanian, then the rocks mapped by Churkin and Brabb (1965) as the Nation River Formation in the Calico Bluff area would be probably better assigned to a new formation. The writers of this paper, however, believe that the rocks in both areas are the same age (Late Devonian) and the same formation (Nation River).

2. Post-Mississippian deformation and erosion may have been followed in Pennsylvanian time by unconformable overlap of the Nation River Formation on the Mississippian Calico Bluff Formation near Calico Bluff and on the Devonian McCann Hill Chert near McCann Hill.

This explanation by Laudon and others is not supported by field observations inasmuch as the Nation River Formation has not been found stratigraphically or structurally above the Calico Bluff Formation.

3. The Nation River Formation of Pennsylvanian age may have been moved to its present position on the Devonian McCann Hill chert near McCann Hill by a low-angle thrust sheet from the south.

The writers of the present paper believe, on the other hand, that the Nation River Formation near McCann Hill contains spores of Late Devonian age, and that it probably grades downward into the underlying McCann Hill Chert.

Laudon and others (1966) also expressed considerable doubt that the distinctive chert and shale of the Devonian McCann Hill Chert could be repeated by sedimentary processes during the Mississippian to form the unit that we refer to as an unnamed siliceous shale and chert formation. They infer, therefore, that

the McCann Chert and the unnamed siliceous shale and chert are the same formation.

STRATIGRAPHIC RELATIONS

The stratigraphic relations of the Nation River Formation to other formations described here are based on geologic mapping in the Calico Bluff area (fig. 3) and the adjoining Nation River area (fig. 4). Little information regarding the lower and upper contacts of the formation has been previously published.

Calico Bluff area

Mertie (1933, p. 409, pl. 7) mapped an unnamed argillite, chert, and cherty grit formation of Middle Devonian age directly beneath the Nation River Formation near McCann Hill, about 5 miles east of Calico Bluff (fig. 3). He did not recognize this unnamed formation near Adams Peak, 4 miles north of Calico Bluff, or in the Nation River area (fig. 4), where he thought that the Nation River Formation rested unconformably on rocks of Precambrian age. The writers, on the other hand, have mapped this chert and siliceous shale formation, which we named (Churkin and Brabb, 1965, p. 180–182) the McCann Hill Chert, from McCann Hill nearly continuously to Adams Peak and to the Nation River area, 15 miles northwest of McCann Hill (figs. 3 and 4). The McCann Hill Chert and the overlying Nation River Formation are accordant throughout this area, and there is no evidence to suggest that the Nation River Formation rests unconformably on rocks older than the McCann Hill Chert. The rocks in the vicinity of the contact are homoclinal, have moderate dips, and are fairly well exposed.

Near McCann Hill and Hillard Peak (VABM 4065 and formerly called triangulation station Chief) the so-called basal conglomerate of the Nation River Formation mentioned by Cairnes (1914, p. 89) and Mertie (1933, p. 425) is underlain by approximately 450 feet of sandstone that contains several interbeds of siltstone and conglomerate. The sandstone and its interbeds are similar to those of the overlying Nation River Formation and should be included in that unit. The sandstone is underlain in turn by the McCann Hill Chert, which contains a varied shelly fauna of Early and possibly Middle Devonian age near its base (Churkin and Brabb, in press). The contact between the chert and siliceous shale of the McCann Hill Chert and the overlying Nation River Formation is abrupt where it is exposed, but there is no evidence for a stratigraphic break. Instead, the upper part of the McCann Hill Chert contains a few thin interbeds of siltstone, sandstone, and chert conglomerate whose similarity to rocks of the Nation River Formation suggests a gradational relationship.

By contrast, the upper contact of the Nation River Formation in the Calico Bluff area has been generalized through rubble and alluvium-covered slopes in the general vicinity of outcrops where the rocks are tightly folded and (or) steeply dipping. Most evidence suggests, however, that the Nation River Formation is overlain by an unnamed shale and chert formation of Late Devonian and Mississippian age which in turn is overlain by the Calico Bluff Formation of Late Mississippian age. For example, Laudon and others (1966, fig. 2), Mertie (1930, p. 110), and the writers all interpret the dip of Paleozoic rocks southwest of the mouth of the Seventymile River (fig. 3) to be predominantly to the northeast, albeit steep or vertical. If this interpretation is correct, then the sequence is Nation River Formation (oldest) overlain by unnamed chert and shale formation overlain by Calico Bluff Formation (youngest). This area has not been adequately mapped, however, and some of the rocks, such as those near Sinnot Creek may not be correctly identified. Nevertheless, a similar sequence is also indicated by attitudes near the mouth of Shade Creek and in cliffs on the north bank of the Yukon River southwest of Adams Peak.

The area from 1 to 2 miles southwest of Adams Peak (locality *A*, fig. 1) is especially important because it has a homoclinal sequence of rocks ranging in age from Cambrian to Permian, all dipping moderately or steeply to the southwest. Mertie (1933, pl. 7) thought that his unnamed chert, slate, and shale formation of Mississippian age in that area rested directly on limestone of Cambrian age, but we believe (fig. 3 and Churkin and Brabb, 1965, fig. 2) that the Road River Formation, McCann Hill Chert, and Nation River Formation intervene. The formations crop out along wooded slopes around the north rim of an abandoned river channel, and they were overlooked in previous investigations.

Mertie also overlooked the occurrence of about 100 feet of conglomerate and sandstone of Permian age in this sequence. These rocks are overlain unconformably by similar conglomerates and sandstones of Cretaceous age. Fossils from the Permian rocks have been listed by Laudon and others (1966, p. 1873) and compared by them to those of the Tahkandit Limestone. The Permian rocks rest directly and probably unconformably on shale and limestone that has long been mapped as the Calico Bluff Formation (for example, see Mertie, 1933, pl. 7) and from which J. S. Williams

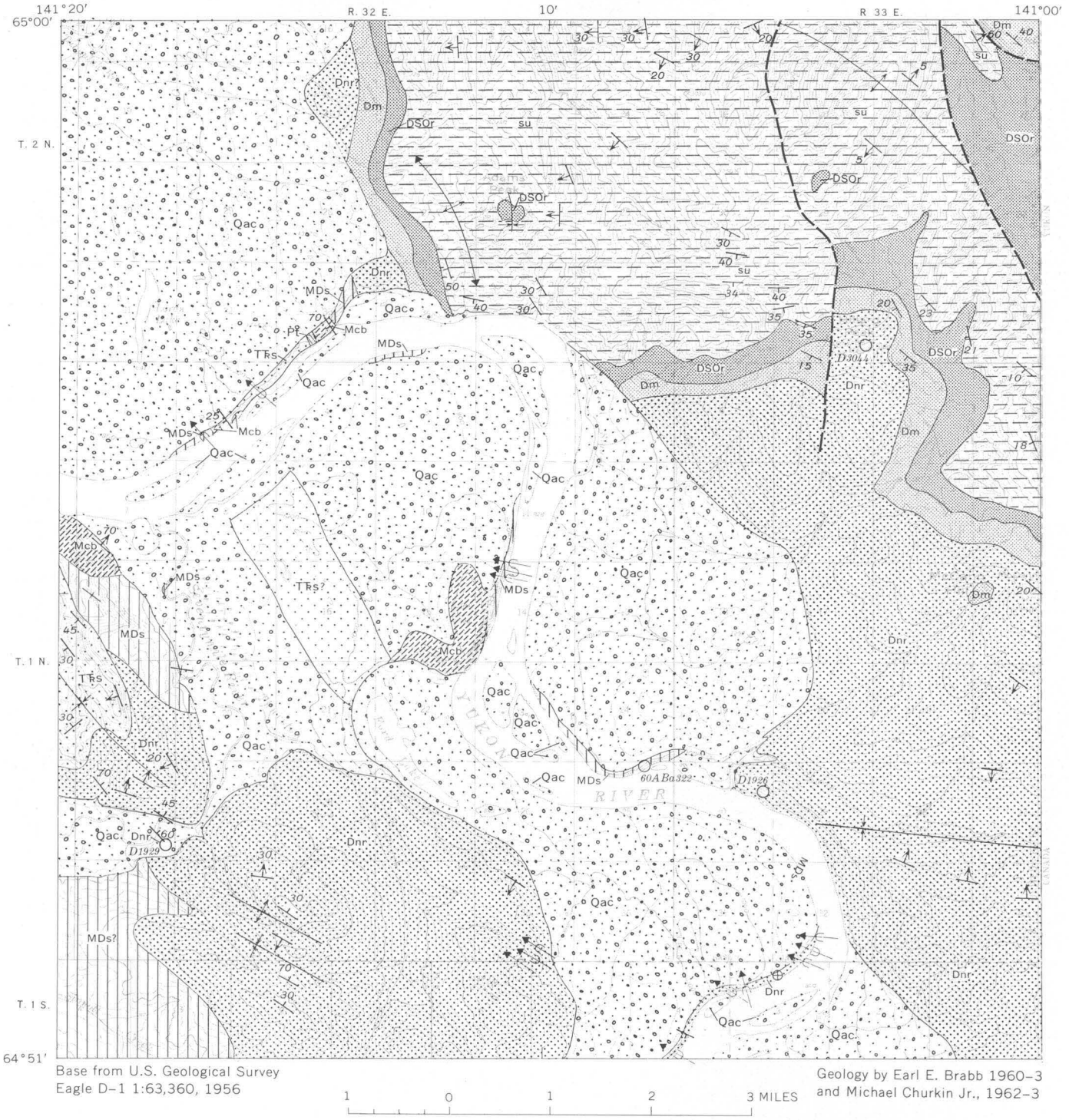

FIGURE 3.—Geologic map of the Calico Bluff area, east-central Alaska. Location of the area is shown in figure 1.

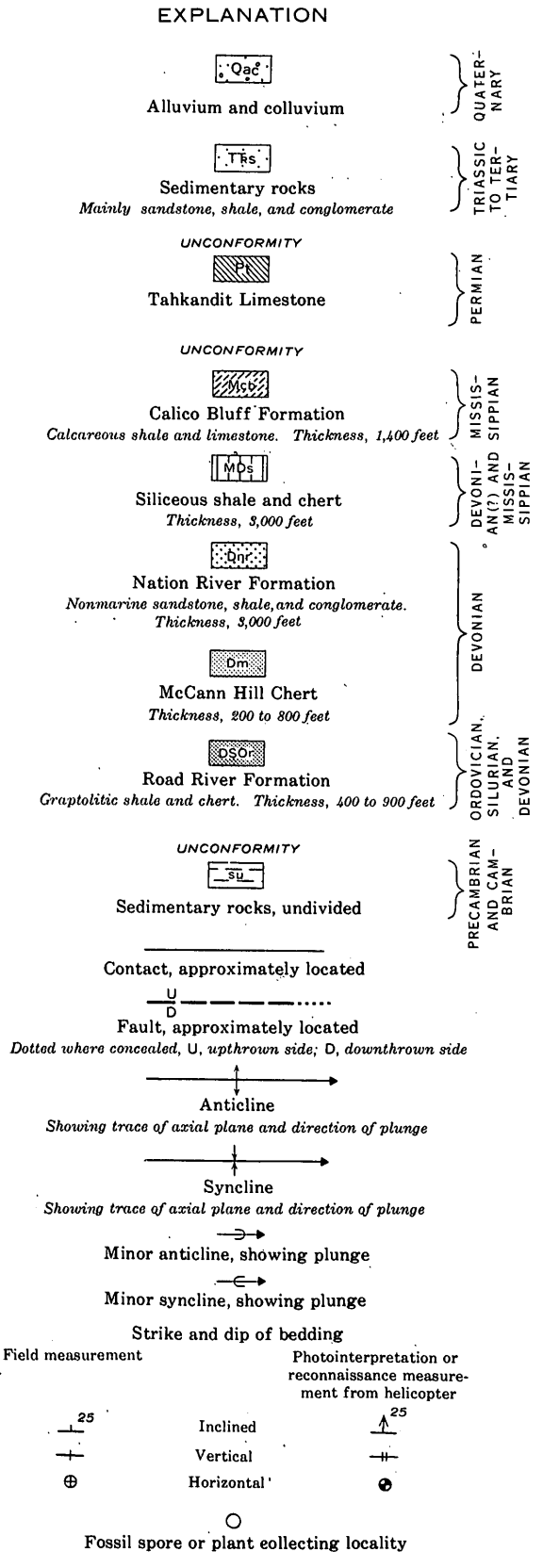

FIGURE 3.

collected the youngest known Mississippian cephalopods in Alaska (Gordon, 1957, p. 13).

Evidence from fossils to support the Devonian age of the Nation River Formation in the Calico Bluff area is meager but consistent. The McCann Hill Chert underlying the Nation River Formation has a fauna of Early and possibly Middle Devonian age near its base (Churkin and Brabb, in press). Fragmentary plant material from the Nation River Formation in the Calico Bluff area (fig. 3) and in the type area (fig. 4) was considered by David White (*in* Mertie, 1930, p. 120) to be Mississippian, and (*in* Mertie, 1933, p. 427) to be Upper Devonian or Lower Mississippian. The following new material was collected in 1960 and 1961 and identified by Richard A. Scott, of the U.S. Geological Survey, whose comments follow the locality descriptions given below (see also fig. 3).

USGS paleobot. loc. D3044 (field No. 61ABa1271). Sandstone of Nation River Formation, about 200 feet above base; lat 64°57.4′ N., long 141°03.0′ W. Collector, Earl E. Brabb, 1961.

"Late Devonian. The spores are badly preserved but are recognizable as the The Nation River assemblage."

USGS paleobot. loc. D1929 (field No. 60ABa723). Nation River Formation, SE¼ sec. 30, T. 1 N., R. 32 E., Seventymile River. Collector, Earl E. Brabb, 1960

"Middle or Late Devonian. This assemblage has been significantly metamorphosed. The remnants include fragments of forms comparable to some of those present at locality 60ABa687, including those spores with bifurcated appendages. There is no evidence of younger forms to suggest reworking of Devonian sediments."

USGS paleobot. loc. D1926 (field No. 60ABa316). Nation River Formation, NW¼ sec. 29, T. 1 N., R. 33 E., lat 64°53.3′ N., long 141°5.3′ W. Collector, Earl E. Brabb, 1960.

"Devonian(?). The spore flora in this sample has been metamorphosed so that most grains are broken and opaque. The possible age assignment is an educated guess based on shapes and fragments of spores."

Fossils from the lower part of the unnamed siliceous shale and chert formation which we believe overlies the Nation River Formation include brachiopods considered by G. H. Girty (*in* Mertie, 1930, p. 94) as possibly Devonian but more probably Mississippian. Fossil wood was collected near the brachiopod locality (see 60ABa322, fig. 3) and identified by Richard A. Scott as follows:

Field No. 60ABa322. Unnamed siliceous shale and chert formation. North bank of Yukon River, lat 64°53.5′ N., long 141°08.3′ W. Collector, Earl E. Brabb, 1960.

"Late Devonian or Early Mississippian. Only one of the 3 specimens of fossil wood could be sectioned because of coalification and degradation. The third specimen is *Callixylon*, a genus of large trees that reproduced by spores but had wood much like the conifers. The genus is widespread in Upper Devonian rocks, occurring in Russia, western and central New York, Oklahoma, Texas. It is also present in the New Albany Shale of Indiana and Kentucky, which is thought to

transgress the Devonian-Mississippian boundary. Hence, the age is most probably Late Devonian, but may also be Early Mississippian."

The upper part of the unnamed siliceous shale and chert formation grades upward into the Calico Bluff Formation of Late Mississippian age at its type locality (Mertie, 1930, p. 88).

In summary, stratigraphic relations and fossils indicate: that the Nation River Formation in the Calico Bluff area is Late Devonian; that it is underlain by the McCann Hill Chert of Early, Middle(?), and Late Devonian age, and that it is overlain by an unnamed siliceous shale and chert formation with fossils of Late Devonian or Early Mississippian age near its base. The Calico Bluff Formation of Late Mississippian age is overlain unconformably by sandy beds of the Tahkandit Limestone of Permian age.

Correspondingly, there was a repetition of distinctive siliceous shale and chert deposition during the Devonian and Mississippian. Similar chert and siliceous shale also occur in both the Ordovician and Silurian parts of the Road River Formation (Churkin and Brabb, 1965, fig. 5 and p. 173), and they are thus not restricted to a single formation or a single system.

Nation River area

The Cambrian to Permian sequence exposed southwest of Adams Peak strikes northward and is exposed again along the lower part of the Tatonduk River and its valley slopes between Pass Creek and Windfall Mountain (fig. 1). A partial measured section including limestone of Cambrian and Ordovician age at the base, the Road River Formation and McCann Hill Chert in the middle part, and the Nation River Formation at the top is shown by Churkin and Brabb (1965, fig. 4, column 3). These rocks all dip moderately and uniformly to the west. The Nation River Formation is overlain in succession by the unnamed siliceous shale and chert, the Calico Bluff Formation, and the Tahkandit Limestone. The Tahkandit is preserved at Windfall Mountain as an erosional remnant along the trough of a north-trending syncline. The rocks west of Windfall Mountain dip uniformly and gently to the east except near the mouth of the Tatonduk River where there are minor folds.

No distinctive fossils were found in the McCann Hill Chert immediately underlying the Nation River Formation in the vicinity of the Tatonduk River, but a well-preserved spore assemblage was found in the Nation River Formation at locality D1927 (see fig. 4). Richard A. Scott provided the following information about this assemblage:

USGS paleobot. loc. D1927 (field No. 60ABa451). Nation River Formation; NW¼ sec. 10, T. 2 N., R. 32 E.; lat 65°1.3′ N., long 141°13.2′ W.; north bank Tatonduk River. Collector, Earl E. Brabb, 1960.

"Late or Middle Devonian. This sample contains a well-preserved spore assemblage generally comparable to, but less diverse than that present at locality 60ABa687 (USGS loc. D1928)."

A. E. Waters, Jr., collected plants near Windfall Mountain (fig. 4) from the unnamed siliceous shale and chert which we believe overlies the Nation River Formation. David White (*in* Mertie, 1933, p. 419) commented at length on these plants and indicated that their age is probably Devonian or at latest, Early Mississippian.

The Calico Bluff Formation near Windfall Mountain has long been dated as Late Mississippian (Mertie, 1933, p. 421–422; Gordon, 1957, p. 13) and the Tahkandit Limestone as Permian (Mertie, 1933, p. 431). Mertie (1933, p. 430) explained the absence of conglomeratic beds at the base of the Tahkandit Limestone and the absence of his "Pennsylvanian" Nation River Formation as due to thrust faults, but the lack of conglomerate at the base of the Tahkandit could be a facies change and the absence of the Nation River Formation is easily explained if it is Late Devonian and not Pennsylvanian.

The Nation River Formation exposed along the Tatonduk River (fig. 4) strikes generally northward for about 10 miles and then strikes northwestward and westward along the south flank of a major anticline. Formations stratigraphically beneath the Nation River Formation are last seen in sequence near Montauk Bluff (fig. 1) because to the west they are concealed by younger formations, and on the north flank of the anticline they are extensively faulted.

Corals and other fossils of Early or Middle Devonian age were reported by Churkin and Brabb (1965, table 3) from the McCann Hill Chert directly beneath the Nation River Formation near Montauk Bluff. Several spore assemblages were collected by the writers from the Nation River Formation in the same area (see fig. 4) and identified by Richard A Scott, whose comments follow:

USGS paleobot. loc. D1928 (field No. 60ABa687). Nation River Formation; SE¼NE¼, sec. 10, T. 3 N., R. 31 E.; lat 65°6.3′ N., long 141°24.2′ W.; north bank Yukon River. Collector, Earl E. Brabb, 1960.

"Late or Middle Devonian. This sample contains an abundant, diverse, and excellently preserved assemblage of spores. There are probably more than 25 genera represented, among them, *Leiotriletes*, *Leiozonotriletes*, *Hymenozonotriletes*, *Verrucosisporites*, *Retusotriletes*, *Reticulatisporites*, *Stenozonotriletes*, and *Convolutispora*. Of particular interest is the pres-

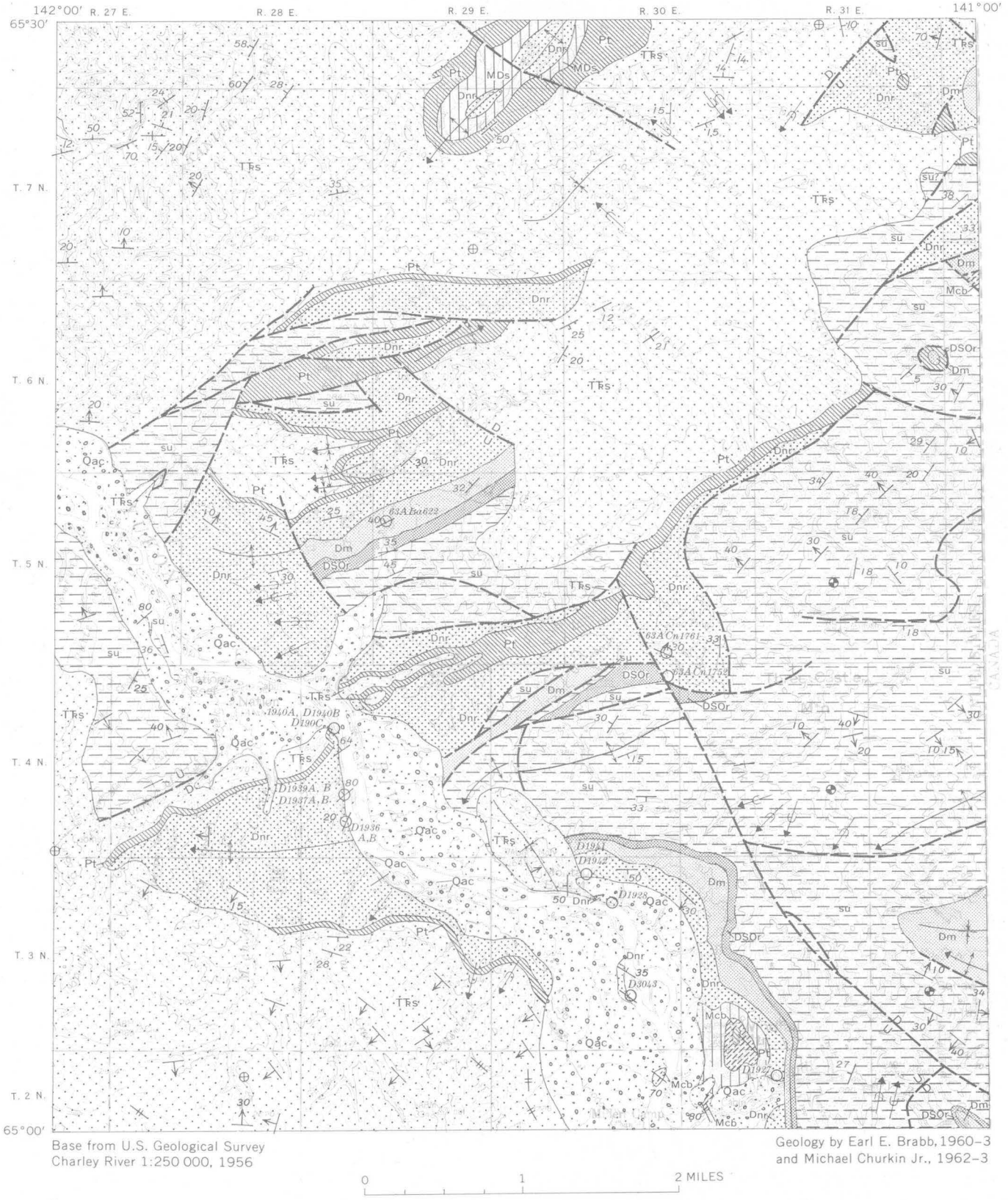

FIGURE 4.—Geologic map of the Nation River area, east-central Alaska. Location of the area is shown in figure 1. Explanation of geologic units and symbols is given in figure 3.

ence of a group of large, trilete spores with bifurcated appendages belonging to the *Archeotriletes-Hystricosporites-Ancyrospora* complex. This group is prominent in Middle and Late Devonian floras from various parts of the world. More detailed study of this assemblage may determine if it is Late or Middle Devonian. My preliminary impression is that it is probably Late Devonian."

USGS paleobot. loc. D3043 (field No. 60ABa981). Olive-gray claystone of Nation River Formation; lat 65°03.8′ N., long 141°23.2′ W., Collector, Earl E. Brabb, 1960.

"Late Devonian. This sample contains essentially the Nation River assemblage."

USGS paleobot. loc. D1941 (field No. 62ACn1023). Nation River Formation. Medium-dark-gray shale bearing plant fragments; NW¼NE¼ sec. 4, T. 3 N., R. 31 E.; lat 65°7.3′ N., long 141°24.6′ W.; west bank of second creek east of Montauk Bluff. Collector, Michael Churkin, Jr., 1962.

"Late or Middle Devonian. This assemblage is poorly preserved. However, the remains of the spores are recognizable as about the same group present in 62AA311A (D1937–A) and most of the other Late Devonian samples (except 62ACn1101, 62ACn1102, and 62ACn1204)."

USGS paleobot. loc. D1942 (field No. 62ACn1031). Nation River Formation. Medium-dark-gray shale stratigraphically below 62ACn1023; Center of SE¼ sec. 33, T. 4 N., R. 31 E.; lat 65°7.7′ N., long 141°26.4′ W. About ½ mile upstream from 62ACn1023. Collector, Michael Churkin, Jr., 1962.

"Devonian(?). A number of spores are present in this sample, but they are badly corroded and broken. Some of the remains suggest Devonian forms, and nothing recognizable is incompatible with this age, but there is no conclusive evidence."

In summary, stratigraphic sequence and fossils indicate that the Nation River Formation in the area from the Tatonduk River to Windfall Mountain and Montauk Bluff is probably Late Devonian; that it is underlain by the McCann Hill Chert, which has fossils of Early or Middle Devonian age; and that it is overlain by an unnamed siliceous shale and chert formation, which has plants of probable Devonian age.

West of Montauk Bluff, the sequence above the Nation River Formation is different and herein lies the problem. The Nation River Formation in the vicinity of the mouth of the Nation River (locality *B*, figs. 1 and 4) is overlain by the Tahkandit Limestone of Permian age, not the unnamed siliceous shale of Devonian and Mississippian age. Nearly all previous investigators have assumed that the Nation River is overlain conformably by the Tahkandit and therefore must be only slightly older, or Pennsylvanian(?). They have then used structure to explain the absence of this "Pennsylvanian(?)" formation in the Calico Bluff area (fig. 3) and near Windfall Mountain (fig. 1). They have overlooked the possibility of an unconformity at the base of the Tahkandit Limestone.

The contact between the Nation River Formation and the Tahkandit Limestone in the type area of these formations can be seen on the southwestern bank of the Yukon River about 1 mile south of the mouth of Nation River (figs. 1, 4, 5). The uppermost shale and siltstone beds of the Nation River Formation, perhaps 100 feet of section, are exposed along the crest of a small anticline, and the older part of the formation is exposed along the river bank farther upstream in the core of a major anticline. The lowest 75 feet of the overlying Tahkandit Limestone consists of sandstone and chert-pebble conglomerate. Unlike the sandstone and conglomerate in the Nation River Formation, these detrital rocks contain abundant productid brachiopods, they have a calcareous matrix, and most of them are glauconitic. Some of the beds are bright green because of abundant glauconite. The contact between the Nation River Formation and the Tahkandit is mostly covered, but the beds on both sides are accordant. In July 1962 the writers dug out the contact and found a 6-inch layer of light-bluish-gray clay separating the top of the Nation River Formation from the basal Tahkandit. This unstratified clay that becomes plastic when wet is interpreted as a residual deposit or paleosol developed by weathering of the Nation River shale prior to Tahkandit sedimentation. In the basal Tahkandit the abundance of glauconite suggests that the contact is disconformable and the associated varicolored chert, sand, and pebbles in the Tahkandit probably represent reworked Nation River conglomerate and sandstone.

The Tahkandit beds shown in figure 5 have furnished a prolific invertebrate fauna (see Mertie, 1930, p. 125-127 for list) which has long been considered Permian, but no fossils had previously been found in the Nation River Formation at this locality. In 1962, several shale samples were collected from which Richard A. Scott eventually extracted the following spore assemblages, arranged with the stratigraphically highest (most northerly localities) first (see figs. 4 and 5):

USGS paleobot. loc. D1940C (field No. 62ACn1204). From 6-inch layer of light-bluish-gray clay separating very top of Nation River Formation from overlying Tahkandit Limestone; NW¼NW¼ sec. 17, T. 4 N., R. 30 E., lat 65°10.6′ N., long 141°41.8′ W. Stratigraphically just above sample 62ACn1012. Collector, Michael Churkin, Jr., 1962.

"Late or Middle Devonian. Excellently preserved assemblage like that in sample 62ACn1011, (D1940A)."

USGS paleobot. loc. D1940B (field No. 62ACn1012). Top of Nation River Formation; from highest stratified shale below Tahkandit Limestone; NW¼NW¼, sec. 17, T. 4 N., R. 30 E., lat 65°10.8′ N., long 141°41.8′ W. West bank of Yukon River. Collector, Michael Churkin, Jr., 1962.

"Late or Middle Devonian. Essentially the same assemblage as in sample 62ACn1011 (D1940A), but slightly less well preserved.

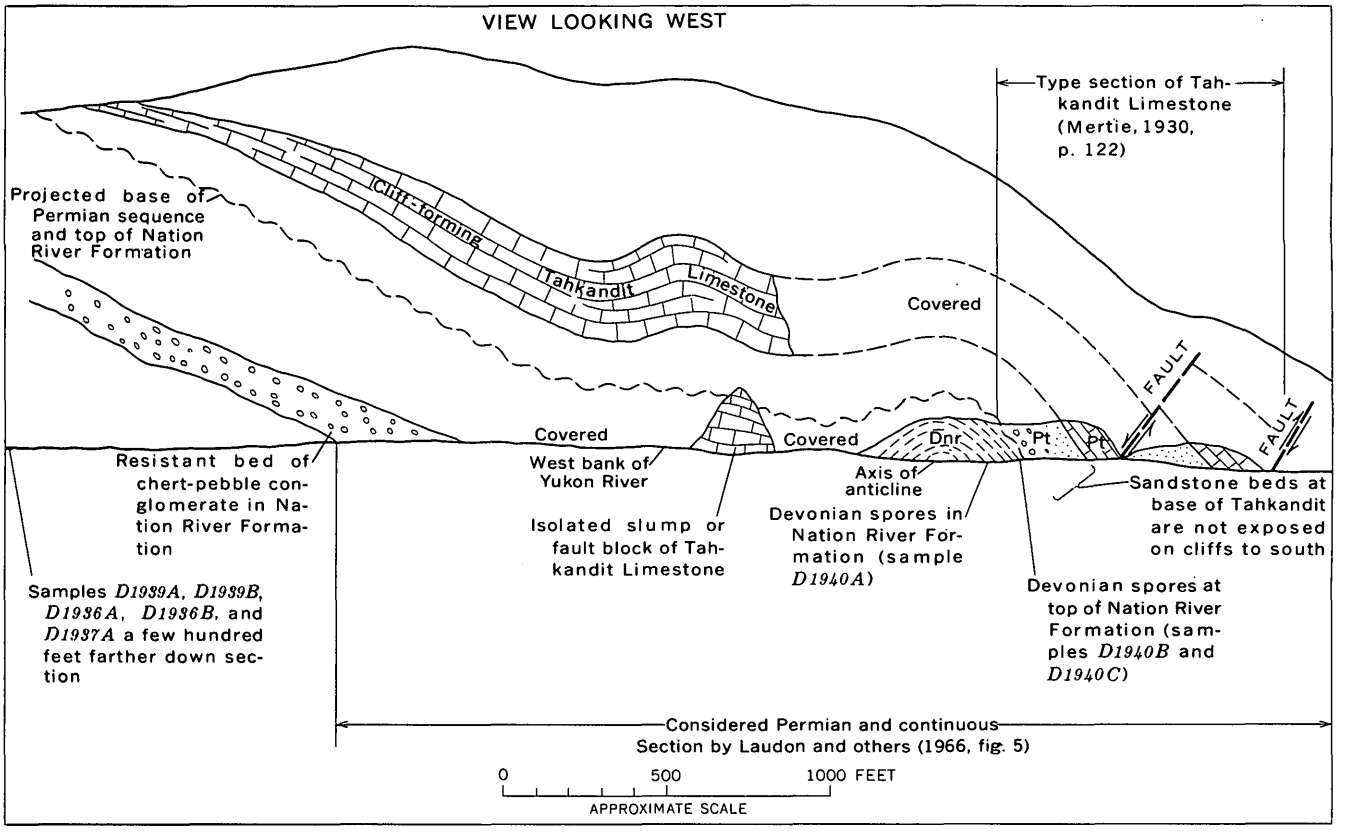

FIGURE 5.—Sketch of geology at type locality of Nation River (Dnr) and Tahkandit (Pt) Formations opposite mouth of Nation River.

USGS paleobot. loc. D1940A (field No. 62ACn1011). Nation River Formation; from shale about 75 feet below contact with Tahkandit Limestone; NW¼NW¼, sec. 17, T. 4 N., R. 30 E., lat 65°10.8′ N., long 141°41.8′ W; West bank of Yukon River. Probably several thousand feet stratigraphically above 62ACn1001. Collector, Michael Churkin, Jr., 1962.

"Late or Middle Devonian. This assemblage has much in common with the Devonian samples listed from the Nation River; however, it contains some new forms and can readily be distinguished from the samples occuring lower in the formation."

USGS paleobot. loc. D1939A (field No. 62ACn1001). Nation River Formation. Olive-gray plant-bearing silty shale thinly interbedded with fine-grained, medium-gray graywacke, NE¼SW¼, sec. 20, T. 4 N., R. 30 E.; lat 65°9.5′ N., long 141°41.3′ W. West bank of Yukon River. Many hundreds of feet stratigraphically higher than 62ACn1002. Collector, Michael Churkin, Jr., 1962.

"Late or Middle Devonian. This assemblage is substantially the same as that in sample 60ABa687."

USGS paleobot. loc. D1939B (field No. 62ACn1002). Nation River Formation. From shale at top of thick conglomerate; SE¼SW¼, sec. 20, T. 4 N., R. 30 E.; lat 65°9.3′ N., long 141°41.3′ W. West bank of Yukon River. Many hundreds of feet stratigraphically higher than 62AA311A. Collector, Michael Churkin, Jr., 1962.

"Late or Middle Devonian. A good assemblage of well-preserved spores essentially similar in composition to 62AA311A. (D1937A)."

USGS paleobot. loc. D1937A (field No. 62AA311A). Nation River Formation. From silty claystone interbedded with chert-pebble conglomerate and graywacke; NE¼NW¼, sec. 29, T. 4 N., R. 30 E.; lat 65°9.0′ N., long 141°41.5′ W. West bank of Yukon River. Several hundred feet stratigraphically above 62AA281. Collector, Arne Aadland, 1962.

"Middle or Late Devonian. A well-preserved and abundant assemblage of spores. All remarks for age and composition under locality 60ABa687 (D1928) apply for this sample."

USGS paleobot. loc. D1937B (field No. 62AA311B). Nation River Formation. NE¼NW¼, sec. 29, T. 4 N., R. 30 E.; lat 65°9.0′ N., long 141°41.5′ W. West bank of Yukon River 15 feet stratigraphically below 62AA311A. Collector, Arne Aadland, 1962.

"Late or Middle Devonian. Basically the same flora as in 62AA311A, (D1937A), but fewer forms recognizable and much poorer preservation."

USGS paleobot. loc. D1936B (field No. 62AA281). Nation River Formation. Interbedded silty shale and graywacke. SE¼SW¼, sec. 29, T. 4 N., R. 30 E,; lat 65°8.3′ N., long 141°41.2′ W. Above west bank of Yukon River and about 150 feet stratigraphically above 62AA251(C). Collector, Arne Aadland, 1962.

"Middle or Late Devonian. This assemblage consists of badly corroded spores. Fragments indicate that the forms present are substantially those of locality 62AA251(C), (D1936A)."

USGS paleobot. loc. D1936A (field No. 62AA251C). Nation River Formation. Silty claystone. SE¼SW¼, sec. 29, T. 4 N.,

R. 30 E.; lat 63°8.3′ N., long 141°41.2′ W. Above west bank of Yukon River. Collector, Arne Aadland, 1962.

"Middle or Late Devonian. A spore assemblage essentially similar to that from locality 60ABa687, (D1928), but less well preserved. The group of spores with bifurcated, anchor-like appendages appears to be lacking; however, this may be a preservation problem because the appendages break off easily. In any case, presence of extremely large, trilete spores approaching the megaspore size range provides independent evidence for Middle or Late as opposed to Early Devonian age. As for locality 60ABa687 (D1928), my feeling is that the age is Late rather than Middle Devonian, but I cannot document this now."

The spores substantiate the physical evidence for an unconformity and indicate that near the mouth of the Nation River, at least, the unnamed siliceous shale and chert formation and the Calico Bluff Formation were removed prior to deposition of the Tahkandit Limestone, if indeed they were ever deposited there in the first place.

If this interpretation is correct, then

(1) There is no unnamed formation beneath the Tahkandit on the south bank of the Yukon River across the mouth of the Nation River, as proposed by Laudon and others (1966, p. 1870). This "unnamed" formation must, by definition, remain the Nation River Formation in this, its type, locality.

(2) There is no need for "unusual structural complications" in the Nation River area, as alleged by Laudon and others (1966, p. 1870).

(3) There is no need for a thrust fault in the Windfall Mountain area, as mentioned by Mertie (1933, p. 430).

(4) There is no need for thrust faults or a post-Mississippian and pre-Pennsylvanian unconformity in the Calico Bluff area, the other alternatives proposed by Laudon and others (1966, p. 1871).

The Nation River Formation is overlain by the Tahkandit Limestone over an area of at least 400 square miles extending from 4 miles southwest of Montauk Bluff (fig. 4) northward to tributaries of the Kandik River about 15 miles north of the mouth of the Nation River, and northeastward to the Alaska-Yukon Territory boundary. The unnamed siliceous shale and chert formation stratigraphically above the Nation River and below the Tahkandit appears also along an anticline in the north-central part of figure 4, suggesting that the 400-square-mile area mentioned above may have been upwarped to form a broad arch during the late Paleozoic.

Three spore samples collected in this 400-square-mile area contribute additional proof that the Nation River Formation is Devonian and is closely related in age to the McCann Hill Chert (see fig. 4 for localities):

Field No. 63ACn1761. Nation River Formation. From medium-gray chert wacke interbedded with light-green to olive-gray micaceous shale containing abundant plant fragments. Center of SE¼, sec. 33, T. 5 N., R. 31 E.; lat 65°12.8′ N., long 141°21.4′ W., High cut bank on east side of Hard Luck Creek. Collector, Michael Churkin, Jr., 1963.

"Late or Middle Devonian. This sample contains less than one-half as many forms as 63ACn1752."

Field No. 63ACn1752. Nation River Formation. From medium-gray micaceous shale thinly interbedded with very fine grained calcareous quartz arenite. SW¼NE¼, sec. 1, T. 4 N., R. 31 E.; lat 65°12.8′ N., long 141°20.7′ W., From high cut bank on east side of Hard Luck Creek. Collector, Michael Churkin, Jr., 1963.

"Late or Middle Devonian. This sample contains an assemblage of Nation River species but preservation is not as good as in the best samples."

Field No. 60ABa622. McCann Hill Chert. Medium-dark-gray fine-grained siltstone. Lat 65°16.3′ N., long 141°38.8′ W.; Collector, Earl E. Brabb, 1960.

"Probably Late Devonian. The broken and highly metamorphosed spores in this sample appear comparable, in so far as their features can be observed, with the assemblage in the Nation River Formation. A variety of trilete forms are present along with the spores with hooked assemblages."

CONCLUSIONS

Recognition that the Nation River Formation is Devonian and not Pennsylvanian makes the geologic history of east-central Alaska more in harmony with that of northern Alaska and the Yukon Territory. The Nation River Formation is similar in lithology to widespread formations of late Devonian age such as the Kanayut Conglomerate in the Brooks Range of Alaska (Brosgé and others, 1962) and the Imperial Formation of the Yukon (Norris and others, 1963), whereas no comparable formations of definite Pennsylvanian age have been recognized in this same area. The Nation River Formation and its lateral equivalents are not associated with a Pennsylvanian orogeny but instead are the record of tectonic instability during the Late Devonian.

REFERENCES

Brabb, E. E., 1962, Preliminary geologic map of part of the Charley River quadrangle (1:250,000), east-central Alaska: U.S. Geol. Survey open-file report.

Brabb, E. E., and Churkin, Michael, Jr., 1964, Preliminary geologic map of the Charley River (1:250,000) quadrangle, east-central Alaska: U.S. Geol. Survey open-file report.

———1965, Preliminary geologic map of the Eagle (D–1) (1:63,360) quadrangle, east-central Alaska: U.S. Geol. Survey open-file report.

Brooks, A. H., and Kindle, E. M., 1908, Paleozoic and associated rocks of the upper Yukon, Alaska: Geol. Soc. America Bull., v. 19, p. 255–314.

Brosgé, W. P., Dutro, J. T., Jr., Mangus, M. D., and Reiser, H. N., 1962, Paleozoic sequence in eastern Brooks Range, Alaska: Am, Assoc. Petroleum Geologists Bull., v. 46, no. 12, p. 2174–2198.

Cairnes, D. D., 1914. The Yukon-Alaska International Boundary, between Porcupine and Yukon Rivers: Canada Geol. Survey Mem. 67, 161 p.

Churkin, Michael, Jr., and Brabb, E. E., 1965, Ordovician, Silurian and Devonian biostratigraphy of east-central Alaska: Am. Assoc. Petroleum Geologists Bull., v. 49, p. 172–185.

———in press, Devonian rocks of the Yukon-Porcupine Rivers area and their tectonic relation to other Devonian sequences in Alaska: Calgary, Alberta Soc. Petroleum Geologists, Proc. Internat. Symposium on the Devonian System.

Collier, A. J., 1903, The coal resources of the Yukon, Alaska: U.S. Geol. Survey Bull. 218, 71 p.

Gordon, Mackenzie, Jr., 1957, Mississippian cephalopods of northern and eastern Alaska: U.S. Geol. Survey Prof. paper 283, 61 p.

Laudon, L. R., Hartwig, A. E., Morgridge, D. L., and Omernik, J. B., 1966, Middle and Late Paleozoic stratigraphy, Alaska-Yukon border area between Yukon and Porcupine Rivers: Am. Assoc. Petroleum Geologists Bull., v. 59, no. 9, p. 1868–1889.

Mertie, J. B., 1930, Geology of the Eagle-Circle district, Alaska: U.S. Geol. Survey Bull. 816, 168 p.

———1933, The Tatonduk-Nation district: U.S. Geol. Survey Bull. 836–E, p. 347–443.

———1937, The Yukon-Tanana region, Alaska: U.S. Geol. Survey Bull. 872, 276 p.

Nelson, S. J., 1961, Permo-Carboniferous of the northern Yukon Territory: Alberta Soc. Petroleum Geologists Jour., v. 9, p. 1–9.

Norris, D. K., Price, R. A., and Mountjoy, E. W., compilers, 1963, Northern Yukon Territory and northwestern District of MacKenzie: Geol. Survey Canada Map 10–1963.

Scott, R. A., and Doher, L. I., 1967, Palynological evidence for Devonian age of the Nation River Formation, east-central Alaska, *in* Geological Survey Research 1967: U.S. Geol. Survey Prof. Paper 575–B, p. B45–B49.

FOSSILIFEROUS LOWER PALEOZOIC ROCKS IN THE CUPSUPTIC QUADRANGLE, WEST-CENTRAL MAINE

By DAVID S. HARWOOD and WILLIAM B. N. BERRY,
Washington, D.C., Berkeley, Calif.

Abstract.—The Taconic unconformity in the Cupsuptic quadrangle separates conglomerate, limestone, and calcareous slate of Silurian age (Llandovery and Ludlow) from a eugeosynclinal sequence of slate, greenstone, and graywacke of Middle Ordovician and older age. Middle Ordovician graptolites, indicative of zone 12, *Climacograptus bicornis*, in black slate of an unnamed unit establish the equivalence of this unit to the Beauceville Formation near Magog, Quebec; the lower part of the Normanskill Shale of New York; various fossiliferous units in northeastern Maine; and date the Partridge Formation, and at least part of the Dixville Formation, of New Hampshire and Maine.

A highly folded eugeosynclinal sequence consisting predominantly of slate, graywacke, and greenstone, dated in part as late Middle Ordovician by newly discovered graptolites, lies in a regional anticlinorium in the Cupsuptic quadrangle, west-central Maine (fig. 1). The pre-Silurian stratigraphic sequence is virtually the same as that recognized originally in New Hampshire by Billings (1935) and subsequently extended into Maine by Milton (1960), C. V. Guidotti (written commun., 1965), and Green (1964; written commun., 1965).

Interbedded phyllite, quartzite, and quartz-feldspar granulite,[1] shown on figure 2 as undivided older Paleozoic rocks, are in the core of the regional anticlinorium in the south-central part of the quadrangle. The older Paleozoic rocks are overlain to the southeast by greenstone and slate and graptolite-bearing black slate. To the northwest the older Paleozoic rocks are overlain by black slate, greenstone, and graywacke of the Dixville Formation (Green, 1964), which is correlated with the greenstone and slate and graptolite-bearing slate to the southeast.

[1] Granulite is used here in the sense of Harker (1939, p. 246), to mean an equigranular rock composed of quartz and feldspar, lesser amounts of muscovite and chlorite, and locally biotite and garnet.

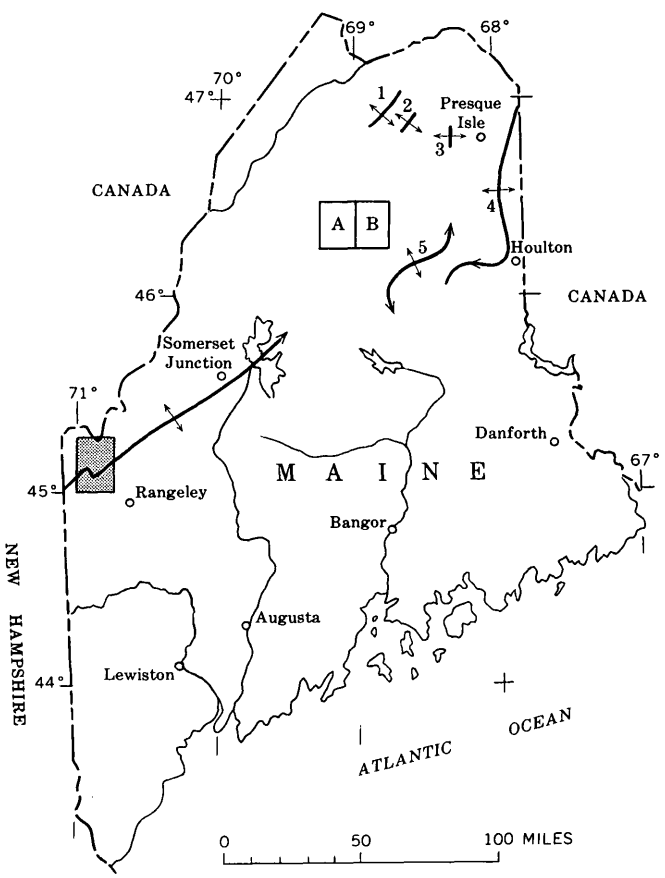

STRUCTURAL FEATURES

1. Pennington anticline
2. Portage anticline
3. Castle Hill anticline
4. Aroostook-Matapedia anticlinorium
5. Weeksboro-Lunksoos Lake anticlinorium

QUADRANGLES

A. Spider Lake
B. Millinocket Lake

FIGURE 1.—Index map of Maine, showing Cupsuptic quadrangle (shaded) and selected structural features in northeastern Maine.

U.S. GEOL. SURVEY PROF. PAPER 575-D, PAGES D16-D23

The pre-Silurian rocks are unconformably overlain by conglomerate and locally by calcareous rocks of Silurian age in the southeast, west-central, and northwest parts of the quadrangle. The rocks of Silurian age lie below, and interfinger with, well-bedded gray slate and quartzite of Silurian or Devonian age or both, shown as undivided younger Paleozoic rocks on figure 2.

There is a marked difference in the type and degree of folding in the rocks above and below the unconformity. The pre-Silurian rocks are characterized by northeast-, and locally northwest-trending isoclinal folds that have steep-dipping axial surfaces and variable but steep-plunging axes. In contrast to this, the Silurian and younger rocks contain northeast- to east-trending open folds that have gently dipping limbs, steep-dipping axial surfaces and gently plunging axes. North-trending, steep-dipping slip cleavage deforms bedding, early axial plane cleavage, and early minor folds adjacent to the three quartz monzonite plutons and along the southern border of the quadrangle. The differences in trend and plunge of folds in the pre-Silurian and Silurian rocks, coupled with the fact that the Silurian rocks truncate both the Middle Ordovician and the older Paleozoic rocks, indicate that at least local folding along northwest trends, uplift, and erosion accompanied the Taconic orogeny in the Late Ordovician to earliest Silurian time. The main period of regional folding, however, was along northeast trends and probably was related to the Acadian orogeny in Middle Devonian time. The north-trending slip cleavage was developed after the main period of regional folding and is tentatively related to the intrusion of the plutonic bodies in late Middle to Late Devonian time.

The metasedimentary and volcanic rocks of the region are in the chlorite zone of regional metamorphism. A body of metadiorite and serpentinite, probably of Late Ordovician age, intrudes the Dixville Formation in the northeast part of the quadrangle. Three quartz monzonite plutons of probable late Devonian age intrude the pre-Silurian rocks and produce a maculose to equigranular hornfels. Three contact metamorphic zones marked by the first appearance of biotite, andalusite, and sillimanite, respectively, have been mapped around the Cupsuptic pluton.

STRATIGRAPHY

Middle Ordovician and older rocks

Older Paleozoic rocks.—Purple, green, and black phyllite; quartzite; quartz-feldspar granulite; and minor greenstone make up the undivided older Paleozoic rocks. These rocks, most recently described in the area adjacent to the southwest by Green (1964), have been mapped as a continuous belt from north-central New Hampshire, where they were named the Albee Formation by Billings (1935). The phyllite and arenaceous rocks, interbedded in variable proportions in the Cupsuptic area, are similar to the Albee of the type section except for hematite-bearing purple phyllite. It is possible that the absence of hematite, and thus of the purple coloration of the phyllite, are due to the higher grades of regional metamorphism in New Hampshire. The purple phyllite and quartzite are overlain by mappable units of green phyllite and quartzite, green phyllite, and black phyllite. Discontinuous greenstone layers generally less than 100 feet thick are scattered in the predominantly pelitic rocks but tend to be more abundant at or near the contact between green and black phyllite. Quartzite and granulite beds range in thickness from a few inches to about 3 feet and contain characteristic paper-thin micaceous partings referred to as the "pinstripe" structure by geologists in northern New England. Locally the arenaceous beds make up 40 percent of an exposure, but the average is about 10 percent.

Fossils have not been found in the older Paleozoic rocks in the Cupsuptic area nor in the Albee Formation with which they are correlated. Billings (1956, p. 95) inferred from regional correlations that the Albee was Middle Ordovician or older, an age consistent with the data in this report.

Greenstone and slate unit.—Dark-green massive to crudely foliated greenstone overlies the older Paleozoic rocks in the southeastern part of the quadrangle. The greenstone weathers light rusty tan and consists of actinolite, chlorite, albite, epidote, quartz, sphene, and calcite and minor pyrite and magnetite. Small epidote-calcite-quartz pods are common, and numerous joints and fractures contain calcite-epidote veinlets. Primary volcanic structures are rare, although in one outcrop poorly preserved pillows are present. Light-green, white-weathering felsite occurs locally in the greenstone and is most common as layers a few feet to a few tens of feet thick adjacent to beds of black slate. The greenstone interfingers laterally with black slate. South of Kamankeag Brook (fig. 2) the unit is predominantly greenstone and has a maximum thickness of 7,500 feet. North of Kamankeag Brook, greenstone occurs in the upper 1,400 feet of the unit, which is predominantly rusty-weathering black slate. The slate is highly fissile and sulfidic and contains minor amounts of dark-gray sulfidic quartzite beds as much as 1 inch thick.

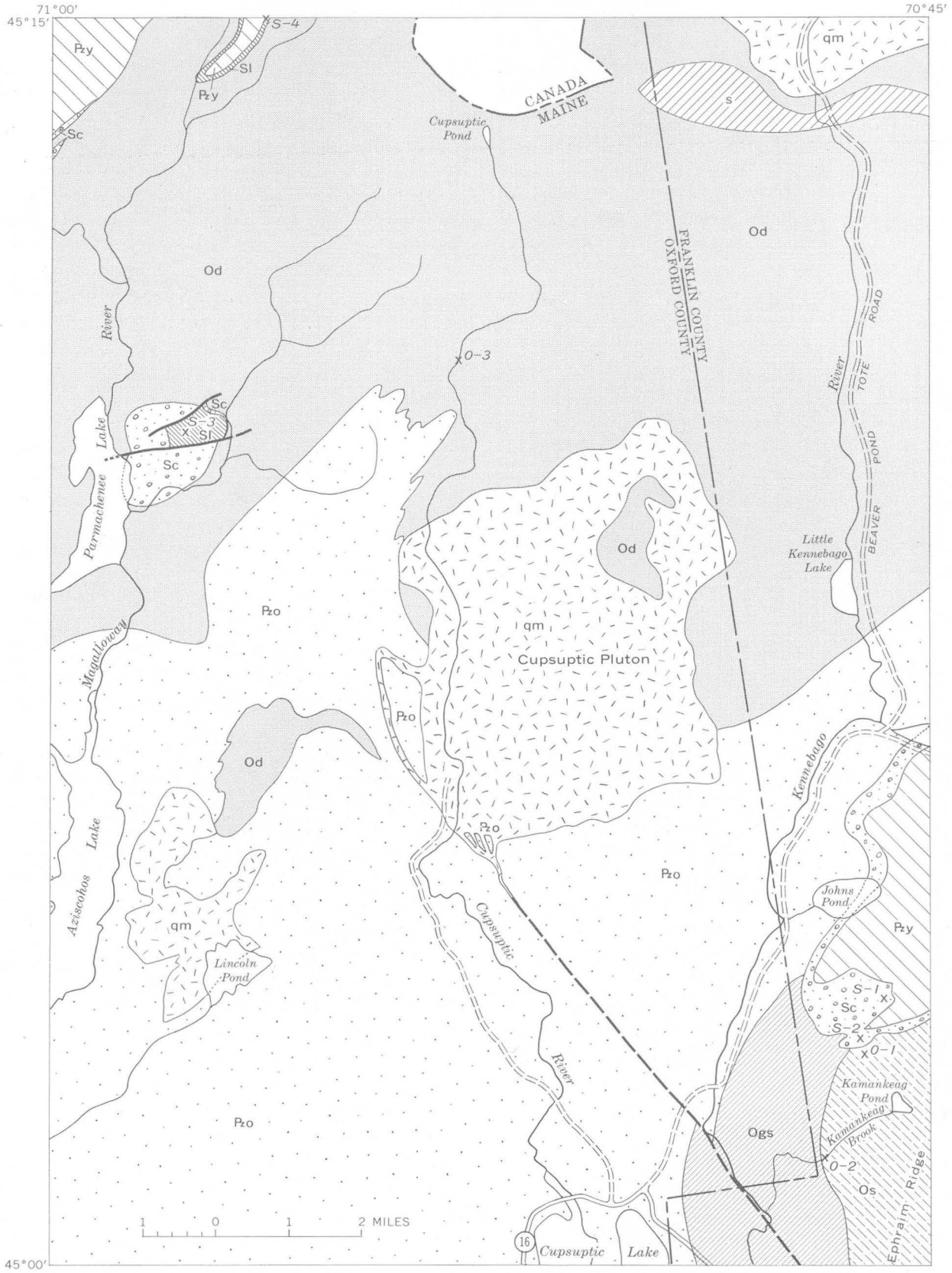

FIGURE 2.—Preliminary geologic map of the Cupsuptic quadrangle, west-central Maine.

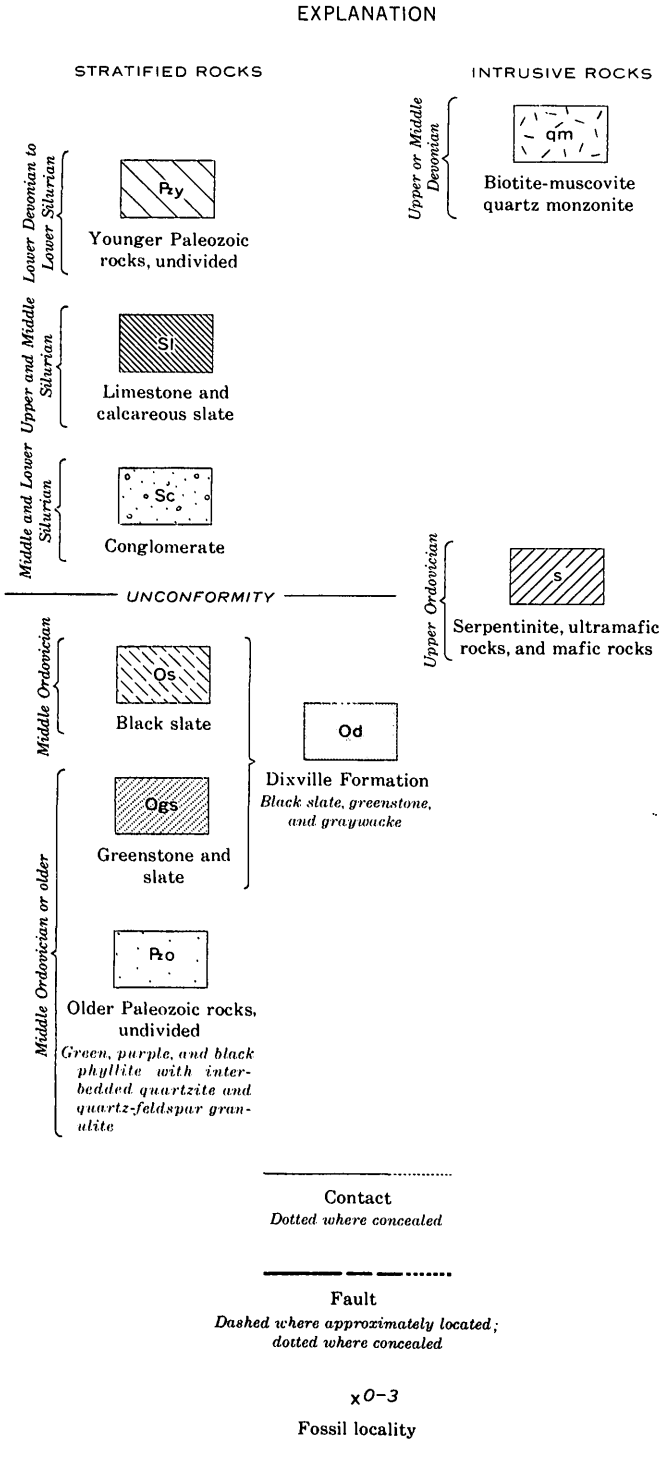

FIGURE 2.

No fossils have been found in the greenstone and slate unit, but it underlies the graptolite-bearing slate described below and therefore must be Middle Ordovician or older.

Black slate unit.—Primarily black slate overlies the greenstone and slate unit in the southeast part of the quadrangle. Typical exposures are found on the low hills northwest of Kamankeag Pond, in Kamankeag Brook east of the Oxford-Franklin County line, and on the prominent ridges at the north end of Ephraim Ridge (fig. 2). In addition to black slate, calcareous lithic graywacke, dark-gray sulfidic quartzite, and minor greenstone are present in variable proportions. Calcareous lithic graywacke in beds and lenses from 1 to 10 feet thick is found locally in the lower 500 feet of the unit. The graywacke generally makes up less than 25 percent of an exposure, except in Kamankeag Brook east of the county line where it is exposed for about 150 feet across strike and contains thin beds and partings of black slate. Here it makes up 85 percent of the section. Dark-gray sulfidic quartzite in beds from 1 to 6 inches thick makes up less than 5 percent of the lower part of the unit but constitutes as much as 30 percent of its upper part. On Ephraim Ridge, quartzite beds as much as 3 inches thick alternate with black slate beds from 6 to 10 inches thick to produce cyclic bedding that is locally graded. A few greenstone lenses less than 50 feet thick are scattered within the black slate.

Black slate in the vicinity of fossil locality O–1 (fig. 2) is hard, siliceous, and poorly cleaved and contains dark-gray pyritic chert laminae as much as 3 millimeters thick. All gradations have been observed between this siliceous slate and the soft sooty-black, highly fissile variety interbedded in the graywacke at fossil locality O–2. On Ephraim Ridge the slate is commonly maculose and contains fine-grained porphyroblasts of biotite and andalusite.

The calcareous lithic graywacke is fine to medium grained and contains lens-shaped fragments of black slate, green slate, and black chert as much as half an inch in maximum diameter. Quartz, plagioclase, calcite, lithic fragments, and minor tourmaline, zircon, and pyrite are set in a matrix of sericite and chlorite. At fossil locality O–2, fragments of shelly fossils are scattered in the graywacke, and the black-slate partings contain poorly preserved graptolites.

The contact between the black-slate unit and the underlying greenstone unit is nowhere exposed, being covered by glacial drift, but is believed to be gradational. The transition into the black slate is shown by alternating layers of greenstone and black slate and

locally is topographically marked by low hogback ridges and depressions a few tens of feet wide. The layers of slate and greenstone are apparently conformable, and the inferred contact is placed east of the easternmost greenstone layer. The top of the black slate unit is not exposed in the Cupsuptic quadrangle. R. H. Moench (written commun., 1964), reported that the black slate unit is overlain conformably by medium- to coarse-grained graywacke immediately southeast of the Cupsuptic quadrangle. The maximum outcrop width of the black slate unit within the quadrangle is 6,500 feet; it therefore has a maximum thickness of about 6,000 feet, if the sequence is homoclinal and the average dip is 70°. The actual thickness cannot be accurately determined from available data, but it may be as little as 3,000 feet if minor folding is prevalent.

The black slate unit has been dated as late Middle Ordovician from graptolites found at locality O–1 and listed in table 1. The graptolite assemblage is characteristic of zone 12 (Berry, 1960). Black slate at locality O–2 contains the graptolites *Climacograptus* sp. and *Dicellograptus* sp. In addition, the graywacke at locality O–2, studied by R. B. Neuman, of the U.S. Geological Survey, contains highly deformed fragments of bryozoans, pelecypods, gastropods, pelmatozoans, and brachiopods. One brachiopod fragment tentatively identified as either *Bilobia* or *Diambonia* is consistent with a Middle Ordovician age determined from the graptolites in table 1.

TABLE 1.—*Middle Ordovician graptolites from locality O–1, Cupsuptic quadrangle, Maine*

Climacograptus bicornis (Hall)
C. scharenbergi Lapworth?
Corynoides sp.
Cryptograptus tricornis (Carruthers)
Dicellograptus gurleyi Lapworth?
D. sp.
Didymograptus sagitticaulis Gurley?
Glyptograptus euglyphus var. *pygmaeus* (Ruedemann)?
G. teretiusculus (Hisinger)
G. sp.
Hallograptus bimucronatus (Nicholson)
H. mucronatus (Hall)?
Orthograptus calcaratus var. *acutus* (Lapworth)
O. calcaratus var. *incisus* (Lapworth)
O. sp. (of the *O. calcaratus* group)

Dixville Formation.—Green (1964) assigned the name Dixville Formation to black phyllite, schist, quartzite, and amphibolite that overlie the Albee Formation immediately southwest of the Cupsuptic area. It is herein proposed that the name Dixville Formation be adopted by the U.S. Geological Survey. The formal member names proposed by Green (1964), however, are not retained because the mafic volcanic unit critical to the original subdivision is not continuous or restricted to one stratigraphic position in the Cupsuptic quadrangle. The Dixville Formation, exposed in the northern half of the quadrangle (fig. 2), is composed of a lower part consisting of rusty-weathering black phyllite and an upper part of fine- to coarse-grained graywacke. Locally, greenstone lenses several hundred feet thick and felsite beds of highly variable thickness are present in both the black phyllite and graywacke. Near locality O–3 the rock is highly fractured, soft, sooty-black slate containing light-greenish-gray felsic tuff beds about 2 inches thick.

One specimen of *Protospongia* sp. found in the black slate on the west bank of the Cupsuptic River at locality O–3 was studied by R. M. Finks, Queens College, New York, but it was too fragmentary to reveal specific characteristics. *Protospongia* ranges in age from Cambrian to Ordovician, but an Ordovician age seems more tenable for the Dixville Formation because similar rocks in the equivalent stratigraphic position contain Middle Ordovician brachiopods in the vicinity of Somerset Junction (fig. 1) (Boucot, 1961; E. V. Post, written commun., 1964).

Silurian rocks

Conglomerate.—Polymict and quartz-pebble conglomerate locally form the basal Silurian units in three widely separated areas of the quadrangle. In the northwest corner, polymict conglomerate lenses as much as 250 feet thick rest unconformably on the graywacke member of the Dixville Formation. Near Parmachenee Lake (fig. 2), polymict and quartz-pebble conglomerate as much as 800 feet thick unconformably overlies the black slate member of the Dixville Formation. In the vicinity of Johns Pond, polymict conglomerate outlines the south limb of an open syncline and is overlain locally by quartz-pebble conglomerate that forms the basal unit on the north limb of the syncline. These basal conglomerates near Johns Pond truncate the black slate unit, the greenstone and slate unit, and part of the undivided older Paleozoic rocks. Although the unconformity is not exposed in the quadrangle, it is inferred from widely divergent dips in the overlying and underlying rocks.

The composition and size of the clasts in the polymict conglomerate vary widely in the Cupsuptic quadrangle. Black slate, quartz, quartzite, granite, green phyllite, minor greenstone, and limestone clasts as much as 2 feet in diameter make up the lower part of the polymict conglomerate near Johns Pond. Quartz, quartzite, granite, green phyllite, and greenstone clasts, generally less than 6 inches in diameter, make up the bulk

of the conglomerate to the north. Black slate, green phyllite, quartzite, and greenstone clasts were apparently derived from the underlying pre-Silurian rocks. The size of the clasts decreases and the relative amount of quartz and quartzite increases in the upper part of the conglomerate. Beds of feldspathic quartzite, gray slate, and locally, near Parmachenee Lake, purple slate beds as much as 3 feet thick are present and tend to be more abundant near the top of the polymict conglomerate. The quartz-pebble conglomerate consists primarily of well-rounded clear to milky-white vein quartz clasts as much as 1 inch in diameter. Minor amounts of dark-gray fine-grained quartzite and black chert pebbles are contained within the conglomerate. Light-gray quartzite beds as much as 10 feet thick are locally interbedded.

The conglomerate is probably of Early and Middle Silurian age. A few corals and scattered brachiopod fragments have been found in the matrix of the polymict conglomerate at locality S–1, and numerous recrystallized halysitid and horn corals were found in a few limestone boulders at locality S–2. A. J. Boucot (written commun., 1966) identified a plectambonitid brachiopod, either *Eoplectodonta* or *Plectodonta*, in the matrix of the conglomerate from locality S–1, and William Oliver (written commun., 1965) identified the halysitid found at locality S–2 as *Catenipora(?)* sp. These fossils are compatible with a late Llandovery (C_4–C_5) age established for similar rocks about 6 miles on strike to the northeast by E. L. Boudette (U.S. Geol. Survey, 1965, p. A74). Calcareous rocks of early Ludlow age (described below) conformably overly the polymict conglomerate near Parmachenee Lake (fig. 2). In turn, the conglomerate here unconformably overlies the Dixville Formation of Middle Ordovician age. Hence, the polymict conglomerate in this area is clearly of post-Middle Ordovician age and probably of early Ludlow or slightly older (Llandovery) age.

Calcareous rocks.—Calcareous gray slate containing lenses of dark-gray limestone and limestone conglomerate as much as 50 feet thick rest unconformably on graywacke and greenstone of the Dixville Formation in the northwest corner of the quadrangle. Light-gray, rusty-tan-weathering argillaceous limestone and greenish-brown, pit-weathering arenacenous limestone form the youngest unit near Parmachenee Lake (fig. 2).

The calcareous slate and limestone unit appears to be of Middle and Late Silurian age. At locality S–4 it is tentatively dated as Ludlow (Naylor and Boucot, 1965, p. 161, locality 19). The arenaceous limestone at locality S–3 is dated as early Ludlow from the brachiopod *Eccentricosta* identified by A. J. Boucot (in Naylor and Boucot, 1965, p. 161, locality 20).

Undivided Silurian and Devonian rocks

Interbedded gray slate and feldspathic quartzite, assigned to an undivided unit of younger Paleozoic rocks, conformably overlie the calcareous slate and polymict conglomerate in the northwest corner of the area (fig. 2) and rest unconformably on the Dixville Formation where the calcareous slate and conglomerate are missing. Gray slate and feldspathic quartzite of this unit interfinger with and overlie the polymict and quartz-pebble conglomerate near Johns Pond. The slate and quartzite here are interbedded in variable proportions. Slate predominates in the lower part of the unit, whereas slate and quartzite in equal amounts are common in the upper part. The quartzite beds range in thickness from ½ to 6 inches and are commonly graded and locally calcareous.

No fossils have been found in the slate and quartzite unit, but because it interfingers with rocks of late Llandovery age near Johns Pond (fig. 1) it is at least in part Silurian. The well-bedded slate and quartzite in the northwest corner of the quadrangle are stratigraphically and lithologically equivalent to rocks in the Moose River synclinorium that have been dated as Early Devonian (Boucot, 1961). These rocks in the Cupsuptic quadrangle may be Silurian or Devonian in age, or both.

REGIONAL CORRELATIONS

Correlation of the Silurian rocks at localities S–3 and S–4 with calcareous rocks of Ludlow age in the northern Appalachians has been done by Naylor and Boucot (1965), and the Silurian rocks near Johns Pond have been discussed briefly by E. L. Boudette (U.S. Geol. Survey, 1965, p. A74). Therefore, only the pre-Silurian correlations will be discussed in this report.

The *Climacograptus bicornis* zone is the probable correlative of at least part of the Porterfield and the Wilderness stages established by Cooper (1956). Berry (1963, p. 29 and chart on p. 21) suggested, on the basis of graptolite and shelly fossil collections from the Normanskill Shale, that the youngest part of the *C. bicornis* zone may be correlative with the earliest part of the Middle Ordovician Trenton stage as defined and discussed by Cooper (1956). The graptolite association diagnostic of the *C. bicornis* zone collected from locality O–1 (fig. 1) in the lower part of the black slate unit falls within a Porterfield-earliest Trenton age span. Correlation between graptolite zones

and Cooper's stages (1956) was discussed by Berry (1960, 1963).

The beds in the black slate unit bearing graptolites diagnostic of the *Climacograptus bicornis* zone are equivalent to part of the Beauceville Formation near Magog, Quebec, Canada, and part of the Normanskill Shale in eastern New York because these units contain graptolites indicative of the same zone (Berry, 1962a, b). As noted by Pavlides and others (1964, p. C31–C32), *C. bicornis* zone graptolites occur (1) in northeastern Maine in the Pennington and Portage anticlines, (2) in the northeastern side of the Weeksboro-Lunksoos Lake anticline, and (3) in an area southeast of the Aroostook-Matapedia anticlinorium near the international boundary south and east from Houlton (fig. 1). Ruedemann (*in* Ruedemann and Smith, 1935) identified graptolites which are probably the same age as those diagnostic of the *C. bicornis* zone from rocks on the southwest side of the Weeksboro-Lunksoos Lake anticline (fig. 1). Graptolites diagnostic of the *C. bicornis* zone have been found near the northwest side of the Weeksboro-Lunksoos Lake anticline in the Millinocket Lake and Spider Lake quadrangles in central Maine and in the Danforth area (fig. 1).

Graptolites indicative of the zone of *Orthograptus truncatus* var. *intermedius*, which is the next youngest zone from the *Climacograptus bicornis* zone, have been identified by Berry (Pavlides and others, 1961) from the Carys Mills Formation of the Meduxnekeag Group (formerly the ribbon rock member of the Meduxnekeag Formation) in the Aroostook- Matapedia anticlinorium and from black slate in the Castle Hill anticline west of Presque Isle, Maine (fig. 1). Part of both the Beauceville Formation and the Normanskill Shale (Berry, 1962a, b) also bear graptolites diagnostic of this zone. At least a part of the black slate unit that stratigraphically overlies the graptolite-bearing rocks in the Cupsuptic quadrangle may be correlative with these units.

The Ammonoosuc Volcanics and Partridge Formation have been mapped to within 20 miles of the Cupsuptic quadrangle (Billings, 1956; Milton, 1960). These formations cannot be mapped directly into the Cupsuptic area because intrusive rocks and Silurian and Devonian rocks crop out in the intervening area (C. V. Guidotti, written commun., 1964). On the basis of lithologic similarity and stratigraphic succession, however, the Partridge Formation is considered correlative with the black slate unit (fig. 2) and the Ammonoosuc Volcanics is probably correlative with the greenstone and slate unit. The Partridge Formation, therefore, may be assigned a Middle Ordovician age in the span from the Porterfield to the early part of the Trenton (stages as used by Cooper, 1956). Billings (1956, p. 98) reached a similar conclusion concerning the age of the Partridge by correlation with lithologically similar units in northern Vermont that are on strike with the graptolite-bearing rocks near Magog, Quebec.

Protospongia, obtained from the Dixville Formation, has too great a range to date the rocks from which it comes more precisely than Cambrian or Ordovician. Green (1964, p. 25) correlates the Dixville Formation with the Ammonoosuc Volcanics and Partridge Formation because of the lithologic similarity the Dixville has to these two formations and because it and the Ammonoosuc and Partridge occur in the same stratigraphic position, namely, above the Albee Formation. In the northern part of the Cupsuptic quadrangle, the Dixville Formation occupies the same stratigraphic position above the older Paleozoic rocks as the greenstone and slate unit and the black slate unit on the southeast. The units northwest and southeast of the older Paleozoic rocks are apparently lithofacies although the relationships are not as yet completely understood. Volcanic rocks equivalent to the greenstone and slate unit are missing from the base of the Dixville but appear scattered within that formation. Graywacke, volcanic rocks, and black slate near Somerset Junction (fig. 1) tentatively correlated with the Dixville Formation by E. V. Post (U.S. Geol. Survey, 1961, p. A12) contain Middle Ordovician brachiopods (Boucot, 1961; E. V. Post, written commun., 1965) apparently equivalent to the graptolites in the Cupsuptic quadrangle. Part of the Dixville thus appears to be coeval with the black slate unit; however, part may be somewhat older.

REFERENCES

Berry, W. B. N., 1960, Correlation of Ordovician graptolite-bearing sequences: Internat. Geol. Cong., 21st, Copenhagen, 1960, pt. 7, p. 97–108.

———1962a, On the Magog, Quebec, graptolites: Am. Jour. Sci., v. 260, p. 142–148.

———1962b, Stratigraphy, zonation, and age of the Schaghticoke, Deepkill, and Normanskill shales, eastern New York: Geol. Soc. America Bull., v. 73, p. 695–718.

———1963, Ordovician correlations in the Taconic and adjacent regions, *in* Bird, J. M., ed., Stratigraphy, structure, sedimentation and paleontology of the southern Taconic region, eastern New York: Albany, N.Y., Guidebook for fieldtrip three, Geol. Soc. America 1963 Ann. Mtg., New York, p. 21–31.

Billings, M. P., 1935, Geology of the Littleton and Moosilauke quadrangles, New Hampshire: New Hampshire State Plan. Devel. Comm., 51 p.

———1956, Bedrock, geology, pt. 2 *of* The geology of New Hampshire: Concord, New Hampshire State Plan. Devel. Comm., 203 p.

Boucot, A. J., 1961, Stratigraphy of the Moose River synclinorium, Maine: U.S. Geol. Survey Bull. 1111–E, p. 153–188.

Cooper, G. A., 1956, Chazyan and related brachiopods [U.S.-Canada]: Smithsonian Misc. Colln., v. 127, pt. 1, p. 1–1024; pt. 2, 1025–1245, 269 pls.

Green, J. C., 1964, Stratigraphy and structure of the Boundary Mountain anticlinorium in the Errol quadrangle, New Hampshire-Maine: Geol. Soc. America Spec. Paper 77, 78 p.

Harker, Alfred, 1939, Metamorphism, 2d ed.: London, Methuen and Co., Ltd., 362 p.

Milton, D. J., 1960, Geology of the Old Spec Mountain quadrangle, Maine: Harvard Univ. unpub. Ph.D. thesis, 190 p.

Naylor, R. S., and Boucot, A. J., 1965, Origin and distribution of rocks of Ludlow age (Late Silurian) in the northern Appalachians: Am. Jour. Sci., v. 263, p. 153–169.

Pavlides, Louis, Neuman, R. B., and Berry, W. B. N., 1961, Age of the "ribbon rock" of Aroostook County, Maine: Art. 30 *in* U.S. Geol. Survey Prof. Paper 424–B, p. B65–B67.

Pavlides, Louis, Mencher, Ely, Naylor, R. S., and Boucot, A. J., 1964, Outline of the stratigraphic and tectonic features of northeastern Maine, *in* Geological Survey Research 1964: U.S. Geol. Survey Prof. Paper 501–C, p. C28–C38.

Ruedemann, Rudolph, and Smith, E. S. C., 1935, The Ordovician in Maine: Am. Jour. Sci., v. 30, no. 178, p. 353–355.

U.S. Geological Survey, 1961, Geological Survey Research 1961: U.S. Geol. Survey Prof. Paper 424–A, 194 p.

———1965, Geological Survey Research 1965: U.S. Geol. Survey Prof. Paper 525–A, 376 p.

PHYSICAL EVIDENCE FOR LATE CRETACEOUS UNCONFORMITY, SOUTH-CENTRAL WYOMING

By MITCHELL W. REYNOLDS, Denver, Colo.

Abstract.—Local physical evidence in the Lamont-Bairoil area, south-central Wyoming, corroborates regional stratigraphic and paleontologic evidence of an unconformity at the base of the Teapot Sandstone Member of the Mesaverde Formation. The new evidence includes low-angle truncation of beds beneath the Teapot Member, channels cut into underlying beds, and pebble conglomerate at or near the base of the Teapot. Clasts in the conglomerate were derived from Mesozoic, Paleozoic, and possibly Precambrian rocks eroded from the rising ancestral Wind River Range.

Uplift across much of Wyoming in Late Cretaceous (late Campanian) time caused erosion of as much as 3,600 feet of Upper Cretaceous strata prior to deposition of the Teapot Sandstone Member of the Mesaverde Formation and its equivalents. Without specific physical evidence, faunal and stratigraphic relations led recently to recognition of the unconformity (Gill and Cobban, 1966, p. B21), and to identification of an area of local truncation of beds beneath the Teapot Member (Reynolds, 1966). In the past, failure to recognize this unconformity locally has contributed to misinterpretation of stratigraphic thinning beneath this unconformity and a local unconformity at the base of the Lewis Shale, and of paleogeography during Late Cretaceous time (Weimer and Guyton, 1961). Local physical evidence is, therefore, critical to establish the presence of the unconformity. Detailed mapping in south-central Wyoming has disclosed such physical evidence. This report summarizes the new evidence and presents data regarding the provenance of the Teapot Member in part of Wyoming.

The area herein discussed covers about 250 square miles centered around the communities of Lamont and Bairoil, Wyo. (fig. 1). The Mesaverde Formation is exposed in a narrow belt across the center and northeastern parts of the area. In the southeastern part of the area, the formation has been removed by recent erosion; in the western and northwestern parts, it is absent by truncation beneath a local unconformity at the base of the Lewis Shale (Reynolds, 1966).

General characteristics of the Teapot Sandstone Member have been summarized elsewhere (Reynolds, 1966, p. B70, B73). Lithologic variations not previously described occur across the southern part of the area (fig. 1). The Teapot Member thickens from 65 feet in sec. 15, T. 24 N., R. 89 W., to 205 feet in sec. 17, T. 25 N., R. 89 W. In sec. 17, the lower part is a massive-weathering white sandstone, and the upper part is a slope-forming sequence of carbonaceous siltstone and sandstone beds that weather reddish brown and white. Part of this upper sequence is lithologically similar to the "Rusty zone" of the Ericson Formation described by Hale (1950, p. 53) in the Rock Springs uplift, about 80 miles to the west-southwest. From a thickness of 205 feet, the Teapot thins northward to about 60 feet in sec. 26, T. 26 N., R. 90 W., partly by depositional thinning, partly by facies change into overlying beds (equivalent to the Almond Formation of the Rock Springs uplift), and, where the overlying brackish-water beds are absent, by truncation beneath the Lewis Shale.

EVIDENCE OF THE UNCONFORMITY

Three lines of evidence establish the presence of an unconformity at the base of the Teapot Sandstone Member: (1) low-angle truncation of beds beneath the member, (2) channels cut into underlying beds, and (3) conglomeratic sandstone beds, referred to hereafter as the coarse facies, in the lower part of the member.

Low-angle truncation of beds

Low-angle truncation of beds underlying the Teapot is evident from Separation Rim northward to Lost Soldier Rim. At Separation Rim (Reynolds, 1966, p. B72, section B), beds of sandstone, carbonaceous siltstone, and lignite compose the 200-foot-thick interval beneath

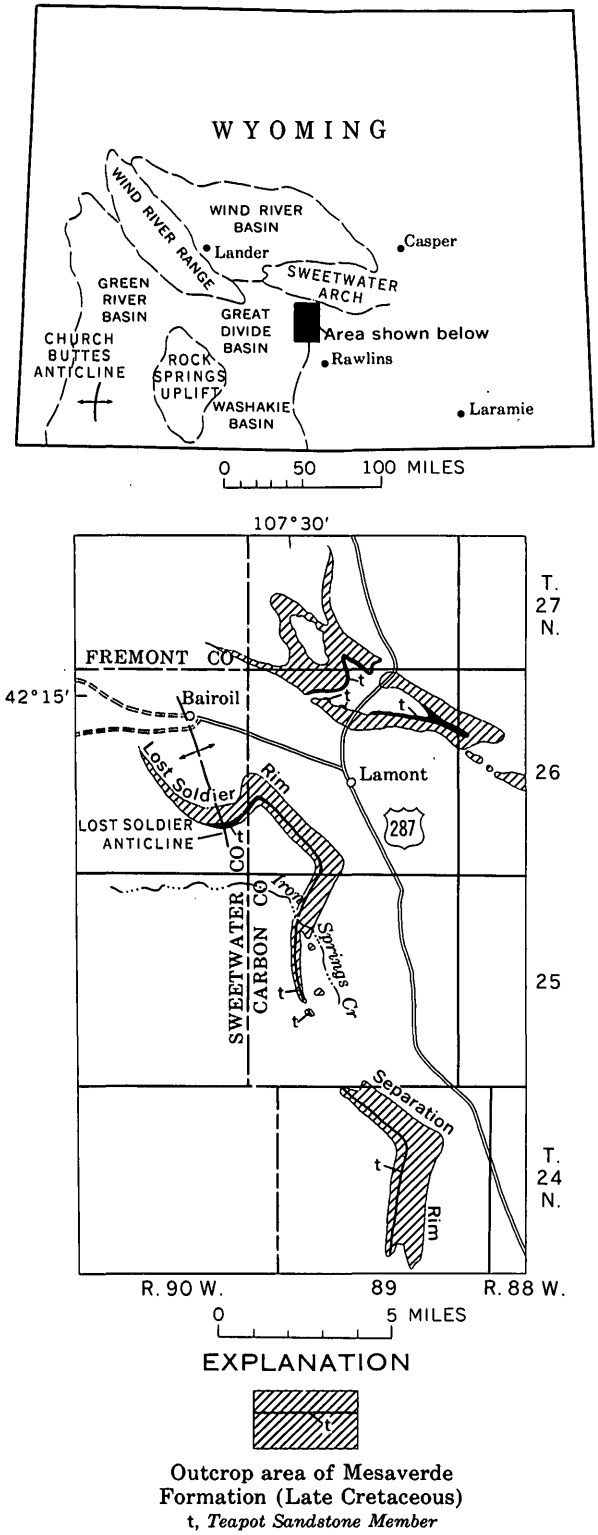

FIGURE 1.—Index maps showing the areal distribution of the Mesaverde Formation and Teapot Sandstone Member in the Lamont-Bairoil area, Wyoming, and tectonic features referred to in the text.

the Teapot. The base of the Teapot is sharp, nearly planar, and lies nearly parallel to bedding planes in the underlying rocks. About 8 miles north of Separation Rim at Iron Springs Creek, the Teapot Sandstone Member directly overlies thick nonmarine sandstone beds which at Separation Rim lie about 200 feet beneath the Teapot; the intervening carbonaceous and lignitic beds have been truncated by erosion. Here the base of the Teapot is undulatory with as much as 15 inches of irregular relief between crests and troughs. From Iron Springs Creek to Lost Soldier Rim, the Teapot Sandstone Member cuts progressively downward across the thick nonmarine sandstone beds in the underlying part of the Mesaverde Formation. At Lost Soldier Rim the thick sandstone beds are also absent by truncation. A thin littoral marine sandstone bed, which lies about 600 feet above the base of the Mesaverde and 1,280 feet beneath the Teapot at Separation Rim (Reynolds, 1966, p. B72, section B), can be traced to its depositional edge on Lost Soldier Rim. There the bed lies only 350 feet beneath the Teapot and 450 feet above the base of the Mesaverde, providing additional control on low-angle truncation beneath the Teapot.

Sharp local truncation at the base of the Teapot Sandstone Member can be seen on the south flank of Lost Soldier anticline. Figure 2 shows the contact between the Teapot and an underlying white silty sandstone bed in the Mesaverde Formation in sec. 26, T. 26 N., R. 90 W., where the contact is conspicuously irregular. From the gully in the center of the photographed area, the silty sandstone bed thins and is truncated within about 300 feet to the southeast and 500 feet to the northwest.

Similar pronounced local truncation occurs in secs. 3, 4, and 5, T. 26 N., R. 89 W., and sec. 34, T. 27 N., R. 89 W. In this area a white littoral marine sandstone bed underlying the Teapot thins by truncation from about 60 feet in the SE¼ sec. 5 and the SW¼ sec. 4 to about 15 feet in the SE¼SW¼ sec. 34. The truncated edge of the littoral marine sandstone bed trends about N. 20° E. in the SE¼ sec. 33, T. 27 N., R. 89 W. In this area of truncation north of Lamont, the coarse facies of the Teapot is also best developed.

Other areas of more abrupt truncation may have been present on the west and northwest flanks of the Lost Soldier anticline prior to truncation of the Teapot and remaining parts of the Mesaverde Formation by post-Teapot-pre-Lewis erosion (Reynolds, 1966, p. B74). The present truncated edges of the Teapot Sandstone Member occur in the NW¼ sec. 26, T. 26 N., R. 90 W., and in the N½SE¼ sec. 33, T. 27 N., R. 89 W.

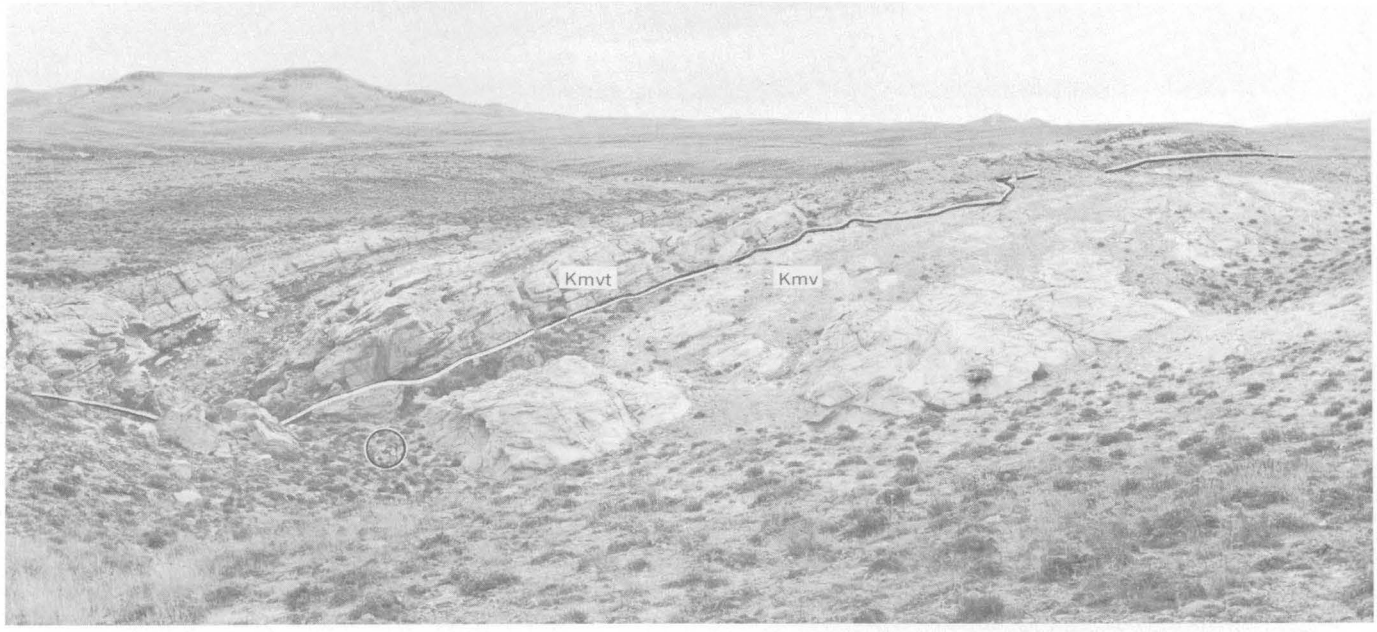

FIGURE 2.—Unconformity between the Teapot Sandstone Member of the Mesaverde Formation (Kmvt) and underlying beds of part of the Mesaverde (Kmv). View is west in the S½SW¼NE¼ sec. 26, T. 26 N., R. 90 W. Backpack (circled) in left center for scale.

Channels cut into underlying beds

Channels cut into underlying beds and filled by younger sediment may not in themselves be evidence of a regional unconformity, for channels and channel-filling sandstone beds are common in nonmarine rocks in other parts of the Mesaverde Formation. When combined with low-angle truncation described above and the coarse facies described below, channeling at the base of the Teapot is persuasive evidence. On a small scale the base of the Teapot is undulatory with an amplitude as much as 2 feet (fig. 3*A*); irregularities increase in size as areas of maximum truncation are approached. Thus a small channel about 5 feet deep and 20 feet across is present on the south flank of the Lost Soldier anticline in sec. 26, T. 26 N., R. 90 W. Similar channels, 2–4 feet deep and as much as 10 feet across, are evident at the base of the Teapot in sec. 4 and 5, T. 26 N., R. 89 W. Underlying beds terminate abruptly against the sides of small channels (fig 3*A*). In most cases the channels are filled with interbedded coarse-grained sandstone and granule-pebble conglomerate.

Coarse facies

A progressive increase of grain size in sand lenses occurs from the southern part of the area, northward to the west flank of Lost Soldier anticline and north of Lamont (fig. 1). At Separation Rim clasts in the Teapot are generally fine grained and well sorted. At Iron Springs Creek, lenses of poorly sorted, very coarse sand (grains 1–2 millimeters in diameter) containing scattered granules (2–4 mm across) are common in the lower 70 feet of the member. Farther northwest in sec. 26, T. 26 N., R. 90 W., pebbles as large as 15 mm across occur at the base (fig. 3*B*). At this locality most clasts are 5–8 mm in diameter. North of Lamont very coarse sand and granules with scattered pebbles occur in the lowermost 10 feet of the Teapot (Reynolds, 1966, p. B73), and lenses of coarse material persist eastward to the NW¼NW¼ sec. 18, T. 26 N., R. 88 W., the easternmost outcrop of the Teapot (fig. 1). Clasts coarser than fine grained were not observed in strata of the Mesaverde Formation beneath the Teapot Sandstone Member.

The coarsest clasts occur in areas where the Teapot abruptly truncates the underlying part of the Mesaverde Formation. Fine-grained sand is dominant in the Teapot from Separation Rim to Iron Springs Creek where the underlying Mesaverde strata thin by deposition and truncation from about 2,000 to 1,375 feet, a rate of about 78 feet per mile. The striking increase in grain size northward from Iron Springs Creek occurs where thinning by truncation increases to about 130 feet per mile.

Granules and pebbles consist for the most part of resistant rock types weathered from older sedimentary, igneous, and metamorphic terranes. Dark-gray to white chert pebbles are common and appear to be derived from Carboniferous and Permian cherts in adja-

A

B

FIGURE 3.—Views of unconformity at base of Teapot Sandstone Member. *A*, irregular surface of unconformity (about middle of tripod legs) between Teapot Sandstone Member and underlying beds of the Mesaverde Formation at south-center edge of SW¼NE¼ sec. 26, T. 26 N., R. 90 W. *B*, closeup view (right center of *A*) of pebble lenses near the base of the Teapot Sandstone Member; unconformity is beneath knife in lower left corner of photograph.

cent areas. Siliceous and volcanic mudstone pebbles, lithologically similar to the Mowry and Aspen Shales of Early Cretaceous age, are abundant. Erosion of some lower Mesozoic strata is suggested by the rare occurrence of pale-reddish-brown siltstone and very fine sandstone pebbles derived possibly from the Chugwater Group. Near the base, scattered buff or white sandstone and siltstone pebbles, and locally abundant gray shale pebbles probably are derived from the underlying part of the Mesaverde Formation.

Quartz is quantitatively the most important constituent of the coarse facies. Very angular grains of quartz as much as 4 mm across were derived from intrusive igneous and metamorphic rocks possibly of Precambrian age. Quartz grains with one or more rounded faces bounded by angular, fractured faces were derived from older well-rounded clasts, probably recycled from older sedimentary rocks. Euhedral dipyramidal crystals of quartz may have been derived from volcanic eruptions in western Montana. Rare feldspar grains, as much as 7 mm across, suggest a source area of Precambrian rocks for some clasts in the coarse facies.

The increase of grain size in the Teapot to the north and northwest in the Lamont-Bairoil area suggests source areas in those directions, very likely along the trend of the present Wind River Range. Clasts derived from Mesozoic and Paleozoic rocks indicate that these rocks were exposed; erosion may have breached these rocks to expose the Precambrian core which provided metaquartzite and very coarse quartz and feldspar clasts. Absence of pebbles and cobbles of most Phanerozoic rocks and any Precambrian granite in rocks immediately adjacent to the Sweetwater arch suggests that, although the arch may have been active (Pryor, 1961, p. 45; Reynolds, 1966, p. B74), relief was low so that only Upper Cretaceous rocks were eroded from it.

A nearly identical conglomeratic sandstone facies forms part of the Ericson Formation at the north end of the Rock Springs uplift (Hale, 1950, p. 53). There, also, grain size increases northward. The coarse clasts are similar in composition to those in the Lamont-Bairol area. Both the northward increase of grain size and similarity of clasts in the Ericson Formation and Teapot Sandstone Member suggest a common source to the northwest and north. Some clasts in the Ericson at Rock Springs were doubtless derived from the west because the conglomeratic facies is also present in the area of the Church Buttes anticline (Roehler, 1965). The close lithologic and stratigraphic similarities substantiate the correlation (Gill and Cobban, 1966, p. B25) between at least part of the Ericson Formation and the Teapot Sandstone Member of the Mesaverde Formation as used in this report.

REFERENCES

Gill, J. R., and Cobban, W. A., 1966, Regional unconformity in Late Cretaceous, Wyoming, *in* Geological Survey Research 1966: U.S. Geol. Survey Prof. Paper 550–B, p. B20–B27.

Hale, L. A., 1950, Stratigraphy of the Upper Cretaceous Montana Group in the Rock Springs uplift, Sweetwater County, Wyoming, *in* Wyoming Geol. Assoc. Guidebook 5th Ann. Field Conf., southwest Wyoming, 1950: p. 49–58.

Pryor, W. A., 1961, Petrography of Mesaverde sandstones in Wyoming, *in* Wyoming Geol. Assoc. Guidebook 16th Ann. Field Conf., Green River, Washakie, Wind River, and Powder River Basins, 1961: p. 34–46.

269–274 O—67——3

Reynolds, M. W., 1966, Stratigraphic relations of Upper Cretaceous rocks in the Lamont-Bairoil area, south-central Wyoming, *in* Geological Survey Research 1966: U.S. Geol. Survey Prof. Paper 550–B, p. B69–B76.

Roehler, H. W., 1965, Summary of pre-Laramide Late Cretaceous sedimentation in the Rock Springs uplift area, *in* Wyoming Geol. Assoc. Guidebook 19th Ann. Field Conf., Rock Springs uplift, 1965: p. 10–11.

Weimer, R. L., and Guyton, J. W., 1961, Geology of the Muddy Gap–Lamont area, Wyoming, *in* Wyoming Geol. Assoc. Guidebook 16th Ann. Field Conf., Green River, Washakie, Wind River, and Powder River Basins, 1961: p. 139–147.

MISSISSIPPIAN DEPOSITIONAL PROVINCES IN THE NORTHERN CORDILLERAN REGION

By WILLIAM J. SANDO, Washington, D.C.

Abstract.—Biostratigraphic studies permit the recognition of the Wyoming, Montana, and Idaho depositional provinces in the Mississippian System of the northern Cordilleran region. The Mississippian rocks record two major marine transgressions separated by a widespread episode of epeirogenic emergence. The earlier, or Madison, transgression began actually in latest Devonian time and pulsated eastward over a broad cratonic shelf. The Madison sea gradually shallowed from Osage to early Meramec time and withdrew from the area during the early or middle Meramec. During later Meramec and Chester time, the sea returned, and the region was differentiated into a miogeosynclinal belt and a cratonic platform. Deposition continued uninterruptedly into the Pennsylvanian except in an emergent area (Bannock Highland of Williams) that developed in southeasternmost Idaho and westernmost Wyoming during latest Mississippian or earliest Pennsylvanian time.

Several geologists (Sloss and Moritz, 1951, p. 2153, 2160; Scholten and others, 1955, p. 363–366; Scholten, 1957, table 1) have noted significant lithic differences between the Mississippian sequences of central Idaho and adjacent southwestern Montana. Nomenclaturally, these differences are reflected by Madison–White Knob (beds now referred to the White Knob Limestone in this area were previously called Brazer Limestone) or Milligen–White Knob terminologies in central Idaho and by a Madison–Big Snowy–Amsden terminology in southwestern Montana, separated by a northwestward-trending line of demarcation in the Beaverhead Range. The observed relationships led Scholten and others (1955, p. 365) to differentiate an "Idaho facies" representing miogeosynclinal deposition and a "Montana facies" representing cratonic shelf deposition.

Similar differences between the Mississippian sequences of parts of the overthrust belt south of the Snake River Plain in western Wyoming, southeastern Idaho, and northeastern Utah have been largely obscured by former confusion regarding the age and correlation of the Mississippian rock units. However, biostratigraphic studies over the past 10 years (for example, Sando and others, 1959; Sando and Dutro, 1960; Dutro and Sando, 1963; Sando, 1967) have provided basic data upon which broad Mississippian depositional provinces can be differentiated throughout most of the northern Cordilleran region. This paper brings together pertinent biostratigraphic data in summary form in an attempt to stimulate further study and thought. The author is indebted to many of his colleagues, particularly J. T. Dutro, Jr., Mackenzie Gordon, Jr., Helen Duncan, C. A. Sandberg, Gilbert Klapper, and J. W. Huddle, for furnishing related data, much of it unpublished.

BASIC CONCEPTS

Three depositional provinces are recognized herein: Idaho province, Montana province, and Wyoming province. The known areal distribution of these provinces is shown on figure 1. Paleotectonically, the Idaho province was a miogeosyncline during some of Mississippian time, whereas the Montana and Wyoming provinces were part of the craton throughout Mississippian time. The Wyoming province is characterized by a relatively thin sequence of rocks deposited in generally very shallow waters. The Montana province includes an area that is transitional between the Idaho and Wyoming provinces in western Wyoming, southeastern Idaho, and northeastern Utah, and also includes a cratonic basin or trough in southwestern and central Montana. Similar areal divisions based on isopach differences were noted by Andrichuk (1955, p. 2182) in the Madison Group of southern Montana and Wyoming, but Andrichuk's "Wyoming positive area" was more restricted than the Wyoming province of this paper. The present approach to definition of province boundaries places emphasis on lithic and temporal differences in the sedimentary sequences representing all of

U.S. GEOL. SURVEY PROF. PAPER 575-D, PAGES D29–D38

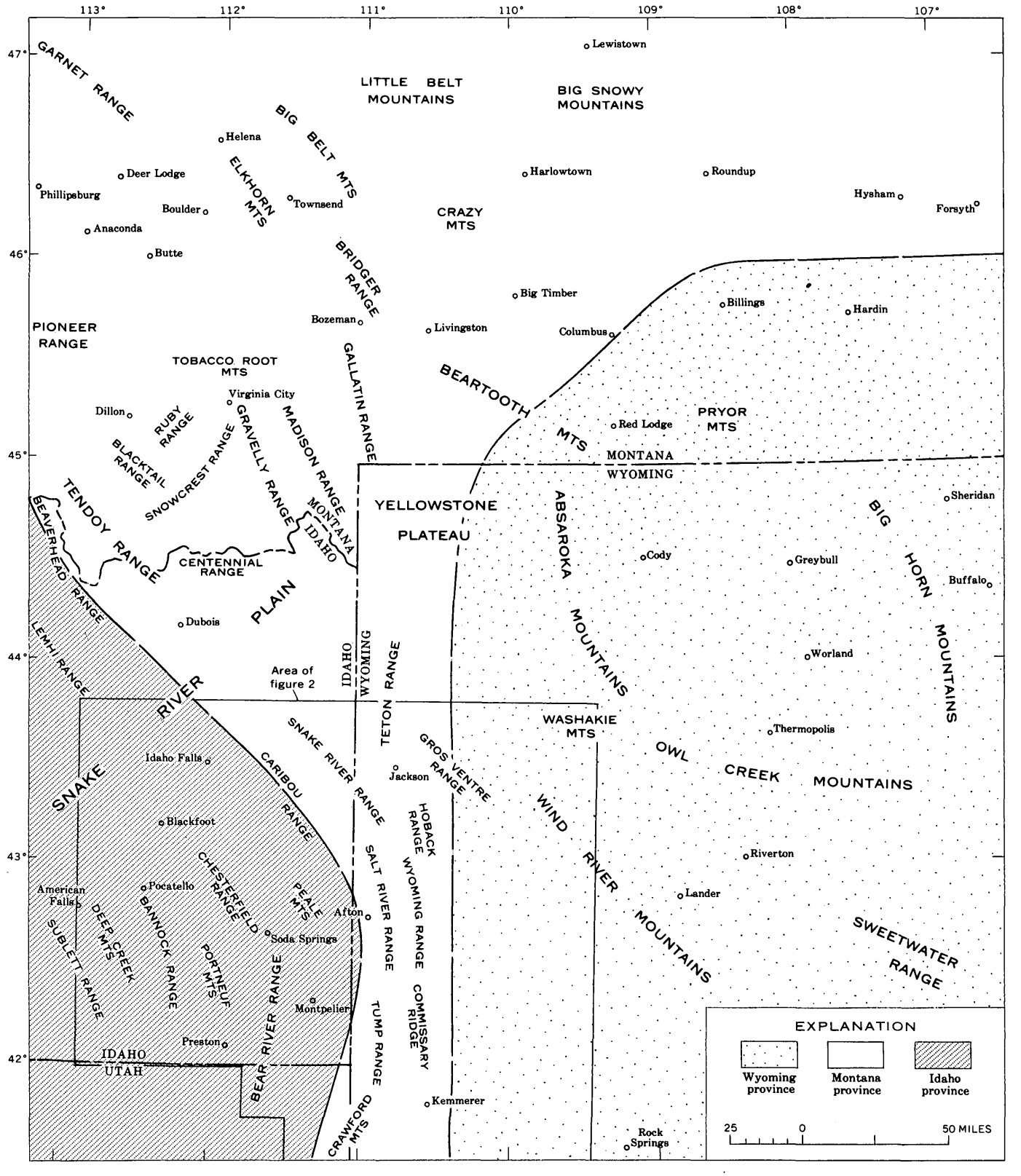

FIGURE 1.—Map of northern Cordilleran region, showing location of principal mountain ranges and Mississippian provinces. Area of figure 2 is outlined.

Mississippian time in the area under study. Reliance on isopach differences as indexes of paleotectonic differentiation is misleading, owing to the variable influence of intra-Mississippian erosion on parts of the area.

Chronologic relationships of the lithic units in the three provinces have been established by dividing the Mississippian of the northern Cordilleran region into 12 faunal zones based mainly on corals, brachiopods, and conodonts (see stratigraphic diagram, fig. 3). The oldest Mississippian zone recognized, herein designated pre-A, is the Mississippian part (*cu*I) of the dark shale unit of Sandberg (1963), whose deposition actually began in latest Devonian (*to*V) time (Sandberg and Klapper, in press). Late Kinderhook time, Osage time, and early Meramec time are represented in the Madison Group by Zones A through D, as recognized by Sando and Dutro (1960). Middle Meramec time is divided into Zone E and an underlying poorly coralliferous zone called pre-E. Zone E was originally defined by Dutro and Sando (1963) in the Chesterfield Range Group. Zone pre-E includes the *Quadratia* Zone and the lower part of *Echinoconchus alternatus* Zone of Dutro and Sando (1963). Zone F of Dutro and Sando (1963) represents upper Meramec time. Chester time is divided into three faunal zones: a poorly coralliferous pre-K Zone, the K Zone of Dutro and Sando (1963), and a post-K Zone suggested by brachiopod studies of Mackenzie Gordon, Jr.

In the discussion that follows, emphasis is placed on key stratigraphic sections from central Wyoming across the overthrust belt of western Wyoming into the deformed belt of southeastern Idaho as far west as the Deep Creek Mountains (figs. 2 and 3). Although a meaningful isopach map cannot be constructed at present, owing to structural complexities in the deformed areas, a general westward thickening of the Mississippian deposits is indicated by the thicknesses shown on figure 2.

Geographic limits of the three provinces are established with reasonable confidence in the area studied, but the total areal extent of the provinces remains to be determined. Furthermore, crustal shortening and other structural complexities in the deformed areas have undoubtedly distorted the original areal relationships of parts of the depositional picture. A reasonable concept of original depositional relationships can only be attained through additional careful study of both rocks and fossils.

WYOMING PROVINCE

The Wyoming province includes all of the State of Wyoming, exclusive of the overthrust belt in the westernmost part, and extends into southern Montana. The Mississippian System of the Wyoming province includes the Madison Limestone and the lower and middle parts of the Amsden Formation. This sequence thickens westward and northward from an erosional zero edge in southeastern Wyoming (Maughan, 1963), to approximately 1,100 feet along the northern and western limits of the province. The Horse Creek section in the Washakie Mountains of central Wyoming (section 1 on figs. 2 and 3) is one of the thickest sections of the Mississippian in the Wyoming province.

In southeastern Wyoming, the oldest Madison strata are transgressive quartz sandstone of supposedly Kinderhook age (Maughan, 1963, p. C24). In central Wyoming, Madison deposition began at some places in latest Devonian (*to*V) time and at others in earliest Kinderhook (*cu*I) time (Sandberg and Klapper, in press), represented by transgressive terrigenous and dolomitic beds of the dark shale unit of Sandberg (1963). The basal Madison strata disconformably overlie rocks ranging in age from Precambrian to latest Devonian in the Wyoming province.

The lower half of the Madison Limestone in central Wyoming is composed of shallow-water marine limestone and dolomite. Shallow-water marine carbonate rocks also dominate the upper half of the formation, but several solution breccia zones suggest the former presence of evaporite interbeds. The Lodgepole and Mission Canyon Limestones of the Montana province are not recognizable as distinct lithic units in the Wyoming province. Time equivalents of both formations appear to be present, however, and possible tongues of Lodgepole-like rocks occur in the lower half of the Madison in the northern part of the province. Madison deposition appears to have been virtually continuous from Kinderhook into Meramec time. The youngest beds in the Madison of the Wyoming province are of early Meramec (Zone D) age; these strata are only locally present because they were removed from much of the area by post-Madison, pre-Amsden erosion. Sinkhole and solution features of a former karst terrane related to the erosional episode extend downward several hundred feet into the Madison at some localities.

In southeastern Wyoming, the Madison is overlain by the Casper Formation of Pennsylvanian age, but over most of the Wyoming province the superjacent beds belong to the Amsden Formation, which includes beds of Mississippian and Pennsylvanian age. The Amsden Formation in most of the Wyoming province is divisible into three units: (1) the Darwin Sandstone Member at the base, (2) a middle red unit composed mainly of siltstone and shale with minor thin beds of

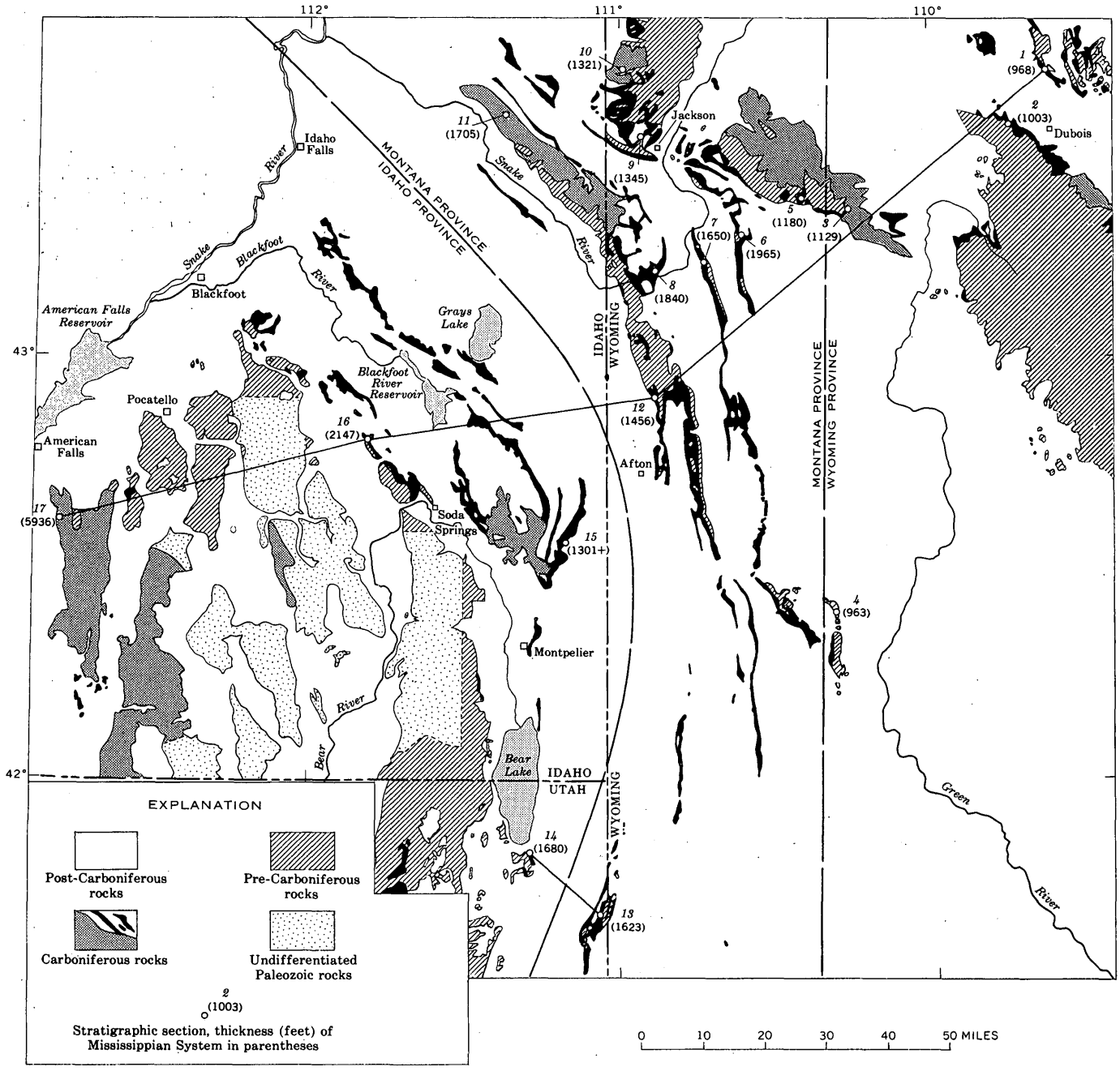

FIGURE 2

quartz sandstone and limestone, and (3) an upper unit of cherty dolomite, dolomitic limestone, and limestone with minor beds of quartz sandstone and shale. The Darwin Sandstone Member lacks diagnostic fossils, but its age can be no older than early Meramec (Zone D) and no younger than late Chester (post-K), on the basis of fossils found below and above it. Regional correlations suggest that the Darwin represents the eastern part of a transgressive sand, which was deposited in middle Meramec (Zones E and pre-E) time in the Idaho province to the west and reached the Wyoming province during Chester (Zone K) time (fig. 3). Fossils found in the middle red unit in the Wind River, Washakie, and Bighorn Mountains are of Chester (post-K) age, whereas the upper cherty carbonate unit has yielded fossils of Pennsylvanian age. Deposition appears to have been virtually continuous from Chester time into the Pennsylvanian except for southeastern Wyoming, where the Casper Formation disconformably overlies the Madison.

FIGURE 2.—Map showing location of key stratigraphic sections of Mississippian rocks in relation to Paleozoic outcrop belts and Mississippian province boundaries in southeastern Idaho, northeastern Utah, and western Wyoming. Geology adapted from Love and others (1955), Ross and Forrester (1947), and Andrews and Hunt (1948).

1. Horse Creek section; sec. 19, T. 43 N., R. 106 W., Fremont County, Wyo. (Sando, 1967, and Shaw, 1955).
2. Warm Spring Canyon section; sec. 31, T. 42 N., R. 107 W., Fremont County, Wyo. (Sando, 1967, and Keefer, 1957).
3. Triangle Peak–Darwin Peak section; sec. 9, T. 39 N., R. 112 W., and sec. 28, T. 40 N., R. 112 W., Teton County, Wyo. (after Love and others, 1951, fig. 3).
4. Mobil Oil Co. test well 22-19-G, Tip Top unit; sec. 19, T. 28 N., R. 113 W., Sublette County, Wyo. (after Marzolf, 1965).
5. Granite Hot Springs section; sec. 4, T. 39 N., R. 113 W., and sec. 33, T. 40 N., R. 113 W., Teton County, Wyo. (after Wanless and others, 1955).
6. Hoback Canyon section; secs. 2 and 3, T. 38 N., R. 115 W., Teton County, Wyo. (after Wanless and others, 1955).
7. Grayback Ridge section; secs. 22 and 27, T. 38 N., R. 116 W., Lincoln County, Wyo. (after Wanless and others, 1955).
8. Wolf Creek and Red Creek sections; sec. 4, T. 37 N., R. 117 W., and sec. 1, T. 37 N., R. 118 W., Lincoln County, Wyo. (after Wanless and others, 1955).
9. Glory Mountain section; sec. 7, T. 41 N., R. 117 W., Teton County, Wyo. (after Wanless and others, 1955).
10. Darby Canyon section; secs. 14, 15, and 23, T. 43 N., R. 118 W., Teton County, Wyo. (Sando and Dutro, 1960).
11. Black Mountain–Sheep Creek–Canyon Creek section; secs. 23 and 24, T. 3 N., R. 43 E., Bonneville County, Idaho (Sando and Dutro, unpub. data; and Staatz and Albee, 1966).
12. Haystack Peak–Covey Cut-off section; sec. 19, T. 34 N., R. 117 W., Lincoln County, Wyo. (after Sando and Dutro, 1960, and Sando and Dutro, unpub. data).
13. Brazer Canyon section; sec. 20, T. 11 N., R. 8 E., Rich County, Utah (Sando and Dutro, 1960).
14. Old Laketown Canyon section; sec. 32, T. 13 N., R. 6 E., Rich County, Utah (Sando and others, 1959).
15. Wells Canyon section; secs. 10 and 11, T. 10 S., R. 45 E., Caribou County, Idaho (after Gulbrandsen and others, 1956).
16. Little Flat Canyon section; secs. 17, 20, and 29, T. 7 S., R. 40 E., Bannock County, Idaho (Dutro and Sando, 1963).
17. Water Canyon–Hunter Canyon section; secs. 35 and 26, T. 9 S., R. 31 R., Power County, Idaho (after Carr and Trimble, 1961).

MONTANA PROVINCE

The Montana province occupies southwestern and central Montana and extends southward across eastern Idaho and into the overthrust belt of western Wyoming (fig. 1). Rocks of the Mississippian System in this area range from about 1,100 to 2,500 feet in thickness and are represented mostly by the Madison Group, which is composed of the Lodgepole Limestone and the Mission Canyon Limestone. Younger strata of Mississippian age have been assigned to a variety of nomenclatural units. In western Wyoming, these Mississippian beds form the lower part of the Amsden Formation. In parts of southeastern Idaho, approximately equivalent beds have been included in the lower part of the Wells Formation (Staatz and Albee, 1966, p. 31). Throughout much of southwestern and central Montana, the Madison is overlain by the Big Snowy Group, which is at least partly equivalent to the lower part of the Amsden Formation of western and central Wyoming. Elsewhere in southwestern Montana, the Madison is overlain by beds of probable Pennsylvanian age referred to the Amsden. The exact relationships of the post-Madison Mississippian and Pennsylvanian age beds of Montana to the Amsden Formation of Wyoming are not known.

The Crawford Mountains of northeastern Utah constitute a curious southern appendage of the Montana province. Here the Mississippian System is composed of the Lodgepole Limestone and the Brazer Dolomite. The Brazer is overlain disconformably by beds of Pennsylvanian age assigned to the Wells Formation. Although this unique Mississippian sequence is of about the same age as other sequences in the Montana province, its lithology might form the basis for regarding it as a separate depositional province.

Stratigraphic sections studied near Haystack Peak and along the Covey Cut-off Trail in the Salt River Range are representative of the Mississippian sequence in the southern extension of the Montana province into the overthrust belt of western Wyoming (section 12 on figs. 2 and 3). Here the Lodgepole Limestone rests disconformably on beds of Late Devonian age which were assigned to the Three Forks Formation by Benson (1966). The base of the Lodgepole at this locality is slightly younger than the base of the Madison in the Wyoming province. The Lodgepole in western Wyoming is divided into a lower unit of mostly fine-grained poorly fossiliferous cherty argillaceous limestone assigned to the Paine Shale Member and an upper unit, the Woodhurst Limestone Member, in which coarse bioclastic debris is scattered through fine-grained limestone beds and interbeds of crinoidal limestone are common. With the exception of a thin but widespread crinoidal limestone unit at the base of the Paine Member, the Lodgepole records deposition in moderately deep water, which becomes progressively shallower. The overlying Mission Canyon Limestone is composed of shallow-water marine limestone and dolomite with a thick zone of probable evaporite-solution breccia at the top. Madison deposition appears to have been virtually continuous from early (but not earliest) Kinderhook time into early Meramec time (Zones A through D).

After an episode of emergence, the Darwin Sandstone Member of the Amsden was deposited on the eroded surface of the Madison. The solution breccia was reworked, and sand and silt infiltrated the interstices of the breccia. The Darwin grades upward into a sequence of cherty fossiliferous marine limestone

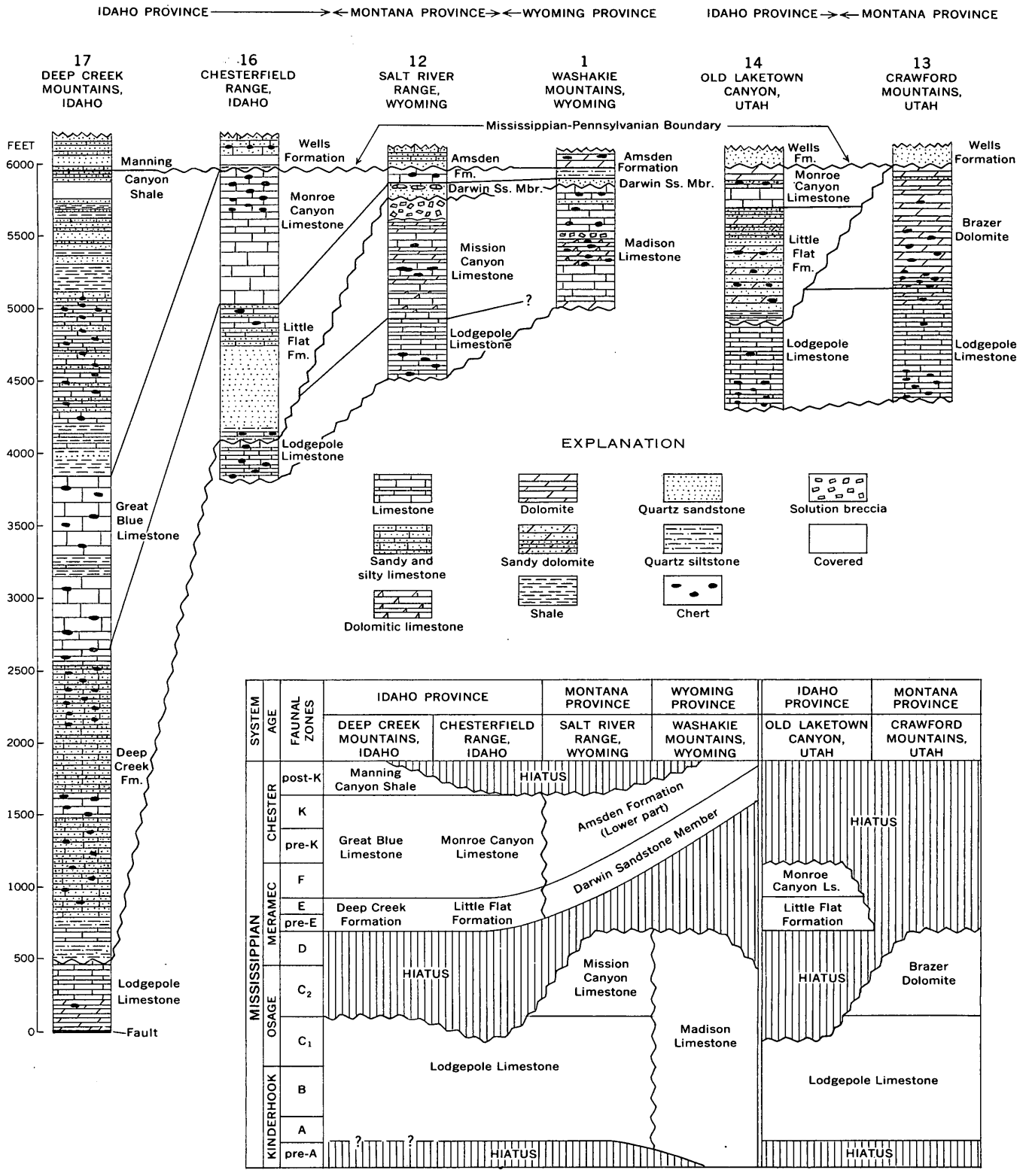

FIGURE 3.—Stratigraphic sections and diagram showing correlation and age relationships of selected sections of Mississippian rocks in southeastern Idaho, northeastern Utah, and western Wyoming. Numbers of stratigraphic sections refer to locations indicated on figure 2.

containing subordinate shale and sandstone. These cherty limestone beds of the Amsden contain fossils representative of the K Zone of Chester age, suggesting a Meramec and (or) early Chester age for the underlying Darwin Member. Beds of quartz sandstone and sandy limestone containing fossils of Pennsylvanian age disconformably overlie the limestone in the lower part of the Amsden. The absence of post-K fossils suggests a hiatus within the Amsden Formation.

In the Brazer Canyon section of the Crawford Mountains in northeastern Utah (section 13 on figs. 2 and 3), the Mississippian System again begins with the Lodgepole Limestone resting disconformably on beds of Late Devonian age (Beirdneau Formation according to Benson, 1966). The pre-A Zone is missing at the base of the Lodgepole; however equivalents of the Paine and Woodhurst Members can be recognized, and all the younger Lodgepole faunal zones are represented. Aside from a concentration of dolomite beds in the uppermost part, the record of Lodgepole deposition is very much like that of sections to the north.

The age and correlation of the overlying Brazer Dolomite have been a source of considerable confusion. Despite a detailed biostratigraphic and structural study of the Crawford Mountain Mississippian sequence (Sando and others, 1959), which provided the basis for a modern interpretation of the Brazer, the term continues to be misused. It seems necessary to reiterate that the Brazer is now regarded as a dolomitized sequence of shallow-water marine carbonates approximately equivalent to the Mission Canyon Limestone. Deposition of the Brazer appears to span late Osage and early Meramec time (Zones C_2 and D). The Brazer is overlain disconformably by the Wells Formation of Pennsylvanian age, and post-early Meramec, pre-Pennsylvanian rocks are absent either because of nondeposition or erosion.

IDAHO PROVINCE

An arcuate belt of Mississippian rocks with as yet undefined western and southern limits extends across eastern Idaho southward into northern Utah (fig. 2). Structural complexities and a paucity of detailed biostratigraphic studies permit only broad generalizations concerning the history of Mississippian deposition in the area north of the Snake River Plain. Most of the published data on that area were summarized by Ross (1962), and a discussion of that area is beyond the scope of this paper. The present analysis of the Idaho province is confined to southeastern Idaho and northeastern Utah, where three carefully studied stratigraphic sections form the basis for most of the interpretations.

The Mississippian sequence is about 1,700 feet thick at Old Laketown Canyon at the south end of Bear Lake (section 14 on figs. 2 and 3). This section is the easternmost control point in the Idaho province. A previous tentative correlation of the Old Laketown Canyon section (Sando and others, 1959, fig. 5), made largely on physical evidence, was later revised when similar sequences to the north and west were studied (Dutro and Sando, 1963, figs. 5 and 6). The section illustrates a striking change from the Brazer Canyon section, which is only about 14 miles to the east. At Old Laketown Canyon, the age of the Lodgepole extends from Kinderhook to early Osage (Zone A into Zone C_1) time, but the uppermost beds of the Lodgepole are missing. The entire Brazer (Mission Canyon equivalent) also is missing. After post-Lodgepole emergence the sandy Little Flat Formation and the Monroe Canyon Limestone were deposited successively. Deposition was continuous through middle and late Meramec time (Zones pre-E to F). Beds of Chester age are not present in this section, and the Monroe Canyon is overlain by the Wells Formation of Pennsylvanian age, indicating a post-Meramec, pre-Pennsylvanian hiatus.

A somewhat thicker (about 2,150 feet) and more complete section at Little Flat Canyon in the Chesterfield Range (section 16 on figs. 2 and 3) was established by Dutro and Sando (1963) as a reference section for the Mississippian of southeastern Idaho. As in the Old Laketown Canyon section, the Madison Group at Little Flat Canyon is represented by an abbreviated section of Lodgepole Limestone that lacks the pre-A Zone at the base and a part of Zone C_1 in the upper part. The Lodgepole is largely represented by the Paine Member, but a few beds of the Woodhurst Member are present at the top. The Lodgepole is overlain disconformably by the Little Flat Formation, a transgressive sequence of marine siltstone, sandstone, and sandy limestone of middle Meramec age. The Little Flat grades upward into marine limestone of the Monroe Canyon Limestone, which ranges in age from late Meramec well into the Chester. Beds of youngest Chester (post-K) age are not present in this section, indicating a period of pre-Pennsylvanian or Pennsylvanian erosion before deposition of the overlying Wells Formation.

The section described by Carr and Trimble (1961, fig. 213.1) in the Deep Creek Mountains (section 17 on figs. 2 and 3) is the westernmost control point in the Idaho province. Unpublished studies of the fossils

collected by Carr and Trimble form the basis for the present chronology of this area, where nearly 6,000 feet of Mississippian sedimentary rock was deposited. The lowest unit is the Lodgepole Limestone, which begins with 190 feet of dolomite that resembles the Paine Member but contains Zone C_1 fossils. On the basis of the fossils, the Paine Member appears to be younger than lithically equivalent beds to the east. Zones A and B have not been identified in this section, but a range-front fault separates the Lodgepole from the underlying Devonian strata (C. A. Sandberg, written commun., 1967) so that these lower zones may be present in the Deep Creek Mountains. The upper part of the Lodgepole appears to belong to the Woodhurst Member. Zones C_2 and D are absent, indicating a hiatus between the Lodgepole and the overlying Deep Creek Formation, which is a temporal and lithic equivalent of the Little Flat Formation to the east. The Deep Creek Formation grades upward into the Great Blue Limestone, an equivalent of the Monroe Canyon Limestone. The Great Blue is conformably overlain by the Manning Canyon Shale, which contains fossils of youngest Chester age (post-K) in the lower part and fossils of Early Pennsylvanian age in the upper part and represents virtually continuous deposition across the Mississippian-Pennsylvanian boundary.

PALEOTECTONIC SUMMARY

The Mississippian Period of the northern Cordilleran region was characterized by two major eastward transgressions of the sea from a geosyncline that extended northward across central Idaho. The older of the two advances is represented by the predominantly carbonate strata of the Madison Group. However, the earliest pulses (latest Devonian to earliest Mississippian) of the Madison advance are represented by the dark shale unit of Sandberg (1963), which now occupies a narrow belt in western Wyoming extending into north-central Wyoming and as far north as southwestern and south-central Montana (Benson, 1966, fig. 16; Sandberg and Klapper, in press). Data compiled by Benson (1966, fig. 16) suggest that the sea entered this early Madison basin through a relatively narrow inlet between the areas of the present Crawford Mountains and Uinta Mountains. At this time, much of southeastern Idaho as far west as the Deep Creek Mountains was apparently a land area of low relief, and most of Wyoming was similarly emergent. Two transgressive pulses are distinguished by Sandberg and Klapper (in press) in the dark shale unit: an earlier pulse in latest Devonian time (upper *to*V to *to*VI), and a later pulse in earliest Mississippian time (*cu*I to *to*IIα). According to Sandberg and Klapper (in press), parts of the early Madison basin were effected by mild orogenic movements related to the Antler orogeny between the two transgressive pulses.

Early Kinderhook (Zone A) time provides evidence of a considerable enlargement of the area of Madison deposition. Limestone deposits dominated by crinoidal debris spread from the Idaho province eastward over a large area of the Montana and Wyoming provinces. Superjacent argillaceous limestone beds of the Paine Member record a slight deepening of the Lodgepole sea in the Montana and Idaho provinces during late Kinderhook (Zone B) time. In the Wyoming province, shoaling conditions prevailed at the same time.

Early Osage (Zone C_1) time was characterized by continued widespread marine deposition in all three provinces. However, the character of the rocks deposited during this time (Woodhurst Member of the Lodgepole) suggests that the depositional environment was becoming progressively shallower.

Continued shallowing of the sea during late Osage and early Meramec time (Zones C_2 and D) is recorded in the carbonate strata of the Mission Canyon Limestone and Brazer Dolomite of the Montana province and equivalent beds in the upper part of the Madison Limestone of the Wyoming province. Gypsum beds both in surface and subsurface sections and widespread solution breccias indicate that evaporite deposition occurred over a large area at several times during this period. The former western extent of Mission Canyon deposition is unknown; if beds of C_2 and D age were ever deposited in the Idaho province, they were removed by subsequent intra-Mississippian erosion.

After the Mission Canyon Limestone and its equivalents had been deposited, the gradual shallowing of the Madison sea culminated in an episode of epeirogenic uplift throughout the northern Cordilleran region. In the Montana and Wyoming provinces, a karst topography was developed on the uplifted Madison rocks. Related solution effects extended down into the evaporite beds, leached out the soluble constituents and produced collapse breccias. In the Idaho province, beds of Zones C_2 and D are absent from the top of the Madison, and the overlying sedimentary rocks are of middle Meramec age. In the Montana and Wyoming provinces, however, the youngest Madison beds belong to Zone D, and the overlying strata are probably of late Meramec and Chester age. These relationships suggest that erosion may have begun earlier or been more intense in the Idaho province than in the cratonic areas to the east.

The second major advance of the Mississippian sea is represented by the Chesterfield Range Group and its equivalents. The early phase of this transgression,

reflected by deposition of quartz sandstone and sandy limestone, began in middle Meramec time in the Idaho province and spread eastward, reaching the Wyoming province in Chester time. The arenaceous beds thin eastward, suggesting a western, or possibly southwestern source. In the Idaho province, the transgressive sandy beds (Deep Creek and Little Flat Formations) contain marine fossils, whereas in the Montana and Wyoming provinces homotaxially equivalent beds (Darwin Sandstone Member of Amsden Formation) are unfossiliferous and may represent near-shore conditions. The Darwin locally fills sinkholes in the Madison of the Wyoming province, but its irregular distribution cannot everywhere be related in any simple way to the topography of the underlying erosional surface.

The thickness and lithic character of the sediments deposited during the earlier transgression (Kinderhook to early Meramec time) do not indicate a marked differentiation of the area into miogeosyncline and craton. The entire region seems to have been characterized by cratonic shelf deposition during Madison time. However, marked facies changes and thickness variations during the Late Mississippian transgression indicate a differentiation into a miogeosynclinal Idaho province bordering cratonic Montana and Wyoming provinces. The Chesterfield Range Group and its western equivalents are shallow-water open-marine deposits several thousand feet thick. In western Wyoming (Montana province), the same time interval is represented by a much thinner sequence of nonmarine or marginal-marine shale, siltstone, and sandstone and marine limestone in the lower part of the Amsden Formation above the Darwin Sandstone Member. At about the same time, an even thinner sequence of highly ferruginous red siltstone and shale containing a few marine limestone beds was deposited in the Wyoming province. The provenance of these red terrigenous deposits in the lower part of the Amsden Formation is unknown, but Keefer and Van Lieu (1966, p. 40) suggest that they may have been derived from regolithic soils developed on an emergent area of Precambrian rocks in southeastern Wyoming.

In the western part of the Idaho province, the sea deepened somewhat in latest Mississippian (post-K) time, and a thick terrigenous sequence, the Manning Canyon Shale, was deposited; these conditions prevailed without interruption into the Pennsylvanian. The easternmost extent of the Manning Canyon sea is unknown because a disconformity separates Pennsylvanian rocks from the Monroe Canyon Limestone in the eastern part of the Idaho province. This eastern area (Bannock Highland of Williams, 1962) was evidently emergent during latest Mississippian or earliest Pennsylvanian time. The emergent area extended into the Montana province in western Wyoming, where the Mississippian-Pennsylvanian disconformity occurs within the Amsden Formation. Farther east, however, on the cratonic platform of the Wyoming province, deposition of red terrigenous sediments continued through latest Mississippian (post-K) time, and was followed by deposition of shallow-water cherty carbonates of the upper part of the Amsden Formation during Early Pennsylvanian time.

REFERENCES

Andrews, D. A., and Hunt, C. B., 1948, Geologic map of eastern and southern Utah (scale 1:500,000) : U.S. Geol. Survey Oil and Gas Inv. (Prelim.) Map 70.

Andrichuk, J. M., 1955, Mississippian Madison Group stratigraphy and sedimentation in Wyoming and southern Montana: Am. Assoc. Petroleum Geologists Bull., v. 39, no. 11, p. 2170–2210, 12 figs.

Benson, A. L., 1966, Devonian stratigraphy of western Wyoming and adjacent areas: Am. Assoc. Petroleum Geologists Bull., v. 50, no. 12, p. 2566–2603, 16 figs.

Carr, W. J., and Trimble, D. E., 1961, Upper Paleozoic rocks in the Deep Creek Mountains, Idaho: Art. 213 *in* U.S. Geol. Survey Prof. Paper 424–C, p. C181–C184.

Dutro, J. T., and Sando, W. J., 1963, New Mississippian formations and faunal zones in Chesterfield Range, Portneuf quadrangle, southeast Idaho: Am. Assoc. Petroleum Geologists Bull., v. 47, no. 11, p. 1963–1986, 6 figs.

Gulbrandsen, R. A., McLaughlin, K. P., Honkala, F. S., and Clabaugh, S. E., 1956, Geology of the Johnson Creek quadrangle, Caribou County, Idaho: U.S. Geol. Survey Bull. 1042–A, 23 p., 2 pls., 1 fig.

Keefer, W. R., 1957, Geology of the Du Noir area, Fremont County, Wyoming: U.S. Geol. Survey Prof. Paper 294–E, p. 155–221, 25 figs., 2 pls.

Keefer, W. R., and Van Lieu, J. A., 1966, Paleozoic formations in the Wind River Basin, Wyoming: U.S. Geol. Survey Prof. Paper 495–B, 60 p., 6 pls., 23 figs.

Love, J. D., Keefer, W. R., Duncan, D. C., Bergquist, H. R., and Hose, R. K., 1951, Geologic map of the Spread Creek–Gros Ventre River area, Teton County, Wyoming: U.S. Geol. Survey Oil and Gas Inv. Map OM–118.

Love, J. D., Weitz, J. L., and Hose, R. K., 1955, Geologic map of Wyoming (scale 1:500,000) : U.S. Geol. Survey.

Marzolf, J. E., 1965, Stratigraphy of the Mobil Oil Company Paleozoic test well No. 22–19–G, Tip Top unit, Sublette County, Wyoming: U.S. Geol. Survey open-file rept. 805, 39 p., 3 figs.

Maughan, E. K., 1963, Mississippian rocks in the Laramie Range, Wyoming, and adjacent areas: Art. 66 *in* U.S. Geol. Survey Prof. Paper 475–C, p. C23–C27, 2 figs.

Ross, C. P., 1962, Paleozoic seas of central Idaho: Geol. Soc. America Bull., v. 73, no. 6, p. 769–794, 3 figs., 1 pl.

Ross, C. P., and Forrester, J. D., 1947, Geologic map of the state of Idaho (scale 1:500,000) : U.S. Geol. Survey and Idaho Bur. of Mines and Geology.

Sandberg, C. A., 1963, Dark shale unit of Devonian and Mississippian age in northern Wyoming and southern Montana: Art. 64 *in* U.S. Geol. Survey Prof. Paper 475–C, p. C17–C20.

Sandberg, C. A., and Klapper, Gilbert, in press, Stratigraphy, age, and paleotectonic significance of the Cottonwood Canyon Member of the Madison Limestone in Wyoming and Montana: U.S. Geol. Survey Bull. 1251–B.

Sando, W. J., 1967, Madison Limestone (Mississippian), Wind River, Washakie, and Owl Creek Mountains, Wyoming: Am. Assoc. Petroleum Geologists Bull., v. 51, no. 4, p. 529–557, 8 figs.

Sando, W. J., and Dutro, J. T., Jr., 1960, Stratigraphy and coral zonation of the Madison group and Brazer dolomite in northeastern Utah, western Wyoming, and southwestern Montana, *in* Wyoming Geol. Assoc. Guidebook, 15th Ann. Field Conf.: p. 117–126, 3 figs., 1 pl.

Sando, W. J., Dutro, J. T., Jr., and Gere, W. C., 1959, Brazer dolomite (Mississippian), Randolph quadrangle, northeast Utah: Am. Assoc. Petroleum Geologists Bull., v. 43, no. 12, p. 2741–2769, 5 figs.

Scholten, Robert, 1957, Paleozoic evolution of the geosynclinal margin north of the Snake River Plain, Idaho-Montana: Geol. Soc. America Bull., v. 68, no. 2, p. 151–170, 7 figs., 1 pl.

Scholten, Robert, Keenmon, K. A., and Kupsch, W. O., 1955, Geology of the Lima region, southwestern Montana and adjacent Idaho: Geol. Soc. America Bull., v. 66, no. 4, p. 345–404, 6 figs., 6 pls.

Shaw, A. B., 1955, The Amsden Formation in southwestern and south-central Wyoming, *in* Wyoming Geol. Assoc. Guidebook, 10th Ann Field Conf.: p. 60–63, 1 fig.

Sloss, L. L., and Moritz, C. A., 1951, Paleozoic stratigraphy of southwestern Montana: Am. Assoc. Petroleum Geologists Bull., v. 35, no. 10, p. 2135–2169, 12 figs.

Staatz, M. H., and Albee, H. F., 1966, Geology of the Garns Mountain quadrangle, Bonneville, Madison, and Teton Counties, Idaho: U.S. Geol. Survey Bull. 1205, 122 p., 2 pls., 16 figs., 5 tables.

Wanless, H. R., Belknap, R. L., and Foster, H. L., 1955, Paleozoic and Mesozoic rocks of Gros Ventre, Teton, Hoback, and Snake River Ranges, Wyoming: Geol. Soc. America Mem. 63, 90 p., 23 pls., 6 figs.

Williams, J. Stewart, 1962, Pennsylvanian System in central and northern Rocky Mountains, *in* Pennsylvanian System in the United States—A symposium: Tulsa, Okla., Am. Assoc. Petroleum Geologists, p. 159–187, 11 figs.

RELATION OF NUSSBAUM ALLUVIUM (PLEISTOCENE) TO THE OGALLALA FORMATION (PLIOCENE) AND TO THE PLATTE-ARKANSAS DIVIDE, SOUTHERN DENVER BASIN, COLORADO

By PAUL E. SOISTER, Denver, Colo.

Abstract.—Alluvial sand and gravel deposits about 145 feet thick and assignable to the Nussbaum Alluvium lie on an erosion surface that slopes southward toward the Arkansas River from near the Platte-Arkansas divide. The arkosic Dawson Formation was the main sediment source. The Nussbaum is partly overlapped by similar younger alluvial deposits. Local post-Nussbaum shifts of the divide are indicated by some deposits on it. Near the divide, the Ogallala Formation may have been overlapped by the Nussbaum. Restored contours on the base of the two formations indicate that the pre-Nussbaum surface diverged from about the same altitude as the pre-Ogallala surface near the divide to several hundred feet below the pre-Ogallala surface near the present Arkansas River.

Delineation of heretofore unrecognized deposits of the Nussbaum Alluvium (earliest Pleistocene) permits preliminary statements as to the relation of the Nussbaum to the Ogallala Formation (Pliocene). Recognition of the Nussbaum and similar younger deposits of Pleistocene age is significant to ground-water geology as well as to late Tertiary and early Quaternary geology and physiography of the Colorado plains and Front Range. In the present study, no attempt was made to correlate the Nussbaum with erosion surfaces in the Front Range described by Lee (1923), Van Tuyl and Lovering (1935), Powers (1935), Lovering and Goddard (1950), and others; however, Scott's (1963) use of surfaces at Canon City as correlative with the Ogallala and Nussbaum is adapted in this report.

The Nussbaum Alluvium was regarded by Gilbert (1897) as pre-Pleistocene when he named it and assigned it to the "Neocene" from deposits at and near Nussbaum Spring on Baculite Mesa just northeast of Pueblo. Stose (1912) changed the age designation to Pliocene(?). Until recently, geologists in Colorado and adjacent States correlated the Nussbaum with the Ogallala Formation (compare Darton, 1905, p. 179; Merriam, 1963, p. 32). Scott (1963) changed its age designation to Pleistocene(?) after his studies of the formation in the type locality showed that the Nussbaum is (1) post-Ogallala and (2) the earliest of a "closely spaced sequence of nearly identical alluvial deposits" (Scott, 1963, p. C52). These statements are supported by this writer's observations, but physiographic and lithologic evidence warrants a definite age designation of Pleistocene. Except for unidentifiable bone fragments on Baculite Mesa (Scott, 1963, p. C50), no fossils have yet been found in the Nussbaum.

Gilbert did no mapping outside the Pueblo quadrangle in this region. Assignments of the name Nussbaum to other deposits were made by other geologists, and some such assignments are erroneous. However, some deposits of the Nussbaum have not heretofore been mapped, and parts of these deposits have been included in the upper arkosic Paleocene part of the Dawson Formation or in the Ogallala Formation.

DEPOSITS ON CORRAL BLUFFS

During mapping of the Corral Bluffs quadrangle, Colorado, the writer found that as much as 145 feet of poorly consolidated sand and gravel caps the Corral Bluffs. These deposits (figs. 1, 2) are unconformable on the north- and northeast-dipping Dawson Formation of Paleocene and Late Cretaceous age and lie on a south-sloping erosion surface (fig. 3) that, to the south, truncates the Laramie, Fox Hills, and Pierre Formations of Late Cretaceous age. The erosion surface is rather irregular and locally hilly on the Dawson Formation but smoother on the Laramie, Fox Hills, and Pierre. It correlates with the surface under the Nussbaum on Baculite Mesa (Scott, 1963, p. C50; 1964), which is

U.S. GEOL. SURVEY PROF. PAPER 575-D, PAGES D39-D46

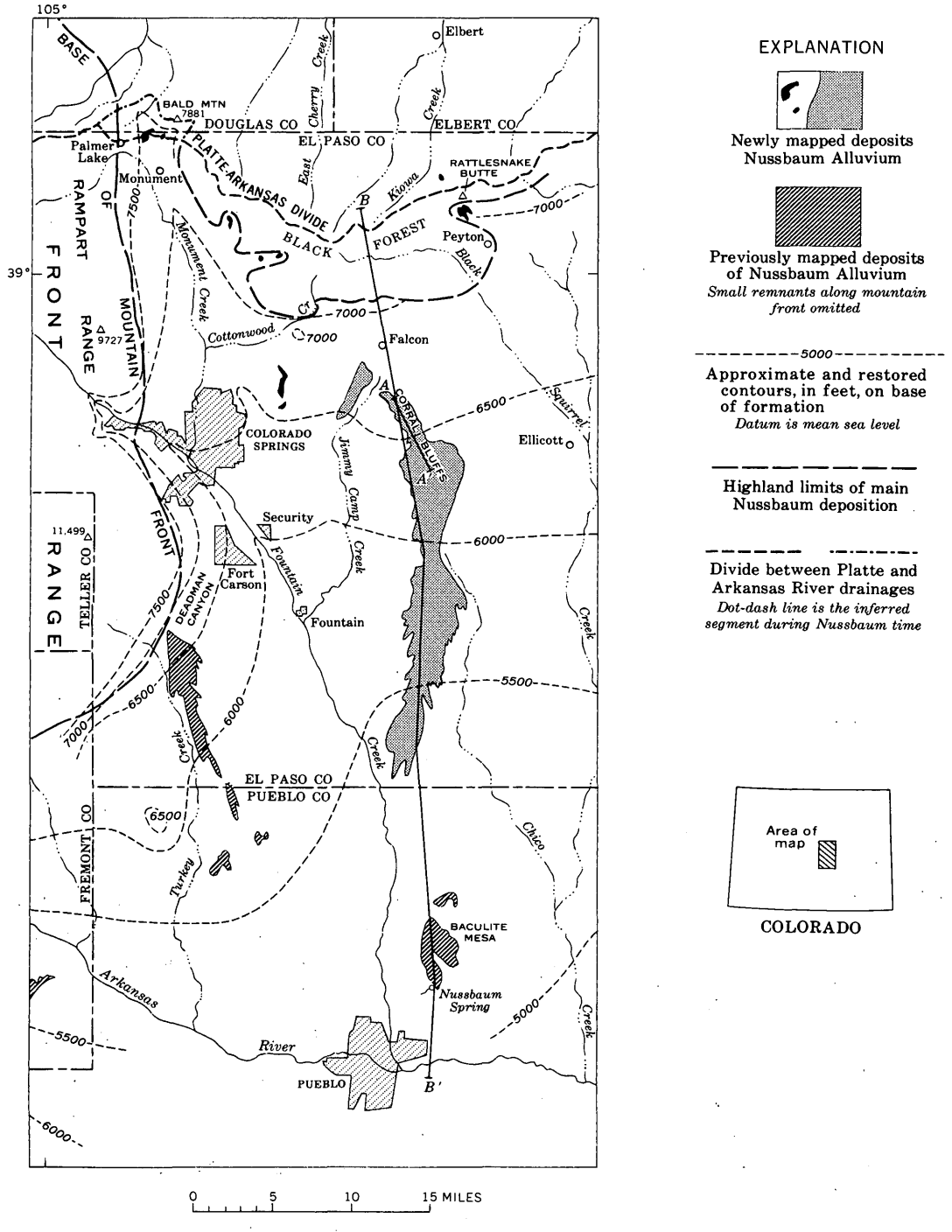

FIGURE 1.—Map showing deposits of Nussbaum Alluvium between the Platte–Arkansas divide and the type locality (Nussbaum Spring) near Arkansas River, Colo.

graded to a point about 400 feet above the present Arkansas River. Because of lithologic and physiographic similarities of the deposits on Corral Bluffs to the Nussbaum of the type locality at Baculite Mesa, they are here assigned to the Nussbaum. Brown (1943, p. 75) and Reichert (1954, pls. 4, 6; 1956, pls. 1, 2) considered the deposits on the Corral Bluffs to be the basal part of the upper, coarse half of the Dawson Formation.

On Corral Bluffs a detailed section of the Nussbaum was measured 0.25 mile south of State Highway 94 in NE¼ sec. 17, T. 14 S., R. 64 W. There, the formation is

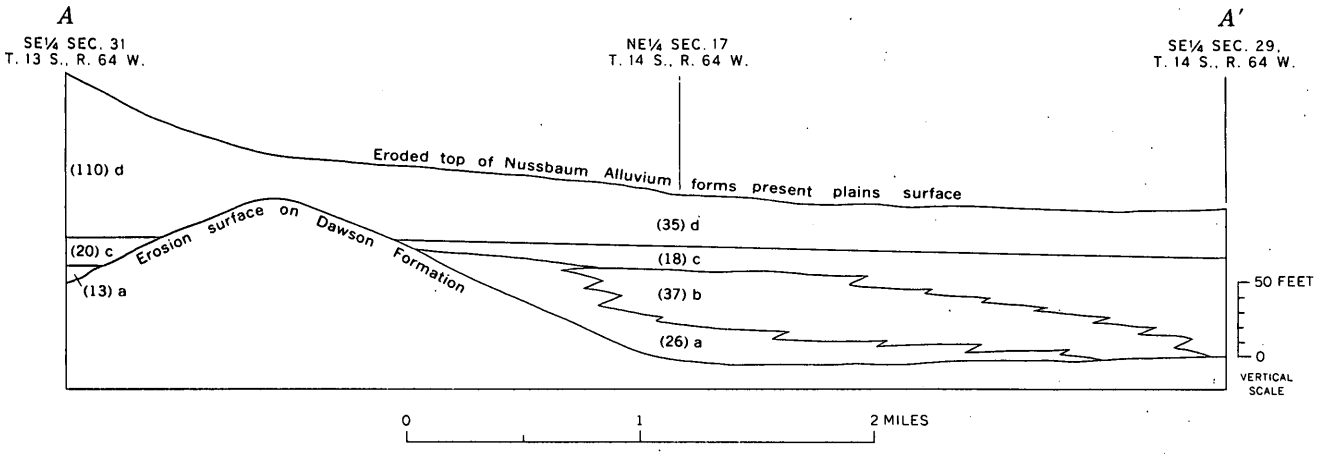

FIGURE 2.—Generalized stratigraphic section of the Nussbaum Alluvium on the Corral Bluffs. Figures in parentheses show thickness, in feet, of lithologic units of the Nussbaum at two measured sections, one of which is described in text. a, coarse arkosic sand; b, fine-to-medium white arkosic sand; c, sandy gravel; and d, medium to very coarse arkosic sand.

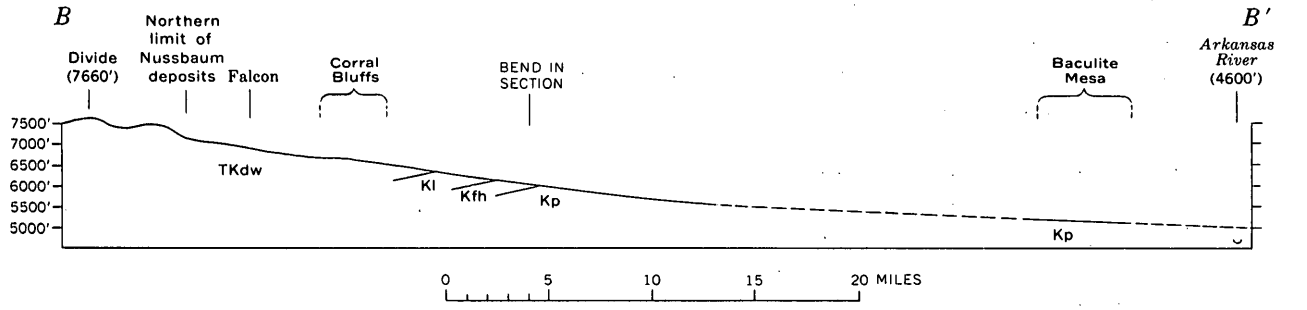

FIGURE 3.—Profile on base of Nussbaum Alluvium from near the Platte-Arkansas divide through Corral Bluffs and Baculite Mesa to the Arkansas River. Dashed line shows inferred approximate position where Nussbaum has been removed by erosion. Formations below Nussbaum are: Kp, Pierre Shale; Kfh, Fox Hills Sandstone; Kl, Laramie Formation; TKdw, Dawson Formation.

116 feet thick. Another 143-foot section was measured at the highest part of the Corral Bluffs, 2 miles north of the highway in SE¼ sec. 31, T. 13 S., R. 64 W. The original thickness of the formation in the Corral Bluffs area was probably about 150 to 200 feet or more. The section near the highway includes all the principal lithologic units noted in this area and is described as follows:

Measured section of the Nussbaum Alluvium on Corral Bluffs. Location about 8 miles east of Colorado Springs and 0.25 mile south of State Highway 94, in NE¼ sec. 17, T. 14 S., R. 64 W.

	Thickness (feet)
Top of section.	
d. Sand, arkosic, medium to very coarse, silty; granules and scarce small pebbles; grayish orange to grayish yellow; partly or mostly thinly laminated. Caps bluffs and forms plains surface. A few miles to the south, unit has caliche ($CaCO_3$) related to present surface	35
c. Gravel, sandy; granules and pebbles mostly of red and gray granite, quartz, and feldspar; some andesite and sandstone pebbles from Dawson Formation; grayish orange to light yellowish gray; basal 1 ft commonly very limonitic, or locally calcareous and hard; top and bottom contacts conformable but unit is abruptly gradational up into unit d	18
b. Sand, arkosic, fine to medium, silty; very light yellowish gray to white; evenly bedded in thin to thick flat beds; has some limonitic laminae generally an inch thick, and upper 5 ft has ¼- to 1-in. soft limonitic sandstone concretions. Pinches out a short distance to the north	37
a. Sand, arkosic, coarse, silty; has granules and small pebbles mostly of granite, quartz, and feldspar, especially near base; very pale orange to grayish orange; locally limonitic in thin layers; flat bedded; alternating soft and slightly consolidated layers produce a thinly laminated appearance	26
Base of section.	

Units c and d (fig. 2) are the most widespread and typical lithologies of the Nussbaum in the Corral Bluffs area, where the formation generally consists of coarse sand above granule and pebble gravel. Locally, the basal few inches to about 2 feet of the Nussbaum is cemented by calcite or by iron oxides. Diffused calcite (caliche) occurs in a few to several indistinct layers locally, most commonly in the upper sand (unit d).

OTHER DEPOSITS

Brief reconnaissance checks of widely separated points in the southern Denver basin were made for remnants of the Nussbaum. Many deposits whose lithology and physiographic position (fig. 4; note contours on figs. 1, 5) are compatible with a correlation with the Nussbaum were noted, and several of these are shown on figure 1. Most are on the south side of the Platte-Arkansas divide, where almost all the reconnaissance was undertaken. Most of these deposits include fragments of rhyolite, arkosic conglomerate, petrified wood, and other materials from the Dawson and Castle Rock (Oligocene) Formations in predominantly arkosic sand and granite pebble gravel.

At the northeast edge of Colorado Springs (fig. 1) 30 feet or more of alluvium similar to the deposits on Corral Bluffs is well exposed in and near gravel pits; its base is more than 500 feet higher than Monument Creek about 5 miles to the west. Between this area and Corral Bluffs, a ridge west of Jimmy Camp Creek is partly capped by more than 100 feet of the Nussbaum.

The broad and gently sloping area of several square miles around Falcon has many outcrops of the Dawson Formation, but the surface is mostly composed of Pleistocene sand and gravel that includes Nussbaum and younger deposits.

About 3 miles north of Falcon, an east-west contact separates predominantly Quaternary deposits and small inliers of the Dawson Formation on the south from almost entirely coarse arkose of the Dawson on the north. This contact roughly coincides with a break in slope from the steeper highland on the north. This higher area, which includes the Black Forest, has many small remnants of alluvium, several of which are believed to be Nussbaum, draped over low ridges and filling small valleys eroded into the Dawson a few hundred feet below the Platte-Arkansas divide.

North of Monument where the main highway (U.S. Highway 85–87, Interstate 25) crosses the Platte-Arkansas divide, and about 1 mile west of the highway also, remnants of alluvium interpreted as Nussbaum lie athwart the divide.

Just south of Rattlesnake Butte, remnants of probable Nussbaum Alluvium are within 1 mile of the Platte-Arkansas divide. The original top of these deposits must have been within about 100 feet of the present divide. About 2¼ miles to the northwest of these deposits a small deposit of Pleistocene alluvium, possibly Nussbaum, lies about 120 feet above Kiowa Creek. This alluvium is north of the Platte-Arkansas divide and a mile east of Kiowa Creek.

Downcutting of several hundred feet by Black Squirrel Creek and its tributaries separates the Nussbaum on Corral Bluffs from probable Nussbaum deposits 17 miles northeast. The latter deposits, more than 100 feet thick, cap a prominant escarpment just south of Calhan and underlie much of the high surface sloping south from the escarpment (figs. 4, 5). Data from water-well logs, together with topography, indicate that the Nussbaum occurs in a narrow southward-trending remnant from the area just south of Calhan to near the Arkansas River. The Nussbaum there is bordered on the east and west mostly by younger deposits. At least some of the Pleistocene deposits east of the long strip are Nussbaum.

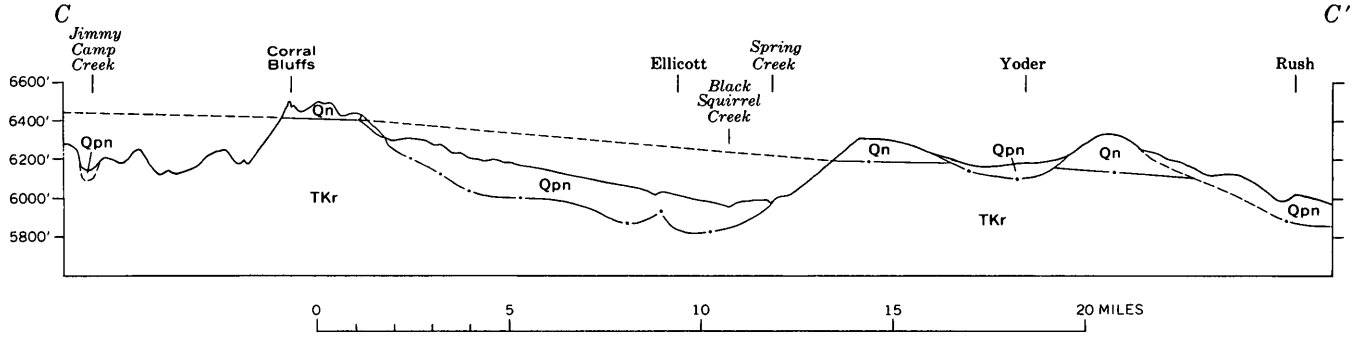

FIGURE 4.—Cross section along State Highway 94, showing interpretation of relation of Nussbaum Alluvium to later deposits. Geologic and topographic control is excellent west of Spring Creek but only fair to the east. Short-dashed line is inferred former position of base of Nussbaum; dots on base of alluvium show data from water wells within 1 mile of section. TKr, Paleocene and Cretaceous formations; Qn, Nussbaum Alluvium; Qpn, post-Nussbaum deposits of Pleistocene age.

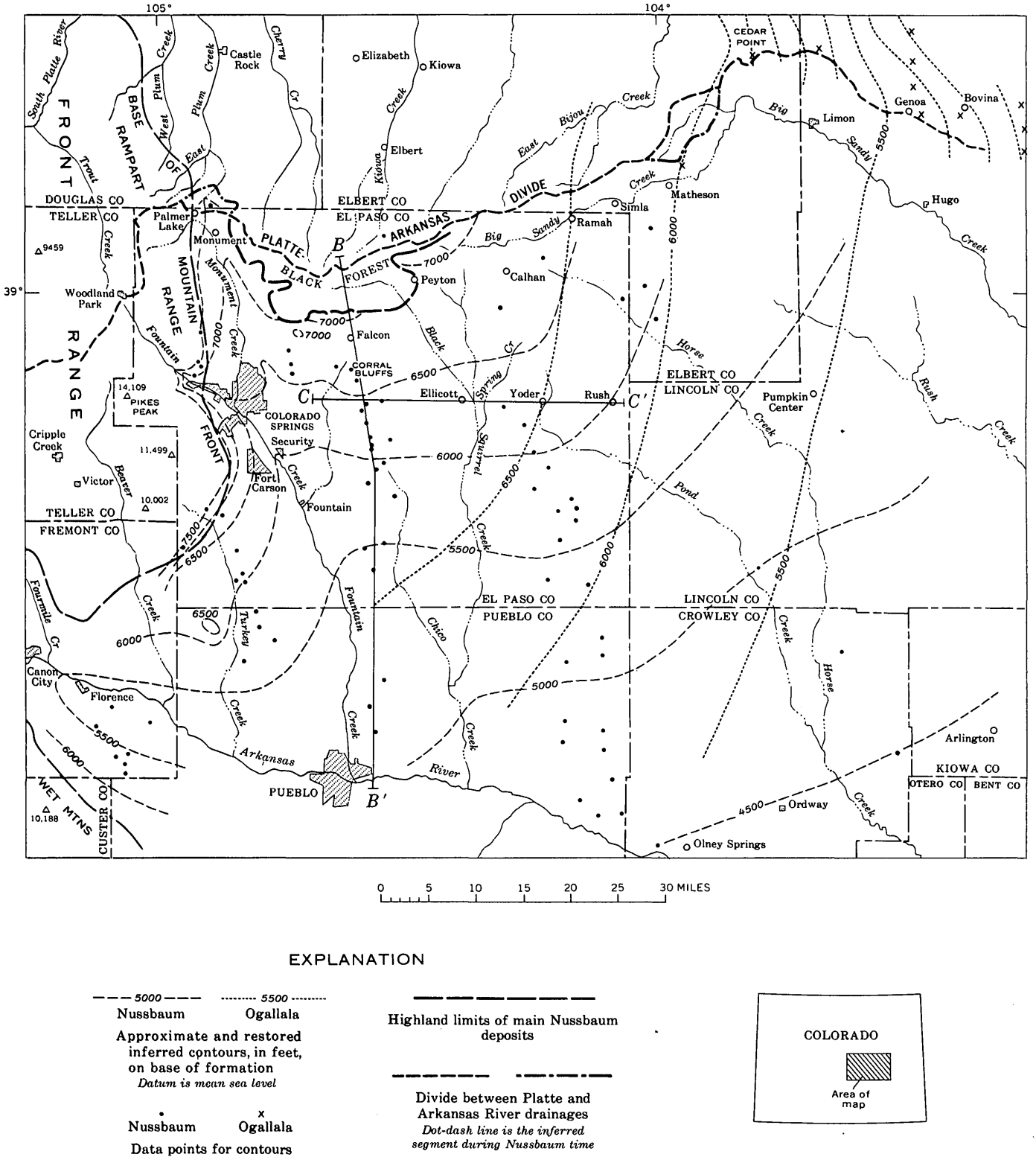

FIGURE 5.—Map comparing contours on base of Nussbaum and Ogallala Formations, southern Denver basin and vicinity, Colorado.

269-274 O—67——4

Seven miles north of Matheson (fig. 5) a deposit of high-level sand and granule gravel more than 20 feet thick closely resembles the Nussbaum of Corral Bluffs and is believed by the writer to be Nussbaum; bedding apparently dips northeast. The exposure examined is at the northwest end of deposits about 1 mile long on the Platte-Arkansas divide that are shown as an outlier of the Dawson Formation on the State geologic map (Burbank and others, 1935), and as the upper part of the Dawson by Dane and Pierce (1936, fig. 3) and McLaughlin (1942, pl. 1) in reconnaissance reports. The present writer believes the entire outlier is probably a remnant of Nussbaum, and has noted other remnants with similar lithology and physiographic position farther north and west.

RELATION TO OTHER PLEISTOCENE DEPOSITS

Eastward and northeastward from Corral Bluffs, the Nussbaum has been removed by erosion in the valley of Black Squirrel Creek, and the edges of the Nussbaum are mostly overlain by younger Pleistocene deposits. Inasmuch as the younger deposits were derived mostly from the Nussbaum and its main source, the Dawson, and were apparently deposited in similar environments, the almost identical lithology makes it difficult to distinguish between them in this area of generally low relief. Greater differences in lithology exist within the Nussbaum than between its most widespread units and some of the younger deposits. However, the younger deposits in Black Squirrel Creek valley lie on a steeper south-sloping surface than does the Nussbaum, so that a few miles to the south there is complete topographic separation between the Nussbaum and the younger deposits.

Drawing contours on the base of the Quaternary deposits, mainly from water-well data, helps to differentiate materials deposited at various times during the Pleistocene. However, this is complicated because of overlapping of deposits, uncertainties as to exact direction of slope of the surface, and presence of tributaries to the main streams during deposition of the various deposits.

Most of the deposits shown on the latest State geologic map (Burbank and others, 1935) as Ogallala in the region between the Arkansas River and Big Sandy Creek are the Nussbaum Alluvium and younger Pleistocene deposits. The earliest Colorado State geologic map (George, 1913) shows most of this area as Arikaree (Miocene), Ogallala, and Nussbaum, undivided. Dane and Pierce (1936, fig. 3) dated this sand and gravel as Pliocene and Pleistocene(?). The deposits form a complex overlapping and crosscutting sequence, with the oldest being higher topographically in some areas but beveled and overlain by younger deposits in others.

From about a mile southeast of Monument (fig. 1), south to the vicinity of Cottonwood Creek, unmapped thick sandy pebble gravel quite similar in lithology to the Nussbaum lies on surfaces which are cut on the Dawson Formation and are graded westward toward Monument Creek. The south-southeastward-sloping Nussbaum has been removed by erosion here. The sandy pebble gravel is of post-Nussbaum age, was derived from the Dawson and Nussbaum, and is equivalent to one or more of the poorly sorted and very coarse bouldery pediment deposits west of Monument Creek. Although approximately the same age as the coarse bouldery deposits, the pebble gravel differs from them in source, grain size, sorting, and partly in color.

PALEOGEOGRAPHY

Preliminary contours were drawn on the base of the extended Nussbaum Alluvium (figs. 1, 5). Contours east of the Corral Bluffs area were drawn by using data from water well logs and by fitting topographic contours of the Army Map Service 1:250,000-scale maps (Denver, Lamar, Limon, and Pueblo sheets) to the geologic map of Colorado (Burbank and others, 1935). Tator (1952, p. 272) correlated his Deadman Canyon surfaces with the Nussbaum of the Pueblo quadrangle, and the altitudes on his surfaces were used in drawing the contours west of Fountain and Monument Creeks. Scott's (1964) mapping on Baculite Mesa was used in that area. An erosion surface at about 6,100 feet, about 7 miles west of Canon City, is described by Powers (1935, p. 190–191), and it is believed by Scott (1963) to correlate with the Nussbaum; this appears to fit the contours shown in figures 1 and 5.

The contours show a surface sloping generally southward in the western part and southeastward in the eastern part of the area between the Arkansas River, Big Sandy Creek, and the Platte-Arkansas divide. This indicates radial drainage from the Platte-Arkansas divide highland area. The Nussbaum of the Corral Bluffs area is graded southward to a point about 400 feet above the present course of the Arkansas River; Scott (1963, p. C50) believes that, in Nussbaum time, the river was about 5 miles south of its present course.

Physiographic positions of probable Nussbaum deposits indicate that a major tributary to the Arkansas River in Nussbaum time flowed south-southeastward a few miles east of Monument and Fountain Creeks, as indicated by curves on the contours (figs. 1, 5). After Nussbaum time, this tributary drainage system shifted

west, closer to the foot of the mountains. During and since Nussbaum time, this drainage line has prevented areas to the east in the southern Denver basin from receiving sediments directly from the mountains. Therefore sediments were supplied from the plains and from the highland area along the Platte-Arkansas divide to form the extensive Quaternary deposits that blanket much of the area between the Arkansas River and Big Sandy Creek. Probably, numerous streams with courses similar to those of today radiated from the highland area toward the Arkansas River in Nussbaum and later time.

The Nussbaum was apparently the thickest and most extensive of the Pleistocene deposits in the area of this report, as evidenced by the remnants cited herein and by the thick correlative deposits on the Deadman surfaces of Tator (1952, p. 270).

PLATTE-ARKANSAS DIVIDE

The relation of the Nussbaum Alluvium to the divide between the South Platte and Arkansas Rivers on the plains of Colorado can now be appraised from the evidence at hand. In the Black Forest area, the present divide is a few hundred feet above the main depositional areas of the Nussbaum and probably occupies about the same position as during Nussbaum time. The occurrence of deposits believed to be Nussbaum on the lower parts of the divide west and east of the Black Forest indicates a shift of these parts in post-Nussbaum time.

It is tentatively suggested that near Palmer Lake the divide in Nussbaum time was a short distance to the north, running from Bald Mountain to Spruce Mountain and then rejoining the present divide about 1½ miles west of the present mountain front.

Bedding in the probable Nussbaum deposit on the present divide (about 5,950 feet altitude) north of Matheson indicates that the divide in Nussbaum time was locally south of its present position. It is here suggested that it lay along the top or a short way south of the first high ridge north of Big Sandy Creek, a ridge now partly capped by a probable remnant of the Ogallala Formation and higher (about 6,050 feet altitude) than the ridge line of the present divide. The divide here was probably very low in Nussbaum time.

RELATION TO OGALLALA FORMATION

About 2 miles northeast of Matheson, arkosic conglomerate capping the high ridge, mentioned above, is interpreted as being a remnant of the basal bed of the Ogallala Formation because of a close resemblance to the Ogallala at Cedar Point; it contains reworked ironstone fragments from immediately underlying beds of the Dawson Formation. The base of this possible remnant of the Ogallala Formation is at an altitude of about 6,000 feet, only about 100 feet higher than probable Nussbaum deposits 4 miles to the north and at about the same altitude as the base of probable Nussbaum deposits a few miles to the southwest.

Using this remnant and the good outcrops of the formation north and east of Limon, approximate and restored inferred contours were drawn on the base of the Ogallala Formation. Water-well data of Cardwell (1953, pl. 2) provide a few accurate points.

West and southwest of the Ogallala remnant, there is no direct evidence as to slope of the surface of the plains during Ogallala time. Powers (1935, p. 190, 195) believed that an erosion surface at about 6,800 feet altitude just west of Canon City is of late Pliocene age; Scott (1963) correlated this surface with the Ogallala Formation, and the present author's contours on the base of the Ogallala (fig. 5) are drawn to approximately fit this interpretation. The contours from the Limon area were drawn to curve in slightly toward the reentrant between the Front Range and the Wet Mountains because such a reentrant must have existed in Ogallala time and may have been reflected in the plains by a broad shallow east-trending valley. The contours indicate a more eastward sloping surface for the Ogallala as compared with a more southward sloping surface for the Nussbaum in the region between the Platte-Arkansas divide and the Arkansas River.

Smith (1940, p. 148) believed that the present course of the Arkansas River in Kansas is of post-Ogallala age. The available evidence suggests that after deposition of the Ogallala Formation a major period of erosion ensued, possibly in latest Pliocene time, during which the Arkansas River was established on the plains of Colorado with approximately the same course as it now has. The erosion involved stripping of the Ogallala, deep cutting into the underlying rocks, and increasing depth of erosion southward toward the Arkansas River. The inferred depth of erosion below the base of the Ogallala in pre-Nussbaum time is indicated by the difference between the two sets of contours (fig. 5). Only the Ogallala on and near the Platte-Arkansas divide was preserved.

In earliest Pleistocene time, any Ogallala deposits remaining west of Limon were partly to completely buried or surrounded by sediments of the Nussbaum. Where contours on the base of the two formations nearly coincide (fig. 5), the Nussbaum has been deposited in juxtaposition to remnants of the Ogallala

or has replaced the Ogallala where the latter was removed by erosion. Where an Ogallala remnant was relatively thin, the Nussbaum could have its base as much as 100 feet or more lower than that of the Ogallala and still overlap it because of the 100- to 200-foot thickness of the Nussbaum. Thus, remnants of the Ogallala Formation may locally underlie the Nussbaum.

REFERENCES

Brown, R. W., 1943, Cretaceous-Tertiary boundary in the Denver Basin, Colorado: Geol. Soc. America Bull., v. 54, no. 1, p. 65–86.

Burbank, W. S., Lovering, T. S., Goddard, E. N., and Eckel, E. B., 1935, Geologic map of Colorado: U.S. Geol. Survey, scale 1:500,000.

Cardwell, W. D. E., 1953, Irrigation-well development in the Kansas River basin of eastern Colorado: U. S. Geol. Survey Circ. 295, 72 p.

Dane, C. H., and Pierce, W. G., 1936, Dawson and Laramie formations in southeastern part of Denver Basin, Colorado: Am. Assoc. Petroleum Geologists Bull., v. 20, no. 10, p. 1308–1328.

Darton, N. H., 1905, Preliminary report on the geology and underground water resources of the central Great Plains: U.S. Geol. Survey Prof. Paper 32, 433 p.

George, R. D., 1913, Geologic map of Colorado: Colorado Geol. Survey.

Gilbert, G. K., 1897, Description of the Pueblo quadrangle [Colorado]: U.S. Geol. Survey Geol. Atlas, Folio 36, 7 p.

Lee, W. T., 1923, Peneplains of the Front Range and Rocky Mountain National Park, Colorado: U.S. Geol. Survey Bull. 730–A, p. 1–17.

Lovering, T. S., and Goddard, E. N., 1950, Geology and ore deposits of the Front Range, Colorado: U.S. Geol. Survey Prof. Paper 223, 319 p.

McLaughlin, T. G., 1942, Geology and ground-water resources of parts of Lincoln, Elbert, and El Paso Counties, Colorado: Colorado Water Conserv. Board. Bull. 1, 139 p.

Merriam, D. F., 1963, The geologic history of Kansas: Kansas State Geol. Survey Bull. 162, 317 p.

Powers, W. E., 1935, Physiographic history of the upper Arkansas River valley and the Royal Gorge, Colorado: Jour. Geology, v. 43, no. 2, p. 184–199.

Reichert, S. O., 1954, Geology of the Golden–Green Mountain area, Jefferson County, Colorado: Colorado School Mines Quart., v. 49, no. 1, 96 p.

———1956, Post-Laramie stratigraphic correlations in the Denver Basin, Colorado: Geol. Soc. America Bull., v. 67, no. 1, p. 107–111.

Scott, G. R., 1963, Nussbaum Alluvium of Pleistocene(?) age at Pueblo, Colorado: Art. 72 *in* U.S.. Geol. Survey Prof. Paper 475–C, p. C49–C52.

———1964, Geology of northwest and northeast Pueblo quadrangles, Colorado: U.S. Geol. Survey Misc. Geol. Inv. Map I–408.

Smith, H. T. U., 1940, Geologic studies in southwestern Kansas: Kansas State Geol. Survey Bull. 34, 212 p.

Stose, G. W., 1912, Description of the Apishapa quadrangle [Colorado]: U.S. Geol. Survey Geol. Atlas, Folio 186, 12 p.

Tator, B. A., 1952, Piedmont interstream surfaces of the Colorado Springs region, Colorado: Geol. Soc. America Bull. v. 63, no. 3, p. 255–274.

Van Tuyl, F. M., and Lovering, T. S., 1935, Physiographic development of the Front Range: Geol. Soc. America Bull., v. 46, no. 9, p. 1291–1350.

AGE OF VOLCANIC ACTIVITY IN THE SAN JUAN MOUNTAINS, COLORADO

By THOMAS A. STEVEN, HAROLD H. MEHNERT, and JOHN D. OBRADOVICH, Denver, Colo.

Abstract.—A review of the evidence supporting the widely quoted interpretation that volcanic activity in the San Juan Mountains took place mostly during the Miocene and Pliocene epochs indicates that this earlier interpretation requires modification. To establish the period of activity more firmly, the ages of six formations in the central and eastern parts of the mountains were determined by the K–Ar method. The results indicate that: (1) The last major intermediate to silicic unit in the San Juans, the Fisher Quartz Latite, was erupted near the end of the Oligocene, about 26 million years ago. Similar rocks were erupted locally and in small volume through the early Miocene. (2) The Creede Formation, which was deposited concurrently with Fisher volcanism, is thus latest Oligocene in age. (3) The span of time between eruption of the oldest and youngest units derived from the central San Juan source area was less than 2 million years. (4) The Hinsdale Formation as previously defined consists of units erupted during widely separated volcanic episodes, and the concept of a single genetically related formation needs to be modified.

The volcanic rocks in the San Juan Mountains, Colo. (fig. 1) have generally been believed largely Miocene and Pliocene in age (Larsen and Cross, 1956, p. 62–64). These ages are based mostly on nondiagnostic plant and gastropod fossils found in a few scattered tuffaceous units in the great volcanic field of the San Juan Mountains. The more recent stratigraphic papers on the San Juans (Luedke and Burbank, 1963, p. C39; Steven and Ratté, 1964, p. D56–57) have used a more general designation of middle to late Tertiary for the rocks. In summarizing the available paleobotanical data from the Creede Formation in more detail, Steven and Ratté (1965, p. 46–47) found that although interpretations by different paleobotanists varied, the bulk of opinion favored a late Tertiary age for the formation.

In an effort to establish the age of volcanic activity more firmly, a number of K-Ar determinations have been made for rocks collected from different volcanic formations in the central San Juan Mountains. In contrast with the interpretations based on paleobotanical evidence, all the K-Ar age data indicate clearly that (1) most of the volcanic rocks had been erupted by the end of Oligocene time, or 26 million years ago, according to the Geological Society of London Phanerozoic time scale of 1964 (Harland and others, 1964, p. 260), and (2) the whole central San Juan sequence (Steven and Ratté, 1964) was erupted within a very brief span of a few million years. Exceptions are scattered local quartz latitic to rhyolitic units erupted during the Miocene, and widespread basaltic flows of the Hinsdale that in the central San Juan, at least, appear to have been erupted near the end of the Miocene.

SUMMARY OF VOLCANIC HISTORY

Although some volcanic centers in southwestern Colorado were active in Late Cretaceous and possibly early Paleocene time, the bulk of volcanic rocks in the San Juan Mountains was erupted in Tertiary time following Paleocene or later folding of the Uncompahgre arch, Needle Mountain uplift, and related structures. This Tertiary volcanism occurred after a period of erosion had stripped the sedimentary rocks from the more highly upwarped areas. Streams responsible for much of this erosion deposited an apron of gravels, sands, and clays around the margins of the higher areas of exposed Precambrian rocks to form the Telluride and Blanco Basin Formations. The age of these formations has never been determined more closely than post-Animas Formation (Late Cretaceous

U.S. GEOL. SURVEY PROF. PAPER 575-D, PAGES D47-D55

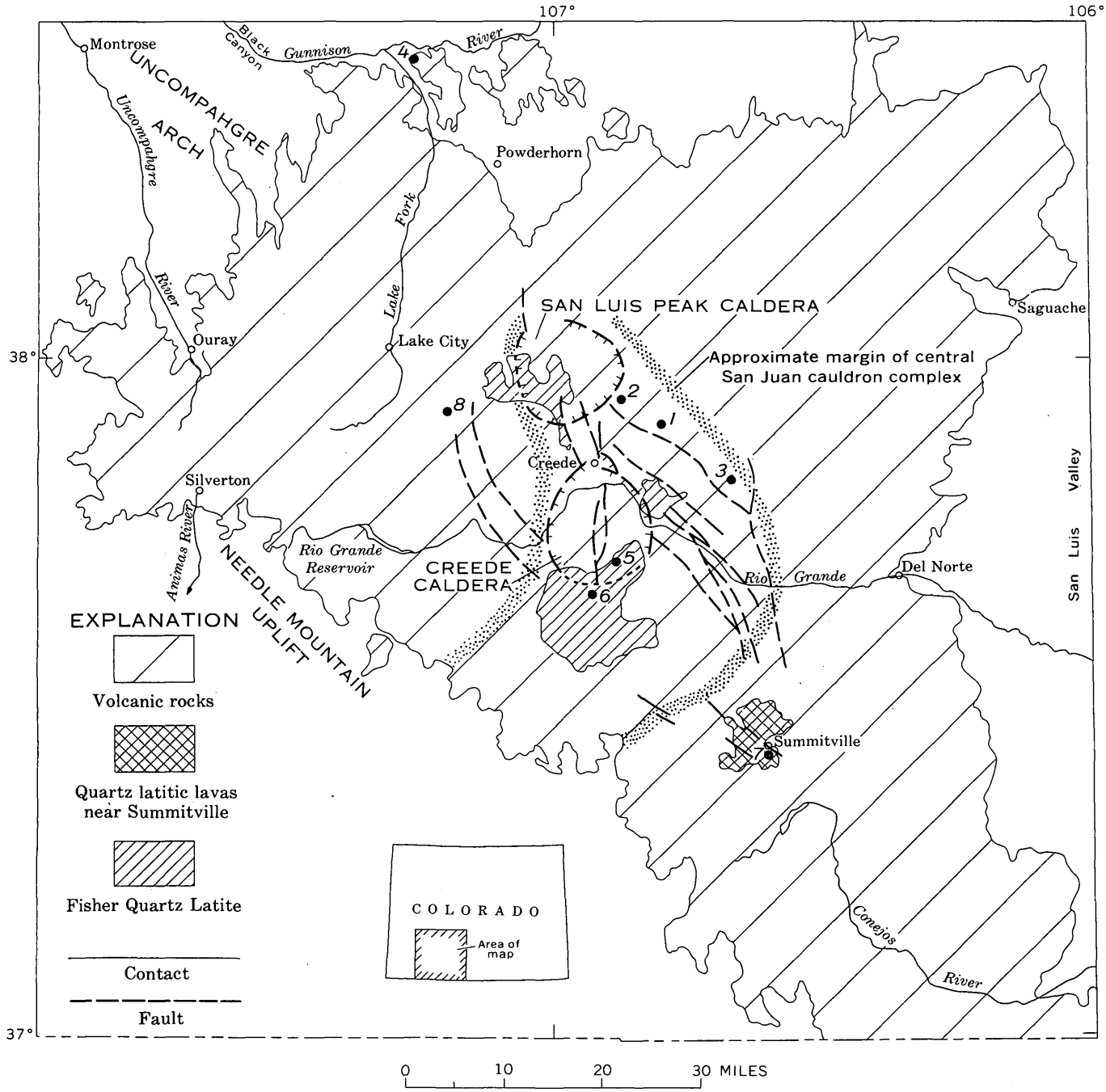

FIGURE 1.—Map of the San Juan volcanic field, Colorado, showing sample localities: *1*, S292; *2*, S318; *3*, Ds28; *4*, BC5793; *5*, S333; *6*, S332, Ds10; *7*, Ds29c; and *8*, S342 A,B.

and Paleocene) and prevolcanic (middle? Tertiary), although in recent years they have been correlated on lithology and stratigraphic position with the San Jose Formation of early Eocene age in the central part of the San Juan Basin (Kelley, 1952; Van Houten, 1957; Simpson, 1948; Dunn, 1964).

After deposition of the Telluride and Blanco Basin sediments, volcanism broke out over a fairly wide area in the San Juan region of southwestern Colorado. In the western part of the region (Luedke and Burbank, 1963), early volcanism built a cluster of volcanoes in the present headwater areas of the Uncompahgre and Animas Rivers, and of the Lake Fork of the Gunnison River, and deposited a great sheet of chiefly rhyodacitic tuff breccia in adjacent areas to form the San Juan Formation. The vent areas of these volcanoes apparently collapsed after the explosive eruptions, thus forming the San Juan depression. Continuing volcanic activity resulted in the accumulation, largely within the San Juan depression, of the alternating lava flow and pyroclastic deposits of the Silverton Volcanic Group. This volcanism in turn was followed by pyroclastic eruptions that deposited great volumes of mostly ash-flow deposits to form the Potosi Volcanic Group as redefined by Luedke and Burbank (1963, p. C43). The more localized Silverton and Lake City cauldrons were formed within the earlier San Juan depression as a consequence of the Potosi eruptions.

According to Larsen and Cross (1956, p. 62–63), early volcanism in the eastern San Juans built scattered local volcanic piles. These were followed by accumulation of a great mass of andesitic to rhyodacitic lavas, breccias, and reworked volcanic debris from a number of volcanic centers to form the widespread Conejos Formation. Although Larsen and Cross (1956, p. 61) state that the San Juan Formation is "much older" than the Conejos Formation, they cite no evidence to support this conclusion. Inasmuch as both formations rest directly on prevolcanic fluviatile deposits of the Telluride and Blanco Basin Formations over wide areas, it seems plausible that both may have formed during the same general time interval.

After the Conejos eruptions, volcanic activity shifted to the central part of the San Juan region (table 1), and a thick sequence of volcanic formations (Ratté and Steven, 1964; Steven and Ratté, 1964; 1965) accumulated in and adjacent to a concurrently forming cauldron complex (fig. 1) that is at least 50 miles N–S and 25 miles E–W across within the central part of the volcanic field. Most of the rocks erupted from this source area are welded ashflow tuffs. Lavas and breccias also accumulated around local centers and are increasingly more abundant among the younger units (Rattè and Steven, 1964, p. D50). The last major units in this sequence are the quartz latitic to rhyolitic lavas and breccias of the Fisher Quartz Latite, and the concurrently deposited sedimentary rocks of the Creede Formation.

TABLE 1.—*Age relations of rock units in the central San Juan Mountains, Colo., showing positions of dated units*
[Many units have limited distribution, and location on the chart does not necessarily represent local superposition]

Basalt flow under Jarosa Mesa (Hinsdale Formation as used by Larsen and Cross, 1956)—age 12.5–15.6 m.y.

Quartz latite flow near Summitville—age 20.2 m.y.

Rhyolite welded tuff under Jarosa Mesa (Hinsdale Formation as used by Larsen and Cross, 1956)—age 22.4 m.y.

Fisher Quartz Latite (flows and breccias)—age 26.4 m.y.

Creede Formation (sedimentary rocks)

ASH-FLOW SEQUENCE

Dark flows and breccias similar to those in the Conejos Formation intertongue with much of the ash-flow sequence

Snowshoe Mountain, Nelson Mountain, and Rat Creek Quartz Latites

Wason Park Rhyolite

Tuff of Sevenmile Creek

Tuff of Carpenter Ridge

Tuff of Fish Canyon—age 27.2 m.y.

Mammoth Mountain Rhyolite

Farmers Creek Rhyolite

Thick quartz latite and rhyolite flows similar to those in the Fisher Quartz Latite intertongue with the ash-flow sequence in and near the central San Juan cauldron complex

Treasure Mountain Rhyolite (Age relative to Farmers Creek Rhyolite, Bachelor Mountain Rhyolite, and La Garita Quartz Latite not known)

Bachelor Mountain Rhyolite
Windy Gulch Member
Campbell Mountain Member
Willow Creek Member

La Garita Quartz Latite
Phoenix Park Member
Outlet Tunnel Member—age 27.8 m.y.

Dark andesitic to rhyodacitic flows and breccias of the Conejos Formation

Eruptions in the central and western parts of the San Juan volcanic field, in part, overlapped; some of the younger ash flow tuffs of the Potosi Volcanic Group (Luedke and Burbank, 1963) intertongue with some of the lower and middle units of the central San Juan sequence (Steven and Ratté, 1964).

Eruption of the Fisher Quartz Latite lavas around younger subsidence structures in the central San Juan cauldron complex marked the end of major intermediate to silicic volcanism in this part of the San Juan volcanic field. Similar rocks were erupted subsequently in the central and eastern San Juan Mountains, but from scattered local centers and in relative small volume. Widespread erosion intervened between eruption of the great bulk of intermediate to silicic rocks and eruption of basaltic lavas of the later Hinsdale Formation. The Hinsdale lavas range from scattered highly eroded remnants in the central part of the volcanic field to widespread sheets surmounted by relatively fresh-appearing cinder cones near the Rio Grande along the southeastern margin of the field. Butler (1946) reports basaltic lavas of several ages interbedded at different places in the younger deposits of the Tusas–Tres Piedras area of New Mexico in the southeastern part of the field. Overall, the late basaltic volcanism appears to have extended over a considerable but as yet undetermined span of time.

EARLIER AGE INTERPRETATIONS

Earlier age assignments for the rocks in the San Juan Mountains were based on a few plant and gastropod fossils found in tuffaceous beds in the upper part of the Burns Formation in the western part of the mountains or on abundant plant fossils found in the lacustrine beds in the Creede Formation in the central part of the mountains. None of these fossils have proven diagnostic. Older and younger formations were dated by extrapolation and by deductive reasoning.

Blanco Basin and Telluride Formations

No fossils have been reported from either the Blanco Basin or Telluride Formations, and all early age assignments of these units were on the basis of lithologic correlation or on assumed structural-stratigraphic relationships. Rocks now called the Telluride Formation (San Miguel Conglomerate of former usage) were originally assigned by Cross and Purington (1899, p. 4) to the Eocene, largely "because of the great unconformity at its base and because it underlies the volcanic complex of the San Juan, which is thought of Eocene age in the portions here developed." The assignment of the volcanic rocks to the Eocene was admittedly tenuous, and became even more so after fossils thought to be late Oligocene or early Miocene in age were found in the Burns Formation of the Silverton Volcanic Group (Cross and others, 1905, p. 2).

Additional complications were introduced when Atwood (1915) described the Ridgway Till and Atwood and Atwood (1926) the Gunnison Tillite, both units of Eocene age, along the northern flank of the San Juan Mountains. Assignment of these units to the Eocene caused Cross and Larsen (1935, p. 47) and Larsen and Cross (1956, p. 61) to reassign the Telluride and Blanco Basin Formations to the Oligocene(?) and the overlying San Juan Formation to the Miocene(?) without citing any supporting evidence. Van Houten (1957) and Mather and Wengerd (1965), however, have demonstrated that the original evidence for a glacial origin for some of these deposits was misinterpreted, and that the so-called Gunnison Tillite is actually a volcanic mudflow deposit. Mather and Wengerd also present convincing arguments that the Ridgway Till consists of glacial till of Pleistocene age overlain by a younger debris slide or mudflow.

Recently, Van Houten (1957, p. 386) and others have correlated the arkosic fluviatile beds of the Blanco Basin Formation underlying the Conejos Formation in the southern part of the volcanic field with similar arkosic beds forming the San Jose Formation in the central part of the San Juan Basin. As summarized by Dunn (1964, p. 43), the Blanco Basin and San Jose Formations are similar in lithology, mineralogy, and stratigraphic position, and can reasonably be considered equivalent. Simpson (1948) believes the San Jose Formation is early Eocene in age on the basis of vertebrate fossils.

Burns Formation

As reported by Cross and others (1905, p. 9), a few plant and gastropod fossils were collected from tuffaceous calcareous shales in the upper part of the Burns Formation in the western San Juan Mountains. As these fossils provide the only factual basis for a long succession of references assigning ages to the older volcanic rocks of the San Juan field, the original statement is quoted:

> Concerning the specimens collected, Dr. F. H. Knowlton reports the identification of *Pinus florissanti* ? Lesq. and *Crataegus Holmesii* Lesq., several cones of Pinus, and one form with leaves in threes. Of the species named the former occurs in the Oligocene lake beds of Florissant, Colo., while the type of the latter was obtained by Mr. Cross in a local rhyolitic tuff near Silver Cliff, Colo.
>
> The suggestion of an Oligocene age for these tuffs receives a degree of confirmation from the gastropod shells found by Mr. Clements in a thin limestone layer of what is clearly the same horizon on the divide between Cleveland and Schafer gulches. Concerning these, Mr. T. W. Stanton reports two species of a

fresh-water shell, *Limnoea*. While not able to identify the species with certainty, Mr. Stanton states that the two species most nearly resemble *L. Meekii* Evans and Shumard, and *L. Shumardi* Meek, which occur in the White River beds, usually assigned to the Miocene but considered by some paleontologists as Oligocene. Therefore, according to the concurrent evidence of plant remains and of invertebrate fossils, the calcareous tuffs and shales of the top of the Burns complex may be regarded as probably Oligocene or early Miocene in age.

Interestingly, both the Florissant and White River Formations referred to above are now firmly considered to be Oligocene in age.

This qualified statement was misconstrued by Cross and Larsen (1935, p. 59) who state that "the tuffs [in the Burns Formation] carry well preserved plant remains, which determine their age as Miocene." As the oldest volcanic rocks are bracketed between the Telluride Formation, which had arbitrarily been interpreted as Oligocene(?) in age, and the Burns Formation of presumed Miocene age, they postulate that volcanic activity commenced in early Miocene time. These conclusions were reiterated without modification by Larsen and Cross (1956, p. 62), and have served as the basis for most references to the age of volcanic activity in the San Juans.

Creede Formation

Abundant well-preserved plant fossils occur in lacustrine beds in the Creede Formation in the central part of the San Juan Mountains (table 1). These have been examined by many paleobotanists, who assigned various ages to them that range through the Miocene and Pliocene. Details concerning the different interpretations have been summarized by Steven and Ratté (1965, p. 46–47) who conclude, "Thus, the more recent opinions based on paleobotanical evidence favor a late Tertiary age for the Creede Formation."

In answer to a query concerning the wide divergence in interpretations of age from the same fossils, R. W. Brown (written commun, 1954) stated that

no one knows definitely what the age really is. The reason for this is clear. We now have a large collection from the Creede formation and the specimens are well preserved so that, theoretically, we should be able to snap right out with a definite age determination. The catch, however, is that the flora is from an isolated area and so few of the species occur in any other fossil flora or in the living flora of a specific region. Many of the Creede species remain to be accurately identified in terms of known species.

Mr. Brown went on to suggest that the real need was to find diagnostic mammalian fossils in the Creede Formation. These were searched for diligently but without success, and in their stead we are presenting the K–Ar data in this report.

Hinsdale Formation

The Hinsdale Formation is younger than the Creede Formation and older than Pleistocene glaciation. The surfaces on which the various remnants of the formation rest were interpreted by Atwood and Mather (1932, p. 21) to be parts of their San Juan peneplain, which supposedly was cut across the area in late Tertiary time. In addition, Hinsdale lavas were tilted and considerably eroded by early Pleistocene time (Florida cycle of Atwood and Mather, 1932, p. 27). After assessing the probable relative lengths of the erosional intervals required to form the San Juan peneplain versus the Florida surface, Cross and Larsen (1935, p. 100) concluded that the Hinsdale Formation probably was erupted in Pliocene, and probably late Pliocene time.

Three major assumptions are implicit in the reasoning outlined above. First, Cross and Larsen assumed on paleobotanical evidence that the age of the Creede Formation was Miocene and probably late Miocene. The K-Ar data presented later in this report indicate that the Creede is late Oligocene in age. Second, the concept of a San Juan peneplain should be abandoned. Independent investigations by the senior author, still in progress, show that the high-level areas of low relief interpreted by Atwood and Mather (1932, pl. 2) as parts of their peneplain were formed at different times by different processes, and were never integrated into a single surface having the attributes of a peneplain; and structures mapped in the bedrock show little or no similarity to structures postulated on the basis of the peneplain concept. Finally, there is no reason known why all the lavas previously included in the Hinsdale should have been erupted within any given brief interval of time. They occur in many widely scattered remnants, and may well represent eruptions extending over a significant segment of time. Data presented later in this report indicate that this is definitely true for the so-called Hinsdale rhyolites and basalts in the west-central part of the San Juan volcanic field.

PRESENT INVESTIGATIONS

Samples were collected from six major units in the central and eastern parts of the San Juan volcanic field. These represent only the upper part of the volcanic pile, and the K–Ar data obtained bear only on the ending of major volcanic activity.

The samples represent the oldest and youngest units in the central San Juan sequence of Steven and Ratté (1964), the La Garita and Fisher Quartz Latites, as well as a widespread welded ash-flow tuff of intermediate age that has been called the tuff of Fish Canyon (Olson, J. C., written commun., 1966). In addition,

a sample was collected from one of the youngest flows of so-called Fisher Quartz Latite from near Summitville in the eastern part of the volcanic field, and two samples, one of rhyolite and one of basalt, were collected from the Hinsdale Formation as used by Larsen and Cross (1956) in the west-central part of the field.

The La Garita Quartz Latite is a crystal-rich ash-flow tuff that forms a compound cooling unit more than 3,000 feet thick under La Garita Mountain (sample localities *1*, *2*, Fig. 1) northeast of the town of Creede, Colo. Most of the rock is densely welded and devitrified, and about half of it consists of a light red lithoidal matrix and the other half of phenocrysts and rock fragments. Plagioclase constitutes about 30 percent; sanidine, 6 percent; quartz, biotite and hornblende about 4 percent each; and accessory minerals about 2 percent of the rock. Cognate inclusions of collapsed pumice appear as irregular more coarsely porphyritic clots, and in these the sanidine phenocrysts commonly attain diameters of a quarter inch to a half inch.

The La Garita Quartz Latite is the oldest known unit derived from the central San Juan source area, and its eruption led to the first known volcano-tectonic disruption in the area that later became a great cauldron complex more than 50 miles long and 25 miles wide. Sanidine concentrates from coarse phenocrysts in collapsed pumice fragments in two samples from near the top of La Garita Mountain were separated and analyzed. The mean age of 27.8 million years (table 2) establishes the beginning of volcanic activity in the central San Juan source area.

The tuff of Fish Canyon is one of the most widespread ash-flow units in the San Juan volcanic field. It has been traced from the vicinity of the Black Canyon of the Gunnison through the Powderhorn district in the north-central part of the field, southward across the west-central part of the field to the southern margin of the mountains, and eastward to the edge of the San Luis Valley near Del Norte. The source area of the tuff was near the present edge of the volcanic rocks at the southern end of the central San Juan cauldron complex. It was not deposited in the vicinity of the Creede mining district; however, its stratigraphic position there is between the Mammoth Mountain and Wason Park Rhyolites (Steven and Ratté, 1964, 1965).

The tuff of Fish Canyon is a granular-appearing crystal-rich welded ash-flow tuff that ranges in thickness from 0 to more than 3,500 feet in different parts of the sheet, and is several hundred feet or more thick over wide areas. Phenocrysts make up about half the rock and consist of predominant plagioclase and lesser quantities of sanidine, quartz, biotite, and hornblende. A large sample, collected from the top of Agua Ramon Mountain (sample loc. *3*, fig. 1) north of South Fork, Colo., was separated into concentrates of plagioclase, sanidine, biotite, and hornblende, and each concentrate was analyzed separately. In addition, a sample of the formation from near the Black Canyon of the Gunnison (sample loc. *4*, fig. 1) was submitted earlier by W. R. Hansen (written commun., 1966), and the contained biotite was separated and analyzed. Mr. Hansen has kindly permitted us to incorporate his data with ours. The tuff of Fish Canyon is an excellent marker unit over a large area, and its mean age of 27.2 m.y. (table 2) has wide application.

Fisher Quartz Latite from Fisher Mountain and adjacent areas consists of quartz latitic to rhyolitic lava flows and related breecias that were erupted around the margins of the youngest volcano-tectonic subsidence structures in the central San Juan cauldron complex. The type Fisher lavas are localized along the southern margin of the resurgent Creede caldera (Steven and Ratté, 1960a, 1965, p. 58; Steven, 1964), and intertongue laterally with the sedimentary deposits in the Creede Formation that accumulated concurrently elsewhere in the lowland around the margin of the caldera. Samples from the capping flows of the Fisher Quartz Latite on Fisher Mountain (sample loc. *6*, S332, fig. 1) and on Copper Mountain (sample loc. *5*, fig. 1) about 4 miles northeast yielded sanidine concentrates that gave late Oligocene ages of about 26 m.y. The basal vitrophyre of the capping flow on Fisher Mountain (sample loc. *6*, Ds10, fig. 1) was re-collected, and plagioclase, sanidine, biotite, hornblende, and glass concentrates also gave a late Oligocene age of 27.3 m.y. The Fisher and Creede are the youngest units in the central San Juan sequence of Steven and Ratté (1964); the mean age of the type Fisher from Fisher Mountain, 26.4 m.y. (table 2), thus marks the end of a major volcanic episode, and also fixes the age of the abundant plant fossils in the Creede Formation.

The widely scattered relatively young local accumulations of coarsely porphyritic lavas heretofore called Fisher Quartz Latite (Larsen and Cross, 1956, p. 172) are not equivalent. To check one of these possible equivalencies, a sample (sample loc. *7*, fig. 1) of one of the youngest flows of so-called Fisher Quartz Latite in the Summitville district (Steven and Ratté, 1960b) was collected, and plagioclase, sanidine, biotite, and hornblende concentrates were separated and analyzed for comparison with the type Fisher Quartz Latite from Fisher Mountain (sample loc. *6*, fig. 1). The difference in the mean age obtained, (table 2), indicates that they are not correlative.

As mapped by Larsen and Cross (1956, pl. 1) the Hinsdale Formation in the west-central part of the San Juan volcanic field consists of a basal white rhyolite ash-flow tuff overlain by thin widespread flows of basalt. This association extends for more than 25 miles north-northeast from the vicinity of the Rio Grande Reservoir (fig. 1). Samples of both rock types were collected along the eastern edge of Jarosa Mesa (sample loc. *8*, fig. 1), that is near the center of this 25-mile span. A plagioclase concentrate from the basalt and a sanidine concentrate from the rhyolite were separated and analyzed for comparison, and contrasting ages (table 2) of 22.4 m.y. for the rhyolite and 12.4–15.6 m.y. for the basalt were obtained.

DISCUSSION OF RESULTS

Standard techniques for potassium and argon analysis were employed (Kistler and others, 1965; Evernden and Curtis, 1965). The analytical data for the K–Ar age determinations are listed in Table 2. The

TABLE 2.—K-Ar *analytical data for mineral separates, central San Juan Mountains, Colo.*

[Analysts, except where otherwise noted: H. H. Mehnert, J. D. Obradovich, R. F. Marvin, H. Collins Whitehead, Lois Schlocker, and H. H. Lipp. Static mode employed in mass spectrometer analysis of argon, except where otherwise noted]

Formation	Map No.	Field No.	Mineral	K_2O[1] (percent)	Radiogenic argon (10^{-10} moles/g)	Radiogenic argon (percent)	Age (m.y.)	Mean age (analytical uncertainty given at 95-percent confidence level)
La Garita Quartz Latite, Outlet Tunnel Member.	1	S292	Sanidine	9.54	3.96	63	27.9±0.8	27.8±1.3
	2	S318	do	10.06	4.15	81	27.7±0.8	
Tuff of Fish Canyon	3	Ds28	do	11.3	4.68	95	27.8±0.8	27.2±0.7
			Biotite	8.31	3.42	73	27.7±0.8	
			Hornblende	0.89	0.351	68	26.5±1.9	
			Plagioclase	0.82	0.334	86	27.4±1.9	
	4	BC5793[2]	Biotite	8.40	3.35	72	26.8±2.7	
Fisher Quartz Latite	5	S333	Sanidine	6.22	2.48	20	26.8±1.4	26.4±0.6
	6	S332	do	9.38	3.70	49	26.5±1.0	
		Ds10	do	8.60	3.49	95	27.3±0.8	
			Biotite	5.66	2.21	80	26.3±0.8	
			Hornblende	0.87	0.334	68	25.9±1.8	
			Plagioclase	0.89_5	0.344	88	25.9±1.8	
			Glass	5.54	2.03	90	24.7±0.7[3]	
Quartz latite flow near Summitville.	7	Ds29c	Sanidine	9.70	2.77	93	19.2±0.8	20.2±1.1
			Biotite	8.29	2.50	62	20.3±0.8	
			Hornblende	0.81	0.244	74	20.3±0.8	
			Plagioclase	0.94	0.292	75	20.9±0.8	
Hinsdale Formation (Larsen and Cross, 1956).	8							
Rhyolite		S342 B	Sanidine	7.26	2.33	95	22.9±0.6	22.4±5.7
			do	7.54	2.46	94	22.0±0.6	
Basalt		S342 A	Plagioclase	0.45	0.082	60	12.4±1.3	
			do	0.34	0.0787	58	15.6±0.9	

Decay constants K^{40}:

$\lambda\varepsilon = 0.584 \times 10^{-10}$ yr^{-1}.

$\lambda\beta = 4.72 \times 10^{-10}$ yr^{-1}.

$K^{40} = 1.22 \times 10^{-4}$ g/gK.

Description of sample localities:

Map No.

1. Sample S292. La Garita Quartz Latite. Wall of south-facing cirque near E. end of La Garita Mountain, 3 miles W. of Half Moon Pass. Altitude 12,800 feet.
2. Sample S318. La Garita Quartz Latite. Ridge marking SW wall of cirque near NW end of La Garita Mountain, 2½ miles NNE of junction of East Willow and Whited Creeks. Altitude 12,800 feet.
3. Sample Ds28. Tuff of Fish Canyon. Divide between Alder Creek and Embargo Creek, 10 miles N. of South Fork, Colo.
4. Sample BC5793. Tuff of Fish Canyon. Collected by W. R. Hansen from Sapinero Mesa, Gunnison County, Colo.
5. Sample S333. Fisher Quartz Latite. West side of Copper Mountain near divide between Lime Creek and Roaring Fork, 3½ miles E. of Spar City. Altitude 10,950 feet.
6. Sample S332. Fisher Quartz Latite. Wall on W. side of north-facing cirque on Fisher Mountain, ½ mile S. of Emma mine. Altitude 11,600 feet.
   Sample Ds10. Fisher Quartz Latite. Base of cliff on ridge extending N. from Fisher Mountain, ½ mile E. of Emma mine. Altitude 11,400 feet. Two-thirds mile NNE of S332, and on same lava flow.
7. Sample Ds29c. Quartz Latite flow from Summitville area. Upper member of so-called Fisher Quartz Latite (Steven and Ratté, 1960b, p. 22–23) from ridge crest about halfway between Cropsy Peak and South Mountain.
8. Sample S342A. Basalt of Hinsdale Formation (Larsen and Cross, 1956). From eastern part of Jarosa Mesa, 2 miles W. of Spring Creek Pass.
   Sample S342B. Rhyolite of Hinsdale Formation (Larsen and Cross, 1956). From eastern part of Jarosa Mesa, 1½ miles W. of Spring Creek Pass.

[1] Average of duplicate determinations, flame photometer, lithium internal standard.

[2] Data from W. R. Hansen (written commun., 1966). Analysts: H. H. Thomas, R. F. Marvin, Paul Elmore. Dynamic mode employed in mass spectrometer analysis of argon.

[3] Purposely omitted from determination of mean because of known tendency for glass to lose radiogenic argon and thereby provide a minimum age.

associated analytical uncertainties express the cumulative errors arising from the potassium and argon determinations but do not include the uncertainties of the decay constants. The uncertainties for the means of the various samples are given at the 95-percent confidence level. Student's t factor, suitable for the statistical treatment of small samples, is employed to define a confidence interval for the population mean (see Hoel, 1954).

The mean age for each volcanic unit or member and the assigned analytical uncertainties permit the following conclusions to be drawn.

1. The Fisher Quartz Latite, the last major intermediate to silicic unit in the central San Juan sequence of Steven and Ratté (1964), was erupted near the end of the Oligocene, about 26 million years ago.

Present evidence gives no clue concerning the beginning of volcanism, and so far as we can now tell, it could have begun any time between deposition of the Blanco Basin Formation in probable early Eocene time and deposition of the central San Juan volcanic sequence in late Oligocene time. A major part of the volcanic activity seems inescapably Oligocene in age.

The flora in the Creede Formation, which was deposited concurrently with eruption of the Fisher Quartz Latite, is by this token, latest Oligocene in age.

However, whereas the bulk of the volcanic activity in the central San Juans is restricted to Oligocene time, the rhyolite welded tuff under Jarosa Mesa (22.5 m.y.), included in the Hinsdale Formation by Larsen and Cross (1956), and the quartz latite flow at Summitville (20.2 m.y.) indicate that sporadic, but minor, intermediate to silicic volcanism continued into early Miocene time.

2. The span of time between eruption of the oldest and youngest units in the sequence derived from the central San Juan source area was short, perhaps only about 1.4 million years.

With the means and the uncertainties given in table 2 we can state that the age of both the La Garita Quartz Latite (Outlet Tunnel Member) and the tuff of Fish Canyon are significantly different from the age of the Fisher Quartz Latite at 95-percent confidence level but not at the 99-percent level. Although the difference of the means of the ages for the La Garita Quartz Latite and the Fisher Quartz Latite is 1.4 million years, an uncertainty of $\pm$ 1.0 million years is assigned to this difference (see Hoel, 1954, p. 227–229). This indicates that at the 95-percent confidence level we can state that the volcanic activity can be restricted to a period of time ranging from 400,000 to 2,400,000 years.

The fact that the mean for the La Garita Quartz Latite is the result of two age determinations separated by only 0.2 m.y. may lead some to question the validity of the assigned uncertainty. The same conclusion, though, is reached if we consider the time separating the tuff of Fish Canyon and the Fisher Quartz Latite where the means are based on five and six analyses respectively. The time interval separating the middle and top of this volcanic sequence is 800,000 years. Again, at the 95-percent confidence level we can state that this segment of the volcanic activity occurred during a period of time which ranged from 50,000 to 1,600,000 years.

The calculated mean ages indicate the precision rather than accuracy of measurements and may, because of unknown bias, deviate significantly from the true age for these rocks. However, it is likely that such a bias would affect all measurements in the same direction and thus that the difference between any two means would not be significantly affected.

Clearly, the volcanic activity in the area must have been intense during this brief interval.

3. Although similar in lithology and gross stratigraphic position to the type Fisher Quartz Latite, the coarsely porphyritic lavas at Summitville are significantly younger and should no longer be called the Fisher Quartz Latite.

Larsen and Cross (1956, p. 172) correlated a number of local piles of relatively young porphyritic lavas in the central and eastern San Juan Mountains on the basis of lithology and gross stratigraphic position, and called them all Fisher Quartz Latite. Steven and Ratté (1960b) followed this usage for the porphyritic rhyodacitic to quartz latitic lavas that form a relatively young local accumulation in the Summitville mining district in the eastern San Juans, but after extended studies in the Creede mining district and adjacent areas (Steven and Ratté, 1965, p. 93–98) recognized that the type Fisher Quartz Latite on Fisher Mountain (sample loc. *6*, fig. 1) represents merely the last in a sequence of related volcanic eruptions from a local source. On the question of possible equivalences with the so-called Fisher Quartz Latite at Summitville, they stated (p. 44) "Conceivably it might be the same age as the post caldera flows [on Fisher Mountain] and thus would truly correspond to the Fisher at its type locality, or it might be equivalent to similar earlier flows interlayered with the intercaldera welded tuff near Wagon Wheel Gap or be completely independent in time and genesis."

The mean age of 20.2 m.y. for the young lava flow at Summitville compared to the mean age of 26.4 m.y. for the type Fisher Quartz Latite on Fisher Mountain

(sample loc. *6*, fig. 1) clearly indicates that the two accumulations were erupted during significantly different intervals of time, and should not be included in the same formation.

4. The Hinsdale Formation, thought by Larsen and Cross (1956) to be a single genetically related formation in the central San Juan area consists of two distinct units erupted during widely separated and unrelated episodes.

The nearly coextensive white rhyolitic welded ash-flow tuff, and overlaying basalt flows underlying Jarosa Mesa (sample loc. *8*, fig. 1), and adjacent mesas in the west-central part of the San Juan volcanic field were included together in the Hinsdale Formation by Larsen and Cross (1956, pl. 2) along with many other scattered remnants of late rhyolites and basalts throughout the field. An age of 22.4 m.y. for the rhyolite compared to 12–15 m.y.[1] for the basalt, makes any genetic relation between these contrasting rock types unlikely and their association in the present erosional remnants fortuitous.

These ages can be extrapolated only to those erosional remnants immediately adjacent to Jarosa Mesa (sample loc. *8*, fig. 1) where the samples were collected. Whether this basalt can be grouped with the other late basalts in the San Juan region into a single formation fitting the concept of the originally proposed Hinsdale Formation is a question that cannot be answered until additional data have been gathered. The present data indicate, certainly, that previous ideas concerning the Hinsdale Formation need modifying.

REFERENCES

Atwood, W. W., 1915, Eocene glacial deposits in southwestern Colorado: U.S. Geol. Survey Prof. Paper 95, p. 13–26.

Atwood, W. W., and Atwood, W. R., 1926, Gunnison tillite of Eocene age: Jour. Geology, v. 34, no. 7, p. 612–622.

Atwood, W. W., and Mather, K. F., 1932, Physiography and Quaternary geology of the San Juan Mountains, Colorado: U.S. Geol. Survey Prof. Paper 166, 176 p.

Butler, A. P., Jr., 1946, Tertiary and Quaternary geology of the Tusas-Tres Piedras area, New Mexico: Harvard Univ., unpub. Ph.D. thesis, 188 p.

Cross, Whitman, Howe, Ernest, and Ransome, F. L., 1905, Description of the Silverton quadrangle [Colorado]: U.S. Geol. Survey Geol. Atlas, Folio 120.

Cross, Whitman, and Larsen, E. S., Jr., 1935, A brief review of the geology of the San Juan region of southwestern Colorado: U.S. Geol. Survey Bull. 843, 138 p.

Cross, Whitman, and Purington, C. W., 1899, Description of the Telluride quadrangle [Colorado]: U.S. Geol. Survey Geol. Atlas, Folio 57.

Dunn, D. E., 1964, Evolution of the Chama Basin and Archuleta anticlinorium, eastern Archuleta County, Colorado: Univ. Texas, unpub. Ph.D. thesis, 112 p.

Evernden, J. F., and Curtis, G. H., 1965, The potassium-argon dating of Late Cenozoic rocks in East Africa and Italy: Current Anthropology, v. 6, p. 343–385.

Harland, W. B., Smith, A. G., and Wilcock, B., eds., 1964, The Phanerozoic time-scale—a symposium: Geol. Soc. London Quart. Jour., v. 120 s, 458 p.

Hoel, P. G., 1954, Introduction to mathematical statistics: New York, John Wiley & Sons, 331 p.

Kelley, V. C., 1952, Tectonics of the Rio Grande depression of central New Mexico, *in* The Rio Grande country, 1952, New Mexico Geol. Soc. Guidebook, 3d Field Conf.: p. 93–105.

———1955, Regional tectonics of the Colorado Plateau and relationship to the origin and distribution of uranium: Univ. New Mexico Pub. Geology, no. 5, 120 p.

Kistler, R. W., Bateman, P. C., and Brannock, W. W., 1965, Isotopic ages of minerals from granitic rocks of the central Sierra Nevada and Inyo Mountains, California: Geol. Soc. America Bull. v. 76, p. 155–165.

Larsen, E. S., Jr., and Cross, Whitman, 1956, Geology and petrology of the San Juan region, southwestern Colorado: U.S. Geol. Survey Prof. Paper 258, 303 p.

Luedke, R. G., and Burbank, W. S., 1963, Tertiary volcanic stratigraphy in the western San Juan Mountains, Colorado: Art. 70 *in* U.S. Geol. Survey Prof. Paper 475–C, p. C39–C44.

Mather, K. F., and Wengerd, S. A., 1965, Pleistocene age of the "Eocene" Ridgway Till, Colorado: Geol. Soc. America Bull., v. 76, p. 1401–1408.

Ratté, J. C., and Steven, T. A., 1964, Magmatic differentiation in a volcanic sequence related to the Creede caldera, Colorado: Art. 131 *in* U.S. Geol. Survey Prof. Paper 475–D, p. D49–D53.

Simpson, G. G., 1948, The Eocene of the San Juan basin, New Mexico: Am. Jour. Sci., v. 246, no. 5, p. 257–282, and v. 246, no. 6, p. 363–385.

Steven, T. A., 1964, Geologic setting of the Spar City district, San Juan Mountains, Colorado: Art. 146 *in* U.S. Geol. Survey Prof. Paper 474–D, p. D123–D127.

Steven, T. A., and Ratté, J. C., 1960a, Relation of mineralization to caldera subsidence in the Creede district, San Juan Mountains, Colorado: Art S *in* U.S. Geol. Survey Prof. Paper 400–B, p. B14–B17.

———1960b, Geology and ore deposits of the Summitville district, San Juan Mountains, Colorado: U.S. Geol. Survey Prof. Paper 343, 70 p.

———1964, Revised Tertiary volcanic sequence in the central San Juan Mountains, Colorado: Art. 132 *in* U.S. Geol. Survey Prof. Paper 475–D, p. D54–D63.

———1965, Geology and structural control of ore deposition in the Creede district, San Juan Mountains, Colorado: U.S. Geol. Survey Prof. Paper 487, 90 p.

Van Houten, F. B., 1957, Appraisal of Ridgway and Gunnison "tillites," southwestern Colorado: Geol. Soc. America Bull., v. 68, p. 383–388.

[1] The results for the Hinsdale basalt are considered only as tentative. The widespread age results for the basalt are due to widely differing potassium values; the most valid age cannot be ascertained until a new sample is prepared and analyzed.

CALLAGHAN WINDOW—A NEWLY DISCOVERED PART OF THE ROBERTS THRUST, TOIYABE RANGE, LANDER COUNTY, NEVADA

By JOHN H. STEWART and ALLISON R. PALMER [1],
Menlo Park, Calif., Stony Brook, N.Y.

Work done in cooperation with the Nevada Bureau of Mines

Abstract.—A previously undescribed window in the Roberts thrust, here named the Callaghan window, covers about 40 square miles of the northern part of the Toiyabe Range, 15 miles north of Austin, Nev. A regionally important quartzite, limestone, and shale sequence which is over 10,000 feet thick and of Cambrian, Ordovician, and Silurian age is exposed in the window. Strata above the thrust comprise chert and quartzite probably of Ordovician and Devonian age. The strata in the window are cut by many low- and high-angle faults, and the central part of the window is a north-trending horst.

A previously undescribed window in the Roberts thrust, here named the Callaghan window, lies about 15 miles north of Austin, Nev., in the northern part of the Toiyabe Range (fig. 1). The window contains a sequence about 10,000 feet thick of Cambrian, Ordovician, and Silurian strata. The closest comparably complete section of Cambrian rocks is near Eureka, 50 miles to the east. The Ordovician sequence contains a nearly complete section of the Pogonip Group. The mapping provides information on the character and extent of the Roberts thrust, a low-angle fault of wide regional extent in central and north-central Nevada (Roberts and others, 1958).

STRATA OF THE LOWER PLATE

Strata in the lower plate are probably over 10,000 feet thick and consist of quartzite, limestone, and minor amounts of siltstone and shale. These strata are considered to belong to the autochthonous carbonate (eastern) assemblage rocks that characterize lower

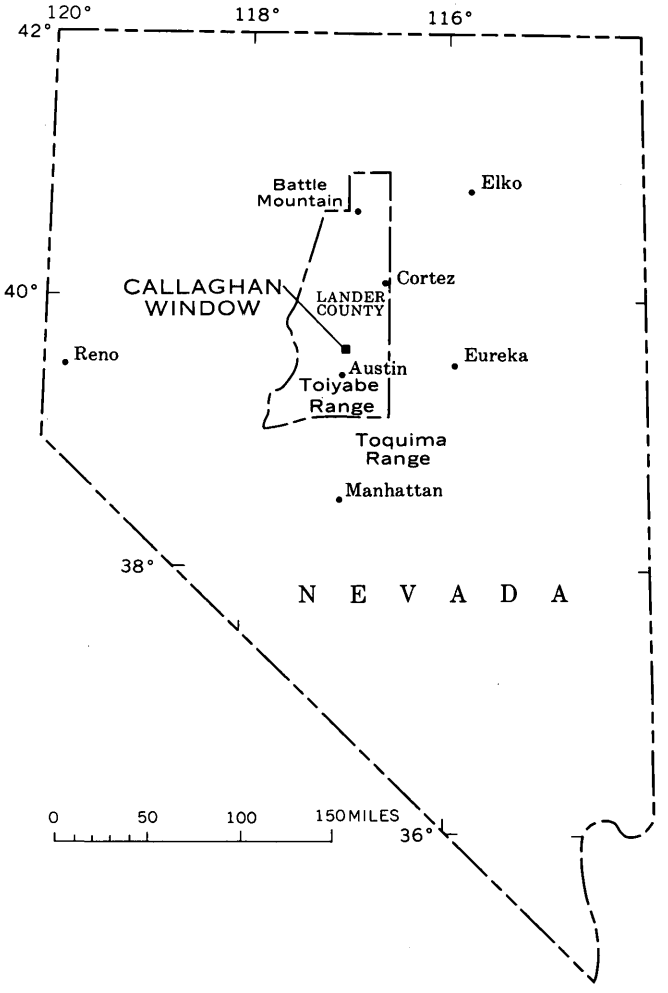

FIGURE 1.—Index map showing location of Callaghan window.

[1] State University of New York.

Paleozoic strata in eastern and central Nevada and are in contrast to the allochthonous siliceous and volcanic (western) assemblage rocks that characterize the strata of comparable age in western and central Nevada (Roberts and others, 1958; Roberts, 1964; Gilluly and Gates, 1965). Some geologists (Roberts and others, 1958; Roberts, 1964) recognize that a transitional assemblage between the eastern and western assemblages and part of the strata in the Callaghan window, particularly the Middle and Upper Cambrian rocks, could be placed in the transitional rather than in the eastern assemblage. Most of the Middle and Upper Cambrian rocks are a part of an outer belt of detrital sediments as defined by Palmer (1960, 1966) that lie to the west of clean carbonate deposition.

LOWER CAMBRIAN STRATA

The Lower Cambrian strata are widely exposed in the central part of the Callaghan window (fig. 2) and are the resistant rocks that underlie the highest part of Mount Callaghan. Three units are recognized in this sequence (fig. 3). The lowest is composed of cliff-forming vitreous quartzite and minor amounts of phyllitic siltstone, and is at least 600 feet thick. The base of this unit is not exposed. The middle unit, which is poorly exposed and slope forming, consists of siltstone, shale, silty sandstone, and very minor amounts of limestone. The middle unit is about 540 feet thick. The upper unit is dominantly cliff-forming limestone in the upper and lower parts (subunits A5 and A3) and slope-forming limestone and siltstone in the middle part (subunit A4). It is about 320 feet thick.

Trace fossils, mostly worm borings and castings parallel to bedding, are common throughout the lower unit, and unidentifiable scraps of trilobites occur about 100 feet below the top of the lower unit and in parts of the middle unit. The Lower Cambrian trilobite *Bristolia* occurs near the base of subunit A3 at locality 2 (fig. 2) (5974–CO) and locality 4 (5975–CO) and is common elsewhere in the area at this stratigraphic position. *Paedeumias* sp. and Olenellus (?) sp. occur in subunit A5 at locality 3 (6003–CO). Concretionary algal structures ("*Girvanella*") are a common and distinctive part of the upper unit. (Numbers used here and elsewhere in this paper are U.S. Geological Survey collection numbers.)

MIDDLE AND UPPER CAMBRIAN STRATA

A poorly exposed faulted and folded sequence of Middle and Upper Cambrian limestone, shale, and siltstone, about 6,000 feet thick, crops out mainly in the southern part of the Callaghan window. The succession of units in this sequence is difficult to unravel because of the structural complexity of the area, the scarcity of outcrops, and the lithologic similarity of many of the units. Study of well-exposed areas, however, suggests that at least 10 lithologic units are present (fig. 4)

Units B1–B6 are best exposed along section *B–B'* (fig. 2) where thicknesses were calculated on a topographic map, using contacts and attitudes plotted in the field. More refined methods probably would not have led to more meaningful results owing to the possibility of concealed faults. The lowest unit in the section (B1) consists predominantly of siltstone from which indeterminate kochaspid trilobites, *Oryctocephalus* sp., indeterminate acrotretid brachiopods, and sponge spicules were collected at locality 5 (6004–CO). This fauna indicates a position low in the Middle Cambrian in beds equivalent to the upper part of the Lower and Middle Cambrian Pioche Shale, a unit recognized at Eureka (Nolan and others, 1956) and elsewhere in eastern Nevada.

Unit B1 is overlain by a thin laminated limestone (unit B2), followed by a poorly exposed sequence (unit B3) of siltstone, limy siltstone, silicified siltstone, and scarce silty limestone. The next higher unit (B4) is probably about 2,100 feet thick and consists of homogeneous and unfossiliferous evenly laminated aphanitic limestone. The position of this unit in the stratigraphic section suggests that it might be equivalent to the Eldorado Dolomite, a thick carbonate unit in the Eureka district (Nolan and others, 1956), although a major facies change from massive dolomite at Eureka to laminated limestone in the Callaghan window would be required if this correlation is correct.

Unit B4 is overlain by interbedded limestone and siltstone or limy siltstone (unit B5), which is in turn overlain by a dark-gray shale (unit B6). The position of unit B6 in the stratigraphic sequence and its lithologic character suggest that it might be equivalent to part of the Secret Canyon Shale of the Eureka area (Nolan and others, 1956), although no fossils have been found to confirm this correlation.

The relationship of units B7, B8, and B9 to one another and to underlying and overlying units is nowhere clear, and the column presented on figure 4 is tentative. The lowest of these units (B7) consists of dark-gray platy limestone weathering light gray or grayish orange. *Centropleura* occurs in this unit at locality 17 (5973–CO) and is the first reported occurrence of a paradoxidid trilobite in western North America. This trilobite is late Middle Cambrian in

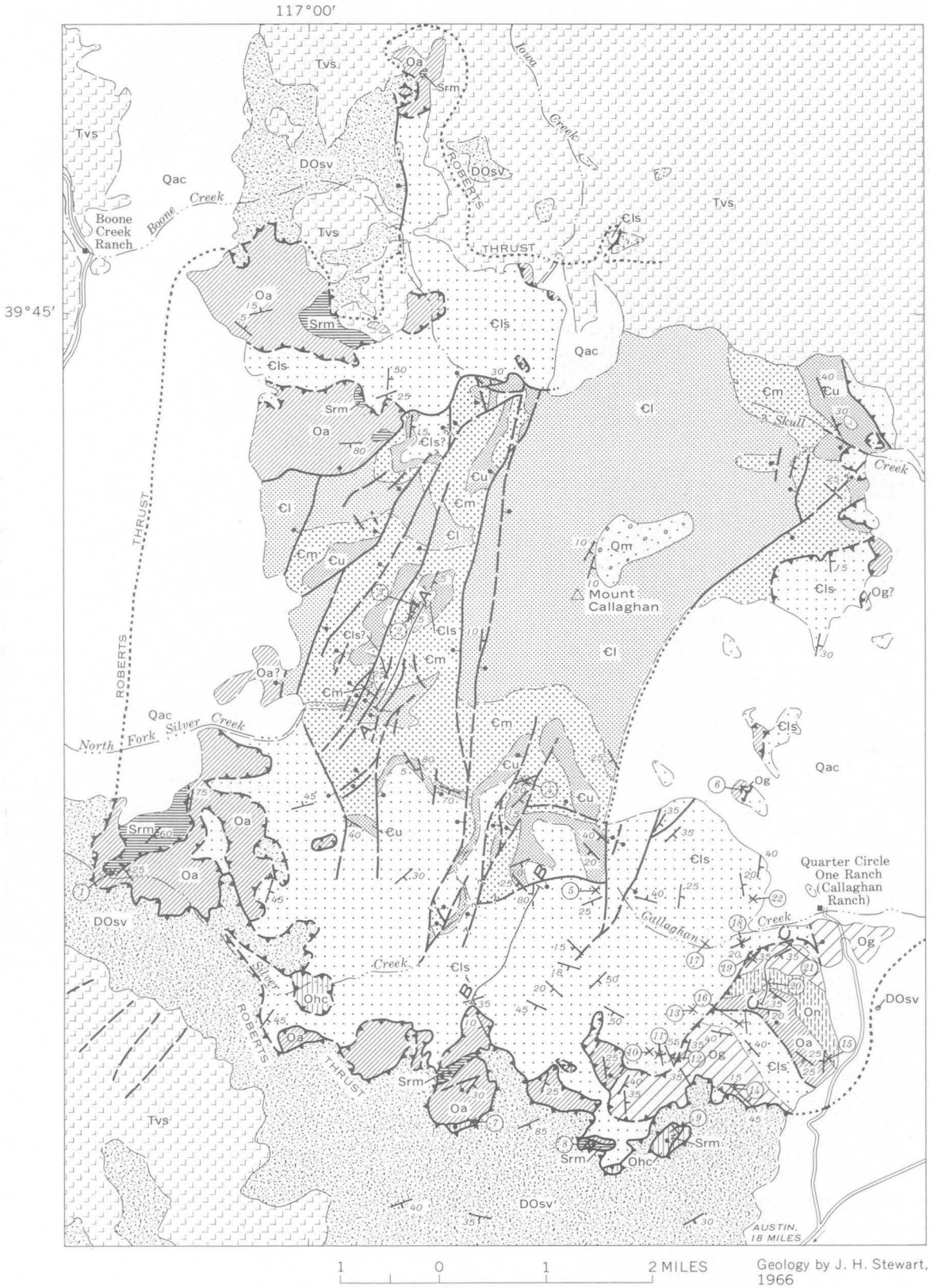

FIGURE 2.—Geologic map of Callaghan window, Toiyabe Range, Lander County, Nev.

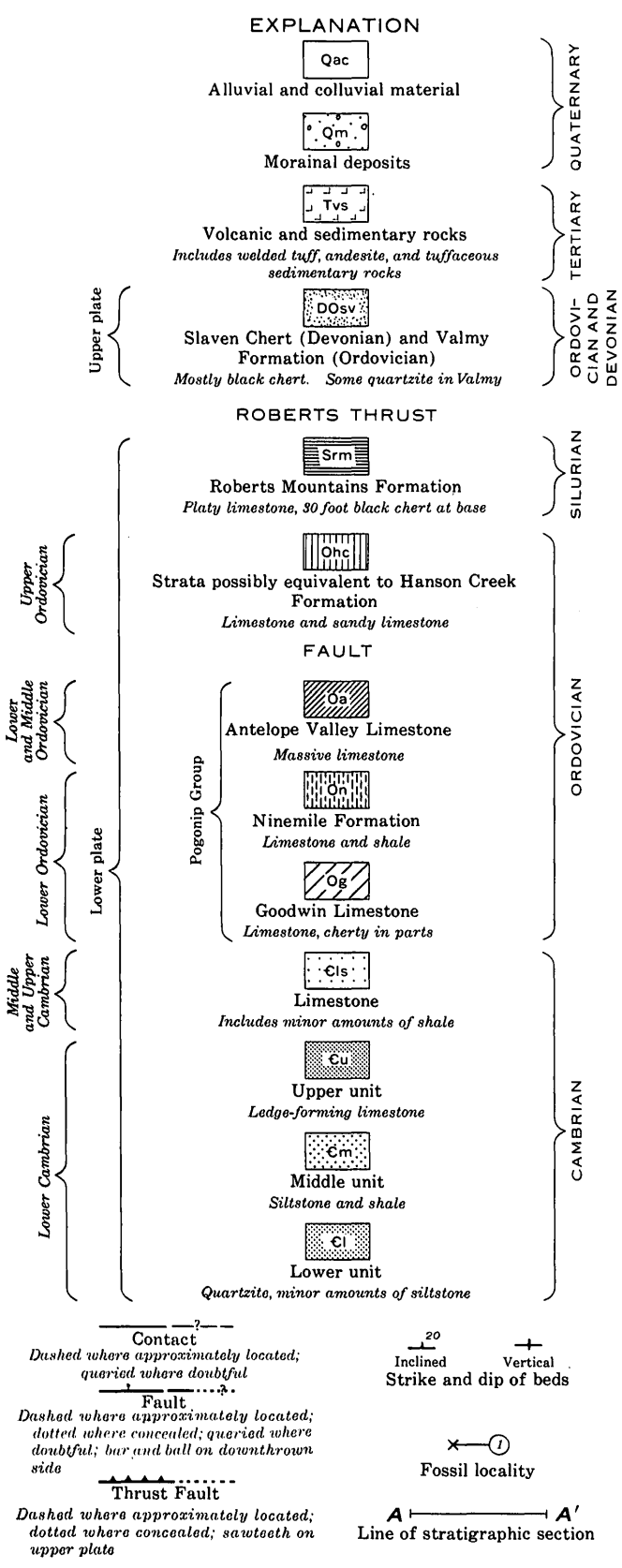

FIGURE 2.

SERIES	UNIT	SUBUNIT THICKNESS, IN FEET	LITHOLOGY	DESCRIPTION
MIDDLE CAMBRIAN	B1			Dark-greenish-gray and olive-gray micaceous siltstone. Rare limestone in lower 80 feet. Shown on figure 4.
LOWER CAMBRIAN, 1460 FEET	Upper unit, 320 feet	A5 160		Medium-dark-gray limestone. *Paedeumias* sp. and *Olenellus*(?) sp., 5 feet above base. Common "*Girvanella*" in upper half. Cliff forming.
		A4 95		Mostly covered, probably siltstone and limestone.
		A3 65		Medium-dark-gray limestone. Common *Bristolia* and *Girvanella* near top.
	Middle unit, 540 feet	A2 540		Greenish-gray phyllitic siltstone and pale-yellowish-brown coarse siltstone to silty sandstone. Rare limy siltstone and limestone. Rare olenellid trilobites. Poorly exposed. Slope forming.
	Lower unit, 600 feet	A1 600		White and yellowish-gray, thin-bedded and, rarely, cross-stratified, medium-grained quartzite with minor amounts of greenish-gray phyllitic siltstone. Worm borings and castings parallel to bedding common. Rare scraps of trilobites in quartzite about 100 feet below top. Cliff forming. Base not exposed.

FIGURE 3.—Stratigraphic column of Lower and Middle Cambrian strata. Measured along *A–A'*, figure 2.

age and the temporal equivalent of the upper Secret Canyon Shale or lower part of the Hamburg Dolomite. If the suggested correlation of unit B6 with the Secret Canyon is correct, then unit B7 probably is equivalent to the lower part of the Middle and Upper Cambrian Hamburg.

Unit B8 consists of shale, silty limestone, and limestone, and lithologically and faunally is equivalent to the Dunderberg Shale of the Eureka area (Nolan and others, 1956) and elsewhere in Nevada. *Glyptagnostus reticulatous* (Angelin) occurs in the lower part of the unit at locality 22 (5972–CO) and at locality 18 (5976–CO), and *Housia* sp., *Irvingella* sp., and *Litocephalus* sp., occur in the upper part of the unit at locality 11 (5971–CO); the latter two fossils also occur at locality 10 (6000–CO).

Unit B9 consists of limestone and minor amounts of shale, and contains *Irvingella* sp. at locality 12 (5970–CO) and *Elvinia* sp. at locality 13 (5977–CO).

269–274 O—67——5

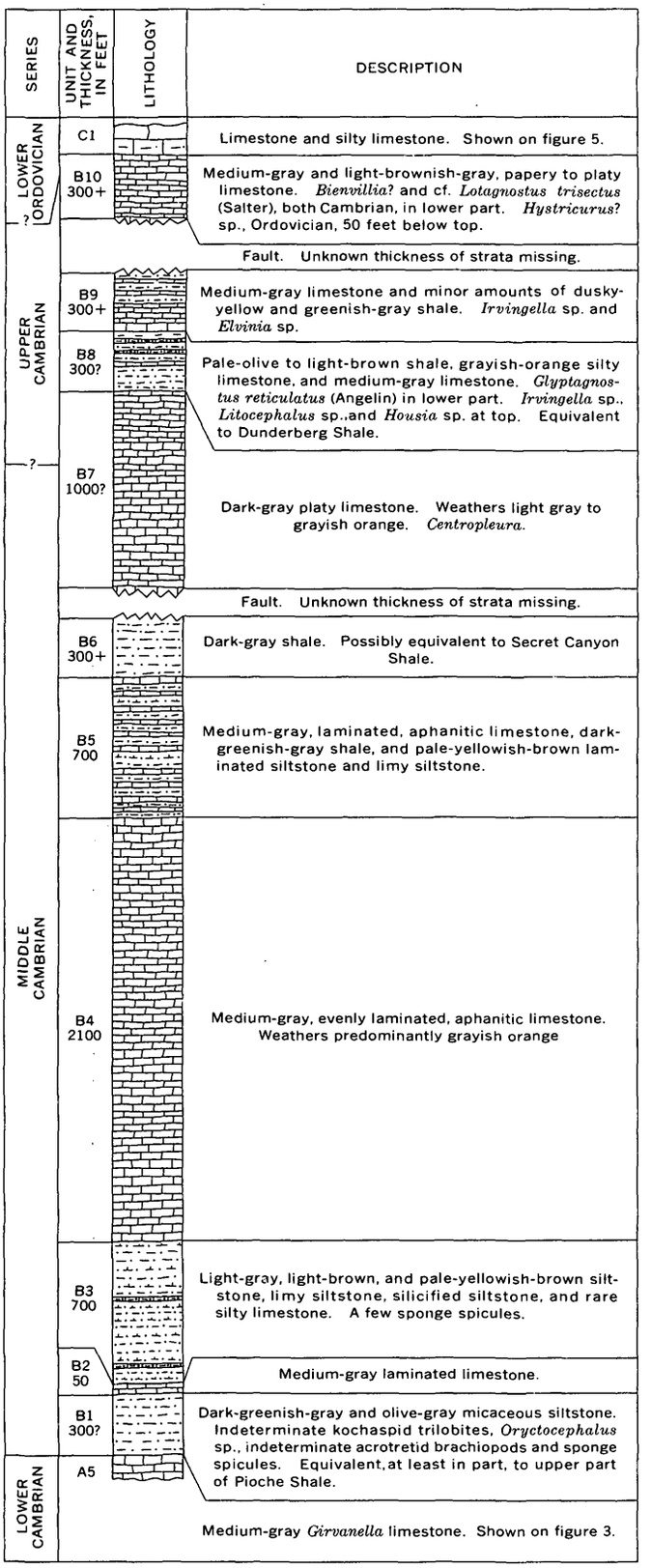

FIGURE 4.—Stratigraphic column of Lower, Middle, and Upper Cambrian and Lower Ordovician strata. Thicknesses of units B1–B6 calculated along section *B–B'*, figure 2. Thicknesses of units B7–B10 estimated.

Unit B10 occurs only in association with Ordovician strata and above a conspicuous thrust in the southern part of the window. It consists of platy limestone and contains *Bienvillia*? and cf. *Lotagnostus trisectus* (Salter) in the lower part at locality 16 (5967–CO, 5968–CO, and 5969–CO). Although the preservation of these fossils is poor, they are definitely Cambrian and indicate equivalence to the Upper Cambrian Windfall Formation of the Eureka area (Nolan and others, 1956). Other poorly preserved trilobites assigned to *Hystricurus*? occur 50 feet below the top of unit B10 at locality 21 (6006–CO); these are probably Early Ordovician.

The Middle Cambrian sequence in the Callaghan window is characterized by carbonate rock that is almost entirely evenly laminated platy limestone. Such rock is in marked contrast to the dominantly massive dolomite in rocks of comparable age to the east near Eureka. The rocks in the Callaghan window are in a more westerly position in the Cordilleran geosyncline and thus the laminated limestone may be a deep-water facies, whereas the dolomite may be a shallow-water shoreward facies.

ORDOVICIAN STRATA

Strata of Ordovician age are at least 2,300 feet thick and consist of the Pogonip Group and some strata possibly correlative with the Hanson Creek Formation. These strata crop out primarily in the southernmost and northernmost parts of the window. The Pogonip Group, as elsewhere in the region, is divided into three formations—the Goodwin Limestone at the base, the Ninemile Formation in the middle, and the Antelope Valley Limestone at the top.

Goodwin Limestone

The Goodwin Limestone, a very distinctive unit lithologically, is about 1,100 feet thick and consists of medium-gray limestone, some yellowish-brown-weathering silty limestone, and scarce very light gray chert (fig. 5). The lower contact of this formation (fig 2) is placed at the lithologic change from platy limestone (unit B10) to more massive but very thin bedded medium-gray limestone and silty limestone. The Cambrian-Ordovician boundary, which in most areas is at the base of the Goodwin, is here within unit B10, and apparently some of unit B10 is temporally equivalent to strata elsewhere included in the Goodwin. The Goodwin Limestone in the Callaghan window has a sparse fauna which consists of *Leptella* n. sp., *Paraboliella*? sp. and a kainellid(?) pygidia in unit C2 at at locality 19 (D1752–CO), *Asaphellus* sp. in unit C3 or C4 at locality 14 (D1747–CO), and *Xenostegium* sp.,

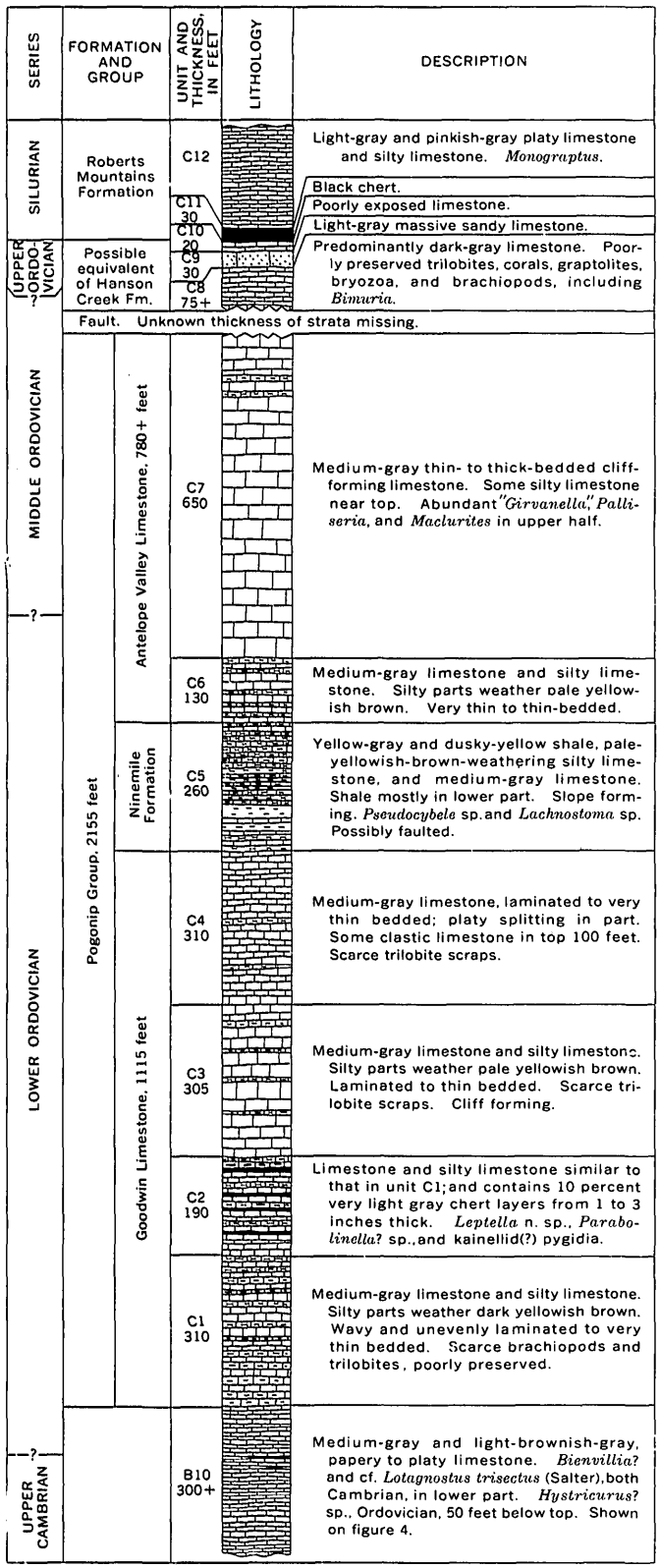

FIGURE 5.—Stratigraphic column of Cambrian, Ordovician, and Silurian strata. Thicknesses of units C1–C7 measured along section *C–C'*, figure 2. Thicknesses of units C8–C12 estimated.

Leiostegium sp., *Shumardia* sp., *Psalikilus spinosum* Hintze, *Hintzeia*? sp., and *Asaphellus* sp. from an unknown part of the Goodwin at locality 6 (D1751–CO) (all identifications by R. J. Ross, Jr., written commun., 1966).

Ninemile Formation

The Ninemile Formation is about 260 feet thick in a possibly faulted section and consists of shale, silty limestone, and minor amounts of limestone. It forms a nonresistant middle part of the Pogonip Group. The Ninemile contains a fairly abundant fauna including *Pseudocybele* sp. and *Lachnostoma* sp. from the middle of the formation at locality 20 (D1753–CO) and *Hesperonomea* sp., *Ptyocephalus* sp., *Lachnostoma* sp., a megalaspid? pygidium, and *Pseudocybele*? sp. from the topmost part of the formation, or possibly the basal part of the Antelope Valley Limestone, at locality 15 (D1746–CO) (all identifications by R. J. Ross, Jr., written commun., 1966).

Antelope Valley Limestone

The Antelope Valley Limestone is at least 780 feet thick as measured in an incomplete section and consists of medium-gray thin- to thick-bedded cliff-forming limestone. Concretionary algal structures ("*Girvanella*") and large gastropods (*Palliseria* and *Maclurites*) are distinctive fossils in the upper half of the formation.

Possible equivalent of the Hanson Creek Formation

In the southern part of the window, the top of the Antelope Valley Limestone everywhere is probably a fault, and the sequence of strata above the Antelope Valley is uncertain. Strata considered to be possibly equivalent to the Hanson Creek Formation are, however, in close association with the Antelope Valley in the southern part of the window and perhaps these possible Hanson Creek strata overlie the Antelope Valley Limestone. If this is true, the Eureka Quartzite is missing; the Eureka elsewhere occurs between the Antelope Valley and Hanson Creek. If the Eureka Quartzite were present in the Callaghan window, it certainly would have been recognized because in most places in central and eastern Nevada the Eureka is the most resistant and easily recognized formation in the lower Paleozoic sequence.

The possible equivalent of the Hanson Creek Formation consists, in ascending order, of dark-gray limestone (unit C8), light-gray massive limestone containing abundant rounded fine to medium quartz grains (unit C9), and limestone which is poorly exposed (unit C10). At locality 9 (D1754–CO), unit C8 contains a

poorly preserved coral, a proetid trilobite, a possible homalonotid trilobite, and a poorly preserved graptolite. At locality 7 (D1755–CO), it contains a few brachiopods, including *Bimuria*, and some bryozoans. Identifications are by R. J. Ross and G. Arthur Cooper. *Bimuria* indicates an Ordovician, possibly Middle Ordovician, age. Units C8 to C10 are everywhere much faulted and have not been sufficiently studied to be confident of stratigraphic details or of regional correlations. Lithologically they most closely resemble strata included in the Hanson Creek Formation elsewhere in north-central Nevada.

In the northwestern part of the Callaghan window (fig. 2), the possible Hanson Creek strata are not recognized and the Antelope Valley Limestone appears to be stratigraphically overlain by the Roberts Mountains Formation of Silurian age, although this contact could be a fault. If the Antelope Valley Limestone-Roberts Mountains Formation sequence is unfaulted, the absence of the possible Hanson Creek strata may be due to an unconformity.

The presence of the Pogonip Group and absence of the Eureka Quartzite in the Callaghan window is unusual when one considers the stratigraphic section at Cortez, about 35 miles to the north. At Cortez, the Eureka Quartzite is present, but the Pogonip is missing apparently owing to erosional truncation (Gilluly and Masursky, 1965, p. 16 and 64) at the base of the Eureka. The Eureka Quartzite is, however, absent in some other areas in central Nevada (Kay and Crawford, 1964, p. 430–437), such as the Toquima Range (fig. 1).

SILURIAN STRATA

The Silurian Roberts Mountains Formation occurs in scattered outcrops in the southern and northwestern parts of the Callaghan window. It consists of a basal black chert unit (unit C11) about 30 feet thick overlain by an unknown thickness of light-gray and pinkish-gray platy limestone and silty limestone. *Monograptus* occurs in the limestone and silty limestone at locality 1 (D213–SD) and locality 8 (D212–SD).

Chert, similar to that in the Callaghan window, is generally present at the base of the Roberts Mountains Formation in Nevada (Merrim, 1963, p. 39). Such a chert layer and a sandy limestone, lithologically similar and probably correlative to unit C9, are included by Kay and Crawford (1964, p. 437–438) in their Gatecliff Formation in the Toquima Range.

STRATA OF THE UPPER PLATE

Strata above the Roberts thrust consist of siliceous (western) assemblage rocks composed of black chert and light- and dark-gray quartzite assigned to the Valmy Formation of Ordovician age and black chert assigned to the Slaven Chert of Devonian age. The lithologic character of these formations is the same as elsewhere in the region. Some poorly preserved fossils consisting of possible tentaculids resembling *Styliolina* or possibly *Nowakia* (identified by Michael Churkin, oral commun., 1966) occur in limestone interstratified with black chert in the Toiyabe Range about 2 miles south of the mapped area. These fossils, which occur in strata mapped as the Slaven Chert, have a possible age of Late Silurian or Devonian and thus support the assignment to the Slaven Chert. No other fossils have been found in the upper-plate rocks near the Callaghan window.

STRUCTURE

The dominant structure in the Mount Callaghan area is the Roberts thrust (fig. 2) along which siliceous (western) assemblage strata have overridden carbonate (eastern) or transitional assemblage limestone and shale. Other thrusts occur within the window; the most conspicuous one is in the southern and northwestern parts of the window and, in most places, brings Ordovician in thrust contact with Middle and Upper Cambrian strata. Most commonly the massive and competent Antelope Valley Limestone forms the sole of this thrust.

North- to northeast-trending high-angle normal faults are common within the window. These are downthrown to the west on the west side of the window and to the east on the east side. The central part of the window, including Mount Callaghan itself, is a horst.

REFERENCES

Gilluly, James, and Gates, Olcott, 1965, Tectonic and igneous geology of the northern Shoshone Range, Nevada, *with sections on* Gravity in Crescent Valley, by Donald Plouff, *and* Economic geology, by K. B. Ketner: U.S. Geol. Survey Prof. Paper 465, 153 p.

Gilluly, James, and Masursky, Harold, 1965, Geology of the Cortez quadrangle, Nevada: U.S. Geol. Survey Bull. 1175, 117 p.

Kay, Marshall, and Crawford, J. P., 1964, Paleozoic facies from the miogeosynclinal to the eugeosynclinal belt in thrust slices, central Nevada: Geol. Soc. America Bull., v. 75, no. 5, p. 425–454.

Merriam, C. W., 1963, Paleozoic rocks of Antelope Valley, Eureka and Nye Counties, Nevada: U.S. Geol. Survey Prof. Paper 423, 67 p.

Nolan, T. B., Merriam, C. W., and Williams, J. S., 1956, The stratigraphic section in the vicinity of Eureka, Nevada: U.S. Geol. Survey Prof. Paper 276, 77 p.

Palmer, A. R., 1960, Some aspects of the early Upper Cambrian stratigraphy of White Pine County, Nevada and vicinity, *in* Guidebook to the geology of east-central Nevada: Intermountain Assoc. Petroleum Geologists 11th Ann. (1960) Field Conf., p. 53–58.

———1966, Regional relationships in Cambrian of the Cordilleran region [abs.]: Geol. Soc. America, Rocky Mtn. Sec., 1966 Mtg., Program, p. 46–47.

Roberts, R. J., 1964, Stratigraphy and structure of the Antler Peak, quadrangle, Humboldt and Lander Counties, Nevada: U.S. Geol. Survey Prof. Paper 459–A, 93 p.

Roberts, R. J., Hotz, P. E., Gilluly, James, and Ferguson, H. G., 1958, Paleozoic rocks of north-central Nevada: Am. Assoc. Petroleum Geologists Bull., v. 42, no. 12, p. 2813–2857.

ORDOVICIAN TECTONISM IN THE RUBY MOUNTAINS, ELKO COUNTY, NEVADA

By RONALD WILLDEN and RONALD W. KISTLER,
Denver, Colo., Menlo Park, Calif.

Abstract.—Lower Paleozoic rocks in the southern Ruby Mountains, northeastern Nevada, have undergone two periods of tight folding that did not affect the middle and upper Paleozoic rocks of the range. The two structural terranes are separated by a surface of discontinuity interpreted to be an angular unconformity. Stratigraphic evidence indicates that the Lower Paleozoic deformation, which was accompanied by at least some regional metamorphism and plutonism, took place between Early Ordovician and Silurian time. Strong deformation of early Paleozoic age has not previously been recognized in the Great Basin.

The Cambrian and Lower Ordovician rocks in the southern part of the Ruby Mountains contain appressed recumbent folds ranging in size from a few inches in hand specimens to a fold with a recumbent limb more than 1 mile long. These rocks also show the effects of a regional metamorphism which presumably accompanied the folding. Chloritic phyllites are found in shaly units in the upper part of the section; and comparable units in the lower part of the section have been converted to quartz-mica schists. These folded and metamorphosed rocks are unconformably overlain by the Lone Mountain Dolomite, which is succeeded conformably by Devonian and Mississippian strata. The Lone Mountain Dolomite and younger rocks lack small-scale structural features, and their gross structural trend is different from trends in the older rocks.

These relations are different from those commonly reported in surrounding parts of Nevada. To the west of the Ruby Mountains the earliest period of strong deformation appears to be the Antler orogeny of Late Devonian to Early Mississippian age (Gilluly and Gates, 1965, p. 92–98; Roberts, 1964, p. A8–A11, A78). To the east of the Ruby Mountains the earliest important deformation is commonly reported to be of mid-Mesozoic age (Misch, 1960, p. 33–34; Misch and Hazzard, 1962, p. 319; Armstrong and Hansen, 1966, p. 119–120; Drewes, 1958, p. 230–238; Thorman, 1962, p. 152–153), and angular unconformities in the Paleozoic section are generally unrecognized. Contrasts in metamorphic grade and tectonic style between older and younger Paleozoic rocks have been observed in the eastern Great Basin and have been attributed to Mesozoic deformation of the rocks with increasing mobility with depth in the sequence (Armstrong and Hansen, 1966, p. 125–126). In the southern Ruby Mountains these contrasts are adequately explained by an unconformity separating deformed and generally weakly metamorphosed lower Paleozoic rocks from relatively undeformed and nonmetamorphosed middle and upper Paleozoic rocks.

STRATIGRAPHIC EVIDENCE OF DEFORMATION

The rock units and gross structural features of part of the southern Ruby Mountains are shown in figure 1. Thermal metamorphism due to Tertiary and Mesozoic plutons has obscured stratigraphic relations in the northern part of the area shown in figure 1. The thermal effects of these plutons die out southward in the range, however, and in the southern part of the area the rocks can be readily identified and dated by fossils. Fossiliferous units can be traced northward into their metamorphosed equivalents, and some tentative correlations with standard sections in other areas can be made, but a formal terminology for many of the stratigraphic units is premature.

Lower Paleozoic rocks

The Prospect Mountain Quartzite, the oldest unit shown on figure 1, is generally thick bedded and cross stratified and characterized by shale partings between beds. The shale partings become shale beds, which are

generally micaceous, in the lower part of the section. Comparable beds in the lower part of the section to the north of the area of figure 1, on Green Mountain, are schistose. The overlying Middle Cambrian undivided unit is dominantly thin-bedded shaly limestone that grades into a thin- to medium-bedded limestone at the top. The basal few hundred feet of the Middle Cambrian, which everywhere within the area of figure 1 shows the thermal effects of the Harrison Pass pluton, consists of hornfels and dark- to light-gray, sometimes mottled, coarsely recrystallized carbonaceous limestone, and some fine-grained quartzite.

The Upper Cambrian undivided unit also clearly shows the thermal effects of the Harrison Pass pluton. In the north part of the area the Upper Cambrian unit consists of several recognizable sequences of hornfels and hornfels interbedded with recrystallized limestone. The hornfels grades southward into phyllite, and the limestone is progressively less recrystallized to the south. The lower part of the Upper Cambrian is probably a lateral equivalent of the Hamburg Dolomite and Dunderberg Shale as exposed at Eureka, Nev. (Palmer, 1960, p. 54). The uppermost part matches rather closely the Windfall Formation of the Eureka district (Nolan and others, 1956, p. 19–23). It consists of a lower part of gray limestone in beds a few inches to about 1 foot thick with thinner interbeds of recrystallized chert and an upper part of alternating light-brown shaly or silty limestone and light-gray limestone in beds a fraction of an inch to about 2 inches thick. The upper part grades upward by a decrease in the amount of shaly limestone into the lower beds of the Pogonip Group.

The Ordovician rocks within the area of figure 1 consist entirely of the Pogonip Group, which we have divided into two map units. The lower unit is further divisible into a lower gray thin- to medium-bedded shaly limestone and an upper medium- to thick-bedded cherty limestone that includes some beds of intraformational conglomerate. The upper unit is sandy dolomite and limy fissile siltstone overlain by platy limestone. The sandy dolomite, although light gray on a fresh surface, weathers to dark brown and forms one of the most conspicuous marker horizons in the area.

In the south part of the range south of figure 1, where we have not mapped in detail, the Pogonip is locally overlain by a few feet of white quartzite which grades upward into a brown somewhat cherty fine-grained dolomite. Sharp (1942, p. 660) included the quartzite and the brown dolomite in the Lone Mountain Dolomite, but we have obtained conodonts (identified by J. W. Huddle, written commun., June 1965) and brachiopods (identified by R. J. Ross, Jr., written commun., Mar. 1967) from the brown dolomite that indicate it is of Middle or Late Ordovician age. We, therefore, assign the brown dolomite to the Ely Springs Dolomite and the underlying quartzite to the Eureka Quartzite. The quartzite appears to be conformable on the Pogonip, but Sharp (1942, p. 659) reported that the upper platy limestone beds of the Pogonip are missing in this part of the range and cited this as evidence of a possible unconformity between the Pogonip and the Lone Mountain Dolomite.

Figure 2, which shows a considerable increase in thickness by folding throughout the length (about 20 centimeters) of the specimen, illustrates the difficulty of estimating thicknesses of the Cambrian and Lower Ordovician strata in the area. The small-scale folding is less intense in the upper part of the stratigraphic section; thus the 3,650-foot thickness for the Pogonip given by Sharp (1942, p. 657) appears reasonable, but his 6,650 feet for the Middle and Upper Cambrian and more than 1,400 feet for the Prospect Mountain Quartzite are uncertain (Sharp, 1942, p. 651–657).

Unconformity at base of Lone Mountain Dolomite

The Cambrian and Lower Ordovician formations in the area of figure 1 are separated from the Lone Mountain Dolomite by a surface of discontinuity which we believe is an angular unconformity. This surface has been mapped as a fault in the part of the range in White Pine County by R. K. Hose and M. C. Blake (written commun., Feb. 1967), but in the same area Sharp (1942, pl. 1) mapped it as a depositional contact and cited some evidence, as noted above, to show that it might be an unconformity, although he nowhere mentions angular discordance at this surface.

Beds above the unconformity are laterally continuous, whereas those beneath it are discontinuous. A persistent fossil horizon about 100 feet above the base of the Lone Mountain has been observed for a distance of more than 5 miles. The upper subdivision of the Pogonip Group appears and disappears beneath the unconformity (fig. 1) from the range front south of Indian Creek to the North Fork Mitchell Creek. On a ridge south of South Fork Mitchell Creek a westward-dipping high-angle fault separates the Lone Mountain from Upper Cambrian rocks. At one locality south of the area of figure 1, we found the Lone Mountain Dolomite resting with an angular unconformity on the Ely Springs Dolomite. This contact, shown in figure 3, is knife sharp with a coherent regularly bedded gray dolomite resting on a blocky-weathering jointed brown dolomite.

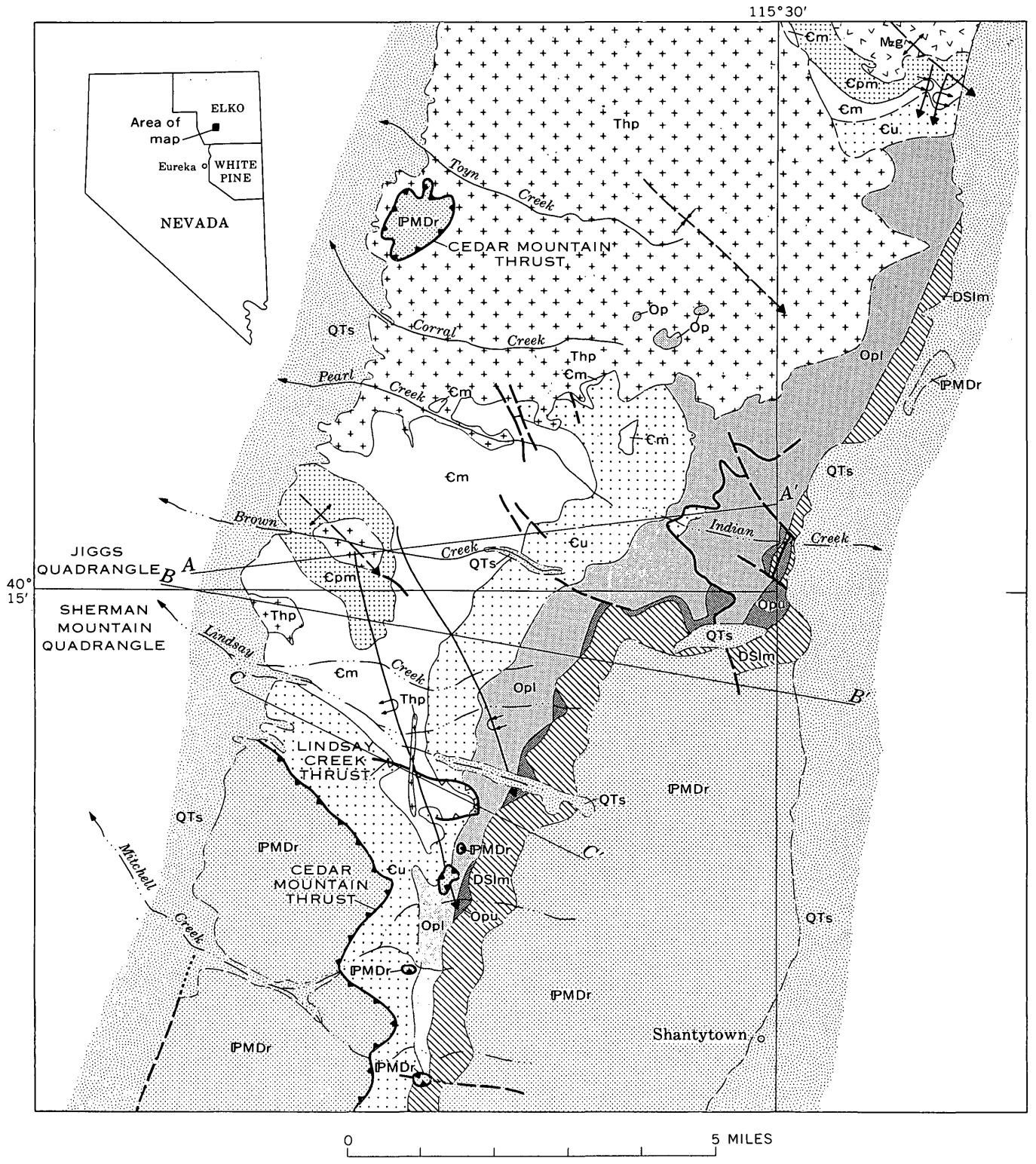

FIGURE 1.—Geologic map and sections of the central part of the southern Ruby Mountains, Elko County, Nev.

EXPLANATION

QTs — Quaternary and Tertiary sediments

Thp — Tertiary granodiorite of Harrison Pass pluton

Mzg — Mesozoic granite

PMDr — Pennsylvanian, Mississippian, or Devonian rocks

DSlm — Devonian and Silurian Lone Mountain Dolomite

Op / Opu / Opl — Ordovician Pogonip Group
Opu, *upper part*
Opl, *lower part*

Cu / Cm / Cpm — Cambrian rocks
Cu, *Upper Cambrian rocks*
Cm, *Middle Cambrian rocks*
Cpm, *Lower Cambrian Prospect Mountain Quartzite*

Contact
Dashed where approximately located; short dashed where projected on sections to show inferred shape of fold

Normal fault
Dashed where approximately located; dotted where concealed

Tertiary / Paleozoic
Thrust faults
Sawteeth on upper plate

Overturned anticline / Overturned syncline / Anticline / Syncline
Fold axes
Showing direction of dip of limbs and direction of plunge. Solid symbols indicate first-generation folds; dashed, second generation

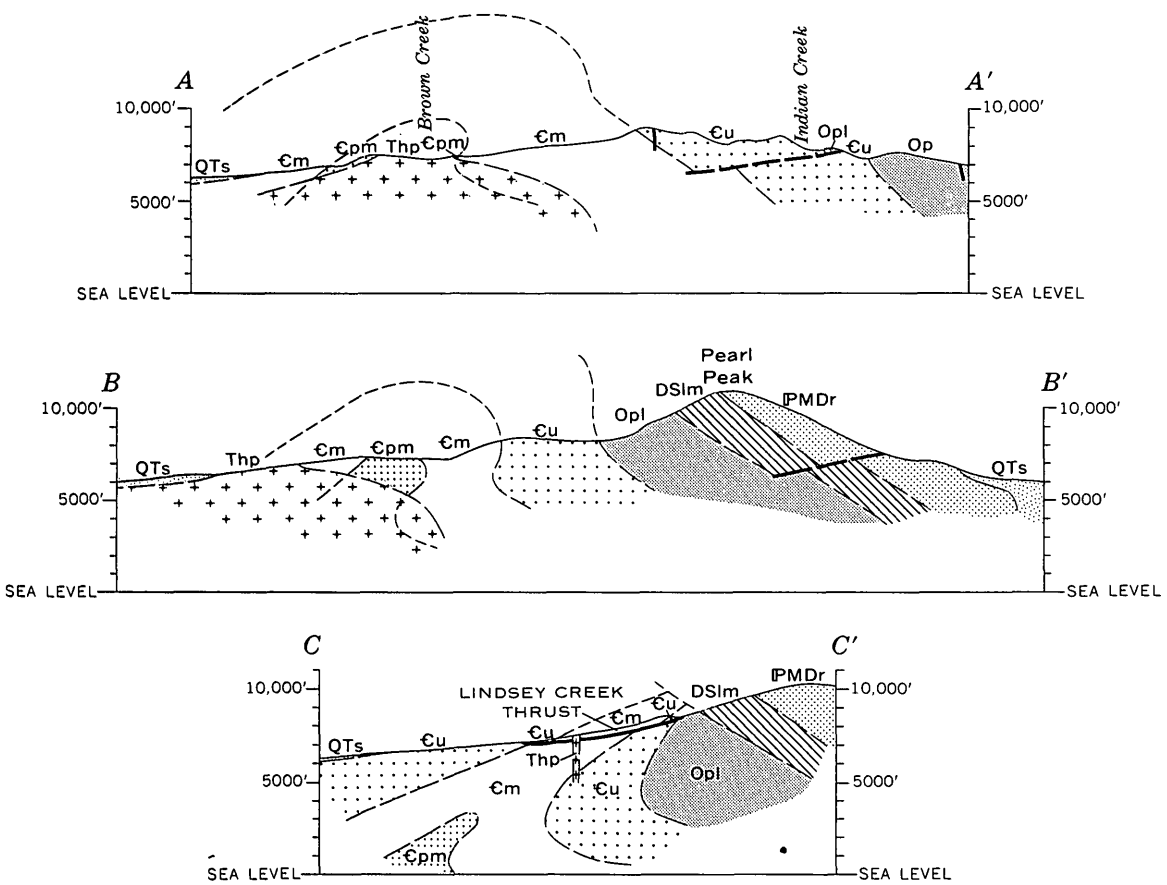

FIGURE 1.

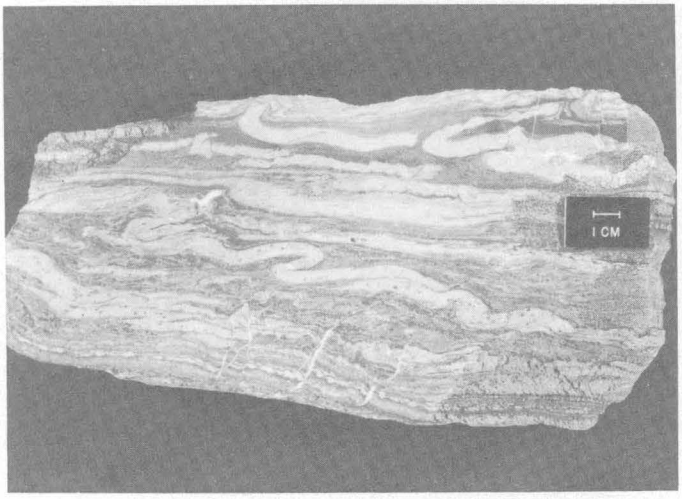

FIGURE 2.—Specimen of argillaceous limestone of the upper part of the Middle Cambrian, showing original thickness nearly doubled by folding.

FIGURE 3.—Lone Mountain Dolomite (light-gray rocks in upper half of picture) resting on blocky-weathering Ely Springs Dolomite. Contact indicated by arrows. Lone Mountain strikes N. 70° W. and dips 11° SW; Ely Springs strikes N. 10° E., and dips 17° W.

The apparently small thickness of the lower part of the Pogonip on the north side of the North Fork Mitchell Creek (fig. 1) is due to pronounced tectonic thinning of lower units of the Pogonip and Upper Cambrian units along the limb of a major first-generation fold. Sharp (1942, pl. 1, p. 682) showed a high-angle thrust fault separating the Upper Cambrian rocks from the Pogonip, but we have been unable to trace any continuous structural discontinuity in this area.

The degree of angular discordance between the Lone Mountain Dolomite and the older rocks has a wide range, depending on proximity to axial regions of folds in the older rocks. The eastward trend of the trace of the unconformity in the east-central part of the area is due mainly to topography, and the angular discordance is slight. At other localities differences in dip of as much as 80° occur between rocks above and below the unconformity.

A basal conglomerate above this unconformity is well exposed on the ridge south of South Fork Mitchell Creek. The conglomerate, one outcrop of which is shown in figure 4, consists of subangular to subrounded dolomite clasts a fraction of an inch to about 8 inches in greatest dimension in a sandy dolomite matrix. The conglomerate appears to be filling a channel cut in the pre-Lone Mountain erosion surface. The lower part, which lacks distinctive bedding, is about 80 to 100 feet thick; above this is an interval about 200 feet thick in which conglomerate beds a few feet thick are interlayered with light-gray dolomite. The conglomerate beds in the upper part of this upper interval are monolithologic and may be intraformational conglomerates. The conglomerate unit thins rapidly to the south and to the north of the ridge south of South Fork Mitchell Creek. On the north side of South Fork Mitchell Creek the contact between the Lone Mountain and the Pogonip is covered by colluvium. Any conglomerate beds in this covered zone could not be more than 500 feet thick. A few beds of monolithologic conglomerate near the base of

FIGURE 4.—Outcrop of dolomite-clast conglomerate near base of Lone Mountain Dolomite on ridge south of South Fork Mitchell Creek.

the Lone Mountain are all that remain of the basal conglomerate at the south boundary of figure 1.

The clasts in the basal conglomerate, although all dolomite, have been derived from diverse sources. Grain size in the clasts ranges from fine to coarse. Nearly all color gradations from pale buff through brownish gray and light gray to nearly black are present. Some clasts are from detrital carbonate rocks, and some appear to be from bioclastic units, although the only fossil material found thus far is some algal-like bodies. Whether the dolomite clasts represent dolomitized limestone fragments derived from the Pogonip Group, or older units, or represent original dolomite fragments is unknown, but their heterogeneity strongly suggests to us that the clasts have been derived from the older rocks. This heterogeneity and the absence of shearing phenomena in the conglomerate beds indicates a basal conglomerate, and not a tectonic breccia.

A basal conglomerate does not crop out at other localities, but at several places beneath outcrops of the Lone Mountain Dolomite we found rounded quartzite boulders that we believe have weathered out of a thin basal conglomerate. A thin section cut from one such boulder showed the rock to be composed of well-sorted well-rounded quartz grains and sparse small rhombic crystals of dolomite. There is no evidence of shearing or cataclasis in the rock as might be expected if the quartzite boulders were from a tectonic breccia rather than a basal conglomerate. The rock is nearly identical to the Eureka Quartzite from farther south in the range.

Further indication that the surface of discontinuity at the base of the Lone Mountain Dolomite is not a thrust fault is given by a study of the two faults in the area that can be clearly recognized as thrusts. These thrusts, shown on figure 1, are the Cedar Mountain thrust of Tertiary age (Willden and others, 1966) and the Lindsay Creek thrust, which we herein assign to the Ordovician Period. In both these thrusts, it is clear that strata above the thrust surface have been eliminated and that brecciation or shearing of rocks above and below the thrust surface has occurred. Structures and beds are truncated and offset by the thrusts. Rocks on either side of the Lindsay Creek thrust fault are made up of tectonitic marble in which the bedding is completely transposed by strong axial-surface schistosity. Where the Cedar Mountain thrust fault cuts the Harrison Pass pluton, the granodiorite exhibits strong cataclasis, which decreases in intensity away from the thrust but is still recognizable as much as 300 feet from the thrust surface. Carbonate rocks on the upper plate of the Cedar Mountain thrust, where they occur at the thrust surface, are strongly brecciated and recemented with calcite and silica veinlets. Conglomerate beds of the Diamond Peak Formation are so disrupted that they do not crop out. The absence of such features at the base of the Lone Mountain Dolomite together with the positive evidence for an erosion and depositional origin such as conglomerate at the surface of discontinuity, abundant sand in the overlying dolomite (see below), and the continuity of beds above the surface, seem to us to indicate that the surface is an angular unconformity.

Lone Mountain Dolomite

The Lone Mountain Dolomite, as we use the term, includes nearly 2,000 feet of generally medium- to thick-bedded sugary textured light-gray dolomite. Some beds are finely laminated and others are massive and make cliff-forming units in the section; these cliff formers, however, generally consist of several layers. Coarsely crystalline units occur in some places and sublithographic units in others. The dolomite beds in the lower part of the formation are generally sandy, and some contain as much as 30 percent quartz grains.

Sharp (1942, p. 660) gave a thickness of 1,350 feet for the formation and we have probably included beds that Sharp mapped as part of the Devonian Nevada Formation in our Lone Mountain. However, Merriam (1963, p. 40) gave a thickness of 2,190 feet for the Lone Mountain at Roberts Creek Mountain about 40 miles to the southwest, and 2,000 feet may be a reasonable estimate for its thickness in the Ruby Mountains. Sharp included in the Lone Mountain in the south end of the range (south of our map area) beds that we regard as more properly assigned to the Ely Springs Dolomite. We have not found beds with the distinctive lithology of the Ely Springs Dolomite within the area of figure 1.

The lowermost part of the Lone Mountain Dolomite —with the exception of the basal conglomerate, which is well developed at only the one locality—consists of platy, medium- to fine-grained locally nearly porcellaneous dolomite that weathers to a light pinkish gray. At a few places beds a few feet thick of dark-gray fine- to medium-grained vuggy dolomite have been found in the platy unit. The thickness of the platy unit is varied, but we have not found it to exceed 100 feet.

Above the platy dolomite is another unit of varied thickness consisting of dark-gray to nearly black medium- to thick-bedded and generally medium-grained fossiliferous dolomite. Where we have ob-

served this unit on the west side of the range, throughout a distance of about 5 miles, its thickness is about 40 to 60 feet. At the mouth of Indian Creek on the east side of the range, the unit appears to be about 200 feet thick, but part of this may be repetition by unmapped normal faults which are common at the range front.

Fossils from the dark unit have been collected at 5 localities all within a distance of about 5 miles of each other, on the west side of the range and at a sixth locality near the mouth of Indian Creek on the east side of the range. In only one of the collections from the west side of the range were the forms sufficiently well preserved to be definitely assigned to a period. The material, studied by W. A. Oliver, Jr. (written commun., Dec. 1966), and R. J. Ross, Jr. (written commun., Aug. 1966), included pentameroid brachiopods, *Syringaxon*-like horn corals, *Favosites?* sp., and halysitid corals, and is definitely of Silurian age. The other collections from the west side of the range contain simple horn corals which cannot be identified definitely because of poor preservation, but Oliver has suggested that three of these collections are more likely of late Ordovician than of Silurian age. The collection from near the mouth of Indian Creek has been reported on by R. J. Ross, Jr. (written commun., Mar. 1965), as follows:

> Amongst the 8 to 9 very scrappy fragments of brachiopods in the residue there is a single brachial hinge bearing an enormous cardinal process of very distinctive form. This seems to belong to some sort of orthotetinid brachiopod, although I have considered that it might be assigned to a triplesiacinid. Because I am unable to identify any of the fragments as to genus I am reluctant to put a definite age on this collection. I do think it much more likely to be Silurian than Ordovician, but would suggest that it might be Carboniferous.

Until additional collections can be made to resolve this apparent conflict we cannot dismiss the possibility that the lower part of the Lone Mountain Dolomite as we have mapped it may be of Upper Ordovician age. We think it more likely, however, that if the poorly preserved forms are indeed Upper Ordovician they represent reworked material.

Devonian and younger rocks

The detailed stratigraphy of the middle and upper Paleozoic rocks in the southern Ruby Mountains is still poorly known. Sharp (1942, p. 686) reports an aggregate thickness of 4,750 feet for the section from the base of the Lone Mountain Dolomite through a cherty limestone unit he assigns a Mississippian(?) age. By scaling thicknesses from our cross sections, we find that the section is even thicker than 4,750 feet, but we have not as yet studied the upper part to determine why the difference exists.

The Devonian and younger rocks in the report area include the Nevada, Devils Gate, Pilot, and Joana Formations. All are conformable, both with one another and with the underlying Lone Mountain Dolomite. Sharp (1942, p. 667–669) did not name the massive cherty limestone that we call Joana, and he (Sharp, 1942, p. 664–667) mapped what we call the Pilot Shale as an upper subdivision of the Devils Gate Limestone. At one locality the Joana is overlain by about 30 feet of green to dark-gray shale that might be assigned to the Chainman Shale of Mississippian age; this in turn is overlain by a thin brown quartzite which may be a part of the Chainman or of the Diamond Peak Formation—also of Mississippian age. Sharp (1942, p. 668) included both these units in his unnamed limestone of Mississippian(?) age.

A thick sequence of conglomerate, quartzite, and siltstone, and some limestone that has been assigned to the Diamond Peak Formation, and which rests on a sequence of Devonian carbonate rocks, is present on the upper plate of a thrust in the southwest part of figure 1. These rocks and the thrust fault are described elsewhere (Willden and others, 1966).

Pennsylvanian rocks consist of medium- to thick-bedded cherty limestone overlain by platy argillaceous limestone both of which are assigned to the Ely Limestone. These rocks are exposed on a low hill east of the range and probably are separated from the Lone Mountain Dolomite immediately to the west by a high-angle fault of large displacement.

STRUCTURAL EVIDENCE OF DEFORMATION

The rocks in the southern Ruby Mountains have undergone at least two and more probably three periods of compressive deformation. Two of these periods are well recorded in the Cambrian and Lower Ordovician rocks and are clearly older than the Harrison Pass pluton of Tertiary age. The oldest period, which is characterized by appressed recumbent folds, predates the deposition of the Lone Mountain Dolomite. The effects of the second period of deformation, which is characterized by open folds with vertical or near-vertical axial surfaces, are more intense in the northern part of the report area where the Lone Mountain Dolomite and younger rocks are not preserved, and its age with respect to these rocks is uncertain. Evidence for a third period of compressive deformation is less definite, but the Cedar Mountain thrust, which cuts the Harrison Pass pluton and shows strong cataclastic features in both the upper and lower plates, has been interpreted to be a compressive feature (Willden and others, 1966).

Structural style of older rocks

The style of folding commonly observed in the Cambrian and Lower Ordovician rocks is shown in the photographs of figure 5. First-generation folds—those produced in the first period of folding and which will hereafter be referred to as first folds—are appressed, recumbent, and asymmetric with one limb several times longer than the other. The map pattern of Cambrian and Lower Ordovician rocks south of the Harrison Pass pluton is controlled by the large-scale first folds whose axes are shown on figure 1. In the Jiggs quadrangle and the north half of the Sherman Mountain quadrangle only one pair of major first folds, which trend south-southeast and plunge about 20° S., was found (fig. 1). To the east and northeast of the Jiggs quadrangle, where the relationships between the individual rock units become complicated by abundant intrusive rocks, other large-scale recumbent folds are present. The sharp bends in the contact between the Middle Cambian rocks and older and younger units in the northeast part of figure 1 are the result of a pair of first folds.

Second-generation folds—produced during the second period of folding—are open and have approximately equal length limbs and vertical or steeply dipping axial surfaces, but the axes commonly plunge as much as 40°. Large-scale second-fold axes have been obscured in part by the emplacement of the Harrison Pass pluton and Mesozoic granite bodies in and beyond the northeast part of figure 1. The second-fold axes shown in the northeast part of figure 1 are only approximately located. We have recognized no large-scale second folds south of Brown Creek.

Small second folds that cross first folds have been observed at several places. One of the better examples of these crossing folds is shown in figure 5*D*.

Small-scale first folds have been found in the Cambrian and Lower Ordovician rocks throughout the southern Ruby Mountains. They are most abundant, however, in axial regions of larger folds. In these areas the small-scale folds are found in all types of rocks. On the limbs of the larger folds, small-scale folds generally are confined to thin-bedded units. The small-scale folds become less abundant upward in the section, and in most large hinge areas (tens of feet or more across) in the Pogonip Group, small-scale fabric elements consist only of strong axial-plane cleavage (fig. 5*C*) and a lineation that lies in the bedding planes; it is due to the intersection of the cleavage and bedding.

The small-scale first folds in the southern Ruby Mountains are similar in style and orientation to the F_2 set of folds described by Howard (1966, p. 78–83, 111–113, fig. 14) in the metamorphic terrane of the northern Ruby Mountains. Howard recognizes three sets of small-scale fabric elements of which F_2 folds are the dominant features, and he assigns all three to a single major period of deformation and metamorphism in Jurassic or Cretaceous time (Howard, 1966, p. 120–134).

Small-scale second folds in the Combrian and Lower Ordovician rocks are abundant only in the extreme northeast part of the map area where they occur on the nose of a major second-generation anticline. This anticline is clearly cut by an intrusive body of weakly foliated muscovite-biotite granite that is of Jurassic age according to preliminary whole-rock rubidium-strontium radiometric age determinations.

One large low-angle reverse fault is associated with the major first-fold hinge in the southwest part of the area (fig. 1, section *C*–*C'*). This fault, which we have named the Lindsay Creek thrust, is parallel to the axial planes of the fold pair, lies in the overturned limb of the fold pair, and has displaced the contact between the Middle and Upper Cambrian rocks several hundred feet. No other major faults related to the first deformation have been observed, but the almost universal strong axial-plane cleavage in all hinge areas suggests that considerable movement may have taken place by slippage on small faults or cleavage planes. Pronounced tectonic thinning of units in the Upper Cambrian section and in the lower part of the Pogonip Group along the common limb of the major first folds from Lindsay Creek to south of Mitchell Creek may be due to this sort of movement. Sharp (1942, pl. 1, p. 682) interpreted this thinning to be due to a high-angle reverse fault.

The first period of folding is clearly older than the Lone Mountain Dolomite because the unconformity at the base of Lone Mountain truncates first folds. Furthermore, regional stratigraphic relationships suggest that the first folding may be a great deal older than the Lone Mountain Dolomite. The widespread hiatus at the base of the Eureka Quartzite (Webb, 1958; Gilluly and Gates, 1965, p. 14–15), which has been recognized in the south part of the Ruby Mountains (see above and Webb, 1958, p. 2365), might reflect the beginning of the crustal unrest that culminated in the tight folding observed in the Cambrian and Lower Ordovician rocks of the southern Ruby Mountains. Deformation was not completed until sometime after the Ely Springs Dolomite was deposited, however, because it is separated from the overlying Lone Mountain by an angular unconformity.

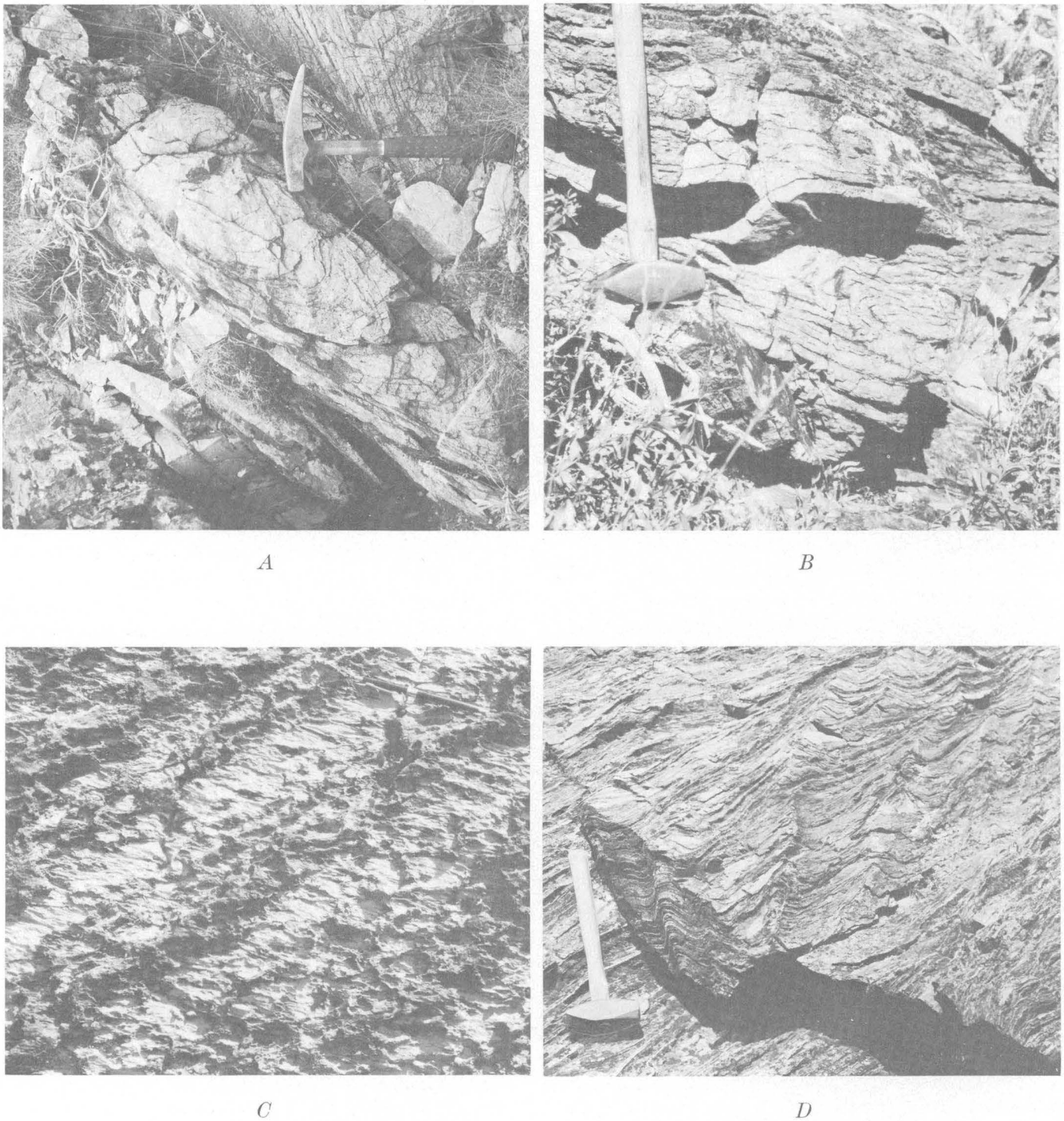

FIGURE 5.—Folds and cleavage in Cambrian and Ordovician rocks. *A*. First-fold hinge in Prospect Mountain Quartzite. *B*. Small first fold in upper part of Middle Cambrian sequence. This fold, which has same style as major first folds, illustrates noncylindrical character of first folds. *C*. Strong axial-surface cleavage in limestone of Pogonip Group. *D*. Second folds crossing first folds in hornfels in lower part of Upper Cambrian sequence. Hammer lies on plane parallel to axial surface of first folds. Second-fold axial surfaces are vertical and normal to plane of picture.

The second period of folding may also predate the deposition of the Lone Mountain Dolomite because there are no structural elements in the Lone Mountain and younger rocks comparable to those produced during the second folding. The second folds are best developed north of the Harrison Pass pluton where the Lone Mountain and younger rocks are not preserved however, and so the structural contrasts may not be definitive. The postulate that both the first and second folds predate the Lone Mountain Dolomite is compatible with the stratigraphic evidence that indicates an unconformity at the base of the Lone Mountain and another beneath the Eureka Quartzite.

Structural style of younger rocks

The Lone Mountain Dolomite and younger rocks have a homoclinal structure that strikes northeast and dips southeast throughout the part of the southern Ruby Mountains shown on figure 1. No small-scale folds have been found in these rocks. Small-scale folds might not be expected in the medium- to thick-bedded carbonate rocks that predominate in the younger sequence, but the Pilot Shale and thinly laminated carbonate units in the section should show the folds if they were present. However, local drag features related to small offsets on high-angle faults have been observed in the Pilot Shale at the range front near Shantytown and are probably present at other places.

The westward-dipping Silurian rocks mapped by Sharp (1942, pl. 1) at the south end of the range suggest that the structure of the Lone Mountain Dolomite and younger rocks is a broad anticline whose western limb has been almost completely removed by erosion or faulting or a combination of the two. If this fold is real it probably is wider than the mountain range and has a gently southwestward-plunging axis to account for the present distribution of Silurian and younger rocks. The remarkably simple structure of the younger rocks is incompatible with the structures observed in the older rocks. We believe that this simple structure is much younger; possibly mid-Tertiary and related in some fashion to the deformation that produced the Cedar Mountain thrust.

Structure diagrams

Figures 6 and 7 are collective structure diagrams constructed by plotting the structural elements, poles to bedding, poles to axial surfaces, and first- and second-fold axes and lineations, as lower hemisphere projections on equal-area nets and contouring the resulting projections. These two illustrate the contrast in structural style between the Cambrian and Lower Ordovician rocks and the Lone Mountain Dolomite and younger rocks to the south of the Harrison Pass pluton. A detailed structural analysis of the deformation of the Cambrian and Ordovician rocks is beyond the scope of this paper, but the diagrams for the Cambrian and Ordovician rocks (fig. 6*A*, *B*, *C*) represent noncylindrical folds. A single rectilinear fold axis trending about S. 15° W. and plunging about 6° is represented in the diagram for the Lone Mountain Dolomite and younger rocks (fig. 7). The very strong maximum in the diagram of figure 7 is completely incompatible with the diagrams for the Cambrian and Lower Ordovician rocks (figs. 6 and 8) and shows that the deformational history of these younger rocks has been relatively simple. The geometry of the macroscopic second-generation folds in the northeast part of the map area (fig. 1) is represented in figure 8.

ASSOCIATED PLUTONISM AND METAMORPHISM

Strongly foliated muscovite-biotite granite sills, deformed along with the enclosing Prospect Mountain Quartzite into second folds on the southeast side of Green Mountain (about 1½ miles north of north boundary of the area of fig. 1), are Early Ordovician in age on the basis of preliminary whole-rock rubidium-strontium dates. These sills are mineralogically similar to granite gneiss which is widely exposed in the area north and northwest of Green Mountain between Rattlesnake Creek and Lamoille Canyon and which has also yielded Early Ordovician dates in three samples. Interpretation of the presently meager data from widely separated localities is conjectural at best, but it seems reasonable to us that much of the northern Ruby Mountains is underlain by a granite body of batholithic proportions that was emplaced during or immediately prior to the folding of the Cambrian and Lower Ordovician rocks.

Much of the metamorphism in the Ruby Mountains is probably more properly related to thermal effects of the various plutonic rocks than to regional deformation. But we have observed chloritic phyllite in the Cambrian rocks, particularly in the lower part of the section, as far south in the range as these rocks are exposed. The chloritic phyllite is most conspicuously developed in the axial regions of first folds on cleavage surfaces that parallel the axial surfaces of the folds. We regard this as strong evidence that the chloritic phyllites are a metamorphic product of the regional deformation that produced the folds, not a distant effect of the Harrison Pass pluton or its offshoots.

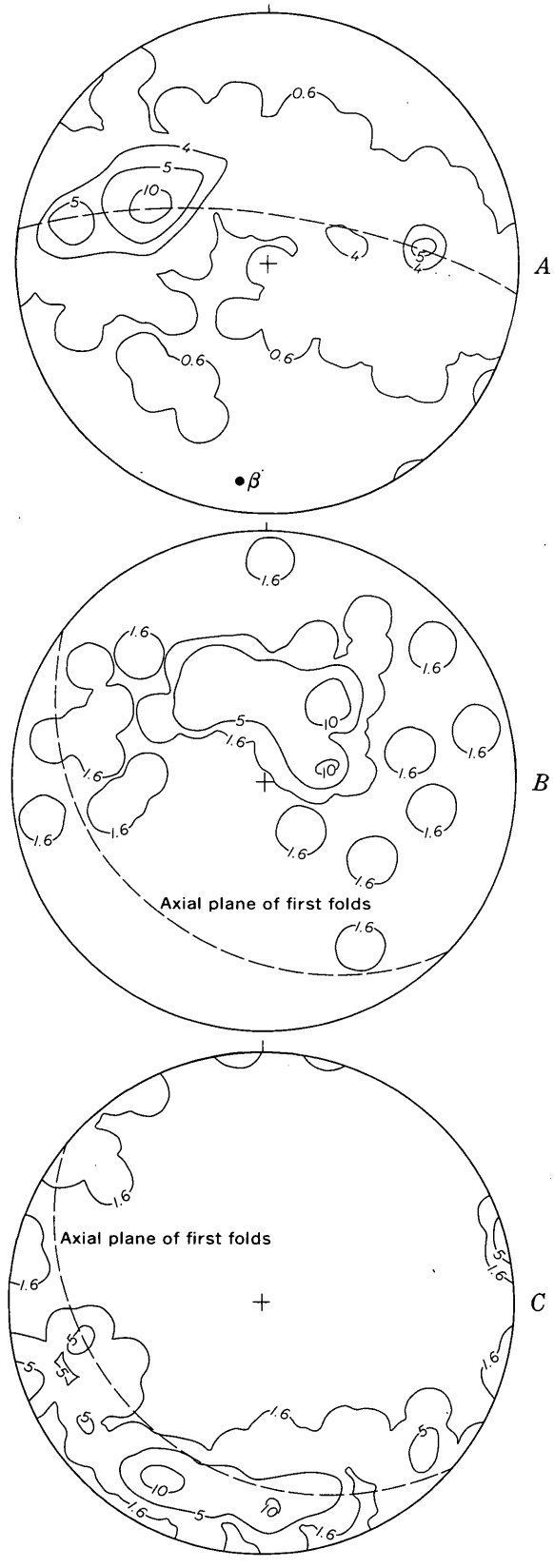

← FIGURE 6.—Geometry of first folds in Cambrian and Ordovician rocks south of the Harrison Pass pluton. *A*. Poles to bedding (165 poles); contours are 10, 5, 4, and 0.6 percent per 1 percent area; β is pole for girdle (dashed line) along which maxima lie. *B*. Poles to axial surfaces of small folds (61 poles); contours are 10, 5, and 1.6 percent per 1 percent area; dashed line shows statistical position of axial plane of first folds. *C*. Axes of small folds (61 axes); contours are 10, 5, and 1.6 percent per 1 percent area; dashed line from *B*.

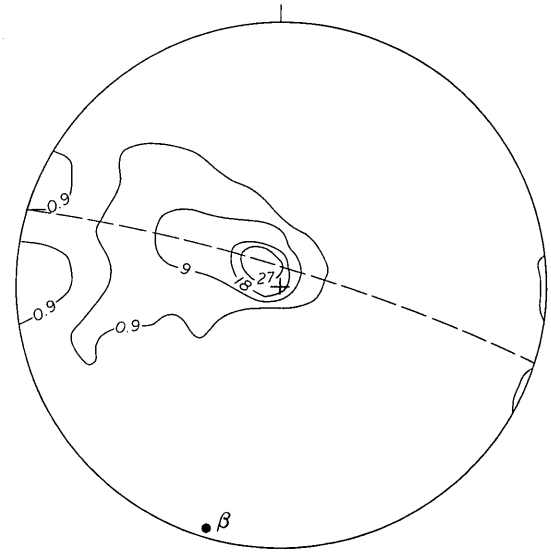

FIGURE 7.—Poles to bedding (111 poles) in Silurian and younger rocks south of Harrison Pass pluton. Contours are 27, 18, 9, and 0.9 percent per 1 percent area; β, pole for plane of symmetry (dashed line) through maximum, plunges 6° in a S. 15° W. direction.

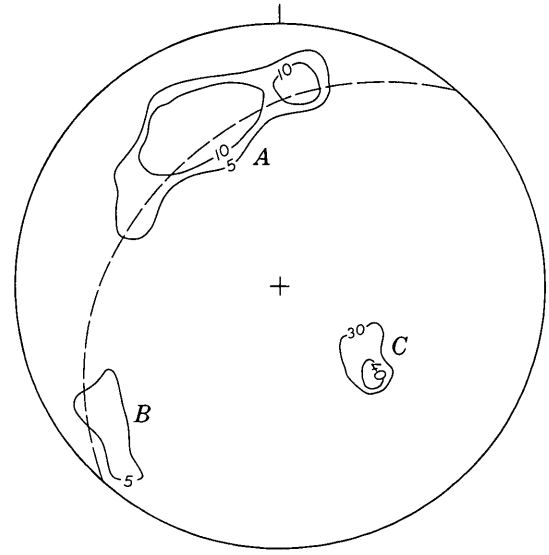

FIGURE 8.—Geometry of second folds in Cambrian and Ordovician rocks northeast of Harrison Pass pluton. *A*. Poles to bedding (50 points); contours are 10 and 5 percent per 1 percent area. *B*. Poles to axial surfaces of small folds (26 points); contour 5 percent per 1 percent area. *C*. Axes of small folds (20 points); contours are 40 and 30 percent per 1 percent area.

SUMMARY

The lower Paleozoic rocks in the southern Ruby Mountains record a period of crustal unrest characterized by development of superposed fold systems and low-grade metamorphic rocks and by associated plutonism of as yet undetermined extent. The deformation began after deposition of the Pogonip Group of Early and Middle Ordovician age and appears to have been completed prior to deposition of the Lone Mountain Dolomite, the age of which is somewhat uncertain in the Ruby Mountains although the lower part is most likely Silurian. The structure of the middle and upper Paleozoic rocks is by contrast remarkably simple and is most likely much younger.

This Ordovician deformational event, although perhaps confined to the Ruby Mountains, was so intense as to warrant a name. We therefore propose that it be called the Ruby disturbance.

REFERENCES

Armstrong, R. L., and Hansen, Edward, 1966, Cordilleran infrastructure in the eastern Great Basin: Am. Jour. Sci., v. 264, p. 112–127.

Drewes, Harald, 1958, Structural geology of the southern Snake Range, Nevada: Geol. Soc. America Bull, v. 69, p. 221–239.

Gilluly, James, and Gates, Olcott, 1965, Tectonic and igneous geology of the northern Shoshone Range, Nevada: U.S. Geol. Survey Prof. Paper 465, 153 p.

Howard, K. A., 1966, Structure of the metamorphic rocks of the northern Ruby Mountains, Nevada: Yale Univ. unpub. Ph.D. thesis, 170 p.

Merriam, C. W., 1963, Paleozoic rocks of Antelope Valley, Eureka and Nye Counties, Nevada: U.S. Geol. Survey Prof. Paper 423, 67 p.

Misch, Peter, 1960, Regional structural reconnaissance in central-northeast Nevada and some adjacent areas:—Observations and interpretations, *in* Geology of east central Nevada, Guidebook 11th Ann. Field Conf., 1960: Intermountain Assoc. Petroleum Geologists, Salt Lake City, Utah, p. 17–42.

Misch, Peter, and Hazzard, J. C., 1962, Stratigraphy and metamorphism of Late Precambrian rocks in central northeastern Nevada and adjacent Utah: Am. Assoc. Petroleum Geologists Bull., v. 46, p. 289–343.

Nolan, T. B., Merriam, C. W., and Williams, J. S., 1956, The stratigraphic section in the vicinity of Eureka, Nevada: U.S. Geol. Survey Prof. Paper 276, 77 p.

Palmer, A. R., 1960, Some aspects of the early Cambrian stratigraphy of White Pine County, Nevada, and vicinity, *in* Geology of east central Nevada, Guidebook 11th Ann. Field Conf., 1960: Intermountain Assoc. Petroleum Geologists, Salt Lake City, Utah, p. 53–58.

Roberts, R. J., 1964, Stratigraphy and structure of the Antler Peak quadrangle, Humboldt and Lander Counties, Nevada: U.S. Geol. Survey Prof. Paper 459–A, 93 p.

Sharp, R. P., 1942, Stratigraphy and structure of the southern Ruby Mountains, Nevada: Geol. Soc. America Bull., v. 53, p. 647–690.

Thorman, C. H., 1962, Structure and stratigraphy of the Wood Hills and a portion of the northern Pequop Mountains, Elko County, Nevada: Univ. Washington, unpub. Ph.D. thesis, 218 p.

Webb, G. W., 1958, Middle Ordovician stratigraphy in eastern Nevada and western Utah: Am. Assoc. Petroleum Geologists Bull., v. 42, p. 2335–2377.

Willden, Ronald, Thomas, H. H., and Stern, T. W., 1966, Oligocene or younger thrust faulting in the Ruby Mountains, northeastern Nevada, *in* Abstracts for 1965: Geol. Soc. America Spec. Papers 87, p. 239.

269–274 O—67——6

ARAGONITE AND CALCITE IN MOLLUSKS FROM THE PENNSYLVANIAN KENDRICK SHALE (OF JILLSON) IN KENTUCKY

By ELLIS L. YOCHELSON, JOHN S. WHITE, JR.,[1]
and MACKENZIE GORDON, JR., Washington, D.C.

Work done in cooperation with the U.S. National Museum

Abstract.—In X-ray studies of a representative of each of 18 molluscan species to determine the mineral composition of the shell, three genera of cephalopods, nine genera of gastropods, and three genera of pelecypods show only aragonite in the shell. Two genera of pelecypods show an outer shell layer of aragonite and calcite. One gastropod genus has an outer calcitic shell layer and an inner aragonitic layer.

D. C. Alvord, of the U.S. Geological Survey, has made an extensive collection of marine invertebrates from the Kendrick Shale (of Jillson, 1919) in eastern Kentucky. This unit lies within the Breathitt Formation of Early and Middle Pennsylvanian age. The invertebrate assemblage contains a large number of mollusks, which are unusual and not typical of those found at most Paleozoic localities in that their shells are chalky white in color and chalky in texture. X-ray studies have shown that much of the molluscan shell material is aragonite, confirming previous reports of aragonite in Kendrick mollusks (Stehli, 1956; Grandjean and others, 1964). The diversity of this fauna enables us to provide additional data on the original shell composition of a number of Pennsylvanian mollusks.

LOCALITY, FOSSIL ASSEMBLAGE, AND CORRELATION

Alvord's collection (U.S. Geol. Survey colln. 22512–PC) was made in the central part of the Pikeville quadrangle, between Long Branch and Road Branch of Island Creek. The fossils were obtained from the high wall of a strip mine. The stripping operation is not indicated on the quadrangle map because production from the mine began after the map was published, but it is indicated on the geologic map of Alvord and Holbrook (1965).

The base of Jillson's Kendrick Shale is at about 1,470 feet elevation just above the Amburgy (Williamson) coal zone. The fossils occur through at least the lowest 20 feet of the Kendrick Shale, with their greatest abundance in the upper 5 feet of this interval. The entire zone is a calcareous silty-clay shale and is disconformably overlain by a channel sandstone. The Kendrick Shale interval is somewhat thinner here than in the adjacent Lick Creek quadrangle where a basal member of sandy siltstone and shale is present.

The X-rayed mollusks are listed in table 1. Four other mollusks wre identified in the faunule: *Nucula* sp. B, *Nuculopsis* aff. *N. girtyi* Schenk, *Nuculopsis*? sp. indet, and *Donaldina* sp. indet. Although the faunule is predominately molluscan, other fossils occur in small numbers. These include the following:

Lophophyllidium sp.
Crinoid stems, indet.
Derbyia sp. indet.
Tornquistia? sp.
Desmoinesia n. sp.
Linoproductus aff. *L. nodosus* (Newberry)
Hustedia sp. indet.

Recent studies of the Kendrick ammonoids by Furnish and Knapp (1966, p. 297) show that the formation is late Morrow in age. In further confirmation of this age assignment, Gordon finds the *Linoproductus* species listed above commonly in the upper part of the Bloyd Shale of Arkansas.

[1] U.S. National Museum.

TABLE 1.—*Aragonite and calcite composition of shells of 18 genera of mollusks*

[Specimens from USGS colln. 22512-PC]

Sample No.	USNM No.	Name	Shell layer or deposit	Composition
		Pelecypoda		
1	158431	*Nucula* sp. A	Inner	Aragonite.
2	158431	----do	Outer	Do.
3	158432	*Yoldia* sp	Outer (differentiation of layers not apparent).	Aragonite and minor calcite.
4	158433	*Parallelodon* sp. indet	Inner	Aragonite.
5	158433	----do	Outer	Aragonite and minor calcite.
6	158434	*Volsellina* sp. indet	Inner	Aragonite.
7	158434	----do	Outer	Do.
8	158435	*Astartella* sp	Outer (differentiation of layers not apparent).	Do.[1]
		Gastropoda		
9	158436	*Bellerophon* (*Pharkidonotus*) sp	Inner, thick	Aragonite.
10	158436	----do	Outer, thin	Do.
11	158437	*Knightites* (*Retispira*) sp. indet	Inner	Do.[2]
12	158437	----do	Outer	Do.[2]
13	158438	*Euphemites* cf. *E. multiliratus* Sturgeon	Inner, thin	Do.
14	158438	----do	Outer?, thin	Do.
15	158438	----do	Inductra deposit on shell	Do.
16	158439	*Trepospira* (*Trepospira*) cf. *T.* (*T.*) *illinoisensis* (Worthen).	Inner, thick	Do.
17	158439	----do	Outer, thin	Do.
18	158440	*Glabrocingulum* (*Glabrocingulum*) n. sp.	Inner, thick	Do.
19	158440	----do	Outer, thin	Do.
20	158441	*Shansiella carbonaria* (Norwood and Pratten)	Inner, thin	Do.
21	158441	----do	Outer, thick	Do.
22	158442	*Glyptotomaria* (*Dictyotomaria*) cf. *G.* (*D.*) *scitula* (Meek and Worthen).	Inner, thick	Do.
23	158442	----do	Outer, thin	Do.
24	158443	*Straparollus* (*Amphiscapha*) sp. indet	Inner, thin	Do.
25	158443	----do	Outer, thick	Calcite.
26	158444	*Ianthinopsis* sp	Inner, thick	Aragonite.
27	158444	----do	Outer, thin	Do.
28	158445	*Meekospira* sp. indet	Inner	Do.
		Cephalopoda		
29	158446	*Mooreoceras colletti* (Miller)?	Inner	Aragonite.
30	158446	----do	Outer	Do.
31	158446	----do	Septum	Do.
32	158447	*Metacoceras* sp	Inner	Do.
33	158447	----do	Outer	Do.
34	158447	----do	Septum	Do.
35	158448	*Gastrioceras occidentale* (Miller and Faber)	Inner	Do.
36	158448	----do	Outer	Do.

[1] Minor amounts of quartz and clay or laumonite present; probably surface contaminant.

[2] Minor amounts of quartz present; probably contaminant as specimen was smal and difficult to sample.

PROCEDURE

X-ray diffraction powder patterns from samples of selected specimens were obtained by using nickel-filtered copper radiation and 114.59 millimeter diameter Debye-Scherrer cameras. A 4-hour exposure at 35 kilovolts and 20 milliamperes was sufficient to produce good pictures. Sampling was performed by powdering material in place on the shell with a fine needle. The powder was picked up on the tip of a thin wedge of cellulose acetate which had been dipped in a slow-setting rubber cement. The wedge was then inserted into the spindle holder of the camera. Thin layers of light-brown calcite occur on some of the shells, and care was taken to avoid their contaminating the sample.

By way of a check on the results of the X-ray determinations given in table 1, a fragment of the brachiopod *Tornquistia*? which lay next to a mollusk was X-rayed. The molluscan material showed an aragonite pattern, and the brachiopod material showed the expected pattern of calcite.

DISCUSSION

Of the five pelecypod genera examined, *Yoldia* and *Parallelodon* (samples 3–5, table 1) were tested twice to confirm that both aragonite and calcite are present in the outer shell layer. The spottiness of the powder patterns indicates that the calcite crystals are relatively large. Whether the outer shell layer in Paleozoic pelecypods is aragonite or aragonite combined with calcite may be a significant taxonomic criterion only at the family level or lower levels. Information from more genera is needed to draw any definite conclusions.

The pleurotomariacean gastropods are represented by four genera (samples 16–23) which give a consistent aragonite composition for both shell layers, in keeping with available information on the shell of living representatives of this superfamily. Stehli (1956) reported a thick inner aragonite layer and a thin outer calcite layer on an unidentified species of Pennsylvanian *Bellerophon*; whether he was dealing with a specimen from Jillson's Kendrick Shale or from the "Buckhorn Asphalt" of Oklahoma is not clear. Our data (samples 9 and 10) do not support this finding, and possibly Stehli may have been misled by the thin coating of secondary brown calcite which simulates an outer shell layer on some specimens. The consistent aragonite in the shell of two other bellerophontacean genera (samples 11 through 15) supports this alternative interpretation.

Stehli's (1956) finding of an inner aragonite layer and an outer calcite layer in *Amphiscapha* is confirmed. The calcite outer shell layer may be a familial or superfamilial characteristic, for at outcrops in the Pennsylvanian of north-central Texas where pleurotomariaceans are represented only by steinkerns, well-preserved euomphalaceans can be collected; this implies a difference in shell mineralogy between the two superfamilies. The aragonite in the remaining two genera (samples 26–28) of more advanced gastropods confirms Stehli's findings. Although he identified the taxa which he investigated as *Sphaerodoma* and *Soleniscus*, respectively, they are probably the same as the two we examined.

In general, the two nautiloids examined (samples 29–34) confirm Stehli's observations. Our material has consistently shown aragonite to be the only material in both shell layers and septa; Stehli reported some calcite in the cameral deposits and aragonite exclusively in the shell. These findings are not necessarily conflicting. The ammonoid *Gastrioceras* examined by both Stehli and ourselves (samples 35 and 36) also has a shell of aragonite.

A problem which has been generally overlooked is the variety of conditions necessary for preservation of aragonite in shale. If one can use the chalky appearance and fibrous texture of molluscan shells as suggestive indication of original aragonite, it is apparent that the mineral is widespread in Pennsylvanian shales of different ages in the Eastern United States. Similar material has been observed in western Pennsylvania at two localities, in eastern Ohio at two localities by Yochelson, and at several other localities in eastern Kentucky by Gordon. The matrix in which these aragonite-shelled mollusks have been found is consistently a dark fine-grained shale, but its precise mineralogy has not been established. If consistent petrographic features can be found among the various localities, they should aid in the search for older Paleozoic aragonite-bearing shales.

REFERENCES

Alvord, D. C., and Holbrook, C. E., 1965, Geologic map of the Pikeville quadrangle, Pike and Floyd Counties, Kentucky: U.S. Geol. Survey Geol. Quad. Map GQ–480.

Furnish, W. M., and Knapp, W. D., 1966, Lower Pennsylvanian fauna from eastern Kentucky, pt. 1, Ammonoids: Jour. Paleontology, v. 40, p. 296–308.

Grandjean, J., Grégoire, Ch., and Lutts, A., 1964, On the mineral components and the remnants of organic structures in shells and fossil molluscs: Acad. Royale Belgique Bull. Cl. Sci., ser. 5, v. 50, no. 5, p. 562–595, 7 pls.

Jillson, W. R., 1919, The Kendrick shale—a new calcareous fossil horizon in the coal measures of eastern Kentucky: Kentucky, Dept. Geology and Forestry, Mineral and Forest Resources of Kentucky, ser. 5, v. 1, no. 2, p. 96–104.

Stehli, F. G., 1956, Shell mineralogy in Paleozoic invertebrates: Science, v. 123, p. 1031–1032.

DIGITAL RECORDING AND PROCESSING OF AIRBORNE GEOPHYSICAL DATA

By G. I. EVENDEN, F. C. FRISCHKNECHT, and J. L. MEUSCHKE, Denver, Colo.

Abstract.—The U.S. Geological Survey operates a geophysical research aircraft equipped with a magnetometer, gamma-ray spectrometer, Input electromagnetic system, and a flight-path recovery system that includes a Doppler navigation system. The outputs from all these systems are digitized at a rate of 10 observations per second and are recorded on magnetic tape. Computer programs have been written to compute the flight path of the aircraft, to prepare profiles, to locate intersections of transverse and base lines, and to make drift corrections. The final program for aeromagnetic data yields a plot of the flight path, intersections of the desired magnetic contours with the flight path, and maximums and minimums along the flight path.

In 1963 the U.S. Geological Survey undertook a program to improve its methods of acquisition and processing of airborne geophysical data. A digital magnetic-tape recording system together with a new magnetometer and flight-path recovery system have been installed in a Convair CV–240 aircraft. A digital computer and plotter are now used to accomplish about 90 percent of the task of data processing which was formerly done by hand.

Acknowledgments.—W. L. Anderson, as Chief Scientific Programmer for the U.S. Geological Survey, and P. P. Hoffman, of the Branch of Regional Geophysics, prepared most of the programs during 1964 and 1965 referred to in this report.

MAGNETOMETER SYSTEM

The basic element of the magnetometer system is an ASQ–10 fluxgate magnetic detector. The detecting head is located at the end of the retractable tail boom. Compensating coils, Permalloy strips, and copper rings compensate for the permanent, induced, and eddy current fields of the aircraft to within about ± 0.1 gamma when the boom is extended. The compensation equipment is set up and adjusted according to techniques developed for compensation of antisubmarine patrol aircraft.

The output signal of the ASQ–10 magnetic detector passes through a band-pass filter so that the system had to be modified for total-intensity measurements. Two different methods for recording total intensity have been used. In the manual system, shown within the rectangle enclosed by a dashed line in figure 1, an analog output voltage is derived from a point before the band-pass filter and is amplified using a separate direct-current amplifier, which also serves as a sensitivity control. Bias current for the fluxgate element is derived from a separate and highly stable power supply (programmable power supply, fig. 1). Base levels are changed by remote programming of the supply. The orienting mechanisms and associated circuits which keep the fluxgate element alined with the earth's field have not been modified.

In the automatic system now used, the fluxgate element is part of a servo loop (fig. 1). The action of the phase discriminator and motor is such as to continuously reposition the programming potentiometer on the power supply so that the net field through the fluxgate element is always near zero. Thus, the position of the servo shaft indicates the intensity of the earth's field. A shaft encoder having 1,024 counts per turn is used to digitize the shaft position. Three sensitivities are provided so that the maximum rotation of the shaft, which is 40 turns, can represent 4,000, 20,000, and 80,000 gammas. The base level of the potentiometer which programs the power supply can be shifted so that measurements can be made within the range of about 15,000–100,000 gammas on any sensitivity.

In addition to the digital output, an analog voltage is available from a 40-turn potentiometer attached to

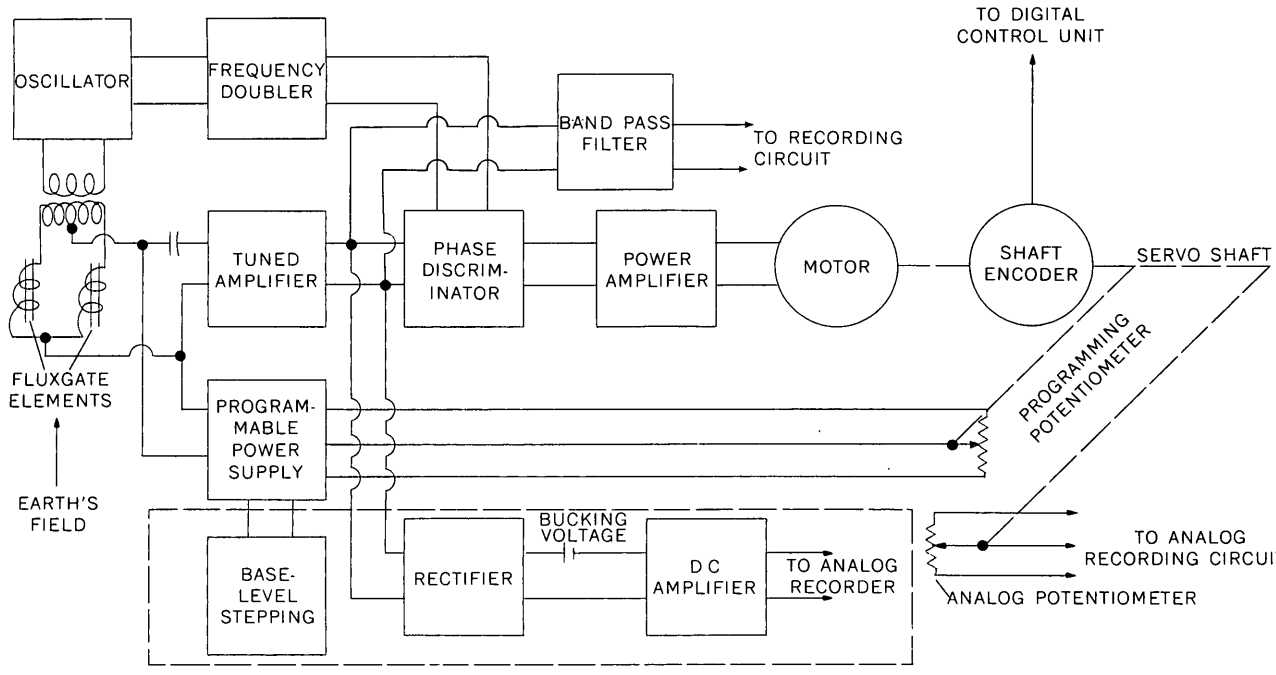

FIGURE 1.—Block diagram of magnetometer system.

the servo shaft. This voltage is recorded on a rectilinear strip-chart recorder with full-scale sensitivities ranging from 20 to 2,000 gammas. Base-level switching is automatic for the analog output.

The noise level in flight when using the automatic system is ±2 counts, corresponding to about ±0.2 gammas on the most sensitive range. With the manual recording system, a noise level of about ±0.1 gamma, or less, can be achieved. Noise levels are a little higher when simultaneously making Input electromagnetic measurements; however, the ASQ–10 magnetic detector operates satisfactorily with the Input system without time sharing, as is required with proton and other types of fluxgate magnetometers.

The magnetometer was originally adjusted and calibrated using Helmholtz coils. Calibration is maintained by periodic checks and calibrations of the bias power supply and by frequent comparisons of the fluxgate magnetometer with a proton magnetometer.

GAMMA-RAY MEASURING EQUIPMENT

Dectectors for the gamma-ray spectrometry system are two 11½- × 4-inch sodium iodide crystals with seven 3-inch photomultiplier tubes each. A 400-channel analyzer is used to take complete spectra between about 0.4 and 2.8 million electron volts. Spectra can be read out from the analyzer to an X–Y recorder in flight. In addition, the spectra are recorded automatically on magnetic tape.

Four single-channel analyzers and count-rate meters are used in addition to the 400-channel analyzer. One of the single-channel analyzers is set to measure a "window" of energies from 0.4 to 2.8 Mev. The other three analyzers are set to measure windows about 0.25 Mev wide centered at (1) the 1.46-Mev photopeak of K^{40}, (2) the 1.76-Mev photopeak of Bi^{214} in the U^{238} decay series, and (3) the 2.62-Mev photopeak of Tl^{208} in the Th^{232} decay series (J. Pitkin and J. Hand, written commun., 1966). Outputs from the individual ratemeters are compensated for altitude variations and are recorded on strip charts. Uncompensated outputs from the ratemeters are digitized by means of an analog-to-digital converter in the aircraft and recorded on magnetic tape.

ELECTROMAGNETIC EQUIPMENT

A six-channel Input electromagnetic system, as designed by Barringer (1962), is employed. The source for this system is a large vertical-axis loop energized by half-sine-wave pulses of alternating polarity. The detectors are small vertical- and horizontal-axis loops towed in a "bird" about 300 feet behind and 70 feet below the aircraft. To date the only other types of aircraft which have been used with the Input system are the Canso and the PBY. The Convair installation is almost the same as the Canso installation except that a special high-drag bird is employed. Use of the PBY bird with the relatively high speed Convair

might have led to destructive oscillations of the tow cable and bird.

The "primary" field of the source loop induces eddy currents in the earth which continue to flow for some time following the ends of the primary pulses. The secondary field associated with these eddy currents is sampled at six different times during the interval between pulses by means of six individual gates and associated circuitry. The output of each channel is recorded on a strip chart, and selected channels may be digitized and recorded on magnetic tape.

FLIGHT-PATH RECOVERY SYSTEM

An APN–147 Doppler system operating in the K_e band and having a roll- and pitch-stabilized antenna is the primary means of tracking the path of the aircraft. Outputs from the Doppler system are a frequency which is proportional to the ground speed of the aircraft and a synchro signal, which is the "drift" angle, the difference between the direction of flight and the heading of the aircraft. A C–12 compass system is used to determine the heading of the aircraft. This system can be operated as a gyrocompass having a drift rate of about 1/4° per hour, or the gyro can be slaved by a fluxgate compass so that the system determines magnetic north. The latter mode of operation is ordinarily employed except in areas of large magnetic variations. The output of the compass system is a synchro signal. To obtain the actual track angle of the aircraft, the drift angle is added or subtracted from the compass signal by means of a synchro differential.

The raw Doppler frequency is counted and recorded directly on magnetic tape. An analog signal corresponding to ground speed is available within the Doppler sensor and is recorded on a strip chart when desired. The actual track angle is digitized by means of a synchro-to-digital converter and recorded on tape. Originally a solid state converter was used; it proved to be unreliable so now a servo repeater and shaft encoder are used. The servo repeater also drives a potentiometer which provides an analog signal which is recorded on a strip chart.

Outputs from the Doppler system also are fed to an ASN–35 computer which displays the track of the aircraft relative to any desired starting point. The computer is used principally for pilot guidance. The output of the computer could be digitized and recorded in place of the raw Doppler information; however, the method used allows greater flexibility in flight techniques and yields greater accuracy.

An APN–22 radar altimeter determines the height of the aircraft above terrain with an accuracy of about 5 percent. The output of the altimeter is a synchro signal which drives indicators and a servo repeater. Five potentiometers, which are driven by the repeater, are used in the altitude-compensation circuits for the single-channel gamma-ray analyzers and to provide an analog voltage which is recorded on a strip chart and also is digitized and recorded on tape.

A strip-film camera is used to photograph "documentation" points and to serve as a backup system in case the Doppler system should fail during a flight. Fiducial marks and numbers are placed on the film, on the strip-chart recorders, and on magnetic tape when the documentation-point switch is activated. Additional fiducial marks are automatically placed on the film, strip charts, and magnetic tape at 6-second intervals.

MAGNETIC-TAPE RECORDING SYSTEM

One incremental magnetic tape recorder is used to record the outputs of the magnetometer system, Doppler system, and 10 channels of information from analog sources. The tape unit records at a density of 200 characters per inch on standard 7-track, 1/2-inch magnetic tape. Maximum character-recording rate is 400 characters per second. Selectable odd or even parity is generated by the unit and recorded as the seventh bit of the tape character. Interrecord gaps are recorded automatically on external command from a digital control unit. Slightly more than 4.5 hours of data can be recorded on a standard 2,400-foot reel of tape.

A digital control unit buffers and puts into a format all digital data and generates the necessary commands for recording the data. All digital data are in binary form and are packed into a 192-bit (32 six-bit characters) observation which is recorded every 0.1 second. This recording rate, corresponding to an observation about every 30 feet, is required for adequate resolution of all data during low-level surveying and for accuracy of the Doppler data at all flight elevations.

Because data from the Doppler system and magnetometer are rapidly varying in comparison with the character recording rate, is it necessary to use buffers of flip-flop type in these channels (fig. 2). This allows almost instantaneous sampling and storage of the data channel at the beginning of the observation cycle. The Doppler frequency is digitized by means of a binary counter. At the beginning of the observation cycle, the input is blocked from entering the counter and the counter value is stored in the buffer. After the buffer is loaded, the counter is reset and allowed to resume summing the Doppler frequency until the next observation.

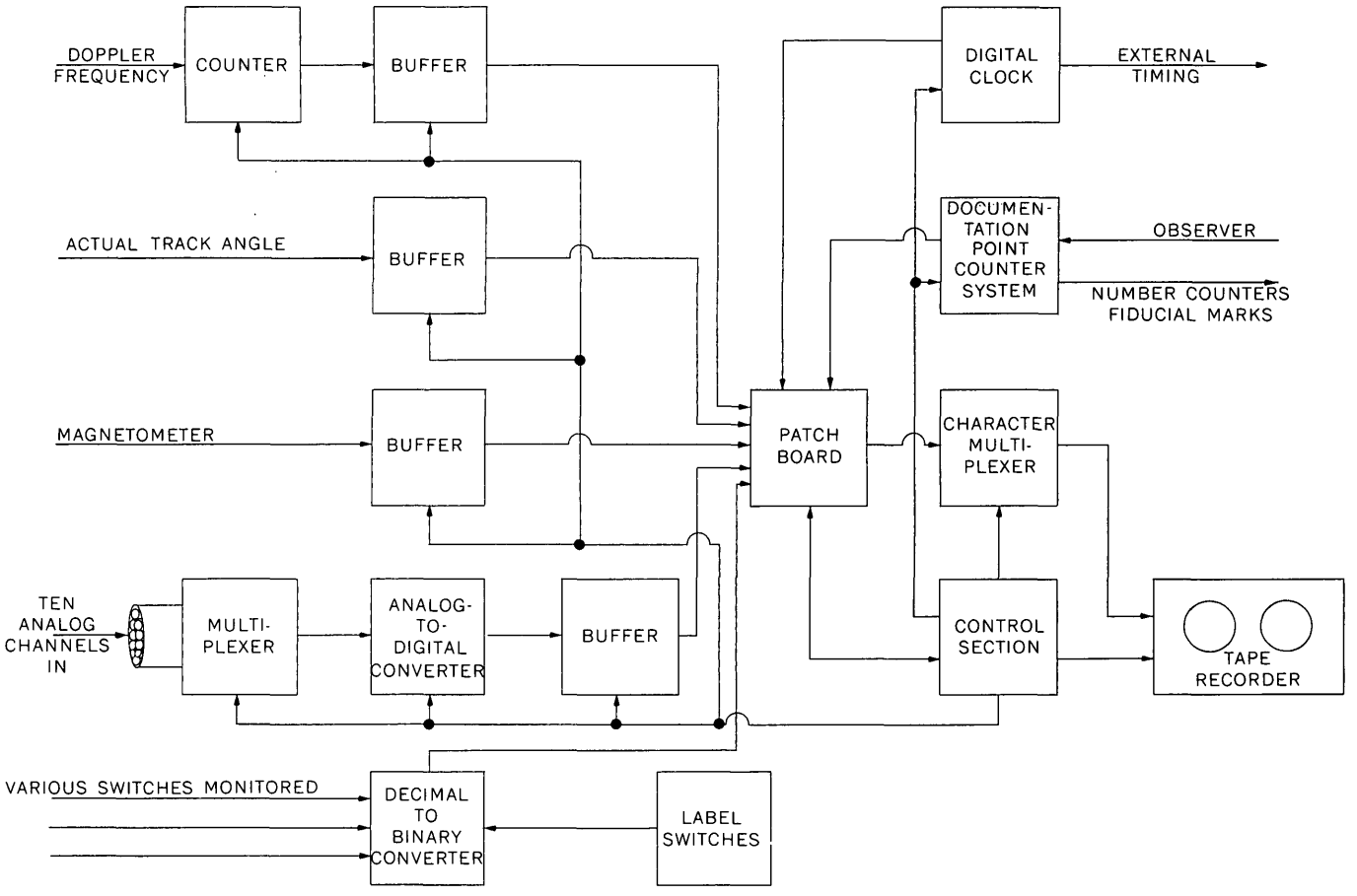

FIGURE 2.—Magnetic-tape recording system.

An analog-to-digital converter selects and encodes each of the 10 analog channels during an observation cycle. After each channel is digitized, the output is buffered allowing the next channel to be digitized while the previous one is being written on tape. The input range of the converter is 0 to 200 millivolts, corresponding to a digitized output of 0 to 255 counts.

Positions of several switches external to the digital control unit, which determine such quantities as the magnetometer sensitivity and base level and sensitivity of the altimeter and other analog channels, are converted to binary form for recording. The positions of switches located on the digital control unit, which are used for identification of the tape, also are converted for recording.

The output from a 12-bit digital clock contained within the control unit is displayed for the operators and is recorded on magnetic tape. Because the clock is synchronous with the recording cycle, buffering is not required. The clock advances every 6 seconds, at which time it provides pulses that activate the aircraft fiducial-mark system.

The documentation point system includes a six-bit counter. When the system is activated, the counter is advanced and at the start of the next observation-recording cycle this counter value is recorded on tape. Also, external mechanical display counters are advanced, and a numbered fiducial mark is recorded on the strip film and strip charts.

All data channels, input to the character multiplexer, and various control functions are connected to the patch-board receptacle. The date are put into format by jumpers on the interchangeable patch boards. At the beginning of each tape, the "tape label" patch board is used to wire the labeling switches to the character multiplexer. A tape-label record of 32 characters, which consists of the date, project number, tape number, and tape type (traverse or base) is recorded on tape. After the label is recorded, the "data" patch board is inserted, which connects the data channels to the character multiplexer, and recording action is started.

Under command of the control section, the multiplexer sequentially selects and transfers the 32 six-

bit characters to the tape recorder and gives a record command. During data recording, 255 observations are recorded for each physical record. Because the tape recorder requires 0.3 second to generate an interrecord gap, three observations are deleted at the end of each record. It should be noted that the Doppler frequency counter remains in operation during this period so that ground-speed information is not lost. The loss of other data during the interrecord gap is rarely significant because the recording rate is much higher than that ordinarily required for all data channels except the Doppler frequency and actual track angle.

A separate tape recorder system (not illustrated in this report) is used to record gamma-ray spectra from the 400-channel analyzer. Output from the digital clock in the main system is recorded on the radiation system in order that the radiation data can be related to the flight path. The radiation-recording system is highly specialized and will not be described in further detail.

OPERATIONAL TECHNIQUES AND DATA PROCESSING

The desired flight lines are laid out on two sets of maps or photomosaics. In most cases the pilots use one set of maps or mosaics in following the flight lines. However, in areas where recognizable landmarks are scarce, the ASN–35 computer for the aircraft Doppler system is used for pilot guidance. The documentation-point system is activated every 20–40 miles over an easily recognizable point by a member of the crew. Besides being recorded on the strip film, magnetic tape, and strip charts, the points are plotted as accurately as possible on a set of the maps using a drift sight. This aids in plotting the locations of the documentation points from the strip film to maps; sometimes the observer's points are used directly in the data processing. Base or drift lines are flown across the traverse lines for correction of diurnal and instrumental drift. For large projects, base lines are closed on themselves. In addition to the base lines, a short test line is selected in a magnetically flat area near the project and flown at the beginning and end of each flight.

Data tapes from the aircraft are read directly into a digital computer as input to the DIAGNOSIS program (fig. 3), where the data are checked for possible errors. Errors such as tape parity and improper sequence of clock or documentation-point counters are listed in terms of their position on tape. Long sequences of abnormal data which may indicate equipment malfunctions are listed.

The listings from the DIAGNOSIS program are examined, and if there are no serious errors or suspected erroneous data, the tape goes directly as input to the REDUCTION program. If some of the data are erroneous, they are corrected by means of one of several CORRECTION programs. If, for instance, part of the Doppler data from a flight are erroneous, the corresponding

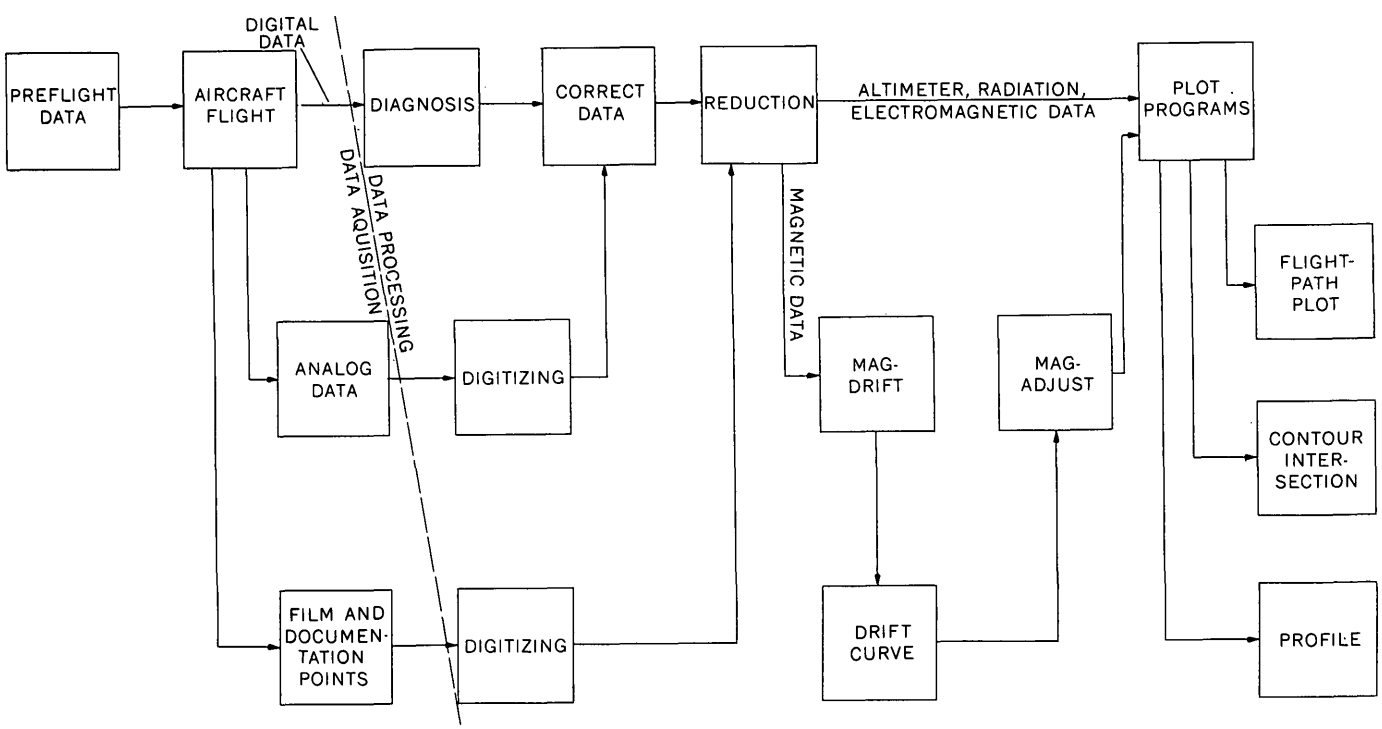

FIGURE 3.—Generalized data flow diagram.

part of the flight path is plotted from the strip film, digitized by means of an X–Y digitizer, and inserted in place of the erroneous Doppler data. Erroneous magnetometer data or other data are handled in a similar manner using data from the strip charts.

Documentation points are plotted on maps from the strip film, and their coordinates are digitized in terms of latitude and longitude. The documentation points plus the original or corrected data tape are the input to the REDUCTION program. In this program, magnetometer and other data are converted to gammas, counts per second, or other appropriate units. Each Doppler observation represents the small segment of the flight path between observations. Starting at a documentation point, these small segments are summed vectorially to obtain the position of the aircraft. Linear corrections are made to the Doppler flight path so that each end of the portion of the path between documentation points fits the points exactly. After all data have been adjusted, they are converted to latitude and longitude coordinates.

From the REDUCTION program all data except magnetic are processed directly by various plotting programs. Magnetic and flight-path data are input to the MAG-DRIFT program which locates the intersections of the traverse lines with the base lines and calculates the difference between the base-line and the traverse-line magnetic readings at these intersections. These differences are plotted out as a function of digital time. If the resulting drift curve appears to be normal, the data tape and the drift curve are used directly as inputs to the MAG-ADJUST program. If the drift curve appears to include some abnormal points, the data are examined in the vicinity of these points to determine the cause. The most common reason for erroneous points is an extreme magnetic gradient in the vicinity of the intersection. In such cases the curve is adjusted before being used.

In the MAG-ADJUST program, linear corrections are applied as a function of time along the traverse lines so that the traverse-line values match the base-line values at their common intersections. The MAG-ADJUST program also lists minimum and maximum values of intensity for later use in plotting profiles

The FLIGHT PATH PLOT program projects the latitude and longitude coordinates of the path into cartesian coordinates for output to an X–Y plotter. The flight path can be plotted out at any standard map scale together with the location of documentation points and 1-minute intervals of time along the flight path.

Using any desired contour interval, the locations of the intersections of contours with the flight lines are calculated by the CONTOUR INTERSECTION program. Those intersections plus the location and values of the maximums and minimums are projected and plotted. The flight path may be superimposed upon this plot.

The PROFILE program converts the time base of magnetic or other data to a distance base and plots the results in the form of nested profiles. Any desired horizontal or vertical scale can be used.

Final contouring of aeromagnetic maps is done by hand. It is hoped that a suitable automatic contouring program can be devised. The gridding routines used with presently available contouring programs disregard most of the data along flight lines. This is acceptable in contouring some high-altitude surveys but is not acceptable in low-level surveys over near-surface magnetic rocks.

Programs (not shown in figure 3) are available for filtering of magnetic profiles. Programs which will correct electromagnetic and radiation data for altitude variations are being developed.

REFERENCE

Barringer, A. R., 1962, New approach to exploration—the Input airborne electrical pulse prospecting system: Mining Cong. Jour., v. 48, no. 10, p. 49–52.

A SEISMIC AND GRAVITY PROFILE ACROSS THE HUECO BOLSON, TEXAS

By ROBERT E. MATTICK, Denver, Colo.

Work done in cooperation with the city of El Paso, Tex., and the Texas Water Development Board

Abstract.—In February and March, 1966, the U.S. Geological Survey obtained seismic and gravity data on a 20-mile profile extending from the base of the Franklin Mountains to near the base of the Hueco Mountains near El Paso, Tex. The geophysical data indicate that a deep structural trough bounded on the west by a large normal fault and filled with unconsolidated Hueco bolson deposits parallels the base of the Franklin Mountains. The maximum thickness of the Hueco bolson fill in the center of this trough is calculated to be about 9,000 feet.

The Hueco bolson is in the extreme western part of Texas and southernmost New Mexico. The area includes parts of El Paso County, Tex., and Dona Ana and Otero Counties, N. Mex. In February and March, 1966, the U.S. Geological Survey conducted geophysical surveys(gravity, seismic, and resistivity) in the Hueco bolson area near El Paso, Tex. The purpose of the surveys was to obtain data that could help resolve some of the existing ground-water problems in the area. In cooperation with the U.S. Geological Survey, the city of El Paso drilled a test well to a depth of 4,363 feet to aid in the interpretation of the geophysical data. This paper is concerned with the results of a 20-mile seismic-refraction and gravity profile that extends across the Hueco bolson from the base of the Franklin Mountains to near the base of the Hueco Mountains (fig. 1).

GENERAL GEOLOGY

The description of the general geology of the Hueco bolson area has been compiled mainly from the following sources: King (1935), Knowles and Kennedy (1956), Nelson (1940), Richardson (1909), and Sayre and Livingston (1945).

The Hueco bolson is a typical bolson by definition. It is a broad gently tilted intermontane lowland bounded on the west by the Franklin Mountains, on the east by the Hueco Mountains, and on the north, about 12 miles north of the Texas–New Mexico border, by the Tularosa Basin, which is another large intermontane basin. The Hueco bolson extends southward into Mexico where it is bounded by a part of the Sierra Madre Oriental chain of Mexico.

The Franklin Mountains extend northward from just north of El Paso to about 4 miles north of the

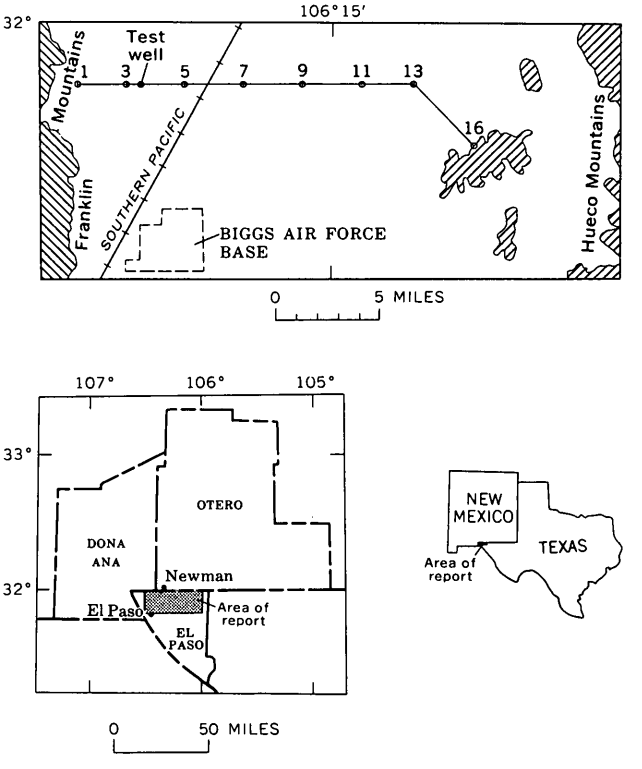

FIGURE 1.—Index map showing location of the seismic and gravity profile and intermediate shotpoints. Pattern indicates upland areas.

Texas–New Mexico border. These mountains are typical eroded block mountains. According to Nelson (1940), the Paleozoic stratigraphic section of the Franklin Mountains is approximately 8,000 feet thick and includes rocks of the Cambrian, Ordovician, Silurian, Devonian, Mississippian, Pennsylvanian and Permian Systems. These Paleozoic sedimentary rocks rest in places on Precambrian rocks, represented by the Red Bluff Granite of Nelson (1940) and Lanoria Quartzite of Richardson (1909).

The Hueco Mountains, like the Franklin Mountains, are composed mostly of stratified sedimentary rocks (predominantly limestone) of Paleozoic age. According to King and others (1945), the oldest rocks of the Hueco Mountains are red granites of Precambrian age.

Richardson (1909) concludes that during the Tertiary Period the Franklin and Hueco Mountains were uplifted and the Hueco bolson was formed between them as a deep structural trough. The subsequent history of the area has been erosional removal of Cretaceous deposits from the Franklin and Hueco Mountains and the filling of the adjacent basin with a great thickness of later Tertiary and Quaternary deposits.

The floor of the Hueco bolson near the base of the Franklin Mountains is topographically lower by about 300 feet than the basin floor near the base of the Hueco Mountains. King (1935, p. 254) has suggested that this gentle slope of the basin floor may be the result of tilting along a fault plane near the base of the Franklin Mountains. The present study shows that this conclusion is supported by geophysical evidence.

The unconsolidated Tertiary and Quaternary sediments of the Hueco bolson are mostly gravel, sands, and clays. According to Sayre and Livingston (1945, p. 45) these were probably deposited by occasional torrential streams and sheet wash from the adjacent Franklin and Hueco Mountains. The deepest well in the area, drilled about 2 miles south of Newman, N. Mex. (fig. 1), was reported by King (1935) to have penetrated unconsolidated deposits to a depth of 4,920 feet.

FIELD PROCEDURES

Seismic

Four reversed lines, each about 5 miles in length, were shot along the profile shown in figure 1. Twelve vertical seismometers were spaced 650 feet apart on a cable extending 7,150 feet along the profile. Recording was on photographic paper. The scheme for shooting each 5-mile line was as follows: First the cable was laid at one end of the profile and the output from a dynamite charge exploded at each end of the line was recorded. Then the cable was moved forward 7,150 feet and the previously used shotpoints at each end of the line were reloaded and reshot. This procedure of moving the cable and reshooting at the same shotpoints was continued until the entire distance along the line was covered. In addition, intermediate shots at about 7,150-foot intervals were used to record velocity changes in the near-surface sediments. The dynamite charges varied from 50 to 600 pounds and were loaded in holes dug to a depth of about 14 feet with a backhoe.

Gravity

Gravity measurements were made along the seismic profile with a Worden gravimeter at intervals approximately half a mile apart. A gravity station at the El Paso airport, reported by Behrendt and Woollard (1961), was used as a datum. A density of 2.67 grams per cubic centimeter was used in computing the Bouguer anomaly, and the values were corrected to a sea-level datum. Terrain corrections were made through zone I using the Hayford-Bowie system as modified by Swick (1942) for those stations located near the Franklin and the Hueco Mountains. The largest terrain correction was about 1 milligal. Horizontal control was determined by odometer readings between section corners spaced at 1-mile intervals. Vertical control was obtained from bench marks, spot elevations, and interpolation between map contours where the contour interval was 5 feet. Theoretical gravity was computed from the international formula. Messrs. Donald L. Peterson and Dallas Jackson, of the U.S. Geological Survey, performed the gravity fieldwork and reduced the data.

TEST WELL

A deep test well, located near the west end of the profile (fig. 1), was drilled by the city of El Paso in cooperation with the Geological Survey to aid in the interpretation of the geophysical data. The well did not penetrate to the basement and was bottomed in unconsolidated Hueco bolson deposits at a depth of 4,363 feet beneath the surface (Marvin Davis, U.S. Geological Survey, oral commun., 1966). The sonic log of this well was made available to the author, and a plot of average velocity against depth is shown in figure 2. The plot shows six velocity zones of sufficient thickness to be "seen" by seismic waves.

SEISMIC RESULTS

Field seismograms were of good quality and show easily identifiable first arrivals on most of the records. No attempt was made to determine second and later arrivals. The traveltimes from shotpoint to seismometers were picked to the nearest 0.005 second.

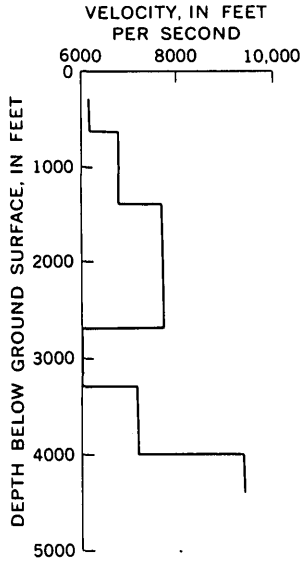

FIGURE 2.—Graph showing average velocity of P waves as a function of depth (taken from sonic log of deep test well drilled by the city of El Paso).

Traveltime curves were constructed for each of the four lines constituting the 20-mile traverse (fig. 3), and velocities were determined by visual fitting of straight-line segments to the traveltime data. In most places the ground level along the profile remained relatively constant and no corrections for elevation were necessary. The first-arrival times on all the traveltime curves show an intercept on the time axis ranging from about 0.18 to 0.25 seconds. This intercept time can be explained by the presence of a thin layer (about 250 feet thick) of low-velocity weathered material (weathering layer). The base of this layer probably corresponds to the top of the water table.

Conventional seismic-interpretation techniques were used in calculating depths and dips of the different refracting zones. Along the east half of the seismic profile (near the Hueco Mountains), where the basin fill is relatively thin, the method of Hawkins (1961) was used. For the remaining part of the profile, where the depths to "basement" are of the order of several thousands of feet and where the overlying material consists of several refracting horizons, the method of Slotnick (1950) was used. In all cases the final interpretation was checked by fitting theoretical ray paths to the computed model.

Figure 3 is a plot of first-arrival times (shotpoint to geophone) against distance. Shotpoints are situated about 7,000 feet apart. The westernmost (shotpoint 1) is located about 2,200 feet east of a granite outcrop at the base of the Franklin Mountains. The easternmost shotpoint (shotpoint 16) is located about 50 feet northwest of a limestone outcrop near the Hueco Mountains.

A study of the time-distance plot reveals a difference in the character of the plot west of shotpoint 9 as compared with that east of it. This difference is attributed to the fact that east of the point, the basin fill is composed of a single refracting unit, whereas to the west the unconsolidated Hueco bolson deposits are composed of several refracting horizons (as shown by the drill data from the El Paso well).

Shotpoints 9–16

Interpretation of the seismic data along the east part of the profile is relatively straightforward and can be interpreted as a "simple two-layer case." Reference to the time-distance plot shows that the P-wave velocity through the unconsolidated Hueco bolson deposits between shotpoints 9 and 16, as measured along nine spreads, ranges from 6,250 feet/sec to 6,950 feet/sec. However, at shotpoint 13 the overburden arrivals were recorded on only two geophones, and at shotpoint 14 on one geophone. Hence, it is reasonable to disregard these two measurements. The remaining seven velocities range from 6,440 to 6,950 feet/sec, and average about 6,570 feet/sec. In the final computations the latter velocity was assumed to remain constant from shotpoint 9 to shotpoint 16.

Between shotpoints 9 and 13 the apparent velocity, measured in the westward direction, of the deepest recorded refractor is about 13,700 feet/sec, whereas the apparent velocity measured in the reverse direction is about 20,200 feet/sec. Hence, a true velocity for this refractor is computed to be about 16,500 feet/sec. In the same manner, between shotpoints 13 and 15, and between 14 and 16, the true velocity of the deeper refractor is calculated to be about 15,900 feet/sec and 15,700 feet/sec, respectively. An average of the three velocities is about 16,100 feet/sec ($\pm$ 2.5 percent difference). This latter velocity was used in the final computations and assumed to remain constant from shotpoint 9 to shotpoint 16.

The method of Hawkins (1961) was used to calculate depths between shotpoints 9 and 16. This method yields depth estimates at 650-foot intervals (equal to geophone spacing). The computed cross section on figure 4 shows the thickness of the unconsolidated Hueco bolson deposits.

Shotpoints 1–9

The sonic log of the El Paso test well located east of shotpoint 3 shows six distinct velocity zones in the upper 4,363 feet. Figure 2 is a graph showing the variation of the average velocity as a function of depth as recorded in this well. An examination of the graph

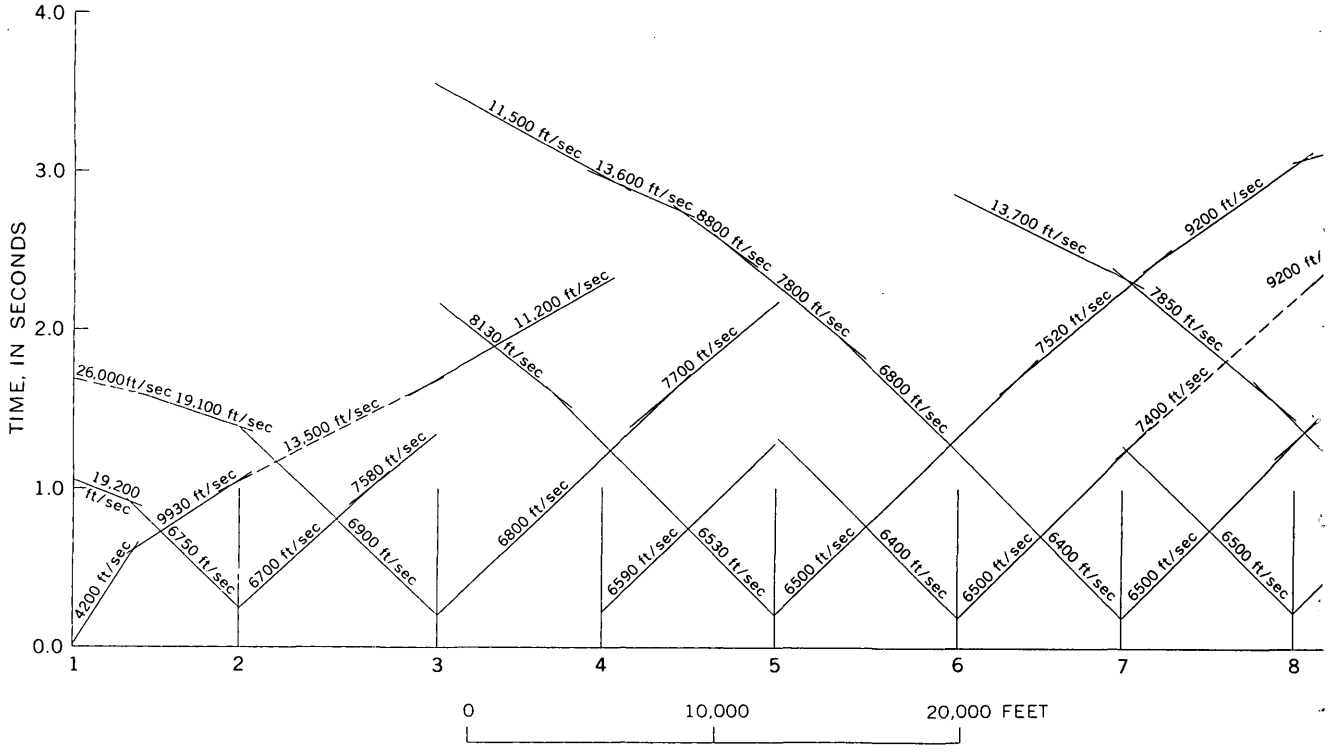

indicates the following: The near-surface 6,200-feet/sec layer might be "overlooked" in seismic profiling owing to its small thickness in comparison to the geophone spacing. Also, the 6,000-feet/sec and 7,200-feet/sec layers recorded in the well at depths of about 2,700 and 3,300 feet, respectively, will be "masked" on a time-distance plot. This is due to the relatively higher velocity layers directed above and below these layers. Let us now assume that the 9,400-feet/sec layer at a depth of about 4,000 feet extends down to the top of the "basement" surface, and that the velocities shown by the well data represent an average section along the west half of the seismic profile. If these assumptions are correct, then a seismic refraction time-distance plot would reveal four distinct velocity zones with the following velocities: 6,800 feet/sec, 7,700 feet/sec, 9,400 feet/sec, and a higher velocity representing waves refracted along the "basement" surface.

Inspection of the obtained time-distance plot (fig. 3) supports the hypothesis that four distinct velocity zones are present. Between shotpoints 1 and 4 the near-surface recorded velocity is about 6,800 feet/sec, and between shotpoints 1 and 9 the near-surface recorded velocity is about 6,500 feet/sec. From shotpoints 2, 3, 5, 6, 7, and 9, apparent velocities ranging from 7,400 feet/sec to 8,130 feet/sec (with an average velocity of about 7,700 feet/sec) were recorded immediately after the 6,800 and 6,500 feet/sec arrivals. Similarly, after the 7,700-feet/sec arrivals, the time-distance plots from shotpoints 5, 6, and 7 show apparent velocities of about 9,200 feet/sec, and 8,800 feet/sec, respectively. An average of these three velocities is about 9,100 feet/sec (about 3 percent lower than the assumed 9,400 feet/sec). Hence, the above velocities recorded on the time-distance plot are seen to be in good agreement with those expected from the study of the sonic log.

Higher apparent velocities (between about 11,000 and 13,000 feet/sec) were recorded when shooting eastward from shotpoint 1 and westward from shotpoint 7. Because of the crossover of these velocity segments (between shotpoints 3 and 4) it might be reasonable to hypothesize the existence of a nearly flat lying layer with a velocity of about 12,000 feet/sec. The computed depth to such a zone would be about 3,000 feet. As already shown, however, a 12,000-feet/sec velocity at a depth of less than 4,400 feet is inconsistent with the velocity data gathered from the El Paso well. Furthermore, a velocity of about 12,000 feet/sec is normally indicative of an indurated sedimentary rock with low porosity. Resistivity data obtained by vertical electri-

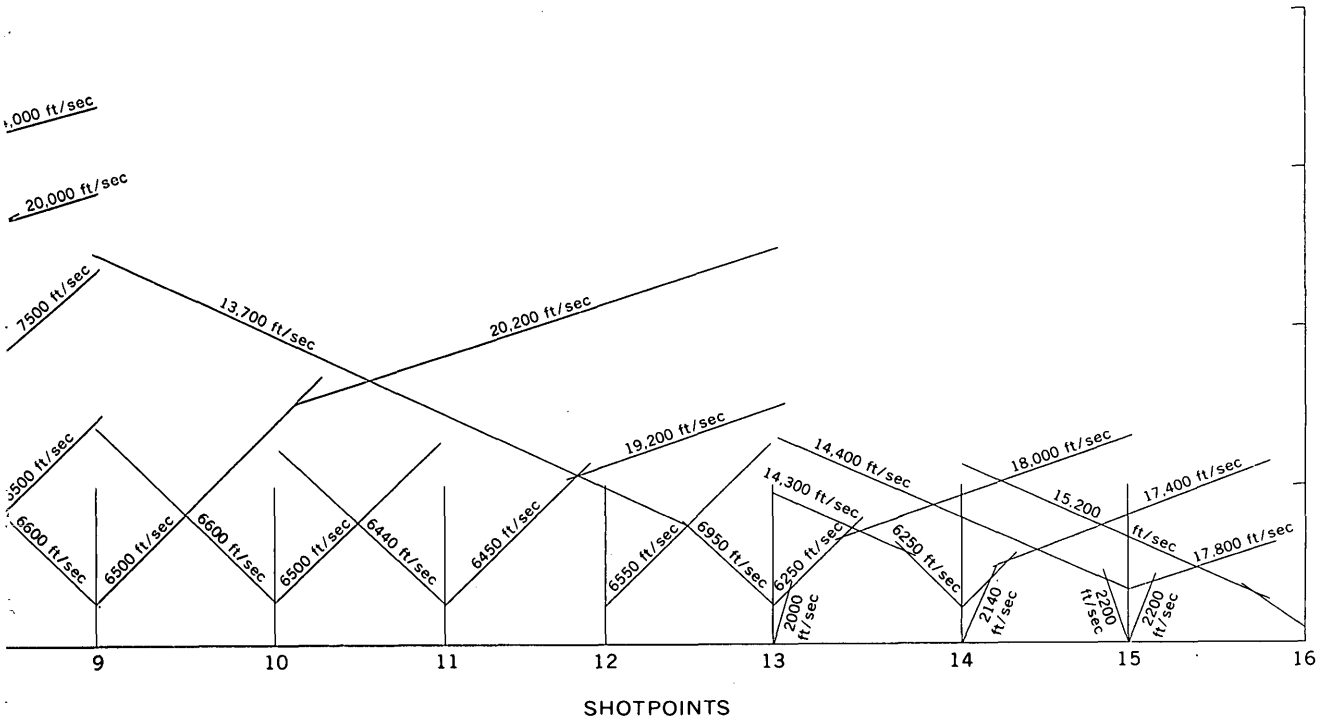

FIGURE 3.—Seismic refraction time-distance plot, showing first arrivals. Dashed lines indicate where records were of poor quality and arrival times were inferred.

cal soundings in this area suggest that the minimum depth to such a horizon is greater than 7,000 feet (Zohdy, 1966). Hence, an alternative interpretation of the seismic data which is consistent with all the other data considers that the segments of the velocity curve with velocities of about 12,000 feet/sec represent seismic waves traveling downdip on the "basement" surface. If it is assumed that the true velocity of the P waves through this surface is about 16,000 to 17,000 feet/sec (a reasonable assumption for either limestone or granitic rock), then the 12,000-feet/sec velocities recorded in both an eastward and westward direction suggest that the seismic waves traveled downdip on the limb of a syncline. The axis of this trough, as shown on the cross section, would be located at about shotpoint 4.

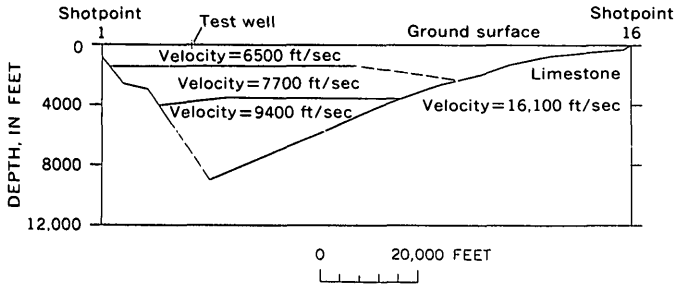

FIGURE 4.—Seismic cross section showing velocity distribution in unconsolidated bolson deposits.

The hypothesis that the high-velocity interface dips eastward from shotpoint 1 and westward from shotpoint 9 is substantiated by the fact that velocities of more than 20,000 feet/sec were recorded (refer to fig. 3) at shotpoints 1 and 9 when shooting from shotpoints 3 and 5, respectively. Several computed P-wave travel paths originating at a shotpoint and traveling along the "basement" surface to a geophone were computed. The traveltimes used along these paths, as computed from the cross section, were in good agreement with the actual arrival times at the corresponding geophone.

GRAVITY DATA

Figure 5 shows the observed gravity anomaly. At the west end of the profile near the base of the Franklin Mountains, the gravity values are about—124 mgals. At the opposite end of the profile, near the Hueco Mountains, the gravity values are about —136 mgals. The axis of a wide gravity minimum of about 40 mgals occurs near the west-center of the profile. Comparison of the observed gravity with the computed seismic cross section shows that the axis of the gravity minimum is located about 3½ miles east of the thickest computed section of unconsolidated Hueco bolson

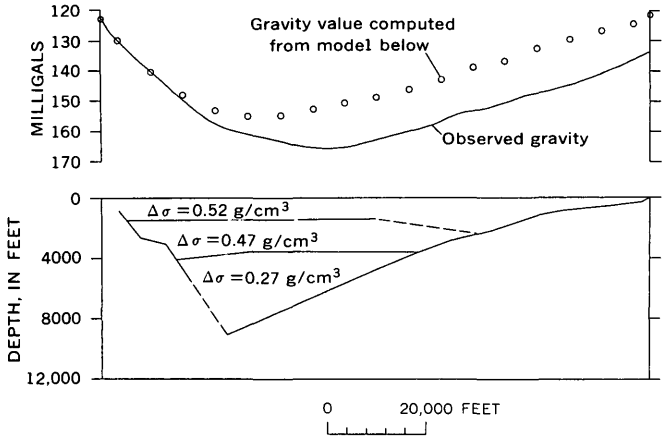

FIGURE 5.—Cross section of unconsolidated bolson deposits, showing assumed relative density distribution, observed gravity, and computed gravity due to bolson deposits.

deposits. This large offset suggests that the source of the gravity low cannot be attributed entirely to the low-density Hueco bolson deposits.

The computed gravity anomaly due only to Hueco bolson deposits as calculated from the seismic cross section is shown in figure 5. Because density is one of the physical parameters that determine seismic velocity, the recorded seismic-velocity distribution was used as a basis for density estimation. Four densities of 1.55, 2.15, 2.20, and 2.40 g/cm³ corresponding to recorded velocities of 2,000, 6,500, 7,700, and 9,400 feet/sec were used. The density estimations are from empirical density-velocity relations for clastic sediments compiled by Woollard (1962). The density of underlying Precambrian basement rocks was assumed to be 2.67 g/cm³.

The computed anomaly due to the unconsolidated Hueco bolson deposits and the observed gravity are in good agreement at the west end of the profile. Along the remainder of the profile, however, there is an apparent discrepancy or residual anomaly of about 15 mgals. If one assumes a flat regional gradient, the pinching out of the residual anomaly near the west-center of the profile suggests that the source of this anomaly is a wedge-shaped body. Because the measured velocity in the Hueco bolson deposits seems to remain horizontally constant along the western half of the profile, it is reasonable to assume that the source of the residual anomaly is located below the Hueco bolson deposits. A reasonable assumption is that this anomaly can be attributed to a density difference between the prebolson sedimentary rocks and the underlying Precambrian basement rock. For this assumption an idealized cross section can be constructed.

A maximum estimate of thickness of prebolson deposits (precluding the occurrence of Cretaceous deposits) is about 8,000 feet (Robert L. Harbour, U.S. Geol. Survey, oral commun., 1966). Although the thickness of the prebolson deposits is undeterminable from existing geophysical data, an estimation of this thickness will allow the shape of the body causing the residual anomaly near the west center of the profile to be computed. An estimated thickness of 10,000 feet was used to compute an idealized model.

In order to account for the difference between the computed anomaly due to the unconsolidated bolson deposits and the observed gravity anomaly, the density difference between the estimated 10,000 feet of prebolson rocks and the underlying Precambrian rock must be about 0.12 g/cm³. It should be noted that an increase or decrease of this density difference would allow the estimated thickness of the prebolson deposits to be decreased or increased, respectively. The resulting cross section is shown in figure 6. This idealized model, which assumes a relatively flat regional gradient, with the prebolson deposits wedging out against a fault dipping eastward at about 25°, is consistent with the observed gravity anomaly.

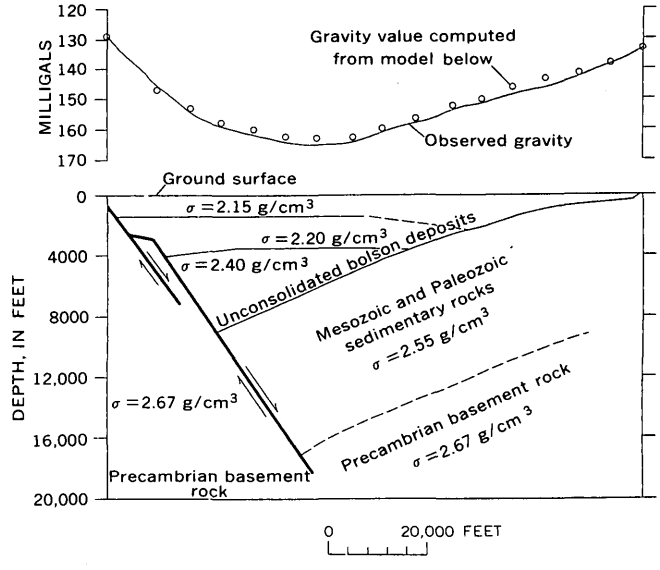

FIGURE 6.—Complete cross section, showing assumed density distribution, observed gravity, and gravity anomaly computed from model.

REFERENCES

Behrendt, J. C., and Woollard, G. P., 1961, An evaluation of the gravity control network in North America: Geophysics, v. 26, no. 1, p. 57–76.

Hawkins, L. V., 1961, The reciprocal method of routine shallow seismic refraction investigations: Geophysics, v. 26, no. 6, p. 806–819.

King, P. B., 1935, Outline of structural development of trans-Pecos Texas: Am. Assoc. Petroleum Geologists Bull. v. 19, p. 221–261.

King, P. B., King, R. E., and Knight, J. B., 1945, Geology of Hueco Mountains, El Paso and Hudspeth Counties, Texas: U.S. Geol. Survey Oil and Gas Inv. (Prelim.) Map 36.

Knowles, D. B., and Kennedy, R. A., 1956, Ground-water resources of the Hueco bolson, northeast of El Paso, Texas: Texas Board of Water Engineers Bull. 5615, 265 p.

Nelson, L. A., 1940, Paleozoic stratigraphy of Franklin Mountains, West Texas: Am. Assoc. Petroleum Geologists Bull. v. 24, p. 157–172.

Richardson, G. B., 1909, Description of the El Paso district [Texas]: U.S. Geol. Survey Geol. Atlas, Folio 166.

Sayre, A. N., and Livingston Penn, 1945, Ground-water resources of the El Paso area, Texas: U.S. Geol. Survey Water-Supply Paper 919, 190 p.

Slotnick, M. M., 1950, A graphical method for the interpretation of refraction profile data: Geophysics, v. 15, no. 2, p. 163–180.

Swick, C. H., 1942, Pendulum gravity measurements and isostatic reductions: U.S. Coast and Geod. Survey Spec. Pub. 232, 32 p.

Woollard, G. P., 1962, The relation of gravity anomalies to surface elevation crustal structure and geology: Wisconsin Univ. Geophys. and Polar Research Rept Series, Rept 62–9, p. 41–43.

Zohdy, Adel, 1966, Geoelectrical exploration for ground water in the southwestern United States [abs.]: Geophysics, v. 31, p. 1216.

269-274 O—67——7

THE U.S. GEOLOGICAL SURVEY–LaCOSTE AND ROMBERG PRECISE BOREHOLE GRAVIMETER SYSTEM—INSTRUMENTATION AND SUPPORT EQUIPMENT

By T. H. McCULLOH [1]; L. J. B. LaCOSTE [2]; J. E. SCHOELLHAMER, and E. H. PAMPEYAN, Pasadena, Calif.; Austin, Tex.; Menlo Park, Calif.

Abstract.—A special modification of the LaCoste and Romberg astatized spring-type geodetic meter is the gravity sensor of the precise borehole gravimeter system. The sensor and certain support components are insulated and operate normally at a thermostatically controlled 101°C. Power, telemetry, and control signals are transmitted through a 13-conductor double-armored cable to a 46-in.-long and 5.5-in.-diameter instrument package that is housed in a steel cylinder with an outside diameter of 6.453 in. and capable of withstanding up to 4,000 psi. An electrically driven and controlled wire-line hoist permits stopping the gravimeter exactly at any point marked on the cable and provides continuously variable cable speeds of 12–400 fpm. Heavy damping of the gravimeter beam and the generally quiet conditions in the borehole permit the gravimeter to be leveled and read remotely in the unanchored sonde. When gravity and depth measurements are carefully made and reduced, the usual overall precision of gravity determinations is better than 0.016 mgal for all depths. A single gravity reading requires less than 10 and generally 3–5 minutes.

Some of the many potential uses of borehole gravimetry were recognized long ago (Airy, 1856; Lorenz, 1938; Smith, 1950) and were partly illustrated by early reports of gravity measurements made in mine shafts (Jung, 1939; Hammer, 1950; Cook and Thirlaway, 1951) with manually operated surface gravity meters. Despite these theoretical and experimental studies, the severe constraints imposed by the small sizes and high temperature ranges of most boreholes (Dolbear, 1959) delayed development of a working borehole gravimeter until the early 1950's.

Gilbert (1952) first described a successful field test of a borehole gravimeter. A specially constructed vibrating-filament instrument package of moderate size (5 in. outside diameter) and low precision (±0.7 milligal or lower) was tested to a depth of 1,226 feet in a well in Eakring, Nottingham, England. Lukavchenko (1962) reported the results of experiments using an even larger (175-millimeter OD) astatized quartz-spring gravimeter in Russian wells down to 1,200 meters and with an apparent precision ranging between ±0.3 and ±1.6 mgal. Goodell and Fay (1964) described a vibrating-filament instrument of moderate size (4.5-in. OD) and low precision (about ±0.5 mgal) which was developed entirely independently of Gilbert's instrument; it has been field tested to depths of at least 10,000 feet in the gulf coast of the United States. Although this instrument is an unquestioned advance over the other two instruments, the long reading time (20 minutes per measurement), the high drift rate (necessitating two measurements for one observation), and the low precision combine to make the Goodell and Fay instrument appear impractical. Lastly, Howell and others (1965; 1966) and Oil and Gas Journal (1966) reported a third vibrating-filament gravimeter of small size (4-in. OD), high precision (±0.012 mgal), and low drift characteristics, but slow reading speed (20 minutes or more per observation). Of these four borehole gravimeters, only the one described by Howell and others appears to be sufficiently precise for most industrial applications.

The purpose of this report is to describe another novel borehole gravimeter. This instrument is relatively large (about 6-in. OD), and has high precision (about ±0.016 mgal) and high reading speed (10 minutes or less per reading). The gravity sensor is a

[1] Present address: Chevron Research Co., La Habra, Calif.
[2] LaCoste and Romberg, Inc.

U.S. GEOL. SURVEY PROF. PAPER 575-D, PAGES D92-D100

specially modified LaCoste and Romberg geodetic gravimeter (number G–95) designed and fabricated as an experimental prototype for the U.S. Geological Survey. It is of the astatized spring type, and although its size restricts somewhat the range of its usefulness, the high precision and quick reading characteristics of this experimental model indicate that it has potential industrial value. Future developments could result in a decrease in size without loss of speed or precision if sufficient incentives are provided.

Acknowledgments.—Persons and organizations that have contributed significantly to the successful design and development of the instrument system described are more numerous than can be recounted here. Particularly important contributions were made by A. W. Sanders and H. B. Parks of LaCoste and Romberg, Inc., Victor Reyna of the Reyna Electric Works, L. H. Austin of the U.S. Geological Survey, M. P. Wennekens of the Office of Naval Research, J. C. Taylor of the Shell Oil Co., Harley Latson of the Dia-Log Co., Cliff Strozier and W. C. Humfeldt of Lane Wells, Inc., Verlin Stanton, M. E. Kliewer of Baker Oil Tools, Inc., R. J. Brown of the Apex Machine Works, and the Christian Manufacturing Engineers.

Appreciation is also expressed to R. P. Sharp and the Division of Geological Sciences of the California Institute of Technology. Finally, financial assistance earlier granted the senior author by the Research Corporation helped stimulate work leading toward this development.

HISTORY AND BASIS OF THE GRAVIMETER DEVELOPMENT

The impetus for the development of the instrument system described here arose mainly from insight gained from investigations of the rocks and structures of the Los Angeles basin of California and their gravimetric effects (McCulloh, 1957, 1960), a part of a larger U.S. Geological Survey investigation of the geology of the Los Angeles basin (Yerkes and others, 1965).

Awareness in the late 1950's of the desirability of using a high-precision borehole gravimeter for evaluating conclusions reached from laboratory measurements of core samples intensified by the early 1960's to a conviction that such an approach was essential. By late 1963, it seemed apparent to the senior author that the LaCoste and Romberg geodetic gravimeter might be suitably modified for this purpose, and experiments undertaken at his initiative at sea in deep water (Beyer and others, 1966) showed that control of the gravimeter and telemetry was possible through 4,000 feet of multiconductor cable.

Consequently, early in 1964, simultaneous decisions (in which Arnold Romberg of LaCoste and Romberg, Inc., and V. E. McKelvey of the Geological Survey played important roles) were made to undertake experiments to determine whether a LaCoste and Romberg "zero-length spring"-beam-microscrew assembly could be built to operate at 100°C, and to begin planning of the support equipment that would be required to operate and test such an instrument in the field.

By late spring of 1964 auxiliary and support equipment was being designed and acquired, and experiments by LaCoste and his staff (particularly A. W. Sanders) were sufficiently encouraging to justify initiation of designs of components such as gimbals, levels, electronic control, and telemetry elements. By this time it was apparent that the downhole cylindrical instrument package could have a diameter of 5.5 inches, that the gravity sensor could be thermostated at about 100°C and leveled in gimbals permitting operation through instrument angles approaching 7½° from the vertical, and that a 13-conductor armored cable would supply power, control, and telemetry. It was also agreed that a precision of ±0.01 mgal should be a prime objective.

In the early summer of 1965, gravimeter G–95, electrically heated and thermostated to operate at 101°C underwent laboratory and field calibration while support equipment was being completed. Semifinal tests of the support equipment and calibration of depth-measuring equipment took place late in 1965, while the gravity sensor was being tested in the laboratory. The first field tests of the entire system took place in late January 1966, almost 2 years from the date that the decision was made to attempt to design and construct the system. Two months later, after minor modifications of the control electronics, preliminary laboratory and field tests had shown that the system had met nearly all specifications and exceeded most expectations.

THE INSTRUMENT SYSTEM

Two basic quantities, gravity or gravity differences and depth or depth differences, must be measured by any instrument system intended to be used for the determination of gravity in boreholes. Additionally, measurements of both gravity and of depth made in a borehole that deviates strongly from vertical may require corrections for the effects of such deviations. The precision with which the quantities (and any cor-

rections to them) should be measured depends upon the overall precision desired in the determination of gravity and upon those factors that ultimately limit overall precision, such as precision of the gravity sensor and the precision of depth-measuring equipment in relation to the underground vertical gradient of gravity.

A borehole gravity meter system should therefore consist of a gravity sensor suitably encased in a protective housing, provision for instrument control and data transmission or storage, equipment designed to provide precise measurements of depth, a suitable cable and winch for lowering and hoisting the sonde, and related support equipment. The following pages describe the important features of the instrument system assembled for the first field tests of the Geological Survey's borehole gravity meter. Alternative designs are numerous and the system described could doubtless be improved.

The gravity sensor and associated components

The heart of the borehole gravity meter system is the LaCoste and Romberg geodetic model gravity meter G–95, especially constructed to be heated and operated at a thermostated temperature of 101°C. As the instrument location is changed, a mass that is attached to the end of a horizontal beam supported by a "zero-length spring" (U.S. Patent No. 2,293,437) and which pivots about shock-eliminating springs is deflected from its null position in response to changes in gravity. A micrometer screw acting on lever systems (U.S. Patent No. 2,377,889) that support the zero-length spring is used to null the beam and measure the beam deflection. The beam is heavily damped (U.S. Patent No. 2,977,799) to permit operation in the presence of seismic motion and, when adjusted to almost infinite sensitivity, is very quick to null and read because it functions in the manner discussed by Nettleton and others (1962, p. 4399).

The beam-spring suspension is compensated for atmospheric pressure changes and, together with the measuring screw and the beam arrestment system, is mounted inside an aluminum box that is sealed by O-rings against such pressure changes. The box and its contents are heated electrically by external Nichrome windings, with the power consumption (and therefore temperature) controlled by a thermistor thermostat switch. The lightly insulated meter box is mounted in gimbals so that it can be rocked and leveled through angles up to about 6°30′ (empirically determined in wells) from the vertical axis of the cylindrical sonde.

The meter box with its associated components is leveled by means of two high-speed reversible electric motors driving reduction gear trains and worm gears which tilt the transverse and longitudinal gimbal mounts. Transverse and longitudinal pendular levels provide a means for observation at the surface control console and manual control of the attitude of the meter box. The outputs of two pairs of matched sun batteries, activated by direct-current lamps, are sensitively affected by the positions of the pendular levels. The output signals are monitored on a surface control galvanometer and are brought to a predetermined null (or level position) by driving the leveling motors.

The beam-spring suspension system is clamped and unclamped by a motor-driven gear-train mechanism provided with both mechanical and electrical stops to prevent damage. Although it is performed remotely, the system's operation is analogous to that of a land gravity meter.

In similar fashion, the operator turns the micrometer screw by activating a motor-driven reduction gear train. As the screw turns to counteract spring tension and bring the beam to null position, it turns a step switch that is followed at the surface by a synchro motor. This in turn actuates a six-digit decade counter in the control box providing relative gravity values in terms of gravity-meter counter units.

The position of the beam when at or near the null position is determined by observing on a galvanometer the voltage output of a third pair of sun batteries which are illuminated by light from a mirror fixed to the gravity meter beam. This voltage output is also used to drive an Esterline-Angus recorder on which small deviations from the exact null position can be quickly detected by varying slopes of the continuously recorded trace.

The level and reading-line optics are adjusted to balance the outputs of each pair of sun batteries at the null position so as to make the effects of lamp voltage changes relatively unimportant. Amplification of the very small (about 1 millivolt) signals produced by the sun batteries is required for transmission through thousands of feet of wire. An amplifier (Fairchild MA709C) circuit of high stability is therefore used. A cathode tube follower circuit at the surface permits observing and recording of the undistorted amplified signals from the sun batteries.

The levels, which are somewhat responsive to temperature changes, are mounted in contact with the meter box and are insulated as thoroughly as practicable. The amplifier and associated circuitry are housed in a separate heavily insulated aluminum box

and kept at a constant temperature by electrical heater windings controlled by a separate thermistor thermostat.

Thirteen-conductor double-armored cable (Vector Mfg. Co. A–5000) is used to suspend, power, and control the instrument. The Teflon-insulated conductors have a dielectric strength of 500 volts direct current and a resistance of 11 ohms per 1,000 feet. Both direct and alternating current are required for operation of the control box and instrument package. Twenty-four-volt direct current needed to activate relays and switches in the instrument package and control box is provided from a battery bank at the surface. An input of 48 volts is sufficient for a 10,000-foot length of cable. The basic external power requirement is 110-volt 60-cycle single-phase alternating current. This passes through an isolation transformer and a Sorenson model ACR500 voltage regulator before it is used directly or transmitted to the instrument package through stepping transformers where it is again transformed and rectified to provide power for heating, lamps, motors, and the amplifier circuit. Four of the 13 conductors are used for alternating current transmission and ground. The cable armor serves as a common ground for all direct-current circuits, leaving nine conductors for direct-current power transmission and telemetry and control circuits.

Provision is made at the control box through relay-controlled switches and ancillary gear for (1) clamping the beam when the meter is being moved, (2) tapping the meter box should the beam stick against its stops, (3) moving the beam electrostatically against the resistance of the heavy damping, (4) observing a voltage pulse at every 1 mgal as a counter check, (5) observing a flood indicator, and (6) observing the electrical pulse generated by an externally attached magnetic casing-collar locator. An ammeter provides a means of monitoring the current flux through the heater circuits. The beam arrestment can be monitored when the sonde is in motion, and the surface counter and micrometer screw may be moved in anticipation of the next reading while moving from one station to another.

The gravity sensor has a total range (without resetting) exceeding 7,000 mgal. It was calibrated by the combination of laboratory and field procedures ordinarily used for all standard LaCoste and Romberg geodetic gravimeters (McCulloh, 1965, p. 1116–1119), except that 150 points on the relative calibration curve were determined using an approximately 20-mgal equivalent calibrating mass in addition to the 30 points normally determined using the approximately 200-mgal equivalent calibrating mass. The importance of both precision and accuracy of gravity measurements in borehole gravimetry and the importance of the accuracy of calibration of the LaCoste and Romberg land gravity meter (McCulloh, 1965) pertain in large part to the instrument system discussed here.

The gravity sensor and associated electrical and electronic support components are shown in figure 1. Extensive laboratory and field tests of the gravity sensor, described in detail elsewhere (McCulloh and others, 1967) (p. D101–D112, this chapter), indicate that the precision of gravity measurements in a borehole, using this instrument, is about 0.016 mgal for all depths, when depth measurement errors and gravity measurement errors are considered together.

Depth measuring equipment

The change of gravity underground along a vertical line is governed almost entirely by the local free-air gradient and by the densities of rock near the line (McCulloh, 1966, p. 2–3), provided that the effects of topography are small or negligible and no pronounced irregularities in underground isopycnic surfaces are nearby. Within the range of rock densities ordinarily expectable in boreholes (1.4–2.8 grams per cubic centimeter), the error in a determination of gravity produced by an error of 1 foot in the measurement of depth ranges from a maximum of about 0.06 to a minimum of about 0.02 mgal, respectively. To be consistent with data from a gravimeter having a precision of ± 0.01 mgal, precision of depth measurements must therefore range from ± 0.2 feet or better at shallow depths to ± 0.5 feet or better at moderate to great depths.

The importance of depth-measurement errors in underground gravity determinations is clearly not quite so critical as elevation errors are in reduction of surface gravity data. However, if borehole gravimeter measurements are to be used for underground or three-dimensional gravity mapping, high precision and absolute accuracy of calibration of depth measuring equipment are essential. If the borehole gravimeter measurements are to be used for determining relative gravity differences over restricted depth intervals, the precision of depth measurement should depend upon the objectives, and absolute accuracy is not so critical.

If measurements are made to determine the vertical gradient of gravity underground for purposes of measuring rock density in situ, the precision of the resultant density determinations will be a curvilinear function of the overall precision of the gradient determinations, and will be controlled by gravimeter precision, preci-

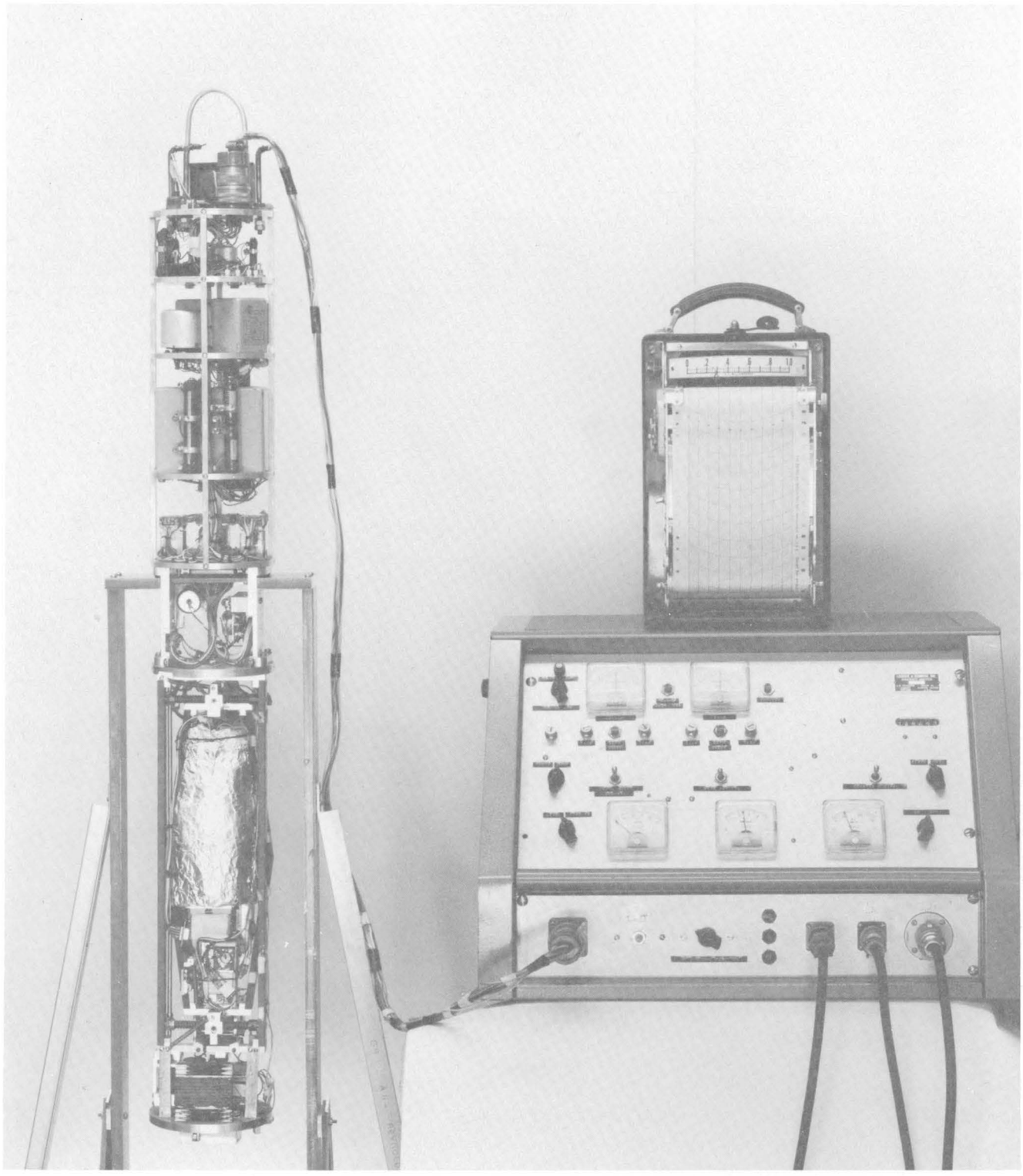

FIGURE 1.—Downhole instrument package (left) and surface control box and recorder (right) that constitute the gravity sensing portion of the instrument system.

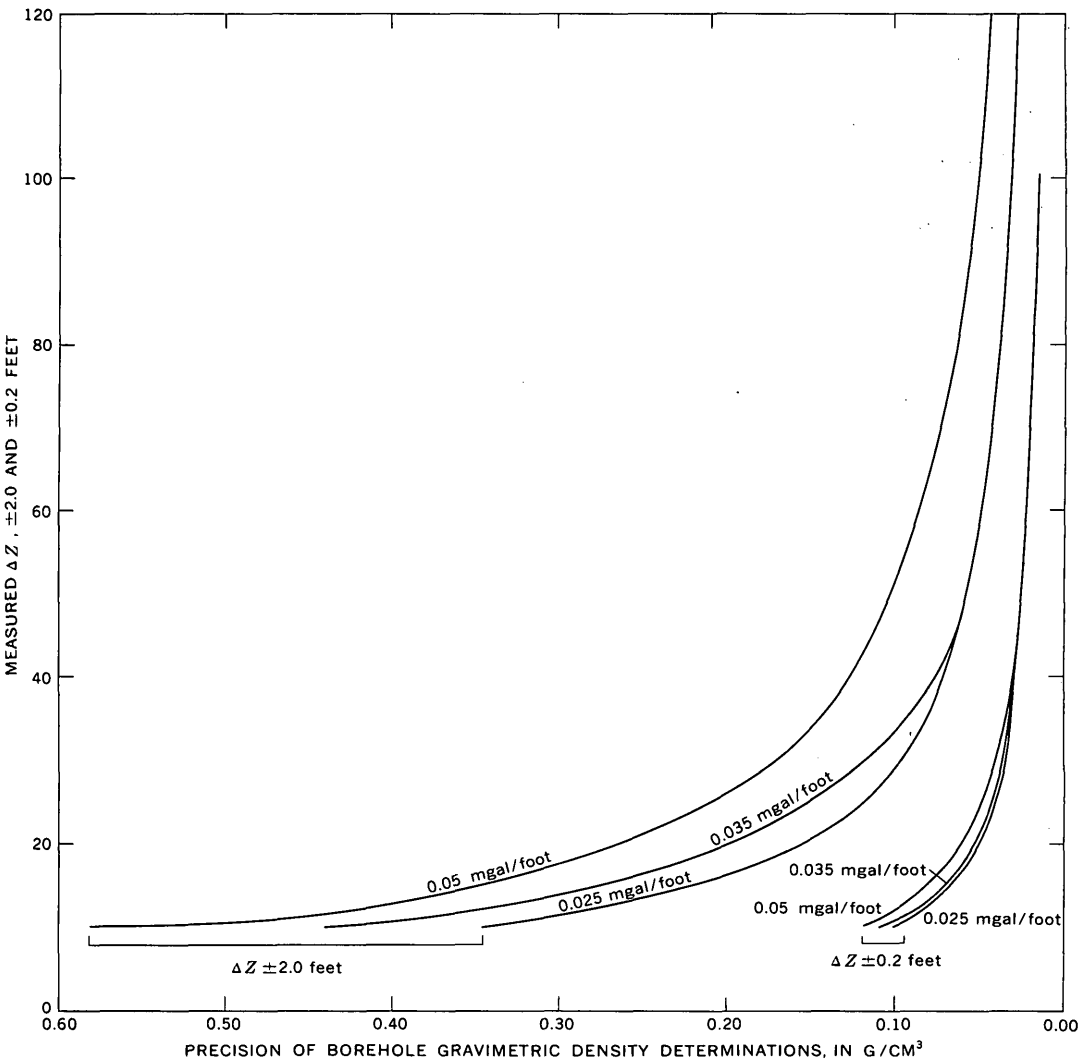

FIGURE 2.—Precision of determination of borehole gravimetric density as a function of size of ΔZ for various underground gravity gradients. Two sets of curves are drawn corresponding to different errors in depth measurements. A free-air gradient of 0.09406 mgal/ft and a gravimeter precision of ±0.01 mgal have been assumed.

sion (errors) of depth measurement, and underground vertical gradient of gravity (rock density in large part). Figure 2 is a plot of precision of density determination as a function of precision of depth-difference (ΔZ) measurements for different underground gravity gradients. This plot assumes that a gravimeter having a reading precision of ±0.01 mgal is used, that the "normal" free-air gradient prevails, and that other gravitational effects are negligible.

In the system described here, depth is measured by the cable passing over the carefully calibrated measuring sheave of a specially constructed wire-line measuring and spooling assembly (designed and manufactured by The Dia-Log Co.). Because wire-line depth measurements are noteworthy for their unreliability (Reistle and Sikes, 1938, p. 92–93) it was necessary to make comparisons between the known depths to casing collars, located by means of a magnetic casing-collar locater, and the depths given by the measuring sheave for the calibration.

The sonde

The instrument sonde consists of four basic parts (fig. 3). Shear screws attach the cable head to the uppermost mandrel on which are fastened three centralizer springs. This mandrel screws into the upper end of the fluid-tight and pressure-resistant instrument housing. The housing, in turn, is attached to either one or two 250-pound sinker bars at its lower end, and a magnetic casing-collar locator may be

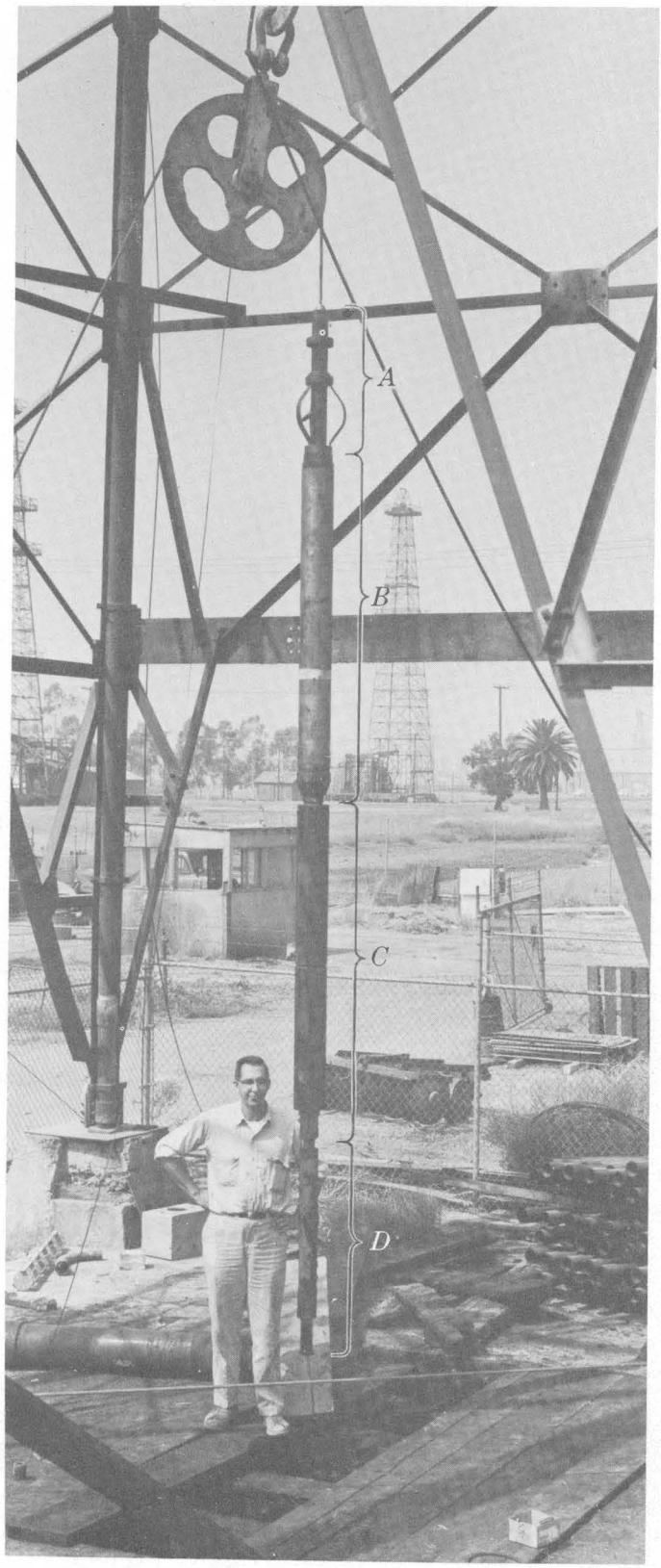

FIGURE 3.—Sonde assembly, consisting of *A*, mandrel and centralizer springs; *B*, fluid-tight gravity meter housing; *C*, sinker bars; and *D*, magnetic casing-collar locator.

screwed onto the lowermost sinker bar to make up the fourth and lowest element of the sonde.

The instrument package, consisting of the gravity sensor and its required mechanical, optical, and electrical gear, has a cylindrical shape and is about 46 inches long and 5.5 inches in diameter. Spring-loaded guides hold it snugly in the 48-inch long and 5.510-inch diameter cavity of the cylindrical steel housing. The upper and lower ends of the cavity are sealed by O-rings borne on steel interior plates.

Fluid-tight entry for the 13 conductors of the cable (plus four conductors used for auxiliary heater power when the main cable is disconnected at the surface) is provided through the top plate of the housing by 17 joy-plug high-pressure connectors. One joy plug through the bottom plate provides the electrical connection to the magnetic casing-collar locator on the bottom of the sonde.

The sonde (extensively modified from one manufactured in part by Baker Oil Tools, Inc.) used in early tests of the system has a maximum outside diameter of 6.453 in. and can withstand pressures up to 4,000 psi. The overall length of this sonde ranges from about 132 in. to 196 in., depending upon the use of 1 or 2 sinker bars and the casing-collar locator. Similarly, the overall weight of the sonde ranges from about 500 to 700 pounds. Experimental data have shown that the gravity meter is least disturbed by seismic motions imparted by the cable when the mass of the sonde is great.

The gravity meter is leveled and read with the sonde hanging freely and unanchored in the well. Experiments conducted using centralizer springs smaller than the inside diameter of the casing indicate that rigid support of the sonde is not required. Similarly, fluid in the hole is not necessary for precise measurements.

Hoisting equipment

The sonde and cable are lowered and raised by a trailer-mounted electrically powered gear-driven hoist modified from a military surplus cargo winch. A General Motors Corp. model 6–71 two-cycle diesel engine (90 horsepower continuous at 1,200 revolutions per minute) drives a 60 kilowatt 250-amp 120/240 volt d-c generator to supply power to the 50-hp hoist motor. A specially designed variable-voltage control system (designed and built by Reyna Electric Works, San Francisco) provides positive yet sensitive regulation of cable speeds ranging from 12 to about 400 feet per minute. A Westinghouse magnetic brake mounted on the end of the motor shaft is self-activating; when the hoist motor is running it is disengaged, and when the hoist control is in the neutral position it is automati-

cally engaged. Any motor overrun while lowering is automatically controlled by dynamic braking through the regenerative electrical system. The hoist drum has a capacity of more than 13,000 feet of 0.580-inch-diameter double-armored cable with an ultimate strength of 21,000 pounds and a weight in air of 0.45 pound per foot. The cable can be stopped exactly at any desired position in a well by an experienced operator. A hand-operated brake on the cable drum provides for emergency stops.

OPERATIONAL CHARACTERISTICS AND LIMITATIONS

The large size of the present sonde (6.453 inches OD) restricts the instrument to wells cased with 7-inch 20-pound casing or larger, or to uncased wells of equal or larger diameter. By using suitable materials and a slightly different design, one could make a 5.9-inch-diameter sonde capable of withstanding static pressures up to 4,000 psi. Such a sonde could be run to depths of 8,000 feet in water-filled casings larger than the heaviest weight 7-inch casing, and could go deeper in gas- or petroleum-filled wells. Increased pressure tolerance would require an increase in housing-wall thickness and therefore tool diameter, with a proportionate resultant decrease in the range of accessible casing sizes. A tool capable of withstanding pressures up to 12,000 psi could be run in all 7⅝ inch casings or larger.

No attempt has yet been made to reduce the size of the limiting instrumental component, the gravity meter beam-suspension system. Reduction of size would almost certainly be possible, but would be costly and might result in reduced accuracy. However, such a reduction would not only greatly expand the useful range of such instruments, but would permit more insulation and thereby simplify somewhat the problem of operating at high temperatures.

Operating the present gravity sensor at temperatures higher than 101°C would not damage the instrument, but would yield meaningless measurements. Inasmuch as subsurface temperatures vary widely (Moses, 1961), the depth limit imposed by the operating temperature of the present experimental prototype ranges from perhaps 5,000 to about 15,000 feet, with 7,000 to 8,000 feet possibly being a limit in the majority of locations.

Although the problems of maintaining a gravity sensor constantly at such a high temperature are severe because of the limited space for insulation, it is apparent that 101°C is not the upper limit achievable for instruments of this design and material. With sufficient incentive, an instrument thermostated to operate at 125°C or possibly even 150°C probably could be built. An even more attractive possibility is to cool the instrument package so that the gravity sensor could be thermostated at a temperature below 100°C but still be operated in much higher environmental temperatures.

When the sonde is quickly lowered or raised several thousand feet, events are observed in the response of the gravimeter beam that are similar to seismic pulses. These are probably caused by "working" of the cable armor in response to change in temperature while under load. Increasing the mass of the sonde greatly diminishes these effects, and they can be further reduced by lowering the sonde gradually while making measurements sequentially from the surface down. Furthermore, the frequency of such events rapidly diminishes with time if the sonde is held at one depth.

There is no need to anchor the sonde in the well to obtain a precise measurement. The heavy damping of the gravity sensor makes reading possible even when the sonde is hanging from a derrick in quiet air above the well. Actually, except for the vibrations apparently caused by cable armor expansion or contraction, the borehole environment appears to be very quiet, and once the sonde is brought to stop, all swaying and swinging motion ceases.

The gimbal mounts of the gravity sensor permitted leveling through angles of 4½° from vertical during early tests of the instrument. This angle has been enlarged to 6½° and could be further increased without basic modification of either the gravity sensor or the protective housing. In deviated wells that are appreciably larger than the sonde, use of large centralizer springs at the top of the tool and of sinker bars at the lower end cause the sonde to hand as a pendulum, thereby extending slightly the tolerable range of departure of holes from the vertical.

REFERENCES

Airy, G. B., 1856, Account of pendulum experiments undertaken in the Harton Colliery for the purpose of determining the mean density of the earth: Royal Soc. [London] Philos. Trans., v. 146, nos. 14 and 15, p. 297–342 and p. 343–355.

Beyer, L. A., von Huene, R. E., McCulloch, T. H., and Lovett, J. R., 1966, Measuring gravity on the sea floor in deep water: Jour. Geophys. Research, v. 71, no. 8, p. 2091–2100.

Cook, A. H., and Thirlaway, H. I. S., 1951, A gravimeter survey in the Bristol and Somerset coalfields: Geol. Soc. London Quart. Jour., v. 107, pt. 3, p. 255–286.

Dolbear, D. W. N., 1959, Design considerations of a borehole gravimeter: Geophys. Prosp., v. 7, no. 2, p. 196–201.

Gilbert, R. L. G., 1952, Gravity observations in a borehole: Nature, v. 170, no. 4523, p. 424–425.

Goodell, R. R., and Fay, C. H., 1964, Borehole gravity meter and its application: Geophysics, v. 29, no. 5, p. 774–782.

Hammer, Sigmund, 1950, Density determinations by underground gravity measurements: Geophysics, v. 15, no. 4, p. 637–652.

Howell, L. G., Heintz, K. O., and Barry, A., 1965, The development and use of a high-precision downhole gravity meter [abs.]: Geophysics, v. 30, no. 6, p. 1237.

———1966, The development and use of high-precision downhole gravity meter: Geophysics, v. 31, no. 4, p. 764–772,

Jung, Heinrich, 1939, Dichtebestimmung im anstehenden Gestein durch Messung der Schwerebeschleunigung in vershiedenen Tiefen unter Tage: Zietschr. Geophysik, v. 15, p. 56–65.

Lorenz, H., 1938, Bieträge zur Theorie des Erdaufbaus: Zeitschr. Geophysik, v. 14, p. 142–152.

Lukavchenko, P. I., 1962, Observations with gravimeters in boreholes and mineshafts: Rasvedschnaya i Promyslovaya Geofizika, no. 43, p. 52–64 [in Russian].

McCulloh, T. H., 1957, Simple Bouger gravity and generalized geologic map of the northwestern part of the Los Angeles basin, California: U.S. Geol. Survey Geophys. Inv. Map GP–149, scale 1:48,000.

———1960, Gravity variations and the geology of the Los Angeles basin of California: Art. 150 *in* U.S. Geol. Survey Prof. Paper 400–B, p. B320–B325.

———1965, A confirmation by gravity measurements of an underground density profile based on core densities: Geophysics, v. 30, no. 6, p. 1108–1132.

———1966, The promise of precise borehole gravimetry in petroleum exploration and exploitation: U.S. Geol. Survey Circ. 531, 12 p.

McCulloh, T. H., Schoellhamer, J. E., Pampeyan, E. H., and Parks, H. B., 1967, The U.S. Geological Survey–La Coste and Romberg precise borehole gravimeter system—test results *in* Geological Survey Research 1967: U.S. Geol. Survey Prof. Paper. 575–D, p. D101–D112.

Moses, P. L., 1961, Geothermal gradients: Am. Petroleum Inst., Drilling and Production Practice, 1961, p. 57–63.

Nettleton, L. L., LaCoste, L. J. B., and Glicken, Milton, 1962, Quantitative evaluation of precision of airborne gravity meter: Jour. Geophys. Research, v. 67, no. 11, p. 4395–4410.

Oil and Gas Journal, 1966, Esso licenses down-hole gravity meter: Oil and Gas Jour., v. 64, no. 26, p. 101–102.

Reistle, C. E., Jr., and Sikes, S. T., Jr., 1938, Well-depth measurements: Am. Petroleum Inst. Drilling and Production Practice, 1938, p. 80–95.

Smith, N. J., 1950, The case for gravity data from boreholes: Geophysics, v. 15, no. 4, p. 605–636.

Yerkes, R. F., McCulloh, T. H., Schoellhamer, J. E., and Vedder, J. G., 1965, Geology of the Los Angeles basin, California—An introduction: U.S. Geol. Survey Prof. Paper 420–A, p. A1–A57.

THE U.S. GEOLOGICAL SURVEY–LaCOSTE AND ROMBERG PRECISE BOREHOLE GRAVIMETER SYSTEM—TEST RESULTS

By T. H. McCULLOH [1]; J. E. SCHOELLHAMER, E. H. PAMPEYAN, and H. B. PARKS [2], Pasadena, Calif.; Menlo Park, Calif.; Austin, Tex.

Abstract.—The U.S. Geological Survey and LaCoste and Romberg, Inc., have developed a borehole gravimeter system and components characterized by precision of (1) depth measurements in the range of 0.05 to 0.2 ft. between the surface and 9,500-ft depth, and (2) downhole gravity measurements ranging from a high of 0.008 mgal to a low of 0.02 mgal. An average precision of 0.016-mgal is attainable at all depths and includes both precision of gravimeter readings and of depth measurements. Time tests suggest that, during normal routine operation, detailed (one station every 100 ft) and precise (±0.01 mgal) gravimeter surveys of wells less than 10,000 ft deep may be made at 300 to 500 ft per hour (including base checks for drift control) by a skilled three-man crew. In the laboratory, an increase or decrease in environment temperature of 60°C on the gravity sensor produces a maximum change in apparent gravity reading of 0.1 mgal. Reliability of the gravity sensor and certain of its key components has been a problem that is undergoing gradual improvement.

In a companion article (McCulloh and others, 1967) (p. D92–D100, this chapter) the functions, characteristics, and arrangement of the essential components of the U.S. Geological Survey – LaCoste and Romberg borehole gravimeter system are described, and a brief history of their development sketched. The purpose of this report is to present a summary and selected sampling of results obtained prior to October 1966 of laboratory and field tests of key components and the entire system.

Laboratory tests of components of the gravity sensor began as early as April 1965, and the first tests of the assembled gravimeter under simulated well-temperature conditions took place during the fall of 1965. Field tests and calibration of the depth-measuring equipment and gravimeter housing were made during January 1966, and field tests of the entire system began late in January 1966. Field tests in wells to depths as great as 7,800 feet, interspersed with periods of modification and refinement of the gravimeter and housing, continued through September 1966. At that time the entire system had been evaluated and was considered beyond the initial development stage, but the need for further development before the system can be considered routinely operational was suggested by problems associated with reliability of the gravity sensor.

Acknowledgments.—The test results reported here would not have been possible without the ingenuity and insight of Dr. L. J. B. LaCoste and the enthusiastic support of his entire staff.

Wells in which testing has occurred were made acessible by The Shell Oil Co., through the offices of J. C. Taylor; by The Standard Oil Company of California through the assistance of C. D. Fiddler, S. F. Craddock, E. P. Maxwell, and Dr. F. G. Blake; by The Mobil Oil Co., with generous assistance of T. L. Cook, Jr., J. R. Kandle, and B. L. Stitzinger; and by Lane Wells, Inc., through the offices of Cliff Strozier and W. C. Humfeldt.

L. A. Beyer and M. D. Kleinkopf, of the Geological Survey, and G. V. Hamilton, of LaCoste and Romberg, Inc., assisted in certain critical tests, and Dr. R. P. Sharp and the California Institute of Technology encouraged the work.

DEPTH MEASUREMENTS

The position of an instrument lowered in a well by wire line may be determined with an accuracy that depends upon the precision of the depth-measuring equipment, the accuracy of calibration of that equip-

[1] Present address: Chevron Research Co., LaHabra, Calif.
[2] LaCoste and Romberg, Inc.

ment, the exactness of knowledge of the amount that the cable elongates under the loading and temperature conditions at the time and place of the lowering, and the adequacy of information about the deviation of the well from the vertical. In a general and comprehensive review of well-depth measurements, Reistle and Sikes (1938, p. 91–93) give attention to the many factors that affect the first three of these variables, and conclude (p. 94) that "Well depths cannot be measured by any procedure wherein all errors may be determined and corrected" and that "Drill pipe offers the most desirable means of measuring depths of wells * * *."

Our experience indicates that the precision of measurements made with a measuring sheave of good quality is very high if the sheave and the wire line are maintained in good condition and if precision is checked frequently. However, the elasticity of steel-armored cable changes because of use and wear. This, and the variability of cable load and stretch associated with variable well conditions, make accuracy of calibration of depth measurements a serious problem. For these reasons, and because of the importance of depth measurements in precise borehole gravimetry, we have found it highly desirable to (1) extensively precondition the cable, (2) calibrate the measuring sheave carefully and repeatedly against a standard test well in which the depths of key points are known, (3) use a magnetic casing-collar locater to check sheave measurements against casing measurements whenever possible, and (4) use a sensitive cable-load indicator as a means of comparing driller's depths to bottoms or plugs and to changes in casing size or weight with depths measured using the wireline measuring sheave.

Reproducibility (precision) of borehole gravimeter depth measurements has been determined in four ways. First, repeated measurements made while using the wire-line measuring sheave and accurately chaining (under load) lengths of cable up to 531.20±0.02 feet long were compared. At such shallow depths, unaided measuring-sheave determinations are reproducible to ±0.05 foot. Second, unaided measuring-sheave determinations of depths to marks placed on the line are repeatable to ±0.2 foot or better in the range of depths from 0 to 6,000 feet, if measurements are all made while running into the well. Third, measuring-sheave determinations of depth to casing collars (or other casing discontinuities that distinctively affect the magnetic casing-collar locater or the wire-line load indicator) are repeatable to within ±0.1–0.5 foot in the range of depths between 6,000 and 9,500 feet, again, if measurements are made while running into the well. Finally, measuring-sheave determinations of depth differences between points identified by marking the wire line and then chaining the distance between marks are repeatable and accurate to ±0.05 foot at moderate depths. From all of these determinations it may be concluded that borehole gravimeter depths and depth differences are quickly and easily measured with a reproducibility generally ranging between ±0.05 and ±0.2 foot if a prestretched cable in good condition is passed through a wire-line measuring sheave of good quality.

High precision of depth measurements is no guarantee that accuracy be equally high. As noted by Reistle and Sikes (1938, p. 92), drill-pipe measurements corrected for stretch provide the best standard for calibrating wire-line depth measurements. Unfortunately, very few companies take account of stretch of drill pipe (or other tubular goods) as it is lowered under load into a well, and virtually none calculate corrections for thermal expansion of drill pipe (Reistle and Sikes, 1938, p. 81–82). Thus, the ideal standard is rarely available for converting the high-precision gravimeter depth measurements to absolute accuracy. As a practical consequence, the gravimeter depth-measuring equipment has been standardized against driller's depths uncorrected for stretch or thermal expansion of drill pipe. Where more refined estimates of absolute depths may be needed, the measured wire-line depths could be approximately corrected for stretch of drill pipe and for thermal expansion.

Stretch of uniform strings of steel pipe suspended freely in a mud-filled hole ranges from about 1 foot for 4,500 feet of pipe to nearly 5 feet for 10,000 feet (Reistle and Sikes, 1938, fig. 3). In the absence of more complete data, and as a first approximation, if accurate absolute depths are required, precise relative wire-line depth measurements could be approximately corrected from such relationships. However, it is useful to bear in mind that a real difference in depth of 1 foot at a depth of 4,500 feet is equivalent, in most localities, to a difference in gravity of only 0.02±0.04 mgal (depending upon the underground vertical gradient of gravity or the rock density), and that a real depth difference of 5 feet at a depth of 10,000 feet is equivalent to a gravity difference of only 0.15 mgal at most. Thus, the approximate corrections to wire-line depth measurements for the uncorrected effects on driller's depth estimates of stretch of drill pipe or casting strings will have very small absolute and even smaller relative effects on underground values of gravity or vertical gradients of gravity.

The externally double-armored steel cable used with the Geological Survey's instrument system stretches 6.1×10^{-7} feet per foot per pound of load at room temperature (with little change to 212°F), or nearly 4.4 feet in 4,500 feet. However, the difference between its stretch under load and that of freely suspended drill pipe or casing is not pertinent, because it is automatically taken into account by using driller's depths as the calibration standard for the wire-line measuring equipment.

The thermal elongation of steel tubular goods and of steel-armored cable is linear and nearly uniform (approx 1 ft in 4,000 ft under temperature conditions prevailing in many geologically young sedimentary basins), and consequently important differential effects on wire-line depth measurements do not arise. If the goal in a particular borehole gravimetric investigation is to obtain absolute rather than relative depths of gravity stations, corrections for thermal expansion of the depth-measuring standard can be calculated from the coefficient of linear thermal expansion for carbon steel, 6.1×10^{-6} per degree Fahrenheit, and underground temperature data.

Depths of precise gravity measurements made in holes deviated from vertical may require correction for the difference between hole length (measured depth) and true vertical depth. Trial calculations based upon a very detailed directional survey (25-ft intervals) of a moderately crooked hole (hole inclinations up to 6° 37′ from vertical) indicate that standard directional survey data are more than sufficiently detailed for such corrections, which range from negligible to moderate (2 ft in 1,000 ft) in those wells in which the gravimeter can be leveled and read.

THE GRAVITY SENSOR

Laboratory tests

Laboratory tests of the gravity sensor (including its integral support equipment such as levels, optics, power supply, amplifier, and control and readout components) were conducted to determine its response to large temperature changes, to shaking and jolts, and to abrupt changes in input voltage. Some observations were made also of the effects of maladjustment of the levels and of the magnitude of long-term instrumental drift.

Despite excellent control and stabilization of the temperature of the gravity sensor and its output signal amplifier, through the use of (1) electrical heating circuits sensitively responsive to metastatic thermistor thermostats and (2) a maximum of thermal insulation, laboratory tests of the gravimeter under simulated well-temperature conditions reveal a small regular and nearly reproducible dependence of gravity readings upon ambient environment temperature. As the sensor environment is heated, the gravity reading decreases, and as the environment cools, the gravity reading becomes more positive. Over a temperature range of about 60°C (+35°C to + 95°C) the gravity readings change about 0.1 mgal. The rate of temperature change affects slightly the exact response of the sensor, and gravity readings made during the heating part of a laboratory excursion tend to be about 0.03 mgal more positive at intermediate temperatures than readings taken at the same temperature during the cooling part of a cycle. Both of these facts suggest that instrumental thermal gradients, rather than the environment temperature in itself, may affect the response of the gravity sensor. Figure 1 is a representative plot of gravity readings (corrected for earth tides) as a function of environment temperature. The duration of the test was almost 4 hours.

If a geothermal gradient of 1°C per 100 feet of depth is assumed as reasonably representative (Moses, 1961), gravity measurements made using gravimeter number G–95 at a depth of 7,000 feet can be expected to be too low by about 0.1 mgal relative to an absolute standard, unless approximate temperature corrections are calculated and applied. Moreover, the desirability of making all gravity measurements while running into a well is apparent from inspection of figure 1 and from the reproducibility of depth measurements (described above). Whether or not corrections for temperature dependence of gravity readings are to be made in a particular study depends again upon whether high precision of relative gravity measurements or absolute accuracy is needed. Temperature corrections of the small magnitudes indicated are in order only if the utmost in absolute accuracy of depth measurements has been achieved.

Under field conditions rough handling of the borehole gravimeter is the rule rather than the exception. Although the gravimeter beam is clamped whenever the sonde is moved, and although relatively elastic centralizer springs cushion the sonde and instrument against shock while it is in motion in a well, excessive shaking and jolts are a part of normal operation. It is difficult to evaluate the extent of instrument shock while in a well, and therefore virtually impossible to simulate such motion in the laboratory. To investigate the effect of handling, comparisons were made in the laboratory between gravimeter performance without movement of any kind and performance in response to clamping the beam and moving, shaking, and hand-

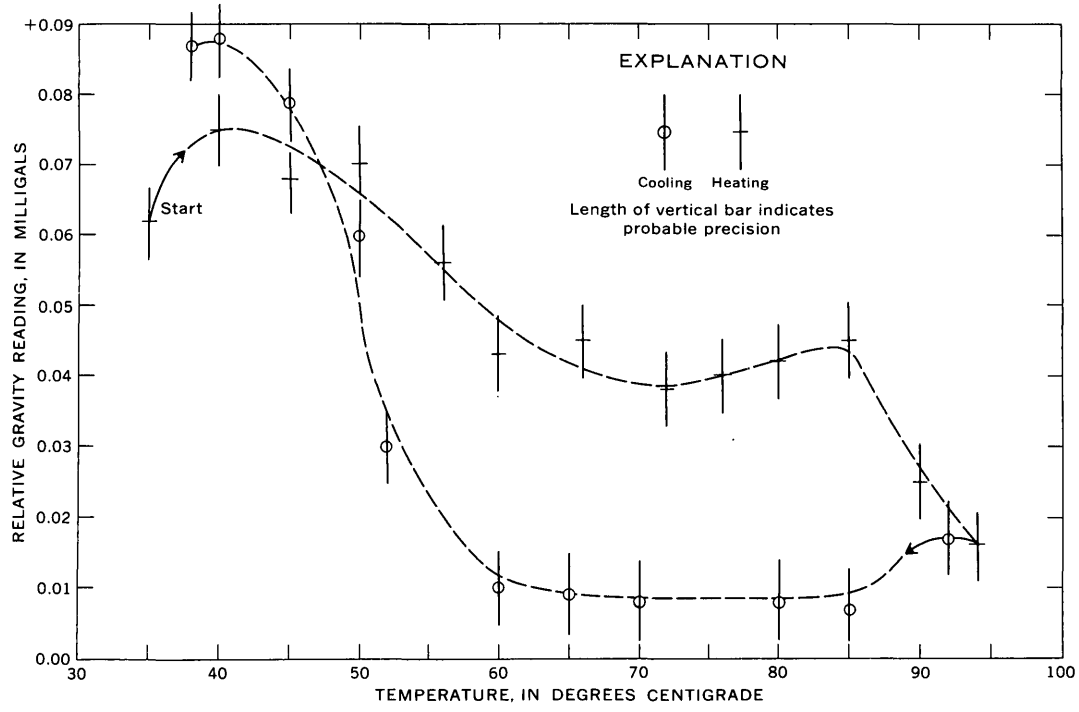

FIGURE 1.—Gravimeter G–95 relative gravity values (tide-corrected) as a function of environment temperature from a representative laboratory test simulating well-temperature conditions.

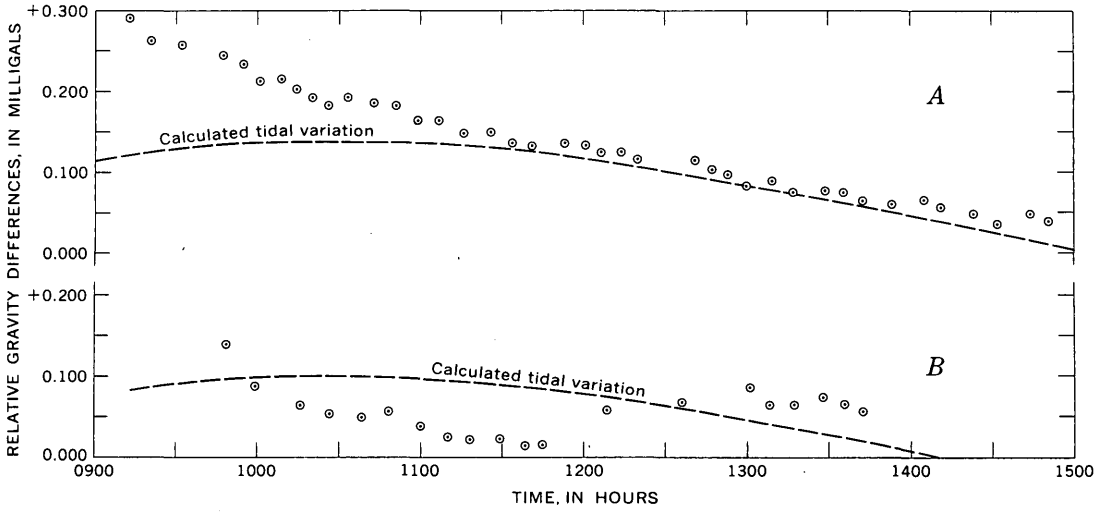

FIGURE 2.—Change of relative gravity versus time for gravimeter G–95 during two laboratory tests that demonstrate the effects of moving, shaking, and disturbing the gravimeter between readings.
A. Temporal variations of gravity readings at one laboratory location; gravimeter unclamped and unmoved. May 10, 1966.
B. Temporal variations of gravity readings at one laboratory location; gravimeter clamped, moved, and shaken between readings. May 17, 1966.

ling the instrument between readings. Figure 2 shows results of two such tests made during May 1966. In each test, the gravimeter readings are plotted against time of reading together with matching earth-tide curves calculated from the tables in Geophysical Prospecting (Service Hydrographique de la Marine and Compagnie Generale de Geophysique, 1965).

When gravity readings are made in a time series without movement of the gravimeter (other than the motions necessitated by moving the leveling and counter motors and those imparted by seismic disturbances within a building in use), individual measurements depart by less than ±0.01 mgal on the average from a fairly smooth curve drawn to represent the

mode of all the readings. Figure 2*A* pictures such a series of 40 readings made during one 6-hour period. Attention is drawn to the fact that the calculated earth-tide curve and the curve of observed gravity values are notably divergent during the first half of the period of observation and then are nearly parallel.

If gravity readings are made in a time series at one location, but the gravimeter is clamped and then moved and shaken between readings, individual measurements define a more irregular line characteristically broken by slight discontinuities. Representative of such results is a second curve of figure 2,*B* based upon 20 measurements made during one 4-hour test. Individual measurements depart in this test also by less than ±0.01 mgal on the average from the two distinct modal lines, but a tare of about 0.05 mgal separates those two parts. Such tares when undetected are probably the principal source of error in downhole gravity measurements, and there is every reason to suspect that the instrument experiences rougher handling during field operation than it was given during this laboratory test. Attention is drawn again to the characteristic divergence between the calculated earth-tide curve and the observed gravity values during the first 2½ hours of the period of observation.

Voltage fluctuations in the 110-volt alternating current input current produce directly dependent fluctuations in gravity readings. Laboratory experiments show that a change of 5 volts produces a change in reading of about 0.02 mgal. Very close regulation accompanied by frequent monitoring enables maintenance of voltage within ±0.5 volts during normal operation, virtually eliminating this source of error.

Considerable care must be taken to determine the optimum attitudes of both cross and long levels (and reading point) to make negligible the effects of slight temperature drifts in the level sensor. Leveling errors are apparently insignificant when the leveling is done carefully as judged by high precision of numerous repeated field and laboratory measurements made before and after releveling. Although of critical importance, the simplicity, sensitivity, and reliability of the pendular levels and electro-optical system used in gravimeter G–95, make both selection of optimum-level positions and reoccupation of optimum positions a simple task for a practiced operator.

During months of interspersed field and laboratory tests of gravimeter G–95, a persistent and remarkably constant positive long-term instrumental drift of approximately 5 mgal per month has been recorded. Although small, this rate of drift is substantially greater than that characteristic of most standard LaCoste and Romberg geodetic gravimeters, presumably because of the much higher operating temperature of the borehole gravimeter. It is clearly not a source of error in field operations that last only a few hours to a few tens of hours, especially because the drift rate is the same or nearly so whether the instrument is in use or at rest.

Field tests in wells

The gravity sensor has been tested extensively in wells during experiments designed to determine the feasibility of leveling and reading the gravimeter without anchoring the sonde against casing; to investigate and counteract the effects of cable and sonde motion; to determine the range of hole deviation from the vertical in which the instrument can be leveled; to determine experimentally the reproducibility under borehole conditions of gravity measurements; and to test the reliability of the gravimeter and its components under operational conditions.

Initial tests of the gravimeter demonstrated conclusively that anchoring of the sonde within casing is not required. Because of deliberately heavy damping of motion of the gravimeter beam, leveling and reading the gravimeter is possible with the sonde hanging freely in the borehole (and in fact even in the open air).

The need for taking a long reading because of the use of high damping is circumvented by making use of the beam velocity in taking readings, as is done with shipboard gravity meters. The reading method is simplified by operating the gravity meter at infinite sensitivity so that the beam position is not needed in taking a reading; otherwise both the beam position and velocity would have to be used. Using the beam velocity rather than its position also reduces errors due to drift in the sensor that measures beam position. Under these conditions, the effects of sensor drift are negligible unless they are so large as to produce a significant error in beam velocity.

Early experiments with a relatively lightweight sonde supported by fairly rigid centralizer springs near the cable head revealed that the unclamped gravimeter beam was disturbed by minute shocks. Shocks, we suspect, are related to extension and contraction ("working") of the cable under variable loads and temperatures. These shocks seriously hampered reading of the gravimeter and when they were severe, readings were altogether prevented for periods of up to 1 hour, the time required for the motion to cease. When the gravity meter is in proper adjustment, substitution of lightweight and more flexible centralizer springs and the addition to the lower end of the sonde of

sinker bars weighing 500 pounds eliminate these effects. Slight swaying motion of the sonde imposes no problems in leveling or reading because of the beam damping.

Experiments in a carefully surveyed crooked well showed that the gravimeter can be leveled and read in an 8⅛-inch cased hole inclined up to 6°37′ from vertical. In a well lined with 7-inch casing, the limiting angle would probably be slightly smaller. On the other hand, a slight instrument design modification would probably permit leveling in wells deviated even more than 6½°.

Reproducibility of gravity measurements in wells can be gaged only if errors or uncertainties in depth measurements can be eliminated. Since this is virtually impossible, demonstrations of repeatability in wells can be taken as indications only of the minimum precision of the gravimeter, complicated by precision of depth positioning. Reoccupation of borehole instrument stations can be accomplished either (1) by marking the wire line at the surface and bringing the mark repeatedly to some fixed surface reference (well head or derrick floor), or (2) by stopping the gravimeter at a station identifiable by the response of the magnetic casing-collar locater (a fixed subsurface reference). In the first procedure, small depth differences may result from differential stretch of the cable. In the second, small depth differences result from inability of the winch operator to stop the sonde at the exact time of the distinctive galvanometer signal. Evaluation of the magnitude of depth differences is equally difficult in the two procedures, but they probably are of the order of 1–2 inches at most, and should be unsystematic in nature. The results of many experiments of both kinds at various depths in three wells consistently indicate that gravity measurements made by a skilled operator, with the gravimeter functioning normally, are reproducible to within ±0.013 mgal, and we suspect that unsystematic depth differences between replicate readings account for perhaps ± 0.004 mgal of this at all depths.

One may partly separate the effects of precision of depth positioning from the effects of precision of gravimeter reading in another way. Repeated measurements at pairs of vertically separated stations marked on the wire line at the surface enable one to obtain differences of gravity over a nearly fixed vertical interval repeatedly. Positioning errors resulting from differential cable stretch affect such small relative depth differences very slightly, if at all. The effects on the measured differences of gravity resulting from differences in absolute depths of each reading are minimal because of the extremely slight change in underground gradient of gravity over a vertical distance of about 100±2 feet. During one 14-hour detailed gravity survey of a deep well, 20 separate measurements of gravity were made at 10 stations arranged in 5 pairs between 720 and 4,550 feet. The deviation of each measured gravity difference from the mean of two independent differences measured for each pair of stations was obtained. The mean of these 10 deviations is 0.016 mgal, and the standard deviation from the mean is 0.007 mgal. Because two measurements of gravity were made to obtain each gravity difference, these data suggest that reading precision of the gravimeter during this test was ±0.008 mgal. Tests of this type at greater depths indicate lower precision, but we are not yet certain whether this is because of the effect of higher temperatures, operator inexperience, or gravimeter malfunction. A precision in well tests of ±0.008 mgal, probably the best that can be expected from gravimeter G–95, agrees well with the precision indicated by laboratory tests described on previous pages.

Early field tests of the gravimeter system encountered problems of reliability of gravity sensor components and related equipment. Increased operating experience and improvements in some components have partly eliminated such problems, but the instrument cannot yet be expected to perform continuously for periods of more than a few tens of hours. Uncertainty remains regarding when the gravity sensor can be expected to function reliably enough under field conditions to be considered routinely operational.

FIELD TESTS OF THE TOTAL INSTRUMENT SYSTEM

Experiments have been conducted in wells of various depths and conditions to evaluate the efficacy of the protective housing of the gravimeter, the reliability of the system as a whole, reproducibility of measurements of all sorts under routine field conditions, and time consumption and costs of operation of the system.

From the outset, the protective instrument housing proved adequate but not perfect. Designed to withstand fluid pressures up to 4,000 pounds per square inch, protracted exposure to pressures almost that high repeatedly caused leakage of a few cubic centimeters of water past the single O-ring seals, but no other ill effects were experienced. At pressures below 3,500 psi, the integrity of the instrument is preserved by this housing. Tests of improved substitutes for the original housing are not yet complete, but are expected to permit operation of the instrument at depths in excess of 13,000 feet, factors other than pressure permitting.

Because the instrument system is a very simple one, problems of overall system reliability, apart from those connected with the gravity sensor, have been minimal. Routine maintenance of the powerplant, hoisting equipment, and wire-line spooling and measuring gear suffices. Normal care in initial spooling, conditioning, and maintaining of the cable is essential. The sonde is simple and rugged, requiring nothing but routine care and inspection. Problems of reliability of the gravity sensor and its associated components have been partly overcome and presumably can be completely or largely eliminated. If so, careful handling and maintenance of these parts of the system should be sufficient to ensure satisfactory routine operation.

Evaluation of reproducibility of gravimeter and depth measurements has been a primary objective of every field test of the instrument system. Inasmuch as separation of the effects of precision of depth measurements and of gravimeter measurements is not practical in a routine operation, the *effective precision*, of the entire system, in terms of repeatability of gravity determinations, is of at least equal importance to that of precision of the gravity sensor in itself. Hundreds of repeat measurements throughout the range of depths from 0 to 7,800 feet, both in fluid-filled and air-filled wells, provide a firm basis for concluding that this bore-hole gravimeter system has the capability, when used carefully, of yielding measurements of gravity that range in overall reproducibility between ± 0.005 and ± 0.02 mgal, depending on depth and operating conditions. If the difference in gravity between two borehole stations 100 feet or less apart is critical, measurements of gravity may be made, the line marked, and then the length of line between marks accurately chained. By this means, that element of uncertainty introduced by the imprecision of depth measurements is greatly reduced, and the precision of effective gravity determination improved to about ± 0.01 mgal.

During what was probably the most meaningful test of the instrument system, in terms of time of normal operation, 96 measurements of gravity were made at 64 stations between depths of 0 and 7,834 feet during two periods, totaling 21 hours. In addition, 4 hours were consumed in adjusting and checking the control electronics, and about 8 hours more in moving in and setting up equipment at the well site, and moving it out again. A single measurement of gravity by a skilled operator requires only 3–5 minutes, but much additional time is spent in traversing between stations, going to and from a base station periodically reoccupied, and making repeat readings to ensure high precision. Two experienced men are essential, and three are desirable, throughout such a survey. Ten traverses were made, the average traverse depth being nearly 4,000 feet. Additional operating experience would doubtless result in a further reduction of total time required. It is, however, difficult to envision circumstances in which gravimeter G–95 could be used to obtain precise detailed (station interval about 100 ft) well profiles of gravity at an average rate exceeding 500 feet of hole per hour, no matter what the depth of operation.

269-274 O—67——8

PROCEDURAL MATTERS

In the course of developing, testing, and evaluating the borehole gravimeter instrument system, certain procedures have been devised for obtaining and reducing data of highest quality with maximum efficiency. Since these procedures have evolved from considerable experience and much trial and error, they are described and explained briefly here.

Observation shows that during the first 1–3 hours of operation after a period of rest, the gravity sensor drifts at an abnormally high rate and is subject to abrupt reading jumps or tares, especially when subjected to excessively rough handling. Following this initial period, low drift rates and generally smooth drift are characteristic. A tendency toward this mode of behavior is seen even in laboratory tests where handling is doubtless more gentle than in the field (fig. 2). These characteristics of gravimeter G–95 make it necessary to break down the survey of a well into traverses or loops, beginning and ending with measurements at a fixed reference or base station. In this way apparent temporal changes of gravity produced by tidal forces and by instrumental drift may be removed to reveal the real differences of gravity between stations. The first traverse should be no longer than about 45 minutes, the second about 1 hour, and the third about 1¼ hours. Subsequent traverses can be as long as 2 hours or even more. By this means, a tare is likely to be more clearly revealed than otherwise, and close control on instrumental drift rates can be maintained while it is most needed.

For these same reasons, it is also highly desirable to complete a survey in one long session of work if possible rather than two or more. Continuous rapid operation of the gravimeter for long uninterrupted periods appears to yield data of appreciably better quality than operation interrupted by notable breaks. Continuous operation is also desirable for optimum operating costs, downtime of producing wells, rig standby time, and costs for a survey conducted during a remedial workover.

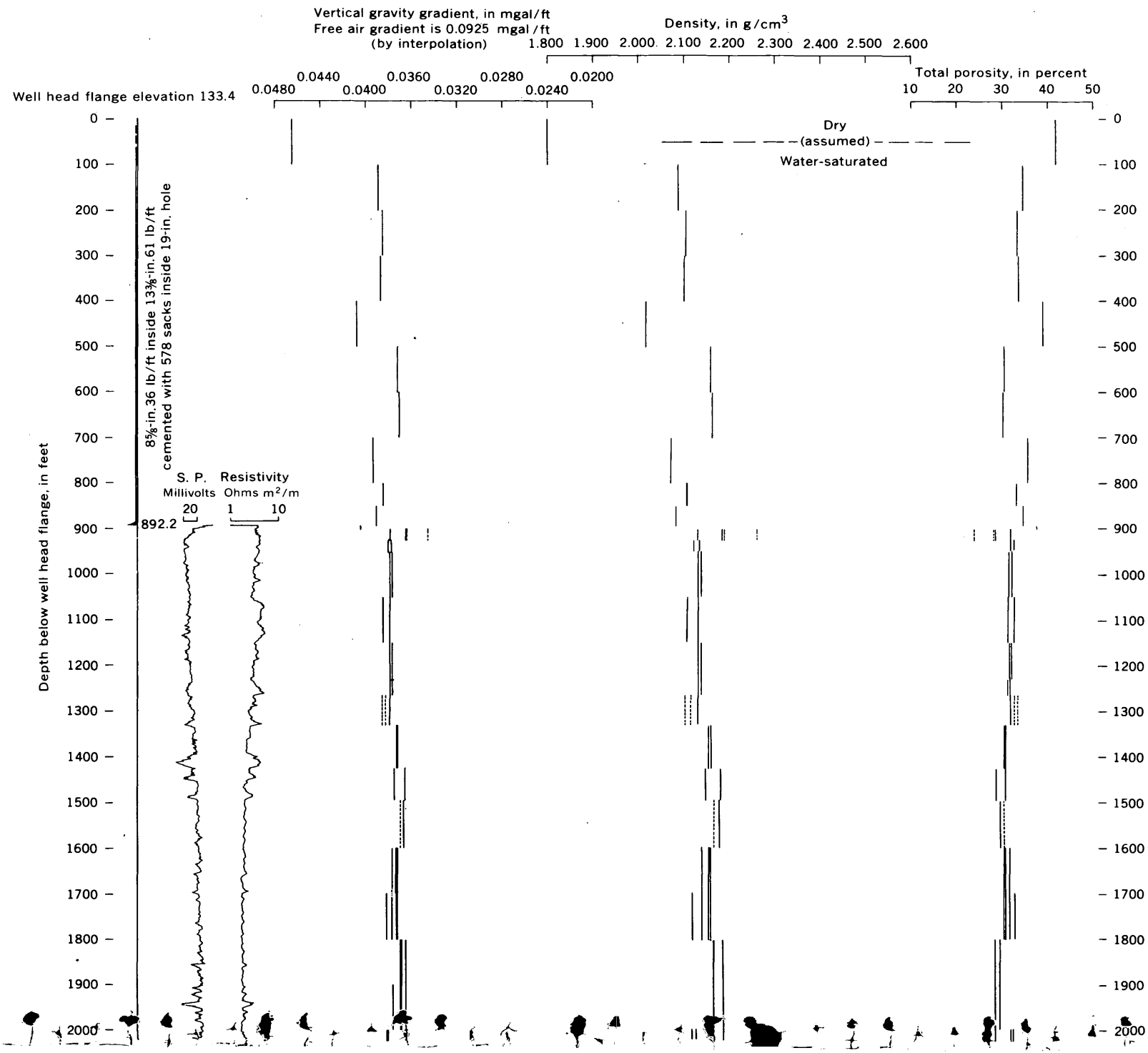
Vertical gravity gradient, in mgal/ft
Free air gradient is 0.0925 mgal/ft
(by interpolation)
0.0480 0.0440 0.0400 0.0360 0.0320 0.0280 0.0240 0.0200
Density, in g/cm3
1.800 1.900 2.000 2.100 2.200 2.300 2.400 2.500 2.600
Total porosity, in percent
10 20 30 40 50
Well head flange elevation 133.4
Dry
(assumed)
Water-saturated
8⅝-in. 36 lb/ft inside 13⅜-in. 61 lb/ft
cemented with 578 sacks inside 19-in. hole
S. P.
Millivolts
20
Resistivity
Ohms m2/m
1 10
892.2
Depth below well head flange, in feet
0 100 200 300 400 500 600 700 800 900 1000 1100 1200 1300 1400 1500 1600 1700 1800 1900 2000

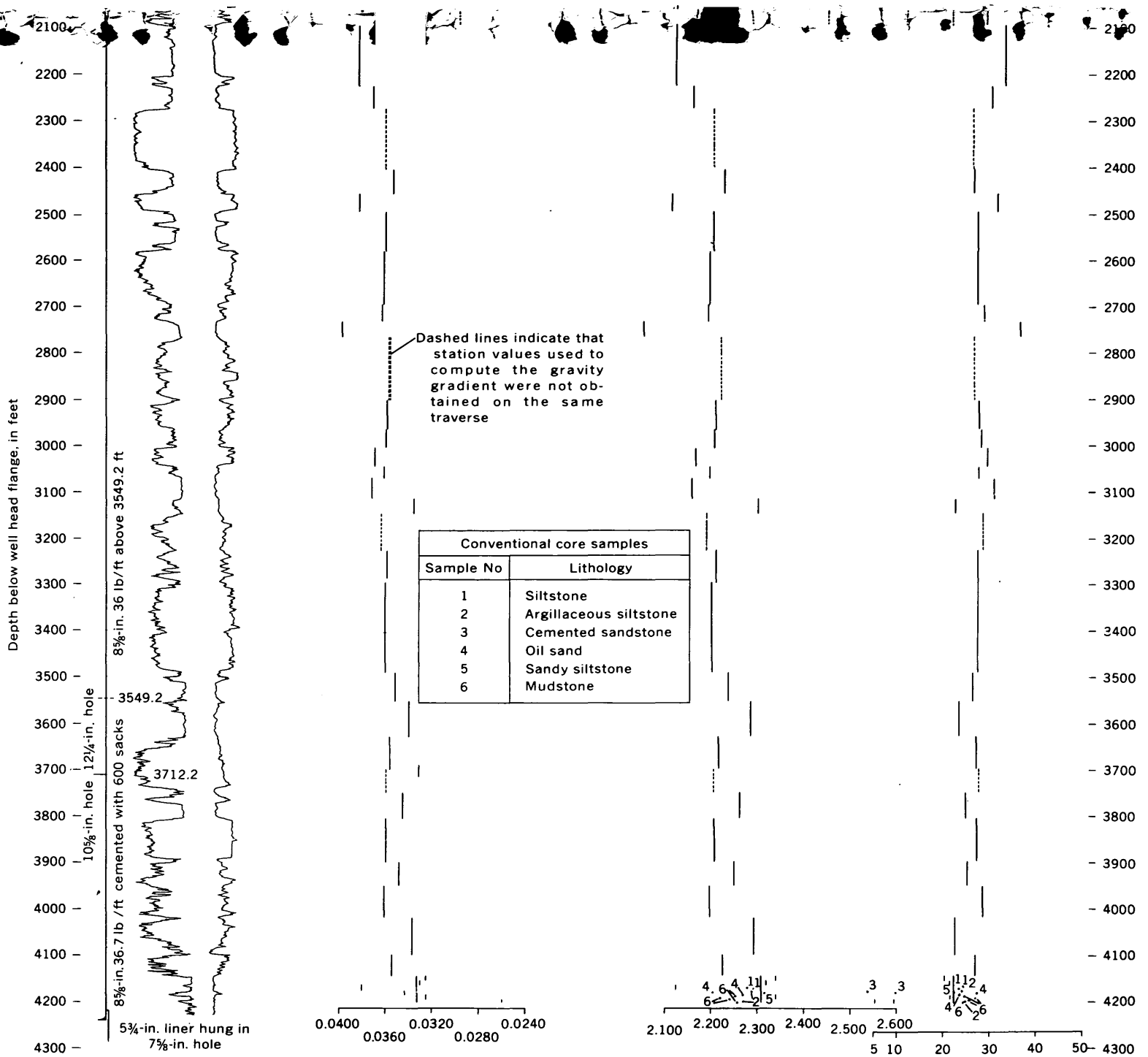

FIGURE 3.—Vertical gravity gradient, calculated average rock density, and derived average interval porosity versus depth for the Shell Oil Co. Slusher No. 28 well, Santa Fe Springs oil field, Los Angeles County, Calif.

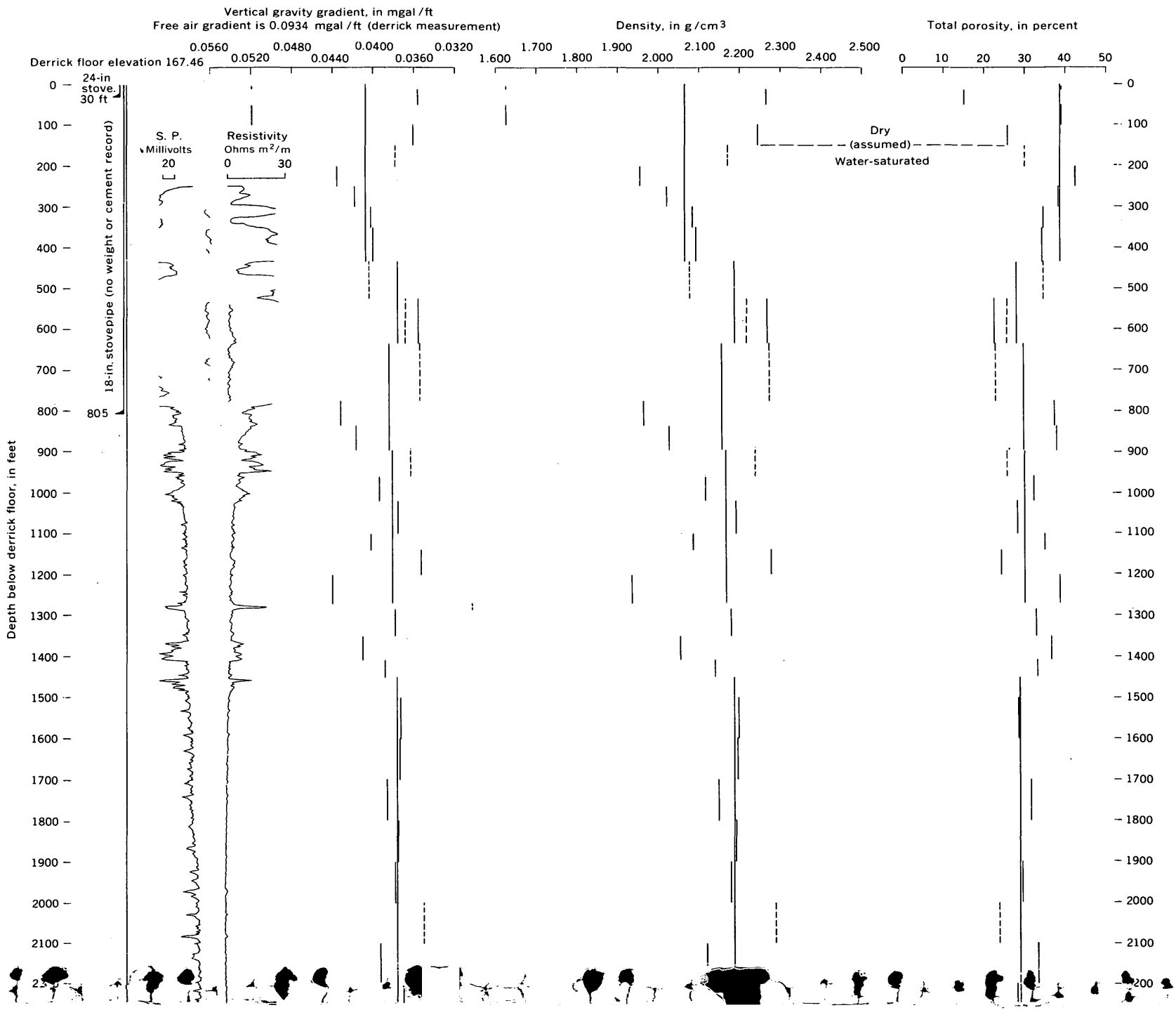
Vertical gravity gradient, in mgal/ft
Free air gradient is 0.0934 mgal/ft (derrick measurement)
0.0560
0.0520
0.0480
0.0440
0.0400
0.0360
0.0320
Density, in g/cm3
1.600
1.700
1.800
1.900
2.000
2.100
2.200
2.300
2.400
2.500
Total porosity, in percent
0
10
20
30
40
50
Derrick floor elevation 167.46
24-in stove, 30 ft
18-in. stovepipe (no weight or cement record)
805
S. P.
Millivolts
20
Resistivity
Ohms m2/m
0
30
Dry
(assumed)
Water-saturated
Depth below derrick floor, in feet
0
100
200
300
400
500
600
700
800
900
1000
1100
1200
1300
1400
1500
1600
1700
1800
1900
2000
2100
2200

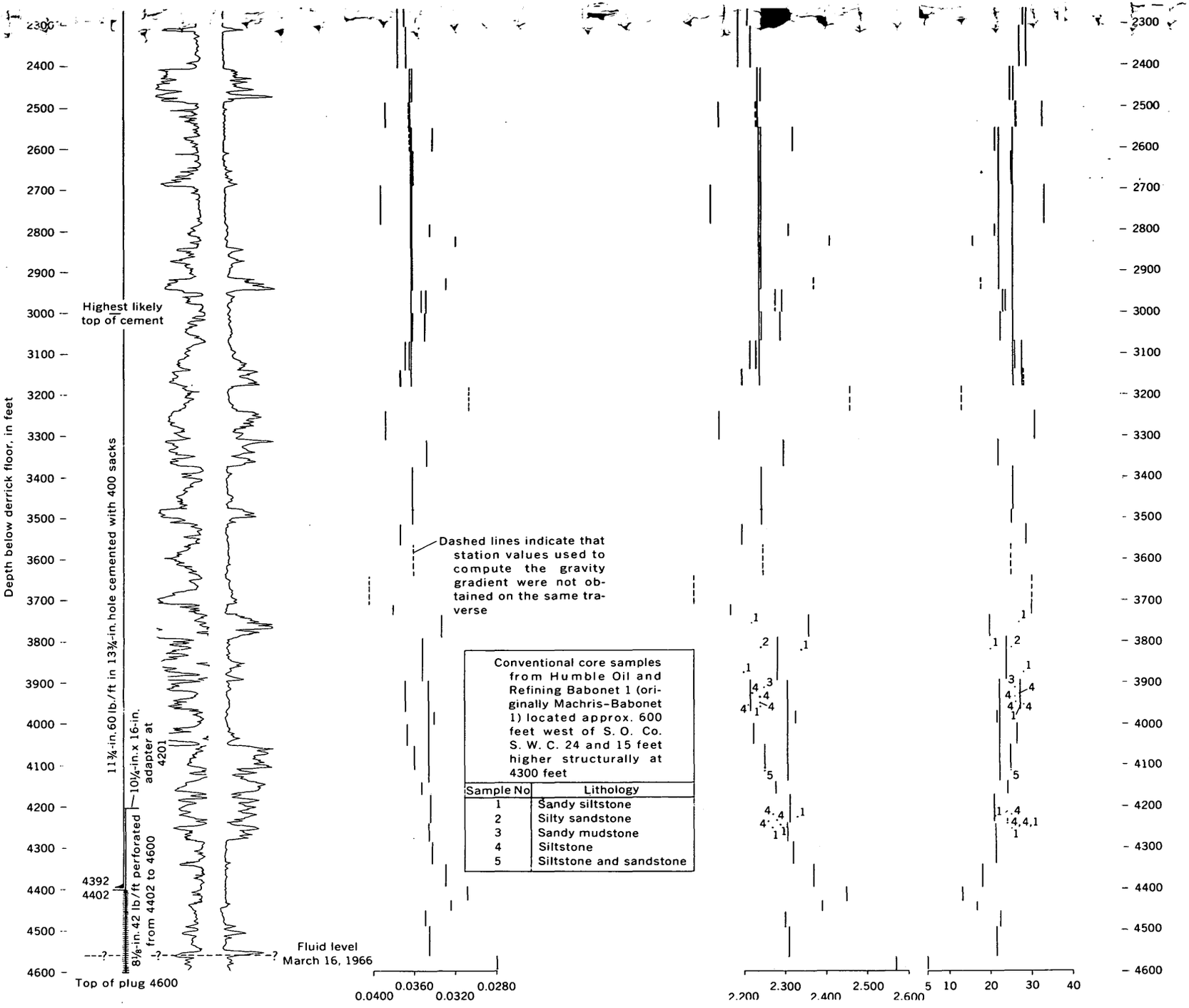

FIGURE 4.—Vertical gravity gradient, calculated average rock density, and derived average interval porosity versus depth for the Standard Oil Co. of California South Whittier Comm. No. 24 well, Santa Fe Springs oil field, Los Angeles County, Calif.

As an additional aid to the calculations of appropriate drift corrections, and as a means of circumventing the problems that arise from uncertainty about depth measurements, the last two stations occupied on each traverse are marked on the wire line and then reoccupied as the first two stations on the next traverse. Excessive drift rates, tares, or malfunction of the gravimeter are immediately revealed by this procedure, without question about depth-measurement errors.

The borehole gravimeter has not yet been tested in open (uncased) holes or in mud-filled holes. However, no evidence has been observed that suggests such operations would not be possible if adequate preparations were made (conditioning drilling fluid; preliminary run with empty sonde).

REPRESENTATIVE ILLUSTRATIVE DATA

Depth profiles of underground vertical gradients of gravity for two wells surveyed in detail during the spring of 1966 are summarized in figures 3 and 4 appearing on pages D108–D111. Observational data for each well are accompanied by the SP (spontaneous potential) and resistivity curves of the standard electrical log, a profile of average interval density (derived from the measurements of underground vertical gradient of gravity), and a profile of average interval porosity computed from the gravimetric interval density using assumptions about grain and fluid densities estimated by inspection of the SP and resistivity curves. Formulas relating bulk-rock density and porosity to underground vertical gravity gradient and procedures of data reduction and interpretation are published elsewhere (McCulloh, 1966, 1967a).

The two wells for which data are presented in figures 3 and 4 are located 7,000 feet apart in the eastern and western parts of the Santa Fe Springs oil field, Los Angeles County, Calif. Brief descriptions of the geology of the oil field are given by Van Couvering (1930), Winter (1943), and Ybarra (1957). The wells illustrated penetrate dominantly marine sandstone interbedded with siltstones and minor polymictic conglomerates of middle early Pliocene to Recent age. Although some oil and gas were produced from sandstones in the lower part of the section surveyed in each well, nearly the entire section surveyed is now water saturated in the vicinity of these locations.

"Natural" densities (Hedberg, 1936) and matching porosities measured and calculated by the senior author from samples of conventional core from one of the wells and from a hole near the other one are plotted in figures 3 and 4 alongside the values calculated from the gravimeter measurements. The discrepancies between the gravimetric and the core density data may result from (1) core samples that do not represent the lithologies penetrated or, the densities of much larger volumes of soft porous rock in situ, or (2) the inappropriateness of assumptions made in conversion of vertical gradients of gravity to rock density in situ, or some combination of these factors. These and related questions are discussed in general terms elsewhere (McCulloh, 1965, 1966, 1967a, b) and are to be examined in detail in relation to the data summarized here in the future.

REFERENCES

Hedberg, H. D., 1963, Gravitational compaction of clays and shales: Am. Jour. Sci., 5th ser., v. 31, no. 184, p. 241–287.

McCulloh, T. H., 1965, A confirmation by gravity measurements of an underground density profile based on core densities: Geophysics, v. 30, no. 6, p. 1108–1132.

———1966, The promise of precise borehole gravimetry in petroleum exploration and exploitation: U.S. Geol. Survey Circ. 531, 12 p.

———1967a, Mass properties of sedimentary rocks and the gravimetric effects of petroleum and natural-gas reservoirs: U.S. Geol. Survey Prof. Paper 528–A, 50 p.

———1967b, Borehole gravimetry—New developments and applications, *in* New geophysical developments and methods: World Petroleum Cong., 7th, Mexico, Sec. 6, p. 85–99.

McCulloh, T. H., LaCoste, L. J. B., Schoellhamer, J. E., and Pampeyan, E. H., 1967, The U.S. Geological Survey–LaCoste and Romberg precise borehole gravimeter system—instrumentation and support equipment: U.S. Geol. Survey Prof. Paper 575–D, p. D92–D100.

Moses, P.L., 1961, Geothermal gradients: Am. Petroleum Inst. Drilling and Production Practice, 1961, p. 57–63.

Reistle, C. E., Jr., and Sikes, S. T., Jr., 1938, Well-depth measurements: Am Petroleum Inst. Drilling and Production Practice, 1938 p. 80–95.

Service Hydrographic de la Marine and Compagnie Generale de Geophysique, 1965, Tidal gravity corrections for 1966: Geophys. Prospecting, v. 13, supp. 1, 53 p.

Van Couvering, Martin, 1930, A comparison between competitive and unit operation in the Santa Fe Springs Field, California: Am Petroleum Inst., 11th Ann. Mtg., Proc., sec. 4 (Production Bull. 206), v. 11, no. 75, p. 54–74.

Winter, H. E., 1943, Santa Fe Springs oil field: California Div. Mines Bull. 118, p. 343–346.

Ybarra, R. A., 1957, Recent developments in the Santa Fe Springs oil field: California Oil Fields, v. 43, no. 2, p. 39–45.

USE OF FAN FILTERS IN COMPUTER ANALYSIS OF MAGNETIC-ANOMALY TRENDS

By EDWIN S. ROBINSON, Salt Lake City, Utah

Abstract.—Potential-field maps for which data are given on a rectangular grid can be analyzed to determine anomaly lineation by means of fan-filtering techniques similar to those applied in seismic-velocity filtering. Filters can be designed to pass only elongate anomalies which strike in a preferred azimuth range. Such filters are useful for defining more clearly subtle anomaly lineations that may not be obvious on unfiltered maps.

FILTER PREPARATION

Fan-filter operators for potential-field maps may be prepared in the same way that such operators are designed for seismic data. A gridded potential-field map is similar to a digitized seismogram in that both give amplitude data at discrete points on a two-dimensional field. Potential fields are described at given X and Y coordinates, and seismic amplitudes are given at rectangular time and distance positions. The derivation of fan-filter operators has been described in detail by Fail and Grau (1963) and Embree and others (1963). The grid values of a fan filter having $2m$ rows and $2n+1$ columns are computed from the following expression which was modified from the equation of Embree and others (1963) by substituting X and Y coordinates for the t and X coordinates applied to seismic data:

$$g(X_n, Y_m)=\left[\pi^2\left[\left(\frac{Y_m}{\Delta Y}\right)^2-\left(\frac{X_n}{K\Delta X}\right)^2\right]\right]^{-1},$$

where ΔX and ΔY are grid intervals and K is an integer. The grid operator is symmetrical in four quadrants. Anomaly-trend filtering is achieved by convolving $g(X, Y)$ with the potential field. Figure 1 shows profiles along rows of a filter having 12 rows and 21 columns. As for most filter operators that theoretically extend to infinity in all directions, practical dimensions are taken at distances where operator amplitudes have diminished to a negligible level. The range of azimuths that are passed by the filter is determined from the expression:

$$\tan\theta=K(\Delta X/\Delta Y).$$

If $K=1$ and $\Delta X=\Delta Y$, then $\theta=45°$ and the filter passes features trending in a $\pm 45°$ range about a center azimuth. For a map having rows extending from west to east, anomalies trending in the range of N. 45° W. to N. 45° E. are passed. If $K=2$ and $\Delta X=\Delta Y$, then $\theta\approx 63°$ and the filter range would be from N. 63° W. to N. 63° E.

The fan-filter response characteristics shown in figure 2 were obtained by two-dimensional Fourier transformation of $g(X, Y)$. Frequency F is given in cycles per grid interval, and wave number $k=F/(\Delta Y/K\Delta X)$. Filter response is plotted in linear units. The filter passes all frequencies of anomalies which strike in the specified azimuth range. FORTRAN IV digital computer programs have been written for computing fan filters and their response characteristics and to convolve these filters with potential fields.

APPLICATION

An aeromagnetic map of part of central Nevada is shown in figure 3. The dominant magnetic anomaly is the linear high striking about northwest. The anomaly is believed to be related to the dike swarm exposed in two locations along the anomaly (Mabey, 1966), but the primary source of the anomaly is probably several kilometers below the surface. The aeromagnetic map was digitized on a 1-mile grid, and a map was prepared by a high-speed printer (fig. 4) from the digital data. Use of a printer to prepare the filtered magnetic maps (figs. 4–6) distorts the horizontal scale somewhat, but the printer is a fast and inexpensive method

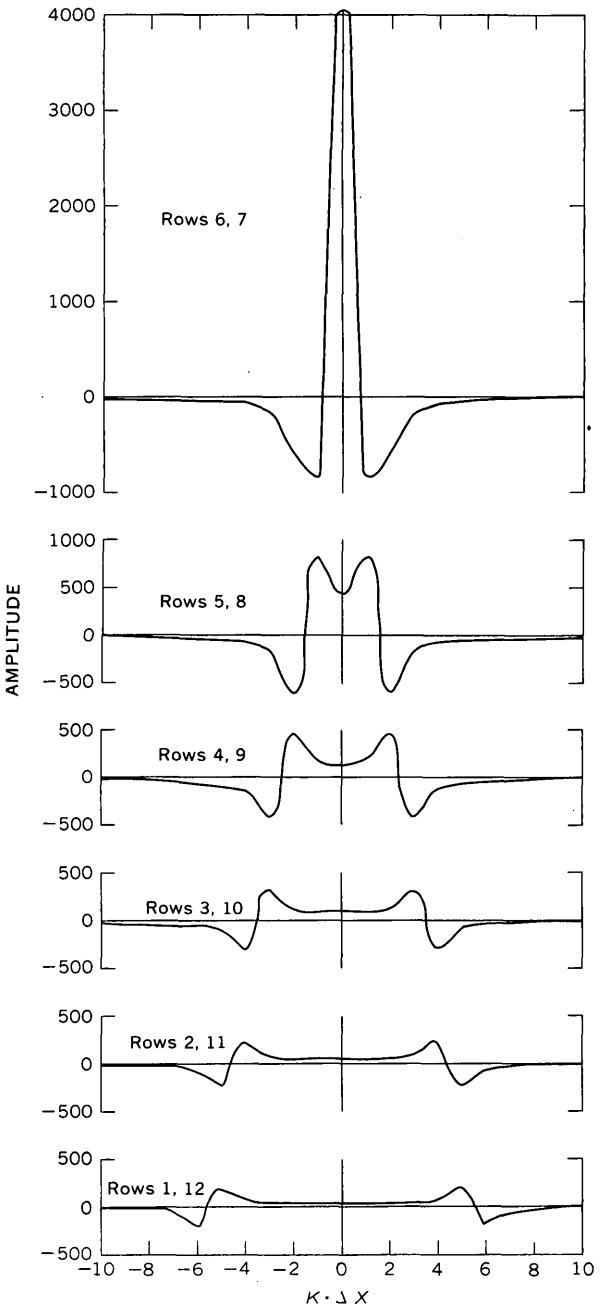

FIGURE 1.—Grid operator designed to pass potential-field features trending in a specified azimuth range.

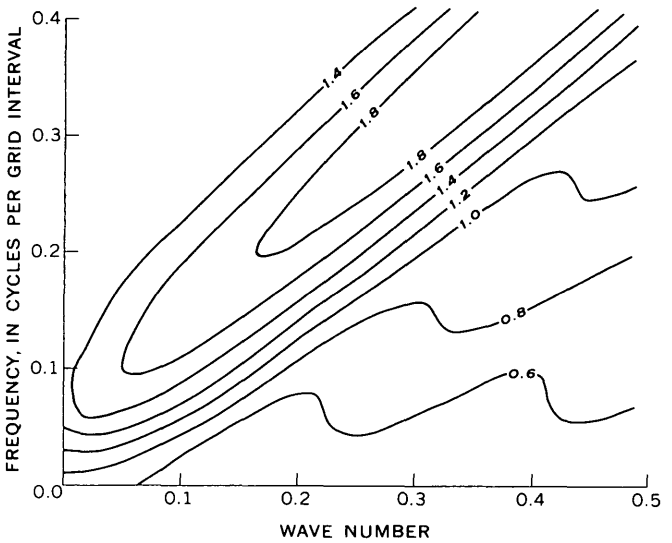

FIGURE 2.—Response characteristics of filter shown in the frequency (F) and wave number (k) domain. Contours are in linear units.

of preparing maps that are adequate for analyzing trends.

Filtered magnetic-field maps on which anomalies trending in the ranges northwest to northeast, west to north, southwest to northwest, and south to west were prepared (figs. 5, 6). The maps filtered to pass anomalies trending in the ranges northwest to northeast and west to north (fig. 5) show the dominant northwest-trending anomaly with most secondary cross trends removed. The dominant northwest-trending feature is effectively suppressed on the maps filtered to pass anomalies trending in the ranges southwest to northwest and south to west, and the secondary features are more obvious (fig. 6). Subtle magnetic patterns probably related to the near-surface geological structure and not obvious on the unfiltered map are suggested by figure 6.

In conclusion, fan-filtering techniques originally developed for processing seismic data may be adapted for potential-field analysis to define subtle anomaly trends which are obscured by more dominant features. Such filters involve data mixing and naturally introduce some smoothing and distortion; therefore quantitative analysis of filtered anomalies should be treated with caution. Anomalies having different lineation but arising from a common source may be distorted, but component trends will be more clearly evident after filtering. Qualitative examination of figures 4, 5, and 6 indicates that the more obvious anomaly shapes have passed through the filter with minimal distortion. Within the specified azimuth range, all frequency components of an anomaly are passed—a feature that is advantageous to the analysis of potential-field features, which usually have a broad spectrum.

ACKNOWLEDGMENT

I would like to acknowledge the helpful discussions with Dr. John K. Costain of the Geophysics Department, University of Utah.

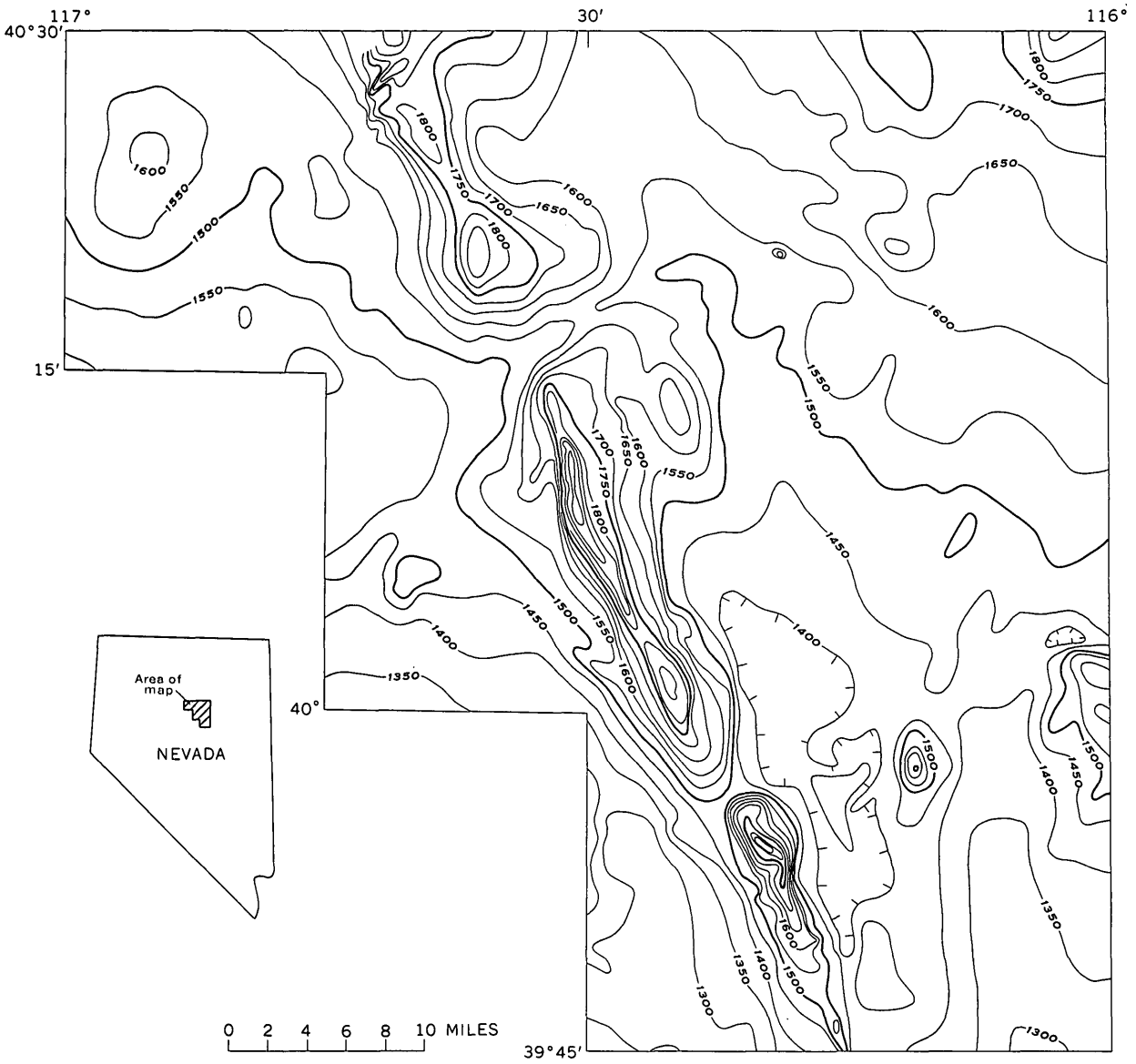

FIGURE 3.—Total-intensity aeromagnetic map of part of central Nevada. Flight lines were 1 mile apart, flown in a north-south direction, and 9,000 feet above sea level. Contour interval is 50 gammas. Hachures indicate closed areas of magnetic lows. (Philbin and others, 1963).

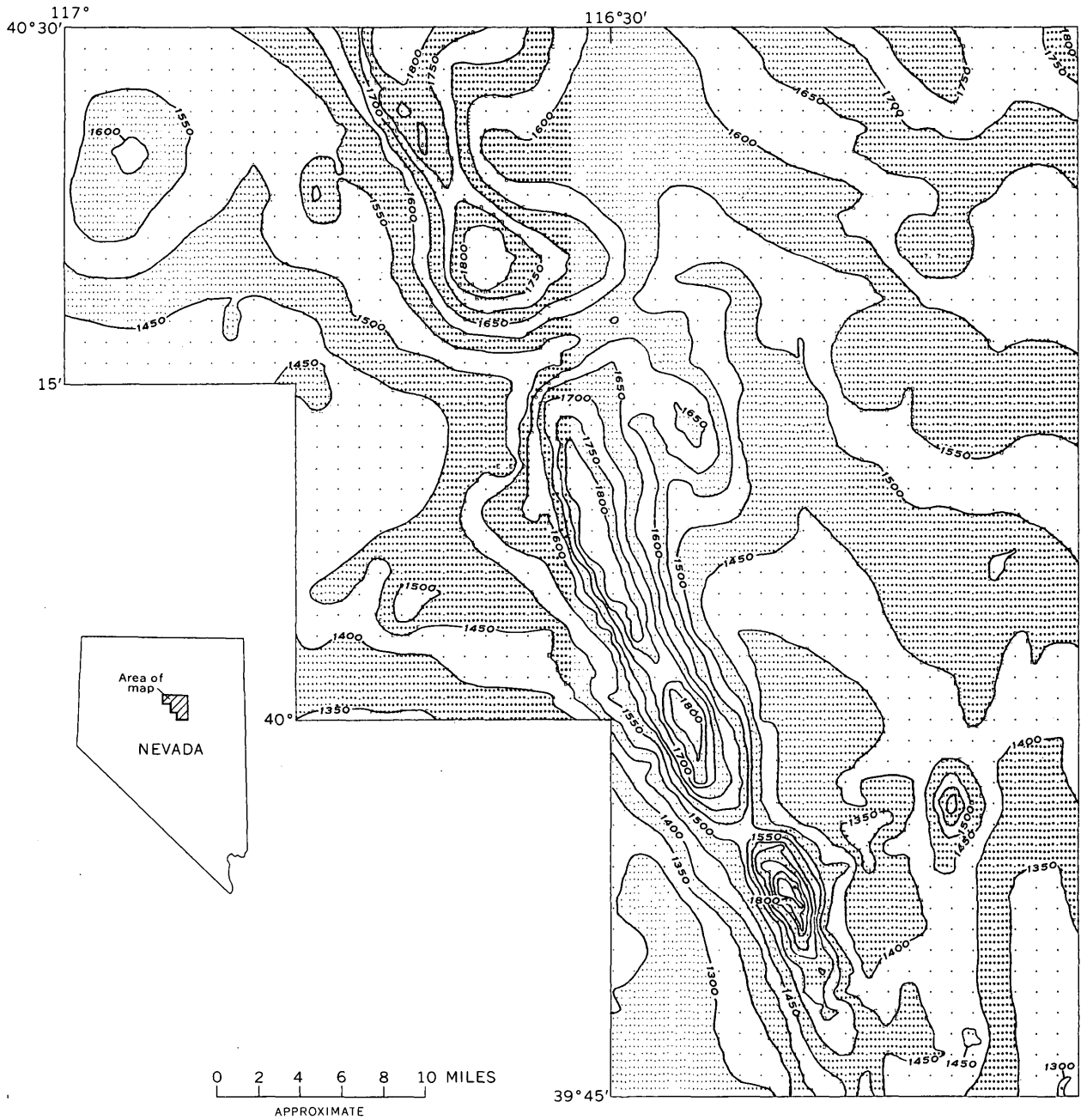

FIGURE 4.—Aeromagnetic map of part of central Nevada digitized on a 1-mile grid and plotted with high-speed printer. Contour interval is 50 gammas. Illustration is a reduced composite of computer printout sheets to which contours have been added.

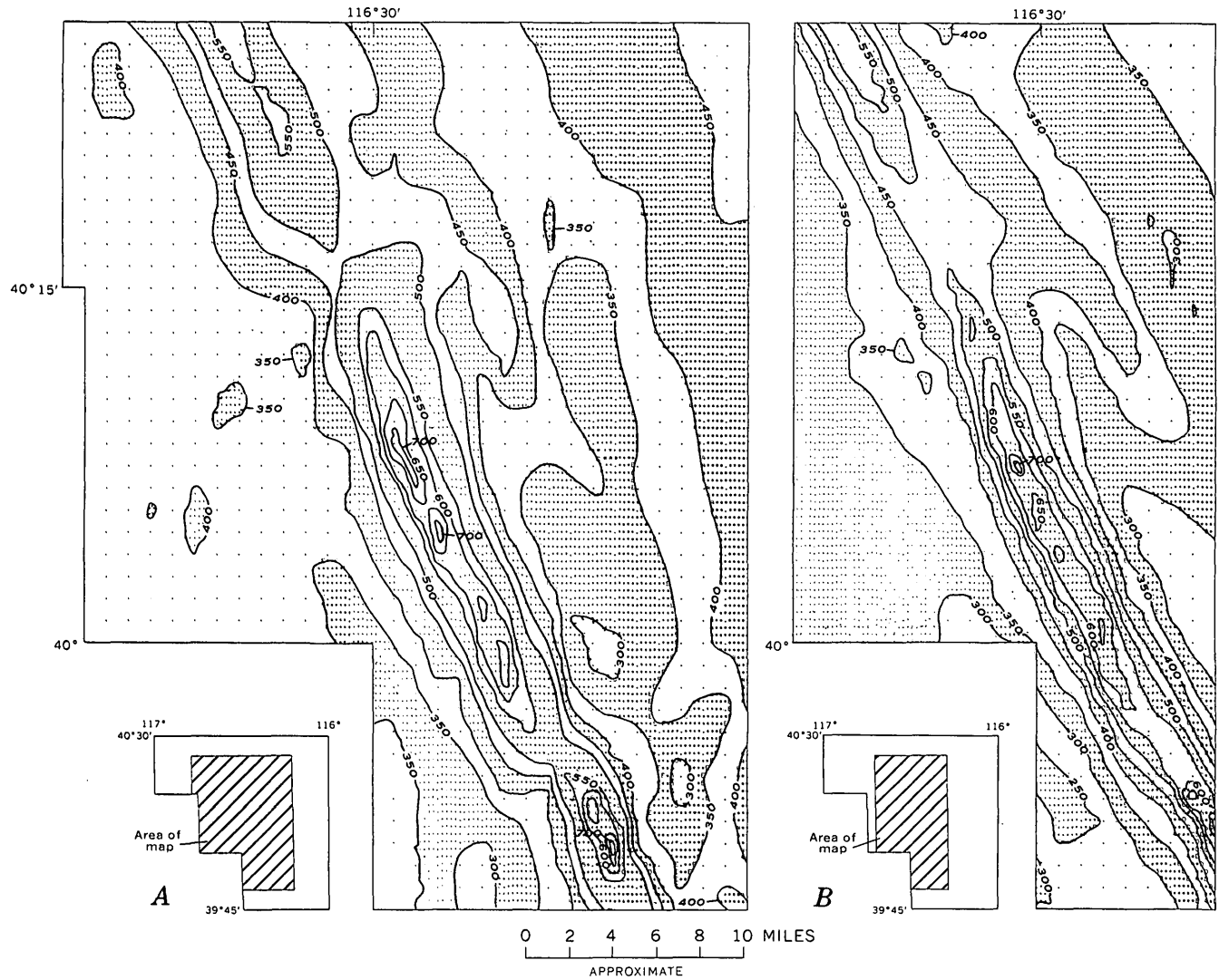

FIGURE 5.—Potential-field maps of part of central Nevada filtered to pass anomalies trending in the ranges (*A*) northwest to northeast and (*B*) west to north. Contour interval is 50 gammas. Illustrations are reduced computer printout sheets to which contours have been added.

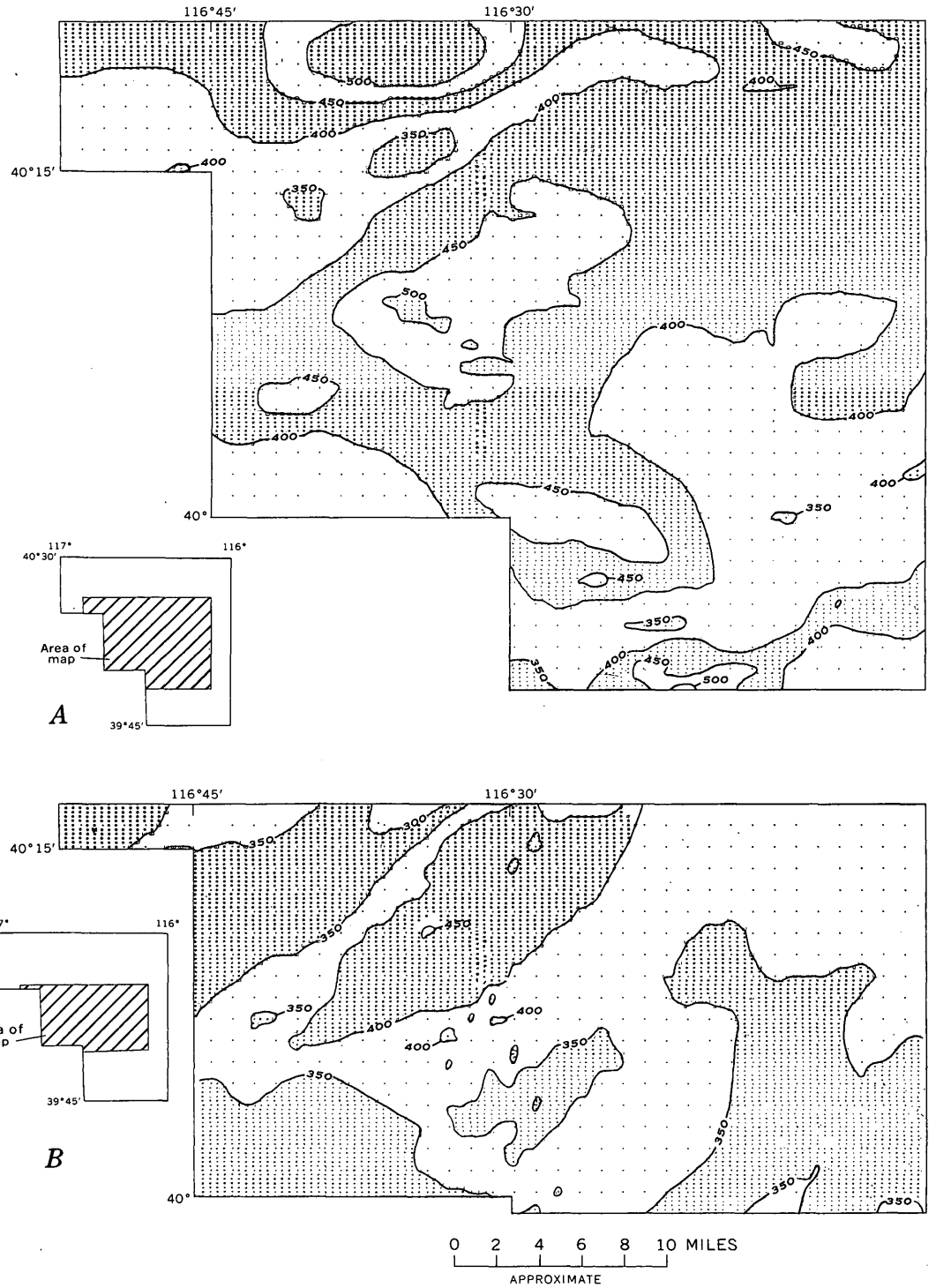

FIGURE 6.—Potential-field maps of part of central Nevada filtered to pass anomalies trending in the ranges (*A*) southwest to northwest and (*B*) south to west. Contour interval is 50 gammas. Illustrations are reduced computer printout sheets to which contours have been added.

REFERENCES

Embree, Peter, Burg, J. P., and Backus, M. M., 1963, Wide band velocity filtering, the pie-slice process: Geophysics, v. 28, no. 6, p. 948–974.

Fail, J. P., and Grau, G., 1963, Les Filtres en eventail: Geophys. Prospecting, v. 11, p. 131–168.

Mabey, D. R., 1966, Regional gravity and magnetic anomalies in part of Eureka County, Nevada, *in* Case histories, v. 1 *of* Mining Geophysics: Tulsa, Okla., Soc. Explor. Geophysics, 492 p.

Philbin, P. W., Meuschke, J. L., and McCaslin, W. E., 1963, Aeromagnetic map of the Roberts Mountain area, central Nevada: U.S. Geol. Survey open-file rept.

TECTONIC INCLUSIONS FROM A SERPENTINITE, EAST-CENTRAL ALASKA

By ROBERT L. FOSTER, Menlo Park, Calif.

Work done in cooperation with the University of Missouri

Abstract.—Mapping in the western Yukon-Tanana Upland has revealed the presence of northeast-trending alpine-type serpentinite masses with associated tectonic inclusions in the general vicinity of Livengood, Alaska. Serpentinite-associated tectonic inclusions have not been documented previously in Alaska.

A discontinuous belt of ultramafic rocks, identified here as the Livengood trend (fig. 1), extends approximately 120 miles northeastward from near Manley Hot Springs (Tanana A–3 quadrangle) through Livengood to Beaver Creek south of Mount Schwatka (Livengood C-2 quadrangle) in east-central Alaska. The linear bodies making up this belt have known maximum widths of as much as 1 mile and lengths of as much as 10 miles. They conform to the regional grain and extend over larger parts of the western Yukon-Tanana Upland than previously believed by Mertie (1937). Detailed geologic investigations on the ultramafic body near Livengood indicate that the ultramafic rocks have alpine-type serpentinite affinities and are characterized by the occurrence of minor amounts of chrysotile and nickeliferous mineral phases. The serpentinites are in fault and unconformable contact with late Middle Devonian metagraywacke strata, and are associated with chert-carbonate units, altered volcanic rocks, and metadiorite. The Livengood body, moreover, is characterized by the sporadic presence of tectonically transported inclusions of a type previously described from near Cassiar, British Columbia.

Tectonically transported calcium silicate-rich rocks, or rodingites (Bell and others, 1911), associated with serpentinites have been described from many parts of the world and reviewed by Coleman (1966). Some of the tectonic inclusions in the Livengood area are similar in mode of occurrence and petrography to the northernmost noted rodingites or "white rock" bodies described by Gabrielse (1963) from the McDame ultramafic rocks near Cassiar, British Columbia, approximately 750 miles to the southeast (fig. 1).

Most of the Livengood inclusions are tabular, blocky, or irregular in shape; are less than 50 feet in maximum dimension; and consist of olive-green, massive, fine-grained rocks. Light-green coarse-grained poikilitic and subophitic gabbroic rocks, dark-gray amygdaloidal volcanic rocks, light-gray foliated chert and quartzite, and white granular quartzite are less common relict characteristics of the inclusions.

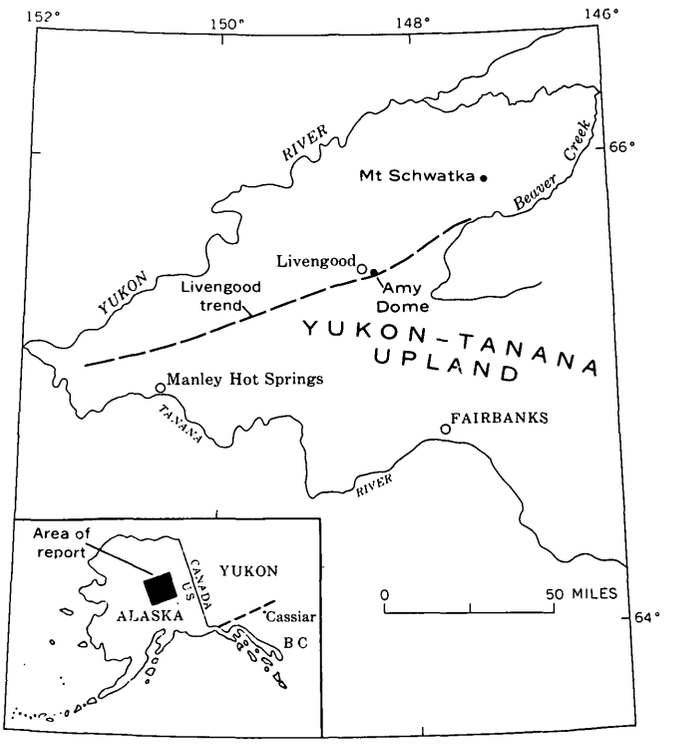

FIGURE 1.—Map of report area, showing trace of Livengood trend.

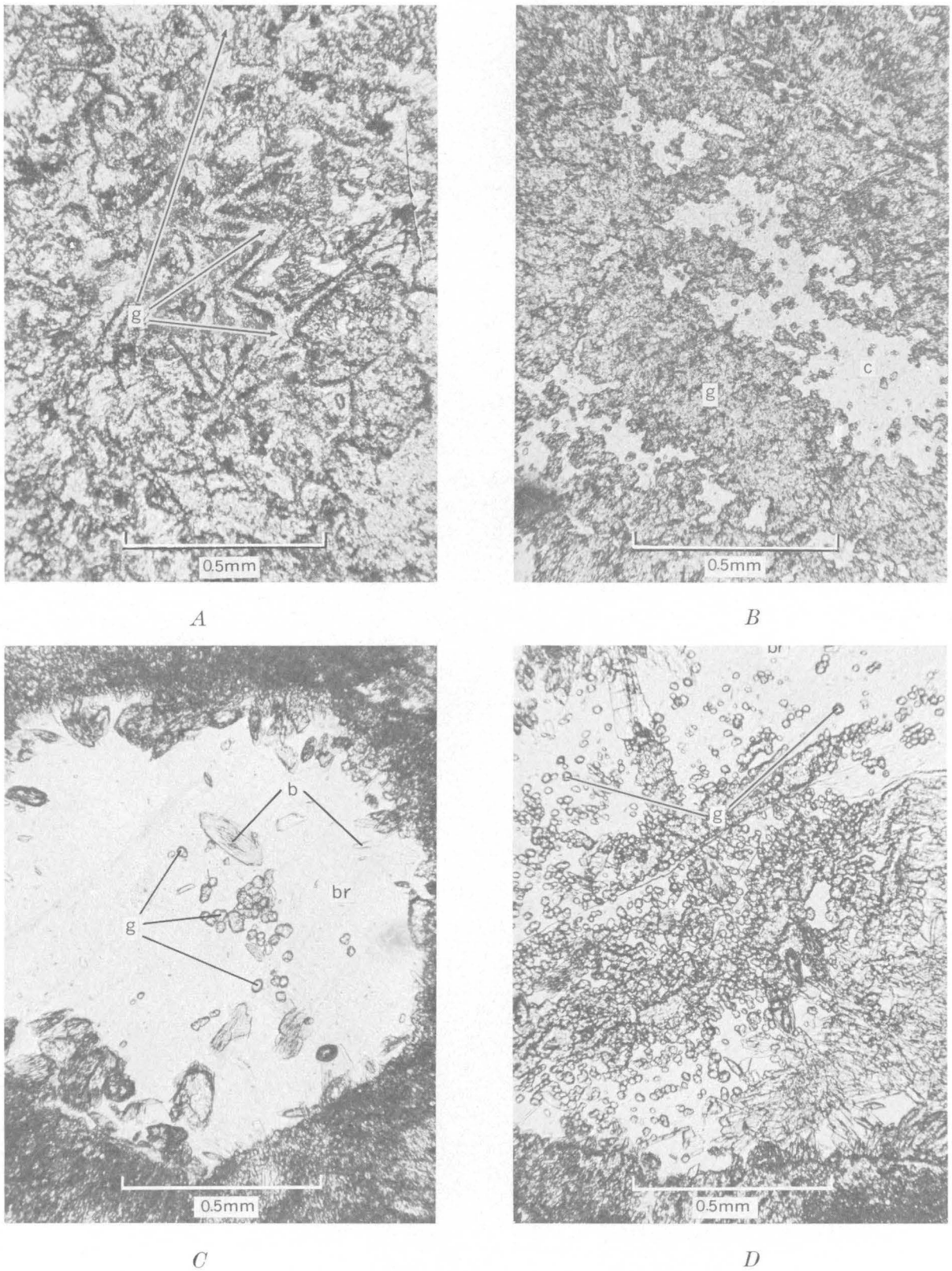

FIGURE 2.—Photomicrographs of tectonic inclusions from a serpentinite in the vicinity of Livengood, Alaska.
A. Garnet (g) pseudomorphous after microlaths of plagioclase. Sample 63AF–99, plane light.
B. Massive garnet (g) in contact with chlorite (c). Sample 64AF–244, plane light.
C. Garnet (g) and unidentified "blades" (b) "floating" in brucite(?) (br) pseudomorphous after olivine. Sample 63AF–108A, plane light.
D. Garnet anhedra (g) "floating" in brucite (br). Sample 63AF–99, plane light.

The fine-grained rocks range from pumpellyite-clinopyroxene-chlorite assemblages to garnet-chlorite-clinopyroxene-vesuvianite assemblages. As much as 50 percent of the volume of the latter is composed of massive garnet, some of which is pseudomorphous after plagioclase laths (fig. 2*A*). X-ray diffraction and optical data indicate that this garnet phase is hydrogrossularite. The coarse-grained rocks range from approximately 70 volume percent garnet that has been partly replaced by chlorite (fig. 2*B*) to (1) mixtures of altered pyroxene anhedra, (2) a pumpellyite-garnet assemblage pseudomorphous after plagioclase, and (3) brucite (pseudomorphous after olivine) surrounded by garnet and an anisotropic brown acicular mineral. The central parts of the brucite pseudomorphs are composed of "floating" garnet anhedra (fig. 2*C*, *D*) and an unidentified colorless mineral with a bladelike habit (fig. 2*C*).

The youngest tectonic inclusions in the serpentinite are semi-randomly oriented blocks derived from dikes that are probably genetically related to a metadiorite stock that makes up part of Amy Dome about 4 miles southeast of Livengood. These inclusions have been metasomatically altered to clinozoisite-epidote-prehnite metadiorite (Foster, 1966).

The Livengood tectonic inclusions (derived from intrusive igneous, volcanic, sedimentary, and metamorphic rocks) were caught up in or intruded into the ultramafic body prior to, or concomitant with final solid emplacement of the mass. The development of rodingite mineral assemblages was genetically associated with the metasomatic metamorphism of the enclosing ultramafic mass during pervasive serpentinization.

Additional detailed geologic investigations of the discontinuous belt of serpentinite masses of the Livengood trend are desirable for a systematic interpretation of the complex structures of the interior of Alaska.

REFERENCES

Bell, J. M., Clarke, E. de C., Marshall, Patrick, 1911, The geology of the Dun Mountain subdivision, Nelson, New Zealand: New Zealand Geol. Survey, v. 12, p. 31–35.

Coleman, R. G., 1966, New Zealand serpentinites and associated metasomatic rocks: New Zealand Geol. Survey Bull., v. 76, 102 p.

Foster, R. L., 1966, The petrology and structure of the Amy Dome area, Tolovana Mining District, east-central Alaska: Columbia, Mo., Missouri Univ. unpub. Ph.D. thesis, 227 p.

Gabrielse, H., 1963, McDame map-area, Cassiar district, British Columbia: Geol. Survey Canada Mem. 319, p. 83–84.

Mertie, J. B., Jr., 1937, The Yukon-Tanana region, Alaska: U.S. Geol. Survey Bull. 872, 276 p.

PRELIMINARY REPORT ON SULFIDE AND PLATINUM-GROUP MINERALS IN THE CHROMITITES OF THE STILLWATER COMPLEX, MONTANA

By NORMAN J PAGE and EVERETT D. JACKSON, Menlo Park, Calif.

Abstract.—Platinum-group minerals, previously known to occur in the layered gabbros of the Banded and Upper zones of the Stillwater Complex, have been found in the Ultramafic zone as well. Laurite and other complex platinum-group sulfides and sulfarsenides are present in at least four of the chromitite zones of the Peridotite member. The economic potential of these occurrences cannot be evaluated at the present time, but the possibility of obtaining platinum-group metals as a byproduct of chrome mining operations should not be overlooked in the future.

The geochemical affinity of the platinum-group metals for layered intrusions of mafic and ultramafic igneous rocks is well documented (Wright and Fleischer, 1965). These metals occur predominantly as sulfide minerals or as alloys spatially associated with sulfide minerals. The presence of sulfide minerals along the base of the Stillwater Complex was known as early as 1883 (Roby, 1949). Although assay values for platinum-group metals have been obtained on samples from these basal rocks (Howland, 1933; Howland and others, 1936), no platinum-bearing minerals have as yet been identified. Sulfide minerals, including the platiniferous mineral sperrylite and the palladium-bearing mineral stibiopalladinite, have also been described in the layered gabbros of the Banded and Upper zones of the complex, and have been compared with similar occurrences in the Merensky Reef of the Bushveld Complex in South Africa (Howland and others, 1936). Sulfide minerals in the Ultramafic zone of the Stillwater Complex, which forms the stratigraphic unit separating the basal rocks from the Banded and Upper zones, have not previously been reported.

Acknowledgment.—The authors are grateful to Michael Fleischer, of the U.S. Geological Survey, for the translation from the Russian original of the paper by Genkin and others (1966).

SULFIDE MINERALS IN THE ULTRAMAFIC ZONE

Jackson (1961) has divided the Ultramafic zone into two stratigraphic units—a lower, Peridotite member, and an upper, Bronzitite member (fig. 1). Scattered individual blebs and small grains of sulfide minerals have been observed in all the ultramafic rock types of both members, from the Benbow area in the east to the Gish area in the west. Field observations suggest, however, that these sulfide minerals are concentrated in the chromitite zones of the Peridotite member (fig. 2).

Thus far, we have found sulfide minerals to be present in the A and B chromitite zones in the Benbow and West Fork areas, in the G zone in the Nye Lip, Mountain View, West Fork, and Gish areas, in the H zone in the Mountain View and Chrome Mountain areas, in the I and J zones in the Mountain View and West Fork areas, and in the K zone in the Nye Lip and Iron Mountain areas (fig. 2). In a few places the sulfide minerals form massive pods subparallel to the footwalls of the chromitite layers, replacing all the silicate minerals and surrounding the chromite grains with a mesostasis of poikilitic sulfide "cement." Most generally, however, they occur as isolated polymineralic aggregates replacing the silicate minerals in the chromitites or, more rarely, as inclusions in the chromite grains.

The most abundant sulfide minerals in the chromitites are pyrrhotite, chalcopyrite, and pentlandite, which are also abundant in the basal rocks and in the Banded and Upper zones (Howland and others, 1936). Electron-microprobe analyses indicate that the range in composition of pyrrhotite is at least from $Fe_{0.96}S$ to $Fe_{0.93}S$. Several types of pyrrhotite are present in some single chromitite layers and can be distinguished from one another by their relative Fe content and textural appearance. The pentlandite contains only minor

U.S. GEOL. SURVEY PROF. PAPER 575-D, PAGES D123-D126

269-274 O—67——9

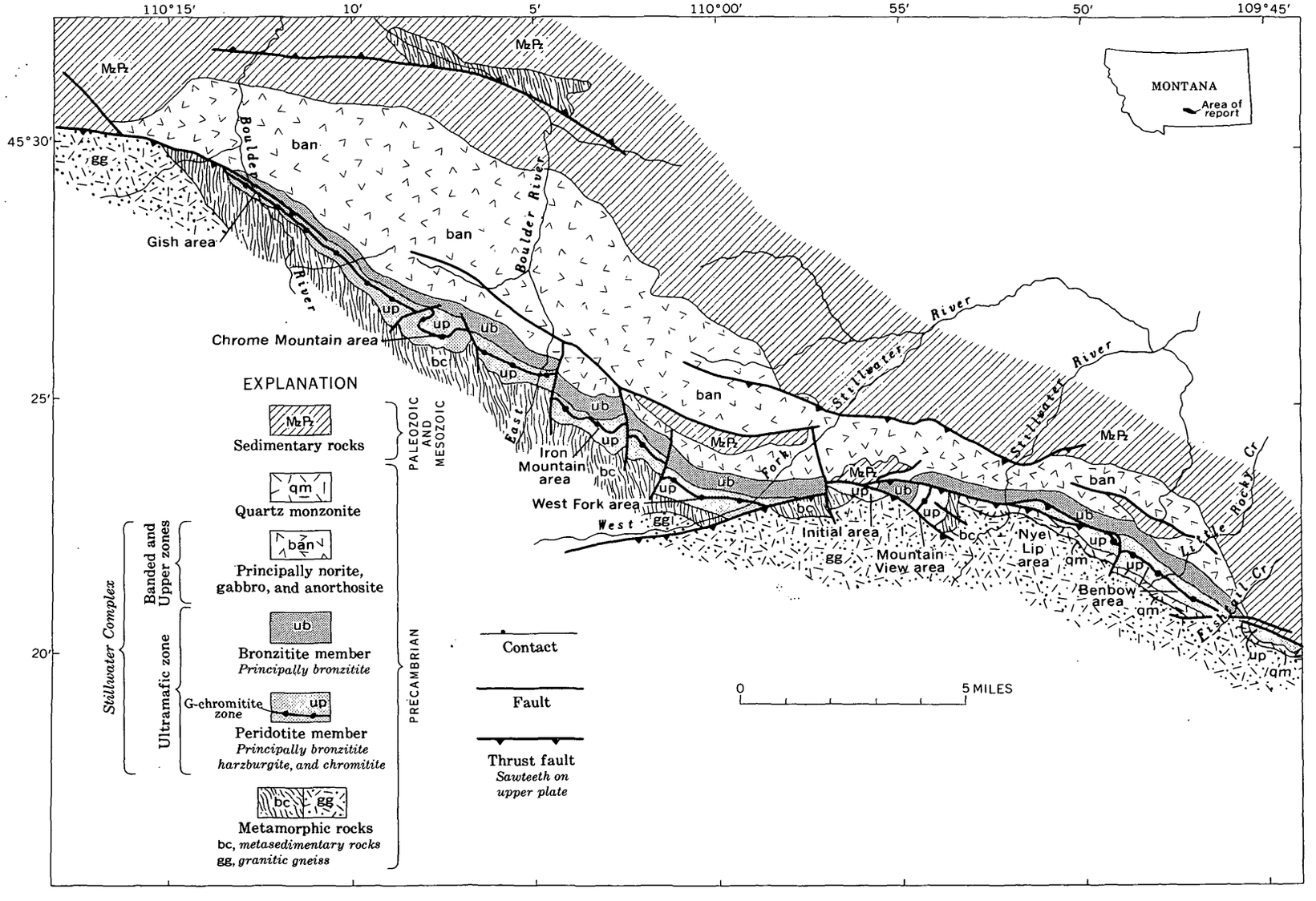

FIGURE 1.—Geologic index map of the Stillwater Complex.

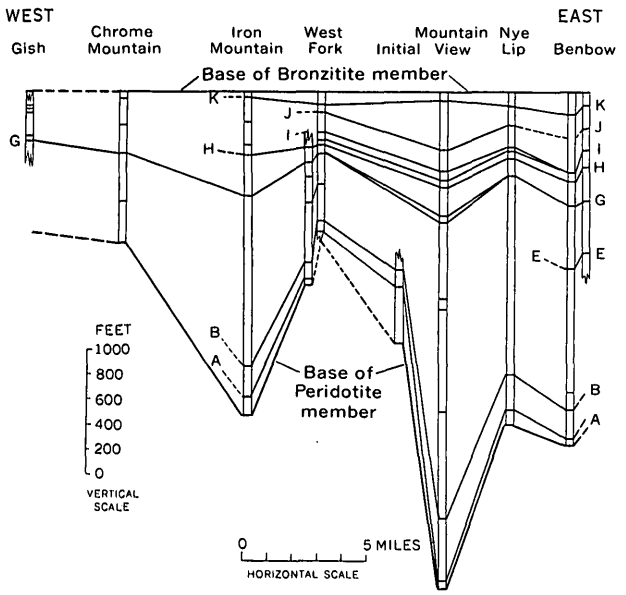

FIGURE 2.—Correlation diagram showing the chromitite zones in the Peridotite member of the Ultramafic zone. Zones are lettered alphabetically from bottom to top of the section.

amounts of Co and has a Ni to Fe ratio of approximately one to one.

Other sulfides and arsenides are present, but appear to have a scattered and limited distribution. These include a member of the cobaltite group, niccolite, molybdenite, and pyrite. Complex arsenosulfo-selenoantimonide minerals have also been found, but their exact identification has not been completed.

The cobaltite-group mineral has heretofore never been described from the Stillwater Complex. Thus far we have observed this mineral in the A-zone and G-zone chromitites and among the sulfides at the base of the complex as well. Uncorrected electron microprobe analyses suggest the following range of composition, in weight percent: 20–22 percent Co, 9–11 percent Ni, 7–8 percent Fe, 16–18 percent S, and 43–49 percent As. Compared with a similar gerdorsffite from Sudbury, Ontario (Hawley, 1962), the Stillwater cobaltite-group minerals contain a greater amount of Co and less Ni.

Niccolite, also previously unknown in the complex, has been found in the A-zone chromitites, but only in small (5–25 micron diameter) polymineralic inclusions in chromite. These inclusions are commonly composed of three phases, having pyrrhotite and chalcopyrite in addition to niccolite. They occur in groups of 5 to 15 per grain, tend to be located near centers of chromite grains, and usually have no visible connections with grain boundaries. Silicate inclusions in the chromites are commonly associated with these sulfide inclusions in the same samples.

Molybdenite, also previously unknown in the complex, is present as small sparsely disseminated grains in the G, H, and K chromitite zones.

PLATINUM-GROUP MINERALS IN THE CHROMITITE ZONES

Platinum-group minerals have been observed in the B chromitite zone of the Benbow area, the G and H zones of the Mountain View area, and in the K zone of the Iron Mountain area. Their presence is also indicated by unpublished assay data from a chromitite very low in the section in the Chrome Mountain area. Thus far, the platinum-group minerals have been recognized only in chromitites and not in peridotites or bronzitites in the Ultramafic zone, and, furthermore, they have been recognized only in those chromitites that contain the more common Fe-, Ni-, and Cu-bearing sulfide minerals.

Texturally, all the platinum-group minerals thus far examined occur as isolated grains, either in the interstitial silicate minerals of the chromitites, or in the chromite grains themselves. They have not been seen in contact with other sulfide minerals, so that their paragenesis cannot be established at this time.

Laurite (RuS_2), also containing Os and Ir, occurs as diamond-shaped inclusions (20–50 microns in diameter) in chromite from the B, G, H, and K chromitite zones. Its identification was confirmed by qualitative electron-microprobe analyses, and it appears to be quite similar to the osmium-rich variety described by Stumpfl and Clark (1964/65) in gold-platinoid concentrates from southeast Borneo.

Other complex platinum-group sulfides and sulfarsenides have been recognized with the microprobe in samples from the G and H chromitite zones. One of these minerals is an Os-Ir-Pt-Ni sulfide in which the metals are listed in order of decreasing abundance based on relative X-ray peak heights from microprobe wavelength scans. Another platinum-group mineral is a complex sulfosalt containing Sn, Os, Ir, Cu, and traces of Pt and Pd. Both minerals are present as 5–20-micron grains. Not enough work has been done to characterize these minerals completely, but they seem similar to platinum-group minerals described by Stumpfl (1961) from the Bushveld Complex and by

Stumpfl and Clark (1965) from the Driekop mine, by Kingston (1966) from the Rustenberg and Union mines in the Merensky Reef, and by Genkin and others (1966) from the Onverwacht deposits.

We have not as yet identified platinum-group alloys in the Stillwater Complex, but in view of their common occurrence in the Bushveld Complex (Cousins, 1964), we plan to look for them.

ORIGIN OF SULFIDE MINERALS IN THE ULTRAMAFIC ZONE

The close association of the sulfide minerals in the Ultramafic zone with the chromitite zones is similar to the distribution of the gabbro pegmatites (Jackson, 1961). It may be that they were localized in much the same way, by the relative impermeability of the fine-grained chromitites to the passage of liquid phases upward through the crystal pile. On the other hand, the chromitites do lie near the bases of the cyclic units of the Ultramafic zone (Jackson, 1961), and it is conceivable that they represent mattes precipitated by the individual batches of magma that formed the cyclic units.

ECONOMIC CONSIDERATIONS

These sulfide minerals, other than those containing platinum-group metals, have no economic potential at this time. The possibility of economic recovery of the platinum-group minerals is more difficult to evaluate. Similar occurrences have been reported in chromitites in the Bushveld Complex, and platinum assays as high as 0.6 ounces per ton have been reported there. However, the values have been spotty and difficult to reproduce, and Wagner (1929, p. 96) said of them "it appears doubtful whether they will ever be worked for their platinum contents." Nevertheless, the Stillwater chromitites have been mined for chrome ore in the past, and about a million tons of concentrates have been produced (Jackson, 1963). In the future, the possibility of obtaining byproduct platinum-group metals during chrome mining operations should not be overlooked.

REFERENCES

Cousins, C. A., 1964, The platinum deposits of the Merensky Reef *in* S. H. Haughton, ed., The geology of some ore deposits in southern Africa, v. 2: Geol. Soc. South Africa, Johannesburg, p. 225–237.

Genkin, A. D., Zhuravlev, N. N., Troneva, N. V., and Murav'eva, I. V., 1966, Irasite, a new sulfarsenide of iridium, rhodium, ruthenium, and platinum: Zapiski Vses. Mineralog. Obshch. v. 95, p. 700–712. [In Russian]

Hawley, J. E., 1962, The Sudbury ores; their mineralogy and origin: Canadian Mineralogist, v. 7, pt. 1, 207 p.

Howland, A. L., 1933, Sulphides and metamorphic rocks at the base of the Stillwater Complex, Montana: Princeton Univ., unpub. Ph.D. thesis, 76 p.

Howland, A. L., Peoples, J. W., and Sampson, Edward, 1936, The Stillwater igneous complex and associated occurrences of nickel and platinum group metals: Montana Bur. Mines Misc. Contr. 7, 15 p.

Jackson, E. D., 1961, Primary textures and mineral associations in the Ultramafic zone of the Stillwater complex, Montana: U.S. Geol. Survey Prof. Paper 358, 106 p.

———1963, Chromium, *in* Mineral and water resources of Montana: Montana Bur. Mines and Geology Spec. Pub. 28, p. 57–60.

Kingston, G. A., 1966, The occurrence of platinoid bismuthotellurides in the Merensky Reef at Rustenberg platinum mine in the western Bushveld: Mineralog. Mag., v. 35, no. 274, p. 815–835.

Roby, R. N., 1949, Investigation of copper-nickel deposits of the Stillwater Complex, Stillwater and Sweetgrass Counties, Montana: U.S. Bur. Mines. Rept. Inv. RI–4431, 10 p.

Stumpfl, E. F., 1961, Some new platinoid-rich minerals, identified with the electron microanalyser: Mineralog. Mag., v. 32, no. 254, p. 833–847.

Stumpfl, E. F., and Clark, A. M., 1964/65, Electron-probe microanalysis of gold-platinoid concentrates from southeast Borneo: Inst. Mining and Metallurgy [London] Trans., v. 74, p. 933–946.

———1965, Hollingworthite, a new rhodium mineral, identified by electron probe microanalysis: Am. Mineralogist, v. 50, nos. 7–8, p. 1068–1074.

Wagner, P. A., 1929, The platinum deposits and mines of South Africa; with a chapter on the mineragraphy and spectrography of the sulphide platinum ores of the Bushweld Complex, by H. Schneiderhöhm: London, Oliver and Boyd, 326 p.

Wright, T. L., and Fleischer, Michael, 1965, Geochemistry of the platinum metals: U.S. Geol. Survey Bull. 1214–A, p. A1–A24.

BISMUTH AND TIN MINERALS IN GOLD- AND SILVER-BEARING SULFIDE ORES, OHIO MINING DISTRICT, MARYSVALE, UTAH

By ARTHUR S. RADTKE, CHARLES M. TAYLOR [1], and JOHN E. FROST [2],
Menlo Park, Calif., Palo Alto, Calif., Houston, Tex.

Abstract.—Large amounts of cuprobismutite and bismuthinite are present in gold- and silver-bearing sulfide ores in the Tunnel Extension Number Two mine near Marysvale, Utah. Significant amounts of cassiterite in small grains are concentrated in the quartz gangue. Most of the silver is present in cuprobismutite, and gold occurs as the native metal. Carbonate beds below the mine, mineralized elsewhere in the district, offer potential exploration targets.

The Ohio mining district, a precious-metal producer, is located on the east flank of the Tushar Range, about 6 miles west-southwest of Marysvale (fig. 1) in Piute County, Utah. Samples collected by J. E. Frost from the 400 level of the Tunnel Extension Number Two mine contain several abundant metallic minerals, and the ore contains abundant bismuth and copper. Bismuth and tin minerals in these ores were not reported in either the early work by Butler and others (1920), or in the recent compilation of minerals in Utah (Bullock and others, 1960). Dasch (1964), in summarizing certain mineral resources for Utah, including bismuth, did not mention the occurrence of this metal in the Ohio district.

Semiquantitative spectrographic analyses by C. M. Taylor and A. S. Radtke, at Stanford University, confirmed the presence of abnormally large amounts of bismuth and copper, in addition to lesser amounts of iron, zinc, arsenic, silver, tin, antimony, gold, lead, and tellurium in ore from the Tunnel Extension Number Two mine.

This paper presents the results of a preliminary study of the mineralogical and chemical associations in this ore and gives a new mineral occurrence for bismuthinite, cuprobismutite, and cassiterite.

[1] Materials Analysis Co.
[2] Humble Oil and Refining Co.

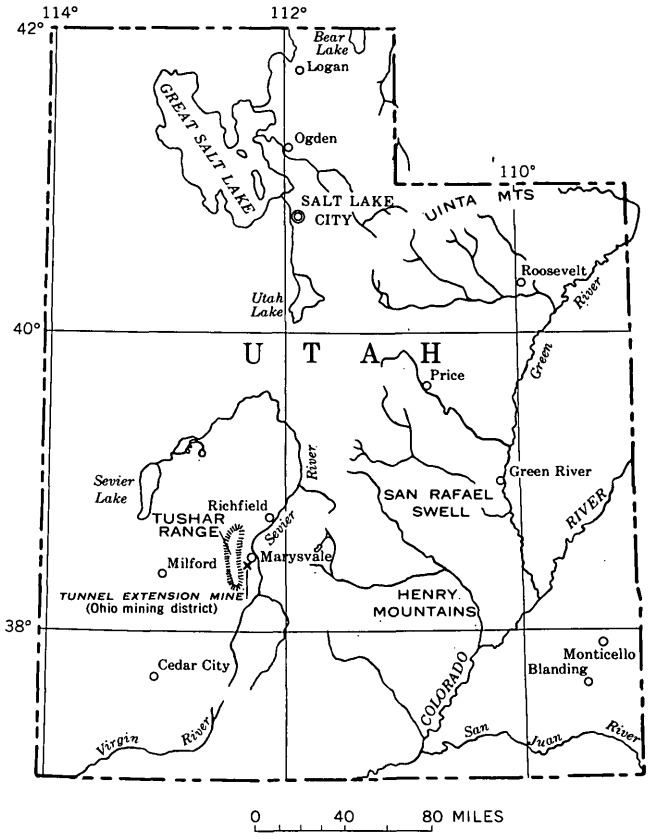

FIGURE 1.—Index map of Utah, showing location of the Tunnel Extension mine (Ohio mining district).

DESCRIPTION OF THE DEPOSIT

Ore bodies in the Tunnel Extension Number Two mine occur in steeply dipping tabular-shaped masses along and in faults or shear zones. Although small amounts of ore locally replace the wallrock, most of the mineralization is confined to the faults or shear zones and the deposits are classified as "fissure-filling type."

U.S. GEOL. SURVEY PROF. PAPER 575-D, PAGES D127-D130

The wallrocks are of the Bullion Canyon Volcanics of middle Tertiary (Miocene?) age. In sequence, underlying the volcanics, although not exposed in the present mine workings, are (1) indurated rocks of the Navajo Sandstone, (2) shale and sandstone of the Chinle Formation with its basal Shinarump Member (conglomeratic sandstone), and (3) siltstone and sandstone of the Moenkopi Formation.

Limestone, dolomite, and interbedded quartzite of the Kaibab Limestone, host rocks for gold-silver ores of the Deer Trail and several other mines in the Tushar Range, underlie the thick sequence of sandstones and shales. Because the ore of the Tunnel Extension mine is believed to be hypogene and because it is possible that the ore-controlling structures extend to depth, the carbonate beds below the mine may be worth exploring for additional gold-silver deposits.

ORE MINERALOGY AND CHEMISTRY

The results of mineralogic studies which included examination of polished sections and thin sections of the ore are described in this report. All polished sections were prepared following the methods described by Taylor and Radtke (1965).

The results of the semiquantitative spectrographic analysis of one specimen of massive sulfide ore (table 1) show that the most abundant elements in the ore are bismuth (>10 percent), silicon (10 percent), copper (7 percent), tin (1.5 percent), and silver (1 percent). Gold content, determined as 0.003 percent, is equal to approximately one ounce per ton. Zinc, arsenic, and tellurium, identified by Taylor and Radtke in previous spectrographic analyses, were not detected in the analysis shown in table 1.

The ore is made up of subhedral to euhedral interlocked grains of quartz and fine-grained intergrowths of sulfide minerals (fig. 2). In hand specimen, only cuprobismutite, bismuthinite, and quartz are sufficiently abundant to be distinguishable. All minerals identified in the ore and their relative abundance are given in table 2.

Primary ore minerals include cuprobismutite, bismuthinite, tetrahedrite, emplectite, chalcopyrite, native gold, and tetradymite. Secondary or alteration minerals include covellite, chalcocite, and a new hydrated bismuth sulfate. Most of the gangue is composed of quartz. Although calcium content is low in the analyzed ore (0.001 percent, table 1), very small amounts of calcite are present.

Cassiterite in two distinct forms is closely associated with and dispersed through the quartz gangue.

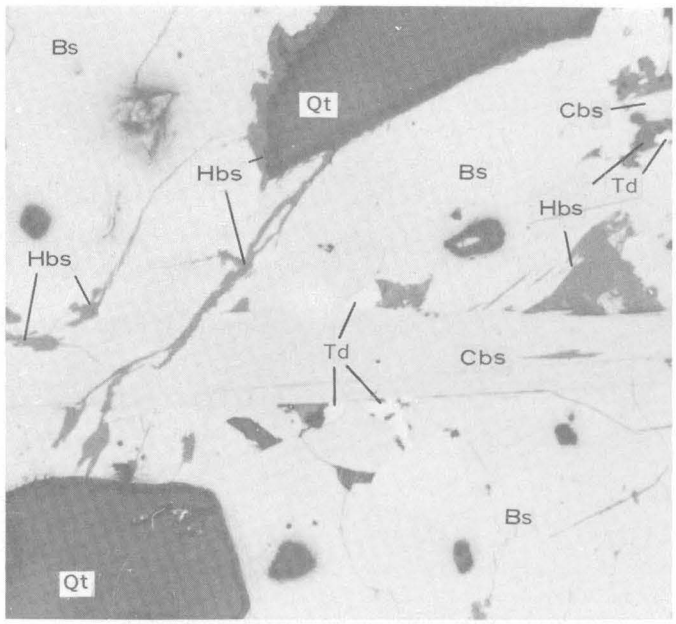

FIGURE 2.—Photomicrograph showing intergrowths of medium-gray bladed cuprobismutite (Cbs) and small white grains of tetradymite (Td) in pale-gray bismuthinite (Bs). Darkest areas are euhedral quartz (Qt) grains. Note alteration of primary bismuth minerals to hydrous bismuth sulfate (Hbs) along fractures and grain boundaries. × 370.

TABLE 1.—*Semiquantitative spectrographic analysis of massive sulfide ore, Tunnel Extension Number Two mine, Marysvale, Utah.*

[In weight percent. M, major constituent, greater than 10 percent. Analyst: Chris Heropoulos, U.S. Geological Survey]

Element	Amount	Element	Amount	Element	Amount
Si	10	Ag	1	Ni	0.001
Al	0.02	Au	0.003	Pb	.3
Fe	.015	Ba	.001	Sb	.1
Mg	.0003	Bi	M	Sn	1.5
Ca	.001	Cr	.0002	V	.005
Ti	.007	Cu	7	W	.01
Mn	.07	Mo	.001		

Other elements looked for but not found: As, B, Be, Cd, Ce, Co, Eu, Ga, Ge, Hf, Hg, In, K, La, Li, Na, Nb, P, Pd, Pt, Re, Sc, Sr, Ta, Te, Th, Tl, U, Y, Yb, Zn, and Zr.

TABLE 2.—*Mineralogy of massive sulfide ore, Tunnel Extension Number Two mine, Marysvale, Utah*

Mineral	Abundance [1]	Mineral	Abundance [1]
Cuprobismutite	+50	Tetrahedrite	1
Quartz	25	Emplectite(?)	<1
Bismuthinite	15	Chalcopyrite	<1
Bismuth-bearing alteration mineral.[2]	5	Gold (electrum ?)	<1
Covellite	2	Tetradymite	<1
Chalcocite	1	Calcite	<1

[1] Visual estimate of percentage of total sample.
[2] New mineral (hydrated bismuth sulfate).

The bulk of the cassiterite is found as small anhedral grains scattered randomly through quartz with lesser amounts as large elongate subhedral grains along the contacts between quartz and sulfide veinlets (fig. 3).

The ore specimens studied show the initial development of extensive oxidation and alteration (fig. 4). Although both bismuthinite and cuprobismutite show alteration, the former is apparently less stable and oxidizes more readily. Along crosscutting microfractures both minerals show alteration to and replacement by secondary phases. In areas with fine-grained intergrowths of both primary sulfides, the alteration may be confined to the binary bismuth sulfide (fig. 4). This is supported by the chemistry and abundances of the secondary or alteration minerals. Cuprobismutite is far more common than bismuthinite; yet secondary copper minerals, including covellite and chalcocite(?), are very scarce. The hydrated bismuth sulfate phase is very common and apparently formed directly from bismuthinite and cuprobismutite. Minor amounts of secondary copper sulfides in submicron particles intergrown with the secondary bismuth sulfate are present near cuprobismutite.

Of specific mineralogical interest is the nature and distribution of gold and silver in the ore. Native gold

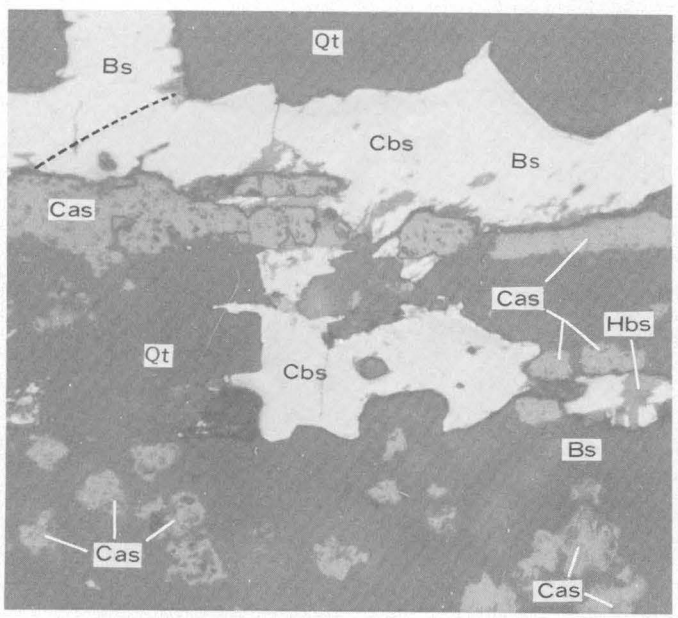

FIGURE 3.—Photomicrograph showing veinlet of white cuprobismutite (Cbs) and bismuthinite (Bs) in dark-gray quartz (Qt). Boundary between the two primary bismuth minerals is marked by dashed line. Note long prismatic subhedral grains of cassiterite (Cas) in quartz along margin of veinlet and small anhedral cassiterite grains scattered through quartz. Slight alteration of primary bismuth minerals to hydrous bismuth sulfate (Hbs) controlled by grain boundaries and microfractures within the grains is apparent. × 180.

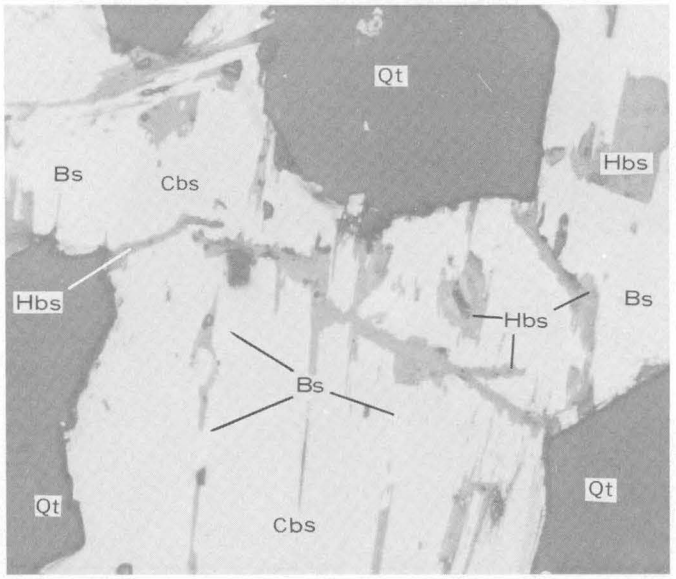

FIGURE 4.—Photomicrograph showing preferential and extensive alteration of pale-gray bismuthinite (Bs) to hydrated bismuth sulfate (Hbs). Cuprobismutite (Cbs), slightly darker than bismuthinite, is altered only along microfractures. Large, dark-gray-black euhedral grains are quartz (Qt) gangue. × 370.

in the ore is virtually confined to small late(?) microfractures cutting large sulfide intergrowths. A photomicrograph of native gold and secondary alteration minerals along a microfracture through cuprobismutite is shown in figure 5. Numerous electron microprobe analyses showed no substitution of gold for other elements in any of the ore minerals. No gold or gold-silver tellurides were recognized. Cuprobismutite, which makes up approximately +50 percent of the samples studied (table 2), contains the bulk of the silver; electron microprobe analyses show that this mineral contains over 1 percent silver. Tetrahedrite, relatively uncommon in the samples studied, is apparently not an important ore mineral of silver. Owing to the extreme small particle size of the gold and the high silver content in surrounding cuprobismutite, quantitative electron microprobe analyses of gold were not attempted. On the basis of color comparisons against known alloys of gold-silver, the gold-bearing phase in the ore is apparently deficient in or virtually free of silver.

In ore from the nearby Bully Boy mine, Butler and others (1920, p. 544) describe a primary unidentified silver mineral with "silvery-white metallic luster * * * coated by a dark grey material of dull luster, apparently an alteration product. The mineral contains free gold in minute fissures." They also reported that cerargyrite forms thin films in the fissures. Although cerargyrite was not recognized in our study, this min-

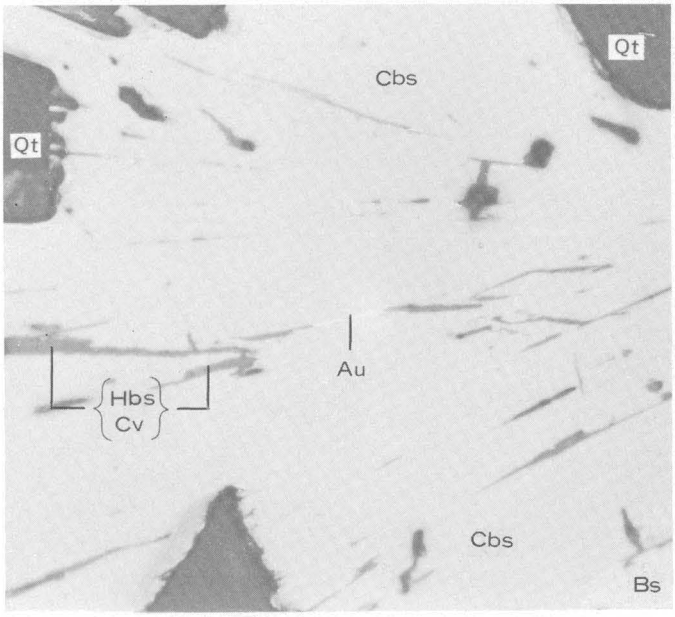

FIGURE 5.—Photomicrograph showing white native gold (Au) in a small microfracture in massive pale-gray cuprobismutite (Cbs). Other minerals in microfractures include admixed covellite (Cv) and hydrous bismuth sulfate (Hbs). Note general lack of alteration of cuprobismutite. Lighter gray mineral in lower right corner is bismuthinite (Bs); dark-gray-black areas are quartz (Qt) gangue. × 370.

eral would account for the silver released from cuprobismutite during alteration.

Butler and others (1920) also suggested that tetrahedrite in the ore was not an important silver mineral. They stated (1920, p. 544), "Material containing several percent of this mineral is said to contain only small quantities of precious metals and is ore only when it contains sufficient copper to be valuable for that metal." This conclusion is supported by the now-recognized concentration of silver in cuprobismutite (copper bismuth sulfide) rather than in tetrahedrite.

REFERENCES

Bullock, K. C., Smouse, DeForrest, and Robinson, G. B., Jr., 1960, Minerals and mineral localities of Utah: Provo, Utah, Brigham Young Univ., Dept. Geology, 170 p.

Butler, B. S., Loughlin, G. F., Heikes, V. C., and others, 1920, The ore deposits of Utah: U.S. Geol. Survey Prof. Paper 111, 672 p.

Dasch, M. D., 1964, Metallic mineral resources—Antimony and other minor metals, *in* Mineral and water resources of Utah: Utah Geol. and Mineralog. Bull. 73, p. 135–149.

Taylor, C. M., and Radtke, A. S., 1965, Preparation and polishing of ores and mill products for microscopic examination and electron microprobe analysis: Econ. Geology, v. 60, no. 6, p. 1306–1319.

CONTRACTION JOINTING AND VERMICULITIC ALTERATION OF AN ANDESITE FLOW NEAR LAKEVIEW, OREGON

By GEORGE W. WALKER, Menlo Park, Calif.

Abstract.—A thick olivine andesite flow near Lakeview, Oreg., is characterized by a well-developed reticulate polygonal system of contraction joints that controlled subsequent moderate- to low-temperature deuteric or hydrothermal alteration. Development of the joints, shortly after flowage ceased, permitted volatile constituents of the lava to escape into them, which resulted in rapid chilling adjacent to joints and formed dense impervious selvages. The selvages acted as effective seals to the exsolving volatiles, which reacted with andesite within the polygonal cells and converted olivine to expandable-lattice vermiculite and magnetite(?).

An unusual reticulate joint and associated alteration pattern in a thick Miocene andesite flow occurs near Lakeview, Oreg. Configuration of joint and alteration patterns indicates that the joints developed shortly after the andesite ceased flowing but before some of the volatile constituents escaped from the lava. The volatiles, which were hermetically sealed within polygonal cells bounded by the rapidly chilled andesite along the joints, deuterically altered the andesite in much the same manner as that described by Fuller (1938).

The andesite is well exposed in several extensive roadcuts along U.S. Highway 395 (lot 42°19′30″ N.; long 120° 18′45″ W.) and quarries just south of the highway, about 10 miles north of Lakeview in the low pass between Goose Lake Valley and Crooked Creek (fig. 1).

The andesite flow is interbedded with tuffaceous sedimentary rocks of probable Miocene age. Neither the upper nor lower contact with the enclosing rocks is exposed in the roadcuts, but the sedimentary rocks and the andesite all dip about 30°E. so that a conformable relationship is indicated. The tuffaceous sedimentary rocks beneath the andesite are fine to medium grained, thinly laminated, and partly pumiceous, whereas those above the flow are coarser grained, more highly pumiceous, and less well bedded. Most of the sedimentary debris is poorly sorted and locally contains abundant pumice lapilli. A few thin beds are made up of poorly sorted andesitic or basaltic debris that is partly altered to palagonite. A greenish-gray, crystal-rich well-indurated tuffaceous grit is exposed near the top of the roadcut sequence.

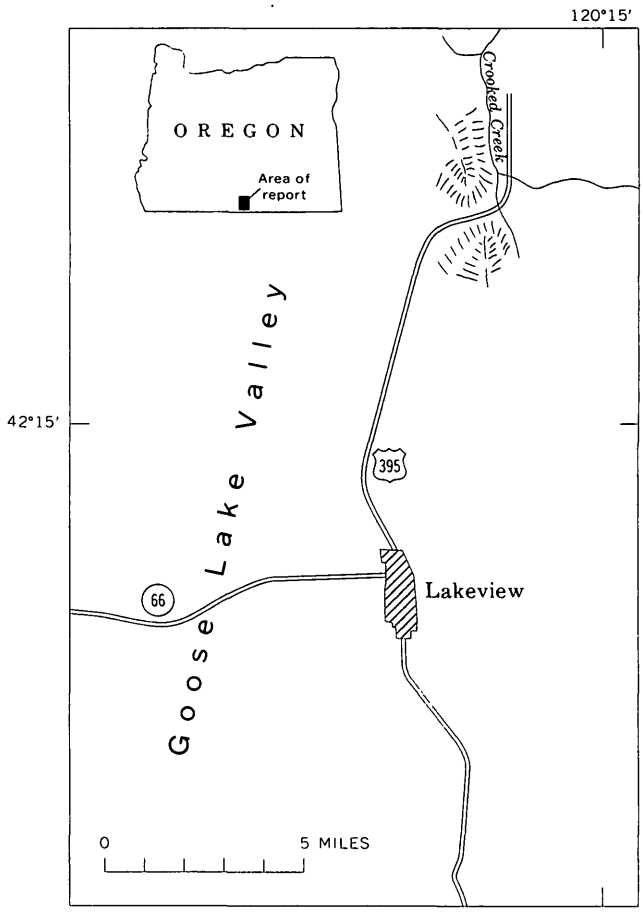

FIGURE 1.—Index map of the Lakeview area, Oregon, showing location of andesite flows discussed in this report. Exposures are in roadcuts (hachured area) along U.S. Highway 395.

U.S. GEOL. SURVEY PROF. PAPER 575-D, PAGES D131-D134

ANDESITE FLOW

The andesite flow cooled as a single thick unit of ponded fluid lava, judging from its lateral continuity, pattern of alteration, and internal structures and textures.

The true thickness of the flow is not known because of inadequate exposures and because of minor faulting, which apparently repeats small parts of the flow in some places. The few data on thickness that are available indicate that it is one of the thickest single mafic flows in south-central Oregon. A minimum thickness of about 200 feet can be established from the more than 450 feet of continuous, eastward-dipping exposure in roadcuts on the north side of the highway. The total thickness may be much more, however, as 150 feet of roadcuts on the south side of the highway expose additional lower parts of the flow that are not visible in the roadcuts on the north side of the highway.

Where unaltered, the andesite is a dense, hard fine-grained and slightly porphyritic flow-banded rock of pale-grayish-brown color. The flow bands are readily traceable into the altered andesite that is friable, lighter in color, and different in mineralogy from the fresh rock. Near its top, the flow has an irregular zone of scoriaceous and flow-brecciated andesite that lacks the reticulate joint pattern and shows little deuteric alteration.

The flow rock is an olivine andesite composed of about 75 percent plagioclase ($\approx An_{50-55}$) microlites, about 10 to 12 percent olivine, minor clinopyroxene, some weakly twinned and zoned calcic labradorite phenocrysts, magnetite, and hematite or martite. Some of the olivine in the fresh andesite is unaltered and is a clear yellow amber; a negative $2V$ estimated at 80° to 85° indicates a composition of about Fo_{65-70}. In fresh to only slightly altered andesite, however, most of the olivine is peripherally or totally altered to bright reddish orange and brownish red, slightly pleochroic "iddingsite" whose exact mineralogic and chemical nature has not been determined, but presumably is comparable in mineralogic properties to some of the "iddingsite" described by Gay and LeMaitre (1961). A silica content of about 55 to 56 percent was determined on several samples by use of the refractive index of fused beads and the "average" and "Lake County" curves presented by Huber and Rinehart (1966).

Plagioclase microlites are less than 0.1 millimeter long in chilled rocks. However, the olivine andesite is typically coarser grained in the central part of the flow and the plagioclase microlites are mostly 0.15 to 0.20 mm, but some are 0.4 mm in length. Olivine and clinopyroxene are slightly more abundant here. Individual flow bands in the andesite are manifest by (1) slightly coarser plagioclase microlites, in contrast to the denser and more finely crystalline andesite between bands, (2) some small irregular vesicles, and (3) less abundant olivine and clinopyroxine. A fine diabasic texture characterizes the coarser parts of the flow, and near the lower and upper margins of the flow the texture is strongly trachytic.

JOINT PATTERN

A conspicuous reticulate joint pattern is manifest by well-defined fractures bounded by hard dikelike ribs of fresh flow-banded andesite; the ribs enclose similar flow-banded andesite that is altered to a soft and friable material (fig. 2). Most of the joints have planar surfaces, so that the cells of altered rock enclosed by the joints are irregular polygons whose faces are only locally curved. Fracture intersections suggestive of both the orthogonal and nonorthogonal "contraction-crack polygon" systems of Lachenbruch (1960) are evident in parts of the andesite flow, but the orthogonal system appears to be dominant. Some of the more noticeable through-going joints are nearly perpendicular to upper and lower cooling surfaces of the andesite flow much in the manner of typical columnar joints, whereas most of the other joints lack preferred orientation and crosscut the flow banding at random angles. The resulting polygonal cells of andesite that are bounded by contraction joints tend to be equidimensional rather than elongate prisms typical of columned flows. The joints apparently formed, after flowage ceased, as a result of contraction during cooling of the lava.

In detail, each major joint is bounded by hard unaltered andesite a few inches to a foot thick. Within the resistant ribs formed by the andesite, the major joint commonly is a conspicuous and sharp median break (fig. 3). Flow bands in the andesite can be traced across both the median joint and the bounding interface between the fresh rib and the altered andesite. The ribs are unaltered throughout, and show little or no gradation from the median joint outward to the soft and friable altered andesite. In fact, the break between the fresh andesite in the ribs and the altered andesite in the cores of polygonal cells is, for some unknown reason, almost as conspicuous and sharp as the median joint. A secondary joint system, probably the result of either further cooling or later tectonic deformation, cuts the dikelike masses of fresh andesite into angular blocks.

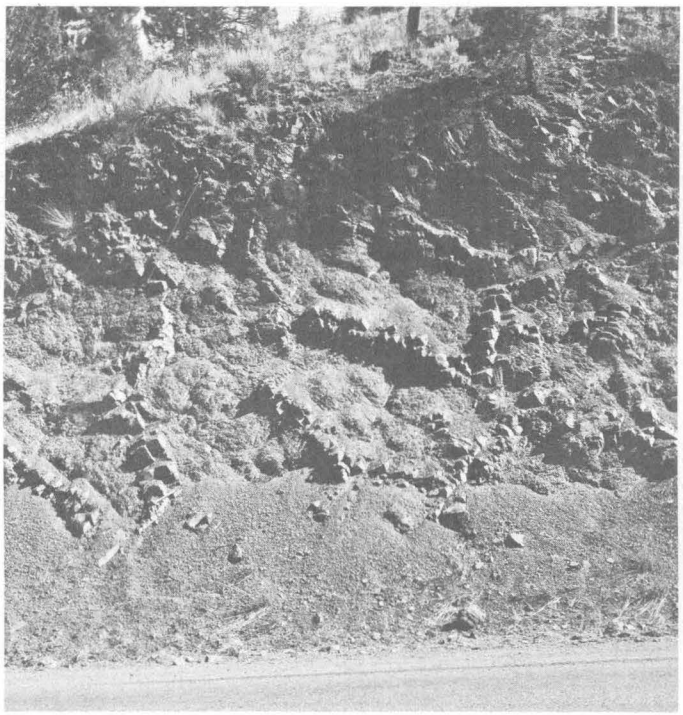

FIGURE 3.—Dikelike mass of unaltered flow-banded andesite with well-defined median joint and sharp boundaries with altered andesite.

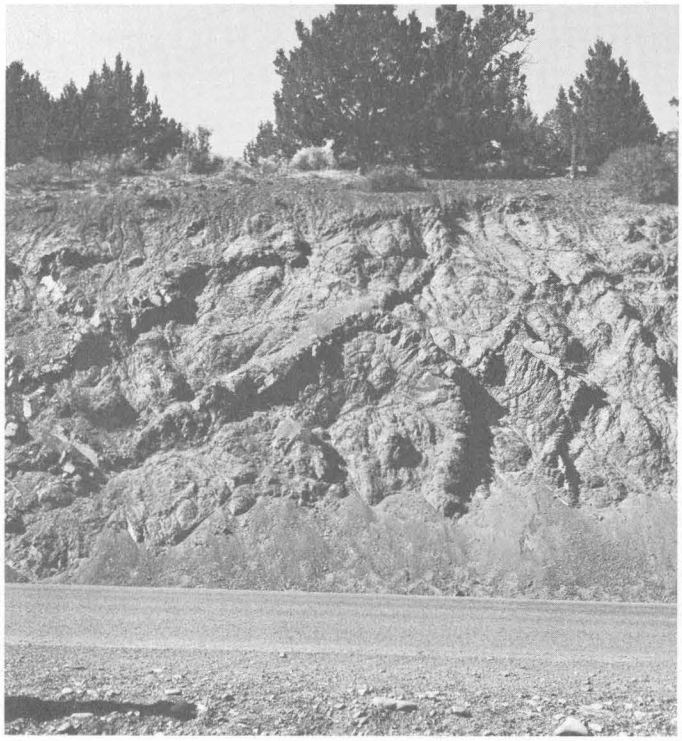

FIGURE 2.—Roadcuts on U.S. Highway 395, showing reticulate dikelike masses of unaltered andesite enclosing masses of soft friable andesite. Photograph at top shows mostly planar joint surfaces that occur on south side of highway near west end of exposure sequence. Photograph at bottom shows an exposure several hundred feet east on north side of highway where both planar and curved joint surfaces are common and are more widely spaced.

ALTERATION

Alteration of the andesite occurred only within the polygonal cells bounded by joints and not in the dense and rapidly chilled andesite along each joint. The alteration, which affected principally the thin flow bands and to a lesser extent the slightly denser rock between the bands, has softened the andesite, thereby making it more friable. It also has changed the color of the andesite to a mottled dusky yellow or light olive brown with intervening dark patches of grayish brown typical of the fresh rock. In thin section, the first sign of alteration is clouding of the "iddingsitized" olivine and the presence of unidentified yellowish-brown, orange, and yellowish-green stains on cleavage planes in the plagioclase. Where alteration is more intense, "iddingsitized" olivine is completely converted to a pale-yellowish-green and grayish-green fibrous to platy aggregate of nonpleochroic and moderately birefringent material that, in places, contains minute opaque grains probably of magnetite. No other changes brought on by alteration are visible, except that the sharp crystal outlines characteristic of the fresh andesite are diffuse and obscure adjacent to the altered olivine crystals.

Comparisons of the fresh and altered andesite, both in thin sections and by X-ray diffraction, indicate that the dominant changes are related to the breakdown of the "iddingsitized" olivine to a poorly defined

mixture of mostly expandable-lattice clay, minor magnetite(?), and hydrated iron oxides. Several samples were studied according to the following procedures in an attempt to identify the clays.

A mixture of material, mostly less than 2 microns in size but including some in the 2- to 40-micron range, was obtained through elutriation and centrifuging of crushed and screened altered andesite. A part of the sized material was used directly to prepare oriented samples for expansion studies using ethylene glycol. Another part that was used to study the reactions of expanding-lattice clay minerals with glycerol, according to procedures outlined by Walker (1958), was first saturated with a 10-percent solution of magnesium chloride and then washed with water until free of chloride.

The basal spacing of sized and oriented but untreated material is 15.2 A (angstroms), probably indicating the presence of calcium and magnesium ions held in ion-exchange positions. Samples treated with ethylene glycol in a vapor bath at 60°C expanded after 1 hour to a basal spacing of 16.1A, and after 12 hours to 17.0A. Saturation with magnesium chloride solution produced a broad diffuse diffraction band, between about 15.2A and 19.0A, which collapsed to form a sharp basal reflection at 14.3A after 12 hours in a glycerol vapor bath at 60°C. The X-ray diffraction measurements obtained are comparable to those given by Walker (1958) for some vermiculite, and the optical data are consistent with those for vermiculite.

Elevated temperatures affected the structure of both treated and untreated material in practically the same way. At 150°C both the 15.2A and diffuse basal reflections between 15.2A and 19.0A had collapsed to about 14.3A. Between 250° and 300°C, the structure of the material was completely destroyed. If this indicates the approximate upper temperature stability limit of the vermiculite, the alteration of the "iddingsitized" olivine must have occurred below about 250°C.

CAUSE OF ALTERATION

The distribution of altered andesite exclusively within polygonal cells bounded by contraction joints and dense unaltered andesite is strong evidence that the alteration took place during and probably late in the cooling history of the lava; there is no spatial relation between the vermiculitic alteration pattern and the ground surface, water table, or postsolidification tectonic faults or fractures.

The reticulate polygonal system of contraction joints developed after movement in the thick olivine andesite flow had ceased. As the joints opened, volatiles escaped into them from the adjoining andesite, which consequently solidified rapidly to a fine-grained dense selvage bordering each joint. The dense selvages apparently were virtually impervious, so they formed a tight hermetic seal to the volatiles that exsolved from the cooling andesite entrapped in the polygonal cells bounded by the joints. As a result, a low-temperature (perhaps less than about 250°C) deuteric or hydrothermal alteration of the andesite took place within the polygonal cells, but not in the impervious crystalline selvages, converting olivine and "iddingsitized" olivine to expandable-lattice vermiculite and magnetite(?). The nature of the alteration, which is essentially a hydration oxidation of the olivine, suggests that the entrapped volatiles were mostly water vapor and that partial pressure of oxygen was relatively high. Minor amounts of hydrate iron oxides now found in the andesite resulted either from the final stages of deuteric or hydrothermal alteration or from later weathering.

Similar patterns of deuteric alteration have been described by Fuller (1938) for columned basalts of Steens Mountain, southeast Oregon. The alteration products of Fuller's basalt are not specifically identified but resulted from the decomposition of olivine to "a soft dark substance which is orange colored in thin section * * *" (Fuller, 1938, p. 162), and thought by Fuller to be chlorophaeite and its oxidation products. A reverse pattern of deuteric alteration, in which the olivine and glass in the peripheral parts of basalt columns are altered to the hydrous mineraloid chlorophaeite but the centers of the columns are fresh, has been described by Smedes and Lang (1955).

REFERENCES

Fuller, R. E., 1938 Deuteric alteration controlled by the jointing of lavas: Am. Jour. Sci., 5th ser., v. 35, no. 207, p. 161–171.

Gay, Peter, and LeMaitre, R. W., 1961, Some observations on "iddingsite": Am. Mineralogist, v. 46, nos. 1–2, p. 92–111.

Huber, N. K., and Rinehart, C. D., 1966, Some relationships between the refractive index of fused glass beads and the petrologic affinity of volcanic rock suites: Geol. Soc. America Bull., v. 77, no. 1, p. 101–110.

Lachenbruch, A. H., 1960, Contraction-crack polygons: Art. 187 *in* U.S. Geol. Survey Prof. Paper 400–B, p. B406–B409.

Smedes, H. W., and Lang, A. J., Jr., 1955, Basalt column rinds caused by deuteric alteration [Oregon]: Am. Jour. Sci., v. 253, no. 3, p. 173–181.

Walker, G. F., 1958, Reactions of expanding-lattice clay minerals with glycerol and ethylene glycerol: Clay Minerals Bull., v. 3, no. 20, p. 302–313.

GEOLOGIC EVALUATION OF RADAR IMAGERY IN SOUTHERN UTAH

By ROBERT J. HACKMAN, Washington, D.C.

Work done in cooperation with the National Aeronautics and Space Administration

Abstract.—A comparison of radar imagery with conventional aerial photography shows that radar imagery has some distinct advantages. It has all-weather, day or night capability of imaging large areas of terrain. Side-looking radar produces a "shadow" enhancement effect that shows greater topographic detail, important to observation of many geologic features. One structural fault that could be only poorly discerned on conventional photography was clearly visible on radar imagery. Calcareous and gypsiferous sedimentary rocks were shown as very light tones of gray in contrast to darker sandstones and shales. These contrasts were reversed and less conspicuous on the conventional aerial photography. However, many of the rock units, readily distinguishable on the photography, could not be positively differentiated on the radar imagery.

The radar imagery evaluated in this report covers a strip approximately 12 miles wide extending 110 miles westward from Dark Canyon Plateau to Table Cliff Plateau in San Juan and Garfield Counties, Utah (fig. 1). This imagery was taken October 4, 1965, at the request of the U.S. Geological Survey and the National Aeronautics and Space Administration. The imagery is the result of reflections obtained from scanning the ground with an airborne energy source in the K band of the electromagnetic spectrum.

The radar imagery is a continuous strip and has an approximate scale of 1:250,000. Both a positive print and transparency were used in this study. The normal 1:250,000 radar strip is in duplicate in a 70-millimeter format. The upper image is the "like" image in which the signal is transmitted and received in the same plane. The lower one is the orthogonal or "unlike" image in which the signal is transmitted in one plane and received in the other (horizontal-vertical, HV; or vertical-horizontal, VH). Parts of the like-image strip were enlarged to an approximate scale of 1:60,000 to facilitate comparison with conventional high-altitude vertical aerial photography (1:50,000 and 1:60,000 scale). All illustrations in this paper are "like" imagery.

GENERAL CAPABILITIES OF RADAR IMAGERY

Radar is an all-weather 24-hour-a-day sensor for gathering geologic data. Unlike conventional aerial photography which generally relies on solar illumination and requires cloud-free skies, radar uses its own energy source for scanning the terrain and has cloud-penetration capabilities.

One of the most advantageous features of radar imagery is the overall view it presents of large areas. Also, as the emitted radar energy is side-looking and does not pass through objects, it produces its own "no show", or shadow effect, on the far side of topographic features away from the flight line, thus enhancing and presenting a three-dimensional view of the terrain in a manner similar to that of a shaded relief map. The radar image is best viewed with shadows falling toward the viewer.

As the radar shadows result from a low-angle (to the horizontal) energy source, small irregularities in the topography of the surface enhanced by the shadows can be seen on the image. These irregularities are readily seen on a radar image but are usually not recognized on a single conventional high-angle illuminated, vertical aerial photograph. Pairs of photographs must be viewed stereoscopically to see many of these same features.

Most conventional aerial photography is taken under high-angle solar illumination (between 10:00 a.m. and 2:00 p.m.). If it were taken early in the morning or late in the day under low-angle illumination it would show a shadow enchancement similar to

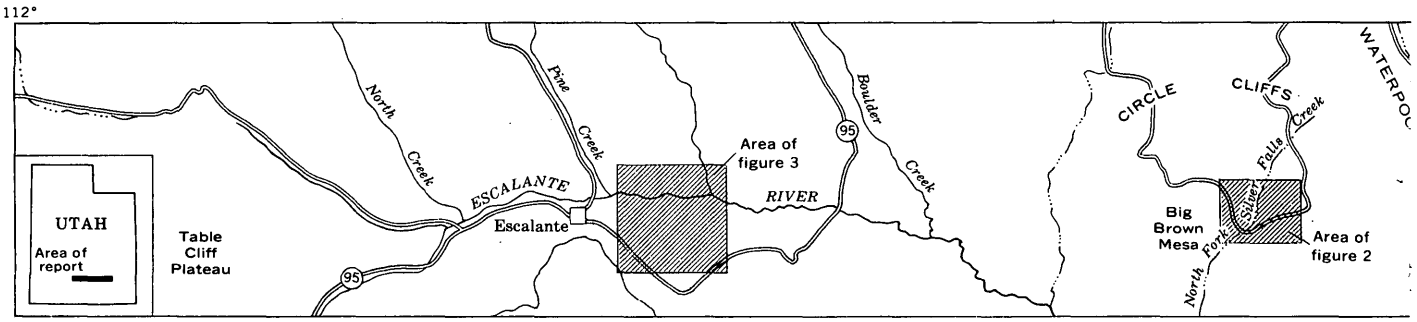

FIGURE 1.—Map showing area covered by radar imagery described in report.

that of radar imagery (Hackman, 1967). However, the direction of solar low-angle illumination and subsequent shadows is restricted by the earth's rotation around the sun and will generally be in an almost easterly or westerly direction, depending on the time of day and the geographic location of the area of interest. Radar, in contrast, has no such limitation because it uses a self-contained energy source which can be flown in any direction.

In studying the tone values of different rock units represented on radar images, one has to consider the angle of "illumination" (here, energy source), for there is a highlight and shadow effect related to the angle at which the radar scan strikes an object. Slopes and cliffs facing the energy source reflect more incident energy than do surfaces that are flat or that slope in other directions. On radar images, values related to different rock types are generally best seen in areas of low relief where the highlight and shadow effect is less evident. Even in such areas the tone value for a certain rock type will vary somewhat from place to place, depending on the angle of illumination and the surface roughness or number of edges (corner reflectors) that are present.

METHOD OF STUDY

Enlarged parts of radar images, at a scale of approximately 1:60,000, were compared with conventional 1:60,000- and 1:50,000-scale aerial photographs to determine what geologic features could be recognized on the radar imagery that were not present or only poorly defined on the conventional photographs. The image was first compared with a single aerial photograph and then, where necessary, with the stereoscopic model of two overlapping photographs of the same area. The radar image and photographs were further compared to the geologic map of the area, and significant geologic features found on the radar image were examined in the field during the summer of 1966. This examination was made in conjunction with field investigation for compilation of the geologic map of the Escalante 2° quadrangle, Utah, by Donald G. Wyant and R. J. Hackman, of the U.S. Geological Survey.

GEOLOGY AND ECOLOGY

Rocks in the Escalante quadrangle area, Utah, range in age from Paleozoic to Tertiary and include extrusive and intrusive igneous rocks and sedimentary rocks. All are covered in part by Quaternary surficial deposits. Major structural features from east to west are: Part of the west flank of the Monument upwarp; the southern part of the Henry Mountains basin, including the Mount Holmes and Mount Ellsworth intrusive structures; the east-dipping Waterpocket monocline; the northern end of the Circle Cliffs upwarp; the west-dipping Escalante monocline; and the Table Cliff syncline, which is a northern extension of the Kaiparowits downwarp.

The western part of the area, west of Escalante, is mostly tree covered. Vegetation zones in descending order from the top of Table Cliff Plateau are the spruce-fir zone (10,000 to 9,000 feet), the Ponderosa pine–Douglas fir zone (9,500 to 6,200 feet), and the pinyon–juniper zone (8,500 to 5,000 feet). East of Escalante, pinyon and juniper grow on the flanks of the Circle Cliffs upwarp, Mount Holmes and Mount Ellsworth, and on the higher parts of Dark Canyon Plateau. The remainder of the area is sparsely covered with a northern desert flora including sagebrush, blackbrush, Mormon tea, shadscale, and some short grasses (Cannon, 1960).

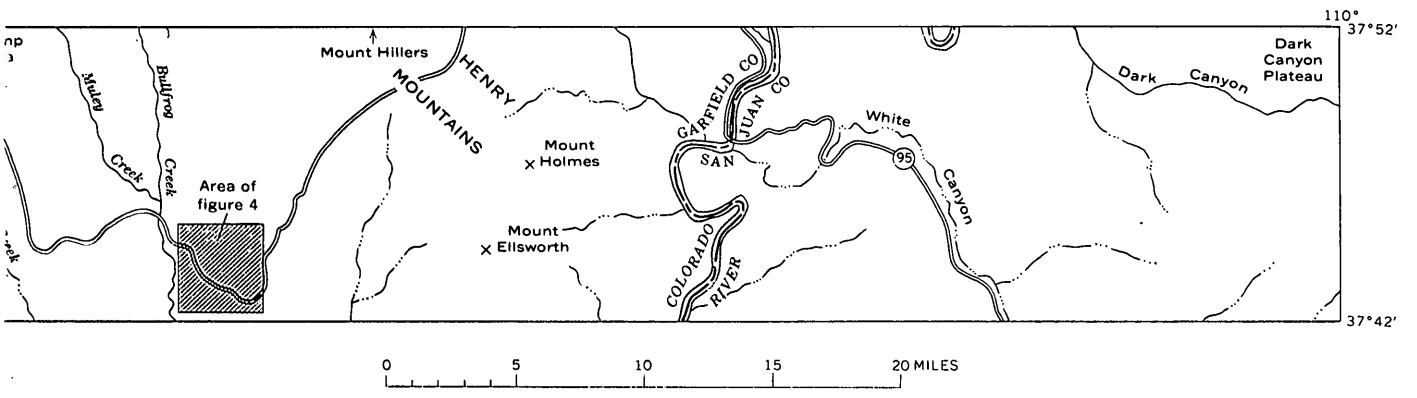

CONTRAST OF LIKE AND ORTHOGONAL IMAGERY

The like and orthogonal images at a scale of approximately 1:250,000 (transparency strip) were simultaneously viewed by means of a binocular stereoscope with adjustable wing mirrors. No significant differences believed to have geologic significance were observed between the two.

GEOLOGIC STRUCTURE SHOWN BY RADAR IMAGERY

Evaluation of radar imagery in this area shows that many geologic structures are clearly defined on the images. This is undoubtedly due to the radar shadow enhancement of topographic expressions of these structures. However, in the area covered by this study, most of these geologic structures are clearly visible on the ground and can also be interpreted in the stereoscopic model of two aerial photographs, with a greater precision. Because of the shadow enhancement and greater area coverage of the radar imagery, it certainly shows more geologic structure at a casual glance than can be seen on a single aerial photograph or photomosaic of the area. One probable structural fault only partly visible on conventional aerial photographs is apparent on the radar images.

The alinement of a concealed fault zone under a thin layer of surficial material (alluvium and windblown sand) shows up on a radar image of a part of the Circle Cliffs area. This fault zone is very poorly expressed on 1:50,000-scale conventional photography (including stereoscopic viewing) where it crosses a canyon floor (fig. 2).

The fault zone crosses the North Fork of Silver Falls Creek, 1 mile east of the northern end of Big Brown Mesa. The geologic map of the area (Carswell and others, 1958) shows the approximate location of a partly concealed fault crossing the canyon floor. The downthrown side of the fault is to the north. The radar image shows a lineation just north of the field-mapped fault. This may be the main fault or a branch of the fault not previously recognized in the field. The topographic expression of the canyon wall just north of the field-mapped fault suggests that the fault dies out to the west before it reaches the canyon wall. The cause of the distinctive tonal break across the fault zone was not determined. The dark tone in the immediate vicinity of the fault may be due to moisture along the fault zone and in the alluvium. The overall dark tone to the south could be due either to greater moisture content or to a difference in lithology of the Moenkopi Formation on either side of the fault.

DIFFERENTIATION OF ROCK UNITS BY RADAR IMAGERY

The differentiation of rock types is, in general, much more difficult on radar images than on conventional photographs. Some surficial deposits are better displayed on radar images than on a single aerial photograph, but, in stereoscopic models of conventional photographs such deposits can usually be delineated more easily. Radar images, however, are definitely superior to conventional photographs (on both the single photograph and in the stereoscopic model) in differentiating rock units in two specific places in the area of study in southern Utah, as discussed below.

Navajo Sandstone and Carmel Formation

A few miles east of Escalante a greater tone difference between the Navajo Sandstone of Triassic(?) and Jurassic age and the Carmel Formation of Jurassic age shows on radar images than is apparent on a conventional photograph (fig. 3). Not only is the contrast about twice as great, but it is a reverse contrast. The

A

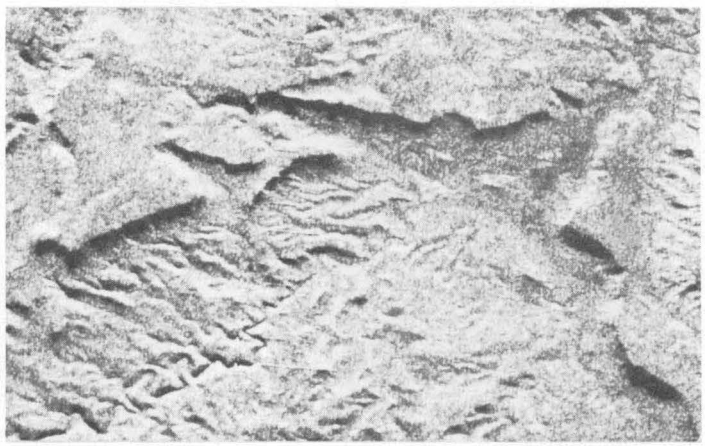

B

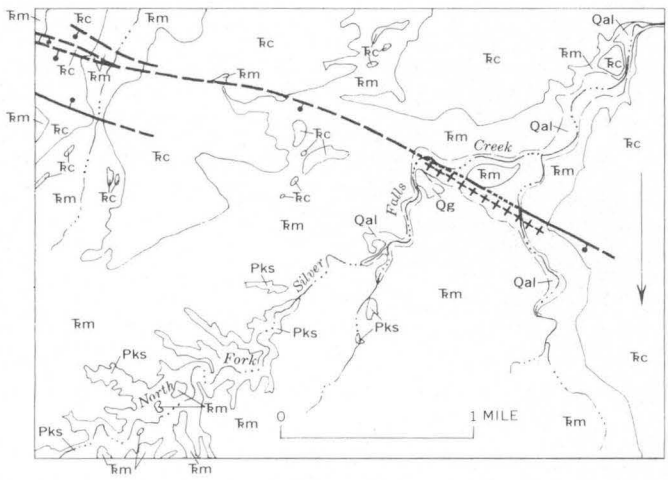

C

FIGURE 2.—Area in the Circle Cliffs region of southern Utah, as shown by *A*, aerial photograph; *B*, radar image; and *C*, geologic map. The radar image shows a sharp tone change just north of the field-mapped fault, where the fault crosses the canyon floor, suggesting that a branch of the fault may be north of the field-mapped one. This tone change is not recognizable on the aerial photograph (including stereoscopic viewing). There is, however, a faint lineation on the aerial photograph about halfway across the canyon floor from the left. The tone change is probably due either to an increase of moisture content south of the fault zone or a reflectivity difference in units of the Moenkopi Formation exposed on opposite sides of the fault zone. Geologic map adapted from Carswell and others (1958) and Davidson and others (1958).

A

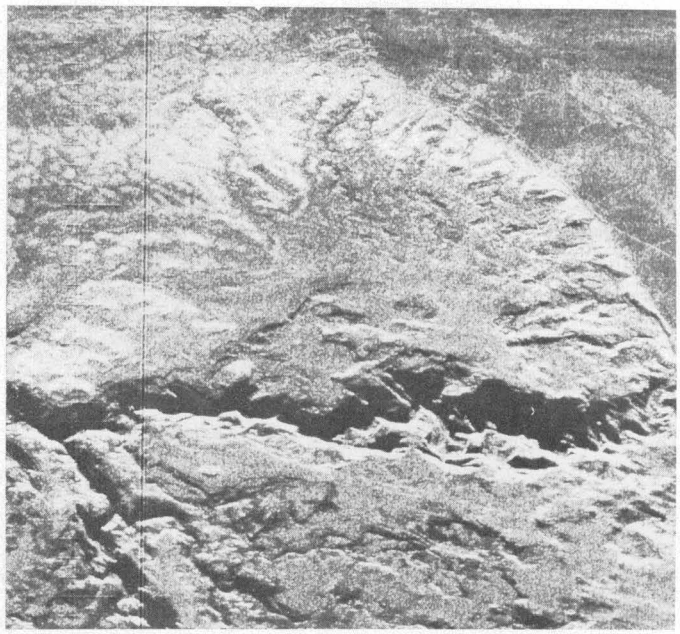

B

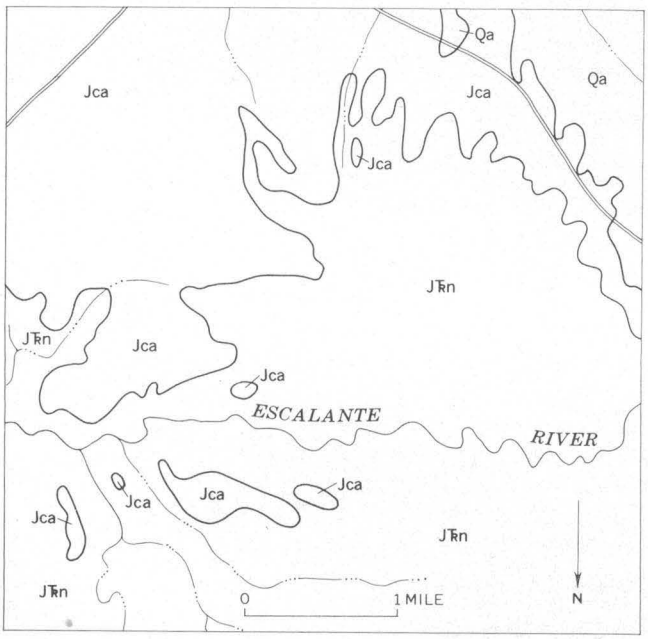

EXPLANATION

Qa —Alluvium Jca —Carmel Formation J℟n —Navajo Sandstone

C

FIGURE 3.—Area in which the Carmel Formation overlies the Navajo Sandstone a few miles east of Escalante, Utah, as shown by *A*, aerial photograph; *B*, radar image; and *C*, geologic map. The tonal contrast between the two formations is much greater on the radar image and is reversed from that on the aerial photograph. The mottled white tone of the gypsiferous and limy beds of the Carmel Formation on the radar image strongly suggests that these beds are a better reflector of radar energy than the rounded quartz sand grains in the Navajo Sandstone. The radar image does not discriminate between the unconsolidated windblown sand (darker toned areas on Navajo Sandstone of aerial photograph) and the consolidated sandstone. Tone contrast between surficial deposits (alluvium top right corner of image) and the Carmel Formation is greater on the radar image than on the aerial photograph. Geologic map adapted from Hintze (1963) and Hintze and Stokes (1964).

269-274 O—67——10

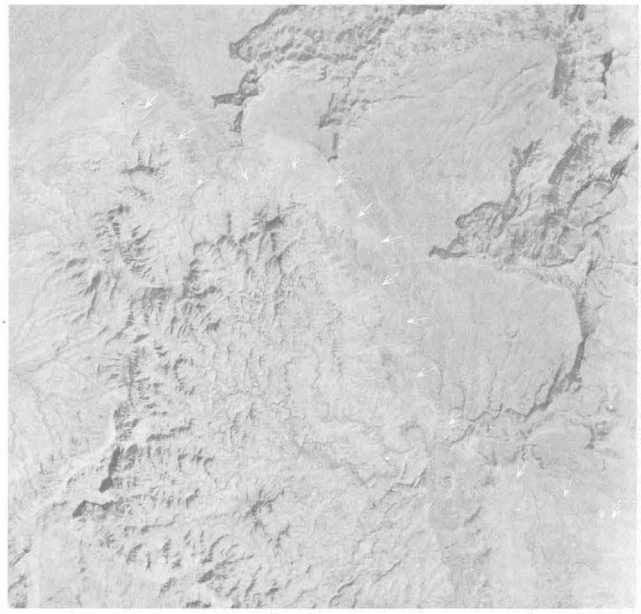

A

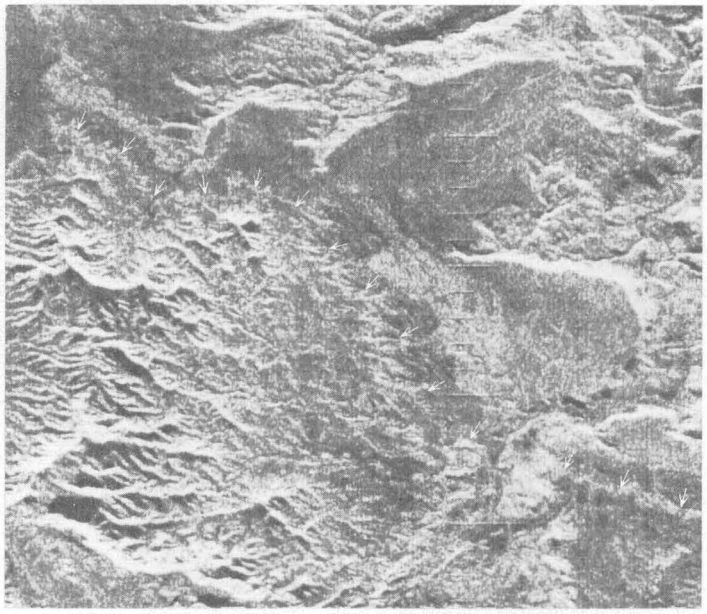

B

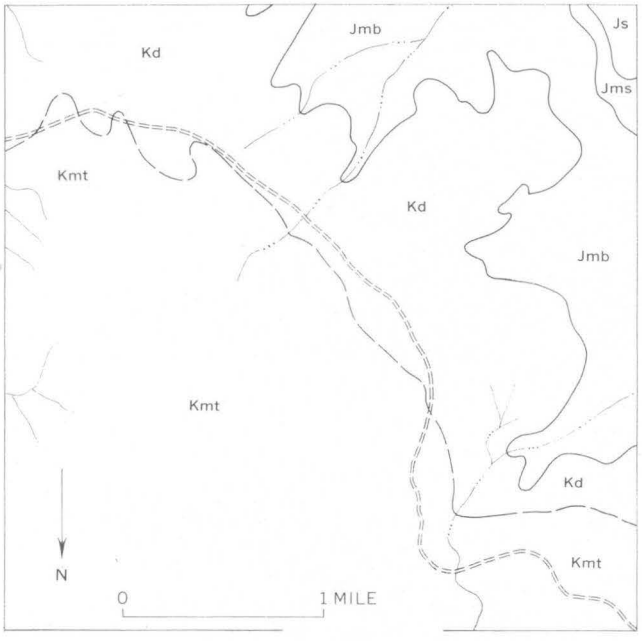

EXPLANATION

Kmt —Tunuk Member, Mancos Shale
Kd —Dakota Sandstone
Jmb —Brushy Basin Member
Jms —Saltwater Sandstone Member
Js —Summerville Formation
Morrison Formation

C

FIGURE 4.—Area 11 miles west of Mount Ellsworth, as shown by *A*, aerial photograph; *B*, radar image; and *C*, geologic map. Field investigations indicate that the light band, indicated by arrows, visible on the radar image and only poorly expressed on the aerial photograph consists of calcareous beds in the Tununk Member of the Mancos Shale. The adjacent dark beds are black fissile shale which weather blue gray. Geologic map adapted from Hunt and others (1953, pl. 1).

radar image shows the Navajo Sandstone to be darker in tone value than the Carmel Formation, whereas the aerial photograph shows the Carmel to be darker than the Navajo but having less contrast.

The Navajo Sandstone in this area is a massive white crossbedded sandstone of eolian origin approximately 1,200 feet thick. The reddish Carmel Formation, on the other hand, is 200 feet thick in this area (Gregory and Moore, 1931, p. 76), and is predominantly gypsiferous with many limy beds and subordinate amounts of sandstone and shale. A massive gypsum bed 45 feet thick is in the lower part of the Carmel, and 85 feet of gypsum and gypsiferous shale are at the top of the unit. The mottled white tone of the Carmel Formation on the radar image is probably the result of a higher reflectivity of radar energy from the generally fine-grained surface texture. In contrast, the darker tone of the Navajo Sandstone on the radar image is probably due to the white rounded and frosted quartz grains acting as spherical reflectors that scatter the radar energy and reduce the reflectivity. It is possible that other chemical and physical properties such as differential absorption of radar energy by gypsum, calcite, and quartz may cause some of this difference in reflectivity.

Some windblown sand present on the Navajo Sandstone bedrock surface is indicated by the darker areas on the aerial photograph. The darkest specks on the photograph are pinyon and juniper trees. The radar image of the area shows no discrimination between the unconsolidated sand and the sandstone.

Calcareous beds in Mancos Shale

Eleven miles west of Mount Ellsworth (Henry Mountains area) the radar image shows a light band in the lower part of the Tununk Member of the Mancos Shale which is generally not traceable on the aerial photograph or stereoscopic model of the area. Field investigation of this area revealed the presence of thin limestone beds and calcareous shale at this horizon. This unit has much higher radar reflectivity than does the adjacent black (weathers blue gray) fissile shale (fig. 4).

CONCLUSIONS

Radar imagery is a useful tool for geologic interpretation as a supplement to present conventional aerial photography, and as an advantageous substitute for photography in specific areas and for specific problems. This statement is restricted to the interpretive use, as the radar imagery used in these investigations does not have the geometric integrity required for making highly precise geologic maps. Radar imagery has the following capabilities:

1. It shows an overall view of a large area of terrain, hitherto not obtainable on a single aerial photograph.
2. It has all-weather capabilities; surfaces of areas usually covered by clouds can be recorded on radar imagery.
3. It shows greater topographic detail resulting from radar shadow enhancement than can be seen on a single conventional aerial photograph. This enhancement results from the low angle of radar illumination as contrasted with the high angle of illumination required for most conventional aerial photography.
4. It does not have the restrictions on direction of shadows as do low-angle-illuminated aerial photographs, where the directions of shadows are controlled by the earth's rotation and the earth-sun relationship. Thus, radar imagery can be flown in any direction and at any time of the day because the direction of flight controls the direction of shadow enhancement.
5. It depicts some geologic faults that are not recognizable for their full length on aerial photographs. This capacity may be due to moisture differences on the two sides of a fault, and (or) to a difference of reflectivity related to the different rock units on the two sides of a fault.
6. It provides some definite rock signatures in this area of study in southern Utah. Calcareous and gypsiferous beds are shown as very light tones of gray in contrast to the darker toned sandstones and shales. The fissile marine shales of the Mancos Shale appear as dark tones in contrast to the medium-toned sandstone members of the Mancos Shale and some light-toned calcareous beds in the lower part of the Mancos Shale. These tonal contrasts in rock units are much less conspicuous on the conventional aerial photographs of the area. On the other hand, many of the other rock units that could be readily distinguished on the photographs could not be positively differentiated on the radar images.
7. It makes Quaternary alluvial deposits in some places more discernible than they are on a single aerial photograph; however, radar imagery does not appear to detect a difference between surficial windblown sand and sandstone.

REFERENCES

Cannon, H. L., 1960, The development of botanical methods of prospecting for uranium on the Colorado Plateau: U.S. Geol. Survey Bull. 1085–A, 50 p.

Carswell, L. D., Davidson, E. S., and Miller, G. A., 1958, Preliminary geologic map of the Circle Cliffs 1 SW quadrangle, Garfield County, Utah: U.S. Geol. Survey Mineral Inv. Map MF–155.

Davidson, E. S., Brew, D. A., and Carswell, L. D., 1958, Preliminary geologic map of the Circle Cliffs 1 SE quadrangle,

Garfield County, Utah: U.S. Geol. Survey Mineral Inv., Map MF–156.

Gregory, H. E., and Moore, R. C., 1931, The Kaiparowits region, a geographic and geologic reconnaissance of parts of Utah and Arizona: U.S. Geol. Survey Prof. Paper 164, 161 p.

Hackman, R. J., 1967, Time, shadows, terrain and photointerpretation, *in* Geological Survey Research 1967: U.S. Geol. Survey Prof. Paper 575–B, p. B155–B160.

Hintze, L. F., 1963, Geologic map of southwestern Utah: Utah State Land Board.

Hintze, L. F., and Stokes, W. L., 1964, Geologic map of southeastern Utah: Utah State Land Board.

Hunt, C. B., Averitt, Paul, and Miller, R. L., 1953, Geology and geography of the Henry Mountains region, Utah: U.S. Geology and geography of the Henry Mountains region, Utah: U.S. Geol. Survey Prof. Paper 228, 234 p.

AN AIRBORNE MULTISPECTRAL TELEVISION SYSTEM

By C. J. ROBINOVE and H. E. SKIBITZKE,
Washington, D.C., Phoenix, Ariz.

Work done in cooperation with the National Aeronautics and Space Administration

Abstract.—Airborne multispectral television images were obtained in the visible and near-infrared ($<2.2\mu$) region of the spectrum and recorded on videotape in a light aircraft. The images are of lower spatial resolution than aerial photographs from equivalent altitude but have the advantages of allowing quite narrow bandpass filtering and instant reproduction of the images for use by interpreters. Such imagery may be quite useful for fast coverage of dynamic events, such as floods, where aerial data are needed quickly but not to the photogrammetric precision of aerial photographs. The use of airborne television imagery by field scientists also will prepare them to use similar but smaller scale data from earth-orbiting satellites.

In November 1966 an airborne multispectral television system was constructed in the Phoenix, Ariz., office of the U.S. Geological Survey, under the direction of H. E. Skibitzke, and flown in a light aircraft. The objectives and purpose of this experiment were:

1. To obtain television imagery from an aircraft and to determine the quality of imagery that can be collected and processed.
2. To determine the lens and filter combinations that should be used with the television system to obtain the maximum clarity of image.
3. To determine the usability of relatively narrow bandpass filters for increasing the contrast of imaged features.

This report describes some preliminary results of the experiments.

Television imagery may be significantly useful in the field of hydrology or in any other fields where aerial imagery is needed and information must be received quickly by persons on the ground. For example, when major floods occur and it is necessary to map the area inundated at the peak of the flood, it would be possible to obtain television imagery from aircraft over the flooded areas and return the videotape records immediately to ground-control parties who could then use them to aid in surveying the inundated areas.

The time usually required for photographic processing would be eliminated because videotapes are immediately usable on television monitors at the site.

DESCRIPTION AND FUNCTIONS OF EQUIPMENT

All the equipment was installed in a high-wing, single-engine aircraft that is well suited for this type of work because of its fairly slow cruising speed of about 105 knots, and its ceiling of about 20,000 feet. Figure 1 is a block diagram of the airborne multispectral television system consisting of cameras, monitors, power supplies, and videotape recorder; the system is simple and uses off-the-shelf-equipment.

Three television cameras were mounted in an aerial photographic camera mount in the belly of the plane. They pointed downward, and the top of the image on the video monitor was toward the front end of the aircraft. Image motion on the television monitors was from top to bottom. The cameras were equipped at various times with three types of 1-inch-diameter vidicon tubes, ML6198, ML7735B, and N156. The spectral response curves for these three tubes are shown in figure 2, and the captions on the imagery shown in figures 6–9 refer to the vidicon tubes and filters used to obtain them. A matched set of three 12.5-millimeter lenses was used on the cameras.

Dichroic absorption filters were used on one of the cameras. Graphs of the selected filter combination used are shown in figure 3. A second camera was used unfiltered; the third camera with the N156 vidicon tube, which is useful to about 2.2 microns in the infrared region was equipped with an 89A red filter which cuts off all wave lengths below about 680 millimicrons.

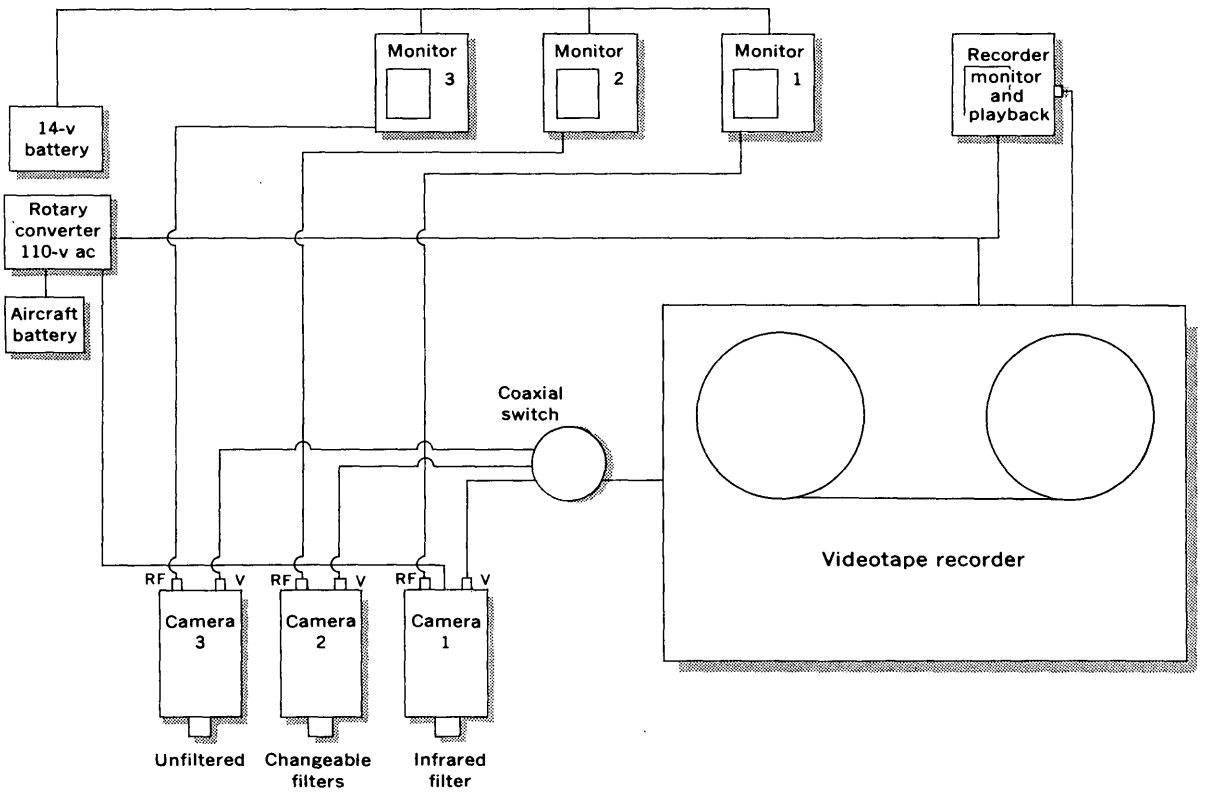

FIGURE 1.—Block diagram of airborne multispectral television system.

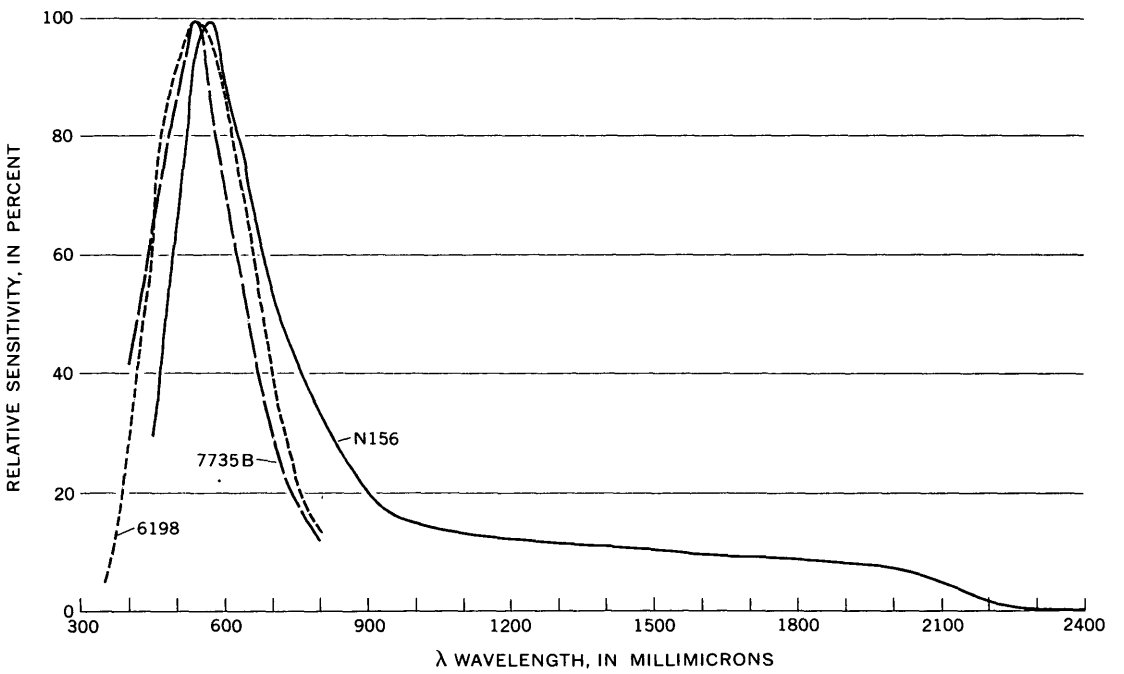

FIGURE 2.—Spectral sensitivity of vidicon tubes (6198, 7735B, and N156) used in airborne multispectral television system (data from manufacturer's specifications).

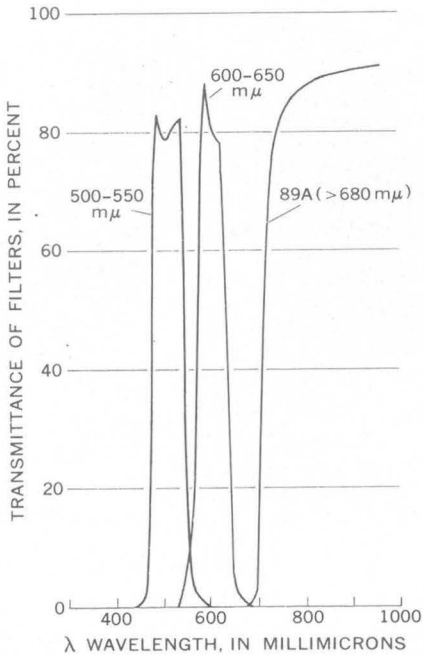

FIGURE 3.—Transmission characteristics of filters used in airborne multispectral television system (data from manufacturer's specifications).

Three standard television monitors with 5-inch picture tubes were used to monitor the in-flight images from each of the three cameras. A fourth monitor was used to view the input to the videotape recorder to assess how well the image was being recorded, and was also used for playback of the videotapes. Figure 4 shows the monitoring and taping equipment and cameras in the aircraft.

A standard videotape recorder was used. The image from any one camera could be recorded at any time by switching a coaxial switch to the desired camera. In addition, an audio channel allows the operator to record comments on the altitude, heading, and terrain conditions.

EXPERIMENTS IN IMAGERY

Three separate flights were made with the multispectral television system—one over the Salton Sea near Brawley, Calif., the second near the coastline of San Diego and LaJolla, Calif., and the third in Eureka County, Nev. All three flights were moderately successful. Some good television imagery was obtained, and it is our hope that the television systems may ultimately obtain almost the operational reliability of aerial camera systems. Figures 5 through 7 illustrate some of the imagery obtained with this system over the three areas. Interpretation criteria for such imagery is identical with that used for aerial photography with the only exception that the spatial resolution of the television systems is limited by the line-scan system.

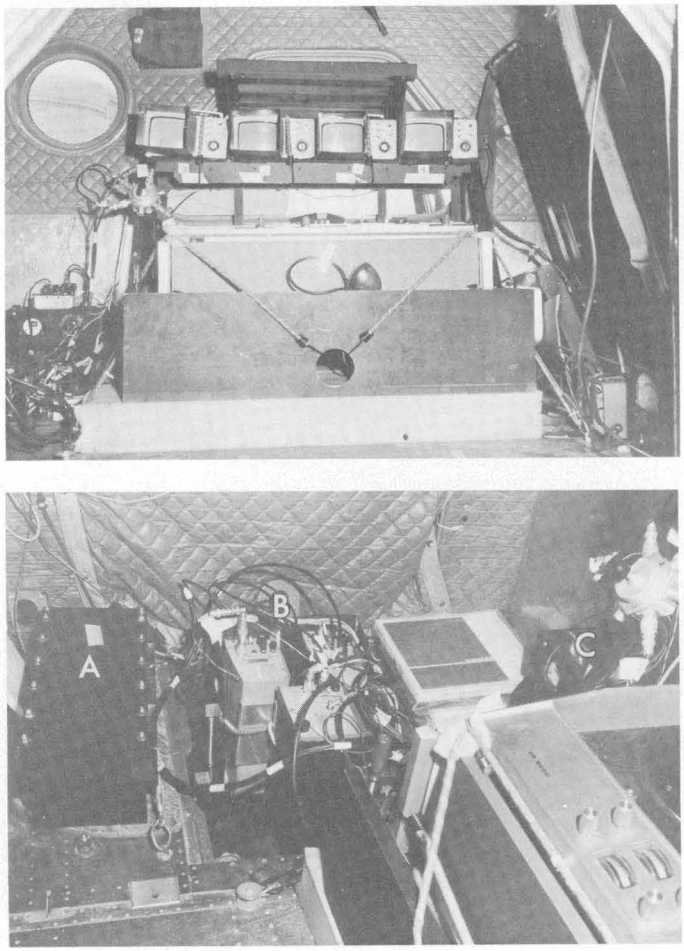

FIGURE 4.—Views of equipment in aircraft. Top, videotape recorder (in box) and television monitors for the three cameras and the recorder. Bottom, battery (*A*), cluster of three television cameras in aerial camera mount (*B*), and rotary converter power supply (*C*).

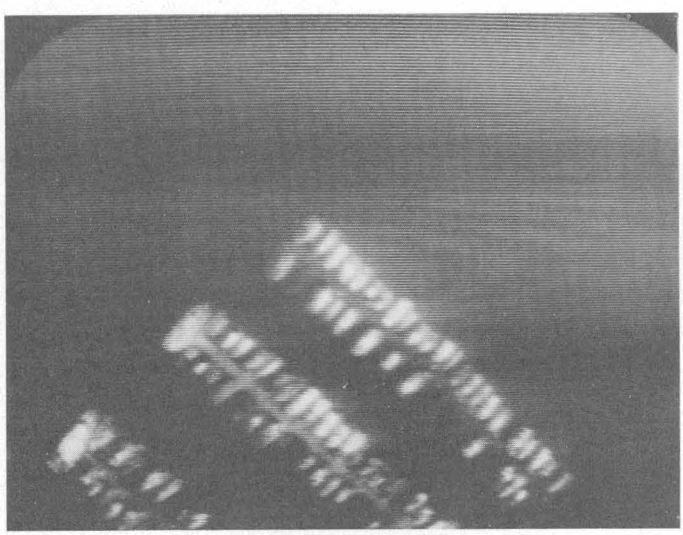

FIGURE 5.—Television images of marina in lagoon near San Diego, Calif. (7735B vidicon tube, 89A filter, altitude 2,000 ft.).

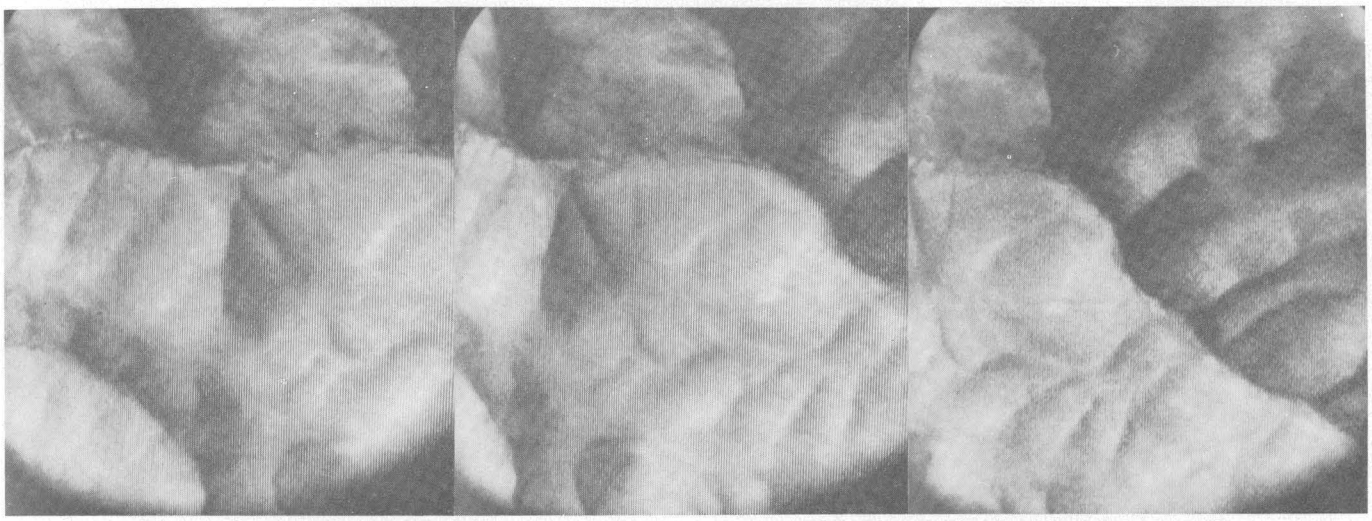

FIGURE 6.—Stereotriplet of television images on the west side of the Tuscarora Mountains, Eureka County, Nev. (7735B vidicon tube, 600–650-mμ filter, altitude 5,000 ft.).

FIGURE 7.—Television images of (top) area west of Elko, Nev. (N156 vidicon tube, 89A filter, altitude 5,000 ft.), and (bottom) Humboldt River, west of Elko, Nev. (7735B vidicon tube, unfiltered, altitude 5,000 ft.).

CONCLUSIONS

1. Multispectral airborne television systems are workable and may be installed and used in light aircraft quickly when needed.
2. The system has the advantage of providing imagery on videotape instantaneously.
3. Recorded comments with the imagery aid the interpreter when looking at the subsequent playback.
4. The exposure and resolution of the imagery may be checked immediately in flight, and the area can be reflown without landing if the imagery is not up to the required standards of clarity.
5. Narrow bandpass filtering is usable for enhancing the contrast of desired features.

Because of some advantages of the airborne multispectral television system over aerial photography it may eventually become a widely used system for identification and mapping of terrain features. It is believed that this is a precursor of television systems for studying the engineering and cultural-resource aspects of natural resources from spacecraft. Such low-altitude use of television systems will prepare scientists to use similar data from earth-orbital satellites.

ACKNOWLEDGMENTS

The authors wish to acknowledge the aid of Raymond Lafferty, Howard Chapman, and other members of the staff of the Phoenix, Ariz., research office, U.S. Geological Survey, for their contributions in the engineering, construction, and flight testing of the airborne multispectral television system described in this paper

USE OF INFRARED IMAGERY IN STUDY OF THE SAN ANDREAS FAULT SYSTEM, CALIFORNIA

By R. E. WALLACE and R. M. MOXHAM,
Menlo Park, Calif., Washington, D.C.

Work done in cooperation with the National Aeronautics and Space Administration

Abstract.—Infrared imagery (in the 8- to 13-micron band) of the San Andreas fault system in the Carrizo Plain area of California shows that the fault can be clearly traced over most of about 200 miles flown. Variations in soil moisture caused by the water-barrier characteristics of the fault zone, as well as vegetation differences related to soil moisture and microtopography, are factors influencing visibility of the fault in the IR imagery. Also identified on the imagery and useful in analyzing offset on the fault are (1) offset segments of ancient stream channels disrupted by movement on the fault, (2) landslide terrain, and (3) numerous soil and Tertiary bedrock units. Imagery obtained 1–2 hours before sunrise is considered most useful for the fault studies.

Infrared imagery in the 8- to 13-micron band obtained in June 1965 is being used to study the San Andreas fault system in the Carrizo Plain area of California. The study is part of a cooperative program with the National Aeronautics and Space Administration to determine the applications of remote sensors and the feasibility of their use in spacecraft.

Movement along the San Andreas fault, a fracture in the earth's crust more than 600 miles long, has been responsible for numerous earthquakes, including the great earthquakes of 1857 in the Carrizo Plain–Tejon Pass area and of 1906 in the San Francisco area. A study of the amounts and frequency of historic and prehistoric displacements on the San Andreas fault is part of a program aimed at developing earthquake-prediction techniques. In the Carrizo Plain area, because of the arid climate, the effects of ancient movements on the fault are exceptionally well preserved. Channels of streams that flow across the fault were offset as much as 30 feet during the 1857 earthquake, and cumulative channel offsets of as much as 3,200 feet are preserved in the Carrizo Plain area. Total cumulative offset on the fault possibly may be hundreds of miles.

Infrared-detection techniques are being applied in this study in anticipation that subtle differences in soil moisture, composition, or physical characteristics that are not readily apparent in black-and-white aerial photographs would be apparent in the IR imagery, thus permitting the positions of ancient offset segments of stream channels, alluvial fans, bedrock units, or other features to be more clearly determined.

The Carrizo Plain (fig. 1), a broad intermontane valley lying at an altitude of 2,000 feet between the Temblor Range on the east and the Caliente Range on the west, is approximately 40–45 miles west of Bakersfield, Calif. Annual rainfall in the Carrizo Plain area is between 3 and 8 inches.

NATURE OF STUDY

Evaluation of the IR imagery is made primarily on an empirical basis by comparing the IR images with geologic maps and with images obtained by other techniques. Geologic maps of the entire area at a scale of 1:125,000, prepared by Dibblee (1962), and of part of the area at a scale of 1:24,000, prepared by J. G. Vedder (in preparation), are important as a basis for analyzing the imagery. In addition, temperature measurements of selected terrane units were made for control during the flights; after the imagery was obtained, further thermal studies of selected soil and rock units were conducted in the field. Graphs (fig. 2) show representative temperature ranges measured during the time the imagery was obtained. Other

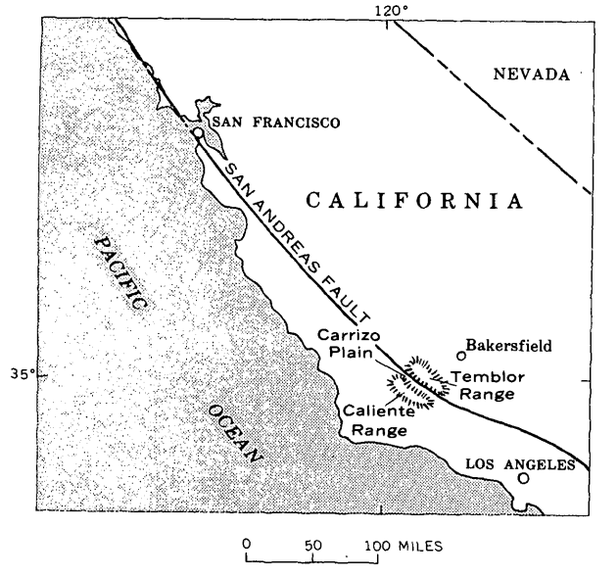

FIGURE 1.—Index map showing location of San Andreas fault and Carrizo Plain in California.

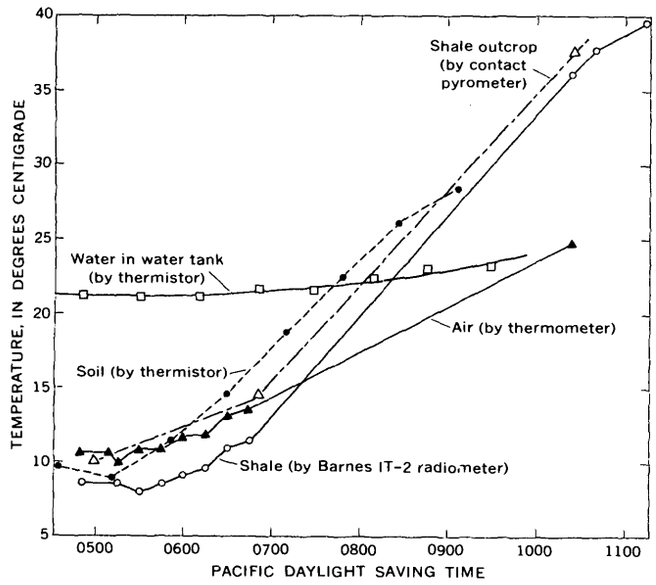

FIGURE 2.—Representative temperature ranges, June 18, 1965.

types of imagery and photography have been obtained of all or parts of the area and include radar, nine-frame enhanced multiband photography, black-and-white photographs at scales of 1:6,000 and 1:24,000, and Aero-Ektachrome color photographs at a scale of 1:12,000. Comparison and evaluation of these different techniques is in a preliminary stage.

No data are available on the emissivity of the surface materials in the report area, and descriptions of relatively cool or warm surfaces are based on radiation temperatures as recorded by the scanning radiometer. Thus the nonquantitative scanning technique permits little more than qualitative discussion of the results.

INFRARED IMAGERY STUDIED

Several sets of IR images were obtained on June 18, 1965, in an area along the San Andreas fault about 80 miles long and 20 miles wide. Some were obtained in a period of a few hours before sunrise and others were obtained within the hour after sunrise. In addition, a continuous strip was obtained within the hour after sunrise. In addition, a continuous strip was obtained on June 3 and 4 during daylight hours of an area along the fault from near San Bernardino to the vicinity of Cholame, Calif. All images were obtained in the 8- to 13-μ band.

The following discussions pertain entirely to the imagery obtained on June 18 because for some reason, yet undetermined, the contrast in the imagery obtained on June 3 and 4 was very low and, although the topography representing the general line of the San Andreas fault was clear, little else of geologic significance has been identified thus far.

GENERAL RESULTS

A comparison of presunrise and postsunrise imagery indicates that presunrise imagery is generally more useful for discriminating rock and soil units and for determining something about their physical characteristics or composition. Postsunrise imagery has the appearance of aerial photography because the sun heats different-facing slopes differently just as it illuminates different slopes differently. A comparison of IR imagery (fig. 3*A*) with aerial photographs taken at the same time (fig. 3*C*) shows this similarity. The wide range in radiation temperatures resulting from topographic differences constitute "noise" through which it is difficult to see thermal differences related to rock characteristics.

During presunrise hours the topographic influence of solar heating is at a minimum and the radiation temperatures represented by the imagery are more closely related to the thermal properties of the rock or soil unit. In the presunrise imagery, striking contrasts can be seen between: (1) plowed ground (relatively cool) and unplowed ground (relatively warm) (see fig. 4*A*); (2) moist ground (relatively cool) and dry ground (relatively warm) (see figs. 6*A* and 7*A*); and (3) areas covered by vegetal material both alive and dead (relatively cool) and barren areas (relatively warm) (see fig. 5*A*).

One marine siliceous shale unit of Pliocene age (informally termed the Bitterwater Creek shale by Dibblee) appears relatively cool in comparison to surrounding and nearby recent alluvial deposits and Pliocene sandstone and conglomerates (see fig. 8).

DISCUSSIONS OF SELECTED EXAMPLES

IR images of selected areas are discussed below and most are compared to black-and-white photographs.

The temperature graphs (fig. 2) show the ranges of temperatures that prevailed during the time that imagery was obtained.

Figure 3

Three images of the same area show the different results obtained from different techniques. Figure 3*A* is a postsunrise (0645 Pacific daylight time) IR image, 3*B* is a presunrise (0535 P.d.t.) IR image, and 3*C* is a panchromatic photograph taken at the same time as the postsunrise IR image. The similarity of the postsunrise IR and the photograph is apparent. The San Andreas fault which controlled the development of a valley shown in this frame, bisects the area from left to right.

In the postsunrise IR image, peculiar scallops appear along the boundary between the lightest area and adjacent dark areas. The cause appears to be instrumental inasmuch as each scallop appears to center on a cluster of dark scan lines. Peculiarly the scallops do not appear along every light-dark boundary. This is one type of instrumental "noise" with which a geologist must become acquainted in using IR imagery for geologic interpretations.

The presunrise IR image appears "flat" and without contrast, but under these conditions the radiation temperatures, which are controlled in large part by the thermal inertia of the rock units, can more readily be seen. For example, recent alluvium on the floors of the meandering valleys in the upper left part of figure 3*B* appears distinctly warmer than the adjacent bedrock.

Figure 4

These images compare a presunrise (0535 P.d.t.) IR image (4*A*) with a panchromatic photograph (4*B*). The San Andreas fault bisects the view from left to right, and several stream channels are displaced along the fault. It is this type of feature from which, hopefully, a history of prehistoric movements on the fault can be developed.

The light wavy line in each image is a dirt road formed by grading and compacting the local surface materials. In the IR image the distinct contrast between light (warm) and dark (cool) areas is between unplowed and plowed ground. Both units were extremely dry. The rock or soil material throughout the area is somewhat similar except for the differences resulting from plowing, although tone differences are discernible on the ground and in the panchromatic photography that cannot be discriminated in the IR image. For the most part the material of the area is unconsolidated alluvium composed of silt, sand, and angular pebble-sized fragments derived from siliceous shale and sandstone units of Pliocene age in the Temblor Range.

The fact that the most compacted material (the road) is warmest and the least compacted material (plowed ground) is coolest seems to be consistent with what might be expected of differences in the thermal inertia of the materials.

Although some boundaries between plowed and unplowed ground show in the panchromatic photograph, discrimination between the two can be made with nowhere near the certainty possible in the IR image.

Figure 5

These images compare a presunrise IR image (5*A*) with a panchromatic photograph (5*B*). The San Andreas fault bisects the area from left to right and has caused segmentation of the drainage. A lack of continuity of drainage can be seen through the three zones in the top, middle, and bottom of imaged areas.

A narrow dark (cool) area can be seen uphill (top of figure) from, and immediately adjacent to, the San Andreas fault. Relatively moist ground, in part accompanied by a stand of green grass, is represented by the relatively cool areas. The fault zone seems to serve as a partial ground-water barrier, although in the area of this view topographic relief also exerts a significant control. Here the light-colored (warm) band through the center of the view is a low ridge bordering the fault.

The deepest black tones in gulches and along the fault represent accumulations of tumbleweeds that have blown into hollows sheltered from the wind. The piles of tumbleweeds are excellent insulators and exhibit the properties of a material having exceptionally low thermal inertia; thus they have relatively cool radiation temperatures before sunrise. During the day, radiant temperatures of the tumbleweed were measured with a Barnes IT–2 radiometer and were found to be relatively high.

Figure 6

These images compare a presunrise IR image (6*A*) and a panchromatic photograph (6*B*). The dark areas (cool) are believed to be related primarily to soil moisture. The San Andreas fault, which bisects the

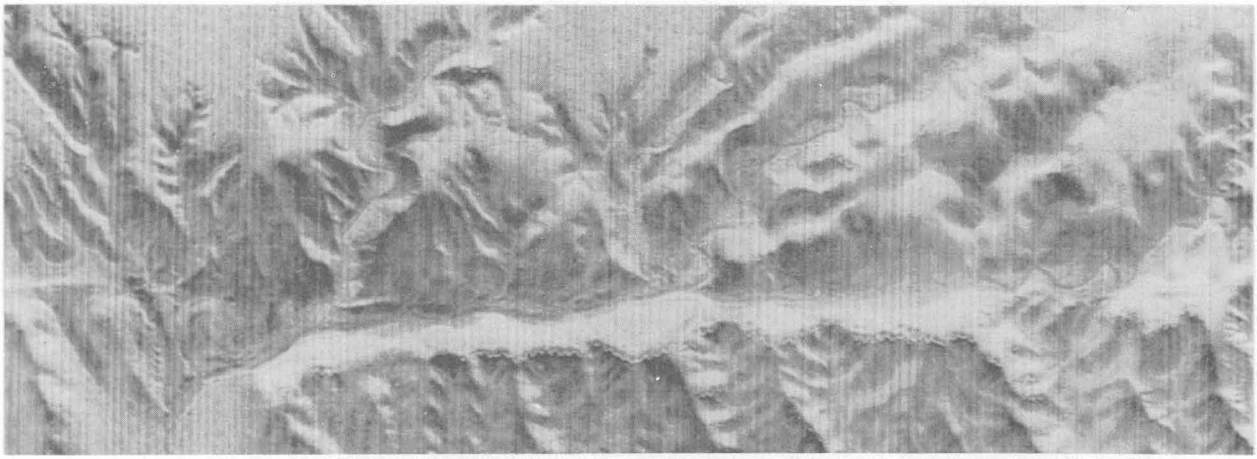

A

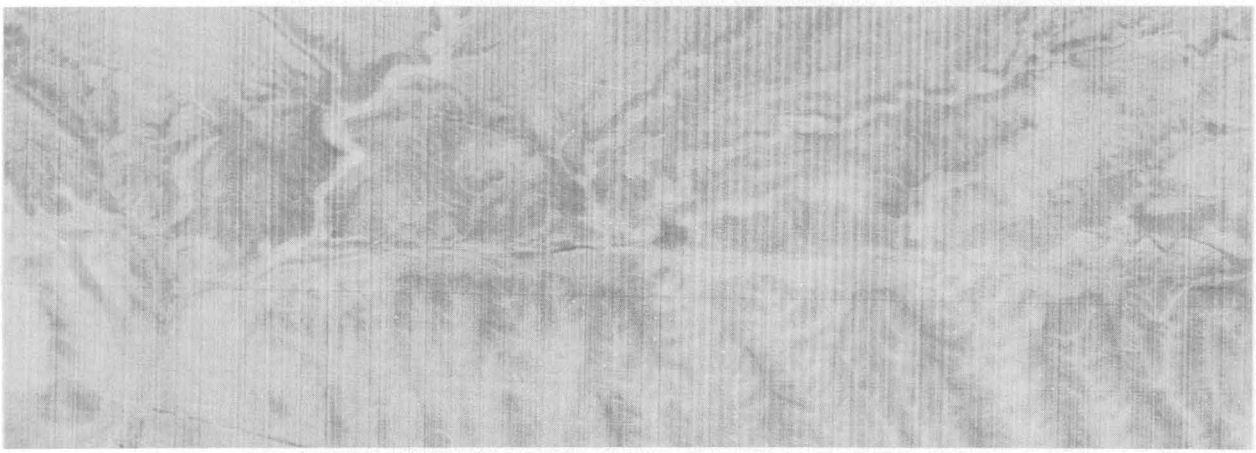

B

C

FIGURE 3.—*A*, postsunrise IR image. *B*, presunrise IR image. *C*, aerial photograph.

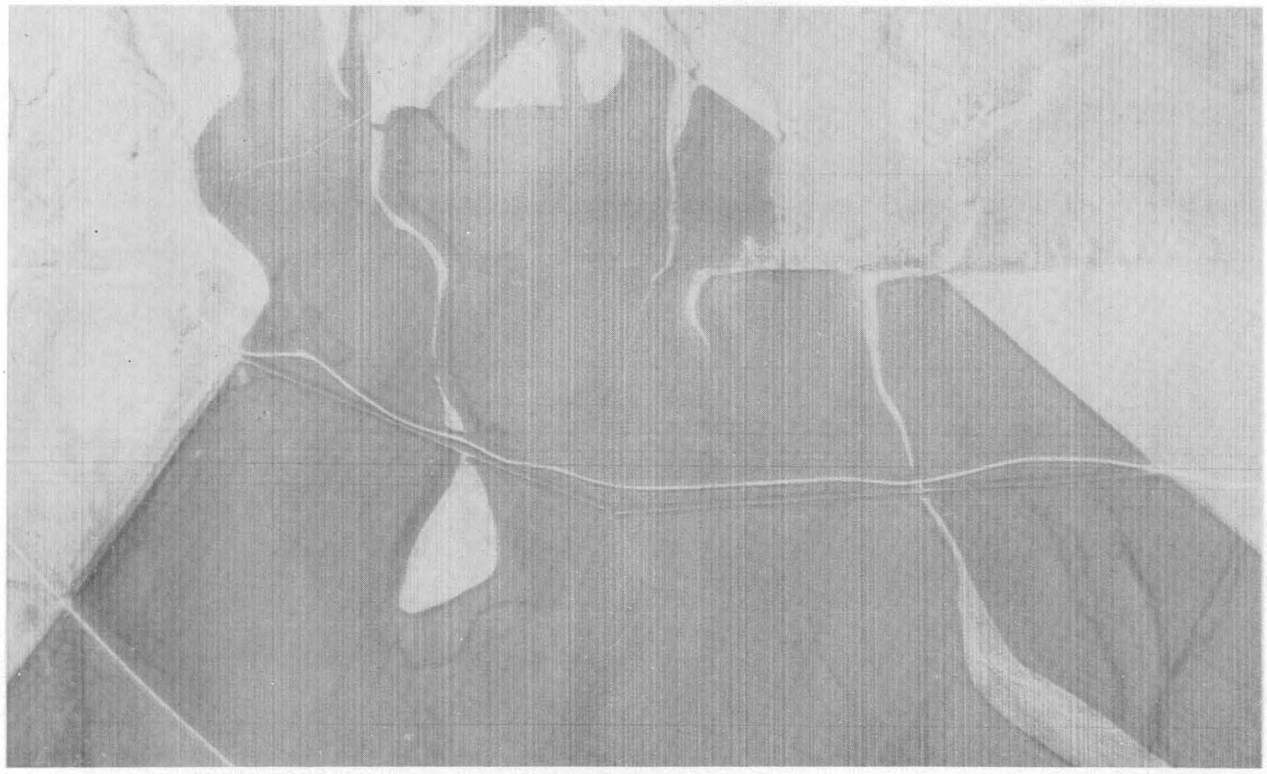

A

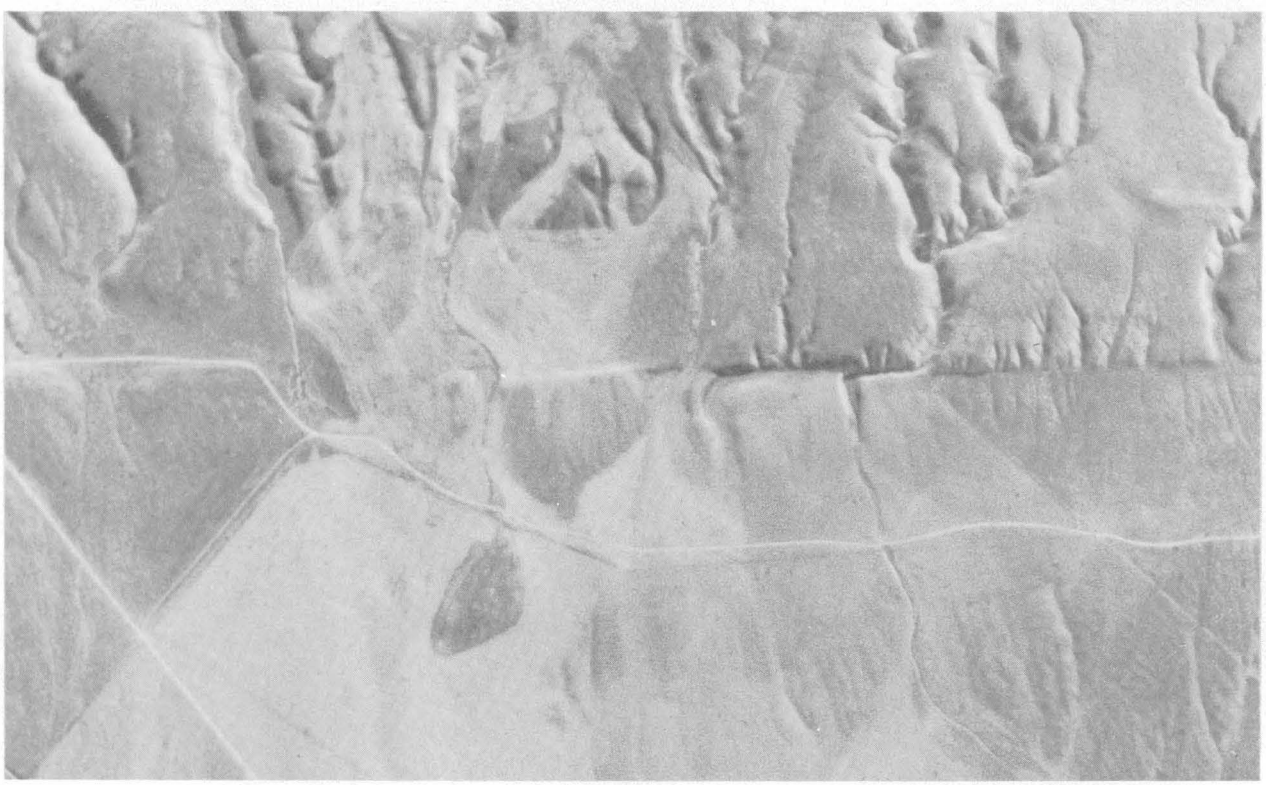

B

FIGURE 4.—*A*, presunrise IR image. *B*, aerial photograph.

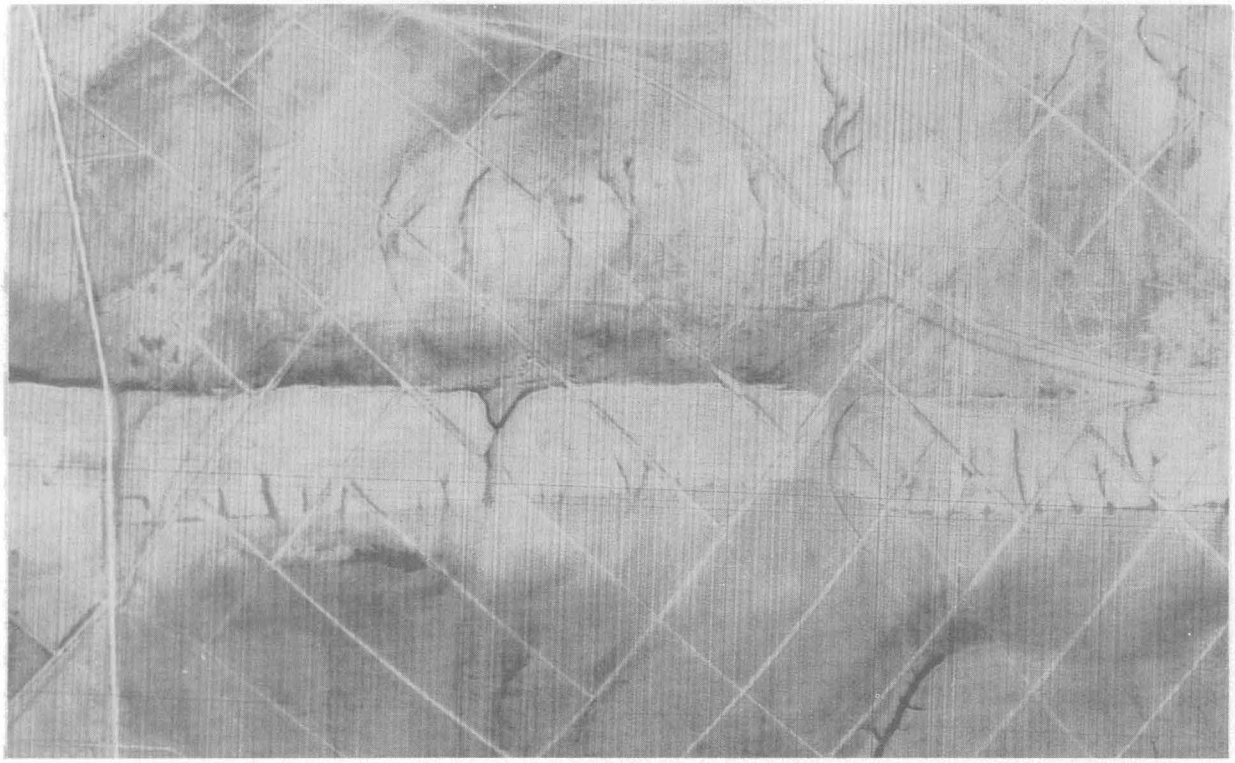

A

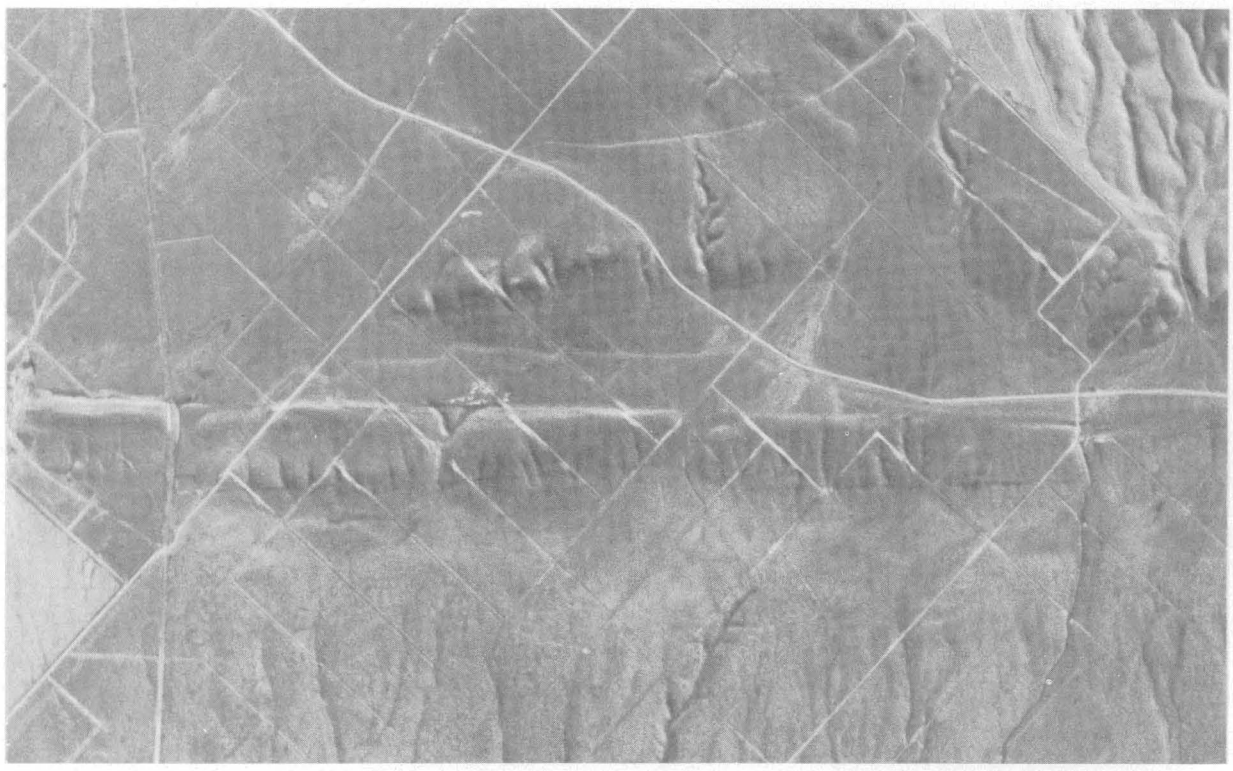

B

FIGURE 5.—*A*, presunrise IR image. *B*, aerial photograph.

A

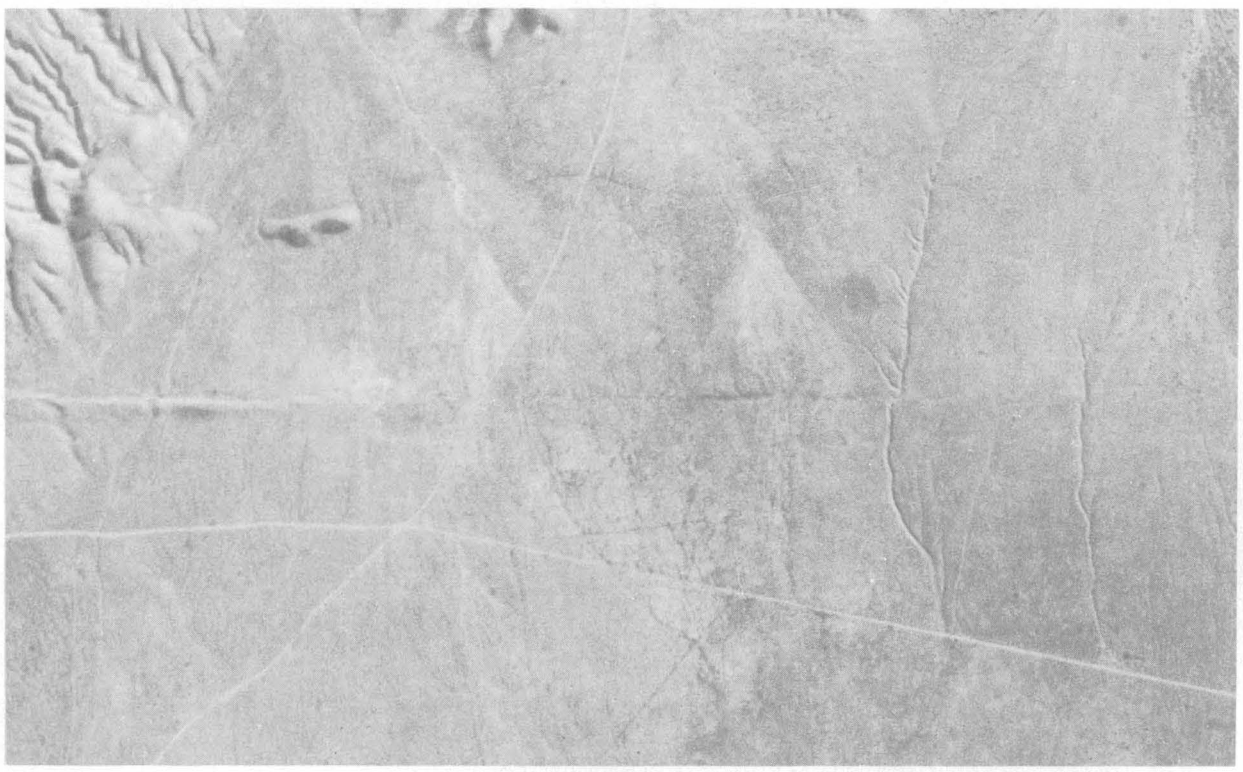

B

FIGURE 6.—*A*, presunrise IR image. *B*, aerial photograph.

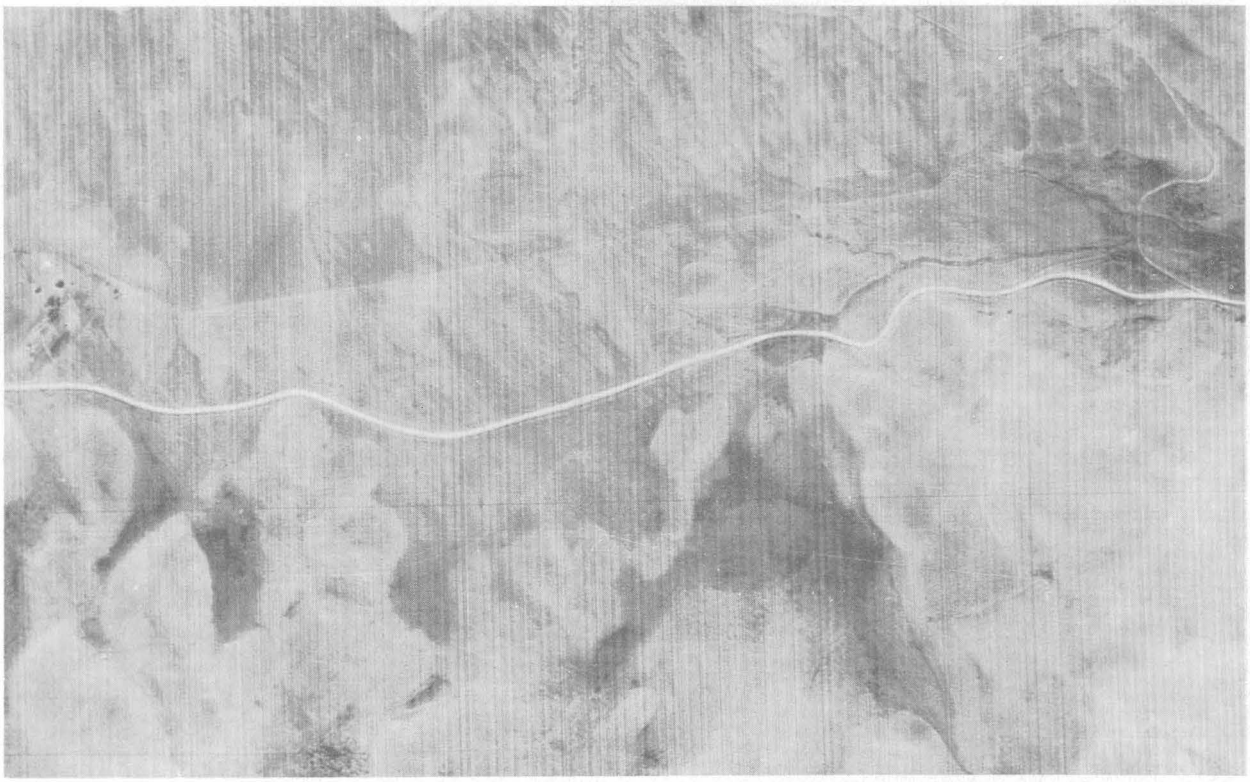

A

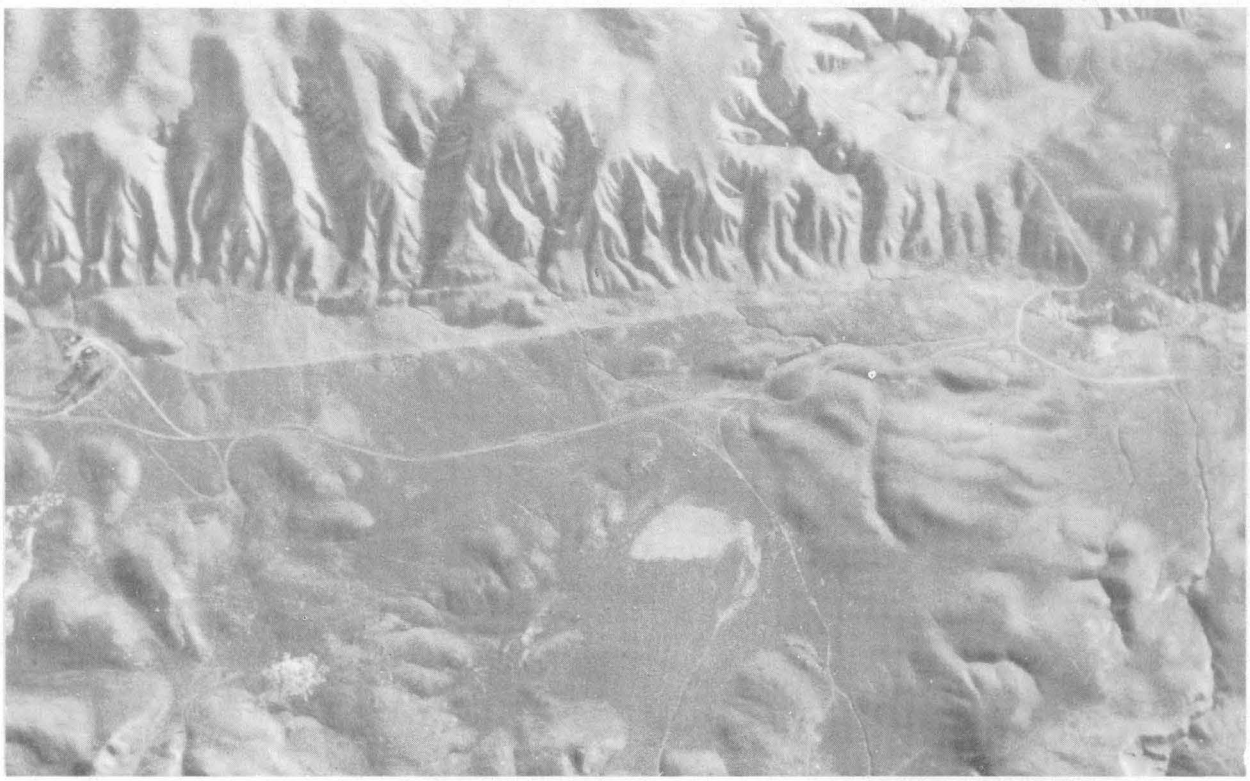

B

FIGURE 7.—*A*, presunrise image. *B*, aerial photograph.

area from left to right, serves as a ground-water barrier and tends to raise the soil moisture on the uphill side (top of frame) of the fault. The fault in this area has little or no topographic expression. Some dead grass and a small amount of green grass were in the darker areas and help to enhance the coolness of the surface. Radiation temperatures of green grass were measured in the field during daylight hours with a Barnes IT–2 radiometer and were found to be as much as 10°C cooler than those of the surrounding barren soil.

Even a small growth of vegetation tends to build up a thin humus mat in these slightly more moist areas. The insulating characteristics of a ¼-inch layer of humus composed of partly decomposed grass, small twigs, and sheep manure was demonstrated by a 9°C temperature difference between the upper and lower surface of the humus layer.

In figure 6*A* a water-tank area shows as a set of dark (cool) spots along the fault zone, left of the road that crosses the fault. The spots represent concentrations of dry cow and sheep manure which are excellent insulators.

Inasmuch as areas of slightly higher soil moisture possibly related to higher water tables can be identified in the IR imagery, IR imagery may prove useful in searching for ground water in desert areas.

Figure 7

These images compare a presunrise IR image (7*A*) with a panchromatic photograph (7*B*). The San Andreas fault trends from left to right at the base of the hills near the top of the frame. High contrast between dark (cool) and light (warm) areas can be seen clearly in the lower half of the IR image. The light (warm) areas are lobelike masses of soil and rocks that have moved as landslides (J G. Vedder, oral commun., 1965) in a direction from the bottom toward the top of the frame. The dark areas are undrained or poorly drained zones between the landslide lobes. Ground moisture was high, and considerable vegetation growing in these poorly drained areas presumably accounts for the relative coolness. No measurements were made to determine the precise temperature difference represented.

Because of its relative warmth, the asphalt road appears as a bright line extending the width of the IR image, but the unpaved roads are obscure. In the aerial photograph, the opposite is true.

The clarity with which the landslide terrain can be discriminated suggests that IR imagery may be useful in preparing an inventory of landslide terrain along and near the San Andreas fault as part of the geologic-hazards study related to the earthquake-study program.

Figure 8

IR images obtained in presunrise hours have shown that some bedrock units display distinctive thermal characteristics. The two elliptical dark-gray (relatively cool) areas shown in figure 8 represent outcrops of a siliceous shale of Pliocene age (informally termed the Bitterwater Creek shale by Dibblee). The differences in physical or chemical characteristics which cause this to be one of the most distinctive bedrock units in the IR imagery is not yet known. These same outcrops also show very low backscatter in side-looking radar imagery. The shaly parting of the rock and resulting platy nature of the fragments which form the outcrop surface may be important in producing low backscatter of the radar energy and in influencing the emissivity of the surface in the 8- to 13-μ range.

CONCLUSIONS

Infrared imagery in the 8- to 13-μ band is potentially useful in the study of the San Andreas fault system, California. The present study shows clearly that certain properties such as degree of compaction, platiness of surface fragments, and soil moisture may influence greatly the thermal inertia and emissivity, and thus the surface temperature of different soil and rock units. A quantitative evaluation of the variables, however, is not yet available.

Relative radiation temperature differences between different rock and soil units are more clearly displayed in imagery obtained in presunrise hours than in postsunrise hours when irregular topography is irregularly heated by solar radiation and effects of the thermal inertia of rock units are masked.

269-274 O—67——11

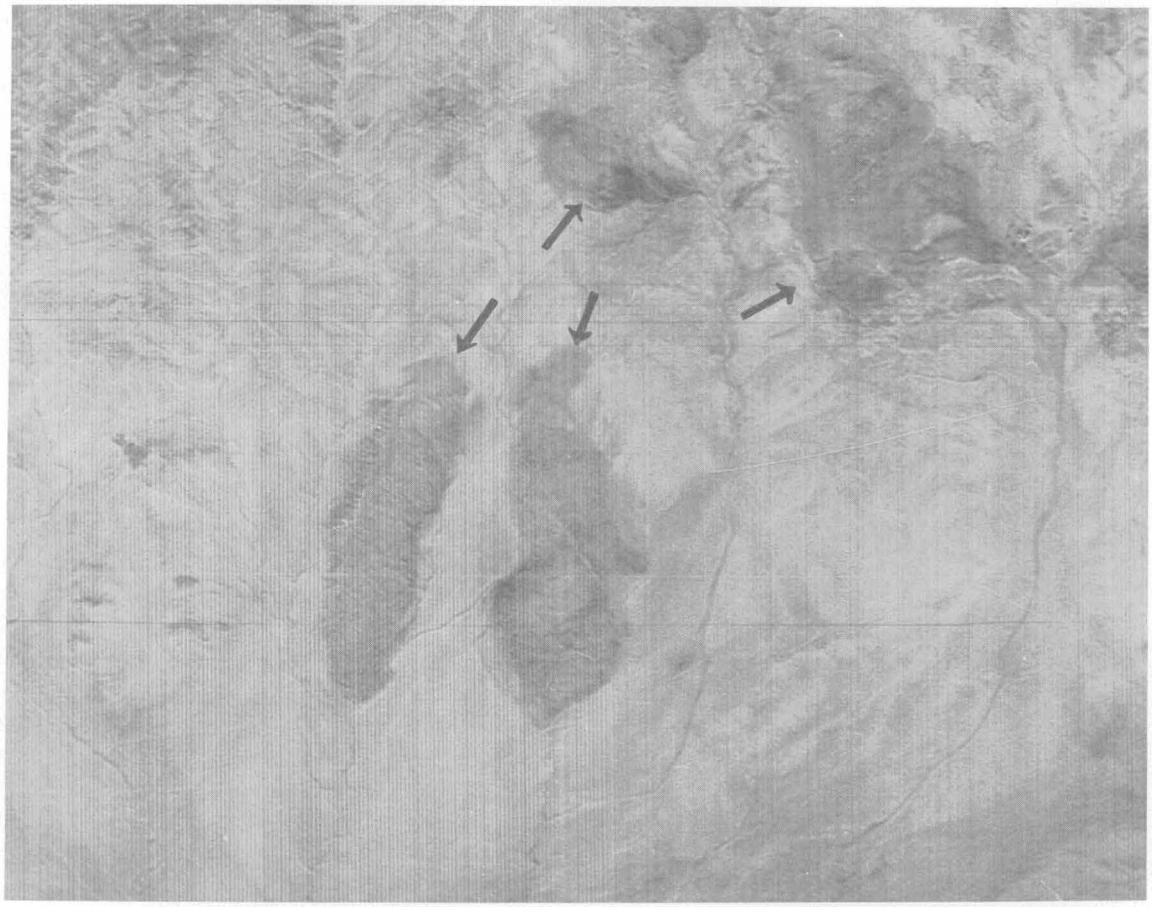

FIGURE 8.—Presunrise IR image. Arrows point to outcrops of the Bitterwater Creek shale of Dibblee.

REFERENCE

Dibblee, T. W., Jr., 1962, Displacements on the San Andreas rift zone and related structures in the Carrizo Plain and vicinity *in* Guidebook, Geology of Carrizo Plain and San Andreas fault: San Joaquin Geol. Soc. and Pacific Sec., Am. Assoc. Petroleum Geologists, Soc. Econ. Paleontologists and Mineralogists, p. 5–12.

ISOTOPIC AGE AND GEOLOGIC RELATIONSHIPS OF THE LITTLE ELK GRANITE, NORTHERN BLACK HILLS, SOUTH DAKOTA

By R. E. ZARTMAN and T. W. STERN, Denver, Colo., Washington, D.C.

Abstract.—The Little Elk Gneissoid Granite of Taylor (1935) in the northern Black Hills, S. Dak., first crystallized 2,560 million years ago and was disturbed about 60 m.y. ago, during Laramide time, as interpreted from isotopic ages of 5 zircon separates. Twelve total-rock Rb-Sr analyses show that extensive open-system conditions have occurred since granite emplacement within the pluton; however, the granite as a whole seems not to have undergone net exchange with its enclosing rocks. Whether all of this element redistribution within the pluton took place in Laramide time, or partly during some Precambrian event, has not been established. Field relationships suggest that the contact between the granite and adjacent Precambrian metasedimentary rocks is an unconformity, although the possibility of a comformable intrusive contact cannot be ruled out.

An approximate age of 2,500 million years was determined from a single U-Th-Pb analysis of zircon during a preliminary radiometric study by Zartman and others (1964) for a gneissic granite occurring near Nemo, S. Dak., in the northern Black Hills. Discordant mineral and total-rock Rb-Sr data, on the other hand, attested to the disturbed nature of this granite. As discussed by Zartman and others, the apparent great antiquity of such a rock is of interest both to the local geologic history of the Black Hills and to a clearer comprehension of the crustal growth of North America. It was therefore decided to pursue the study further in order to define the age of emplacement more precisely and to decipher the effects of the later metamorphic disturbance.

Four additional zircon and nine total-rock samples from the granite were obtained, and the results are reported here. The material was collected to represent as wide a range in lithology and geographic location as possible (fig. 1 and table 1). In addition, geologic mapping was undertaken to better understand the structural relationship of the granite to the surrounding rocks.

The gneissic granite which occupies the valley of Little Elk Creek near the east border of Lawrence County was first described by Runner (1934) and later named the Little Elk Gneissoid Granite by Taylor (1935, p. 280). Neither of these workers, who respectively employed geologic mapping and a primitive chemical-lead dating method, gave conclusive proof of the relationship between the granite and other Precambrian rocks of the Black Hills. The statement by Runner (1934, p. 368) that "the granite is clearly intrusive into the pre-Cambrian sediments . . . . [and] the border zone is dominated by numerous small dikes extending into the sedimentary schists" appears to be unsubstantiated in light of a detailed field study of the area. Because of the ambiguous meaning of the term "gneissoid" and because this rock is clearly igneous in its more massive occurrence, the Little Elk Gneissoid Granite of Taylor (1935) is herein referred to as the Little Elk Granite.

Acknowledgments.—The samples for this study were collected with the assistance of J. J. Norton and J. C. Ratté, and Richard Bayley permitted us access to some of his unpublished geophysical data from the Little Elk Creek area. M. F. Newell aided in the chemical separation and purification of uranium, thorium, and lead from the zircon concentrates.

FIELD RELATIONSHIPS

The Little Elk Granite is exposed over an area of about 2 square miles through 2 windows in Paleozoic sedimentary rocks. Less than a mile of contact between the granite and adjacent Precambrian metasedimentary rocks is observable, and conclusive evidence of geologic relationships along this contact is absent. The metasedimentary rocks consist of mica schist, quartzose schist, conglomerate, and iron-formation. They appear to be extensions of the Nemo and Estes Sys-

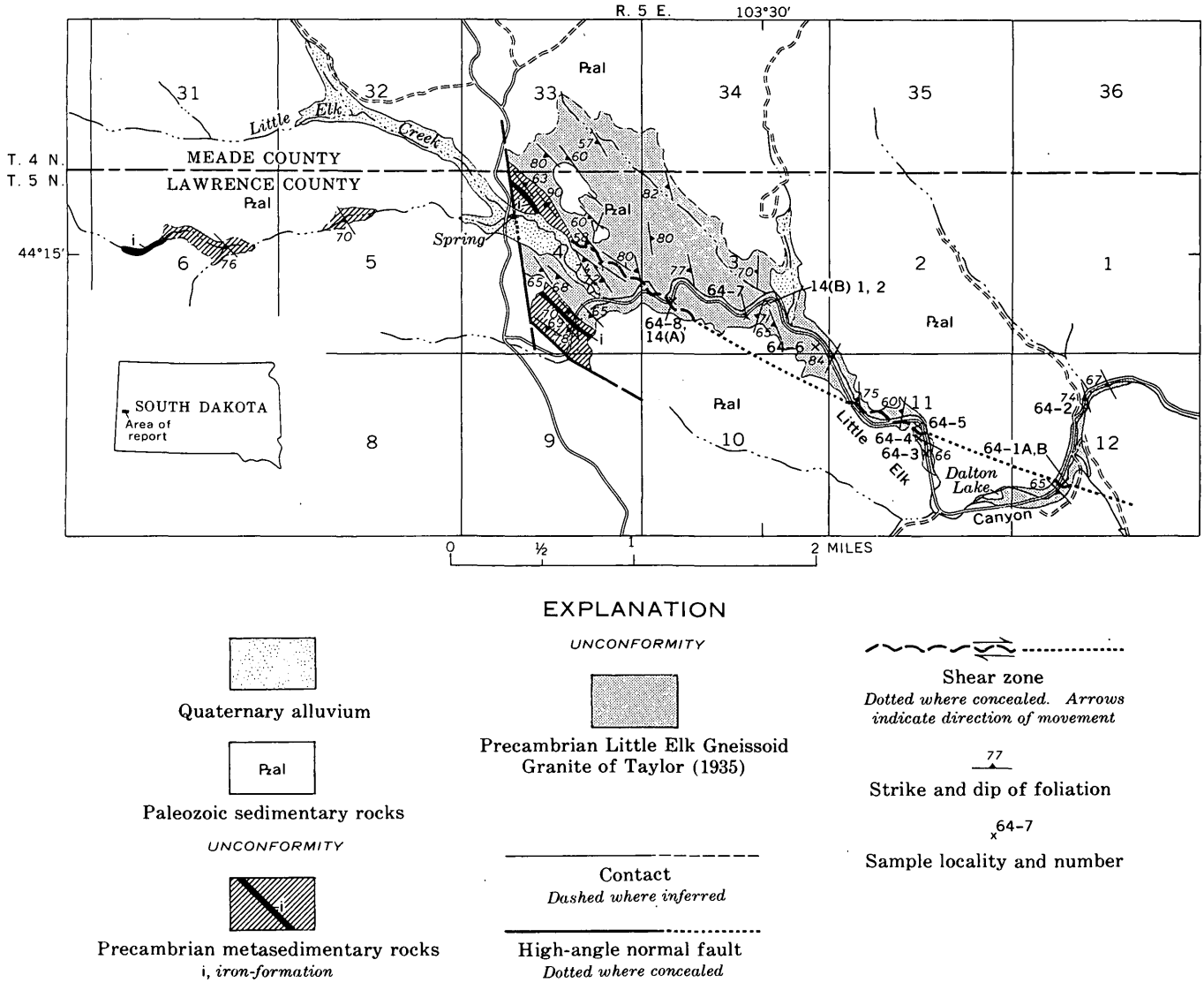

FIGURE 1.—Geologic map of part of the Little Elk Canyon area, northern Black Hills, S. Dak., showing location of samples collected for radiometric dating.

tems as described by Runner (1934), which crop out 2 miles to the southwest in the main Precambrian terrane of the Black Hills. All of the Precambrian rocks have been regionally metamorphosed and show evidence of cataclastic deformation. A prominent shear zone with about 2,000 feet of displacement in the Precambrian rocks crosses the area, but does not cut the overlying Paleozoic sedimentary rocks. Normal faults of Laramide(?) age are also present; however, they have displacements of only a hundred feet or less.

Detailed petrographic descriptions of the Little Elk Granite are given by Runner (1934) and Taylor (1935). The rock is predominantly gneissic in structure, cataclastic in fabric, and granitic in composition. It is light to medium gray and has a grain size ranging from 1 to 10 mm. The dominant minerals are oligoclase (An_{10-15}), microcline, quartz, and biotite. Muscovite is abundant locally. Primary accessory minerals include apatite, sphene, zircon, magnetite, and pyrite-pyrrhotite. Epidote-clinozoisite, calcite, and iron oxides of secondary origin are also present, especially in the more sheared zones. Moderately to well-developed foliation formed by biotite crystals in parallel orientation is common and is distributed in layers and lenses separated by fractured feldspar and quartz. The granite is hypautomorphic-equigranular in its more massive parts; however, it displays a pervasive cataclastic texture, which, where well developed, has changed the rock to a mylonite that consists of small grains and

TABLE 1.—*Location and description of samples of Little Elk Gneissoid Granite of Taylor (1935) used for radiometric dating*

Sample	Location		Description	Mineral content (percent)						
	Lat. N.	Long. W.		Quartz	Microcline	Plagioclase	Biotite	Muscovite	Carbonate	Opaque minerals
64–1A	44°13′54″	103°28′00″	Pinkish-gray moderately foliated biotitic gneissic granite. Large sheared microcline phenocrysts give rock augen texture.	34	38	18	8	2	------	------
64–1B	Same as 64–1A.	Same as 64–1A.	Gray strongly sheared biotitic gneissic granite. Extreme granulation associated with major fault zone.	38	32	20	6	3	------	1
64–2	44°14′17″	103°27′54″	Gray moderately sheared biotitic gneissic granite.	38	42	12	6	1	------	1
64–3	44°14′04″	103°28′56″	Gray weakly foliated biotitic gneissic granite. Unit rather massive, but biotite in subparallel orientation distributed in layers and lenses separated by feldspar and quartz grains.	30	46	16	5	1	1	1
64–4	44°14′08″	103°28′57″	Gray moderately foliated biotitic gneissic granite.	40	34	16	7	2	------	1
64–5	44°14′11″	103°28′58″	Light-gray mylonitic granite. Profound granulation gives rock aplitic texture.	50	20	26	2	1	------	1
64–6	44°14′35″	103°29′38″	Gray moderately foliated biotitic gneissic granite.	32	34	26	6	2	------	------
64–7	44°14′44″	103°30′03″	Gray weakly foliated biotitic gneissic granite. Unit rather massive, with least deformation of any sample included in study.	38	34	20	4	3	1	------
64–8	44°14′46″	103°30′35″	Pink somewhat sheared medium-grained pegmatite.	14	52	32	1	1	------	------
14(A) [1]	Same as 64–8.	Same as 64–8.	Gray strongly sheared biotitic gneissic granite. Extreme granulation associated with major fault zone.	58	18	16	3	4	------	1
14(B)1 [1]	44°14′49″	103°29′57″	Gray weakly foliated biotitic gneissic granite.	38	30	24	7	1	------	------
14(B)2 [1]	Same as 14(B)1.	Same as 14(B)1.	Gray weakly foliated biotitic gneissic granite.	36	34	20	8	1	------	1

[1] Sample from Zartman and others (1964).

veinlet-filled fractures. Taylor (1935, p. 284) concluded that "* * * the presence of calcite-quartz-muscovite veinlets and * * * yellow-brown oxides in the micaceous layers perhaps indicate that some addition or removal of material might have occurred [during metamorphism]."

Runner interpreted the Little Elk Granite as intrusive into the Precambrian metasedimentary rocks; however, it appears more likely that the sediments were deposited unconformably on the granite. Reasons for this conclusion are:

(1) Mappable units within the metasedimentary rocks, such as the iron-formation, parallel the granite contact and thus are compatible with the deposition of sediments on preexisting basement.

(2) Conglomerate within the metasedimentary rocks may reflect the onset of deposition following a period of erosion; however, no pebbles of recognizable Little Elk Granite were found in these conglomerates, which consist almost entirely of quartzite clasts that commonly have a pronounced tectonic elongation.

(3) No evidence of a fine-grained border phase, contact metamorphism, or crosscutting relationships was found at the contact between the metasedimentary rocks and the granite.

All of the Precambrian rocks of this general area of the Black Hills lie within the biotite zone of metamorphism; however, this metamorphism was imposed during a period of deformation subsequent to the formation of both granite and sedimentary rocks and has no bearing on their relative age. Although the above evidence is interpreted to mean sedimentary deposition upon the granite, the possibility of a conformable intrusive contact cannot be conclusively ruled out. Because of the short distance over which the contact is exposed and owing to the obscuring effect of the later metamorphism, it has not been possible to establish conclusively whether the granite is

intrusive into the metasedimentary rocks or was the basement on which they were deposited.

Little is known about the original conditions under which the granite was emplaced. Where least deformed it is massive, coarse grained, and somewhat porphyritic. A magnetic survey suggests that the granite occurs along the southwest flank of a rather extensive dome which is largely buried under Paleozoic sedimentary rocks to the north (Richard Bayley, oral commun., 1967). This dome appears to be related to a period of medium-grade regional metamorphism and cataclastic deformation which occurred sometime in the Precambrian subsequent to both the emplacement of the granite and the deposition of the sediments which now comprise the Nemo and Estes Systems of Runner (1934). A pronounced foliation which appears related to this tectonism is present in the metasedimentary rocks and the granite. This foliation, which parallels the bedding in the sedimentary rocks and extends uninterrupted in orientation into the granite, is the dominant textural feature now seen in the area.

The most extreme cataclastic deformation and accompanying mylonitization occurs adjacent to a pronounced Precambrian shear zone trending northwestward diagonally across the map area. This fault cuts both the granite and the Precambrian metasedimentary rocks and apparently has at least 2,000 feet of right-lateral displacement. Because there is a sharp change in foliation direction across this zone, movement on the fault must have taken place after the area was metamorphosed. Whether the shearing merely represents a waning stage of the metamorphism or occurred at some distinctly later date is not clear.

Laramide(?) normal faults, which cut both the Precambrian and the flat-laying Paleozoic rocks, were not accompanied by any significant metamorphism.

AGE DETERMINATION

For each sample analyzed, approximately 100 pounds of rock was pulverized and a total-rock aliquot was carefully split from it. The remainder of the sample was processed for its zircon concentrate, and, by using alpha activity to estimate uranium and thorium content, four zircon samples of widely differing radioactivity were chosen for analysis.

Results of U–Pb and Th–Pb age determinations on zircon are given in tables 2 and 3. Rb-Sr total-rock analytical data are shown in table 4. All uranium, thorium, and lead concentrations were obtained by isotope dilution. The zircons were decomposed by sintering with borax, and standard ion-exchange and dithizone extraction techniques were used for chemical purification. Rubidium and strontium concentrations were obtained on several of the total-rock samples by standard chemical-isotope dilution methods and, using these samples as standards, the remainder were deter-

TABLE 2.—*Analytical data for* U–Pb *and* Th–Pb *age determinations*

Sample	Concentration (ppm) [1]			Atom percent			
	Pb	U	Th	Pb^{204}	Pb^{206}	Pb^{207}	Pb^{208}
64–1A	181.8	949.0	620.1	0.133	66.93	12.34	20.54
64–3	211.1	504.0	300.1	.029	72.35	12.55	15.07
64–4	158.5	476.3	271.9	.142	70.05	12.89	16.92
64–7	272.4	724.7	369.7	.086	72.06	12.76	15.09
14(B)2	172.7	479.8	315.6	.056	72.15	12.63	15.16

[1] Concentrations are believed to be correct to within 2 percent of the reported value. The isotope ratios of the common lead used to correct for the nonradiogenic lead present in the zircons are $Pb^{206}/Pb^{204}=18.5$, $Pb^{207}/Pb^{204}=15.7$, and $Pb^{208}/Pb^{204}=38.4$.

TABLE 3.—*Zircon ages by the* U–Pb *and* Th–Pb *methods*

Sample	Rock	Age (million years)			
		Pb^{206}/U^{238}	Pb^{207}/U^{235}	Pb^{207}/Pb^{206}	Pb^{208}/Th^{232}
64–1A	Moderately foliated biotite gneissic granite.	870	1, 460	2, 490	1, 010
64–3	Weakly foliated biotite gneissic granite.	2, 180	2, 380	2, 580	2, 430
64–4	Moderately foliated biotite gneissic granite.	1, 520	1, 965	2, 475	1, 500
64–7	Weakly foliated biotite gneissic granite.	1, 730	2, 110	2, 510	1, 870
14(B)2 [1]	——do——	1, 675	2, 100	2, 550	1, 560

Constants: U^{238}:$\lambda=1.54\times10^{-10}yr^{-1}$
U^{235}:$\lambda=9.72\times10^{-10}yr^{-1}$
Th^{232}:$\lambda=4.88\times10^{-11}yr^{-1}$
$U^{238}/U^{235}=137.7$

[1] Sample from Zartman and others (1964).

TABLE 4.—Sr^{87}/Sr^{86} *and* Rb^{87}/Sr^{86} *atom ratios and rubidium and strontium concentrations for some total-rock samples from the Little Elk Gneissoid Granite of Taylor (1935)*

Sample	Sr^{87}/Sr^{86}	Rb^{87}/Sr^{86}	Rb (ppm)	Sr (ppm)
64–1A	0.8576	[1] 4.93	[1] 134	[1] 79.8
64–1B	.9383	8.13	154	54.9
64–2	.8446	4.13	169	119
64–3	.7579	[1] 1.46	[1] 114	[1] 228
64–4	.7790	[1] 2.33	[1] 118	[1] 148
64–5	.7584	[1] 1.28	[1] 54.2	[1] 123
64–6	.7697	[1] 1.92	[1] 131	[1] 199
64–7	.7614	1.28	103	233
64–8	.7361	.94	21.0	64.5
14(A) [2]	.885	6.06	79.7	38.1
14(B)1 [2]	.764	1.61	129	232
14(B)2 [2]	.788	2.34	126	156

Constant: Rb^{87}: $\lambda_\beta=1.39\times10^{-11}$ yr^{-1}

[1] Concentrations determined by X-ray fluorescence and the resultant Rb^{87}/Sr^{86} ratio are believed correct to ±5 percent of reported value. Remaining concentrations are by isotope dilution and are believed correct to within 1 percent of the reported value.
[2] Sample from Zartman and others (1964).

mined by X-ray fluorescence. Independent strontium isotopic compositions were determined on all samples with a precision of ±0.2 percent. All strontium data have been normalized to an Sr^{86}/Sr^{88} ratio of 0.1194.

When, as in these determinations, the Pb^{206}/U^{238} and Pb^{207}/U^{235} ages do not agree within about 5 percent, the sample is considered to be discordant. This lack of agreement is too large to be ascribed solely to analytical errors and uncertainties in the decay constants, and, therefore, must be due to a loss or gain of lead and (or) uranium from the zircon subsequent to its crystallization. Several different models for the interpretation of discordant U–Pb ages have been proposed, and two of these, the episodic-loss (Wetherill, 1956) and the continuous-diffusion (Tilton, 1960) models, will be discussed. On a Pb^{207}/U^{235} – Pb^{206}/U^{238} diagram (fig. 2), the curve drawn through the points where the ages by both decay schemes are equal is known as concordia. The episodic-loss model may be solved graphically by drawing a chord through the points defined by the measured isotopic ratios of two or more cogenetic zircons. The chord intersects concordia in two places. The lower intersection, accepting several qualifying assumptions, represents the time of lead loss or of uranium gain. The upper intersection gives the original age of the mineral. On the other hand, the continuous-diffusion model assumes that lead has been diffusing out of the zircon crystal continuously over the lifetime of the mineral at a rate governed by a diffusion parameter and the concentration gradient. By calculating the present-day Pb^{206}/U^{238} and Pb^{207}/U^{235} ratios as a function of the diffusion parameter, a curve is generated which intersects concordia at the origin and at the original age of the mineral. When, as in the present study, several widely spaced points can be used to define a line, the accuracy in locating intercepts is substantially increased and one can generally determine which of the two models better explains the data.

Figure 2 shows that all of the zircons fall very near to a chord (line A) with lower and upper intercepts of 60 and 2,560 m.y., respectively. A typical continuous-diffusion trajectory (line B) assuming a fixed diffusion constant, D_o, for a primary age of 2,800 m.y. is also shown, but it or any similar trajectory would represent a very poor fit to the data. Since it does not appear possible that these data can be explained by the continuous-diffusion model, they are interpreted as indicating an original age of 2,560 m.y. for a granite that was subsequently disturbed in Tertiary (Laramide?) time. The sharply terminated, euhedral habit and the slender, prismatic shape of the zircons from the Little Elk Granite argue against the incorporation of a detrital component into the granite, and their uniform pale-yellow color and lack of overgrowths suggest that a single population is involved. In short, this study confirms the age assignment of Zartman and others (1964) and verifies the age equivalence of this granite with rocks of the Superior province of Canada and north-central United States and of western Wyoming and Montana.

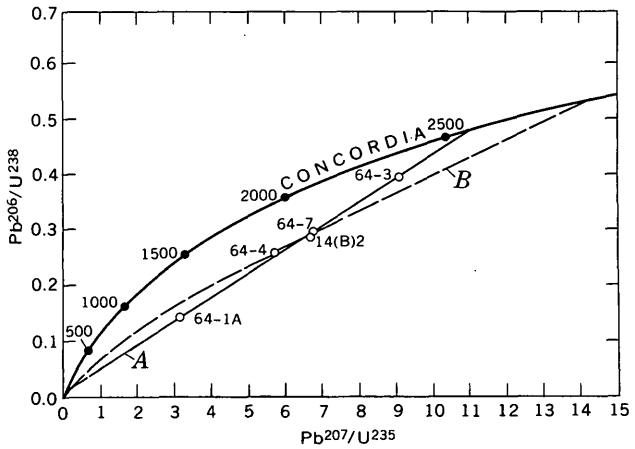

FIGURE 2.—Daughter-parent (concordia) diagram for zircon samples. The chord (line *A*) defines the loci of samples 2,560 m.y. old that lost varying proportions of lead episodically about 60 m.y. ago. A continuous diffusion trajectory (line *B*) assuming a fixed diffusion constant, *Do*, for primary age of 2,800 m.y. is shown for comparison. Labelled ages on concordia diagram are given in million of years.

The total-rock rubidium-strontium data are more difficult to interpret, owing to the disturbed nature of the gneissic granite. Figure 3 shows a Rb^{87}/Sr^{86}–Sr^{87}/Sr^{86} isochron diagram on which all of the samples are plotted. It is obvious that if the Little Elk Granite began with a homogeneous strontium isotopic composition 2.56 b.y. ago, it has been modified considerably by subsequent chemical alteration. Certainly no meaningful age can be calculated from any individual sample. A poorly defined least-squares isochron can be fitted to the data yielding an age of 1,840±70 m.y. and an initial Sr^{87}/Sr^{86} ratio of 0.720±0.004 (90-percent significance level), but no clear-cut meaning can be assigned to such an age. If one accepts the zircon isotopic age of 2,560 m.y. for the Little Elk Granite, perhaps these total-rock Rb-Sr data serve best to show that open-system conditions within the pluton have operated over a scale larger than the size of the samples, or about 1 cubic foot. Lanphere and others (1964) found a similar situation in a metamorphosed gneiss dome in the Panamint Range, Calif., and they suggested that still larger samples were necessary to discover the distances involved in element redistribution.

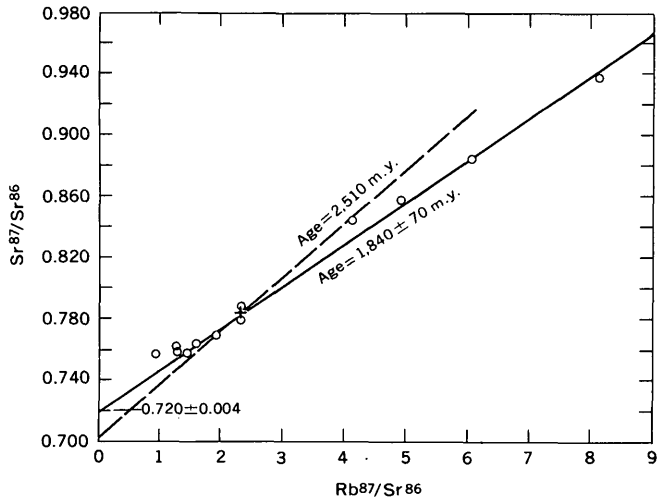

FIGURE 3.—Rb^{87}/Sr^{86}–Sr^{87}/Sr^{86} diagram for total-rock samples. Solid lines show the least-squares isochron fit to the 12 samples. Dashed line represents a 2,510-m.y. isochron calculated to pass through the average total-rock concentration and strontium isotopic composition, assuming an initial Sr^{87}/Sr^{86} ratio of 0.702. (o) individual total-rock samples, (+) average of the 12 total-rock samples.

An interesting question is whether or not the Little Elk Granite body as a whole was effectively a closed system following its emplacement. If we assume that the 12 analyzed total-rock samples are an adequate random sampling of the granite, we may calculate an average total-rock rubidium and strontium concentration and strontium isotopic composition. A hypothetical composite comprised of equal weights of each of the samples would have the following values for these parameters: Rb = 111 ppm, Sr = 140 ppm, Sr^{87}/Sr^{86} = 0.7842. On the assumption that the granite at the time of crystallization had a uniform Sr^{87}/Sr^{86} ratio of 0.702, similar to that commonly found for granites of early Precambrian age in Minnesota and Ontario, we calculate a Rb-Sr age of 2,510 m.y. for the composite sample. This age is in good agreement with the zircon isotopic age and suggests that even though rubidium and (or) strontium were mobile after the time of intrusion, there is no evidence for these elements to have migrated from or into the granite body as a whole.

DISCUSSION OF RESULTS

Although not conclusive, field investigation suggests that the Little Elk Granite unconformably underlies the adjacent metasedimentary rocks of the Nemo and Estes Systems of Runner (1934). The zircon isotopic age of 2,560 m.y. as interpreted by the episodic-loss model makes this granite the oldest rock thus far identified in the Black Hills region. Following the deposition of the Nemo and Estes Systems upon the exposed granite, the entire area was subjected to regional biotite-grade metamorphism and cataclastic deformation. A prominent period of intrusion and metamorphism approximately 1.7 billion years ago is well documented in the southern Black Hills (Wetherill and others, 1956; Eckelmann and Kulp, 1957; Giletti and Gast, 1961; Goldich and others, 1966), and it is possible that this tectonic episode has also been effective here. The close temporal agreement between this event and the total-rock Rb-Sr age of 1,840 m.y. obtained for the granite by the least-squares isochron method may be significant if rather extensive, although imperfect, isotopic homogenization took place throughout the intrusive body at this time.

As pointed out by Zartman and others (1964), Rb-Sr mineral ages on a sample of the Little Elk Granite, which are as young as 1,150 m.y., demonstrate that the mineral phases must have become open systems again at some time later than 1.7 b.y. ago. It is possible that while the area was regionally metamorphosed approximately 1.7 b.y. ago, shearing occurred much later in Precambrian time and was responsible for producing these younger mineral ages. Similar cataclastic shear zones yielding mineral ages of 1,000 to 1,200 m.y. have been recognized in the subsurface of Nebraska (Goldich and others, 1966) and in the central Colorado Rocky Mountains (Pearson and others, 1966; Carl Hedge, oral commun., 1967).

It is somewhat surprising that the zircon isotopic data show no evidence for an episodic loss of lead in the Precambrian, but rather they point entirely to Laramide time for the cause of their disturbance. While broad-scale uplift, minor normal faulting, and the local emplacement of rhyolitic and intermediate composition intrusions occurred during Laramide time (Darton and Paige, 1925; Noble and Harder, 1948; Noble and others, 1949), the Little Elk Granite bears a much stronger Precambrian metamorphic imprint than anything produced in Tertiary time. A possible explanation might be related to the metamictization process within the zircon which occurs because of the cumulative effect of radiation damage. A metamict zircon may be far more susceptible to low-temperature hydrothermal or meteoric-water alteration than to regional metamorphism to remove its radiogenic lead. Medium- or high-grade metamorphism would anneal the zircon lattice, and cause it to become quite impervious to lead diffusion.

REFERENCES

Darton, N. H., and Paige, Sidney, 1925, Central Black Hills, S. Dak.: U.S. Geol. Survey Atlas Folio 219, 34 p.

Eckelmann, W. R., and Kulp, J. L. 1957, North American localities, pt. 2 *of* Uranium-lead method of age determination: Geol. Soc. America Bull., v. 68, no. 9, p. 1117–1140.

Giletti, B. J., and Gast, P. W., 1961, Absolute age of Pre-Cambrian rocks in Wyoming and Montana, *in* Geochronology of rock systems: New York Acad. Sci. Annals, v. 91, art. 2, p. 454–458.

Goldich, S. S., Lidiak, E. G., Hedge, C. E., and Walthall, F. G., 1966, Northern area, pt. 2 *of* Geochronology of the midcontinent region, United States: Jour. Geophys. Research, v. 71, p. 5389–5408.

Lanphere, M. A., Wasserburg, G. J., Albee, A. L. and Tilton, G. R., 1964, Redistribution of strontium and rubidium isotopes during metamorphism, World Beater complex, Panamint Range, California, *in* Isotopic and cosmic chemistry, Urey volume: Amsterdam, North-Holland Publishing Co., p. 269–320.

Noble, J. A., and Harder, J. O., 1948, Stratigraphy and metamorphism in a part of the northern Black Hills and the Homestake mine, Lead, South Dakota: Geol. Soc. America Bull., v. 59, no. 9, p. 941–976.

Noble, J. A., Harder, J. O., and Slaughter, A. L., 1949, Structure of a part of the northern Black Hills and the Homestake mine, Lead, South Dakota: Geol. Soc. America Bull., v. 60, no. 2, p. 321–352.

Pearson, R. C., Hedge, C. E., Thomas, H. H., and Stern, T. W., 1966, Geochronology of the St. Kevin Granite and neighboring Precambrian rocks, northern Sawatch Range, Colorado: Geol. Soc. America Bull., v. 77, no. 10, p. 1109–1120.

Runner, J. J., 1934, Pre-Cambrian geology of the Nemo district, Black Hills, South Dakoto: Am. Jour. Sci., ser. 5, v. 28, no. 167, p. 353–372.

Taylor, G. L., 1935, Pre-Cambrian granites of the Black Hills: Am. Jour. Sci., ser. 5, v. 29, no. 171, p. 278–291.

Tilton, G. R., 1960, Volume diffusion as a mechanism for discordant lead ages: Jour. Geophys. Research, v. 65, no. 9, p. 2933–2945.

Wetherill, G. W., 1956, Discordant uranium-lead ages, I: Trans. Am. Geophys. Union, v. 37, p. 320–326.

Wetherill, G. W., Tilton, G. R., Davis, G. L., and Aldrich, L. T., 1956, New determinations of the age of the Bob Ingersoll pegmatite, Keystone, South Dakota: Geochim. et Cosmochim. Acta, v. 9, nos. 5–6, p. 292–297.

Zartman, R. E., Norton, J. J., and Stern, T. W., 1964, Ancient granite gneiss in the Black Hills, South Dakota: Science, v. 145, no. 3631, p. 479–481.

ESTIMATES OF THE DEVONIAN GEOMAGNETIC FIELD INTENSITY IN SCOTLAND

By PETER J. SMITH, Menlo Park, Calif.

Abstract.—Two hundred and eighty samples from 73 Scottish lower Devonian and Carboniferous basalt lava flows have been investigated to determine the intensity of the ancient geomagnetic field. All but three samples (from two lower Devonian flows) were rejected as unsuitable because of instability of natural remanent magnetization (NRM), alteration in the magnetic minerals during the heating necessary to induce an artificial thermoremanent magnetization (TRM), or remagnetization (probably chemical) since the flows were formed. The samples from the two remaining flows indicated ancient geomagnetic dipole moments of 0.75 and 0.34×10^{25} gauss cm^3, which are considerably smaller than the present dipole moment (8.0×10^{25} gauss cm^3).

Seventy three basalt lava flows have been sampled in the Ochil Hills (lower Devonian) and in the Campsie Fells (Carboniferous), northeast and southwest, respectively, of Stirling, Scotland (fig. 1), for paleomagnetic studies of both direction and field intensity. The geology of these areas has been described by MacGregor and MacGregor (1948). A complete investigation of paleomagnetic directions is at present in progress. This paper presents the results of attempts to determine the intensity of the geomagnetic field during the Carboniferous and part of the Devonian Periods.

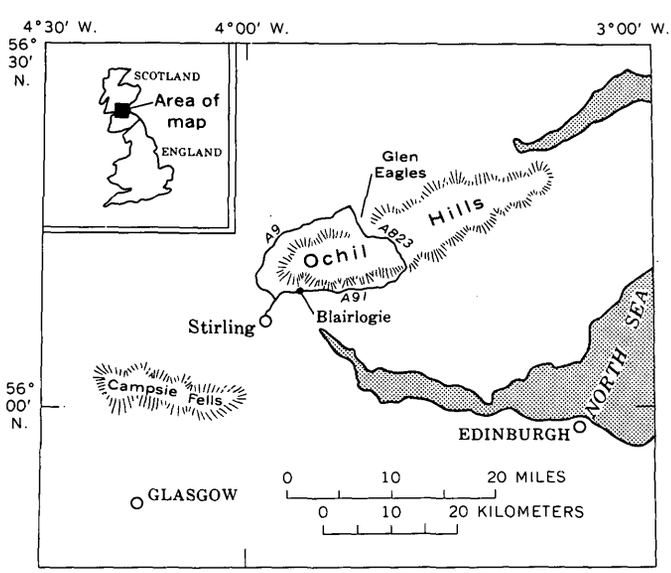

FIGURE 1.—Map of Stirling, Scotland, and vicinity.

The intensity of the ancient geomagnetic field (F) may, in principle, be obtained from any given sample, using the formula $F=H(J_n/J_T)_h$, where J_n is the natural moment remaining after demagnetization to any given alternating-current field h, J_T is that part of an artificially induced thermoremanent magnetization (TRM) remaining after demagnetization to the same field, and H is the magnetic field in which the TRM was produced. Use of this formula assumes that (1) $J_n \propto F$ and $J_T \propto H$, (2) no changes in the magnetic minerals take place during heating, and (3) J_n and J_T are due to the same process. No attempt has been made to check assumption 1, but it is almost certainly valid for the small cooling fields used here (0.50 oersted) (Nagata, 1943). Various selection procedures and tests must be carried out in order to ensure that conditions 2 and 3 are obeyed in any given case.

PROCEDURES AND TESTS

Wherever possible, four independently oriented samples were cored from each of the 73 lava flows which were obtained from nine separate, nonoverlapping stratigraphic sections. The opaque iron-titanium oxides in a polished section from each sample were examined microscopically in reflected light at a magnification of × 1,200, and samples in which grains of the highest oxidation classes 3–5 predominated were selected as being potentially suitable for field-intensity determination. The petrographic classification scheme used was that described by Wilson and Watkins (1967) in which iron-titanium oxides range from class 1, the lowest state of oxidation found in basalts (optically homogeneous titanomagnetites), through progressively higher

U.S. GEOL. SURVEY PROF. PAPER 575-D, PAGES D164-D168

degrees of exsolution and oxidation (classes 2–4) to class 5 (predominately hematite and pseudobrookite). Samples containing highly oxidized magnetic grains were selected for field-intensity determination in an attempt to avoid, as far as possible, the effects of additional oxidation during heating which was carried out in air (Smith, 1967a). Out of a total of about 280 samples, 45 (representing 23 flows) were chosen in this way.

In order to determine the degree of alteration which takes place in the magnetic minerals during heating, the saturation magnetization ($H > 5{,}000$ oersteds) of a small specimen from each of the 45 samples selected was measured in air as a function of temperature. In each case the total time for heating and cooling was about 3 hours. Twenty-five samples were rejected as unsuitable for field-intensity determination because the room-temperature saturation magnetizations had changed by more than 15 percent during the heating process, and two other samples were rejected because their Curie points had changed by 20°C and 40°C, respectively. The remaining 18 samples (representing 10 flows) each possessed saturation-magnetization heating and cooling curves similar in shape. Three examples are shown in figure 2.

The basic field-intensity determination was made on each of the remaining samples, using the method devised by Van Zijl (1961) and later refined by Smith (1967a), in which the natural remanent magnetization (NRM) is compared with an artificial thermoremanent magnetization (TRM) after demagnetization in various a-c fields. In order to get an idea of the stability of the samples with respect to a-c demagnetizing fields, a pilot sample (CA1–4) was demagnetized in 100-oersted steps up to 2,700 oersteds. By the end of this process the natural moment had decreased by only 33 percent — a remarkable degree of stability which subsequently proved to be typical, although this particular sample was later rejected for another reason. However, at fields greater than about 700 oersteds the NRM of this and other samples began to deviate from a smooth curve, presumably due to noise introduced by the demagnetization apparatus; hence, subsequent samples were generally demagnetized in 100-oersted steps to 700 oersteds only. All samples reached uniform directions of magnetization by 100 oersteds, except for two whose directions failed to become con-

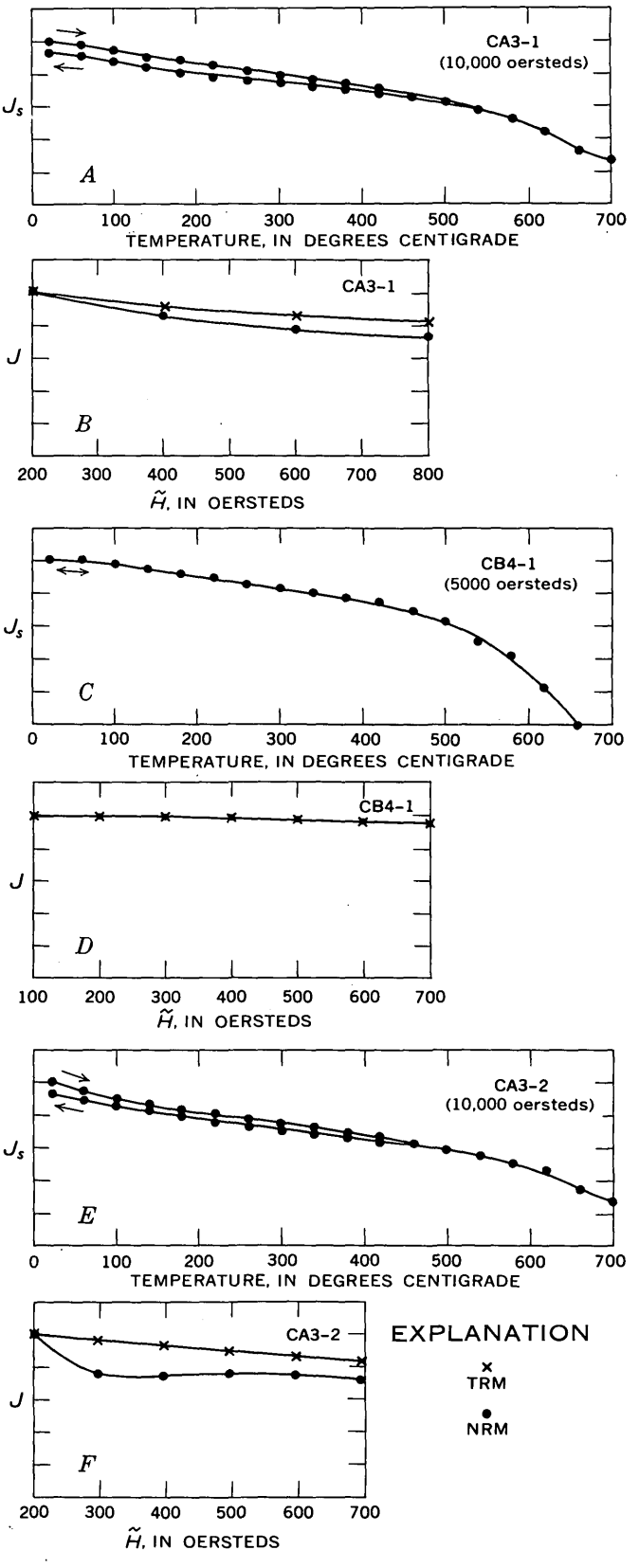

FIGURE 2.—Examples of saturation magnetization, J_s, plotted against temperature, in degrees Centigrade, and normalized NRM–TRM curves, J, plotted against a-c demagnetizing field, $\tilde{H}$, in oersteds. J_s and J in arbitrary units. *A*, *B*, and *C*, *D* represent samples giving acceptable field-intensity values; *E* and *F* represent rejected sample.

stant even by 700 oersteds. These two were rejected as unstable. Each of the remaining 16 samples was then heated in air to a temperature above its Curie point and cooled in a controlled field of 0.50 ± 0.01 oersted, after which it was again demagnetized at the same peak fields as before.

For each sample, NRM and TRM demagnetization curves were compared after normalization at the peak demagnetization field above that at which the direction became uniform; that is, above the effects of secondary components. In five cases in which the curves were dissimilar in shape, the samples were rejected, the implication being that such dissimilarities represented changes in the rock during heating. Examples of NRM-TRM curves for both acceptable and unacceptable samples are shown in figure 2. In the end only 11 samples (from 7 flows) were considered to be reliable; that is, the samples met all the criteria previously listed (Smith, 1967a). For each of these 11 samples, the ancient field intensity was calculated at each a-c field above the effects of secondary components, using the basic formula.

All pertinent magnetic data for the 16 samples which reached uniform directions are given in table 1. These samples were from only two sections, designated CA and CB (see table 1 for locations), both of which belonged to the lower Devonian. (All Carboniferous samples had been rejected.)

In figure 3, directions of magnetization are compared with previously published mean directions of magnetization for British lower Devonian rocks. Whereas directions for flows CA2, CA3, CA9, and CA10 agree well with previous values, the directions from other flows deviate considerably for two possible reasons.

First, it is possible that flows CA1, CB3, CB4, CB5, and CB6 were magnetized during reversals in field polarity, although this is unlikely because:

1. The proportion of deviating flows (56 percent) is much higher than the proportion of transition-zone flows normally found on the earth. In Iceland, for example, the proportion of transition flows is about 5 percent (R. L. Wilson, unpub. data).

2. Within the two single lava flows CB3 and CB6, samples do not give consistent directions, which they should even if magnetized in a transition field.

3. Field intensities obtained from the deviating samples are all higher (by factors of as much as about 18) than those obtained from flows CA2 and CA3, which have characteristic lower Devonian directions,

TABLE 1.—*Magnetic data for 16 samples reaching uniform directions of magnetization*

Section	Flow	Sample	D (degrees east of true north)	I (degrees)	J_s (change, in percent)	T (° C)	F (oersteds)	σ (percent)	n	VDM × 10^{-25} (gauss cm^3)
CA	1	1	26.0	−54.0	0.0	680	0.17	0.0	6	
	1	4	25.0	−52.0	−9.1	680				
	2	1	207.0	−2.0	−13.7	680	.029	3.4	4	0.75
	3	1	201.0	−6.0	−6.4	660	.014	7.1	4	
	3	2	199.0	.0	−7.8	670				0.34±0.03*
	3	3	201.5	+3.0	−10.4	670	.012	8.3	3	
	9	4	216.0	+21.5	−12.0	630				
	10	2	34.0	−20.0	−7.5	580				
CB	3	1	25.0	+66.0	.0	560 660	.073	8.2	7	
	3	4	17.0	+29.0	−3.9	580 670	.11	5.5	7	
	4	1	45.5	+53.5	.0	660	.22	.0	7	
	4	3	48.0	+52.5	−8.9	~660	.19	.0	7	
	4	4	47.5	+53.5	−3.8	660	.19	.0	7	
	5	4	186.0	−63.0	−7.4	560 660	.074	8.1	6	
	6	3	335.0	+73.0	+13.5	~650	.19	4.7	7	
	6	4	260.0	+34.0	−8.0	660				

D = Declination after demagnetization to 200-oersted peak field. } Corrected for tilt of flows.
I = Inclination after demagnetization to 200-oersted peak field. }
J_s = Saturation magnetization at room temperature.
T = Curie point.
F = Mean ancient field intensity for n values.
σ = Standard deviation in F for n demagnetizing fields.
VDM = Virtual dipole moment calculated, using measured I.
* = Standard deviation for 2 samples.
Section locations:
CA, about ¾ mile ENE. of Blairlogie on Road A91 out of Stirling, Scotland (lat 56.2°N., long 3.9°W.).
CB, Glen Eagles, Scotland, on Road A823 2 miles SSE. of junction with Road A9 (lat 56.2°N., long 3.7°W.).

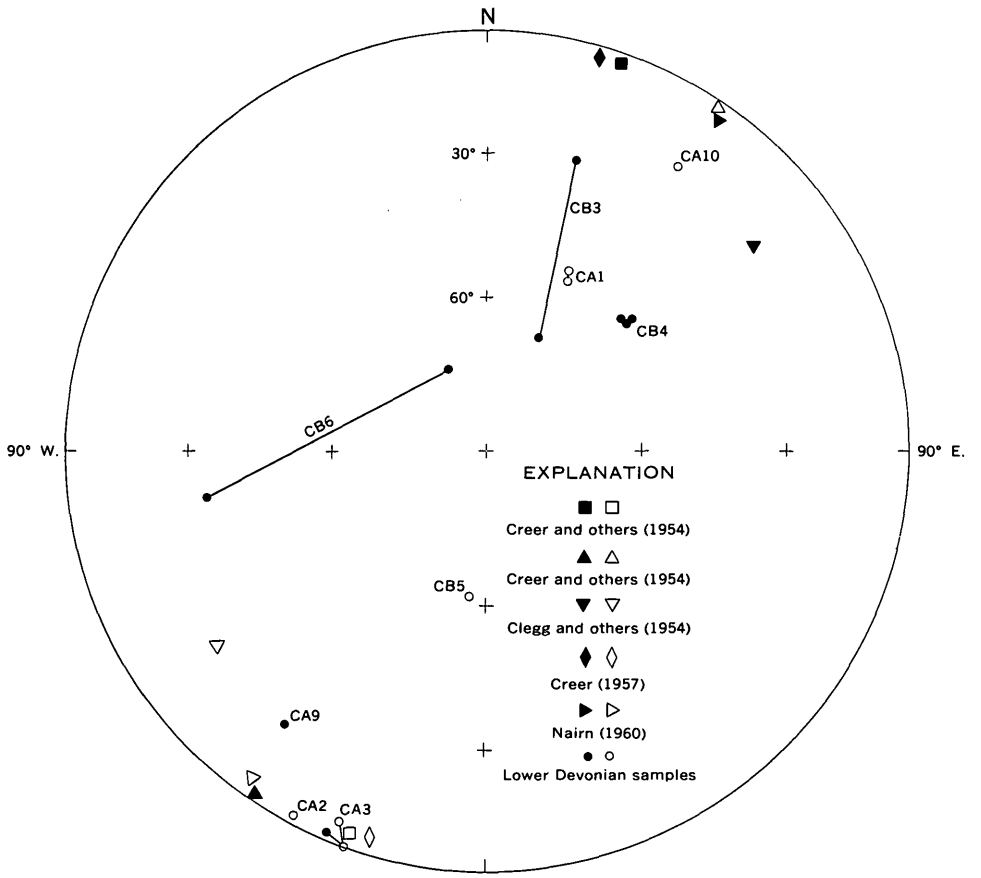

FIGURE 3.—Directions of magnetization of lower Devonian samples compared with mean directions of magnetization for British rocks of similar age. Equal area projection. Solid symbols, dips down; open symbols, dips up. Tie lines join samples from same flow.

whereas during a field transition the field intensity decreases (Van Zijl, 1961; Momose, 1963).

The second and more likely explanation is that the deviating samples have become remagnetized since the early Devonian, probably chemically. This would explain why (1) the inclinations of the deviating samples are much larger than typical lower Devonian inclinations and (2) in flows CB3 and CB6, samples from the same flow disagree in direction. Samples from CB3 also disagree in field intensity. If chemical remagnetization has occurred then the assumption that J_n and J_T are due to the same process is not valid, and the resulting field-intensity values cannot be accepted. It is for this reason that sample CB4-1, for example, which gives excellently reproducible curves (fig. 2*C* and 2*D*), must be rejected.

There is one other possible explanation for the large deviations in direction, namely that they represent the effects of large nondipole field components. In this case the directions would be valid for the lower Devonian, despite the scatter. But again this cannot be considered likely because of the high proportion of flows of this type and because of the within-flow deviations for CB3 and CB6.

From an initial collection of 280 samples, only 3 (representing flows CA2 and CA3) give ancient field intensities which may be considered reliable, although even in these the possibility of remagnetization cannot be ruled out definitely. For flows CA2 and CA3, virtual dipole moments (VDM's) have been calculated using the measured mean field intensities and inclinations (table 1). Although the mean lower Devonian dipole moment may not be deduced from measurements on only two flows, the results imply a much smaller moment than that observed at present (8.0×10^{25} gauss cm^3). The VDMs obtained here (0.75×10^{25} gauss cm^3 and 0.34×10^{25} gauss cm^3) may be compared with four VDMs in the range $1.71 - 3.24 \times 10^{25}$ gauss cm^3 obtained by Briden (1966) from Australian rock samples of similar age. Although the new VDM's are smaller, they are not inconsistent with those from Australia if geomagnetic dipole moment fluctuations are real (Smith, 1967b).

ACKNOWLEDGMENTS

I would like to thank Dr. J. M. Ade-Hall, of Liverpool University, for carrying out most of the petrographic work. I am also grateful to the North Atlantic Treaty Organization for a postdoctoral fellowship.

REFERENCES

Briden, J. C., 1966, Estimates of direction and intensity of the paleomagnetic field from the Mugga Mugga Porphyry, Australia: Geophys. Jour., v. 11, p. 267–278.

Clegg, J. A., Almond, Mary, and Stubbs, P. H. S., 1954, The remanent magnetism of some sedimentary rocks in Britain: Philos. Mag., v. 45, p. 583–598.

Creer, K. M., 1957, The natural remanent magnetization of certain stable rocks from Great Britain: Royal Soc. [London] Philos. Trans. A., v. 250, p. 111–129.

Creer, K. M., Irving, Edward, and Runcorn, S. K., 1954, The direction of the geomagnetic field in remote epochs in Great Britain: Jour. Geomagnetism Geoelectricity, v. 6, p. 163–168.

MacGregor, M., and MacGregor, A. G., 1948, British regional geology. The Midland Valley of Scotland, 2d ed.: Edinburgh, Her Majesty's Stationery Office, 95 p.

Momose, Kanchi, 1963, Studies on the variations of the earth's magnetic field during Pliocene time: Earthquake Research Inst. Bull., v. 41, p. 487–534.

Nagata, Takesi, 1943, The natural remanent magnetism of volcanic rocks and its relation to geomagnetic phenomena: Earthquake Research Inst. Bull., v. 21, p. 1–191.

Nairn, A. E. M., 1960, Paleomagnetic results from Europe: Jour. Geology, v. 68, p. 285–306.

Smith, P. J., 1967a, On the suitability of igneous rocks for ancient geomagnetic field intensity determination: Earth and Planetary Sci. Letters, v. 2, p. 99–105.

Smith, P. J., 1967b, The intensity of the ancient geomagnetic field: A review and analysis: Geophys. Jour., v. 12, p. 321–342.

Van Zijl, J. S. V., 1961, A paleomagnetic investigation on Karroo lavas [South Africa]: Univ. Witwatersrand Ph. D. thesis, 98 p.; *also in* Van Zilj, J. S. V., Graham, K. W. T., and Hales, A. L., 1962, The paleomagnetism of the Stormberg lavas, [pt.] 2, The behaviour of the magnetic field during a reversal: Geophys. Jour., v. 7, p. 169–182.

Wilson, R. L., and Watkins, N. D., 1967, Correlation of petrology and natural magnetic polarity in the Columbia Plateau basalts: Geophys. Jour., v. 12, p. 405–426.

INFRARED RADIATION FROM ALAE LAVA LAKE, HAWAII

By ROBERT W. DECKER [1] and DALLAS L. PECK,
Hanover, N.H., Washington, D.C.

Abstract.—Radiation and contact temperatures of the surface of Alae lava lake, Hawaii, ranged from 15°C to 85°C during the day and night in November and December 1964, shortly after the lake solidified. Hottest temperatures were over fuming joint cracks, and coolest temperatures were from nighttime measurements taken over the cooled thin margins of the lava lake. Surface-radiation heat loss from the central part of the lava lake is greatest at night, averaging 950×10^{-6} cal cm^{-2} sec^{-1}, compared to the total calculated heat flow of approximately $4{,}300 \times 10^{-6}$ cal cm^{-2} sec^{-1}. During the day, solar radiation and other heat-transfer mechanisms mask any net surface-radiation heat loss from the cooling lava lake.

The August 1963 eruption of Kilauea Volcano formed a small ponded flow of lava as much as 48 feet thick in the bottom of Alae pit crater, Hawaii (fig. 1). The lava is tholeiitic basalt containing about 3 percent by volume modal olivine and 50.44 percent by weight SiO_2 (Peck and others, 1966). Temperatures in the cooling lava lake were studied by means of repeated thermocouple measurements in drill holes in the crust of the lake, and the eruption and the cooling history of the lake through February 1964 were reported by Peck and others (1964). The lake cooled at a rate similar to that calculated by Jaeger (1961, p. 730, fig. 11) for the conductive cooling of an extrusive sheet. The last interstitial melt in the lake solidified in late September 1964, and the continued cooling of the lake has been followed by temperature measurements in two drill holes that penetrate to the base of the lake.

RADIATION TEMPERATURE MEASUREMENTS

To better understand the mechanism of surface heat loss by radiation, a series of observations of contact and infrared radiation temperatures of the surface of the lava lake were made during November and December 1964 shortly after the lava body had completely solidified but while the maximum temperatures, at depths of 30–31 feet, were still about 900°C. Surface contact and air temperatures were measured with an Alnor 2300B thermocouple pyrometer; wind speeds with an Alnor hot-wire anemometer; and infrared radiation temperatures (>3 microns wavelength) with a modified Stoll-Hardy HL4 radiometer, which measures radiative energy loss or gain between the measured surface and the sensing unit. The measured radiation temperature is the relative black-body temperature of the measured surface compared to the black-body temperature of the sensing unit. These instruments and instructions on their use were kindly provided by Jack N. Rinker, of the U.S. Army Cold Regions Research and Engineering Laboratories, Hanover, N.H.

Two control stations, C1 and C2, were selected at the edges of the lava lake where the thin layer of lava had completely cooled (fig. 2). Station C1, at the southeast edge of the lake, is shaded the entire day during the winter months by the steep south cliff of the pit crater. Station C2, on the northeast edge, receives direct sunlight after 8^h00^m on clear days. The third control station, H1, is on the northeast end of the measured strip, which is located 20 feet south of, and is parallel to, the line between survey stations 4 and 36 (not shown) on the central part of the lava lake. For interpretive purposes, C1 and C2 can be considered "cold base stations" and H1 the "hot base station."

At each base station, measurements of contact surface temperature, air temperature and wind velocities at 3 millimeters and 1 meter above the surface, and infrared radiation temperatures of the surface and sky were made several times on November 17 and December 18, 1964. The Stoll-Hardy HL4 radiometer

[1] Dartmouth College, Hanover, N.H.

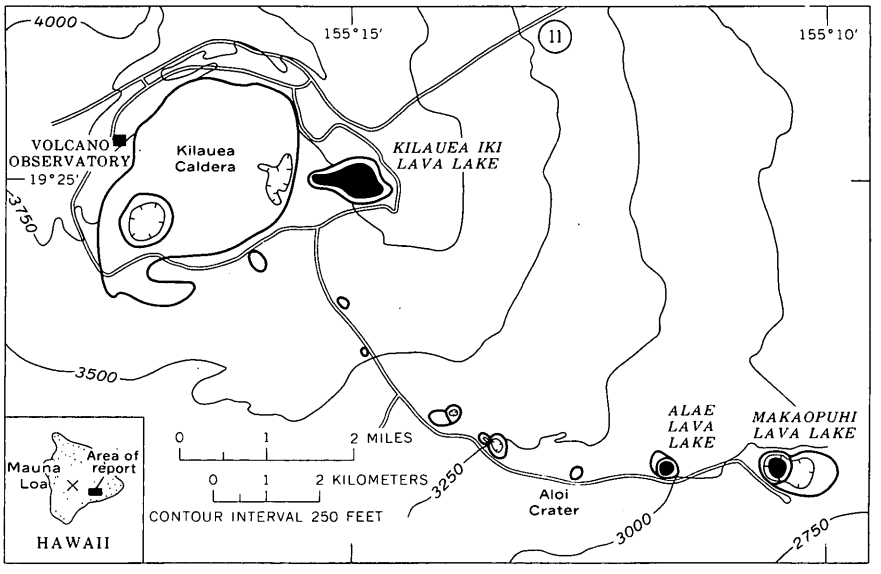

FIGURE 1.—Index map of the summit and the upper east rift zone of Kilauea Volcano, Hawaii. Boundaries of craters and Kilauea Caldera are shown by heavier lines. Recent lava lakes are solid black.

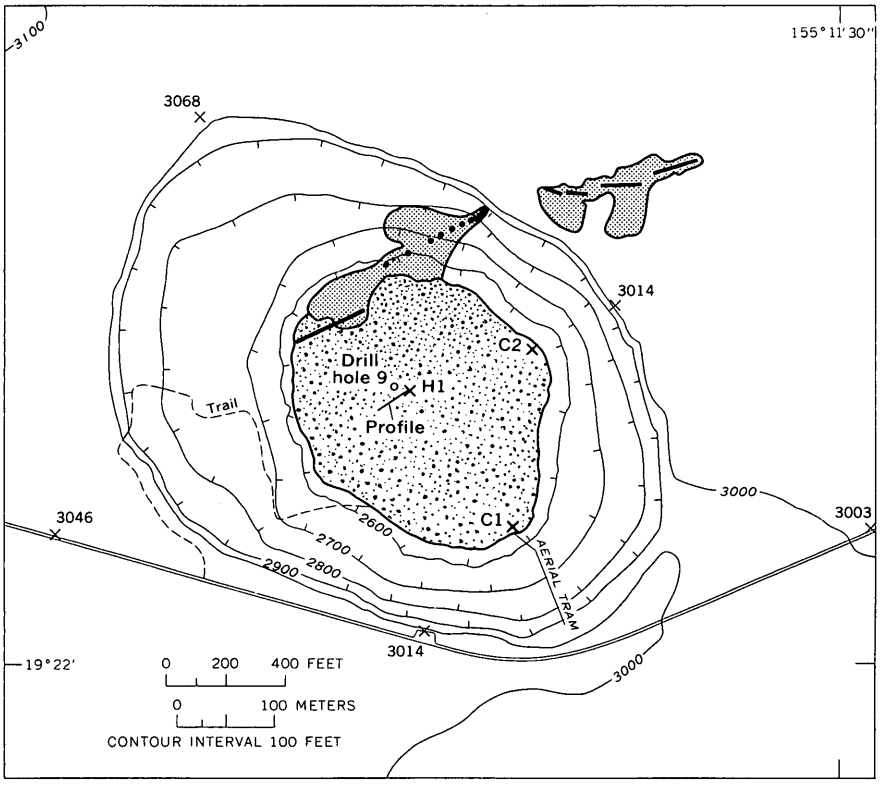

FIGURE 2.—Map of Alae Crater, showing distribution of volcanic rock from the August 1963 eruption and location of control stations C1, C2, and H1, the measured profile, and drill hole 9. Lava lake, random stipple; eruptive vents, heavy lines and dots; spatter, thin flows, and pumice, fine stipple. Location of crater shown in figure 1. Base modified from 1:24,000-scale map of Makaopuhi Crater quadrangle (1963), using a special U.S. Geological Survey map of the crater floor prepared by photogrammetric methods from aerial photographs taken February 1963.

TABLE 1.—*Air, infrared radiation, and surface-contact temperatures, and wind velocities of Alae lava lake, Hawaii*

Date (1964)	Time	Temperatures measured (°C)					Wind velocity above lava lake surface (ft/min)	
		Surface-contact	Air, at indicated distances above lava lake surface		Infrared radiation			
			3 mm	1 meter	Surface	Sky	3 mm	1 meter
Station C1 (cold base, shaded)								
Nov. 17	10h15m	17. 7–18. 3	18. 3	18. 3	15. 5–16. 5	----------	10	100
	11h00m	18. 5–18. 9	18. 3	18. 3	15–16	6. 5	20–40	200
	15h30m	22. 0–23. 0	22. 5	22. 0	----------	----------	10–50	200–500
Dec. 18	4h30m	16. 0	16. 0	16. 0	16	4	10–20	50–100
	6h40m	----------	----------	----------	15	4	----------	----------
Station C2 (cold base, not shaded)								
Nov. 17	11h20m	38. 0–42. 0	24. 0	23. 0	37–40	11–42	10–100	50–400
	15h15m	32. 5–24. 5	24. 0	23. 0	25	25	10–30	100–200
Dec. 18	6h20m	15. 0–15. 9	15. 6	16. 0	16	4	40–70	100–200
Station H1 (hot base)								
Nov. 17	11h40m	38. 0–41. 0	34. 0	28. 0–29. 0	36–38	10–47	10–100	50–400
	12h20m	36. 0–40. 0	33. 0	27. 0	33–35	----------	50–100	300–600
	13h20m	31. 0–34. 0	29. 0	23. 0–25. 0	28–29	22–24	0–30	30–100
	14h55m	29. 0–31. 0	27. 5	22. 0–26. 0	27	24	30–100	300–800
Dec. 18	4h55m	19. 2–21. 0	18. 5	17. 1–18. 3	20	4	50–70	200–300
	6h15m	18. 3–20. 2	18. 0	16. 0–17. 5	20	4. 5	40–70	100–200

views a conic section of 28° and was read at 1 foot above the surface, thereby giving the radiation temperature from approximately 0.2 square foot of area. The measurements are listed in table 1. Surface contact temperatures, shown in column 3 of the table, are in close agreement with the infrared surface temperatures, column 6. This indicates that the black-body approximation is valid for the lava surface in this temperature range. The air temperatures at 3 mm and 1 meter above the surface are shown in columns 4 and 5 respectively. Pronounced air-temperature gradients were found only at station H1, suggesting that convection may be an important heat transfer mechanism over the hot base station. Wind speeds at 3 mm and 1 meter above the surface (columns 8 and 9) were variable at all stations. The sky temperatures in column 7 were measured with the radiometer and represent the major surface to or from which the lava lake was losing or gaining radiative heat. For example, from 4h30m to 5h30m on December 18, the infrared radiation temperature of the sky was 4°C, that of the lake surface at C1 and C2 was 16°C, and that of the lake surface at H1 was 20°C. At that time radiative heat was being lost from the entire lake surface to the sky, the greatest loss being from the H1 area at the center of the lake. At 15h15m on November 17, the lava lake surface at C2 and the sky temperature were both 25°C, and no heat was being transferred by radiation. The 11h20m and 11h40m radiation temperature readings of the sky at C2 and H1 on November 17 include high measurements when the sun's disk was within the 28° view of the radiometer. This illustrates how the lava lake surface can gain radiative heat from the sun while simultaneously losing it to other areas of the sky.

During the early afternoon of November 17, 1964, and before dawn on December 18, 1964, radiation temperatures were measured at every foot along a 102-foot-long line extending southwest from station H1 (fig. 2). The line lies within a 100-foot-wide and 102-foot-long area that was studied in detail. Joint cracks and areas encrusted with sublimates were mapped at a scale of 1 inch equals 10 feet from October to December 1963, in May and November 1964, and in August 1965. The repeated mapping revealed the progressive formation of joint cracks in the crust of the cooling lake, both by the downward growth of preexisting cracks and by the opening of new cracks. After October 1963, most new cracks that formed were marked by encrustations of sublimates deposited from sulfur-

rich gases rising along the cracks from the interior of the lava lake. Sublimates also formed along some of the older cracks, presumably because of the downward growth of the cracks. The joint cracks along the line of infrared temperature measurements are shown in the section in figure 3, together with the temperature measurements. The resulting infrared temperature profiles are compared to the radiation temperatures from control stations C1 and C2 under similar sky conditions interpolated to the time of making the radiation measurements along the line. The straight line of the control base temperature on December 18 (night profile) can be interpolated with confidence because there was practically no change in the radiation temperatures of the control stations or the sky during the predawn measurements. The sloping line of the radiation temperature at the control bases during the daylight measurements on November 17 is less certain. Scattered clouds crossing the sun caused changes in radiation temperature of 1°C to 3°C over periods of minutes at control base C2. Both C2 and the profile area were exposed to intermittent direct sunlight but at different times during the measurements. The general trend was from continuous sunlight at the start to complete cloud cover at the finish of these daylight measurements, and the negative slope of the control base line represents this average trend.

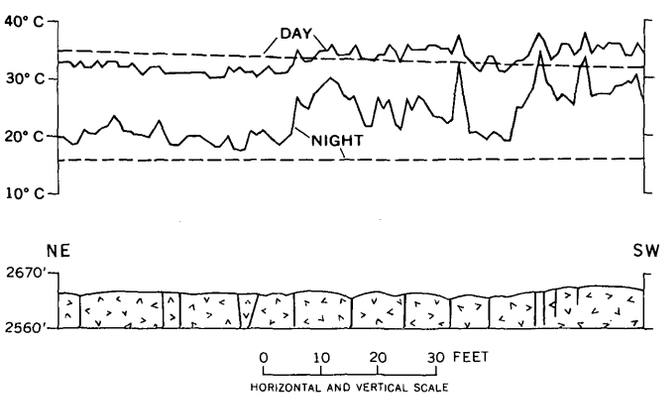

FIGURE 3.—Profile showing joint cracks and infrared radiation temperatures along a line near the center of Alae lava lake. Position of line is shown in figure 2. Solid-line profile "DAY" represents infrared radiation temperatures (>3 microns wavelength) measured during the day between 12^h30^m and 13^h15^m on November 17, 1964; this contrasts with the dashed line representing interpolated infrared radiation temperatures at a control base station at the margin of the lava lake (C2 of fig. 2). Solid-line profile "NIGHT" represents infrared radiation temperatures measured during the night between 5^h10^m and 5^h30^m on December 18, 1964; this contrasts with the dashed line representing interpolated temperatures of two control base stations at the margins of the lake (C1 and C2, fig. 2). The section shows joint cracks extrapolated downward from surface mapping.

Because weather and sky conditions are important, the following remarks on the conditions during the measurements were noted on the days and hours indicated:

Nov. 17, 1964:	
8^h00^m	Clear sky; sun on profile line and C2, open shade at C1.
11^h00^m	Open shade at C1, 5 percent clouds.
11^h20^m	Bright sun all morning at C2.
11^h40^m	Scattered clouds (30 percent) over profile line; sun in and out.
12^h33^m	Start of profile measurements; sun obscured 12^h57^m–13^h15^m with sky radiation temperature 22°C.
13^h15^m	Clouds, 90 percent.
13^h45^m–13^h50^m	Sunny; 13^h50^m–14^h40^m sun obscured.
14^h45^m	Dark clouds, 99 percent with 24°C sky radiation temperature.
15^h30^m	First few rain drops, after 15^h30^m very light rain and mist.
Dec. 18, 1964:	
3^h30^m	Heavy fog along chain of craters.
3^h45^m	Fog dissipating.
4^h20^m	Calm clear moonlight night.
4^h55^m	Moon sets, leaving sky clear and dark.
6^h20^m	Clear sky beginning to lighten, very gentle wind.
6^h40^m	Clear dawn sky.

Calibration checks on the thermocouple contact pyrometer and anemometer were good, but the radiometer check was not entirely satisfactory. The indicated ice-bath black-body temperatures from a Leslie cube were 8°C–10°C instead of 0°. Human body temperature calibrations near 35°C were consistently obtained by checking the radiation temperature inside the mouth. Because the radiometer sensing head actually measures radiation energy input or outflow rather than direct radiation temperatures, a calibration error is to be expected when the ambient temperatures are different from the calibration temperatures. The measured radiation temperatures above 20°C are probably accurate to 1° compared to a body temperature calibration of 35°C. The indicated cold sky temperatures are probably too warm by a few degrees.

Many of the high radiation temperatures along the line were measured at or near conspicuous joint cracks. The other high temperatures probably occurred over hairline cracks concealed beneath the vesicular filamented surface layer of the lava lake. The highest temperatures were measured along the southwest part of the line in an area where a swarm of short sublimate-encrusted cracks were forming. These high temperatures resulted from hot gases rising along the cracks from the interior of the lake. Some of the other high temperatures measured along the line, particularly those over gaping older cracks, may have resulted from heated air circulating in the cracks. Many of the older cracks along the line of measurements did not have high temperatures associated with

them; presumably these had not recently grown at depth at the time of the measurements.

Random radiation temperatures were measured over a large area of the center of Alae lava lake between 13^h50^m and 14^h55^m on November 17, 1964, to determine whether radiation temperatures were related to surface features, and to see if the range of observation made in the detailed profile was representative. The range of measured radiation temperatures was 25°C to 86°C. Except for very local high temperatures over cracks actively depositing sublimates, no correlation was apparent between lava lake topography and radiation temperature. Apparently the detailed profile was representative of the central area of the cooling lava lake.

TRANSMISSION OF RADIANT HEAT

Emission of radiant heat is expressed by the Stefan-Boltzman law (McAdams, 1942, p. 49)

$$W=\sigma T^4,$$

where

W is energy per unit time per unit area,
σ is the Stefan-Boltzman constant (1.354×10^{-2} cal cm^{-2} °K^{-4} sec^{-1}), and
T is temperature in degrees Kelvin.

When the emitting body is not a perfect radiator (black body), the energy emitted is reduced by an emissivity factor (e), which is the ratio of emission between the real surface and an ideal black body. In computing net heat exchange by radiation between surfaces (lava surface and sky), or the excess heat exchange of one surface compared to another, when both are radiating to a third surface (warm lava surface compared to cool lava surface, both radiating heat to the sky), it is convenient to rearrange the equation as follows:

$$W=e\sigma(T_1^4-T_0^4)$$

where

e is emissivity,
T_1 is the warm lava surface temperature, and
T_0 is the cool lava surface temperature.

This can be solved numerically to compare the heat radiation of the profile near the central part of the lava lake with the heat radiation of the cold base stations on the cooled margins of the lake. The unknown factor is the emissivity of the lava. The similarity of the measured contact temperatures to the measured infrared radiation temperatures indicates a high emissivity but does not provide a direct means of calculating emissivity. David L. Daniels (written commun., Feb. 1967) has measured the emittance spectra between 7 and 15 microns wavelength of five vesicular olivine basalt samples from the Pisgah Crater area, California. The measured emissivities ranged from 0.86 to 1.0 and had an average value of 0.95 ± 0.03. A reasonable estimate of the emissivity of the surface of Alae lava lake is 0.95 ± 0.05.

An approximate solution can be obtained for the nighttime radiation heat loss by the profile in excess of the "normal" radiation heat loss of the cold base by using the average radiation temperature (296.5°K) along the profile for T_1 and the constant cold base temperature (289°K):

$$W=(0.95)(1.354\times10^{-12})[(296.5)^4-(289)^4]$$
$$=968\times10^{-6} \text{ cal cm}^{-2} \text{ sec}^{-1}.$$

Because the power function $(T_1^4-T_0^4)$ is not linear, a better solution is obtained with a digital computer by making a numerical integration of the radiation energy flux from each station along the profile:

$$W=e\sigma/n\sum_{i=1}^{n}(T_1^4-T_0^4),$$

where

n is 103 stations of the profile,
$=957\times10^{-6}$ cal cm^{-2} sec^{-1}.

It should be noted that a 1°K temperature error in the measurements can lead to a 10-percent error in these calculations because of the T^4 power term. The combined uncertainty of the measured temperatures and the emissivity estimate indicate that the excess nighttime radiation heat loss from the central surface of the lava lake is approximately 950 $(\pm100)\times10^{-6}$ cal cm^{-2} sec^{-1}.

The percentage of internal heat loss by surface radiation can be obtained by comparing it to the total heat flux in the cooling lava of the lake. The heat flux per unit area is given by:

$$\frac{dQ}{dA}=-K\frac{dT}{dZ}$$

where

Q is heat flow in cal per sec,
Z is depth in cm,
A is area in cm^2,
K is thermal conductivity in cal cm^{-1} °C^{-1} sec^{-1}, and
T is temperature in °C.

The temperature gradient from the surface to the base of the lake was measured on December 8, 1964, in drill hole 9 which is located 21 feet west of reference station H1 at the northeast end of the radiation meas-

urement profile (fig. 2). Temperatures in the drill hole were measured at 3-foot intervals with a 50-foot, 5-junction thermocouple of Chromel-Alumel, using a portable millivolt potentiometer and a 0°C reference junction. The temperature profile is shown in figure 4. Temperatures in the upper part of the hole were slightly lower than those of an equilibrium profile, either as a result of cooling water used in drilling the hole (completed on October 20, 1964), or the 6.4 inches of heavy rain that fell from November 5 to 12.

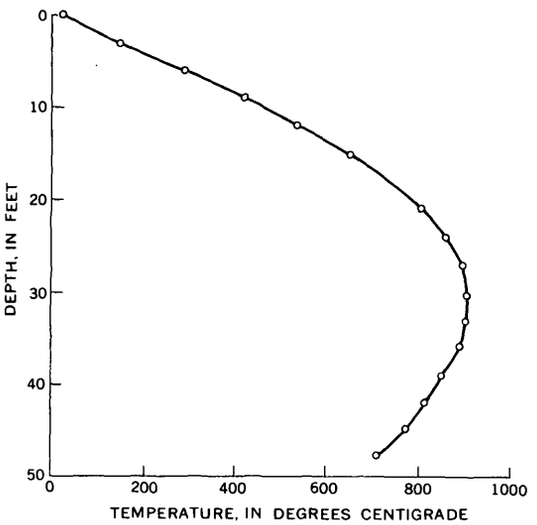

FIGURE 4.—Temperature profile on December 8, 1964, in drill hole 9 near the center of Alae lava lake (fig. 2). The base of the solidified lake is at a depth of 48 feet.

Measurements of thermal conductivity were made at room temperature at the U.S. Geological Survey laboratory at Silver Spring, Md., on 10 samples of basalt from the August 1963 lava lake in Alae Crater and from a petrographically similar prehistoric lake exposed on the walls of the crater. The values of K range from 2.03×10^{-3} to 3.40×10^{-3} cal cm^{-1} °C^{-1} sec^{-1} (Eugene C. Robertson, written commun., Jan. 21, 1966) and show an empirical linear relationship to porosity (P), where $K = 0.00349 - 0.00425\ P \pm 0.00007$. Porosity (which equals vesicularity in the lava) decreases downward in the crust of the August 1963 lava lake from a maximum of 40 percent at or near the surface to a nearly constant minimum of 11 percent below 15 feet, as determined from bulk and grain density measurements of drill core. Between 9 and 15 feet, the porosity decreases from 14 to 11 percent; the room-temperature conductivity, K, calculated from the empirical equation listed above, increases downward from 2.86×10^{-3} to 2.97×10^{-3}, cal cm^{-1} °C^{-1} sec^{-1}, and has an average value of 2.92×10^{-3} cal cm^{-1} °C^{-1} sec^{-1}.

Thermal conductivities of basalt from Alae Crater at higher temperatures were measured by Dr. Kaoru Kawada at the Earthquake Research Institute, University of Tokyo, Japan. The conductivity of two very vesicular samples (porosity 25 and 28 percent) from the surface of the lake increased at a rate of almost 0.1 percent per degree from room temperature to 1,000°C (K. Kawada, written commun., Dec. 13, 1966). The conductivity of a less vesicular sample (porosity 7 percent) increased at a lower rate; the measured conductivity increased at a rate of about 0.03 percent per degree from 32°C to 673°C, the highest temperature studied with the sample. These measurements suggest that the actual conductivity, K, at depths of 9 to 15 feet and temperatures of 420°C to 645°C ranged from 3.23×10^{-3} to 3.53×10^{-3} cal cm^{-1} °C^{-1} sec^{-1}, and averaged about 3.38×10^{-3} cal cm^{-1} °C^{-1} sec^{-1}.

Using the $\Delta T/\Delta Z$ value of 1.22°C cm^{-1} in the interval 9 to 15 feet, an average thermal conductivity of 3.38×10^{-3} cal cm^{-1} °C^{-1} sec^{-1}, and neglecting the slight departure from steady-state conditions in this interval, the heat flux in the lake is found to be:

$Q/A = -(3.38 \times 10^{-3})\ (1.22) = -4{,}310 \times 10^{-6}$ cal cm^{-2} sec^{-1}. Thus the average heat flow by conduction to the surface of the central portion of the cooling lava lake was about $4{,}300 \times 10^{-6}$ cal cm^{-2} sec^{-1}. At night about 950×10^{-6} cal cm^{-2} sec^{-1} were being lost from this surface to radiation, about 20 percent of the conductive heat flow to the surface. These figures contrast with the "normal" heat flow from the earth, which averages about 1.6×10^{-6} cal cm^{-2} sec^{-1} (Lee, 1965, p. 136).

The daytime heat radiation budget is more complex. Theory indicates that the central part of the lake would be heated during the day by insolation the same amount as the sunlit cold base station (Carslaw and Jaeger, 1959, p. 75, 8). However, the daytime profile on figure 3 shows that the spread between the cold base and the profile temperatures has greatly decreased. The temperatures on the northeast end of the profile are even slightly lower than the cold base temperature. The hottest peak temperatures on the profile show the least increase from night to day temperatures. A similar effect is noted on airborne infrared imagery of Kilauea volcano, where thermal anomalies show higher contrast to their surroundings at night (Fischer and others, 1964, p. 734). The increase in rate of heat emission at higher temperatures from the T^4 power term does not adequately explain this temperature limiting effect at 35° to 40°C. Arthur H. Lachenbruch (oral

commun., June 1966) suggests that air convection may become important at about this temperature range in Hawaii. The high air-temperature gradient over H1 in the daytime (table 1) supports this suggestion.

The net effect of the daytime heat budget is that the surface of the central part of the lava lake loses no excess heat by radiation.

Whereas at night the heat loss by radiation from the surface of the central part of the lava lake was 20 percent of the heat conducted through the body of the cooling lava, during the day the heat loss by radiation was no greater than the normal diurnal radiation budget of rock surfaces practically unheated from below. The combined effects of insolation and a limiting surface temperature of 35° to 40°C, possibly caused by air convection, masked any net heat loss by radiation from the central surface of the cooling lava lake in daytime.

Thus during November and December 1964, the net heat loss by surface radiation was about 10 percent of the total heat loss from the cooling lava lake. The remaining heat was lost by evaporation of rain, transfer by escaping gases, and conduction and convection of the contact air layer.

REFERENCES

Carslaw, H. S., and Jaeger, J. C., 1959, Conduction of heat in solids: London, Oxford Univ. Press, 510 p.

Fischer, W. A., Moxham, R. M., Polcyn, Fabian, and Landis, G. H., 1964, Infrared surveys of Hawaiian volcanoes: Science, v. 146, no. 3645, p. 733–742.

Jaeger, J. C., 1961, The cooling of irregularly shaped igneous bodies: Am. Jour. Sci., v. 259, p. 721–734.

Lee, W. H. K., ed., 1965, Terrestrial heat flow: Am. Geophys. Union Mon. 8, 276 p.

McAdams, W. H., 1942, Heat transmission: New York, McGraw-Hill, 459 p.

Peck, D. L., Moore, J. G., and Kojima, George, 1964, Temperatures in the crust and melt of Alae lava lake, Hawaii, after the August 1963 eruption of Kilauea Volcano—a preliminary report *in* Geological Survey Research 1964: U.S. Geol. Survey Prof. Paper 501–D, p. D1–D7.

Peck, D. L., Wright, T. L., and Moore, J. G., 1966, Crystallization of tholeitic basalt in Alae lava lake, Hawaii: Bull. Volcanol., v. 29, p. 629–656.

A GEOCHEMICAL ANOMALY OF BASE METALS AND SILVER IN THE SOUTHERN SANTA RITA MOUNTAINS, SANTA CRUZ COUNTY, ARIZONA

By HARALD DREWES, Denver, Colo.

Abstract.—An area of Jurassic granite northwest of Patagonia, Ariz., altered in Paleocene (late Laramide) time, contains anomalous amounts of Cu, Pb, and Zn, and also contains sporadic anomalous concentrations of Au, Ag, and Mo. Background values of the three base metals are, respectively, about 15, 25, and 25 ppm. Samples in the altered area show concentrations of 2 to more than 100 times these background values, and over a substantial part of the area they are 5–16 times background values. The ore metals were introduced or mobilized during alteration; at the same time B, Sc, Ti, V, and Zr were concentrated in the altered rocks.

Results of current geological investigations in the Santa Rita Mountains southeast of Tucson, Ariz., indicate several groups of geochemically anomalous areas. One group of anomalies occurs largely within a zone of altered plutonic rocks that trends north-northwest roughly along the crest of the range. The location of the altered areas and their relation to various plutonic rocks and to some volcanic host rocks are shown on a preliminary geologic map of the Mount Wrightson quadrangle (Drewes, 1966). Very likely a zone of altered areas continues southeastward along Flux Canyon to Washington Camp in the Patagonia Mountains.

This article briefly describes the anomalous concentration of copper, lead, zinc, and silver in one of the largest and least prospected of these areas with altered rocks, which for brevity will be referred to as altered areas The area is located southeast of the old Ivanhoe mine, about 3 miles west-northwest of Patagonia. The Ivanhoe altered area, as it will be called here, is in a relatively inaccessible region and has not been as intensively studied as some of the other altered areas of this region. As a result, small prospects, common in most of the other altered areas, are virtually absent here. Indeed, most mines and prospects in the southern part of the Santa Rita Mountains are on quartz veins (Schrader, 1915). The only altered area that has received considerable attention is in the upper reaches of Mansfield Canyon, 4 miles north-northwest of the Ivanhoe area. A geochemical reconnaissance of the other altered areas suggests that they, too, contain anomalous concentrations of base metals.

GEOLOGY

The oldest rocks of the Ivanhoe altered area (fig. 1) are Triassic volcanic and sedimentary rocks and consist of intensely indurated and commonly finely laminated reddish-gray siliceous flows and tuffs, intercalated with thin lenses of quartzite. Clastic rocks are more abundant and more quartzose in this unit than in any of the younger ones. In places these clastic rocks contain crossbedding suggestive of an aeolian origin. Near the Ivanhoe altered area the Triassic rocks form a steeply dipping structural block only a few thousand feet thick, but in most of the Santa Rita Mountains these rocks are in a more gently eastward dipping homoclinal sequence about 10,000 feet thick.

Jurassic granite of Squaw Gulch intrudes the older volcanic and sedimentary rocks north of the area shown in figure 1, but locally it is probably faulted against them. The granite is part of a pluton at least 10 miles long; it commonly is a massive coarse-grained moderate-orange-pink rock, whose composition ranges from granite in the south to quartz monzonite in the north. Modes of virtually unaltered granite near the Ivanhoe altered area are listed in table 1. The orthoclase of these rocks is mildly but pervasively kaolinized, and the biotite is mostly chloritized.

Four sedimentary and volcanic rock sequences of Cretaceous and Tertiary age are shown together on figure 1. The oldest two sequences, lying to the east of the altered area, consist of arkosic conglomerate, volcanic conglomerate, rhyolitic tuffs, and dacitic flows,

U.S. GEOL. SURVEY PROF. PAPER 575-D, PAGES D176-D182

TABLE 1.—*Modes of unaltered granite near Ivanhoe altered area*

	Sample No.			
	184	209	229	249
Quartz	37.4	31.2	12.0	23.2
Orthoclase	45.0	57.2	46.2	37.6
Albite	14.9	9.7	35.2	36.1
Biotite	1.3	1.1	2.4	2.0
Magnetite	1.0	.7	.7	.9
Apatite	.2	.05	.6	.05
Zircon	.2	.05	.05	.05
Amphibole(?)	----	----	1.1	----
Sphene	----	----	1.7	----
Tourmaline	.05	----	----	.2
Total	100.05	100.0	99.95	100.1

which lie unconformably on the granite. They are probably of Early Cretaceous age. The granite debris in the arkosic rocks was derived from the Jurassic granite. The third sequence, lying to the west, near the Ivanhoe mine, also contains arkoses derived from the granite, lies unconformably on it, and contains at least some rocks of Late Cretaceous age. These three sequences were mildly chloritized, epidotized, and argillized during emplacement of assorted plutons and dikes of Laramide age that are not exposed in the area shown in figure 1. The youngest sequence of post-granite volcanic and sedimentary rocks occurs south of the granite and consists of rhyodacitic tuffs and volcanic breccia, which unconformably overlie a Cretaceous pluton southwest of the area shown in figure 1.

Quartz veins, here usually only a few feet thick, cut all these rocks, as well as some of the intensely altered granite. However, inasmuch as some hundred similar veins are not surrounded by altered areas, the veins are probably younger than the alteration, rather than contemporaneous with it. Many of the veins carry base metals, and some have been mined for silver in the nearby Wrightson and Tyndall mining districts. The Ivanhoe mine (fig. 1), described by Schrader (1915, p. 216–218), produced some lead, silver, and gold from a quartz vein.

The geologic structure is relatively simple near the Ivanhoe altered area. Vestiges of a pre-Paleocene fault trend north-northwestward within and along the Triassic rocks along Temporal Gulch (lower right-hand side, fig. 1). This fault is probably related to, or was a part of, a major fault(?), along which (1) many intrusives were intruded from Triassic time onward, (2) movement has differentially tilted the blocks on either side of the mountains, and (3) fluids moved that altered and mineralized some rocks (Drewes, 1966). Another group of faults, which splay out to a broad west-trending zone at Temporal Gulch, join west of the area shown in figure 1 to form a major fault that swings northwestward. Some quartz veins lie in this fault system and some are brecciated by late movement along it. These faults are a result largely of Paleocene (Laramide) deformation. The Ivanhoe altered area lies near the intersection of the inferred pre-Paleocene fault and two branches of the younger fault system.

The main altered area, southeast of the old Ivanhoe mine, forms an irregular ellipse slightly more than half a square mile in extent. Several smaller patches of altered granite lie southeast and northwest of the main area. Scrub growth, particularly manzanita, is markedly denser in the altered area than around it. Local relief is about 500 feet, and the gullys are narrower than those in unaltered granite terrane. Outcrops are abundant, small, and irregular on the slopes but are more extensive along the gully bottoms; they are mostly more silicified or less intensely fractured altered rock, resulting in at least one bias in the sampling. The altered rock is vividly colored in reddish-brown, yellowish-brown, and pale-yellowish-gray hues. Relict granitic textures are still discernable in all but the most intensely altered rock. Breccia texture appears only in the two small volcanic bodies at the north edge of the altered areas; presumably these are remnants of a capping sheet, but they may be intrusive bodies. Fractures are much more abundant in the altered than in the unaltered granite, and the most abundant concentration of iron oxides is along this fracture network. Bulk rock X-ray diffraction analyses of 17 specimens show that the altered rocks are made up of at least 25 percent of clay minerals, which consist of about equal amounts of the kaolin and sericite groups. Alunite makes up an additional 5–10 percent of about a third of the specimens. Sulfides have not been seen in outcrop, but pyrite boxwork structures are preserved in some iron oxide fracture filling. A few jasperoid veinlets are also present. The alteration is probably of late Paleocene (late Laramide) age, because some plutons of Paleocene age are similarly altered but younger rocks are not.

SAMPLING AND RESULTS OF ANALYSES

Reconnaissance sampling of alluvium showed the presence of anomalous amounts of base metals in several local basins between Squaw Gulch and Temporal Gulch. The initial chip samples of rock were chosen to show primarily what metals remained in the various types of altered rock rather than their areal distribution; the samples consisted of as many as eight chips each, and each chip was analyzed indi-

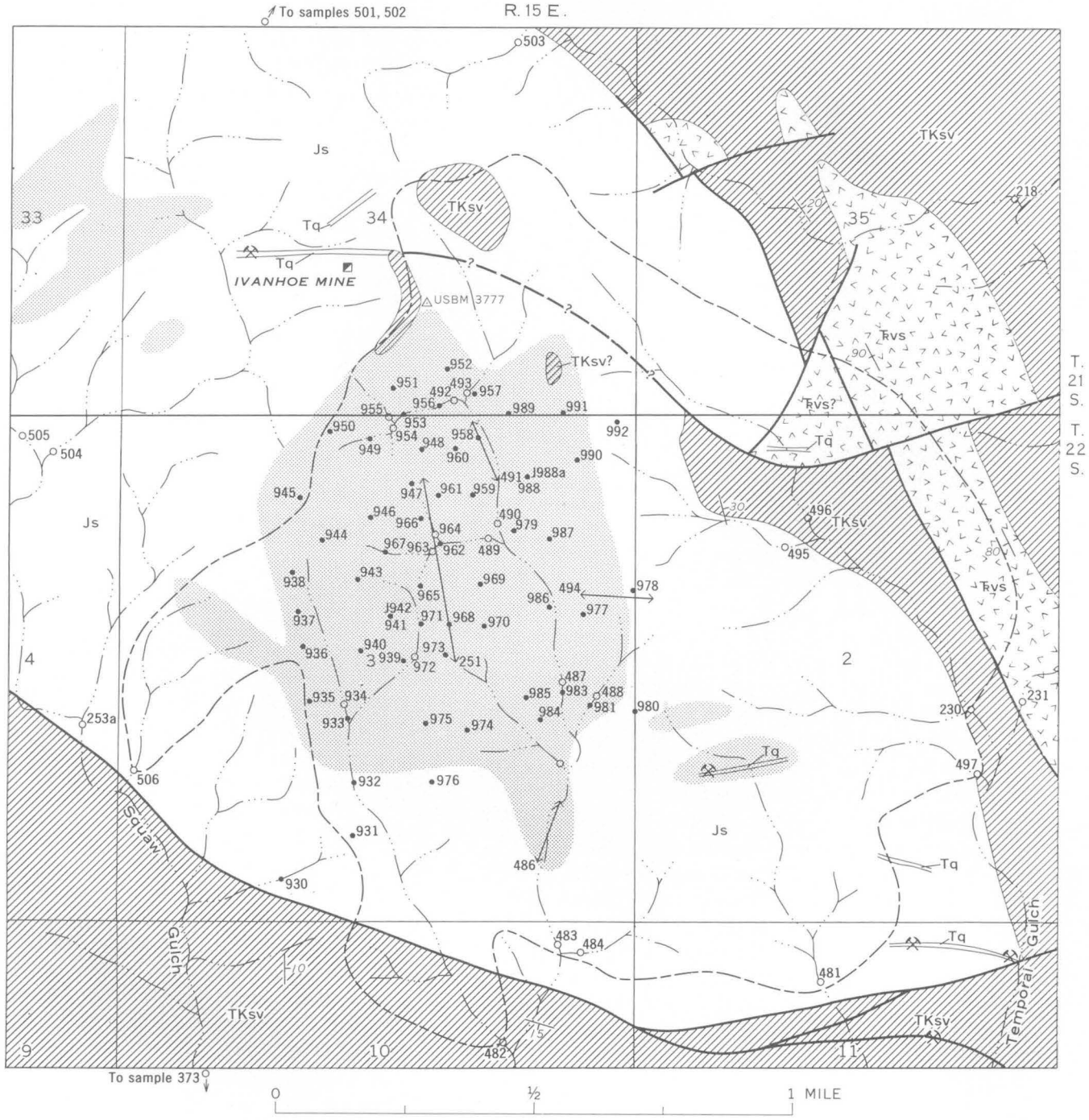

FIGURE 1.—Generalized geologic map of the Ivanhoe altered area, Santa Rita Mountains, Ariz. Index map shows following locations: 1, Wrightson mining district; 2, Tyndall mining district; 3, Mansfield Canyon; 4, Flux Canyon; 5, Washington Camp; 4–5, Patagonia Mountains area.

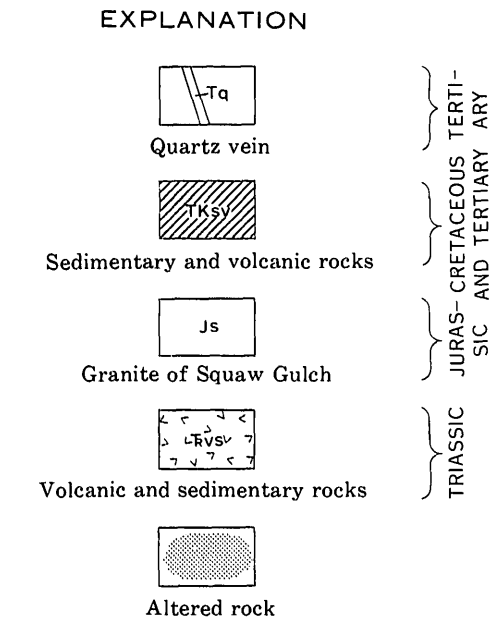

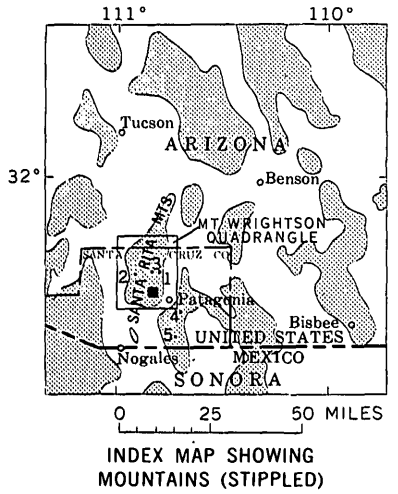

INDEX MAP SHOWING MOUNTAINS (STIPPLED)

vidually. Final sampling was concentrated on the most altered rocks to get a general idea of the distribution of selected metals. Each of these samples consisted of three to six chips of the most altered rock types, such as may appear along fractures, and were collected within about 100 feet of each other. Composites of these chip samples, as well as of the individual alluvial samples and initial chip samples (about 110 in all) were analyzed for copper, lead, and zinc by the wet chemical methods described by Ward and others (1963) and by semiquantitative spectrographic methods. Gold was analysed for only in the altered rock samples, using atomic absorption methods. The chemical analyses were made by T. F. Harms, K. W. Leong, Elizabeth Martinez, J. B. McHugh, C. S. E. Papp, and Eric Welch, and the spectrographic analyses by Jerry Motooka, Elwin Mosier, and D. M. Valiere.

Background values for unaltered granitic rocks of the Santa Rita Mountains are about 15, 25, 25 parts per million, respectively, for copper, lead, and zinc. These values were obtained from many rock analyses and selected alluvial analyses (table 2). They are roughly valid for a total of 46 rock analyses, but certain dioritic rocks, for example, may have slightly higher background values for copper. Thus an estimated average background value for copper is about 15 ppm. However, to be on the safe side, in figure 2 a copper background value of 20 ppm is used. An additional 10 samples of alluvium taken from granitic basins also show about the same background values for copper and lead, and they provide the only detailed values for zinc.

TABLE 2.—*Source of data for background values of copper, lead, and zinc in samples from the Santa Rita Mountains, Ariz.*

Rock type (unmineralized)	Number of samples	Median content of metal (ppm)		
		Cu	Pb	Zn[1]
Semiquantitative spectrographic method				
All plutonic rocks	46	30	15	<200
Granitic rocks	33	~12	15	<200
Jurassic granite	5	7	~25	<200
Wet method				
Jurassic granite	4	10	≦25	25
Alluvium from granitic basins	10	15	<25	25
Estimated background values of Ivanhoe altered area	------	15	25	25

[1] Threshold of detection by semiquantitative spectrographic method is 200 ppm.

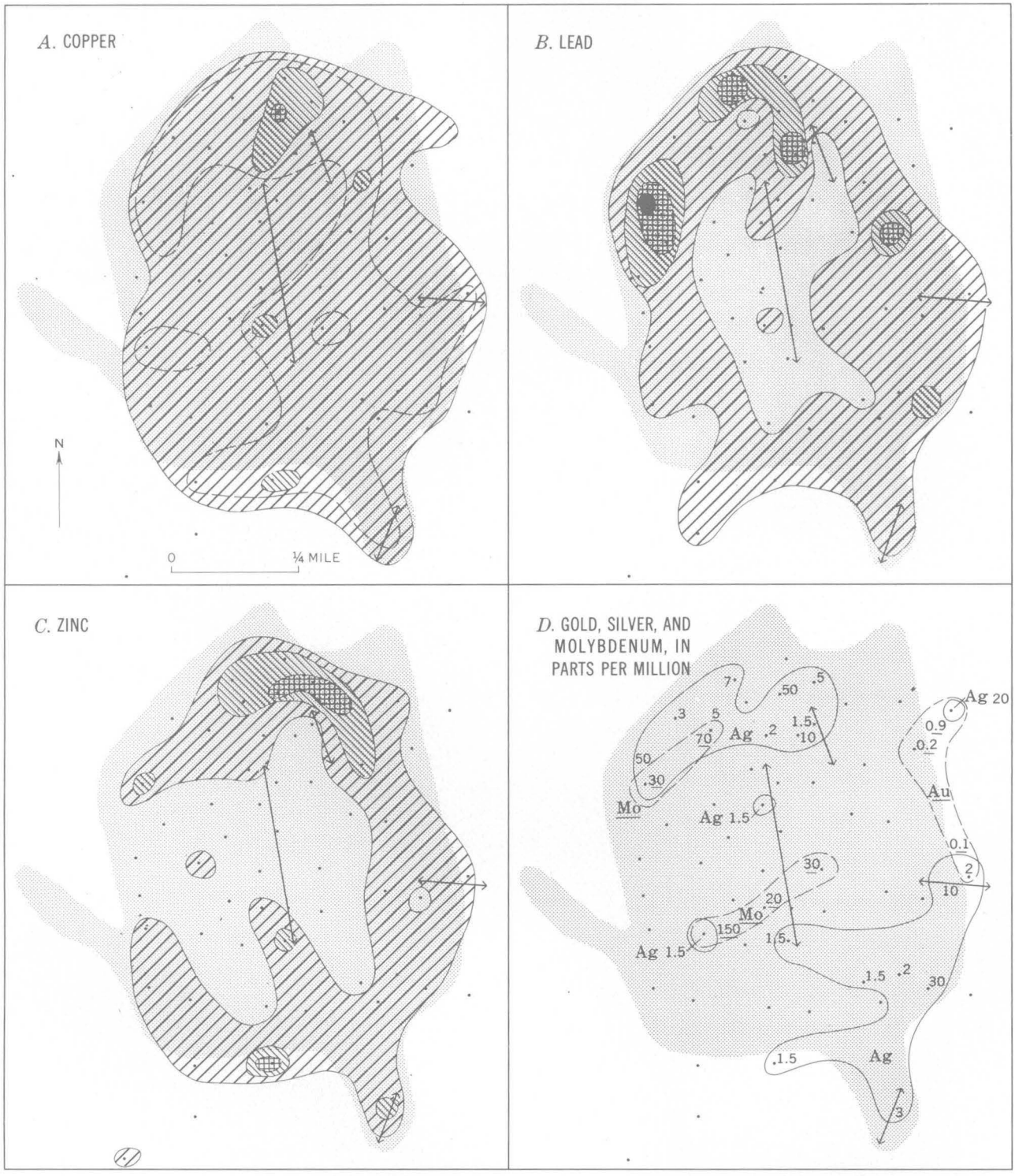

FIGURE 2.—Maps showing the distribution of copper (*A*), lead (*B*), zinc (*C*), and gold, silver, and molybdenum (*D*) in the Ivanhoe altered area, Arizona.

EXPLANATION

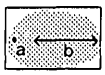

Altered rocks
Showing location of samples (a) *and line of chip samples* (b)

CONTENT OF COPPER, LEAD, AND ZINC, IN PARTS PER MILLION, AND IN RELATION TO BACKGROUND

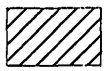

Lead and zinc, 50-150 ppm
Copper, 40-150 ppm
2-6× background

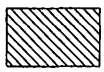

150-400 ppm
6-16× background

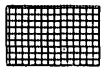

400-2,000 ppm
20-100× background

More than 2,000 ppm
>100× background

Maximum values of copper, lead, and zinc in rocks obtained from the Ivanhoe altered area are 500, 15,000, and 1,200 ppm, respectively. The distribution of copper, lead, and zinc in the Ivanhoe altered area is shown in figures 2*A*–*C*. The values are contoured in terms of the background; that is, the field between the × 2 and × 6 contours, or isopleths, contain only samples having values of a particular metal of 2 to 6 times its background value. In general, data obtained by the wet method are in close agreement with that obtained by semiquantitative spectrographic methods. However, the contours have been constructed to show the highest values where the two methods were not in full agreement.

The base-metal anomalies are crudely annular, the highest values being located near the margin of the altered area. Reasons for this distribution, such as an increase in alteration or fracture density near the margin of the anomalous areas, were not observed in the field. Possibly there has been an outward movement of these metals from the center of the altered area, and zinc and lead retained their mobility after some copper had become fixed.

In addition to the anomalously high values of three base metals, some samples contain silver (as much as 50 ppm), gold (as much as 0.9 ppm), and molybdenum (as much as 150 ppm). The concentration and distribution of these elements are shown in figure 2*D*. A single sample (No. 945) also contains both antimony (300 ppm) and beryllium (30 ppm), and two other samples (Nos. 956 and 981) each contain 150-200 ppm of bismuth. Again, most of the samples with high concentrations of these metals are near the margin of the altered area, especially along the northern and eastern sides. The highest gold content was actually obtained from locally altered rock adjacent to quartz-filled fractures outside the intensely altered area.

Semiquantitative spectrographic analyses for 20 elements are summarized in figure 3. The ranges, shown by the bars, and the median values, shown by the symbols on the bars, are given for four groups of samples, of which two groups are of unaltered rocks to provide background data. Among the values for the unaltered rocks, the abundances of the trace elements are given separately for the 5 samples of Jurassic granite, and to augment the relatively few samples of that granite, abundances for 33 samples of all granitic rocks in the area are also given. These include the Jurassic granite, as well as several bodies of quartz monzonite and of granodiorite and one of monzonite. Thus, in addition to minor compositional variation, the group of 33 samples also represents rocks exposed at different levels in each pluton. Comparison of the first two bars (median values) for each element shows that the elements Ag, B, Ga, La, Mo, Ni, Pb, V, Y, and Zn are about equally abundant in the Jurassic granite and in all granitic rocks of the area. Ba, Co, Cr, Cu, Mn, Sc, Sr, Ti, and Zr are less abundant in the Jurassic granite, and only Be is more abundant in this granite than in the other rocks.

Additional analyses of tellurium on about half of the specimens show a distribution roughly comparable to that of lead or zinc, and show concentrations to 6.3 ppm which is several orders of magnitude more than could be expected in granite.

An increase of the mean values of Ag, B, Cu, Mo, Pb, Sc, Ti, V, and Zr in the altered rocks, compared with the unaltered ones, suggests that these elements were concentrated or added during the alteration. Likewise, the altered rocks were impoverished in La, Be, and Mn. The Ba, Ga, and Y content of the altered rocks and unaltered rocks is about the same. Poor sensitivity of the analytical technique for the other elements does not permit any significant comparison to be made for them.

The higher content of Ba, Cu, Mn, Pb, and Zn in alluvium derived from the altered rocks than in the

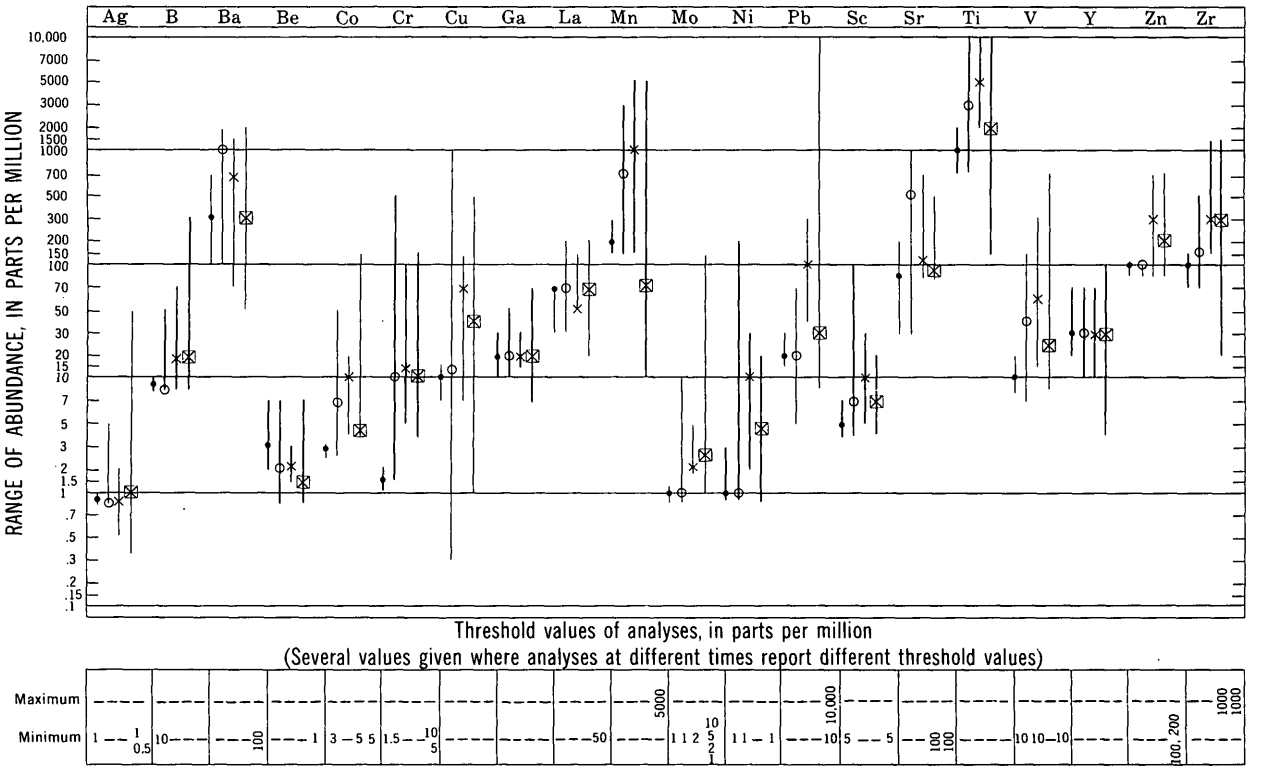

FIGURE 3.—Range of abundance and median value of some trace elements in 5 samples of Jurassic granite of Squaw Gulch (●), 33 samples of all granitic rocks of the Santa Rita Mountains, Ariz. (○), 28 samples of alluvium derived wholly or largely from altered granite of Squaw Gulch (X), and 55 samples of altered granite of Squaw Gulch in the Ivanhoe area (⊠). Trace elements looked for and not found, or found only rarely, include As, Cd, Nb, Sn, and W. Threshold value of analyses only given for elements some of whose reported abundance lie close to that value.

altered rocks themselves is noteworthy, and suggests that in altered areas close comparison between results obtained on alluvium and rock samples may be difficult to make. Possibly some elements are concentrated in organic compounds present only in alluvium derived from altered areas but absent in altered rock.

Samples of two jasperoid veinlets from the altered area were also analyzed. Other than copper (200–300 ppm), they contain much less of the other elements than do the altered rocks in which they appear.

CONCLUSIONS

Reconnaissance indicates that the Ivanhoe altered area has a fairly extensive tract of ground underlain by altered granite that is enriched in copper, lead, zinc, silver, and other elements. Surface examination, and reconnaissance sampling, shows several similar areas of altered and mineralized rocks in a north-northwest-trending belt in the Santa Rita Mountains.

REFERENCES

Drewes, Harald, 1966, Preliminary geologic map of the Mt. Wrightson quadrangle, Santa Cruz and Pima Counties, Arizona: U.S. Geol. Survey open-file report.

Schrader, F. C., with contributions by Hill, J. M., 1915, Mineral deposits of the Santa Rita and Patagonia Mountains: U.S. Geol. Survey Bull. 582, 373 p.

Ward, F. N., Lakin, H. W., Canney, F. C., and others, 1963, Analytical methods used in geochemical exploration by the U.S. Geological Survey: U.S. Geol. Survey Bull. 1152, 100 p.

RELATION OF BUILDING DAMAGE TO GEOLOGY IN SEATTLE, WASHINGTON, DURING THE APRIL 1965 EARTHQUAKE

By DONAL R. MULLINEAUX, MANUEL G. BONILLA, and JULIUS SCHLOCKER,
Denver, Colo.; Menlo Park, Calif.

Abstract.—The strong Puget Sound earthquake of April 29, 1965 caused widespread but generally mild damage. In the city of Seattle, a relation between building damage and the distribution of geologic formations at the surface was locally recognizable, but was imperfectly developed and less well expressed than the marked relation reported for many strong earthquakes. The most severe damage occurred over an area underlain in part by compact Pleistocene sediments and in part by less compact postglacial deposits and artificial fill, in a pattern evidently controlled by some factor other than surface distribution of geologic materials.

At about 7:30 a.m. Pacific standard time on April 29, 1965, a strong earthquake shook the Puget Sound region of western Washington. The shock produced ground cracks, landslides, and building damage over a broad region, and the U.S. Geological Survey immediately sent a team of geologists into the area to evaluate the relation of these earthquake effects to the geologic terrane. This article describes the results of a 1-week investigation of building damage with respect to the distribution of geologic formations in Seattle.

The April 29 earthquake originated beneath the central part of the Puget Sound lowland in the vicinity of Seattle and Tacoma, at a depth of about 60 kilometers (Algermissen and Harding, 1965; Chiburis and others, 1965). Its magnitude of about 6.5 on the Richter scale was as great or greater than that of any other recorded earthquake in the region except for the 7.1 magnitude of the April 13, 1949 temblor, which originated at a comparable depth but a few tens of miles farther southwest (Nuttli, 1952). The foci of both the 1949 and 1965 Puget Sound earthquakes were deep compared to those of typical California earthquakes (Steinbrugge and Cloud, 1965) and the great Alaska earthquake of 1964 (Grantz and others, 1964). In addition, seismograph records show that the duration of strong motion was rather short, from 10 to 20 seconds, in both the 1949 and 1965 Puget Sound shocks (Steinbrugge and Cloud, 1965).

GEOLOGIC ENVIRONMENT

Seattle lies in the central part of a broad structural and topographic lowland that is bounded both east and west by mountain ranges. The lowland is underlain by an extensive fill of Pleistocene sediments, locally as much as a thousand feet thick, which nearly everywhere buries an irregular, ancient erosion surface cut on Tertiary sedimentary and volcanic rocks. The Pleistocene deposits, deeply and repeatedly grooved by southward-moving glaciers and entrenched by rivers, have a topography characterized by deep valleys and broad fluted hills. Locally, troughs or valleys separating the broad hills are occupied by Puget Sound and adjacent lakes, but many valleys have been partly filled by postglacial sediments. Because of repeated glaciation the geology of the lowland near Seattle is complex in detail, but the geologic units can be grouped into three general categories: Tertiary bedrock, Pleistocene sediments, and post-Pleistocene or postglacial deposits (fig. 1). Geologic formations of the first two categories form the hills and underlie the valleys at depth. Postglacial sediments, however, occupy the floors of almost all the lowland valleys. Artificial fill, a nongeologic but important deposit in terms of earthquake response, is also located chiefly on the valley floors.

Tertiary bedrock forms a minor part of the hills at Seattle, cropping out only in the southeast part of the city and at Alki Point in West Seattle (fig. 1). It consists chiefly of folded and faulted sandstone and silt-

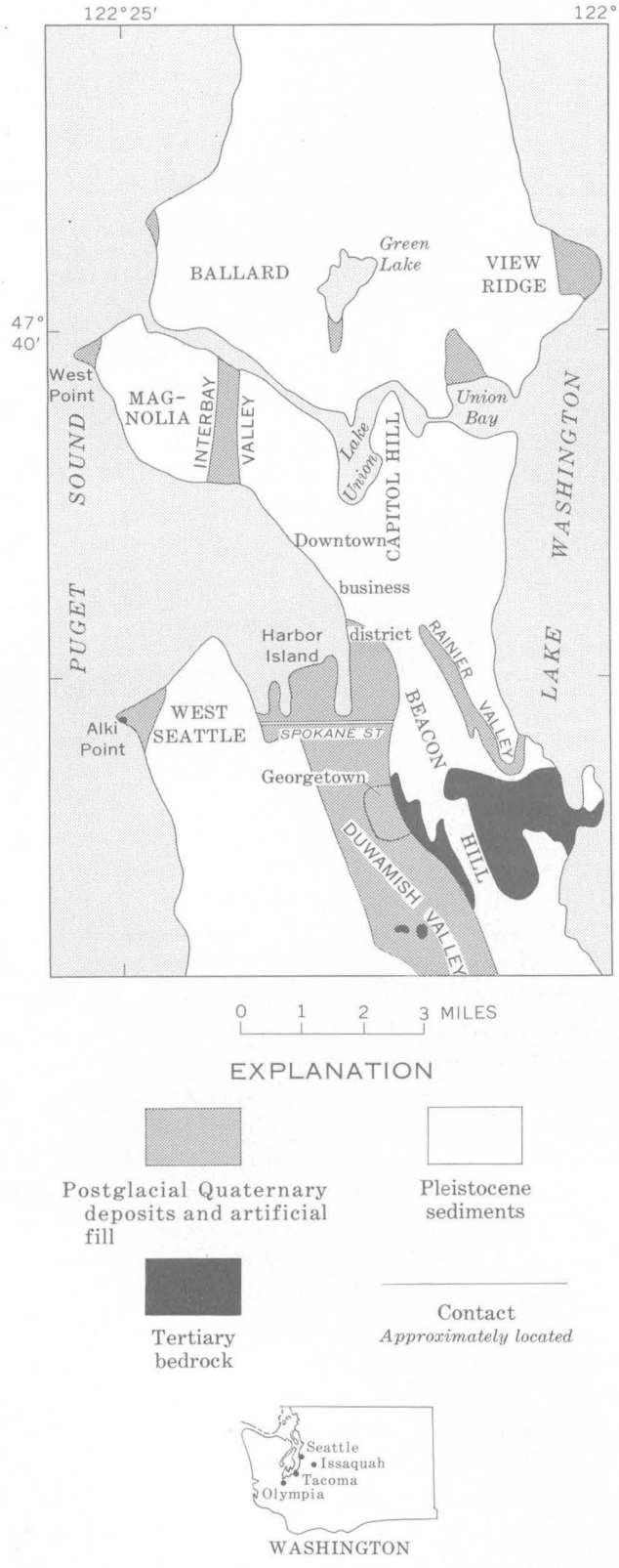

FIGURE 1.—Generalized geologic map of the Seattle area.

stone composed of fragments of volcanic rock. Although these sedimentary rocks are only poorly to moderately lithified, they are relatively dense and contain little water.

The Seattle hills are composed predominantly of nearly horizontal layers and lenses of Pleistocene sand, silt, and clay representing several glacial and interglacial episodes. Sediments predating the youngest interglacial episode of the region, the Olympia Interglaciation, can be separated only locally into recognizable formations. These diverse but generally clayey deposits form the bulk of the uplands in southeast Seattle; however, they are for the most part covered by thick accumulations of younger strata elsewhere in the city. Overlying the pre-Olympia deposits is a stratified sequence of nonglacial beds and advance outwash including, from the base upward, nonglacial sediments of Olympia age, the Lawton Clay Member of Vashon Drift, and the Esperance Sand Member of Vashon Drift (Mullineaux and others, 1965). These sediments constitute most of the upper parts of Seattle's hills (fig. 2), and are overlapped in turn by an irregular mantle of Vashon till spread across the entire area. This stratigraphic sequence is known to underlie much of the West Seattle, Magnolia, Ballard, Capitol Hill, and View Ridge districts, for example, and it probably underlies much of the rest of the city as well. The Esperance Sand Member and Vashon till probably form the surface of 90 percent or more of the city uplands (see Waldron and others, 1962, in which Esperance is mapped as "Older sand"). None of the Pleistocene sediments are lithified, but they have been compacted by the weight of thousands of feet of ice. Consequently, they are overconsolidated or preconsolidated in a soils-engineering sense and, compared to bedrock and postglacial sediments, are of intermediate density and water content.

Postglacial deposits that occupy valley floors and smaller upland basins are chiefly deposits of sand, silt, and clay that locally contain peat. From one valley to another and even within single valleys, these sediments are highly variable in thickness and composition. For example, the postglacial alluvium along the floor of the Rainier Valley (fig. 1) is mostly silt and is only a few feet thick, whereas the alluvium of the much broader Duwamish Valley is predominantly sand and is at least several hundred feet thick. Although within the Duwamish Valley the bulk of the alluvial fill is sand, the most abundant constituent of the upper few to few tens of feet probably is silt. This upper few tens of feet actually consists of a complex assemblage

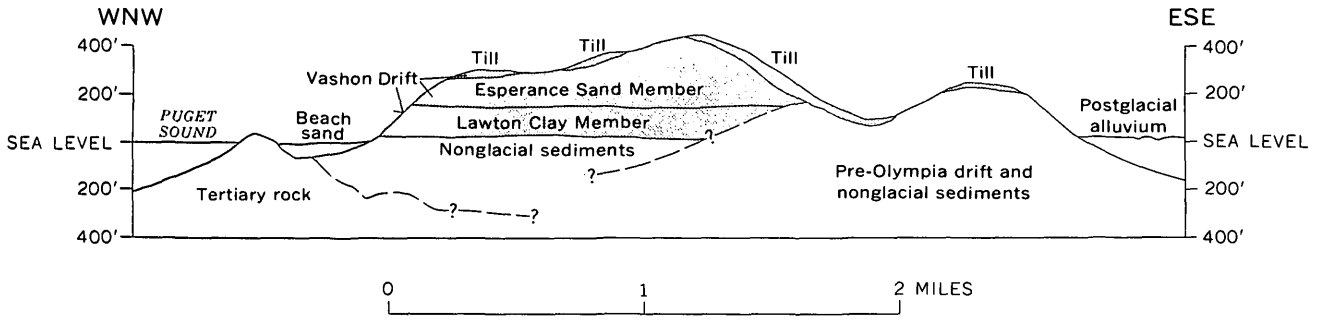

FIGURE 2.—Diagrammatic geologic section of a typical Seattle hill (West Seattle).

of channel sand, flood-plain silt, and thin but extensive swamp deposits of silt, clay, and peat. Despite the wide variety of constituent materials, however, most postglacial sediments do have in common the properties of low density, high percentage of voids, high compressibility, and generally high water content.

Artificial fill occurs locally throughout this area, but most of it has been placed on postglacial sediments. The fill consists of reworked geologic materials, trash, and garbage; some engineered fills are compact, but the fill deposits, like the postglacial deposits, generally are characterized by low density, high percentage of voids, and high compressibility.

BUILDING DAMAGE

Building damage has been widely used as an index of "intensity" or "amount" of earthquake-induced ground motion (Neumann, 1962), even though the relation of such damage to ground movement is complex and not fully understood. Moreover, a precise evaluation of damage is difficult to obtain, for rigorous comparative analyses of damage to buildings of various types would require detailed study by qualified engineers (Edwards, 1951). Nevertheless, a survey of readily apparent building damage was very useful for evaluating the effects of the April 29, 1965, quake within the city of Seattle. At least a few structures on each exposed geologic unit were damaged, a wide variety of sizes, types, and ages of buildings were among those damaged, and visible exterior effects were common enough to allow an approximation of the pattern of certain kinds of damage from a reconnaissance survey. Thus, building damage appeared to be a useful index of ground motion, and was used to relate earthquake effects to geologic terrane.

As in previous relatively strong earthquakes in the Puget Sound lowland (Coombs and Barksdale, 1942; Dirlam, 1949; Edwards, 1951), the overall destruction resulting from the 1965 quake was minor when one considers either the relatively high magnitude or the broad area over which the shock was felt. The intensity reached VIII on the Modified Mercalli scale only in Issaquah and at a few localities in Seattle (Algermissen and Harding, 1965). Scattered areas of damage indicating an intensity nearly as severe, however, extended southward from Seattle as far as Olympia. Overall, only a small proportion of structures was seriously damaged, and no general destruction occurred anywhere in the region. The characteristic of slight damage contrasted with the extensive felt area and large magnitude was attributed to a short period of strong motion by Edwards (1951) for the 1949 earthquake, and to a relatively deep point of origin by Steinbrugge and Cloud (1965) for the 1965 earthquake.

The type of damage caused by the 1965 earthquake was also similar to that resulting from earlier strong earthquakes. Cracking or collapse accompanying the differential subsidence of fill and postglacial sediments was significant locally, but damage attributable to shaking was more widespread. The most severe shattering was sustained by older unreinforced masonry structures and by masonry veneer and chimneys on wood frame buildings. Whereas the majority of damaged buildings were merely cracked, numerous walls, gables, parapets, cornices, and chimneys were broken and partly or wholly thrown down. Typical building damage resulting from the 1949 earthquake has been described by Edwards (1951) and that from the 1965 quake by Steinbrugge and Cloud (1965).

The heaviest damage in Seattle occurred on the part of the Duwamish Valley floor extending from the lower downtown business district south to about Spokane Street, and in West Seattle (fig. 1). The maximum damage to a business and industrial district was represented by that on the Duwamish Valley floor, which is occupied by a wide variety of buildings of highly diverse construction. Falling debris from buildings in this area caused three deaths and several serious injuries. Damage to storage tanks, bridges,

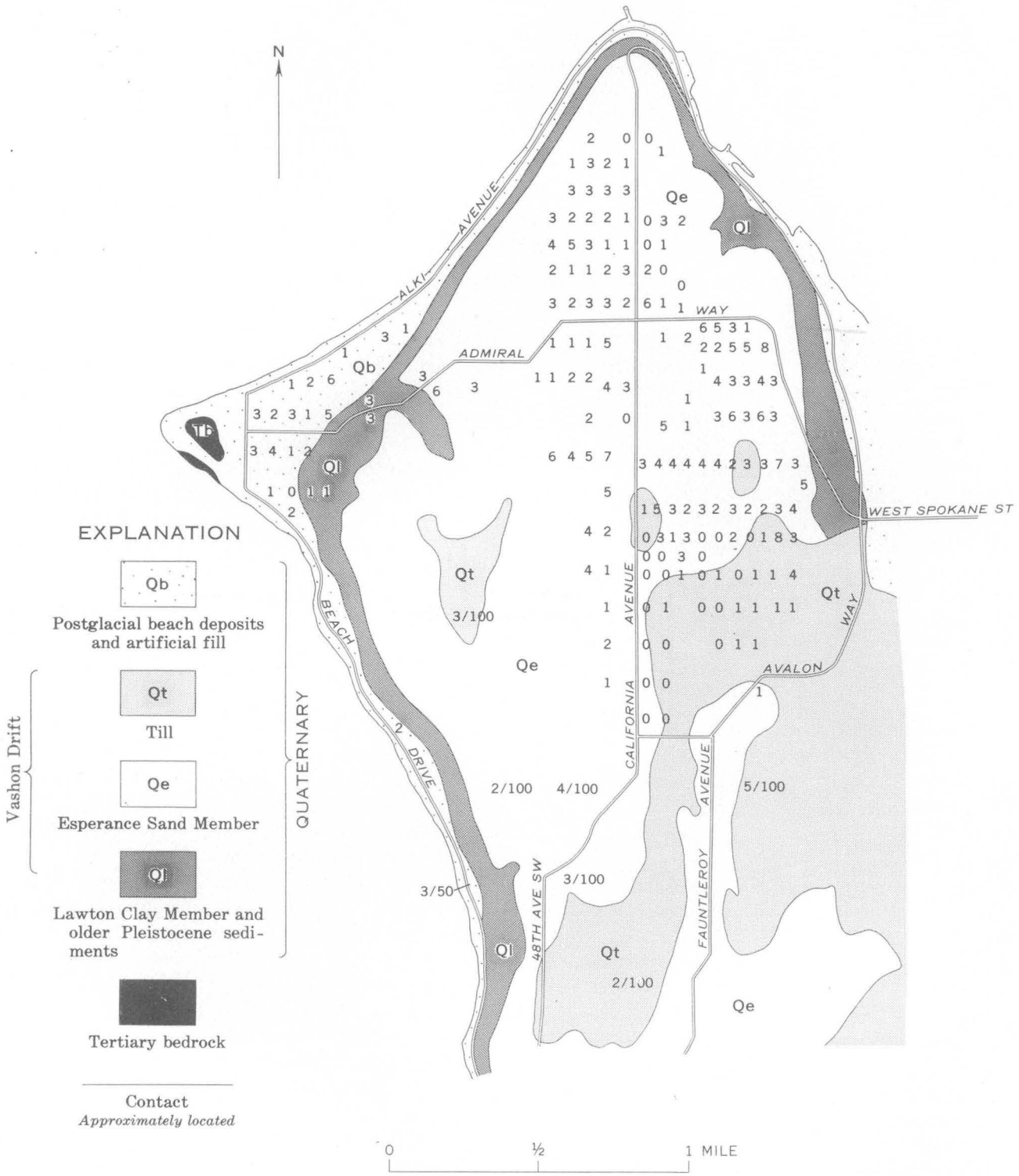

FIGURE 3.—Distribution of chief geologic units and fallen chimneys in part of West Seattle. The approximate percentage of fallen or partly fallen chimneys in counted city blocks is shown by plotted whole numbers that are 1/10 of the actual percentage. Fractions represent the proportion of similarly damaged chimneys in larger areas where less than 10 percent fell. Geology modified from Waldron and others (1962).

utility lines, and port structures also indicated a relatively high intensity on the valley floor. However, because the structures are so varied in design and construction, and because many retained unrepaired damage from previous quakes (Edwards, 1951; Steinbrugge and Cloud, 1965), the ground motion there cannot be compared effectively with that in other districts.

The maximum residential damage occurred in West Seattle, where residences predominate and small commercial and public buildings are common. Numerous masonry walls were cracked or thrown down in this area, but the chief visible destruction was to chimneys. Because the chimneys were readily observable and have been widely used elsewhere as an index of earthquake effects in residential areas, counts of broken chimneys were made over much of the district. Figure 3 shows the proportions of partly or wholly fallen chimneys in the northern part of West Seattle.

RELATION OF DAMAGE TO GEOLOGIC UNITS AT THE SURFACE

The relatively severe damage on the Duwamish Valley floor and in West Seattle occurred over an area underlain in part by compact Pleistocene materials, by thin postglacial beach deposits, and by thick and thin postglacial alluvium, each of which is overlain locally by artificial fill. No consistent difference in degree of damage was evident from one geologic environment to another, and the variation in damage from place to place within each was locally as great as from one environment to another. Hence the damage pattern in these most strongly affected areas did not show an expected relation to the distribution of geologic materials. To investigate that expected relation further, inspections were made of many other less affected districts in the city, and an attempt was made to judge the amount and uniformity of damage on several extensively exposed geologic units. The following discussion describes the damage evident in areas underlain chiefly by bedrock, Pleistocene sediments, and postglacial deposits for each district in which the underlying geologic sequence is relatively well known. Where possible, damage is compared with that on adjacent but dissimilar formations, and with that on similar formations in the Duwamish Valley and in West Seattle.

Areas underlain chiefly by bedrock

Damage to structures situated in areas directly underlain by bedrock was not significantly different from that in immediately adjacent areas underlain by pre-Olympia Pleistocene sediments or by postglacial deposits. Bedrock crops out extensively only in the southeastern part of the city (fig. 1). This area is occupied by residences and commercial and public buildings of a wide variety in size, age, and type of construction. Very few of these buildings sustained obvious damage in the form of broken walls or toppled chimneys. For example, no more than 1 or 2 percent of all the chimneys observed were fallen or partly fallen in the area underlain by bedrock, and only a comparable percentage of fallen chimneys was found in the adjacent area underlain by Pleistocene sediments older than the Olympia Interglaciation. Earthquake damage to buildings appeared comparably slight in areas underlain by postglacial deposits in the part of the Duwamish Valley directly west of the bedrock outcrops. There, old commercial and industrial buildings constructed of masonry showed little damage, and no fallen chimneys were seen in an old residential district of about 30 houses.

Areas underlain chiefly by Pleistocene sediments

In general, building damage was slightly greater throughout Seattle on post-Olympia deposits than on the older Pleistocene sediments that directly underlie the surface only in the southeastern part of the city. Post-Olympia deposits underlie many hills in the northern and central parts of the city, and in West Seattle (fig. 2). Commercial and public buildings are common in these areas, but private residences predominate except in the downtown portion of Capitol Hill, where there are many large commercial buildings. In the Magnolia district, for example, which is underlain by Lawton Clay and Esperance Sand Members partly mantled by Vashon till, no collapsed walls were seen, but a few chimneys had toppled in most parts of the district. The largest proportion of fallen or partly fallen chimneys, ranging up to 10 percent, occurred among brick houses located along a till-covered ridge. The proportion of fallen chimneys elsewhere in the Magnolia district was generally somewhat less than 5 percent, and it did not appear to be significantly different in areas underlain by till and those underlain directly by the Esperance Sand Member.

In Ballard, the pattern was similar to that in Magnolia, except that more damage was evident in its older commercial district where parts of several walls collapsed. Yet in the entire district, which is directly underlain by Vashon till (Waldron and others, 1962), no count of fallen chimneys was greater than 9 percent, and the average was less than 5 percent.

To the east as far as View Ridge, damage was scattered, very irregular, and apparently somewhat less severe than in Ballard. In one small area underlain

269-274 O—67——13

by glacial till, however, a group of nearly identical small houses with tall chimneys sustained relatively severe chimney damage; this localization of destruction probably was related more to characteristics of the houses than to the geologic environment. In another small area, the frequency of broken chimneys on houses underlain partly by glacial till and partly by the Esperance Sand Member was less than 5 percent and approximately the same on both deposits.

In West Seattle, damage on the northern part of the principal hill, which is underlain by the same stratigraphic sequence as that beneath Magnolia, was relatively very severe. The proportion of fallen or partly fallen chimneys in West Seattle was locally as high as 80 percent, and averaged more than 30 percent over an area of about a square mile (fig. 3). The destruction decreased markedly southward along West Seattle hill —along its eastern flank, the decrease coincided roughly with the northern boundary of glacial till at the surface. Yet, along both the crest and western flank of the same hill, a comparable decrease occurred where no till is present (fig. 3). Hence the diminishing damage southward must correlate with some factor other than surficial till. This contrast in damage, as well as the contrast in damage between West Seattle and Magnolia, Ballard, and View Ridge, indicate that the heavy damage at West Seattle is not related to presently recognizable differences within the underlying Pleistocene sequence.

Areas underlain chiefly by postglacial deposits

Damage on valley floors underlain by postglacial deposits was considerable, but assessment of its relation to the natural materials and comparisons with damage on other geologic units are difficult. A major difficulty is attributable to the fact that no sizable built-up districts lie on natural materials alone; nearly everywhere the natural materials have been partly or wholly covered by artificial fill. Comparison with damage in residential districts underlain by Pleistocene deposits is complicated because buildings on the postglacial sediments are mostly commercial and industrial types rather than residential. An additional factor that complicates direct comparison is that much of the damage was caused by subsidence due to compaction, and such damage occurred only on valley floors.

On the Duwamish Valley floor, the relatively heavy damage north of Spokane Street resulted partly from subsidence, but the apparent effects of vibration, such as broken gables and cornices, were also common. Farther south, damage appeared to be more spotty and generally less severe. In the Georgetown district, not only were residential chimneys relatively undamaged but old industrial and commercial buildings constructed of masonry showed few effects of the quake. About a mile still farther south, however, property loss at the Boeing Company was reported to be high. Much destruction there resulted from subsidence, but numerous broken windows attested to vibration damage as well. In the lower downtown area, damage to exterior masonry was much greater on buildings on the valley floor than on similar buildings on the adjacent part of Capitol Hill. In contrast, little difference was evident in damage to comparable buildings on the valley floor and on Beacon Hill at Georgetown. Property loss from subsidence and vibration, combined, on the valley floor appeared considerably greater than that on Capitol and Beacon Hills and probably greater than that on West Seattle Hill. Whether or not vibration damage alone was greater than on West Seattle Hill, however, was not clear.

Buildings on other valley floors showed subsidence or vibration effects, but on none was damage as severe as that on the Duwamish Valley floor. At the northern end of the Interbay Valley (fig. 1), broken windows and cracked walls in commercial and industrial buildings probably resulted from vibration, and differential subsidence caused some foundation damage. The effects generally were slight, however, and, because buildings there are not similar to any on the adjacent hills, no meaningful comparison of damage could be made. Just south of Green Lake (fig. 1), lacustrine sediments overlain by thin fill subsided, apparently as a result of both compaction and lateral movement downslope toward the lake. Here, ground cracks opened as much as 2 inches, breaking the foundation of a small building, fracturing walks and paving, and breaking utility lines. Similar ground cracks were absent on the adjacent hills, which showed only scattered chimney damage. North of Union Bay, a broad fill over alluvial and lacustrine sediments subsided and exhibited scattered ground cracks and sand mounds. Subsidence caused minor damage to paving and walks, and an estimated 10 to 30 percent of shelf goods were shaken down in two stores in the shopping center there. In contrast, virtually no damage was observed at a shopping center on the hill about a mile to the east, and less than 1 percent of shelf goods were thrown down in two stores at that locality. Thus, at least locally, vibration as well as subsidence evidently was greater on postglacial sediments overlain by artificial fill.

Postglacial beach sand, overlain by thin and probably discontinuous artificial fill, underlies the spits at Alki Point and West Point (fig. 1). At Alki Point, many masonry walls and chimneys were shattered and toppled, and waterline breaks were more numerous than anywhere else in the city. The visible damage was highly variable from place to place in this district, but no pattern of variation was discovered. In general, the residential building damage there was greater than at any other place in the city except on the adjacent West Seattle Hill, where the damage appeared to be approximately as severe. Destruction of walls and broken utility pipelines appeared to be greater on the beach, but destruction of chimneys was somewhat greater on the adjoining hill of compact Pleistocene deposits. At West Point, where a complex group of sewage treatment plant structures was under construction on an engineered fill, little damage occurred. Although these structures are greatly different from those on the Alki Point spit, parts of them were not yet strongly supported laterally, so it seems certain that the ground motion at West Point was considerably less than that at Alki Point.

Because large areas of artificial fill exist only over postglacial sediments, it was not generally possible to separate the effects of the two materials. However, several examples of the effect of small deposits of artificial fill were seen where it overlies Pleistocene sediments. Whether vibration damage was greater on these fills was not certain, but differential subsidence from compaction and landsliding produced relatively heavy damage to several houses and to a relatively new commercial building situated partly or wholly on small artificial fills.

CONCLUSIONS

Overall, the degree of damage attributable to the April 29, 1965, earthquake was mild. The relation of damage to the distribution of geologic materials at the surface was not well expressed, and that relation was locally overshadowed by some factor or factors, as yet unrecognized, that concentrated the damage in certain areas. The correlation of damage with surface geology appeared significantly less strong than that commonly reported for California and Japan earthquakes (Duke, 1958), or for the 1964 Alaska earthquake (Hansen, 1965; Kachadoorian, 1965).

Nevertheless, the effects of the Puget Sound quake were generally greater on "soft ground" such as postglacial sediments and artificial fill than on firm Tertiary rock or compact Pleistocene deposits. But the greater damage on "soft ground" was highly variable from place to place, and locally it was not recognizably greater than on nearby "firm" rock and Pleistocene deposits. Part of the damage on "soft" materials obviously was attributable to differential subsidence due to compaction; possibly subsidence alone could account for the greater overall building damage on those materials. At least locally, however, vibration effects also appeared greater on "soft ground" than on firmer sediments. Many of these relations were obscure or equivocal because the interpretation of damage was complicated by the mildness and irregularity of damage distribution, the wide variety of structures involved, and by unevaluated residual damage from previous earthquakes.

Where damage was recognizably greater on "soft ground," natural unconsolidated deposits were overlain by artificial fill, and the response of natural and artificial materials could not be separated. However, in several places, natural postglacial materials overlain by little or no fill showed no greater damage than that on adjacent more compact Pleistocene sediments. As a result, it seems likely that the chief reason for the greater observed damage on "soft ground" was the presence and quality of the artificial fill. This supports the conclusions of several studies reviewed by Duke (1958), which indicate that there is a much greater difference in response between fills and natural "soft" ground than between natural "soft" and "firm" ground. It must be recognized, however, that while a greater response may be typical of most existing artificial fills, some well-engineered fills are more firm and probably would exhibit less response than the natural "soft" ground of these studies.

The factor or factors that restricted the relatively severe damage to West Seattle and nearby parts of the Duwamish Valley floor are not known. The presence of this localized destruction on compact Pleistocene materials on the West Seattle hill indicates that vibration rather than subsidence was the cause; the contrast from north to south along that hill is so marked that a significant difference in ground motion is certainly indicated. The north-south decrease was pronounced across both compact and loose sediments; thus, the geologic materials recognized at the surface apparently were not the controlling factor. Moreover, there is no evidence that the topography, or the type or age of buildings, localized the damage. The concentration of earthquake effects here may possibly have been caused in some way by bedrock, which presumably underlies West Seattle not far below sea

level. The effects were not simply a function of depth to, and lithology of, the rock, however, because the same factors must surely exist both north and south of the bedrock outcrops in southeastern Seattle. But the effects could have been related to the shape or structure of the bedrock mass, either of which might modify the distribution of earthquake energy by reflection, refraction, or other wave interference. Such a suggestion was made by Coombs and Barksdale (1942) for small areas of relatively high intensity in the Puget Sound lowland during an earthquake on November 13, 1939.

An important point shown by a comparison of our results with those of other reconnaissance studies of the same earthquake is that the actual pattern of damage was not unmistakably clear. Our description of the earthquake effects has emphasized a somewhat weak relation of damage to distribution of surface materials and a zone of unexplained high intensity that spread across a variety of sediments. One other study team (Steinbrugge and Cloud, 1965) concluded that high earthquake intensity could almost always be associated with the local geology, and that damage was most pronounced in what is commonly termed "poor ground" areas. Still another team noted a concentration of damage where the sedimentary deposits in the lowland are thickest, and, in Seattle, where the Esperance Sand Member (shown as "Older sand" on the map of Waldron and others, 1962) lies at the surface (N. H. Rasmussen, oral commun., 1966).

The irregular pattern of ground motion and damage of the April 29 earthquake indicates that, for the central part of the Puget Sound lowland, we can predict in only a general way either correlation of damage with surface outcrops of various geologic formations or the relative intensity of damage from place to place on similar formations. For planning purposes, however, most areas underlain by artificial fill can be regarded as relatively susceptible to earthquake damage. The potential hazard probably increases as thickness and water content of a fill increase, and decreases as compactness increases. Even small fills may be hazardous, partly because they tend to be placed under only parts of structures and on slopes.

Building sites on postglacial sediments may or may not be more hazardous than those on compact Pleistocene deposits or Tertiary rock. Experience elsewhere, and past reports of Puget Sound earthquakes, suggest that the postglacial deposits are likely to be, overall, relatively unstable. Yet the 1965 quake showed that structures on the compact materials may be as hard hit as those on adjacent postglacial sediments, or even more severely damaged than those on some nearby postglacial units. Because they form the hill slopes, Pleistocene and older materials are also more susceptible to landsliding than are the postglacial deposits, which generally underlie flat areas.

Whether or not the severely affected area in West Seattle is peculiarly susceptible to earthquake damage is not certain. Some residents have held that the same district was selectively damaged during the strong 1949 earthquake; if true, such a susceptibility would certainly be suggested. However, this area was not described as one of severe damage in published reports of the 1949 quake (Dirlam, 1949; Edwards, 1951), thus recorded evidence of a similar damage pattern in West Seattle for the two events is absent.

The erratic effects of the 1965 earthquake and the widespread but mild damage typical of the last several quakes suggest that the response of the Puget Sound region is somewhat unusual, at least by comparison with regions where most earthquake data have been gathered. The difference could be due partly to the properties of the thick lens of sedimentary material that underlies the lowland.

REFERENCES

Algermissen, S. T., and Harding, S. T., 1965, The Puget Sound, Washington, earthquake of April 29, 1965: U.S. Coast and Geod. Survey Prelim. Seismol. Rept., 26 p.

Chiburis, E. F., Dehlinger, Peter, and French, W. S., 1965, The Tacoma earthquake of April 29, 1965: The Ore Bin, v. 27, no. 5, p. 99–100.

Coombs, H. A., and Barksdale, J. D., 1942, The Olympic earthquake of November 13, 1939: Seismol. Soc. America Bull., v. 32, no. 1, p. 1–6.

Dirlam, C. N., 1949, Reporting the Northwest earthquake—damage to buildings: Building Standards Monthly, v. 18, p. 4–7.

Duke, C. N., 1958, Effects of ground on destructiveness of large earthquakes: Jour. Soil Mech. and Found. Div., Proc. Am. Soc. Civil Engineers, v. 84, no. SM 3, p. 1730–1 to 1730–23.

Edwards, H. H., 1951, Lessons in structural safety learned from the 1949 Northwest earthquake, pt. 1: Western Construction, v. 26, no. 2, p. 70–74.

Grantz, Arthur, Plafker, George, and Kachadoorian, Reuben, 1964, Alaska's Good Friday earthquake, March 27, 1964, a preliminary geologic evaluation: U.S. Geol. Survey Circ. 491, 35 p.

Hansen, W. R., 1965, Effects of the earthquake of March 27, 1964, at Anchorage, Alaska: U.S. Geol. Survey Prof. Paper 542–A, 68 p.

Kachadoorian, Reuben, 1965, Effects of the earthquake of March 27, 1964, at Whittier, Alaska: U.S. Geol. Survey Prof. Paper 542–B, 21 p.

Mullineaux, D. R., Waldron, H. H., and Rubin, Meyer, 1965, Stratigraphy and chronology of late interglacial and early

Vashon glacial time in the Seattle area, Washington: U.S. Geol. Survey Bull. 1194–O, 10 p.

Neumann, Frank, 1962, Engineering seismology, *in* Reviews in engineering geology, v. 1: New York, Geol. Soc. America, p. 161–186.

Nuttli, O. W., 1952, The western Washington earthquake of April 13, 1949: Seismol. Soc. America Bull., v. 42, p. 21–28.

Steinbrugge, K. V., and Cloud, W. K., 1965, The Puget Sound, Washington, earthquake of April 29, 1965: U.S. Coast and Geod. Survey Prelim. Eng. Rept., p. 27–51.

Waldron, H. H., Liesch, B. A., Mullineaux, D. R., and Crandell, D. R., 1962, Preliminary geologic map of Seattle and vicinity, Washington: U.S. Geol. Survey Misc. Geol. Inv. Map I–354.

BOTTOM-WATER TEMPERATURES ON THE CONTINENTAL SHELF OFF NEW ENGLAND [1]

By THOMAS J. M. SCHOPF [2], Woods Hole, Mass.

Abstract.—Approximately 5,300 measurements of bottom-water temperatures collected on cruises of U.S. Bureau of Commercial Fisheries vessels, mostly in 1955, 1956, 1964, and 1965, show a striking similarity of bottom temperatures on Georges Bank and Nantucket Shoals, and distinctly lower temperatures on the nearby Scotian Shelf. An intermediate temperature regime occurs in the Gulf of Maine. Temperature distribution is related to bottom currents that circulate water over the Scotian Shelf, through the Gulf of Maine, and then onto Georges Bank and Nantucket Shoals. Available data indicate that regions of different bottom-temperature regimes have different faunal assemblages.

Water temperatures and substrate are the most important factors controlling the distribution of benthic organisms in open marine waters of the continental shelf in temperate latitudes. Broad-scale work is progressing on the distribution of substrate types (Trumbull and others, 1966; Schlee and Pratt, 1966), but little information is readily available on the distribution of bottom temperatures. This paper was prepared for those interested in using bottom-water temperatures in work on zoogeography, and amplifies the abstract of Schopf and Colton (1966).

The geographic area considered in this report extends from Hudson Canyon (lat 40°N., long 72°W.) to the continental shelf off eastern Nova Scotia (lat 44°N., long 64°W.) (fig. 1). Within this large New England offshore region, several smaller physiographic areas are recognized which have distinctive topographic, temperature, sediment, and biologic characteristics. The areas studied are Nantucket Shoals (20–80 meters depth), Georges Bank (4–100 m depth), most of the Gulf of Maine (100–377 m depth), and the southern Scotian Shelf and Browns Bank (40–140 m depth) (fig. 1).

Acknowledgments.—I am greatly indebted to J. B. Colton, Jr., U.S. Bureau of Commercial Fisheries, Woods Hole, Mass., for providing many of the data from which the maps and interpretations presented here were derived, and for offering several valuable suggestions during the course of the work. S. R. Nickerson, of the Bureau of Commercial Fisheries, Christina Augustyniak, of the Marine Biological Laboratories, and J. B. Nauman, of the U.S. Geological Survey, plotted the positions of most of the stations. Helpful comments on an earlier draft of the paper were generously provided by K. O. Emery and D. F. Bumpus, of the Woods Hole Oceanographic Institu-

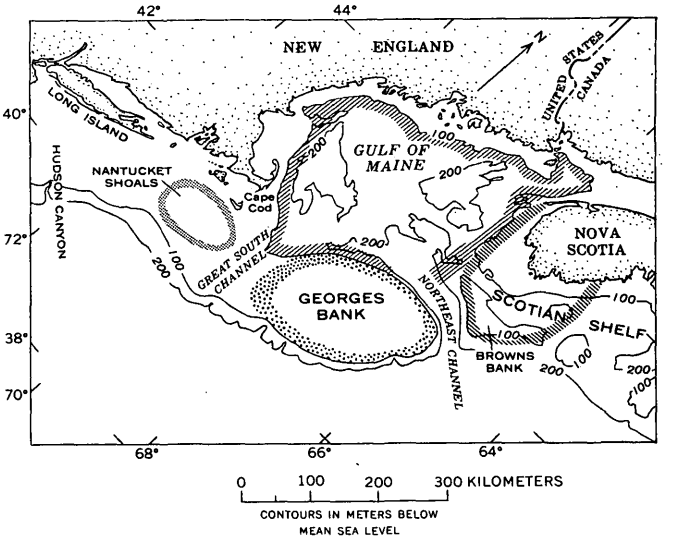

FIGURE 1.—Map of continental shelf off New England showing submarine physiographic regions. Only the southern part of the Scotian Shelf (as shown by the diagonal-line delineation) is included in this report.

[1] Contribution No. 112 of the Systematics-Ecology Program, Marine Biological Laboratory, Woods Hole, Mass.; Contribution No. 1963 of the Woods Hole Oceanographic Institution.

[2] Present address: Lehigh University, Bethlehem, Pa.

tion; R. H. Meade, of the U.S. Geological Survey, Woods Hole; and M. R. Carriker and B. A. Wade of the Systematics–Ecology Program, Marine Biological Laboratory, and R. L. Wigley, U.S. Bureau of Commercial Fisheries. The work was supported by a grant from the Ford Foundation to the MBL Systematics-Ecology Program.

MATERIALS AND METHODS

Bottom-temperature data are based on bathythermograph observations obtained on 37 cruises during the period 1955–66 (table 1). Temperatures from 11 cruises in the fall of years 1955–61 were used as plotted and contoured by Fritz (1965), and those from the 3 cruises in 1966 were used as plotted and contoured in a report

TABLE 1.—*Sources of bottom-temperature data*

Year, and days at sea	Cruise	Number of bottom-temperature readings	Source of data
1955			
Feb. 21–Mar. 2	*Albatross* III–57	160	This report.
Mar. 19–Apr. 1	–58	195	Do.
Apr. 19–May 3	–60	205	Do.
May 16–28	–61	210	Do.
Sept. 7–28	–65	138	Fritz (1965).
	–66		
1956			
Feb. 20–Mar. 2	*Albatross* III–71	160	This report.
Mar. 21–31	–72	165	Do.
Apr. 17–28	–73	220	Do.
May 16–29	–75	235	Do.
June 11–24	–76	250	Do.
Nov. 2–21	–81	94	Fritz (1965).
	–82		
1958			
Sept. 22–Oct. 28	*Albatross* III–118	114	Do.
	–119		
	–120		
1959			
Sept. 23–Oct. 27	*Delaware* 59–12	147	Do.
	59–13		
1960			
Nov. 2–21	*Delaware* 60–12	117	Do.
1961			
Oct. 25–Nov. 20	*Delaware* 61–19	151	Do.
1963			
July 18–Aug. 19	*Albatross* IV–63–5	240	This report.
Dec. 2–27	–63–7	124	Do.
1964			
Jan. 16–28	*Albatross* IV–64–1; a	121	Do.
Feb. 4–13	–64–1; b	122	Do.
July 27–Aug. 22	–64–10	250	Do.
Aug. 31–Sept. 13	–64–11	51	Do.
Oct. 31–Dec. 4	–64–13	275	Do.
Dec. 3–18	–64–14	87	J. B. Colton, Jr., and others. [1]
1965			
Mar. 9–22	*Albatross* IV–65–3	123	Do.
May 19–June 3	–65–7	100	Do.
July 7–Aug. 10	–65–10	260	This report.
Sept. 1–16	–65–12	98	J. B. Colton, Jr., and others. [1]
Oct. 6–Nov. 11	–65–14	420	This report.
Dec. 8–22	–65–15	110	J. B. Colton, Jr., and others. [1]
1966			
Mar. 2–14	*Albatross* IV–66–2	113	Do.
May 24–June 7	–66–7	112	Do.
Sept. 8–23	–66–12	111	Do.

[1] Unpublished information.

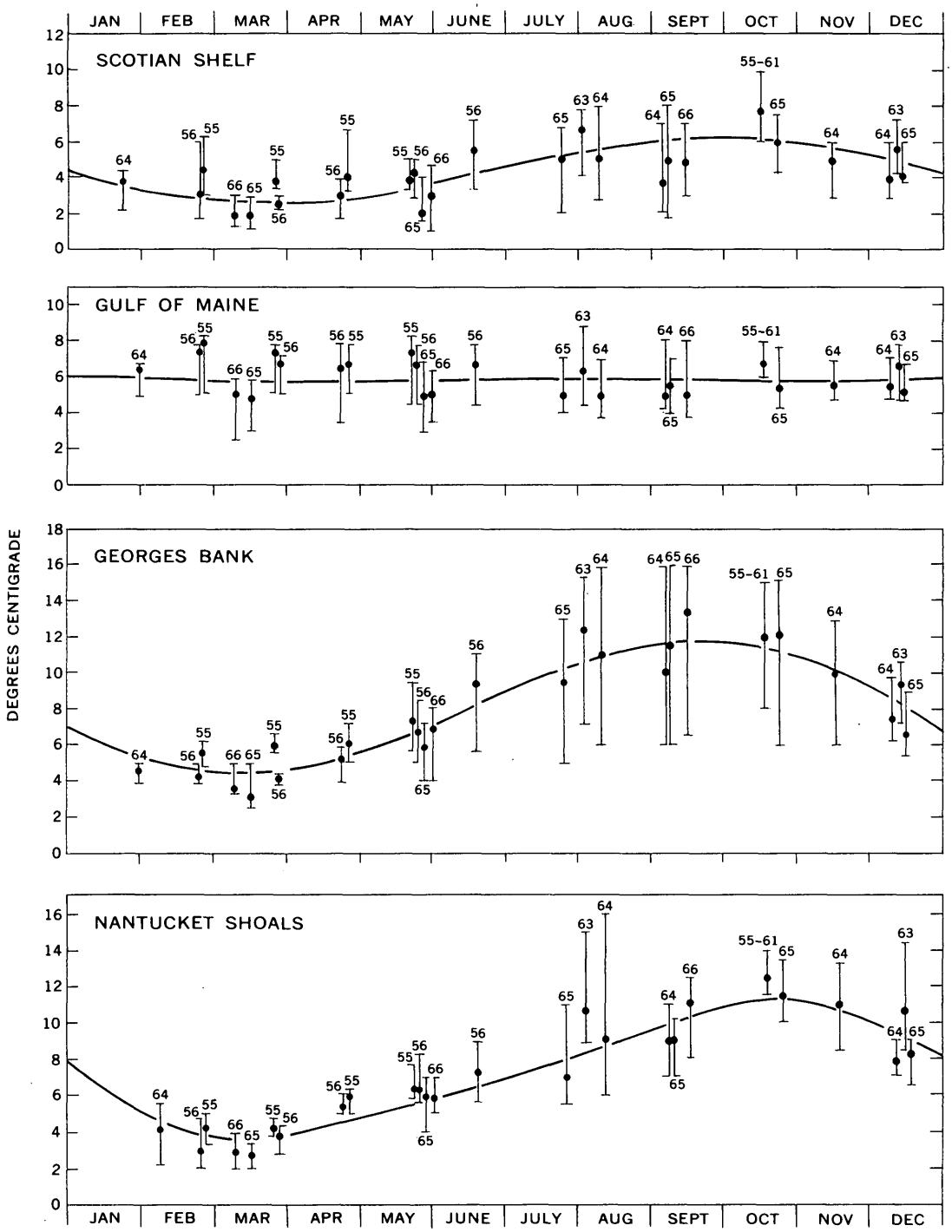

FIGURE 2.—Mean and range of bottom temperatures for each cruise or block of cruises for four physiographic areas and the average yearly temperature cycle. Data are plotted on midpoint of cruise dates. Note large seasonal fluctuations on Nantucket Shoals and Georges Bank, nearly constant conditions in Gulf of Maine, and moderate seasonal fluctuations on Scotian Shelf.

in preparation by J. B. Colton, Jr., and others. Bottom temperatures from the remaining 23 cruises were read, plotted, and contoured for this report. Temperatures supplied by Colton and his associates (see table 1) covered all of the New England continental shelf and were obtained at regularly spaced stations. Data from other cruises were usually obtained incidental to other observations and were unevenly distributed over the region. The best coverage was during the months of February, March, May, September, October, and December.

RESULTS

The range of bottom temperatures for each cruise in the four physiographic areas considered is shown in figure 2. An averaged seasonal cycle of bottom temperatures for each area is shown in figure 3. Due to the buffering effect of strong thermoclines, bottom waters of Nantucket Shoals and the Scotian Shelf reach their maximum temperatures later in the year than do those of Georges Bank. Contour maps of average bottom temperatures for the coldest and warmest parts of the year (mid-February through March, and mid-September through October) are shown in figures 4 and 5. For the coldest part of the year, depending upon the long-term (monthly) trends, values for Georges Bank, Gulf of Maine, and areas off Nova Scotia may be 1° higher or lower than shown, although the relative temperatures and their spatial distribution remain about as indicated in figure 4. Botton temperatures on Nantucket Shoals and in the regions southwest of it are a degree colder in some years than shown. In figure 5, an inshore band of isotherms south of Long Island coincides with the region of inshore movement of currents and high-salinity water (Bumpus, 1965). The warm pockets in the Gulf of Maine change their position yearly but are usually associated with the deeper areas. The region south of Long Island is warmest in November (as much as 14°C in water 30 m deep).

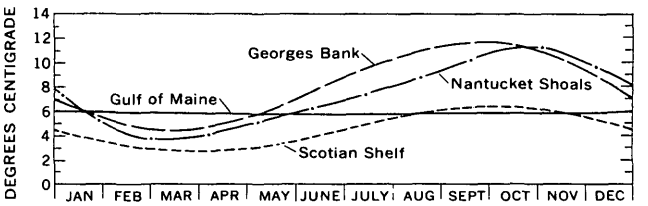

FIGURE 3.—Seasonal cycle of bottom temperatures for Scotian Shelf, Gulf of Maine, Nantucket Shoals and Georges Bank.

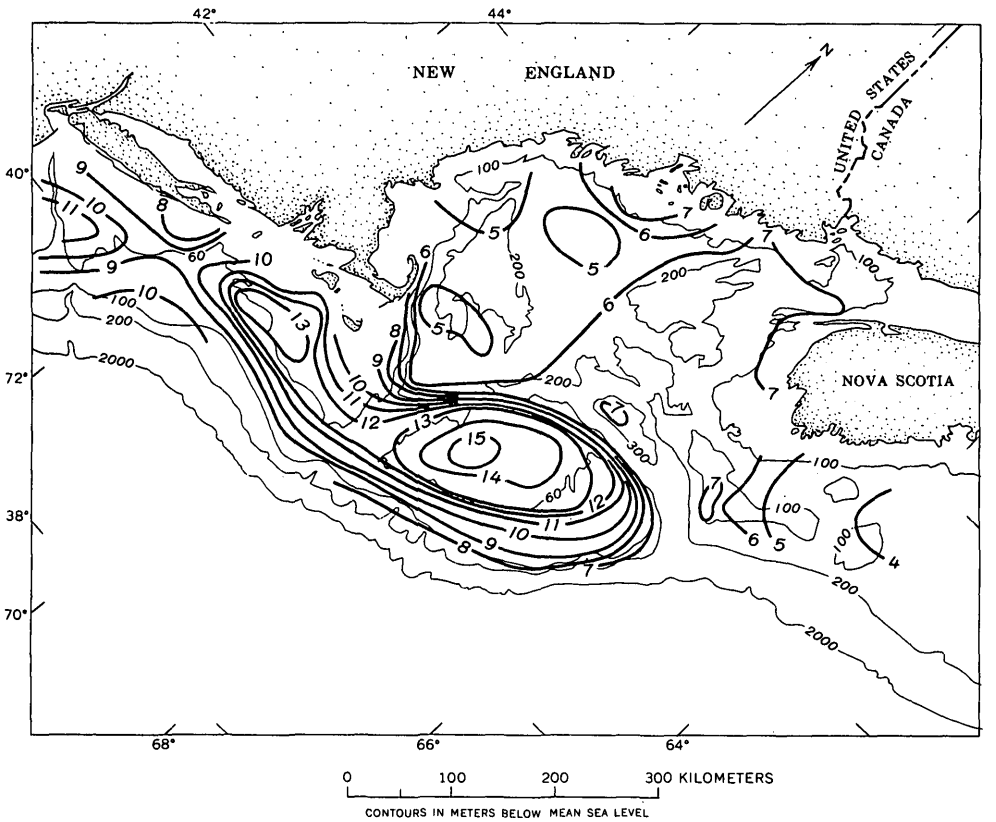

FIGURE 4.—Distribution of bottom-water temperatures for coldest part of year (mid-February through March). Isotherms (heavy lines) in degrees Centigrade.

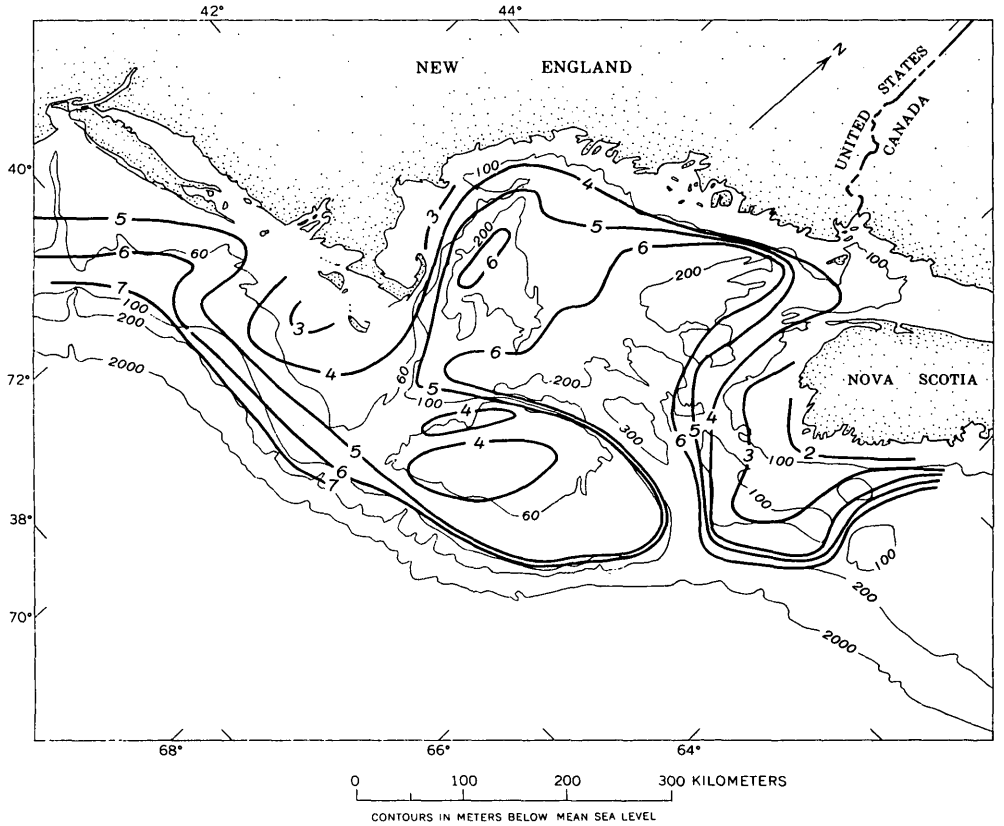

FIGURE 5.—Distribution of bottom-water temperatures for warmest part of year (mid-September through October). Isotherms (heavy lines) in degrees Centigrade.

DISCUSSION

For each place and season in the region under study, temperature conditions vary from year to year. Consequently, absolute values of bottom temperatures for specific locations and times have limited value. Greater importance should be attached to relative differences between physiographic areas, as these remain nearly constant from year to year. For example, 1955 was appreciably warmer than 1956, but the relative difference between temperatures of different physiographic regions remained about the same (fig. 2).

For any given year, Georges Bank and Nantucket Shoals have similar bottom temperatures and both are appreciably warmer than nearby Browns Bank and the Scotian Shelf (1°–5° for any season). The central area of Georges Bank undergoes a pronounced temperature change during the year. It is both warmer and colder than the margins, which remain at about the same temperature. The eastern and most northeastern edge of Georges Bank is more similar to Browns Bank than is the rest of Georges Bank.

Different physiographic regions reach their minimum and maximum temperatures at different times of the year. Nantucket Shoals are coldest in early March. Northward, the areas off Nova Scotia are coldest in late March and early April, seemingly from the influence of late melting snow and ice on the southward-flowing Nova Scotia Current.

In areas where a strong thermocline exists during the summer months (Nantucket Shoals, Browns Bank, and the Scotian Shelf), the bottom-temperature maximum occurs in October at the time of the fall overturn (Bigelow, 1933). On Georges Bank, however, tidal mixing prevents the development of a significant thermocline and the bottom-temperature maximum occurs in September when the surface maximum occurs. As would be expected, bottom temperatures in the central Gulf of Maine vary only slightly with the seasons, as these deeper waters are little influenced by surface-temperature conditions.

Bottom temperatures are probably related to bottom-current patterns, but these are not well known. On the basis of recovery of 14 surface-drift bottles that sank to the bottom on Georges Bank and southeast of Cape

Cod, Day (1958) suggested a southwesterly movement of bottom water along the southern edge of Georges Bank and a generally southerly movement out of the Gulf of Maine, through the Great South Channel, and onto Nantucket Shoals. This pattern agrees with that of surface currents (Bumpus and Lauzier, 1965); thus Georges Bank and Nantucket Shoals probably receive bottom waters from the Gulf of Maine.

Warmer continental-slope water sometimes moves onto the southern edge of Georges Bank or into the Northeast Channel between Georges Bank and Browns Bank. Most likely, pockets of high-temperature water in Georges Basin and the rest of the Gulf of Maine have their origin in this slope water. If colder than normal slope water moves onto Georges Bank, organisms with a very limited temperature tolerance, such as tile fish, can be killed in tremendous numbers (Bigelow and Schroeder, 1953).

Bottom-water temperatures are useful in understanding the distribution of faunal and floral elements because organisms depend directly and indirectly on temperature, both in larval and adult stages (Hutchins, 1947). For offshore areas, data of Fritz (1965) for groundfish, Parker (1948) for benthic Foraminifera, Peterson (1964) for hydroids, and Schopf (1965) for ectoprocts suggest that the faunas north and northeast of Cape Cod are decidedly different from those south, east, and west of it. In general, the fauna of the Gulf of Maine and Scotian Shelf are more similar to each other than is either to the fauna of Georges Bank and Nantucket Shoals. This faunal distribution agrees with that of the bottom temperatures.

Benthic organisms in the area off New England do not seem to be limited by winter temperatures. Rather, potentially southward migrating forms are limited by summer temperatures too high for survival, whereas northward-migrating forms may be limited by summer temperatures that are not high enough for reproduction (type 3 of Hutchins, 1947).

REFERENCES

Bigelow, H. B., 1933, Studies of the waters on the continental shelf, Cape Cod to Chesapeake Bay; I. The cycle of temperature: Papers in Phys. Oceanography and Meteorology, v. 2, no. 4, p. 1–135.

Bigelow, H. B., and Schroeder, W. C., 1953, Fishes of the Gulf of Maine: U.S. Fish and Wildlife Service Fishery Bull. 74, v. 53, 577 p.

Bumpus, D. F., 1965, Residual drift along the bottom on the continental shelf in the Middle Atlantic Bight area: Limnology and Oceanography, v. 10, Supp., p. R50–R53.

Bumpus, D. F., and Lauzier, L. M., 1965, Surface circulation on the continental shelf off eastern North America between Newfoundland and Florida: Am. Geog. Soc., Serial Atlas of the Marine Environment, Folio 7, 4 p., 7 pls.

Day, C. G., 1958, Surface circulation in the Gulf of Maine as deduced from drift bottles: U.S. Fish and Wildlife Service Fishery Bull. 141, v. 58, p. 443–472.

Fritz, R. L., 1965, Autumn distribution of groundfish species in the Gulf of Maine and adjacent waters, 1955–1961: Am. Geog. Soc., Serial Atlas of the Marine Environment, Folio 10, 3 p., 20 pls.

Hutchins, L. W., 1947, The bases for temperature zonation in geographical distribution: Ecol. Mon., v. 17, p. 325–335.

Parker, F. L., 1948, Foraminifera of the continental shelf from the Gulf of Maine to Maryland: Harvard Univ. Mus. Comp. Zoology Bull., v. 100, p. 213–241.

Peterson, K. W., 1964, Some preliminary results of a taxonomic study of the Hydrozoa of the Cape Cod area [abs.]: Biol. Bull., v. 127, p. 384–385.

Schlee, J. S., and Pratt, R. M., 1966, Glacial history of the Gulf of Maine [abs.]: Geol. Soc. America abstracts for American Assoc. Adv. Sci. meeting, Washington, D. C. 1966, p. 32.

Schopf, T. J. M., 1965, Ectoproct (Bryozoa) distribution on the Atlantic continental shelf from the Hudson Canyon to Nova Scotia [abs.]: Biol. Bull., v. 129, p. 421–422.

Schopf, T. J. M., and Colton, J. B., Jr., 1966, Bottom temperature and faunal provinces—continental shelf from Hudson Canyon to Nova Scotia [abs.]: Biol. Bull., v. 131, p. 406.

Trumbull, J. V. A., Schlee, J. S., Ross, D. A., Hülsemann, Jobst, and Hathaway, J. C., 1966, Continental shelf sediments off Northeastern United States [abs.]: Geol. Soc. America Abstracts for American Assoc. Adv. Sci. meeting, Washington, D. C., 1966, p. 35.

PROVENANCE OF RECENT GLACIAL ICE IN LOWER GLACIER BAY, SOUTHEASTERN ALASKA

By A. THOMAS OVENSHINE, Menlo Park, Calif.

Abstract.—Erratics of staurolite schist, chaistolite schist, biotite-quartz schist, amphibolite, gabbro, and pyroxenite are common constituents of beach gravels in lower Glacier Bay west of a line near Sturgess Island, Sandy Cove, and Hutchins Bay. These erratics were derived from the Fairweather Range and their present distribution describes the extent of glacial ice from that source, here termed the Russell drainage, in about A.D. 1740. The Muir drainage area may also have contributed ice to lower Glacier Bay but because ice from the Russell system had a much larger extent, it is suggested that discharge from the Russell glacier greatly exceeded discharge from the Muir. Probably the glacial drainage from the Muir area was partly or completely blocked by flow from the Russell glacier; ponding thus produced may have caused development of the extensive icefield observed in the Muir region by early visitors.

A recent glacial advance and retreat of more than 60 miles has been documented by observation (John Vancouver in 1801, quoted in Klotz, 1899, p. 528–530) and geologic studies (Cooper, 1923; Lawrence, 1958) in the Glacier Bay region (fig. 1). The snow that facilitated the advance accumulated in two source areas, here termed the Muir and Russell drainages (fig. 1). A single glacier issued from each source area, and south of Sebree Island these merged to form the large glacier that once filled lower Glacier Bay. For convenience of expression it is necessary to name glaciers that have now melted away or shrunk appreciably. The glacier that filled Muir Inlet was seen by Reid (1896) and termed the Muir Glacier. The Muir Glacier still exists, but is much smaller. The former glacier that earlier filled the northwest arm of Glacier Bay between Russell and Lone Islands was never named but is here termed the Russell Glacier; it issued from the Russell drainage. Observations on the distribution of erratics indicate that most of the lower bay was occupied by ice drawn from the Russell drainage only. This distribution suggests that Russell ice impeded glacial drainage from the Muir area, causing ponding and development of an icefield.

GLACIAL ERRATICS

Shorelines are tightly armored by cobbles and boulders throughout Glacier Bay and the connecting fiords and inlets. The boulders have been derived from nearby deposits of drift (deposited by the post-A.D. 1740 withdrawal of glaciers) and concentrated on the beaches by wave action, although at places in the Beardslee Islands the boulder armor represents incompletely eroded terminal moraines. Inspection of the boulder beaches reveals the presence of rocks derived from the Fairweather Range 20 to 25 miles west of Glacier Bay. The following list characterizes the principal distinctive erratics attributable to a Fairweather source:

Staurolite schist.—Gray to brown fine-grained mica schist; typically contains 2–5 percent 1-millimeter garnet euhedra and 5–15 percent 3–10-mm brown staurolite euhedra; a third or more of the staurolite crystals are twinned.

Chiastolite schist.—Identical to the staurolite schist but with 3–15 percent chiastolite instead of staurolite.

Biotite-quartz schist.—Fine- to medium-grained biotite (⅓) quartz (⅔) rock, commonly friable; particularly distinctive because of a brick-red hematitic weathering crust.

Amphibolite.—Medium to dark gray; typically with strong lineation and foliation; commonly friable.

Pyroxenite.—Yellow green to green 1-mm grained rock, generally massive but rarely with a primary planar structure; boulders are distinguished by a very smoothly abraded surface.

Gabbro.—Rusty weathering brown to black medium- to coarse-grained gabbro; some erratics show primary layering.

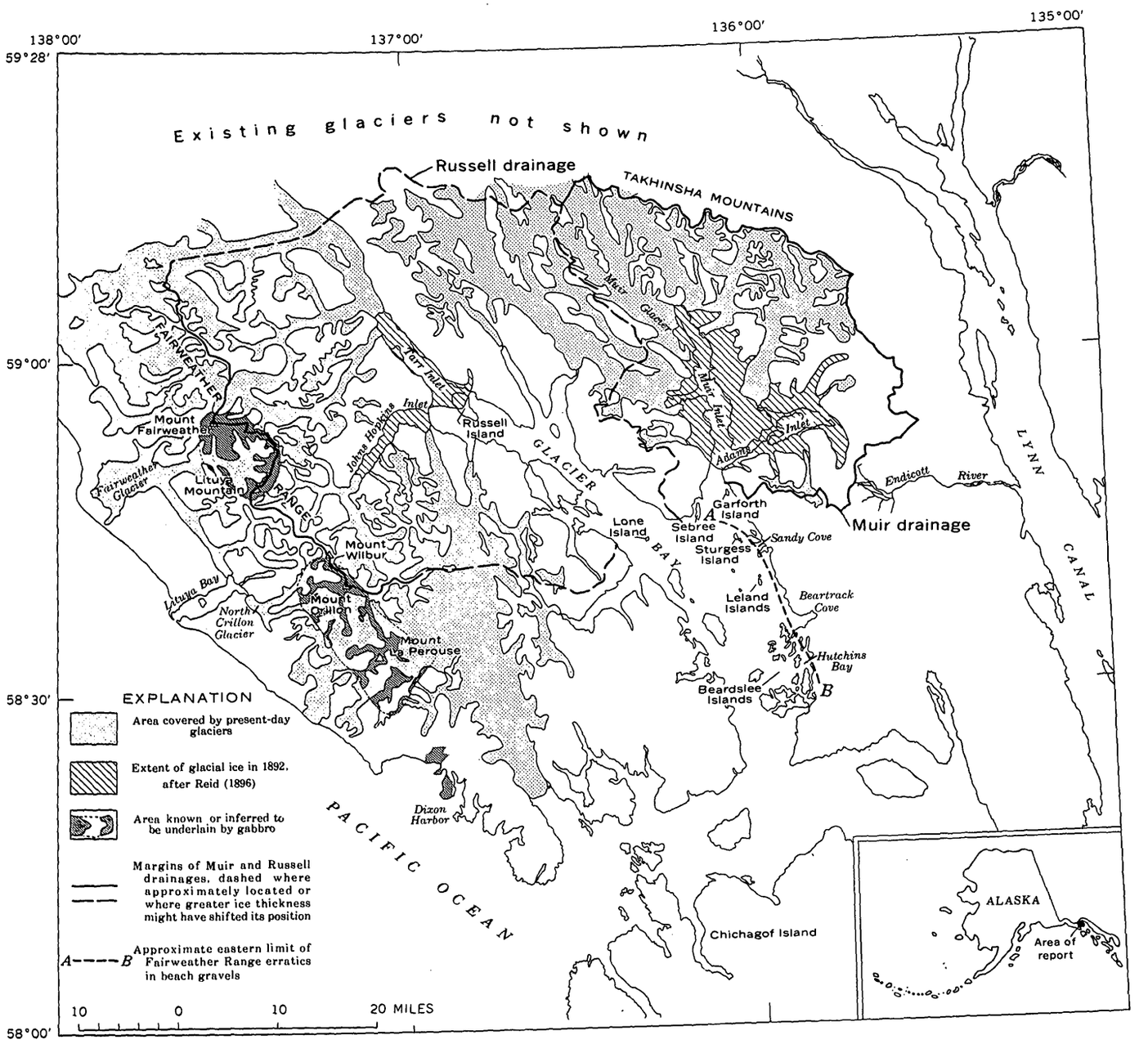

FIGURE 1.—Map of Glacier Bay region, southeastern Alaska.

Two additional types of erratics were recognized as having possible sources in the bedrock of the Johns Hopkins Inlet region:

Greenschist.—Dark- to light-green highly schistose rock; commonly with ¼- to 3-inch milky quartz veins.

Quartz monzonite.—Highly leucocratic with minor biotite or hornblende; typically unfoliated or very weakly foliated; occurs in large angular blocks having subconchoidal fracture faces.

Although the greenschist and quartz monzonite erratics compare most closely with similar bedrock in the Johns Hopkins Inlet region, minor amounts of greenschist and unfoliated granitic rock also occur in the vicinity of upper Muir Inlet (D. A. Brew and others, unpub. data).

Erratics of the crystalline rock types described above are conspicuous constituents of beach gravels in Glacier Bay everywhere west of the line *A–B* shown in figure 1. The erratics suite is totally absent along the east side of the bay between Garforth Island and Beartrack Cove. Differences in the composition of beach boulder armor are especially striking in the Sandy Cove area and in the vicinity of Hutchins Bay. In Sandy Cove, the western shores of the peninsula and the large island east of Sturgess Island exhibit abundant crystalline erratics of the types noted, whereas beach gravels on the eastern and inner shores of the cove are composed of limestone, calcareous graywacke and argillite resembling the bedrock exposed nearby. Similarly, in Hutchins Bay, crystalline erratics occur only along the western shores of the bay.

The present distribution of erratics presumably reflects the former distribution of glacial ice at about the time of the maximum recent extent of glaciers in this region (glaciers may have extended to the mouth of Glacier Bay in about A.D. 1740, according to Goldthwait, 1966, p. 8). As shown in the following paragraphs, the ice and the erratics it carried west of the line *A–B* in figure 1 had their source in the Russell drainage, and the ice and erratics east of the line *A–B* came from the Muir drainage (fig. 1).

SOURCES OF THE ERRATICS

Reconnaissance geologic mapping of the Muir Inlet–Takhinsha Mountains region (D. A. Brew and others, unpub. data) reveals no bedrock source for the relatively high grade metamorphic and mafic igneous rocks found as erratics in lower Glacier Bay; these erratics, therefore, were derived from the Russell drainage. Reconnaissance studies of the Fairweather Range suggest sources of the erratics in the region between Mount Wilbur and Mount Fairweather. Three bodies of mafic igneous rock (principally olivine gabbro) are known in the Fairweather Range (Rossman, 1963, p. 11): (1) the Astrolabe-DeLangle stock near Dixon Harbor, (2) the Crillon-LaPerouse stock which includes the mountains of the same names (also known by Kennedy and Walton, 1946, p. 70), and (3) an unnamed gabbro body in the vicinity of Lituya Mountain and Mount Fairweather known only from boulders in the moraine of the Fairweather Glacier. These areas, which are known or inferred to be underlain by the gabbros, are shown in figure 1. Layered gabbro erratics found in lower Glacier Bay could have come either from the northern part of the Crillon-LaPerouse stock or from the gabbro body of unknown extent in the vicinity of Mount Fairweather. No occurrences of pyroxenite in the Fairweather Range are noted by either Kennedy and Walton (1946) or Rossman (1963), but pyroxenite might well be expected in association with the gabbro (Williams and others, 1955, p. 80).

The high-grade metamorphic rocks found as erratics probably were derived from the contact zones of the olivine gabbros. The Crillon-LaPerouse stock intrudes actinolite, staurolite, biotite-quartz, graphite, and hornblende schists as well as amphibolite northeast of the head of Lituya Bay (Kennedy and Walton, 1946, p. 68). Rossman (1963, p. 9) reports that "amphibole and biotite schists * * * compose most of the bedded rock in the area immediately north of the North Crillon Glacier." Rossman notes further that "in areas that have recently been uncovered from beneath snow and ice, the rock [biotite schist] contains andalusite, or, less commonly, staurolite * * * accompanied by small but abundant garnets." The observations of Kennedy and Walton (1946) and Rossman (1963) pertain to the west flank of the Fairweather Range, but it is probable that rocks of similar metamorphic grade occur at many places near the intrusive contact of the gabbro. Probably, therefore, the high-grade metamorphic rocks of the erratics suite were derived from the east flank of the Fairweather Range near the contact zones of either the Crillon-LaPerouse stock or the gabbro body of unknown extent near Mount Fairweather.

DISCUSSION

The present distribution of erratics, because it reflects the former distribution of ice, provides a measure of the relative glacial discharge from each major source area. Thus it is inferred that the recent glacial ice discharge from the Russell system greatly

exceeded that of the Muir system. An effect of apparently greater discharge of the Russell system could have been produced if the western half of lower Glacier Bay were much shallower than the eastern half; in fact, however, the western half of lower Glacier Bay is deeper than the eastern half (U.S. Coast and Geodetic Survey, 1942).

That the discharge of ice from the Russell glacier exceeded that from the Muir seems surprising in view of the quantities of ice observed at lower elevations in each drainage by early scientific visitors. John Muir, who visited Glacier Bay in 1879, discovered an icefield of impressive size occupying Muir and Adams Inlets and the adjacent lowlands (Muir, 1893). H. F. Reid's topographic map (1896) shows the east-west dimensions of the icefield as 17 miles, the north-south as 14 miles; the surface lay between 1,000 and 2,000 feet above sea level over most of its extent. Reid's limits of the icefield are reproduced in figure 1. At the same time that Muir Inlet was occupied by an icefield, the valley glaciers of Tarr and Johns Hopkins Inlets had termini about 12 miles in advance of their present positions (fig. 1) (Reid, 1896; Gilbert, 1904). On the basis of maps and observations made near the end of the 19th century, therefore, it is clear that at lower elevations, the Muir drainage contained the larger amount of ice. Similar relations persist today, for valley glaciers of the Muir system are broader (fig. 1), probably deeper, and coalesced to a higher degree than valley glaciers in the Russell system.

Thus from the amounts of ice in each drainage at the end of the 19th century and today, observers might infer that glaciers of the Muir system had played the dominant role in the previous advance into lower Glacier Bay. The distribution of erratics, however, indicates otherwise. The following paragraphs explain these apparently contradictory relationships.

The hypothesis proposed is that ice drainage from the Muir region was partly or completely blocked by the relatively larger amount of ice flowing into lower Glacier Bay from the Russell drainage. Under these conditions three observed effects would be expected: (1) Ice from coalescing valley glaciers would form a large icefield. Reid's (1896) map of this icefield has already been noted (fig. 1). (2) Glaciers would seek other exits. Reid's (1896) map portrays a lobe of the Adams icefield extending southeastward into the valley of the Endicott River (fig. 1). (3) Recession of the Muir Glacier would lag behind that of the Russell glacier after recession had reached the junction of the two ice streams.

According to Lawrence (1958, fig. 6, p. 98), the Muir glacier and ice from the northwest arm of Glacier Bay (Russell glacier of this report) separated by 1860; between 1860 and 1899, the Muir retreated about 5 miles while the ice in the northwest arm of Glacier Bay retreated about 22 miles. Rapid recession of the Muir Glacier began only after 1899 (Field, 1947). These effects, which are consistent with the hypothesis of impeded drainage, are also consistent with a hypothesis of snow nourishment in the Muir drainage greater than in the Russell drainage. But if this were the case, it might normally be expected that glaciers would have advanced into Muir Inlet earlier than the Russell glacier would have advanced southward into the northwest arm of Glacier Bay. Goldthwait (1963, p. 42–43; 1966, p. 7–8), however, using carbon-14 dates, argues that glaciers advanced into Muir Inlet from the north and west at a later date than the time at which ice from the northwest arm of Glacier Bay (Russell glacier of this report) dammed the mouth of Muir Inlet and produced the lakes in which the late Wisconsin lacustrine member of the Van Horn Formation of Haselton (1966) was deposited. Thus, the hypothesis remains tenable that the large accumulation of glacial ice in the Muir area was the result of impeded drainage. Possibly also, the large amount of glacial ice present there today (1967) is chiefly relict, reflecting a former strongly positive accumulation caused by the partly or completely ponded drainage.

REFERENCES

Cooper, W. S., 1923, The interglacial forests of Glacier Bay: Ecology, v. 4, p. 93–128.

Field, W. O., Jr., 1947, Glacier recession in Muir Inlet, Glacier Bay, Alaska: Geog. Review, v. 37, p. 369–399.

Gilbert, G. K., 1904, Glaciers and glaciation of Alaska, *in* Harriman Alaska expedition, v. 3: New York, Doubleday, Page and Co., p. 16–39.

Goldthwait, R. P., 1963, Dating the little ice age in Glacier Bay, Alaska: Internat. Geol. Cong. 21st, Norden 1960, Sess. rept., pt. 27, p. 37–46.

———1966, Glacial history; *in* Mirsky, Arthur, ed., Soil development and ecological succession in a deglaciated area of Muir Inlet, southeast Alaska: The Ohio State Univ. Inst. Polar Studies, Rept. 20, p. 1–17.

Haselton, G. M., 1966, Glacial geology of Muir Inlet, southeast Alaska: The Ohio State Univ. Inst. Polar Studies, Rept. 18. 34 p.

Kennedy, G. C., and Walton, M. S., Jr., 1946, Geology and associated mineral deposits of some ultrabasic rock bodies in southeastern Alaska: U.S. Geol. Survey Bull. 957–D, p. 65–84.

Klotz, O. J., 1899, Notes on glaciers of southeastern Alaska and adjoining territory: Geog. Jour., v. 14, p. 523–534.

Lawrence, D. B., 1958, Glaciers and vegetation in southeastern Alaska: Am. Scientist, v. 46, p. 89–122.

Muir, John, 1893, Alaska: Am. Geologist, v. 11, p. 287–299.

Reid, H. F., 1896, Glacier Bay and its glaciers: U.S. Geol. Survey 16th Ann. Rept., 1894–95, pt. 1, p. 415–461.

Rossman, D. L., 1963, Geology and petrology of two stocks of layered gabbro in the Fairweather Range, Alaska: U.S. Geol. Survey Bull. 1121–F, 50 p.

U.S. Coast and Geodetic Survey, 1942, Hydrographic chart of Glacier Bay: Chart 8306, 4th ed.

Williams, Howel, Turner, F. J., and Gilbert, C. M., 1954, Petrography: San Francisco, W. H. Freeman and Co., 406 p.

UPPER PLEISTOCENE FEATURES IN THE BERING STRAIT AREA

By C. L. SAINSBURY, Denver, Colo.

Abstract.—New data on upper Pleistocene deposits east of Bering Strait may solve some problems of correlation. Erratics (Skull Creek erratics) of a widespread pre-Wisconsin glaciation are now recognized; the east limit of the early Wisconsin York Glaciation is defined, as is the northwest limit of Wisconsin glaciers from the Kigluaik Mountains. An anomalous glacial pattern is shown for two adjacent ranges (York and Kigluaik Mountains) and existing glacial correlations are refined. The barrier bar along the northwest coast of Seward Peninsula is migrating landward rapidly. Local destruction of marine terraces of Yarmouth(?) and Sangamon age can be explained by glaciation and dune migration.

Continuing fieldwork on the western Seward Peninsula (fig. 1) has given much additional information on the upper Pleistocene features and deposits. The new information gives additional support to conclusions already presented (Sainsbury 1965) and leads to new conclusions that support earlier ideas (Hopkins and others, 1960). This paper contains more evidence supporting the proposed former existence of two glaciations (York and Mint River) of Wisconsin age, names a Recent glaciation (Esch Creek), and names erratics (Skull Creek) of a widespread glaciation of pre-Wisconsin age. It shows that the Pleistocene features may be traced eastward into the Grantley Harbor area, where important placer gold deposits occur. It further points out that the postulated Wisconsin glacial histories of the two main mountain ranges of the western Seward Peninsula (York and Kigluaik) differ substantially, which leads to the conclusion that either the postulated history is in error or that a very anomalous pattern of glaciation existed.

Acknowledgments.—The author is indebted to D. M. Hopkins and D. S. McCulloch for helpful reviews of this paper. During 1966, Hopkins spent three days in the field, during which time the marine deposits at California River were jointly examined, and other upper Pleistocene features and problems were discussed.

GENERAL GEOLOGY OF THE YORK MOUNTAINS

The general geology of the area is particularly favorable to the analyses of glacial advances by tracing erratics and by studying juxtaposition of moraines and marine strandlines. The entire western Seward Peninsula consists of but three main types of sedimentary rocks, and two highly contrasting types of plutonic rocks. The highest hills (York Mountains) from which the ice advanced northward over the lowlands are composed of fossiliferous limestone, whereas the wide lowlands are underlain entirely by slates, dark phyllites, and schistose argillaceous limestone; this situation allows easy recognition of erratic boulders and their source areas.

The highest peak in the York Mountains is Brooks Mountain, a 2,898 foot-high very coarsely porphyritic biotite granite stock about a mile across surrounded by calc-silicate rock and biotite-andalusite hornfels. It is the only such stock in the York Mountains. Because the main ice sheet in Wisconsin time centered on Brooks Mountain and flowed east, north, and south from it, an uninterrupted train of distinctively diverse erratics (porphyritic granite, hornfels, and limestone) marks the course of glaciers outward from the mountains and across the slate areas. Moreover, the area is a sparsely vegetated tundra where most hills higher than a few hundred feet are completely barren. On these hills, glacial erratics (especially of granite and tactite) are easily discerned. In the lowlands north of the mountains, several rivers have many cutbacks that show complete sections; and along the coastline to the south, marine erosion is exposing the old terrace deposits and valley fill and provides excellent exposures of all deposits younger than Sangamon (Pelukian transgression of Hopkins and others, 1960).

U.S. GEOL. SURVEY PROF. PAPER 575-D, PAGES D203-D213

269-274 O—67——14

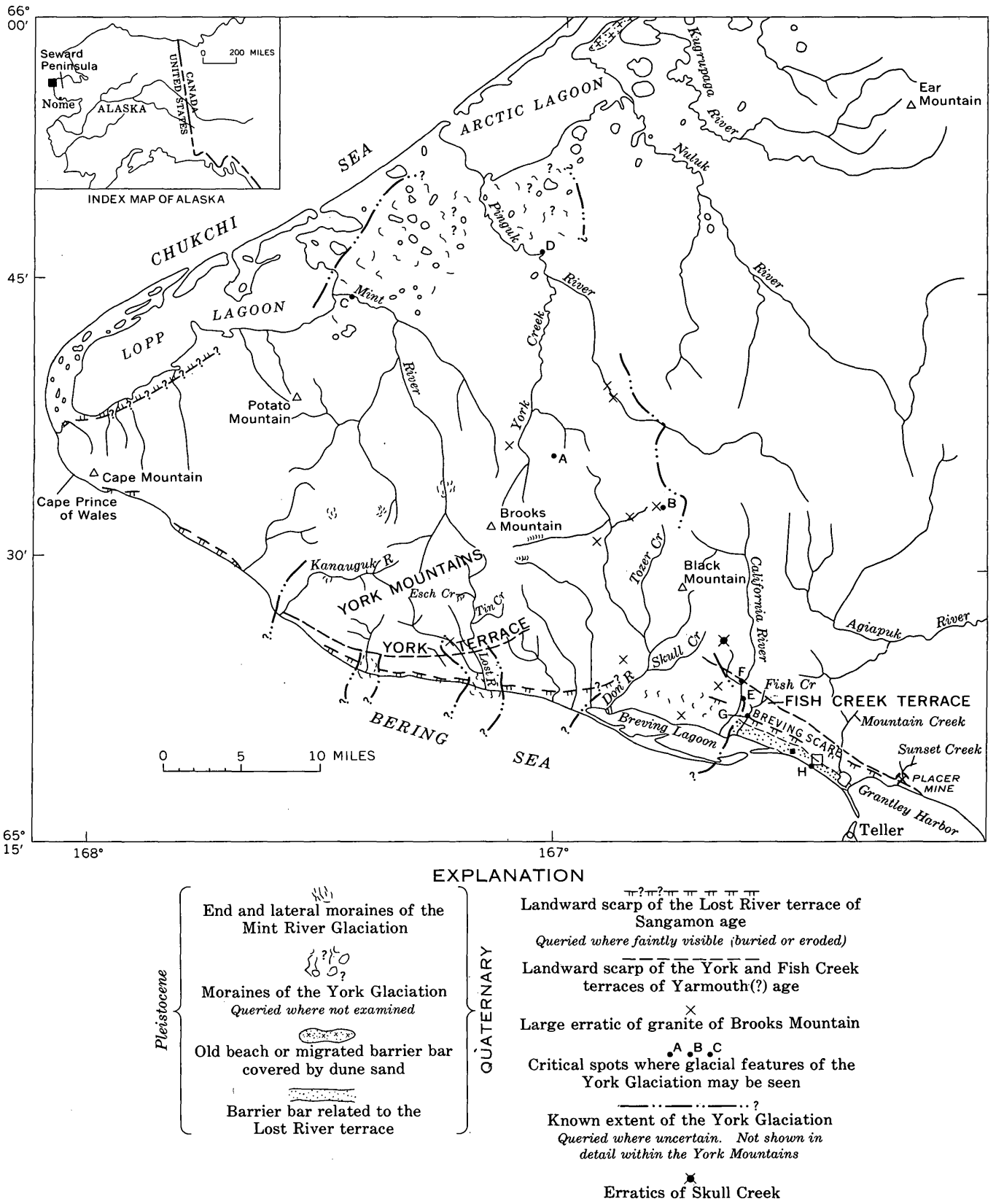

EXPLANATION

Pleistocene

End and lateral moraines of the Mint River Glaciation

Moraines of the York Glaciation
Queried where not examined

Old beach or migrated barrier bar covered by dune sand

Barrier bar related to the Lost River terrace

QUATERNARY

Landward scarp of the Lost River terrace of Sangamon age
Queried where faintly visible (buried or eroded)

Landward scarp of the York and Fish Creek terraces of Yarmouth(?) age

Large erratic of granite of Brooks Mountain

A B C
Critical spots where glacial features of the York Glaciation may be seen

Known extent of the York Glaciation
Queried where uncertain. Not shown in detail within the York Mountains

Erratics of Skull Creek

FIGURE 1.—Map of the western Seward Peninsula, Alaska, showing the upper Pleistocene features discussed in this report.

THE MARINE PLATFORM

Interrelations between glaciations and marine transgressions are well displayed in the Bering Strait region, where two distinct and extensive marine terraces are locally covered by glacial deposits. The older terrace of probable Yarmouth age (Sainsbury, 1965a), an elevated marine platform extending unbroken along the south side of the York Mountains for about 20 miles, is notched on its seaward side by the younger Lost River terrace of Sangamon age which extends east and west of the York (fig. 1). The York terrace was uplifted some 400 feet and gently warped after Yarmouth time; the Lost River terrace is undeformed, and its planed rock surface generally stands between 10 and 20 feet above sea level. A remnant of the York terrace is preserved at Cape Mountain on the Bering Sea (fig. 1) at an altitude of about 500 feet, showing that late Pleistocene uplift of several hundred feet extended into the Bering Strait. Hence, it is probable that during most of the Pleistocene prior to the uplift in late Pleistocene time, the Bering Strait was a seaway rather than a land bridge, as has been postulated by many workers.

GLACIATION REPRESENTED BY THE SKULL CREEK ERRATICS

Fieldwork in 1966 resulted in the recognition of erratics on hilltops near but several hundred feet higher than the terminal moraines of the York Glaciation (large dot and cross, fig. 1). The erratics lie in a saddle at an altitude of 770 feet in limestone hills west of the California River and east of Skull Creek (Teller B–4 quadrangle). Terminal moraines and drift of the York Glaciation mantle the lower slopes of the hills on the south side, reaching a maximum altitude of 250 feet. The high-level erratics consist of angular plates of biotite-andalusite hornfels, presumably from the hornfels zone around the biotite granite of Black Mountain, 5 miles northwest (fig. 1). Nowhere do they form a veneer, and hence they are not a mappable unit. Ice that overrode the saddle would have been unconfined ice several hundred feet thicker than the ice that left the lower moraines, and would, therefore, have extended much farther seaward than the ice of the York Glaciation. Significantly, the direction of ice movement was to the southeast, and the ice, therefore, may have been centered over Brooks Mountain, as was ice of the York Glaciation. The earlier glaciation is not named, but the erratics left by it are referred to as the Skull Creek erratics.

The earlier glaciation predates the Lost River terrace of Sangamon age (if not, drift would have buried the scarp and terrace deposits of that age beyond the limits of the York Glaciation, which it did not do). Unless the scattered cobbles which lie upon the York and Fish Creek terraces, and which are best explained as of marine origin, are in reality drift of the early glaciation, the early glaciation may be pre-Yarmouth in age (for example, it did not mantle the Yarmouth age terrace with drift). If the scattered cobbles on the York terrace are Skull Creek erratics, they may be correlative with an ancient (drift of pre-Illinoian? or early multistage Illinoian? age) glaciation in the Kobuk River area some 300 miles northeast (Fernald, 1964, p. K6; McCulloch, 1965). It is probable that rounded topography impressed on the hills between the western end of the York Mountains and Cape Mountain, and which the writer believes is ice-scoured topography, is correlative with this early glaciation. Pending proof of greater age, the Skull Creek erratics are here considered to be of pre-Wisconsin age, possibly Illinoian. No moraines or till of this glaciation are known, and the evidence for its former existence is the ice-rounded topography and the scattered erratics of hornfels at Skull Creek.[1]

GLACIATIONS OF WISCONSIN AGE

In the western Seward Peninsula, Sainsbury (1965b) has recognized and named two glaciations of Wisconsin age, principally on the basis of a study of the central York Mountains. New work proves that the York Glaciation of early Wisconsin age was centered over the York Mountains (fig. 1). Its ice spread north of the mountains for at least 20 miles, where the ice formed a thick piedmont lobe covering at least several hundred square miles and left moraines that obliterated the Lost River terrace at the present shoreline of the Chukchi Sea. Valley glaciers penetrated south of the mountains only along the major valleys, where they left moraine and outwash over the marine terraces.

After retreat of the York Glaciation, and before the maximum advance of the Mint River glaciers, large alluvial fans and talus cones were built outward into the main glaciated valleys. On the south side of the York Mountains, where no glaciers formed during the Mint River Glaciation, valley fills as much as 100 feet deep were deposited locally; these fills were subsequently trenched deeply by streams.

The Mint River Glaciation, of late Wisconsin age,

[1] High-level erratics were found in 1967 on mountaintops 75 miles east of the York Mountains, and indicate that ice from an unknown source (probably an icecap) flowed south from the Chukchi Sea and overrode this part of the Seward Peninsula. The erratics are correlated with the Skull Creek erratics.

was restricted to north- or west-facing valleys in the York Mountains, and both terminal and lateral moraines are well preserved. Ice flowed down main valleys as much as several miles from cirques, but did not coalesce into piedmont lobes. The larger moraines are shown on figure 1.

A third glaciation is here named the Esch Creek Glaciation from the well-defined moraine at the type locality which is in the large cirque in the headwaters of Esch Creek, a tributary of Lost River. It is presumed to be of Recent age because the moraines lie in or near cirques. The moraines consist entirely of limestone; they are practically undissected and are enclosed by modified end moraines (probably Mint River) about 1 mile downstream.

The Esch Creek Glaciation moraines lie on broken bedrock and have only scattered patches of tundra grass on top. The moraine at the type locality is confined to the cirque and extends only about half a mile from the headwall. During the Esch Creek Glaciation, ice was confined entirely to high-level cirques facing north in the central York Mountains. A large cirque on the southwest shoulder of Brooks Mountain that heads against a ridge 1,400 feet high was extensively glaciated during the Mint River Glaciation, but not during the Esch Creek Glaciation, showing that the perennial snowline was higher during the Esch Creek Glaciation. Most cirques that were ice filled during the Esch Creek Glaciation head against ridges exceeding 1,700 feet in altitude.

CRITICAL POINTS OF OBSERVATION OF THE YORK GLACIATION

Because the moraines of the York Glaciation are not easily observed in the lowlands along the northwestern Seward Peninsula, and because the restricted moraines south of the York Mountains give no clue to the former great extent of ice north and west of the mountains, specific localities that disclose critical relations are marked on figure 1 (points A to E) and are briefly discussed here. The absence of large moraines of the York Glaciation in the York Mountains may be explained by the fact that almost all the bedrock north of the ridge line of the mountains was buried by ice, which probably accounts for a small accumulation of morainal material and, consequently, restricted terminal moraines. Moraines are noticeable only at the extreme terminus and along glaciated valleys on the south side of the mountains, where well-defined terminal and ground moraine is preserved and still contains closed depressions and pools that form subdued hummock and kettle topography. Some of the critical points of observation used to establish the age and extent of the York Glaciation are discussed below (fig. 1).

At point A, at an altitude of 1,050 feet on the northwest shoulder of a rounded mountain on the extreme north front of the York Mountains, scoured and grooved limestone is exposed in several places. Near the grooved limestone are widely scattered erratics of tactite and gravels of polished quartz. The limestone has been exposed since the retreat of the ice. The erratics are from Brooks Mountain, some 7 miles to the southwest. Polished quartz pebbles, which extend to an altitude of 1,250 feet on the adjacent hill and are also foreign to the area, are waterworn—presumably in subglacial streams. The exposures prove (1) that ice no longer confined to valleys was almost 1,000 feet thick along the north front of the mountains and (2) that the ice sheet was Wisconsin in age, for it is inconceivable that glacially grooved limestone continuously exposed could have survived from Illinoian time or ice sheets of an earlier time.

At point B, at an altitude of 470 feet in the low rounded divide between the Don River and Tozer Creek, a cutbank exposes numerous large boulders, some faceted, of granite from Brooks Mountain in a till-like matrix. The exposure proves that ice from Brooks Mountain, 12 miles west, moved upvalley along the Don River and its tributaries for several miles, and that it crossed the divide.

At point C (figs. 1, 2), a high cutbank on the south bank of the Mint River, glacial till containing polished and striated cobbles overlain by shingled outwash gravels and loess is exposed at river level (altitude about 20 feet). The exposure is in a large area of low hummocky hills and many lakes where the Lost River terrace has been obliterated. The hummocky topography extends some 15 miles northeast to the Pinguk River, and several miles southwest. Numerous peat bogs and filled lakes are interspersed among the lakes between hummocks, and drainage is poor. Many of the morainal hills are notched by river terraces indicating widespread fluvial action unrelated to the present drainage, probably during retreat of the ice. The exposure proves (1) that ice moved at least 20 miles north from its source area in the York Mountains and formed a large piedmont sheet, and (2) that, on the basis of all existing evidence, the moraine obliterated the Lost River terrace, and hence is Wisconsin in age.

The relations at point D, a high cutbank on the northeast side of the Pinguk River in an area of low

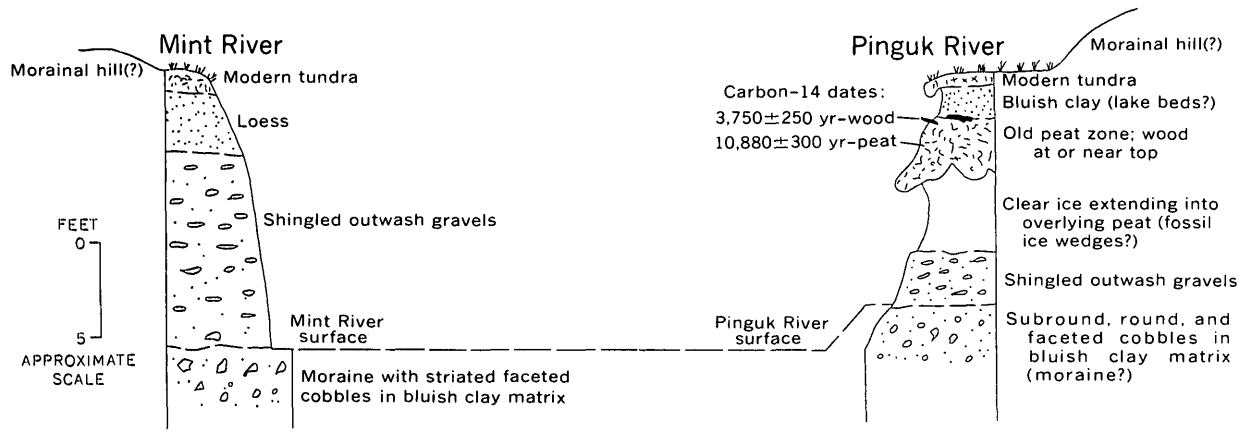

FIGURE 2.—Sections exposed in cutbanks on the Mint (*C*, fig. 1) and Pinguk (*D*, fig. 1) Rivers.

hummocks and lakes, are shown in figure 2. The shingled gravels at the base of the cutbank are similar to those above the till in the cutbank on the Mint River, and are considered to be outwash gravel. The underlying material containing faceted cobbles in a clayey matrix is believed to be moraine. From the air, it can be seen that the cutbank is near the edge of an old flat surface that lies between low hummocky hills, covered by thick tundra, and the Mint River. This surface could be either an old filled lake or a high-level terrace, but is more probably a filled lake.

Wood and peat from the cutbank were dated by the carbon-14 method by Meyer Rubin, U.S. Geological Survey radiocarbon laboratory, to establish the youngest possible age for the outwash gravels (fig. 2). The peat, consisting of grasses and sedges, proved to be 10,880 ± 300 years old, and the wood, 3 feet higher in the section, is 3,750 ± 250 years old (U.S. Geol. Survey Nos. W–1776 and W–1773.) The sequence is interpreted to show (1) the advance of glaciers of the York Glaciation, (2) retreat of the ice and modification of the moraine by fluvial action, or advance of the glaciers of the Mint River Glaciation and deposition of outwash gravel, (3) formation of the peat zone on a bench about 10,000 years ago, (4) increase of water, possibly by blocking of subsurface drainage by permafrost, which created a small lake having a growth of woody shrubs on its banks some 3,750 years ago, and (5) formation of the modern tundra after the lake was filled or was drained by erosion by the Pinguk River.

At point E, a cutbank on the east bank of the California River, angular and faceted cobbles in a blue clay matrix can be recovered by digging with a shovel below river level. The faceted cobbles and the resemblance of the matrix to the clay-matrix till containing striated cobbles on the Mint River, suggest that the material is moraine. This is the most easterly point at which morainal material has been found; significantly, it also marks the eastern margin where the Lost River terrace of Sangamon age has been obliterated. From here eastward to Grantley Harbor, the Pelukian transgression strandline (Lost River terrace) and a corresponding offshore barrier bar are continuously exposed in the present seacliffs (fig. 1.). West of the California River, hummocky topography extends west to the Don River, and moraine is exposed locally in frost boils and along the beach of Breving Lagoon. Observations of the above localities are convincing evidence of the wide extent of ice during the York Glaciation of early Wisconsin age.

DESTRUCTION OF THE YORK TERRACE

The excellent state of preservation of the York terrace along the south front of the York Mountains leads one to seek an explanation for its absence elsewhere. Along the south front of the peninsula, absence of parts of the terrace can be correlated with soft bedrock (slate), for example, in the area west of the Kanauguk River, and between the Don and California Rivers. Its complete absence along the north side of the peninsula cannot be so explained, and leads to the conclusion either that the terrace never existed (unlikely), or that it has been totally destroyed by processes of erosion which did not operate south of the mountains.

Two explanations for the situation above are that (1) a much wider distribution of ice on the north side of the mountains existed during both the early glaciation represented by the Skull Creek erratics and the York Glaciation, and (2) increased erosion was caused

by heavier snowfall and later runoff. Without question, the York Glaciation was much more widespread north of the mountains, for ice reached almost to the present shoreline of the Chukchi Sea, some 25 miles north of its source at Brooks Mountain, whereas it penetrated south of the mountains only along low passes or around the west end where coalescing valley glaciers probably formed a piedmont lobe. On the basis of (1) the absence of moraine at most places on the York terrace, and (2) the undissected surface of the terrace, one can conclude that the York terrace south of the mountains was not covered by ice that left the Skull Creek erratics or ice of the York Glaciation. Therefore, the York terrace north of the mountains probably has been eroded principally by glacial scouring during two widespread glaciations.

At present, snowfall north of the mountains seems both to be heavier, and to last longer, than to the south. From several years of personal observation, it can be stated that deep snow persists about a month longer on the north side of the mountains. During this critical period, seasonal frost thaws and the runoff from melting snow removes the soil more effectively than the snowmelt while seasonal frost persists. This process could have contributed in a minor way to erosion of the York terrace north of the mountains.

Incidentally, we should note the possibility that ice from the Chukotsky Peninsula in Siberia may have pushed southeast through the Bering Strait to meet ice flowing north from the York Mountain and forcing an unusually thick accumulation of ice along the northwestern Seward Peninsula. Reliable information on the eastward extent of ice from the Chukotsky Peninsula is lacking. The sampling methods used by marine geologists and oceanographers (Creager and McManus, 1965) have not been capable of recovering glacial till buried by upper Pleistocene and Recent sediments in the Bering Strait regions. For example, a coring device would have to penetrate as much as 30 feet of Recent sediments, several feet of silt, and several feet of outwash gravels (as shown in fig. 2) before entering till recognized as such only by its content of straited and faceted cobbles. Statements have been made denying the existence of glacial deposits in the Bering Strait areas because piston core samplers neither reached bedrock nor recovered glacial material similar to that exposed near the present shoreline. These statements may be wrong, for they are based on nondefinitive data. Moreover, D. M. Hopkins (oral commun., 1967) stated that divers from the Navy Electronics Laboratory observed striated bedrock off Cape Prince of Wales in 1966, a fact which strongly suggests the possibility of glacial scouring in the Bering Strait.

DESTRUCTION OF THE LOST RIVER TERRACE BY GLACIATION

From figure 1, it is seen that proven or probable till exists in the areas where the Lost River terrace disappears as a distinct topographic feature. At several places, this till (or outwash gravel) is exposed where it overlies the marine platform of the terrace. In areas beyond the probable termini of the glaciers of the York Glaciation, the Lost River terrace is preserved, or obscured by other processes presently operative in the area, for example, dune migration.

POSSIBLE DESTRUCTION OF THE LOST RIVER TERRACE BY DUNE MIGRATION

Between the Kugrupaga River (fig. 1) and Shishmaref (fig. 3), on the offshore barrier bar, there is an extensive lowland with numerous low hummocky hills, many of which are elongated parallel to the coastline.

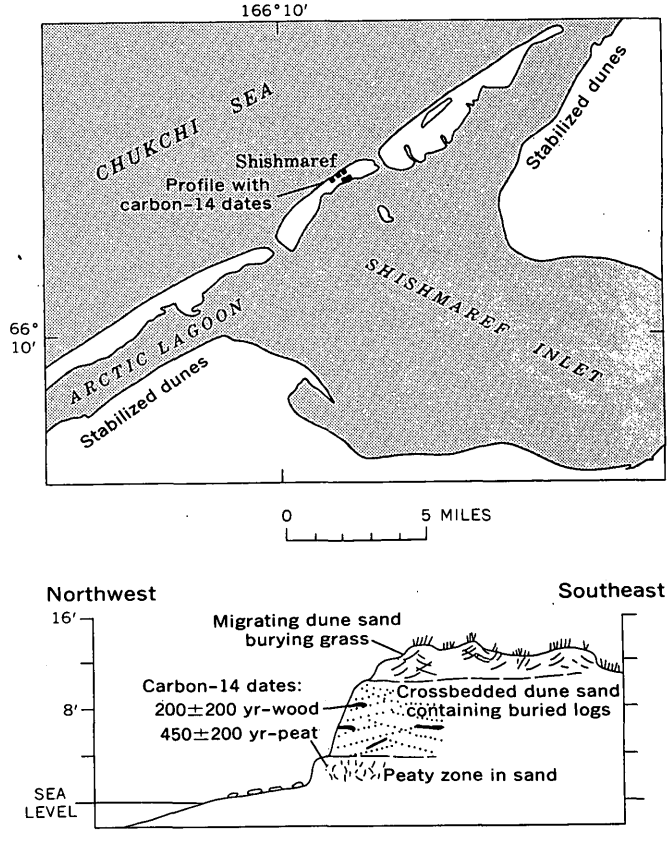

FIGURE 3.—Shishmaref Inlet, and section along modern beach.

Low-level aerial reconnaissance disclosed that most of the trenched hills are composed of stratified sand; some have gravels at the base. These hummocks probably are mostly sand dunes that have been stabilized by tundra, and it is entirely possible that in this area the Lost River terrace was obliterated by migrating sand dunes rather than by glaciation, or alternatively, that moraine is present but covered by dune sand.

Between Shishmaref Inlet (fig. 3) and Arctic Lagoon, an ancient barrier bar composed principally of sand extends along the mainland side of Arctic Lagoon for 12 miles (fig. 1). Because the ancient barrier bar is composed principally of sand, it probably originated by shoreward migration of dune sand on a barrier bar, as is happening to the present barrier bar. This modern bar is about 0.5 mile wide at Shishmaref (fig. 3), and it is migrating landward rapidly. The Eskimos at Shishmaref say that "about 50 feet" disappear from the front of the bar each year (Walter Noyapuk, oral commun., 1965). A cross section of this bar as exposed along the beach southwest of Shishmaref shows logs in dune sand above a peat zone buried beneath cross-bedded dune sand (fig. 3); radiocarbon dating shows the peat to be only 450±200 years old and the logs 200±200 years (U.S. Geol. Survey Nos. W–1778 and W–1771). As the peat and wood represent backslope tundra and beachwood buried by migrating dune sand, it is concluded that the beach is migrating landward at the rate of at least half a mile (the width of the bar) in a few hundred years.

TERRACES EAST OF THE CALIFORNIA RIVER

Two terraces extend east from the California River to Grantley Harbor (fig. 1). The lower terrace can be correlated confidently with the Lost River terrace, but the upper terrace lies well below the York terrace, and has a canyon cut into it that is filled with marine and continental gravels. The higher terrace, which has its landward scarp at an altitude of about 350 feet, as opposed to about 650 feet for the York terrace, is here named the Fish Creek terrace. The lower terrace, here correlated with the Lost River terrace of Sangamon age, is composite, and consists of an outer gravelly barrier bar generally below 80 feet in altitude; it contains numerous fragments of marine shells, and it has an inner scarp, here termed the Breving Scarp, which lies below about 100 feet in altitude. Where exposed along Fish Creek (*G* on fig. 1), the Breving Scarp truncates bedrock. Seaward of the scarp, ground level slopes gently seaward for about a mile, then rises toward the barrier bar. Bedrock is beneath stream level in this area, and is buried by dark, organic-rich muck and silt. The surface expression is that of either an old filled-in lake or a lagoon. Both the scarp and the barrier bar can be traced eastward almost to the modern beach at Grantley Harbor (fig. 1).

The Fish Creek terrace has a bare rock surface sloping up landward at about 100 feet per mile from where it is truncated by the Breving Scarp, and its slope steepens abruptly at about 350 feet altitude. Boulders, angular cobbles, and pebbles of rocks of lithology foreign to the area lie scattered on the terrace surface where bedrock is exposed. At an altitude of about 150 feet in Fish Creek valley, 1.2 miles landward of the Breving Scarp, marine gravels containing large rounded boulders of lava are well exposed, and lie in the streambed below the level of the terrace surface. The marine gravels are not continuous with the marine gravels of the Lost River terrace. The sloping surface of the Fish Creek terrace and the landward slope break can be traced eastward to Mountain Creek (fig. 1), where an abrupt change in bedrock lithology occurs along a fault trending up Mountain Creek. Quartz-mica schists of greenish cast that crop out east of the fault are faulted against the argillaceous limestones to the west. The terrace can be traced east of the fault, but owing to the more rapid weathering of the schist, the hills are lower and more rounded, and the landward scarp is subdued. The terrace ends about a mile east of Sunset Creek where the inner scarp intersects Grantley Harbor. There is no suggestion of the terrace on the south shore of Grantley Harbor.

Owing to the lower altitude of Fish Creek terrace, and the occurrence of marine deposits in a canyon cut into it, the Fish Creek terrace cannot be positively correlated with the York terrace, although additional study probably will prove it to be the same surface but at a lower altitude.

MARINE DEPOSITS IN CANYON OF THE CALIFORNIA RIVER IN FISH CREEK TERRACE

A complex sedimentary fill of a canyon that is cut into the Fish Creek terrace is well exposed on the west bank of the California River where the river issues from the mountains at a point 4 miles from Breving Lagoon. The deposits (fig. 4) consist of wood- and shell-bearing beach deposits which enclose a wedge of conglomerate of continental origin, and which is overlain by thin deposits that contain angular to rounded erratic boulders and cobbles of glacial origin (York

Glaciation). The slopewash conglomerate contains the same lithologies as lithified continental conglomerates that occur on the York terrace to the west (Sainsbury, 1965a). The base of the marine gravels on the California River is below the level of bedrock exposed a few hundred yards downstream, a fact which shows that the gravels were deposited in a canyon trenched below the level of the Fish Creek terrace.

The exposures imply the following sequence of events, oldest first:

1. Cutting of the marine platform represented by the Fish Creek terrace; or, uplift of an older terrace (or eustatic lowering of the sea) and trenching of the terrace by the California River.
2. Rise of sea level and deposition of marine deposits.
3. Temporary lowering of sea level and encroachment of a wedge of nonmarine gravel of local origin.
4. Rise of sea level and final cutting of the seacliff, deposition of the upper marine gravels, and then lowering of sea level.
5. Advance of glaciers of the York Glaciation.
6. Trenching of the valley fill by the modern stream.

The age of the marine deposits in the California River is not certain. No diagnostic fossils were recovered, although a carbon-14 age date on the wood gave the age as greater than 35,000 years (U.S. Geol. Survey No. W–1984). Furthermore, there are not sufficient exposures to prove whether the Fish Creek terrace was originally a continuous surface that was trenched by the California River, or whether a canyon existed prior to cutting of the Fish Creek terrace and was filled by deposition of the marine gravels. The lapping of beach gravels toward the old seacliffs (fig. 4) suggests that the upper gravels were deposited during the final cutting of the terrace. The glacial deposits which overlie the marine deposits prove that the marine gravels are older than the York Glaciation of early Wisconsin age. The fact that the Breving Scarp of probable Sangamon age bevels the Fish Creek terrace suggests a pre-Sangamon age for the gravels. In this report, these marine deposits in the California River are dated only as probably pre-Sangamon. If the Fish Creek terrace is correlative with the York terrace, the deposits may be as old as Yarmouth(?). Whatever their age, the deposits show a two-stage sea-level stand separated by a time interval of unknown, but probably short, length.

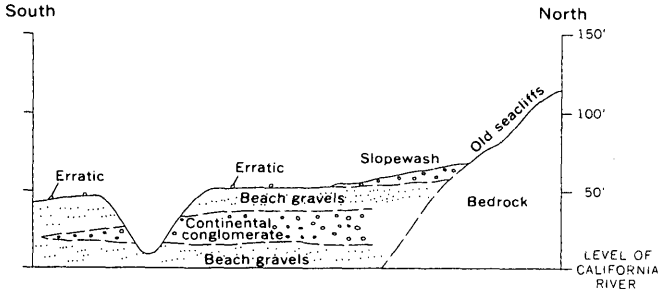

FIGURE 4.—Marine and continental gravels on west side of the California River.

SUNSET CREEK PLACER GOLD DEPOSIT

Near the east end of the Fish Creek terrace on Sunset Creek is a gold placer deposit (fig. 1). It is the most westerly one in a large and important field of gold deposits on the western Seward Peninsula (Brooks and others, 1901). It extends upstream and downstream from the old slope break of the modified seacliffs of the Fish Creek terrace, where deposition occurs because of reduced stream gradient. Greenschists east of the fault along Mountain Creek contain numerous small gold-bearing quartz veinlets, which, on weathering, provide the gold for the placer deposits.

PROBLEMS AND CORRELATIONS

Several problems remain unsolved relative to the late Pleistocene history of the western Seward Peninsula, as summarized below:

1. Age and extent of the glaciation that left the Skull Creek erratics.
2. Age of the marine gravels filling the canyon of the California River, and in upper Fish Creek.
3. Correlation of glacial advances in the York Mountains and the Kigluaik Mountains.

The first can be solved only by considerably more fieldwork in adjacent areas, but the glaciation that left the Skull Creek erratics obviously was widespread. It is perhaps worthwhile to note here that evidence is accumulating in widely separated areas of northwestern Alaska that suggests a very widespread glaciation of pre-Wisconsin age. This glaciation is represented by the unnamed pre-Illinoian glaciation of Fernald (1964, p. K6) in the Kobuk, by the Skull Creek erratics of the writer, and by permissive evidence of glaciation of pre-Sangamon age in the Cape Thompson area (Sainsbury and others, 1965, p. 241–244). Fernald (1964, p. K6) cautiously suggests that his glaciation was "perhaps of ice-cap proportions," Sainsbury and others (1965, p. 244) cautiously suggest that ice from an unknown source may have blocked drainage in lowland areas not formerly considered as glaciated in the Cape Thompson area (although the topography looks ice-scoured to the writer). Also, they suggest that the glaciation that left the Skull Creek erratics must have extended over lowlands far beyond the limits of the York Glaciation which itself was of much greater

extent than postulated recently by Péwé and others (1965). It is perhaps time to state not so cautiously that an icecap may have existed over much of northwestern and northern Alaska.[2] Absolute age dates for the shells in the marine deposits in the California River will give additional information on the age of the deposits.

Correlation of glacial advances between the York and Kigluaik Mountains still presents problems, the major one being the single glaciation of Wisconsin age in the Kigluaiks. Elsewhere in northwestern Alaska, two glaciations of Wisconsin age are recognized (Fernald, 1964, p. K12–K16). If there is a single Wisconsin glaciation in the Kigluaik Mountains, then a very anomalous glacial pattern exists between two adjacent ranges on the Seward Peninsula.

The writer and D. M. Hopkins spent a few days in 1966 in an attempt to resolve the question. With the new information presented here, and the benefit of mutual discussion, the following explanations of the problem were considered:

1. Instead of being of Sangamon age, the Lost River terrace is older and the York drift therefore is older.
2. A drift of early Wisconsin age is present but unrecognized in the Kigluaik Mountains.
3. The glaciation of early Wisconsin age did not extend beyond the limits of the Salmon Lake Glaciation, and hence is everywhere covered by Salmon Lake drift.
4. The Salmon Lake drift can be subdivided into drifts of early and late Wisconsin ages.

The facts warrant agreement on several of these points as follows:

1. The Lost River terrace almost certainly is of Sangamon age, and the terminal moraines of the York Glaciation definitely have covered the terrace and are, therefore, younger and hence Wisconsin.

[2] For additional evidence of this icecap, see footnote 1 on p. D205.

TABLE 1.—*Correlation chart for upper Pleistocene features and events in the Seward Peninsula–Bering Strait–Kobuk area, Alaska*

Age		York Mountains (Sainsbury, this paper)	Kigluaik Mountains (Hopkins and other, 1960)	Central Kobuk region and Baldwin Peninsula (Fernald, 1964; McCulloh, 1965)
Recent		Protalus ramparts		Modern glaciers and recessional moraines in Schwatke Mountains
		Esch Creek Glaciation	Mount Osborn Glaciation	Ulaneak Creek Glaciation
——?——?——		——?——?——?——?——?——?——	?—?—?—?—?—?—?—?—?—	——?——?——?——?——?——
Wisconsin	Late Wisconsin	Mint River Glaciation (two distinct pulses) Alluvial fans, stream terraces, and talus cones	? Alluvial fans, talus cones, and terraces.	Walker Lake Glaciation (2 or 3 pulses)
	Early Wisconsin	York Glaciation	Salmon Lake Glaciation (undivided pulses)	Ambler Glaciation
Sangamon	Pelukian Transgression	Lost River terrace and covering marine deposits	Coastal terrace between Port Clarence and Cape Douglas-Second Beach at Nome	
Pre-Sangamon		Skull Creek erratics	Nome River Glaciation Iron Creek Glaciation	Kobuk Glaciation Earliest glaciation

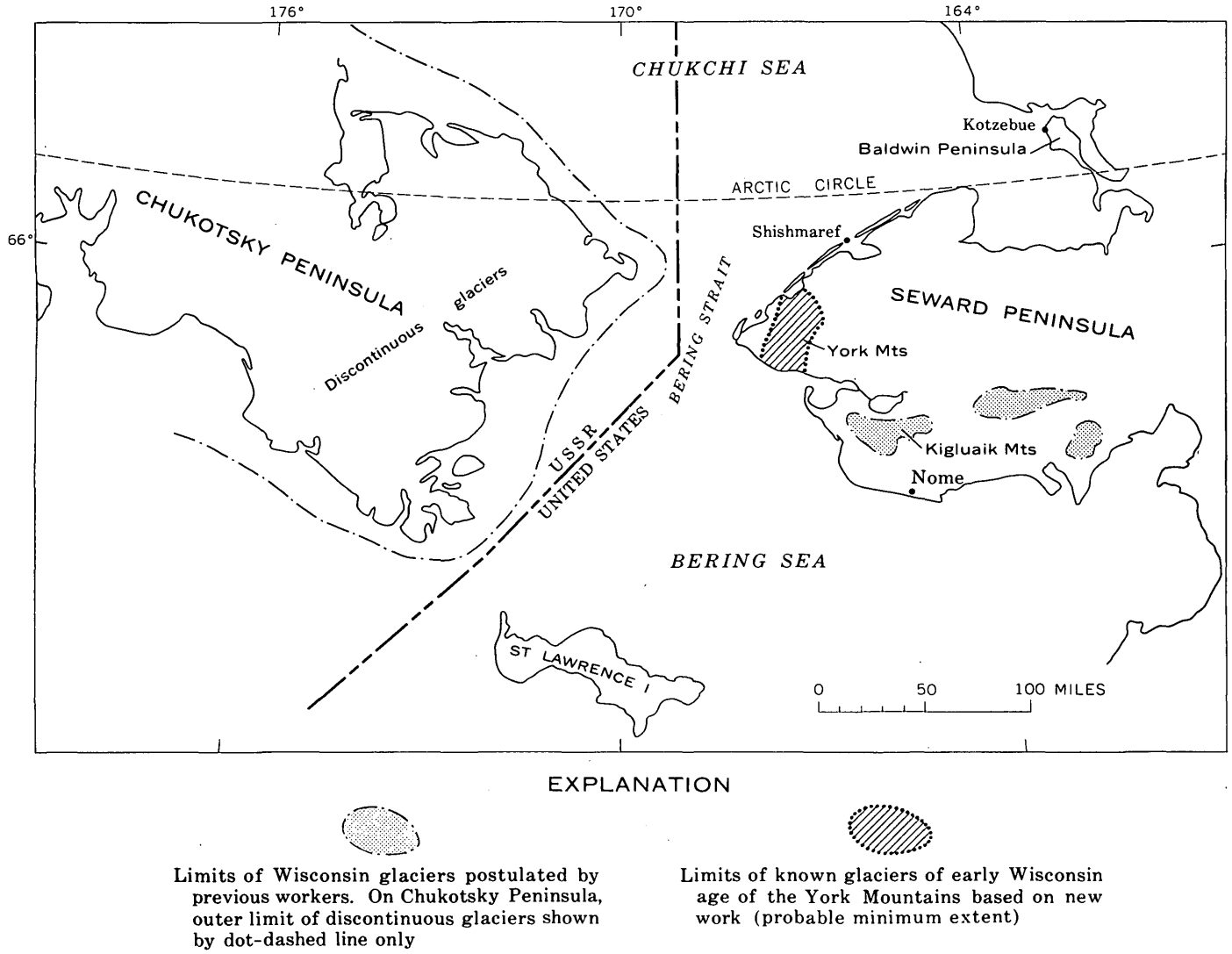

FIGURE 5.—Map of the Bering Strait area, showing the contrast in the postulated extent of glaciations in Wisconsin time on opposite sides of the strait. Source of Russian data: Gerasimov and Baranov (1964, p. 199).

2. Glaciers (Wisconsin) never extended northwest from the Kigluaiks as far as the north shore of Grantley Harbor, as is proved by the preservation of the Lost River terrace (Sangamon). This suggests an anomalous glacial pattern, for the Kigluaiks are, on the average, some 2,000 feet higher than the York Mountains, yet in Wisconsin time ice could not have extended any farther outward than did ice from the York Mountains.
3. The Salmon Lake Glaciation is complex and probably can be subdivided.
4. A till of early Wisconsin age may be present in the Kigluaiks but is not recognizable by current work.

The above four statements largely remove the problem of correlation. Should future work show, however, that ice of Wisconsin age never extended beyond the Salmon Lake moraines, we must find the explanation for the much greater extent of ice from the much lower York Mountains. The only possible factor, climate excepted, that may be significant is late Pleistocene uplift of the Kigluaik Mountains, which are bounded on the north front by a range-front fault showing Recent movement.

On the basis of the information given here, a correlation chart for upper Pleistocene glaciations in the Seward Peninsula-Bering Strait-Kobuk area has been compiled (table 1) using information by Hopkins and others (1960), Fernald (1964), McCulloch (1965), and Sainsbury (this paper), for the three areas. A map showing the correlated extent of glaciers in Wisconsin time on the Alaskan side of the Bering Strait is given in figure 5.

REFERENCES

Brooks, A. H., Richardson, G. B., and Collier, A. J., 1901, A reconnaissance of the Cape Nome and adjacent gold fields of Seward Peninsula, Alaska, in 1900: U.S. Geol. Survey Spec. pub., 222 p.

Creager, J. S., and McManus, D. A., 1965, Geology of the floor of Bering and Chukchi Seas—American studies [abs.]: Internat. Assoc. for Quaternary Research, 7th Internat. Cong., Gen. Sess., Boulder, Colo., Aug. 30–Sept. 5, 1965, p. 81.

Fernald, A. T., 1964, Surficial geology of the Central Kobuk River valley, northwestern Alaska: U.S. Geol. Survey Bull. 1181–K, 31 p.

Gerasimov, I. P., and Baranov, A. N., eds., 1964, Fizikogeograficheskii, atlas mira: Akad. Nauk SSSR i Glavnoe Upravlenie Geodezii i Kartografii, 298 p.

Hopkins, D. M., MacNeil, F. S., and Leopold, E. B., 1960, The coastal plain at Nome, Alaska—A late Cenozoic type section for the Bering Strait region *in* Chronology and climatology of the Quaternary: Internat. Geol. Congr., 21st, Copenhagen, 1960, Rept. pt. 4, p. 45–57.

McCulloch, D. S., 1965, Quaternary geology of the Alaskan shore of Chukchi Sea [abs.]: Internat. Assoc. for Quaternary Research, 7th Internat. Cong., Gen. Sess., Boulder, Colo., Aug. 30–Sept. 5, 1965, p. 333.

Péwé, T. L., Hopkins, D. M., and Giddings, J. L., 1965, The Quaternary geology and archeology of Alaska, *in* Wright, H. E., and Frey, D. C., eds., The Quaternary of the United States: Princeton Univ. Press, p. 355–374.

Sainsbury, C. L., 1965a, Geology and ore deposits of the central York Mountains, western Seward Peninsula, Alaska: U.S. Geol. Survey open-file rept., 146 p., *and* Stanford Univ., Ph.D. thesis 146 p.

———1965b, Quaternary geology of the western part of the Seward Peninsula, Alaska [abs.]: Internat. Assoc. for Quaternary Research, 7th Internat. Cong., Gen. Sess., Boulder, Colo., Aug. 30–Sept. 5, 1965, p. 406.

Sainsbury, C. L., Kachadoorian, Reuben, Campbell, R. H., and Scholl, D. W., 1965, Marine platform of probable Sangamon age, and associated terrace deposits, Cape Thompson area, northwestern Alaska: Arctic, v. 18, no. 4, p. 230–245.

EVIDENCE OF SECONDARY CIRCULATION IN AN ALLUVIAL CHANNEL

By JAMES K. CULBERTSON, Albuquerque, N. Mex.

Abstract.—Evidence of secondary circulation, or helical flow, has been found in the Rio Grande conveyance channel near Bernardo, N. Mex. Sand trails, or ribbons of sand, were deposited on a layer of clay as a result of the effect of helical flow cells which are estimated to have formed at flow depths of 0.15 foot and 0.3 foot. If these features are preserved in sedimentary deposits, they should serve as a diagnostic clue to the hydraulic environment under which the deposits were formed.

Secondary circulation, or helical flow, in natural channels has been discussed in many technical papers and textbooks. Actual documentary evidence of occurrence, however, is meager. Karcz (1966) shows photographs of bed configurations, which he attributes to secondary currents, on beds of several ephemeral streams (wadis) in southern Israel. He describes secondary circulation by saying that "streamflow is transversally unstable and splits into a series of elongated vortex tubes with alternating directions of rotation and with axes parallel to the direction of flow. The individual flow filaments advance helically." In laboratory experiments to determine effects of sediment on velocity distribution in a rectangular flume, Vanoni (1946) found that adding sand to clear-water flow apparently caused secondary circulation. Vanoni describes the pattern of sand transported along the flume bed as "clouds, or ribbons parallel to the flow * * * which were stable regardless of flow rate." He concluded that the secondary circulation was caused by the addition of sediment, and that this type of circulation might also exist in natural channels. Figure 1 is a sketch illustrating the type of secondary flow patterns that is thought to cause the sand trails discussed in this report. The distance between the trails is approximately twice the depth of flow.

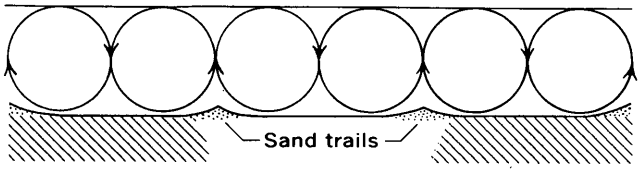

FIGURE 1.—Diagrammatic section showing helical flow cells and resulting sand trails, or ribbons, deposited between cells.

SAND TRAILS AND RELATED CHARACTERISTICS IN THE RIO GRANDE CONVEYANCE CHANNEL

Figure 2*A* is a view of the Rio Grande conveyance channel near Bernardo, about 50 miles south of Albuquerque, N. Mex. The apparent evidence of secondary circulation in the form of longitudinal parallel sand trails can be seen in the upper right-hand corner. Figures 2*B*, *C*, and *D*, are closeup photographs of the sand trails. Similar features have been referred to as harrow marks by Karcz (1966, p. 3109), or ribbons by Vanoni (1946, p. 98).

The conveyance channel is a relatively straight channel with a bed width of about 75 feet. Under ideal conditions the channel will carry about 2,000 cubic feet per second. The channel had been completely dry for several weeks prior to August 17, 1964, when as a result of thundershowers two small flows passed down the channel. The first flow event was characterized by a rapid rise to a discharge of 20 cfs. Discharge remained relatively constant for a period of 20 hours before falling. In the next 12-hour period the discharge dropped, and when it reached about 3 cfs, the second flow arrived (about 2 cfs). After an initial increase flow remained steady at about 3 cfs for another 5 hours, then dropped to zero in the next 18 hours. The two flows carried high clay concentrations and apparently were from different sources as indicated by two different colored clay layers deposited on the bed. The photographs shown in figures 2 and 3 were taken about 3 weeks after the channel bed had completely dried.

U.S. GEOL. SURVEY PROF. PAPER 575-D, PAGES D214-D216

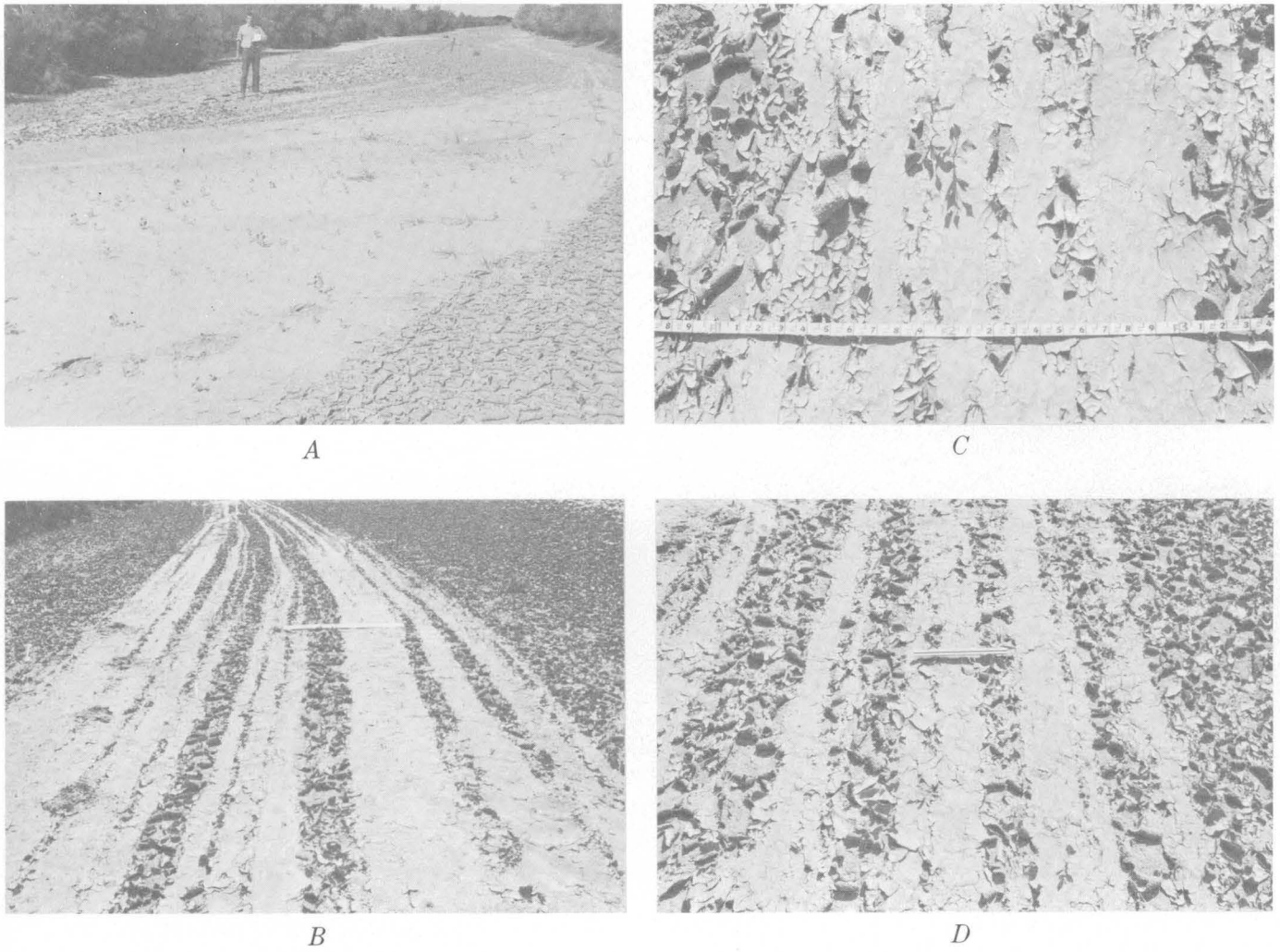

FIGURE 2.—Photographs showing features of the Rio Grande conveyance channel near Bernardo, N. Mex. *A*. General view. Flow is toward the reader. *B*. Sand trails resulting from secondary circulation cells. Flow is toward the reader. Scale is 3 feet long. *C*. Closeup view of sand trails. Flow is away from reader. *D*. Closeup view of sand trails. Flow is away from reader. Scale is 1 foot long.

Examination of the channel bed showed that, as the first flow receded, a ¼-inch to ½-inch layer of dark-red clay was deposited on the preexisting sand bed. This clay layer effectively sealed off the underlying sand. The second flow apparently carried a smaller clay load because the top clay, a light brown, is a considerably thinner 1/16-inch to ⅛-inch layer. The second flow also carried enough sand in suspension to form sand trails which appear similar to those described by Vanoni (1946, p. 98) in his flume experiments. It is logical that secondary circulation formed the sand trails during the relatively steady flow period of 5 hours following the second rise. As the second rise receded, the final deposition of clay covered the sand trails.

Figures 2*C* and 2*D* show that as the channel bed dried in the hot sun, the topmost and thinner clay layer shrank and curled where it covered the sand trails. Between sand trails the top clay layer adhered to the bottom layer and apparently the combined thickness of the clay deposits was sufficient to prevent curling.

The distance between the sand trails is about 0.3 foot at the particular location shown in figure 2*C*. Thus, the depth of flow would have been one-half this distance, or 0.15 foot, as illustrated by figure 1. Figure 2*B* shows several sand trails about 0.6 foot apart, indicating a 0.3-foot depth at this location. High-water marks showed that the average depth of the first flow ranged from 0.3 to 0.5 foot through the reach.

The wide bands of curls are difficult to explain. They occur in the spaces between relatively thick sand trails where the clay layers of the first and second flows may adhere to each other; in these places the clay layers are separated by only scattered sand grains or very thin discontinuous sand deposits. Also, the wide bands of curls may have resulted from breaks between groups of circulation cells.

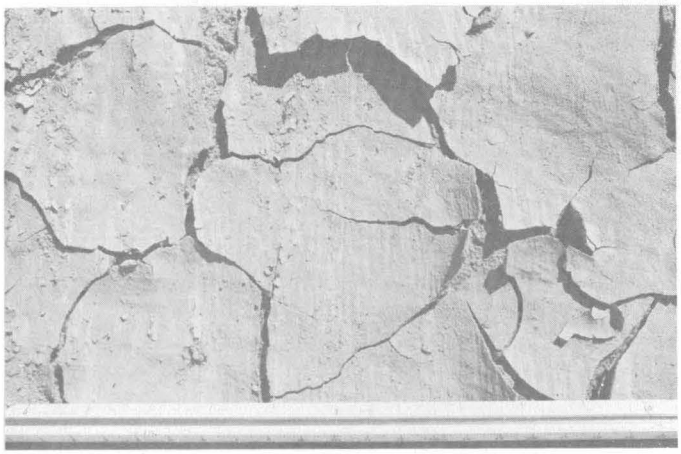

A

B

FIGURE 3.—Photographs of features of the Rio Grande conveyance channel near Bernardo, N. Mex. *A*. Thin dried clay layer of first flow sparsely covered by clay-coated sand grains of second flow. Underlying sand bed is visible under the curled edges of the clay. *B*. Small area of channel-bed scour that probably is the source of sand trails about 60 feet farther downstream.

Figure 3*A* is a closeup photograph showing the dried and curled surface of the clay deposits from the first flow event, and some grains of sand carried by the second flow event. The underlying sand bed is exposed under the curled clay edges. No indication of secondary circulation cells was found at this location, and only an extremely thin layer of clay from the second flow event covered the sand grains.

A small area of scour in the foreground and sand trails downstream are shown in figure 3*B*. This scour area may have been the source of sand that was deposited as sand trails downstream. The distance from the end of the scour hole to the beginning of the sand trails was about 60 feet, indicating that strong secondary circulation cells formed rather quickly in the vicinity of this area of high turbulence. Not all reaches where sand trails were observed, however, were immediately downstream from scour holes to which the trails could be associated.

CONCLUSIONS

The mechanics of formation of helical flow in open channels are not fully understood. However, the observations presented in this paper are important in two respects:

1. The observations constitute almost positive proof of the existence of secondary circulation in open-channel flow.
2. If these sand trails or ribbons are preserved in sedimentary deposits, they should serve as a diagnostic clue to the hydraulic environment under which the deposits formed.

As more evidence of occurrence is documented, the nature and importance of secondary circulation with respect to hydraulics and sediment transport in alluvial channels should become more clear.

REFERENCES

Karcz, Iaakov, 1966, Secondary currents and the configuration of a natural stream bed: Jour. Geophys. Research, v. 71, no. 12, p. 3109–3112.

Vanoni, V. A., 1946, Transportation of suspended sediment by water: Am. Soc. Civil Engineers Trans., v. 111, p. 67–133.

ROCK STREAMS ON MOUNT MESTAS, SANGRE DE CRISTO MOUNTAINS, SOUTHERN COLORADO

By ROSS B. JOHNSON, Denver, Colo.

Abstract.—Rock streams on the west side of Mount Mestas are composed of imbricated tabular fragments of brittle microgranite and microsyenite. One rock stream has an ice matrix. The ice apparently permits flowage of the rock stream in a manner similar to that of an alpine valley glacier. Continuing movement of the rock stream is revealed by bending of pines and the tilting and partial burial of young aspens growing at its toe.

Picturesque rock streams in several stages of development festoon the sides of Mount Mestas (also called La Veta Peak) in south-central Colorado. Mount Mestas is on the eastern flank of the Sangre de Cristo Mountains near La Veta Pass on U.S. Highway 160 about 20 miles west of Walsenburg, Colo. (fig. 1), and is separated from the main mass of the Sangre de Cristo Mountains by South Abeyta (also called South Veta) Creek. The summit of Mount Mestas (elevation 11,569 feet; fig. 2) is actually about 1,000 feet higher than the crest of the main mountain range, which is just 2½ miles to the southwest.

The two most spectacular rock streams are on the west slope of Mount Mestas (fig. 2, *A* and *B*) at elevations between 8,500 and 10,000 feet. They lie within V-shaped valleys that have gradients of about 28° (fig. 3). A panoramic view of both rock streams (fig. 4) is seen when travelling eastward along the old U.S. Highway 160 from Old La Veta Pass.

During the construction of a new highway over La Veta Pass in 1963, a rock-crushing machine was set up on the front of the northernmost rock stream (fig. 2, *A*) to supply material for the highway base. Interstitial ice was first encountered at the level of the valley floor about 30 feet in from the surface of the front of the rock stream. Operations were then moved to the upper surface of the rock stream, which is about 200 feet thick, and ice was encountered at a depth of 10–20 feet. Here, depressions and ridges in the highly irregular surface of the ice closely parallel the flow structures on the surface of the rock stream. The ice forms the matrix of the rock stream and apparently permits the rock stream to flow downhill in a manner

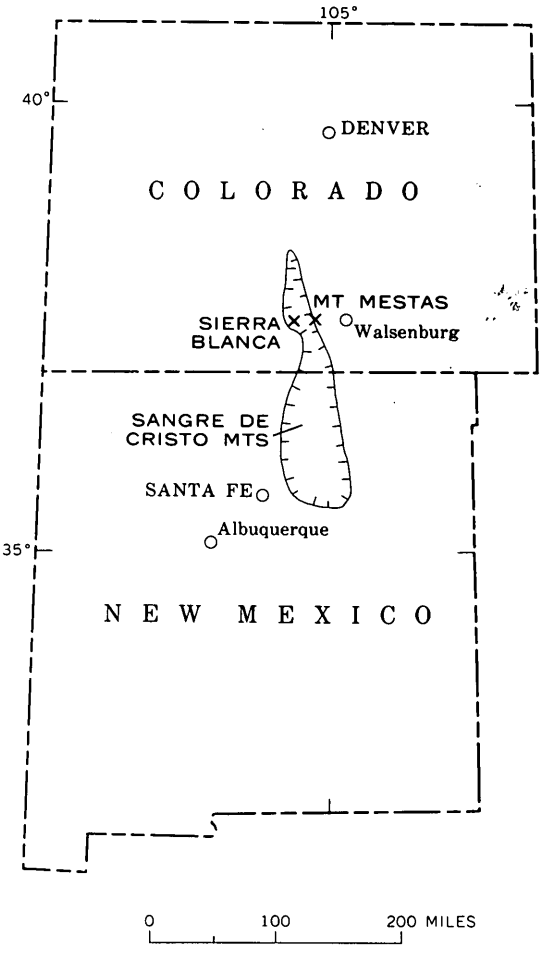

FIGURE 1.—Location map of Mount Mestas, Sangre de Cristo Mountains, southern Colorado.

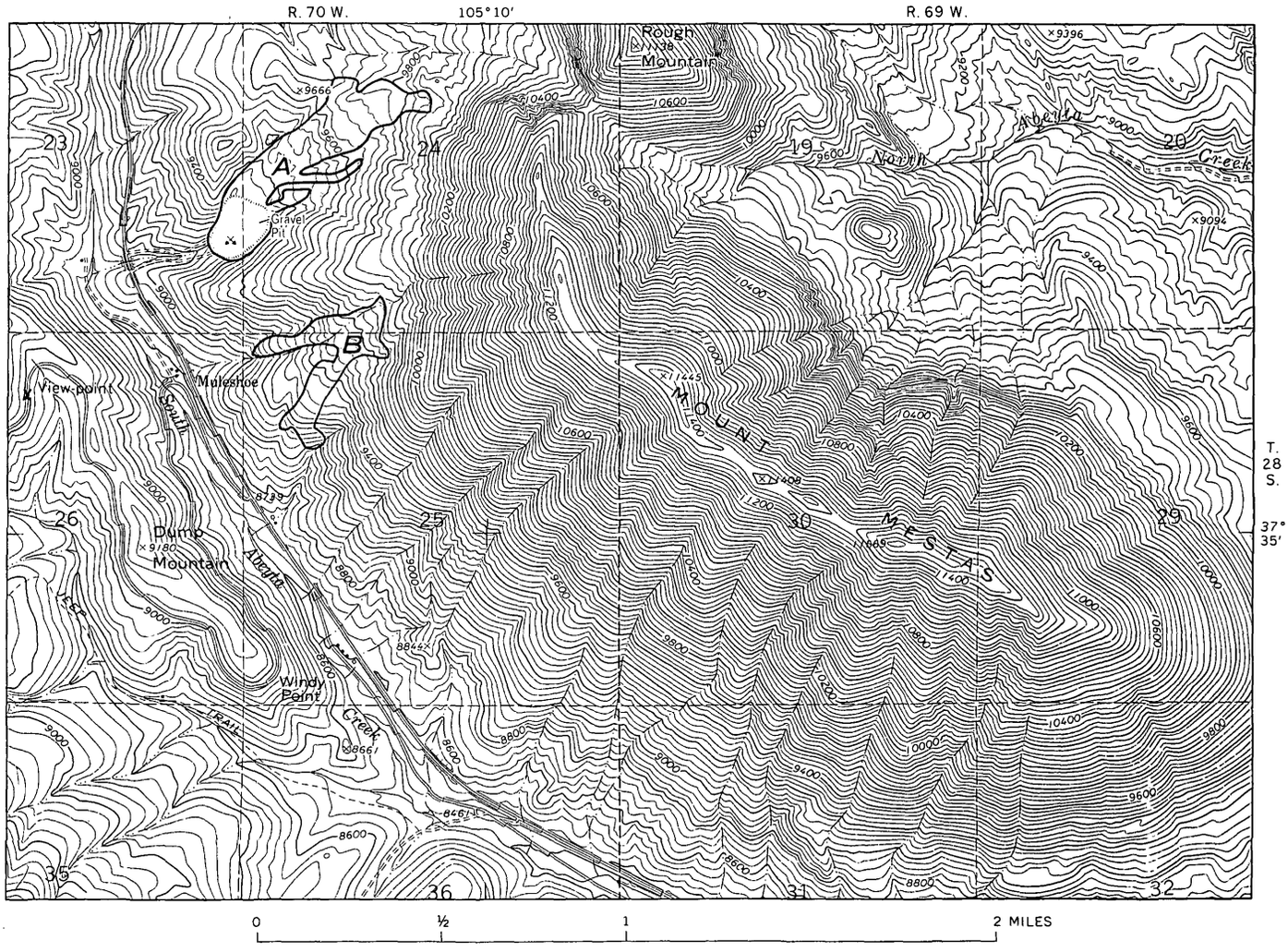

FIGURE 2.—Topographic map of Mount Mestas, showing location of rock streams *A* and *B*. (×, "View-point," at center of left edge of map is point from which fig. 4 was taken.)

similar to that of a normal valley glacier composed entirely of ice.

The interstitial ice in the northern rock stream (fig. 2, *A*) appears blue on the outcrop but is crystal clear in the hand. Below the troughs the ice locally is granular as if structurally crushed during movement. Although the rock stream contains a great deal of fine debris, very little of it seems to have been incorporated in the ice. The ice is dirty locally, but at most places it contains only isolated lineations of silt and clay particles. The ice contains very little air, although small well-defined air bubbles show several directions of lineation. At a few places the ice encloses small twigs. During the summer, melting ice feeds a small stream that issues from the front of the rock stream.

The average annual rainfall here is less than 20 inches, and the mean snowfall is between 125 and 150 inches. Snow does not remain long on west slopes at the latitude and elevation of the rock streams. Water from melting snow drains rapidly downward through the rubble of the rock stream to the top of the interstitial ice, where it may form a new layer of ice.

GEOLOGIC SETTING

The body of Tertiary igneous rock at Mount Mestas is an elliptical mass of microgranite and microsyenite that was injected along the frontal thrust fault of the Sangre de Cristo Mountains (Johnson and others, 1958). Overturned beds of the Sangre de Cristo Formation, dipping 25°–85° W., arch up onto the southwest flank of the intrusive for a short distance but have been eroded from the mass elsewhere. The intrusive is exposed over an area 2½ miles long northwest to southeast and about 1 mile wide.

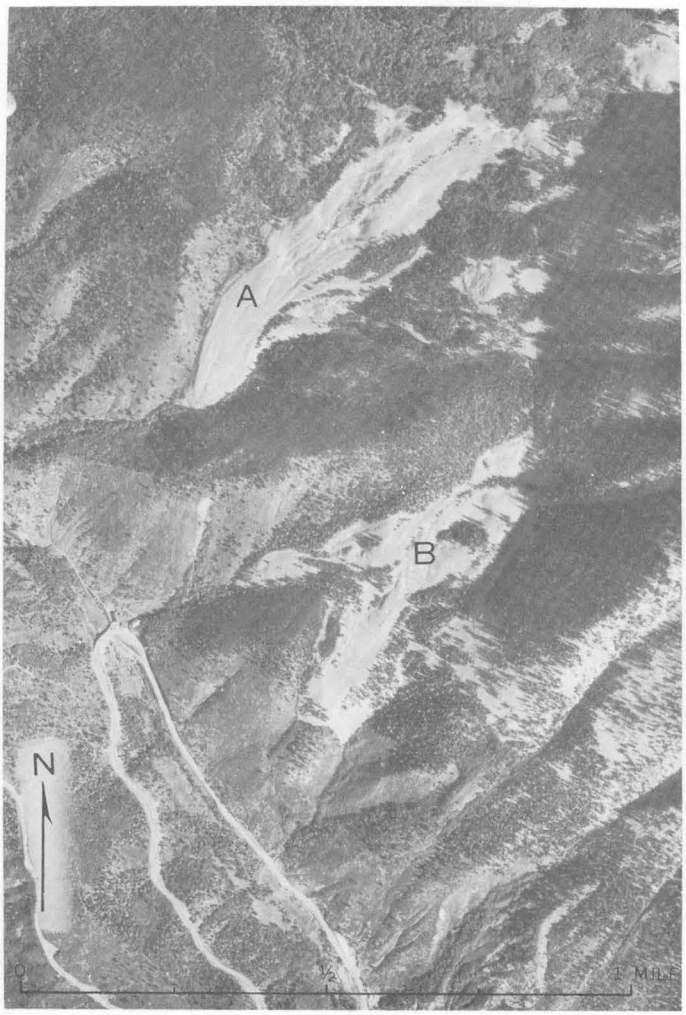

FIGURE 3.—Aerial view of two rock streams (*A* and *B*) on west slope of Mount Mestas. U.S. Forest Service photograph, No. CL 37–25, Sept. 19, 1938.

The intrusive rock is a very light gray leucocratic holocrystalline rock so fine grained that its texture appears porcelaneous to the eye. It is the most siliceous (73.6 percent SiO_2) rock in the region and is very hard and brittle. The rock is highly jointed and breaks up readily into flat tablets that form unstable masses on the steep sides of Mount Mestas. The surface of the entire intrusive is subject to large-scale rockcreep and rockfall. Fragments of the jointed rock are broken off, spall apparently by frost riving, and collect at the bases of cliffs in chaotic masses that form the sources of debris for the rock streams.

Sedimentary beds below the base of the intrusive are part of an imbricate lobate salient in advance of the frontal thrust fault and are made up of steeply dipping and overturned beds of Cretaceous and Tertiary age. Metamorphism extends for at least 500 feet below the base of the intrusive, where shale beds have been altered to slate and phyllite. Overturned beds of the Sangre de Cristo Formation of Pennsylvanian and Permian age for the bulk of the bedrock on the east side of the Sangre de Cristo Mountains in this locality. The light-gray intrusive rock and the debris derived from it contrast markedly with the bright-red conglomerate, sandstone, and shale beds of the Sangre de Cristo Formation.

Evidences of Pleistocene alpine glaciation in the Sangre de Cristo Mountains at this latitude include cirques, U-shaped valleys, and small moraines. Some moraines are found at elevations as low as 8,600 feet, but most are at around 11,000 feet. No evidence of alpine glaciation is found on Mount Mestas.

The only true glacier in the vicinity lies within a large cirque on the north side of Sierra Blanca 8½ miles west of Mount Mestas at about 11,000 feet. The glacier is very small and fluctuates in size yearly according to the annual precipitation.

DESCRIPTION OF THE ROCK STREAMS

Because of their spectacular appearance and ready accessibility, the two tongue-shaped (Wahrhaftig and Cox, 1959, p. 389) rock streams (figs. 3, 4) were examined closely. The northern rock stream (fig. 2, *A*), in which the ice was found, extends for three-quarters of a mile from its source to the tip of its front. Within this distance the surface of the rock stream drops in elevation from 9,900 to 9,200 feet, and has an average gradient of 10°. The maximum width of about 800 feet occurs only one-quarter of a mile from the source area. Here the gradient steepens to form a cascade (Patton, 1910, p. 669; pl. 48, fig. 2). Below the cascade the rock stream narrows (fig. 2), and two small tributaries (fig. 3) merge, but do not mix, with the main rock stream (Patton, 1910, p. 670–672; pl. 51, fig. 2). The southern rock stream (fig. 2, *B*) extends for nearly half a mile from its source to its front. The surface drops from an elevation of 9,740 to 9,120 feet and has an average gradient of 13°. Just below the area where it reaches a maximum width of 600 feet, the rock stream bifurcates (figs. 2, 3, 4). Below the point of bifurcation, both branches steepen and form cascades. These rock streams seem to be similar to frost-sorted rubble streams in the La Sal Mountains of Utah (Richmond, 1962, p. 64–65).

At most places the undulating surfaces of the rock streams are characterized by subparallel troughs and ridges that are also nearly parallel to the sides of the rock streams (fig. 3). The amplitudes of these features

269–274 O—67——15

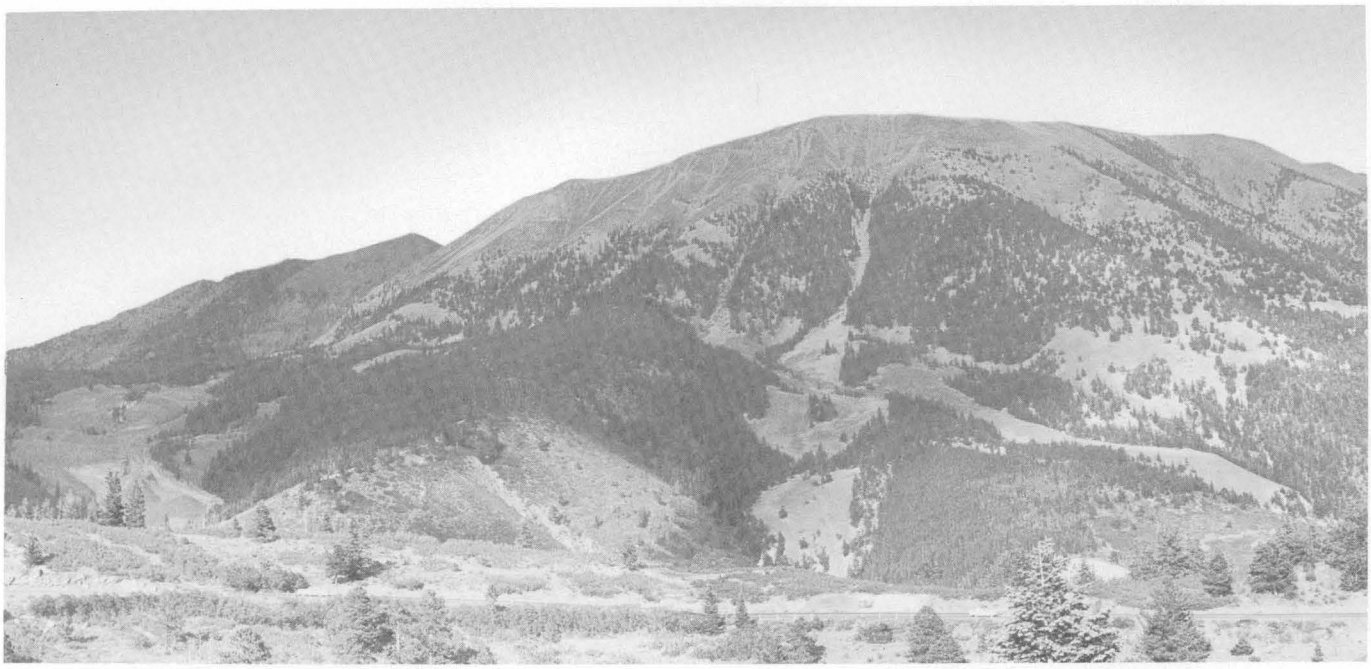

FIGURE 4.—Rock streams on west flank of Mount Mestas. Old U.S. Highway 160 in foreground. View is east from point marked by × on topographic map (fig. 2). The front of the northernmost (at left) rock stream has been partly excavated to provide highway construction material. Composite photograph by R. R. Dutcher, The Pennsylvania State University.

average 4–5 feet. At the cascades, the gradients of the slopes approach 30°, and subconcentric troughs and ridges form across the rock streams (figs. 3, 4; Patton, 1910, pl. 48, fig. 2). The fronts of the rock streams have slopes of nearly 35°, and the sides have slopes of 28°–32°.

The constituent rock fragments range in size from rock flour to tablets more than 5 feet in maximum dimension, and the average size is 2 × 12 × 18 inches. Most of the tabular fragments are flat lying and are imbricated. However, in some of the troughs the tablets are turned on edge and have their longest dimension parallel to the flow lines (Patton, 1910, p. 670; pl. 51, fig. 1). Although overlying the red beds of the Sangre de Cristo Formation throughout most of their extent, the rock streams are composed only of fragments of intrusive rock.

RATE AND MANNER OF MOVEMENT

Comparison of aerial photographs made in 1938 and 1962 shows that the fronts of these two rock streams have moved forward only a few feet in 25 years. A ponderosa pine about 30 feet tall growing on the south margin of the front of the northern rock stream shows less than 2 feet of horizontal compensation by bending. Aspens at the toe of this rock stream are about 20 feet tall and are tilted about 10° from the vertical, and the bases of their trunks are covered by at least 5 feet of tabular rock fragments.

It is therefore apparent that movement continues to a small extent in some of these rock streams. Movements may be due largely to the deformation of the interstitial ice, but some movement may be initiated by the seasonal freezing and thawing of this ice. Because of the absence of cirques on Mount Mestas and of the low latitude and elevation of the Mount Mestas rock streams, probably the original source of the ice was not a true valley glacier. The ice more likely was derived from the freezing at depth of downward moving rainwater and melted snow.

REFERENCES

Johnson, R. B., Wood, G. H., and Harbour, R. L., 1958, Preliminary geologic map of the northern part of the Raton Mesa region and Huerfano Park in parts of Las Animas, Huerfano, and Custer Counties, Colorado: U.S. Geol. Survey Oil and Gas Inv. Map OM–183.

Patton, H. B., 1910, Rock streams of Veta Peak, Colorado: Geol. Soc. America Bull., v. 21, p. 663–676.

Richmond, G. M., 1962, Quaternary stratigraphy of the La Sal Mountains, Utah: U.S. Geol. Survey Prof. Paper 324, 135 p.

Wahrhaftig, Clyde, and Cox, Allan, 1959, Rock glaciers in the Alaska Range: Geol. Soc. America Bull., v. 70, p. 383–436.

AN INTERPRETATION OF PROFILES OF WEATHERING OF THE PEORIAN LOESS OF WESTERN KENTUCKY

By LOUIS L. RAY, Washington, D.C.

Abstract.—The surficial mantle of Peorian Loess in western Kentucky is the parent material for soils of the Memphis catena (Memphis, Loring, Grenada, Calloway, and Henry). These soils have distinct profiles of weathering which are gradational from those of the Memphis to those of the Henry soil. Interpretation of the profiles of weathering and of the silt-clay ratios of their component zones indicates that the profile characteristics result from normal weathering and that it is not necessary to postulate two distinct loess deposits, two separate periods of profile development, or periglacial climatic conditions to explain their genesis. Maturely developed profiles of weathering are believed to be the same age in years as those that are less well developed and seemingly more youthful.

The surficial Peorian Loess, youngest of the loess deposits generally recognized along the Lower Mississippi and Ohio Valleys (Wascher and others, 1948; Leighton and Willman, 1950; Ray, 1960, 1963), has been examined along the Mississippi River from the mouth of the Illinois River to Natchez, Miss., and along the Lower Ohio and Wabash Valleys. Observations indicate that weathering has produced a variety of distinct soils in the Peorian Loess whose profiles of weathering form a gradational series related to the environment of the deposit. For simplicity and for geologic interpretation, the horizons of the soil profiles have been recast into the profile of weathering zonation proposed by Leighton and MacClintock (1930, 1962).

Although the general regional relationships of these soils appeared to be similar, those of the Coastal Plain region of western Kentucky were selected for study because: (1) there the surficial mantle of Peorian Loess is well developed and widespread, (2) the terrain provides a suitable environment for development of distinctive profiles of weathering, (3) the area lies south of the limits of glaciation and is transitional between the north and south climatic zones along the Mississippi Valley, and (4) published reports provide data for determination of silt-clay ratios of the zones of the profiles of weathering derived from the single parent material, the Peorian Loess.

A gradational series of five soils is recognized by soil scientists for the loess-derived soils of western Kentucky—the Memphis, Loring, Grenada, Calloway, and Henry—grouped together as the Memphis catena (table 1). Although not yet confirmed by detailed soil mapping on a regional basis, soils of the Memphis catena appear to have been developed in belts related to thickness of the loess, which is in general related to the distance from the Mississippi Alluvial Plain, the source area for most of the sediments (fig. 1).

Ray (1963) called attention to the general uniformity of the profiles of weathering of the thick, well-drained, buff to yellowish-brown loess deposits close

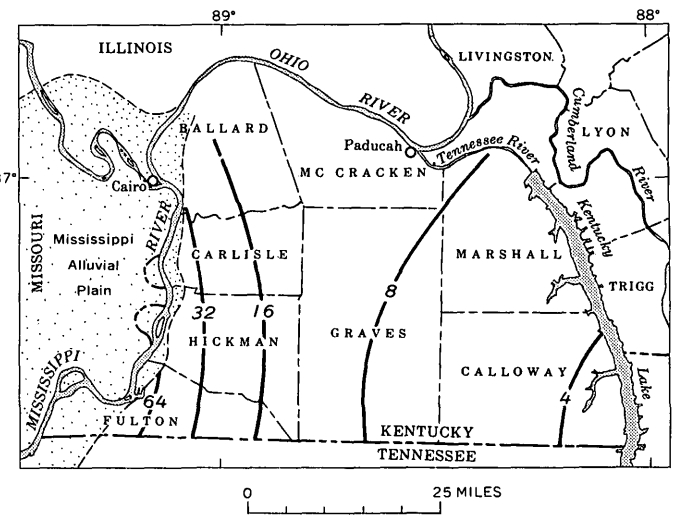

FIGURE 1.—Coastal Plain area of western Kentucky; isopachs in feet of loess (modified from National Research Council, 1952). Mississippi Alluvial Plain (stippled) is source area of most loess sediments.

TABLE 1.—*General characteristics of soils of the Memphis catena*

[Modified from Leighty and Wyatt, 1953]

Soil	Relief	Surficial color	Drainage		Subsoil
			External	Internal	
Memphis	Gently rolling; slopes 5–10 percent.	Buff to yellowish brown.	Well drained	Well to moderately well drained.	Bright yellowish brown; friable; slightly compacted; no hardpan or suprapan.
Loring	Gently undulating; slopes 2–5 percent.	Grayish brown	Moderately well drained.	Moderate to moderately slow.	Bright yellowish brown, mottled at depth; poorly developed, friable suprapan above poorly compacted silty hardpan (depth from 30 to 48 in.) with poorly developed prismatic structure and some gray veins; hardpan slightly plastic when wet.
Grenada	Gently undulating; slopes 2–5 percent.	Grayish brown	Imperfectly drained.	Slow	Yellowish brown, mottled; friable suprapan above compact clayey silt hardpan, or fragipan (depth from 26 to 50 in.) with prismatic structure and gray veins; fragipan hard and brittle when dry, plastic and sticky when wet.
Calloway	Almost level; slopes less than 2 percent.	Brownish gray	Imperfectly to poorly drained.	Very slow	Light gray, mottled; friable suprapan above compact, impermeable silty claypan (depth from 21 to 42 in.) with prismatic structure and gray veins; silty claypan hard and brittle when dry, plastic and sticky when wet.
Henry	Level; slopes less than 1 percent.	Light gray	Generally poorly drained.	do	Medium gray, somewhat mottled; friable, silty suprapan above compact impermeable claypan (depth from 11 to 48 in.) with prismatic structure and gray veins; claypan hard and brittle when dry, plastic and sticky when wet.

to the Ohio River, as revealed by the silt-clay ratios of the component zones. These profiles represent only the Memphis soil, which in western Kentucky is best developed in the loess marginal to the broad Mississippi Alluvial Plain. Away from the source area of the sediments, the Memphis soil is present only in the thicker well-drained loess on ridge crests and hilltops (Leighty and others, 1945; Leighty and Wyatt, 1950, 1953).

As the distance from its source area increases, the loess mantle decreases in thickness, changes from calcareous at depth to noncalcareous, and is less well drained. Its surficial color changes from buff or yellowish brown to a light gray as the Memphis soil is

TABLE 2.—*Silt-clay ratios of profiles of weathering of soils of the Memphis catena, Graves County, Ky.*

[Data interpreted from that of Leighty and Wyatt (1953). Soil zones: I, II, SP (suprapan), P (hardpan), and III]

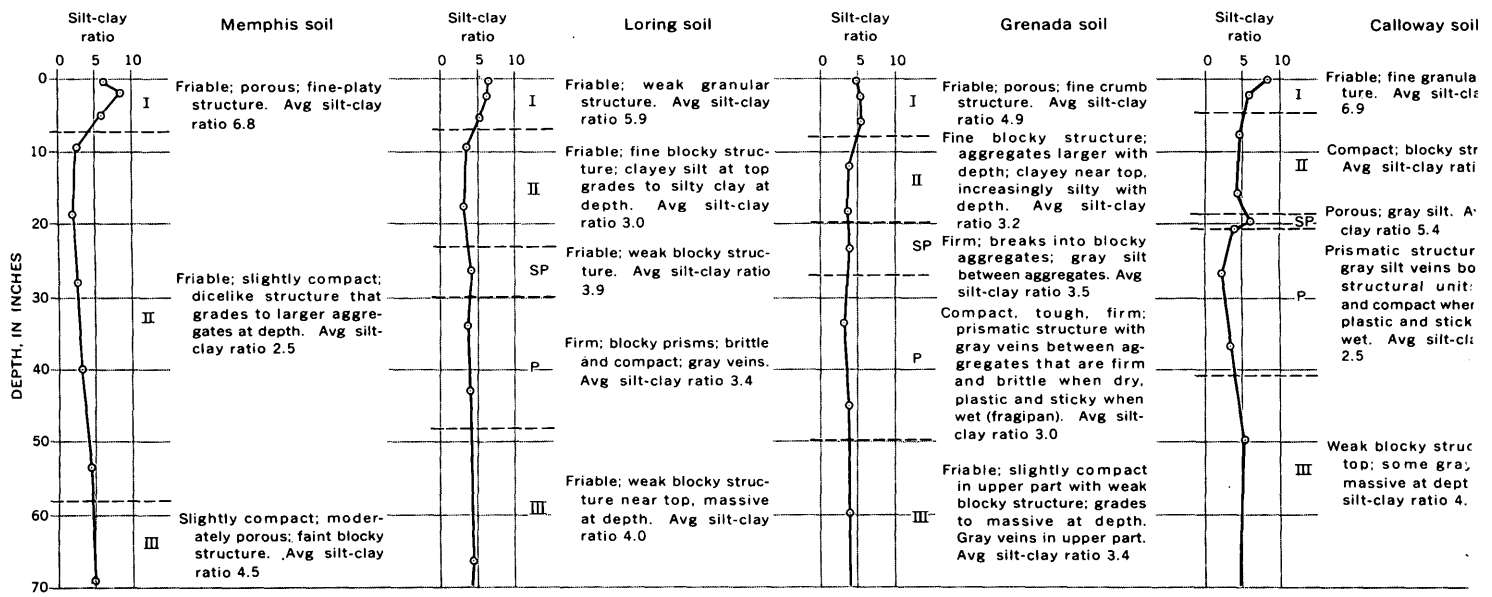

replaced by others of the catena (table 1). Exposures lose their ability to stand in vertical walls and erode to a miniature mature topography of closely spaced, steep-walled gullies.

Changes in the profile of weathering at depth are less obvious. As the thickness decreases and drainage becomes poorer, the loess becomes mottled and veined, and a prismatic structure is developed. A hardpan first appears at depth in the Loring soil as a scarcely recognizable, slightly compacted silty zone. As the Henry soil is approached the hardpan becomes gradually more compact, impermeable, and clayey, and its upper limit is closer to the land surface. Roadcuts through loess sections with a well-developed and impermeable hardpan commonly intersect a light-gray, porous, silty seepage or spring zone immediately above the hardpan.

Differences between the various soils are well illustrated by the silt-clay ratios of the zones of their profiles of weathering (table 2) calculated from grain-size analyses of the Memphis catena in Graves County, Ky. (Leighty and Wyatt, 1953). Two new zones that are especially important for defining and interpreting the genesis of the profiles of weathering have been added to the classification proposed by Leighton and MacClintock (1930, 1962): the hardpan (P) and the suprapan (SP) (table 2; fig. 2).

WEATHERING DURING DEPOSITION OF THE PEORIAN LOESS

The Peorian Loess of western Kentucky is thickest and least weathered at depth nearest its source area,

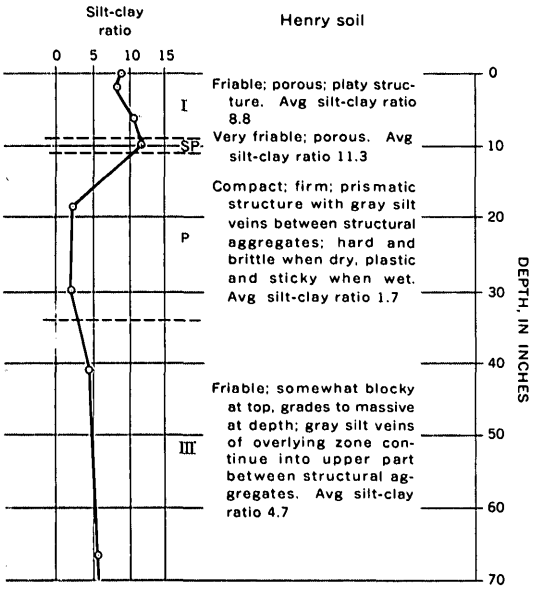

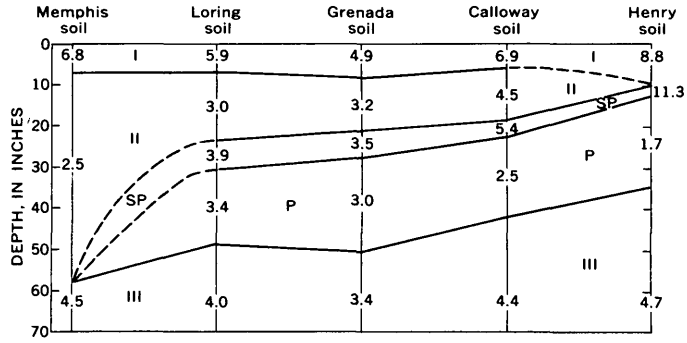

FIGURE 2.—Zonation of the profile of weathering of soils of the Memphis catena, Graves County, Ky. Average silt-clay ratios are indicated for Zones I, II, SP (suprapan), P (hardpan), and III. (Data interpreted from that of Leighty and Wyatt, 1953.)

the valley trains of Wisconsin age in the Mississippi Alluvial Plain (fig. 1). On the basis of the character of the deposits least altered by weathering, it would appear that originally the loess at any given locality had a remarkable textural homogeneity, a uniform grain-size distribution, and a high carbonate content. Analyses of the least altered loess indicate that calcite and dolomite compose 20–30 percent by weight of the loess and are present in both silt and clay fractions. The intimate mixing and simultaneous deposition of silt- and clay-size particles have been attributed by Beavers (1957) to the adsorption of clay by silt-size particles electrostatically charged by friction during eolian transportation. Such a mechanism explains the remarkable uniform mixing of the silt and clay and the open fabric now observable in the least altered deposits, where the larger silt particles are loosely bound together by intergranular "braces" or "bridges" of very fine silt and clay.

Despite the seeming textural uniformity in any one loess section, Smith (1942) has demonstrated subtle variations in grain-size distribution. He has also shown that "within limits there is a linear relationship between particle size and the logarithm of the distance from the source area of the sediments," and that as the distance from the source area increases "the coarser fractions decrease in quantity, the fine fractions increase in quantity, and the intermediate fractions first increase and then decrease" (Smith, 1942, p. 153; see also Leighton and Willman, 1950; Simonson and Hutton, 1954). If the minor amount of sand in deposits adjacent to the source area is disregarded, regional studies indicate that the arithmetic mean of the particle size of both the silt and clay fractions decreases away from the source area. Inasmuch as unaltered parent loess does not exist in western Kentucky, comparison of the original grain-size distribution for the

soils of the Memphis catena is not possible. Silt-clay ratios of leached and oxidized loess (Zone III, table 2; fig. 2) seemingly do not bear out the anticipated grain-size distribution pattern. This discrepancy may be the result of leaching of the carbonate constitutents in all grade sizes.

Weathering of the loess through oxidation, hydration, and leaching of the carbonate-mineral constituents presumably began simultaneously with deposition of the sediments. Decomposition of the silicate minerals proceeded so slowly during the time of deposition that it can be disregarded. Near the source area of the sediments, where the rate of accumulation was greatest, oxidation may have kept pace with sedimentation, because even the thickest deposits are oxidized throughout. Hydration proceeded at a somewhat slower rate, but perhaps more rapidly than the leaching of the carbonate minerals (Droste, 1956). Although oxidation and hydration are important processes in the alteration of the loess, leaching of the carbonate minerals during the time of deposition appears to have been the major process for loess modification.

Apparently the loess originally had a uniform carbonate content. Complete leaching of the carbonate minerals during deposition is believed to have occurred where the rate of accumulation was slower than the rate of leaching. Where accumulation was more rapid, leaching was incomplete; where accumulation was most rapid, most of the carbonates were possibly retained. Mineralogical analyses of loess along the Ohio Valley indicate that clay-size particles of calcite were the first component to disappear, followed by the clay-size particles of dolomite. Silt-size carbonate particles were reduced in both size and number; calcite disappeared first, then dolomite. By the end of loess deposition, presumably a regional gradation in the amount of carbonate mineral was present because of this selective leaching. The gradation of the carbonate-mineral content depended primarily on the rate of accumulation and, to a lesser degree, on grain size and drainage.

Where loess is less than 10 feet thick, evidence for gradation in carbonate content at the close of its period of deposition has been largely destroyed by postdepositional leaching. Smith (1942, p. 173) concluded that where well-drained loess was less than 80 inches thick and was under a forest cover "leaching should have removed the carbonates as rapidly as the loess was deposited. Similarly, under a grass vegetation the well-drained Peorian Loess that was less than 50 in. thick should have been non-calcareous at the close of the period of deposition." No attempt has been made to assess the role of vegetation in western Kentucky, the general assumption being that the area was uniformly forested during loess deposition. Grassland areas (barrens) reported by the first white settlers are believed to have been the result of burning of the flatter areas by Indians (Leighty and Wyatt, 1953; Leighty and others, 1945).

Leaching of carbonates from the loess during deposition presumably resulted in a decrease in its volume. Despite minor increases in volume because of oxidation and hydration of some mineral components, the resultant shrinkage from loss of carbonates caused reorientation of the particles so that the original open fabric of the deposit was destroyed. Therefore, as the distance from the source area increased, the finer grained, more thoroughly leached loess became denser, more compact, and less permeable.

Thus, at the close of loess deposition, the deposit was not a uniform blanket of clayey silt spread evenly over a preexisting terrain, but a blanket that had a wide range of physical characteristics. Postdepositional weathering of the nonuniform loess produced the gradation series of profiles of weathering now represented by the soils of the Memphis catena.

POSTDEPOSITIONAL WEATHERING OF THE PEORIAN LOESS

The following interpretations are based on field observations, especially in western Kentucky, on published descriptions of soil profiles, and on silt-clay ratios derived from published grain-size analyses of the soils of Graves County, Ky. (Leighty and Wyatt, 1953). Soils with similar profile variations have been recognized on Peorian Loess elsewhere (Smith, 1942; Grossman, Fehrenbacher, and Beavers, 1959; Grossman, Stephen, Fehrenbacher, Beavers, and Parker, 1959; Grossman, Stephen, Fehrenbacher, and Beavers, 1959), but no satisfactory explanation of their genesis has been proposed (Vanderford and Shaffer, 1966).

The normal profile of weathering of thick well-drained loess consists of distinct zones that reflect its history of weathering and modification (Ray, 1963). Briefly, Zones I through III are leached of carbonate minerals. The thin surficial Zone I and the underlying Zone II (fig. 2) are most altered chemically and physically. Original clay-size particles in Zone I and those produced through weathering have been in part removed by eluviation and transported into the underlying Zone II which is enriched in clay through illuviation. Zone III, normally below Zone II, is less altered, but is leached and oxidized. Zone IV, which is unleached but oxidized, and Zone V, the unleached and

unoxidized parent material, are not considered in this report.

Where loess is thinner and less well drained, two new zones, a hardpan and a suprapan are present between Zones II and III. The hardpan (P, fig. 2) is a zone of relatively high bulk density, more compact and impermeable than the overlying or underlying zones. Its upper boundary is sharp and its lower boundary is transitional with the underlying Zone III. The suprapan (SP, fig. 2) is a distinct friable gray silty zone that overlies the hardpan and underlies the clay-enriched Zone II.

In the Memphis catena the hardpan is first discernible in the Loring soil where it appears as a zone of relatively compact silt; it becomes gradually more dense, clayey, and impermeaable as the Henry soil is approached. The silt-clay ratios and general gradational relations of the hardpan to the profile of weathering are shown diagrammatically in figure 2 and in table 2. Where the hardpan is hard and brittle when dry, less brittle when moist, and somewhat plastic when wet, it has been termed a fragipan (Soil Survey Staff, 1960). In the Memphis catena the fragipan is characteristic of the Grenada soil.

Vertical fractures in the hardpan have produced a prismatic structure that is especially well developed in its upper part. As the clay content of the hardpan increases, the prismatic structure becomes more pronounced. The fractures are interpreted here as drying cracks (see Yassaglou and Whiteside, 1960; Jha and Cline, 1963).

The polygonal pattern of fractures opened in the hardpan during dry periods is accentuated by the infiltration of ashen-gray silt or clayey silt into the fractures from the overlying suprapan zone (Vanderford and Shaffer, 1966). The introduced gray sediments produced a distinctive and characteristic appearance of "larding" or veining in the hardpan (Grossman, Fehrenbacher, and Beavers, 1959). Where best developed, the fracture filling may be as much as an inch thick and extend through the hardpan into the upper part of the underlying Zone III. Commonly the margins of the filled fractures are bounded by thin bands of iron oxides. Roots, which normally do not penetrate the hardpan, may follow the filled fractures as platy fan-shaped mats.

Eroded outcrops of the hardpan display a distinctive miniature topography consisting of a series of sharp, ridgelike "knees" separated by V-shaped gullies. The small sharply defined ridges are crisscrossed by the veinlike filled fractures; these appear to exert only a modest influence in the development of the erosional pattern.

Immediately above the hardpan is the thinner suprapan (SP) zone (Vanderford and Shaffer, 1966) which is readily separable from the underlying hardpan and the overlying clay-enriched Zone II in outcrops and auger holes. Where best developed it consists of ashen-gray, poorly consolidated or friable, porous silt. From its lower boundary the gray fracture fillings or veins extend into the underlying hardpan (Grossman, Stephen, Fehrenbacher, and Beavers, 1959). In outcrops the suprapan is commonly a seepage or poorly defined spring zone that drains the shallow water table perched on the relatively impermeable hardpan.

Like the hardpan zone, to which it is closely related, the suprapan is not present in the Memphis soil. It is first discernible in the Loring soil (table 2; fig. 2) and is best developed in the Henry soil where it most closely approaches the surface. As the Henry soil is approached, the suprapan zone becomes more silty and the overlying clay-enriched Zone II decreases in thickness until it disappears and the surficial Zone I rests directly on the suprapan (fig. 2).

The general character of the Memphis soil on Peorian Loess adjacent to the source area of the sediments and the silt-clay ratios of its profile of weathering have been discussed by Ray (1963). The gradational profiles of weathering observable today in the five soils of the Memphis catena are attributable to postdepositional weathering which first differentiated Zones I, II, and III. Continued weathering resulted in development of the hardpan and the suprapan zones.

Where loess accumulated slowly and was substantially weathered, leached, and compacted during deposition, and where both internal and external drainage were poor, the zone of illuviated clay particles is thinnest and nearest the surface. Where well-drained loess accumulated so rapidly that there was relatively little weathering during deposition, its open fabric and greater permeability permitted the illuviated clay particles to be distributed throughout a greater depth range. Thus, the thickest clay-enriched Zone II developed in the least compact loess (Memphis soil) and the thinnest in the most compact loess (Henry soil) (fig. 2). The base of Zone II was ill defined and transitional with the underlying Zone III.

The hardpan developed as a relatively impermeable, compact, clay-enriched layer in Zone II, where pore spaces are clogged by illuviated clay that increases the bulk density and impermeability of the loess. In the Loring soil the hardpan is least developed and at greatest depth; progressively toward the Henry soil, as the

loess is more maturely weathered and both internal and external drainage are poorer (Bailey, 1964; Hutcheson and Bailey, 1964), the hardpan becomes more pronounced, at shallower depth, and has a greater clay content (fig. 2). Where the percentage of silt by weight is approximately three times that of the clay, ideally in the Grenada soil, the compact hardpan is relatively impermeable and has a characteristic brittleness when dry. This is the typical fragipan (Soil Survey Staff, 1960). As silt-clay ratios increase, the fragipan grades to a silty hardpan; as silt-clay ratios decrease, the fragipan grades to a claypan.

When the hardpan is sufficiently well developed so that downward percolation of ground water is impeded, a perched water table develops above it. This results in lateral rather than downward movement of ground water. Although some clay and silt are carried from above into the dessication fractures opened in the hardpan during periods of drought, most clay-sized particles are slowly flushed from the layer immediately above the hardpan, leaving it a porous silty zone—the suprapan. This process of degradation affects not only the material immediately above the hardpan, but perhaps the top of the hardpan itself.

The gray to whitish-gray color of the suprapan is believed to result from reduction by humic acid in the lateral-moving ground water. Similarly, the light-colored silty clay carried from the suprapan into the dessication fractures in the underlying hardpan are in sharp contrast to the darker oxidized hardpan. The continuing development of the suprapan is believed to be the most active process in the contemporary modification of the profiles of weathering.

Progressively greater differentiation of the zones of the profile of weathering from the Memphis to the Henry soil gives the false impression of progressively greater maturity and therefore of increasing age. Furthermore, where the suprapan zone is well developed, the overlying material has been mistaken for a younger loess overlying an older loess deposit in which a profile of weathering has been developed.

Silty-loam soils with profile characteristics similar to those of the Memphis catena are widespread, and their evolution has been variously interpreted by the soil scientists. The hardpan, especially if it has the characteristics of a fragipan, is commonly discussed in detail, but the overlying silty layer (the suprapan of this report), although noted, either is not differentiated or is not given its proper consideration as a distinct genetic zone of the profile of weathering.

Nikiforoff and others (1948) described a hardpan soil of the Coastal Plain in southern Maryland; Nikiforoff (1955) suggested the similarity of the hardpan soil to those of western Kentucky, especially the Grenada soil. Furthermore, he suggested that they may have been developed through similar evolutionary steps. The author concurs in the belief that they are due to similar processes but believes that there is no justification for postulating a periglacial climate in either area (Nikiforoff, 1955; Judson, 1965) during development of the profile of weathering in order to explain the fractures of the hardpan.

If the interpretation here suggested for the development of the profile of weathering is applied to silty-loam soils elsewhere that are noncalcareous and poorly drained, it is believed that the characteristic profiles can be shown to be the product of long-continued, normal weathering of a single parent material. Furthermore, if, as suggested, the fractures in the hardpan result from alternate wetting and drying, there is no necessity to attribute them to a former periglacial climate in areas embarrassingly far separated from all other evidence of a rigorous frost climate during the development of the profiles of weathering in postglacial time.

REFERENCES

Bailey, H. H., 1964, Fragipan soils, morphological relationships: Soil Sci. Soc. America Proc., v. 28, p. 680–683.

Beavers, A. H., 1957, Source and deposition of clay minerals in Peorian Loess (Mississippi Valley): Science, v. 86, p, 1–5.

Droste, J. B., 1956, Alteration of clay minerals by weathering in Wisconsin tills: Geol. Soc. America Bull., v. 67, p. 911–918.

Grossman, R. B., Fehrenbacher, J. B., and Beavers, A. H., 1959, Fragipan soils in Illinois, [pt.] 1, general characterization and field relationships of Hosmer silt loam: Soil Sci., Soc. America Proc., v. 23, p. 65–70.

Grossman, R. B., Stephen, I., Fehrenbacher, J. B., Beavers, A. H., and Parker, J. M., 1959, Fragipan soils in Illinois [pt.] 2, mineralogy in reference of parent material uniformity of Hosmer silt loam: Soil Sci. Soc. American Proc., v. 23, p. 70–73.

Grossman, R. B., Stephen, I., Fehrenbacher, J. B., and Beavers, A. H., 1959, Fragipan soils in Illinois, [pt.] 3, micromorphological studies of Hosmer silt loam: Soil Sci. Soc. America Proc., v. 23, p. 73–75.

Hutcheson, T. B., Jr., and Bailey, H. H., 1964, Fragipan soils, certain genetic implications: Soil Sci. Soc. America Proc., v. 28, p. 684–685.

Jha, P. P., and Cline, M. G., 1963, Morphology and genesis of a Sol Brun Acide with fragipan in uniform silty material: Soil Sci. Soc. America Proc., v. 27, p. 339–344.

Judson, Sheldon, 1965, Quaternary processes in the Atlantic Coastal Plain and Appalachian Highlands, *in* Wright, H. E., Jr., and Frey, D. G., ed., The Quaternary of the United States: Princeton, N. J., Princeton Univ. Press, p. 133–136.

Leighton, M. M., and MacClintock, Paul, 1930, Weathered zones of the drift sheets of Illinois: Jour. Geology, v. 38, p. 28–53.

———1962, The weathered mantle of glacial tills beneath original surfaces in north-central United States: Jour Geology, v. 70, p. 267–293.

Leighton, M. M., and Willman, H. B., 1950, Loess formations of the Mississippi Valley: Jour. Geology, v. 58, p. 599–623.

Leighty, W. J., Higbee, H. W., Reed, W. S., and Wyatt, C. E., 1945, Soil survey of Calloway County, Ky.: U.S. Dept. Agriculture, Bur. Plant Industry, Soils and Agr. Eng., ser. 1937, no. 15, 94 p.

Leighty, W. J., and Wyatt, C. E., 1950, Soil survey of Marshall County, Ky.: U.S. Dept. Agriculture, Bur. Plant Industry, Soils and Agr. Eng., ser. 1941, no. 29, 109 p.

———1953, Soil survey of Graves County, Ky.: U.S. Dept. Agriculture, Bur. Plant Industry, Soils and Agr. Eng., ser. 1941, no. 4, 139 p.

National Research Council, Committee for the Study of Eolian Deposits, Thorp, James, and Smith, H. T. U., chm., 1952, Pleistocene eolian deposits of the United States, Alaska, and parts of Canada [map]: Geol. Soc. America, scale 1:2,500,000.

Nikiforoff, C. C., 1955, Hardpan soils of the Coastal Plain of southern Maryland: U.S. Geol. Survey Prof. Paper 267–B, p. 45–63.

Nikiforoff, C. C., Humbert, R. P., and Cady, J. G., 1948, The hardpan in certain soils of the Coastal Plain: Soil Sci., v. 65, p. 135–153.

Ray, L. L., 1960, Significance of loess deposits along the Ohio River Valley: Art. 92 *in* U.S. Geol. Survey. Prof. Paper 400–B, p. B211.

———1963, Silt-clay ratios of weathering profiles of Peorian Loess along the Ohio Valley: Jour. Geology, v. 71, p. 38–47.

Simonson, R. W., and Hutton, C. E., 1954, Distribution curves for loess (Iowa-Mo.): Am. Jour. Sci., v. 252, p. 99–105.

Smith, G. D., 1942, Illinois Loess, variations in its properties and distribution, a pedologic interpretation: Univ. Illinois Agr. Exp. Sta. Bull. 490, p. 139–184.

Soil Survey Staff, 1960, Soil classification, a comprehensive system, 7th approximation: U.S. Dept. Agriculture, Soil Conserv. Service, 265 p.

Vanderford, H. B., and Shaffer, M. E., 1966, Comparison of fragipan and bisequal profiles of the Gulf Coastal Plain with soils of the southern loess belt: Soil Sci. Soc. America Proc., v. 30, p. 494–498.

Wascher, H. L., Humbert, R. P., and Cady, J. G., 1948, Loess in the southern Mississippi Valley, identification and distribution of the loess sheets: Soil Sci. Soc. America Proc., v. 12 [1947], p. 389–399.

Yassaglou, N. J., and Whiteside, E. P., 1960, Morphology and genesis of soils containing fragipans: Soil Sci. Soc. America Proc., v. 24, p. 396–407.

SOILS ON UPPER QUATERNARY DEPOSITS NEAR DENVER, COLORADO

By RICHARD VAN HORN, Denver, Colo.

Abstract.—A study of soil-stratigraphic relationships along Indian Creek south of Denver, Colo., suggests that a previously unrecognized possible soil-forming interval occurred soon after deposition of the Broadway Alluvium and prior to renewed downcutting and deposition of the next younger pre-Piney Creek alluvium. This indicates that 4 intervals of soil-profile development took place in Wisconsin and Recent time, instead of 3 such intervals as previously recognized. The informal designation of early Recent soil should be applied only to the soil that developed after deposition of the pre-Piney Creek deposits.

While investigating surficial deposits in the Golden quadrangle, Colorado, I decided that the early Recent soil of Scott probably represented weathering older than the time assigned in the Littleton and Kassler quadrangles, Colorado (Scott, 1962, p. 32; 1963, p. 41). (See fig. 1.)

According to Scott, this moderately well-developed zonal soil formed about 4,500 years ago on Broadway Alluvium of late Wisconsin age along principal streams and on pre-Piney Creek alluvium of early Recent age along upland tributaries. At no place are the two formations contiguous. Scott has stated (1963, p. 39) that no soil now recognizable formed on the Broadway Alluvium previous to deposition of the pre-Piney Creek alluvium. On the contrary, I believe that the soil on the Broadway Alluvium was developed mostly during two soil-forming intervals, whereas soil on the pre-Piney Creek alluvium was developed mainly during the younger of these two soil-forming intervals. (See fig. 2.)

Direct stratigraphic evidence for two soils is lacking in the Golden quadrangle or in the Denver area, but compelling indirect evidence is found in the Kassler and Castle Rock NW quadrangles. The evidence consists of a moderately well-developed soil on alluvium along Indian Creek and a noticeably less well-developed soil at Scott's archeologic locality 126 along

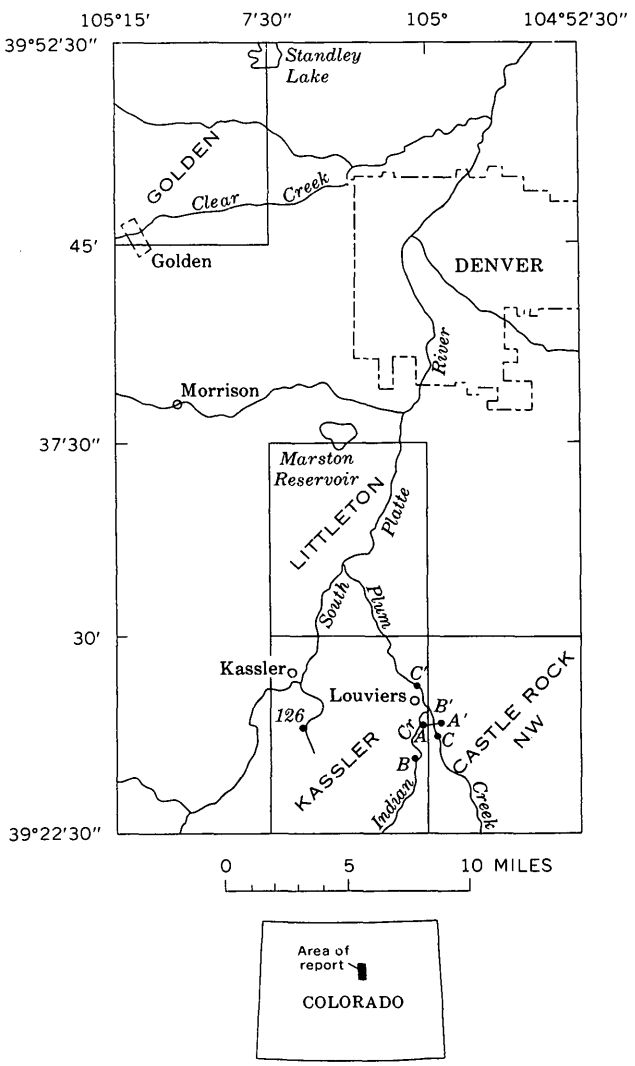

FIGURE 1.—Index map of places mentioned in the text: *126*, archeologic locality 126 along Little Willow Creek; *B*, measured section on Indian Creek. *A–A'*, transverse profile between Indian and Plum Creeks; *B–B'*, longitudinal profile along Indian Creek; and *C–C'*, longitudinal profile along Plum Creek are shown in detail on figure 3.

U.S. GEOL. SURVEY PROF. PAPER 575-D, PAGES D228-D232

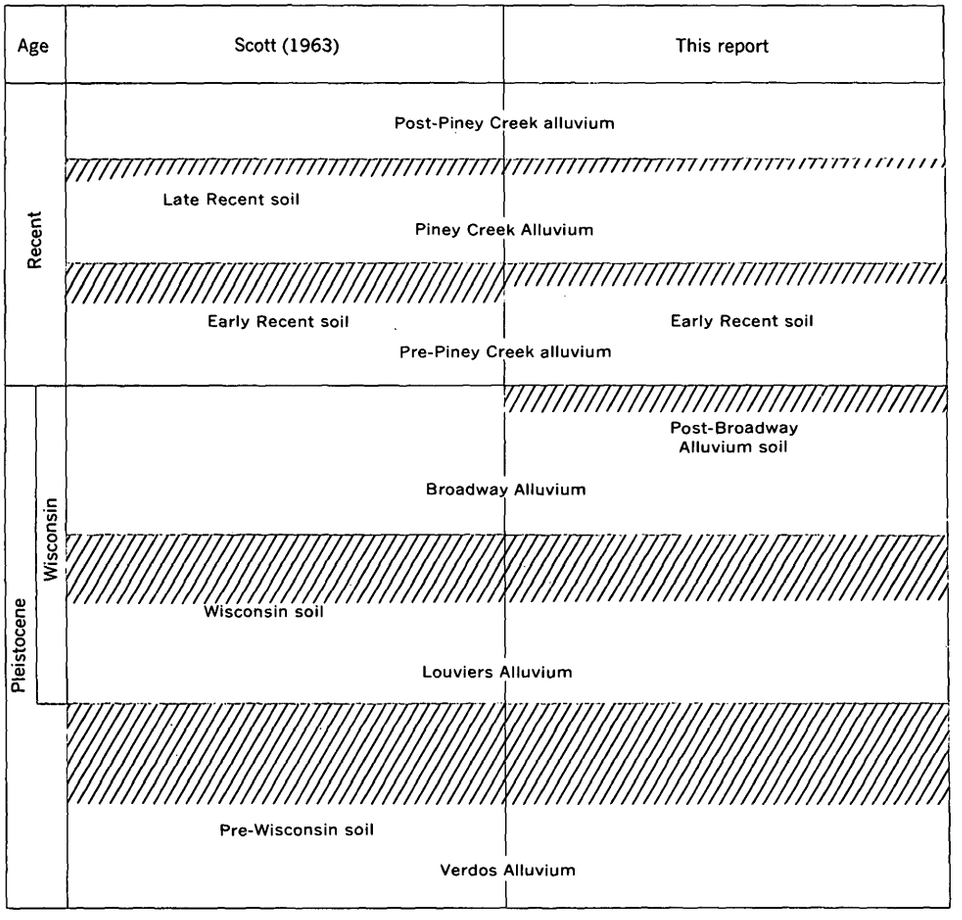

FIGURE 2.—Relation of soils to formations mentioned in text. Longer hachures denote relatively stronger soil development.

Little Willow Creek. The alluvium along Indian Creek probably is Broadway Alluvium, rather than younger pre-Piney Creek alluvium as mapped by Scott (1963). The deposit along Little Willow Creek, however, is demonstrably younger than Broadway Alluvium. Because of this difference in age, I account for a noticeable contrast between soils at these two localities by postulating two soil-forming intervals—that is, the occurrence of stronger soil on the older deposit can be mainly explained as two soils superimposed.

GEOMORPHOLOGY OF INDIAN AND PLUM CREEKS

An extensive alluvial terrace deposit along Indian Creek probably correlates with the extensive Broadway Alluvium along Plum Creek, but a half-mile gap in deposits prevents direct comparison of the two alluviums. Indian Creek is a northward-flowing stream tributary to the northwestward-flowing Plum Creek. A mile upstream from their junction the Verdos Alluvium of Kansan or Yarmouth age forms the divide between the two streams. (See fig. 3.)

Wrapping around and forming a northern extension of this divide is a lower flat-topped ridge of Louviers Alluvium of early Wisconsin age. The Louviers extends a short distance upstream into Plum and Indian Creeks adjacent to the Verdos. The Louviers west of the divide was deposited by Indian Creek, and that east of the divide by Plum Creek. The tongues of Louviers up the two creeks are at comparable altitudes, indicating that the two streams were graded to each other when the Louviers was deposited. Adjacent to the Louviers on the west, and 20 feet below it, is a terrace of probable Broadway Alluvium, of late Wisconsin age, which Scott (1963) mapped as pre-Piney Creek alluvium of early Recent age. This deposit extends along Indian Creek to within half a mile of Plum Creek. In this report it is henceforth called Broadway(?) Alluvium.

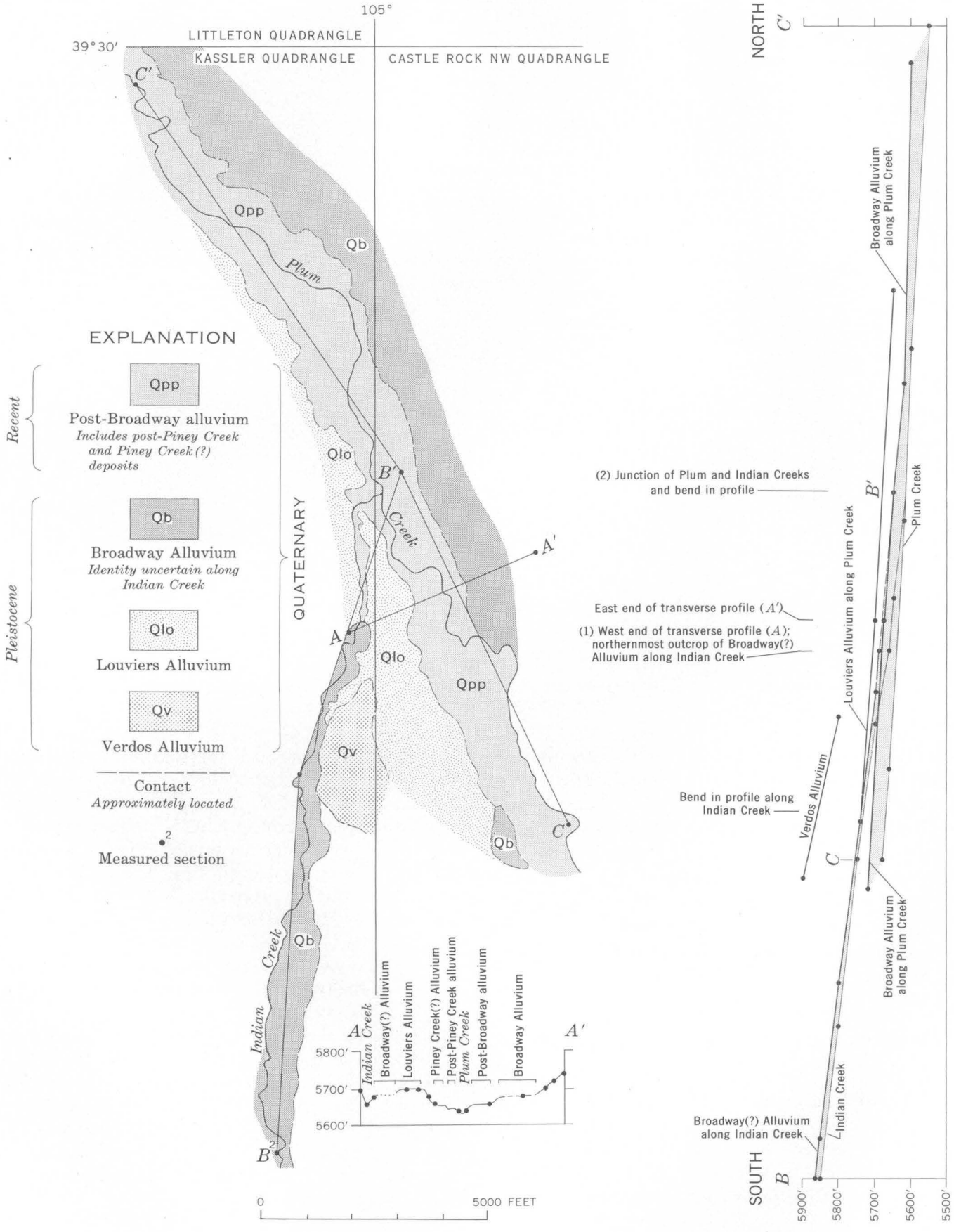
105°
39°30′
LITTLETON QUADRANGLE
KASSLER QUADRANGLE
CASTLE ROCK NW QUADRANGLE
EXPLANATION
Recent
Pleistocene
QUATERNARY
Qpp
Post-Broadway alluvium
Includes post-Piney Creek and Piney Creek(?) deposits
Qb
Broadway Alluvium
Identity uncertain along Indian Creek
Qlo
Louviers Alluvium
Qv
Verdos Alluvium
Contact
Approximately located
Measured section
Plum Creek
Indian Creek
Qpp
Qb
Qlo
Qv
A
A′
B
B′
C
C′
Broadway(?) Alluvium
Louviers Alluvium
Piney Creek(?) Alluvium
Post-Piney Creek alluvium
Post-Broadway alluvium
Broadway Alluvium
5800′
5700′
5600′
0
5000 FEET
NORTH
SOUTH
(2) Junction of Plum and Indian Creeks and bend in profile
East end of transverse profile (A′)
(1) West end of transverse profile (A); northernmost outcrop of Broadway(?) Alluvium along Indian Creek
Bend in profile along Indian Creek
Broadway Alluvium along Plum Creek
Louviers Alluvium along Plum Creek
Verdos Alluvium
Broadway(?) Alluvium along Indian Creek
5900′
5800′
5700′
5600′
5500′

East of the Louviers Alluvium, on the east side of Plum Creek, is an extensive terrace, also 20 feet lower than the Louviers between the two creeks. This terrace can be traced northwestward into the Broadway Alluvium mapped by Scott (1963) northeast of the town of Louviers. The upper part of this terrace deposit of undoubted Broadway Alluvium has been eroded by the many small streams emanating from the rough hilly country to the east. These streams have also deposited small alluvial fans on top of the terrace surface at many places and thus the original terrace surface is effectively obscured. South of the confluence of Indian and Plum Creeks and on the east side of Plum Creek there is a terrace 40 feet lower than the Louviers Alluvium. No soil was found exposed on this terrace or on the terrace of Broadway Alluvium.

A younger alluvial terrace adjacent to Plum Creek is east of, and 48 feet below, the Louviers Alluvium between Indian and Plum Creeks. This terrace is capped by a 2-foot-thick soil consisting entirely of a very dark gray humic massive and pebbly to silty sand that is slightly firmer than an underlying pebbly to silty sand. This soil has no associated Cca horizon or clay skins and is structureless. It is probably equivalent to the Piney Creek Alluvium. Adjoining this terrace on the east is a still lower terrace about 57 feet below the Louviers and 8 feet above Plum Creek. The lower terrace has a humic A horizon similar to the soil on the probable Piney Creek equivalent, but it is only 0.5 to 1 foot thick. The relations of these terraces to each other are shown in profile on figure 3.

The critical points of the foregoing are that the deposits of Louviers Alluvium along Indian and Plum Creeks are graded to each other and that the Broadway(?) Alluvium along Indian Creek and the Broadway Alluvium along Plum Creek are both 20 feet below the Louviers along the line of the profile (*A–A'*, fig. 3). This accordance of altitudes indicates that the two deposits are probably of the same age. The deposit along Plum Creek can be traced into the Denver area, is properly designated the Broadway Alluvium, and is of late Wisconsin age. The geomorphic evidence, then, strongly suggests that the Broadway(?) Alluvium along Indian Creek correlates with the undoubted Broadway Alluvium along Plum Creek. Thus, the upper surface of this alluvium presumably has been subjected to soil-forming processes since the close of deposition of the Broadway Alluvium in late Wisconsin time.

FIGURE 3.—Geologic sketch map of the Indian and Plum Creek areas, transverse profile *A–A'*, showing the accordance in level of the terrace of Broadway(?) Alluvium and Broadway Alluvium, and longitudinal profiles along Plum (*C–C'*) and Indian (*B–B'*) Creeks. The terrace of Broadway(?) Alluvium (pre-Piney Creek alluvium of Scott) along Indian Creek as projected from point 1 to 2 grades to the terrace of Broadway Alluvium along Plum Creek. Topographic control for profiles *A–A'*, *B–B'*, and *C–C'* is from the U.S. Geological Survey Kassler quadrangle, the manuscript map of the Castle Rock NW quadrangle (20-ft contour interval), and from hand-level measurements.

BROADWAY(?) ALLUVIUM ALONG INDIAN CREEK

The Broadway(?) Alluvium along Indian Creek ranges from sandy silt to coarse cobbly gravel. The soil developed on this deposit is exemplified by the following section, from top to bottom, that I measured:

Measured section of the Broadway(?) Alluvium along Indian Creek in the NW¼NE¼ sec. 21, T. 7 S., R. 68 W., Kassler quadrangle, near Denver, Colo.

	Thickness (feet)
1. Silt, sandy, dark-grayish-brown, platy, noncalcareous, humic. Grades into the underlying unit	0.5–1.0
2. Silt, clayey to sandy, dark-brown with reddish cast, noncalcareous, prismatic structure; thin clay skins on prism faces. B horizon. Grades into the underlying unit	1.0–1.5
3. Silt, sandy, pale-reddish-brown, noncalcareous to slightly calcareous, prismatic structure; poorly developed clay skins on prism faces. Lower part of B horizon. Grades into the underlying unit	0.5
4. Silt, sandy, pale-reddish-brown, slightly to moderately calcareous. Contains many vertical vein fillings of very light gray calcium carbonate. Cca horizon. Grades into the underlying unit	1.0–4.0
5. Sand and sandy silt, pale-reddish-brown. C horizon	3.0
6. Sequence covered to streambed	5.0

This soil on the Broadway(?) Alluvium is comparable to the early Recent soil described by Scott (1963, p. 41). Units 2 and 3 make up the B horizon of a soil that has been leached of calcium carbonate and that shows well-formed distinct prismatic structure and moderate accumulation of clay. At the place where the section was measured the terrace of Broadway(?) Alluvium is about 12 feet above Indian Creek; it extends northward for about 2 miles to its end, half a mile upstream from the confluence of Indian and Plum Creeks. At the downstream end, the terrace is about 25 feet above Indian Creek and about 45 feet above Plum Creek, from which it is separated by a low alluvium-capped ridge. The soil on the downstream end of the terrace deposit is partly eroded, but the remaining part of the B horizon consists of 0.7 foot of dark-brownish-gray noncalcareous sandy silt that has a coarse moderately developed prismatic structure. The prism (ped) faces contain faint clay skins. This B horizon is underlain by a faint Cca horizon. The soil

is comparable to the one described in the foregoing measured section on the upstream part of this same terrace.

PRE-PINEY CREEK ALLUVIUM

In the Denver area no deposit of pre-Piney Creek alluvium has been found that has both (1) definitive evidence (fossil or radiocarbon content) of an early Recent age and (2) a moderately or weakly developed zonal soil. At two places in the Kassler quadrangle, radiocarbon dates from pre-Piney Creek deposits have been reported by Scott. At one site the deposit has been eroded and no soil was found. At the other site, colluvium along Little Willow Creek that yielded fossils of still-living species, artifacts, and charcoal radiocarbon dated as 5,780±160 years Before Present (sample W–272) was correlated by Scott (1963, p. 40, loc. 126) with pre-Piney Creek alluvium. I judge that soil on this colluvium is less well developed than the soil observed on Broadway(?) Alluvium along Indian Creek, but more strongly developed than the late Recent soil described by Scott (1963, p. 44, 45). The following section of the pre-Piney Creek colluvium was measured at locality 126:

Measured section of the pre-Piney Creek colluvium in the east side of shale pit at archeological locality 126 in the SE¼SE¼ sec. 11, T. 7 S., R. 69 W., Kassler quadrangle, near Denver, Colo.

	Thickness (feet)
1. Silt, dark-brown, noncalcareous, platy, soft, powdery, humic. A horizon	0.5
2. Silt, pebbly, reddish-brown, calcareous, firm, massive. Vertical joints are present at a few places. B or Bca horizon	1.0
3. Silt, pebbly, pale-reddish-brown, very firm. Contains sparsely scattered, very small threads of very light gray calcium carbonate. At a few places there are slightly greater concentrations of disseminated calcium carbonate. Cca horizon	2.0
4. Red calcareous shale of the Triassic(?) and Permian(?) Lykins Formation.	

Unit 1 of this section is the A horizon of a soil. The calcareous nature, lack of clay skins, and lack of structure of unit 2 indicate that this is a weakly developed B or Bca horizon. Unit 3 is a Cca horizon that contains a relatively minor accumulation of calcium carbonate. The zonal nature of this soil is indicated by the leached A horizon and redeposition of the calcium carbonate in the Cca horizon. The B horizon, although calcareous, is partly leached and seems slightly more plastic than either the A or Cca horizons. The soil is developed on a moderately sloping colluvial surface that extends from the lower part of the Lykins Formation to the lower part of the Permian Lyons Sandstone. The colluvium is principally silt but contains some pebbles. It is derived from sandstone and siltstone of the Lyons Sandstone and from sandy shale and limestone of the Lykins Formation. Even though the physiographic settings are different, and recognizing the fact that the soil on the colluvium may not be typical of weathering that has taken place in the last 5,500 years, I judge that the soil at locality 126 does not show the same degrees of weathering as the soil formed on the Broadway(?) Alluvium along Indian Creek.

CONCLUSIONS

The relict soil developed on the Broadway(?) Alluvium of Indian Creek is a moderately well developed soil. The relict soil developed on colluvium about 5,500 years old at the mountain front is less strongly developed. This suggests to me that the soil on Broadway Alluvium may express more prolonged weathering, or multiple cycles of weathering. Whether soil development took place just after deposition of Broadway Alluvium is not known and cannot be determined from known exposures. The soil formed on the pre-Piney Creek colluvium is also a relict soil, and its degree of development cannot be assessed until a buried example has been found. It seems likely to me, however, that if weathering occurred as a discrete episode just after Broadway time, any soil thus formed would have been relatively weak. The less intense weathering indicated by the soil at locality 126 if added to the inferred effects of weathering first produced on Broadway Alluvium would, I believe, culminate in a moderately well developed soil. If these two soils are found in a buried position, each will, I think, be relatively weakly developed. The fossils and date of the pre-Piney Creek colluvium do not provide a limiting age for the moderately well developed soils. The informal designation, early Recent soil, should be applied only to the soil that developed after deposition of the pre-Piney Creek colluvium.

REFERENCES

Scott, G. R., 1962, Geology of the Littleton quadrangle, Jefferson, Douglas, and Arapahoe Counties, Colorado: U.S. Geol. Survey Bull. 1121–L, 53 p.

———1963, Quaternary geology and geomorphic history of the Kassler quadrangle, Colorado: U.S. Geol. Survey Prof. Paper 421–A, 70 p.

A SIMPLE AND RAPID INDIRECT DETERMINATION OF FLUORINE IN MINERALS AND ROCKS

By LEONARD SHAPIRO, Washington, D.C.

Abstract.—Fluorine is volatilized from a 5-milligram sample in a test tube as H_2SiF_6, using phosphoric acid to decompose the sample. The upper part of the test tube is washed with dilute hydrochloric acid, and the silica in the wash liquid is determined spectrophotometrically as molybdenum blue. With suitable standards, and samples with less than 5 percent F, accuracy is generally ±5 percent relative or ±0.05 percent absolute, whichever is larger.

The determination of fluorine is usually made by first separating the fluorine by distillation (Willard and Winter, 1933), or by diffusion (Frere, 1961). Occasionally a resin separation of cations is used (Shapiro, 1960). In nearly all procedures the fluorine is determined by its bleaching effect on some reagent.

Separation of fluorine together with silica in the volatile form recently was used for determining silica in small samples by transporting silica as volatile SiF_4 and subsequently converting it to silicomolybdate. The molybdate was reduced to the more stable molybdenum blue (Hozdic, 1966).

The possibility of determining fluorine in a sample by its separation as a volatile silicofluoride and measurement of the silicon was investigated. A simple procedure was developed utilizing this approach.

Preliminary attempts to determine fluorine by using bisulphate fusions to drive off the volatile fluoride worked well only with phosphates, which are very easily decomposed by acids, but rather poorly with silicates. At the suggestion of J. I. Dinnin, of the U.S. Geological Survey, sirupy phosphoric acid was tried and found to provide a much more aggressive attack on silicates while at the same time working well on phosphates. Talvitie (1951) studied the decomposition of a number of silicates by boiling phosphoric acid and listed the refractory minerals which are not broken up by this attack. These refractory minerals occur in trace levels in most rocks and, therefore, would rarely present a problem. Phosphate, which is often troublesome in fluoride determinations, does not interfere with the spectrophotometric procedure chosen (Straub and Grabowski, 1944).

EXPERIMENTAL METHOD

Reagents

Sodium molybdate ($Na_2MoO_4 \cdot 2H_2O$): Dissolve 30 grams in 90 milliliters of water. Add 10 ml of 1+1 H_2SO_4. Add the acid just before the solution is needed because the acidified solution is unstable beyond 1 day.

Oxalic acid dihydate ($H_2C_2O_4 \cdot 2H_2O$): Dissolve 10 g in 100 ml of water.

Reducing reagent: Dissolve 30 g of sodium bisulphite ($NaHSO_3$), 1 g of sodium sulphite (Na_2SO_3), and 0.5 g of 1-amino-2-naphthol-4-sulfonic acid in 200 ml of water.

Sirupy phosphoric acid: Prepare from concentrated phosphoric acid by boiling to fumes briefly in a beaker.

Procedure

Transfer 5.0 milligrams of each sample powder to the bottom of a series of borosilicate test tubes (18 × 150 millimeters) with the aid of a long-stemmed funnel. Duplicate the process with one or more standards. Add 3 drops of sirupy phosphoric acid to each tube and to an empty tube which serves as a reference blank. Into each tube insert tightly a one-hole No. 1 rubber stopper bearing a short piece of thick-walled glass capillary tubing. Wrap a 1-inch strip of wet filter paper around the upper part of the test tube.

Carefully heat the bottom of each test tube one at a time over the low flame of a Meker burner. Hold the tube at an angle of about 30° from the horizontal at first; agitate the tube so as to wet the entire sample and move it in and out of the flame to control the

U.S. GEOL. SURVEY PROF. PAPER 575-D, PAGES D233-D235

heating rate. In about 1 minute a thick coating of silica will form from the attack on the test tube by the phosphoric acid, and the liquid will have dried. Increase the flame temperature and, with the tube held horizontally, heat the lower third of the test tube strongly for 30 seconds. Place the test tube on a sheet of asbestos and proceed to heat the other test tubes. The tubes should be allowed to cool for at least 5 minutes but not more than 40 minutes because after 1 hour the value obtained for silica begins to decrease significantly, doubtlessly as a result of the volatility of the fluosilicic acid (H_2SiF_6) which has been formed.

To save time while the tubes are cooling, add 50 ml of hydrochloric acid (4+996) with a pipet to each of a suitable number of 150-ml beakers. Bend a piece of glass tubing of 3-mm outside diameter and about 18 inch length into a U shape with one side about 5½ in. long and the other a little over 12 in. long. The two outer sides of the U should be ½ in. or less apart. After the sample tubes are cool, transfer the 50 ml of acidified water from one beaker to a 100-ml glass graduate having a 1-in. internal diameter. Remove the stopper from the first test tube and invert the test tube. Insert the 5½-in. side of the U-tube into the test tube and, using the longer side as a handle, lower the test tube to the bottom of the graduate. The U-tube allows air to leave the test tube so that its upper part can be washed without wetting the part of the tube containing the sample. The 50-ml quantity of water limits the height to which the washing can take place. Raise and lower the test tube 5 times, then remove and discard it. Transfer the contents of the graduate back into the empty beaker and proceed to wash each of the other test tubes in the same manner.

Using rapid squeeze-type pipets, transfer 2 ml of the molybdate solution to each of the beakers while mixing; allow the beakers to sit 10 minutes; add 5 ml of the oxalic acid solution to each; allow to sit 1 minute; add 2 ml of the reducing reagent, and allow to sit at least 10 minutes. Using the blank solution to set a spectrophotometer at zero, read the absorbance of the other solutions at 640 millimicrons. A 4-percent standard, when one uses a 25-mm path-length absorption cell, should have an absorbance of about 0.5. Calculations are made on the assumption that Beer's law is being followed.

DISCUSSION AND RESULTS

Experiments were run to establish the nature of the fluorine-silicon compound which is evolved. To determine the stoichiometry, a comparison was made between known silica solutions and the silica evolved from a sample of known fluorine content. The atomic ratio for the fluorine and silicon in the evolved compound was found to be 6:1.

An experiment was then run in which the test tube was first freed of all surface moisture by strong heating, after which it was stoppered and cooled to room temperature. A sample was quickly inserted and then run as described above. The amount of silica recovered was identical with that obtained from a sample run in the usual manner.

These results are consistent with the conclusion that H_2SiF_6 is evolved from the sample, condenses on the upper portion of the test tube, and is then dissolved in the dilute hydrochloric acid solution.

The procedure described here yields a straight-line relationship between fluoride and absorbance when applied to phosphate rocks and a straight line of somewhat different slope (approximately 5 percent difference) when used with silicates. Should the material be of an undefined nature, the average obtained with a standard phosphate such as National Bureau of Standards phosphate rock No. 120a (3.92 percent F) and a silicate such as the NBS opal glass No. 91 (5.72 percent F) is used to establish the slope of the calibration curve. If the material is known to be a phosphate or a silicate, only the appropriate standard need be used.

The difference in slopes obtained with phosphates and silicate sample is not unexpected and arises because the phosphate goes entirely into solution before much silica has dissolved. On heating, the fluorine is then driven off almost in its entirety very rapidly and condenses onto the upper part of the test tube. In silicates, as the mineral dissolves, a significant amount of silica builds up in solution as the sample dissolves, and as is well known, this is capable of retarding the fluorine distillation. Grimaldi and others (1955) resolved this problem by a chemical separation of the fluoride from silica prior to its distillation. Modification of the present procedure to ensure a perfect agreement between phosphates and silicates at the expense of simplicity cannot be justified by the slight gain in accuracy that might result.

The procedure is simple and rapid—40 samples or more per day can be easily analyzed. The blank solution has an absorbance corresponding approximately to a 0.4 percent F sample. This varies in repeated runs by less than 5 percent or the equivalent of about ±0.02

percent F, using a 5-mg sample, and thus sets the limitation of accuracy for a single run. This compares favorably with most fluoride procedures which are based on the reduction in color of a strongly absorbing complex. As was pointed out by Ingram (1962), in these procedures "poor pipetting techniques can be a source of error which is very apparent in blank determinations."

In tables 1 and 2 results obtained by the described procedure are compared with results obtained by more conventional procedures. Where samples have a few tenths of a percent or less of fluorine and greater accuracy is desired, a 25-mg sample is employed. This reduces the significance of the blank error from ±0.02 percent to ±0.005 percent and, therefore, improves the accuracy of the sample determination.

A biotite sample was run on six different occasions using one blank tube and NBS opal glass No. 91 (5.72 percent F) as the reference standard for each. The results ranged from 1.38 percent to 1.52 percent fluorine with a standard deviation, s, = ±0.05.

TABLE 1.—*Comparison of quantities, in percent, of fluorine in phosphatic materials determined by rapid and by conventional procedures*

Sample No.	Description	Rapid procedure (this paper) on 5-mg samples	Microdistillation procedure [1]
166888	Human enamel	0.05	0.0075
166889	Human dentine	.04	.012
166890	Manatee rib	.09	.072
166891	Bison enamel	.02	.0076
166892	Mako shark enamel	2.80	2.76
166893	Apatite pellets	2.85	2.99
166894	do	3.00	3.10
166895	Gastropod bone	3.25	2.93
166896	Pelecypod molds	4.00	3.96
166897	White pebble (2d cycle) from Teneroc mine, Florida.	3.90	4.04
166898	White pebble (1st cycle) from Bunny Lake mine, Florida.	3.95	3.94
166899	White pebble (2d cycle) from Bunny Lake mine, Florida.	3.90	3.80

[1] Analyst: Blanche L. Ingram. Method described by Ingram (1962).

TABLE 2.—*Comparison of quantities of fluorine in rocks and minerals determined by rapid and by conventional procedures*

[Quantities in percent, except where otherwise indicated]

Sample No.	Description	Rapid procedure (this paper)	Conventional distillation procedure [1]
D101541	Biotite	[2] 0.15	0.17
D101542	Hornblende	[2] .09	.10
LTS 2	Biotite	1.5	1.5
G-1	Granite	.07	700 ppm (avg)
W-1	Diabase	.02	200 ppm (avg)
D1773	Silicate rock	.11	.13
158933	Biotite	.83	.78
FB-2 (ray 21)	do	.46	.54
Job 6789	do	3.8	3.75

[1] By several analysts using methods described by Grimaldi and others (1955), except analyses for samples G-1 and W-1, which were done by neutron activation.
[2] 25-mg samples; all others, 5 mg.

REFERENCES

Frere, F. J., 1961, Specific microdiffusion method for the determination of fluorine based on the lanthanum alizarin complexone color system: Anal. Chemistry, v. 33, p. 644–645.

Grimaldi, F. S., Ingram, B. L., and Cuttitta, Frank, 1955, Determinations of small and large amounts of fluorine in rocks: Anal. Chemistry, v. 27, p. 918–921.

Hozdic, Charles, 1966, Rapid method for determination of microgram amounts of silicon by colorimetric procedures: Anal. Chemistry, v. 38, n. 1626–1627.

Ingram, B. L., 1962, Spectrophotometric determination of fluorine with thoron: Art. 216 *in* U.S. Geol. Survey Prof. Paper 450–E, p. E130.

Shapiro, Leonard, 1960, Rapid determination of fluorine in phosphate rocks: Anal. Chemistry, v. 32, p. 569.

Straub, F. G. and Grabowski, H. A., 1944, Photometric determination of silica in condensed steam in presence of phosphates: Indust. Eng. Chem., Anal. Ed., v. 16, p. 574–575.

Talvitie, N. A., 1951, Determination of quartz in presence of silicates using phosphoric acid: Anal. Chemistry, v. 23, p. 623–626.

Willard, H. H., and Winter, O. B., 1933, Volumetric method for the determination of F: Indust. Eng. Chemistry, v. 5, p. 7.

A SPECTROPHOTOMETRIC METHOD FOR THE DETERMINATION OF TRACES OF PLATINUM AND PALLADIUM IN GEOLOGIC MATERIALS

By C. E. THOMPSON, Denver, Colo.

Abstract.—A sensitive method for the determination of traces of platinum and palladium in geologic materials is based on the catalytic effect of these metals on the reduction of molybdophosphoric acid to molybdenum blue using formic acid as the reducing agent. The platinum and palladium are dissolved with hydrobromic acid containing free bromine and are separated from most of the rest of the sample by precipitating with stannous chloride using tellurium as a carrier. As little as 0.05 ppm can be detected, and about 25 analyses can be made per man-day.

Geochemical methods of exploration have been little used in the search for deposits of platinum metals because adequate field-type analytical methods have not been available. There is an increasing interest today in exploration for these elements. Accordingly, the present investigation was aimed at developing a method of analysis for trace amounts of platinum, palladium, or the two combined, which can be used under field conditions or in a mobile laboratory.

Among the colorimetric methods available for the platinum-group metals (Beamish and McBryde, 1958; Beamish, 1966), the stannous chloride and the p-nitrosodimethylaniline methods appeared to be the most applicable, but both methods lack the required sensitivity for platinum and are impractical for field-geochemical exploration purposes. Atomic absorption methods have been used for the determination of platinum and palladium, but these methods at present also lack adequate sensitivity.

Catalytic methods appeared to offer the greatest promise because, in general, they have a greater inherent sensitivity than most colorimetric methods. Such methods depend upon the catalytic effect of trace elements on chemical reactions that yield colored compounds or precipitates. The method described below is a procedure of this type.

Formic acid releases carbon monoxide when mixed with another acid or when heated, and this reaction has been used to precipitate platinum in gravimetric procedures. Blackmore and others (1952) state that if a platinum solution containing formic acid is heated for less than 3 hours the elemental platinum formed probably remains in a colloidal form. The method described in the present report is based on the catalytic effect of colloidal platinum and palladium formed in the above manner on the reduction of molybdophosphoric acid to molybdenum blue using carbon monoxide released from formic acid as the only reducing agent. Filippov and Gushchina (1964) used the above reaction for the determination of colloidal platinum, and Feigl (1954) describes a spot test for palladium using the same reaction.

Formic acid, in the method described, is used to reduce both platinum and palladium to a colloidal form, and these colloidal metal particles control the reduction of the molybdophosphoric acid to molybdenum blue. Because both metals have nearly identical catalytic effects, only platinum was used to prepare the standards by which the measurements were obtained. Platinum and palladium are dissolved with hydrobromic acid containing bromine and are initially separated from the bulk of the sample constituents in solution by precipitating them with stannous chloride using tellurium as a carrier. Sandell (1959) reports on the precipitation of platinum with tellurium as a carrier from hydrochloric acid solution. The precipitation is just as satisfactory, however, from the hydrobromic acid solution.

The method is simple, rapid, and can be used in mobile field laboratories. As little as 0.05 parts per million of platinum, palladium, or the two combined can be determined at the rate of 25 analyses per man-day.

U.S. GEOL. SURVEY PROF. PAPER 575-D, PAGES D236-D238

REAGENTS AND APPARATUS

Reagents

Standard platinum solution (0.1 percent): Transfer 0.1140 g of $(NH_4)_4PtCl_6$ into a 150-milliliter beaker containing 5 ml of concentrated hydrocloric acid and 1 ml of concentrated sulfuric acid. Evaporate the solution to fumes of SO_3. Dissolve the residue in a small volume of aqua regia and evaporate the solution to near dryness. Add 10 ml of concentrated hydrochloric acid to the beaker and transfer the solution to a 50-ml volumetric flask and dilute to volume.

Dilute platinum solution (0.001 percent): Dilute 1 ml of the standard platinum solution (0.1 percent) to 100 ml with 3*N* hydrochloric acid. Prepare fresh weekly.

Dilute platinum solution (0.0001 percent): Dilute 10 ml of the platinum standard solution (0.001 percent) to 100 ml with 3*N* hydrochloric acid. Prepare fresh daily.

Hydrobromic acid-bromine reagent: Add 10 ml of bromine to 1 liter of concentrated reagent-grade hydrobromic acid.

Hydrobromic acid, 3*N*: Dilute 342 ml of concentrated hydrobromic acid to 1 liter with water.

Stannous chloride solution, 25 percent: Dissolve 50 g of $SnCl_2$ in 50 ml of concentrated hydrochloric acid and dilute to 200 ml with water.

Tellurium solution, 100 micrograms per ml: Dissolve 0.125 g of TeO_2 in 1 liter of 6*N* hydrochloric acid.

Nitric acid, concentrated, reagent grade.

Hydrochloric acid, concentrated, reagent grade.

Molybdophosphoric acid reagent: Dissolve 10 g of ammonium molybdate in 100 ml of water and add slowly with stirring 4 ml of concentrated phosphoric acid. A clear solution should result.

Gold solution, 100 micrograms per ml: Dissolve 0.100 g of gold in hydrobromic acid-bromine reagent and heat gently to expel bromine. Cool the solution and dilute to 1 liter with concentrated hydrobromic acid.

Formic acid, reagent grade.

Sodium carbonate, anhydrous, reagent grade.

Sodium hydroxide solution: Dissolve 100 g of sodium hydroxide in 500 ml of water.

Apparatus

An apparatus for filtering the precipitate containing platinum and palladium can be assembled from a Millipore metal syringe with a two-way valve; the bottom half of a field monitor, which is a disposable plastic Millipore filter holder; and a 4-inch section of plexiglass tubing machined to fit in the field monitor. Millipore filters (37 millimeters, 0.45 micron) are used in this apparatus. A stand to hold four of these is used in the field.

PROCEDURE

Preparation of sample solution

Roast 2 g of pulverized sample for 15 minutes at red heat in a porcelain dish. Transfer the sample to a 150 ml beaker and add 30 ml of concentrated hydrobromic acid-bromine reagent. Allow to stand at room temperature for 1 hour and then boil the solution for 15 minutes.

Preparation of standard solutions

Add 0, 0.2, 0.5, 1, and 2 μg of platinum to five 75-ml portions of 3*N* hydrobromic acid in 150-ml beakers, add 15 ml of 25-percent stannous chloride solution and heat the solutions to boiling. Add 5 ml of tellurium solution to each hot solution. Stir to mix and allow the beaker to stand for 2–3 hours at room temperature.

Proceed to estimation step.

A standard curve is obtained by measuring the absorbance at 725 millimicrons on a spectrophotometer of the standard solutions after diluting each to 40 ml. Measure the absorbance of each standard several times and plot the average value against concentration.

Separation of platinum and palladium

Transfer the prepared sample solution to a 22 × 175-mm screw-capped culture tube; wash the beaker with water and add the washings to the solution in the tube. Centrifuge the tube for 2 minutes; then transfer the solution to a 150-ml beaker. Wash the residue in the tube with 20 ml of 3*N* hydrobromic acid and again centrifuge. Add the washings to the solution in the beaker. Repeat the wash with a 20-ml portion of 3*N* hydrobromic acid, and add the washings to the beaker. Add 15 ml of 25-percent stannous chloride solution to the sample solution, and heat to boiling. Add 5 ml of 100 micrograms per milliliter tellurium solution, mix, and allow to stand 2–3 hours.

Estimation of platinum and palladium

Filter the solution through a 0.45-μ Millipore filter and transfer the precipitate and filter into a 100-ml beaker. Add 5 ml of aqua regia and heat on a hotplate to dissolve the precipitate. Remove the filter as soon as solution has taken place. Evaporate the aqua regia to near dryness and add 2-ml concentrated hydrochloric acid. Remove the beaker from the hotplate and dilute the solution to 20 ml with water. Then add 0.5 ml of gold solution, 1 ml of molybdophosphoric acid solution, and 5 ml of formic acid. Neutralize with solid sodium carbonate as indicated by the disappearance of yellow color. Add 10 ml of 25-percent sodium hydroxide solution and heat to boiling for 15 minutes. Add two 5-ml portions of formic acid 5 minutes apart while continuing to heat for a total of 25 minutes. Remove the beaker from hotplate, cool, and compare the color of the solution either visually or on a spectrophotometer with standards prepared at the same time.

DISCUSSION

The precision of the results obtained depends upon the amount of boiling of the solutions. Slight differences in temperature can make large differences in the amount of color produced by the same amount of platinum. For instance, no color can be obtained even with 5 μg of platinum at steam-bath temperatures. It is important, therefore, that the temperature be the

same for all samples and standards and that it be high enough to continuously boil the solutions.

The beakers used should be rinsed before use with either hydrobromic acid and bromine or aqua regia to remove any platinum or palladium remaining on the glass from previous samples.

Aqua regia is commonly used to effect solution of the platinum-group metals, but several evaporations may be required to expel oxidizing agents before analysis. The digestion procedure used here requires little evaporation, is less time consuming, and is equally effective in dissolving both platinum and palladium. The detection limit of the method can be lowered starting with a 10-g sample and incorporating an initial hydrofluoric acid digestion step. However, use of hydrofluoric acid is not practical in the field.

In addition to platinum and palladium, gold, mercury, rhodium, and iridium are reduced to the metal with formic acid in boiling solutions. The possible interference of rhodium, iridium, or the other platinum metals is not important when using the method for geochemical exploration for the platinum metals. Ignition of the sample before digestion eliminates the interference of mercury.

Gold is reduced by formic acid but has no effect on the reduction of molybdophosphoric acid to molybdenum blue. However, it does enhance the effect of platinum and palladium. A solution containing 2 μg of platinum but not gold gives an absorbance reading of about 0.3; when 50 μg of gold are added to the solution, a reading of about 0.4 is obtained. To take advantage of this enhancement, gold is added to all standards and samples.

In the precipitation of platinum and palladium using tellurium as a carrier, gold, silver, rhodium, and possibly small amounts of other elements are also precipitated. To assess the possible interference of elements that might precipitate as contaminants with the tellurium, 1,000 μg of Mn, Cr, As, Ni, Pb, U, and Sb; 300 μg of V and Co; 200μg of Ag and Nb; and 100 μg of W, Bi, Cd, and Be were each added to an estimation-step solution. No interference resulted.

To test the possible interference of major rock-forming elements a solution containing 6.3 g of Na_2CO_3, 18 g of $MgCl_2 \cdot 6H_2O$, 48 g of $Al(OH)(C_2H_3O_2)_2$, 6 g of KBr, 9 g of $CaCO_3$, 3.5 g of $K_2TiO(C_2O_4) \cdot 2H_2O$, 0.4 g of $MnCl_2 \cdot 4H_2O$, and 18 g of $FeCl_2 \cdot 4H_2O$ per liter was prepared in a 3*N* hydrobromic acid solution. Various amounts of platinum were added to 75-ml portions of this solution. These solutions were carried through the described procedure. No interference resulted, and the standard curve obtained was nearly identical to one obtained without addition of these elements.

PRECISION

The standard deviation obtained when the standard series is repeatedly run is 5 to 7 percent of the absorbance obtained except for the lowest standard, on which it is about 12 percent.

Three samples were analyzed four times each; the values obtained are listed along with values obtained by a fire-assay–spectrographic method in table 1.

TABLE 1.—*Comparison of repeated spectrophotometric analyses with a combined fire-assay–spectrographic analysis*

Sample No.	Sample type	Pt + Pd (ppm)				
		This method				Fire-assay-spectrographic [1]
		1	2	3	4	
AAE–665	Mine dump	0.8	0.4	0.7	0.7	0.8
AAE–667	do	3.0	2.5	2.5		4.0
D126451	Mineral concentrate.	.6	.5	.6	.6	.8

[1] Analysts: L. B. Riley, O. M. Parker, and J. Haffty.

REFERENCES

Beamish, F. E., 1966, The analytical chemistry of the noble metals, 1st ed.: New York, Pergamon Press, 609 p.

Beamish, F. E., and McBryde, W. A. E., 1958, A critical evaluation of colorimetric methods for the determination of platinum metals: Anal. Chim. Acta, v. 18, p. 551–564.

Blackmore, A. P., Marks, M. A., Barefort, R. R., and Beamish, F. E., 1952, Microgravimetric methods for platinum—A comparative study: Anal. Chem. v. 24, p. 1815.

Feigl, Fritz, 1954, Spot tests, v. I, Inorganic application: Amsterdam, Elsevier Publishing Co., p. 130–131.

Filippov, M. P., and Gushchina, L. F., 1964, Determination of colloidal platinum by a kinetic method: Zhurnal Anal. Khim., v. 19, no. 4, p. 480–483, [in Russian] p. 441–443 [English translation].

Sandell, E. B., 1959, Colorimetric metal analysis, 3d ed.: New York, Interscience Publishers, 1032 p.

ATOMIC ABSORPTION DETERMINATION OF BISMUTH IN ALTERED ROCKS

By F. N. WARD and H. M. NAKAGAWA, Denver, Colo.

Abstract.—Small amounts of bismuth in altered rocks are determined by atomic absorption spectrophotometry after samples are treated with boiling nitric acid. This treatment solubilizes most of the bismuth in the materials being investigated, and the acid solution is atomized directly into an acetylene-air flame without prior enrichment or preconcentration. As little as 10–20 ppm of bismuth can be measured with a relative standard deviation of about 10 percent. The accuracy is comparable to that of existing colorimetric and spectrographic methods. All these features coupled with the speed and simplicity commend the proposed method for scanning large numbers of geologic samples in geochemical exploration programs and related investigations.

As a part of an expanded program in the U.S. Geological Survey to develop new sources of heavy metals now in critical supply, a reasonably rapid and objective analytical method is needed to determine small amounts of bismuth in rocks and other geologic materials. Trace amounts of bismuth are often associated with gold and silver in such minerals as sylvanite, with tellurium in tetradymite, with selenium in guanajuatite, and with lead in most galenas (Goldschmidt, 1954). Because bismuth is not as ubiquitous or abundant as other metals such as copper or zinc, the presence of small amounts of bismuth may serve to pinpoint areas of possible economic importance. Thus, its determination is highly important in geochemical exploration for concealed ore deposits.

The existing colorimetric methods (Ward and Crowe, 1956; Sandell, 1959) are inadequate for scanning large numbers of samples in a short time. Of the several instrumental techniques available, atomic absorption is simplest and is reasonably sensitive for bismuth. Moreover, the technique lends itself to high productivity even in the hands of relatively unskilled analysts.

Briefly, the proposed procedure consists of two steps: (1) sample dissolution accomplished with boiling nitric acid, and (2) measurement of the dissolved bismuth by atomization of the decanted acid in a conventional flame. The percentage of absorption is read out directly and related to the bismuth concentration by various means as recommended for the particular spectrophotometer.

OPERATING CONDITIONS

Wavelength counter	223 (2,231 angstroms).
Source	Hollow cathode.
Lamp current	30 milliamperes.
Range	Ultraviolet.
Slit	3 (0.3 millimeter, 2 angstroms).
Scale	× 1
Boling burner:	
Air	Pressure, 30 pounds per square inch.
Acetylene	Pressure, 8 pounds per square inch.

REAGENTS AND APPARATUS

Bismuth standard solution, 1,000 micrograms per milliliter. Dissolve 0.5 gram bismuth metal in 500 ml concentrated nitric acid. Prepare less concentrated standard solutions by dilution with 1 + 1 nitric acid.

Magnetic stirrer with hotplate fitted with heating block drilled to receive 16- × 150-mm test tubes.

Stirring bars, magnetic, Teflon-coated, ½-inch-long.

Test tubes, 16- × 150-mm, calibrated at 10 ml.

PROCEDURE

Weigh 0.5 g of finely powdered sample into a 16- × 150-mm test tube and add 5 ml concentrated nitric acid. Insert small Teflon-covered magnet into mixture and place the test tube and contents in an aluminum heating block. Place block on hotplate equipped with rotating magnet and heat contents of test tube while stirring until mixture boils gently. Continue heating and stirring for 30 minutes. Remove test tube and contents from heating block, cool, and dilute the acidic solution with water to 10-ml mark on tube. Centrifuge the test tube and contents or allow solid material to settle to bottom. Atomize the supernatant liquid into the flame of the atomic absorption instrument, read the percent absorption, and convert to concentration as directed for the particular instrument.

U.S. GEOL. SURVEY PROF. PAPER 575-D, PAGES D239-D241

DISCUSSION AND RESULTS

In part, the proposed procedure is offered as an alternate to a colorimetric method (Ward and Crowe, 1956) found to be useful in geochemical exploration; therefore, its accuracy should be equal to or better than the other method. In order to establish the accuracy, several samples of altered rocks were analyzed by three methods: (1) the proposed atomic absorption method, (2) the colorimetric method based on the reaction of bismuth with carbamate, and (3) a three-step semiquantitative spectrographic method (Myers and others, 1961). These results are shown in table 1. The general agreement of the results obtained by three different and independent analytical procedures is ample evidence of the accuracy of the proposed procedure.

TABLE 1.—*Comparison of three methods for determination of bismuth, in parts per million, in altered rocks*

Sample	Atomic absorption (this report)	Colorimetric	Spectrographic
G49	15	<10	<10
G3	17	35	<10
G50	29	35	20
G28	48	70	50
G4	63	100	50
G12	60	100	70
G1	91	120	150
G37	280	380	300
G18	370	400	200
G45	350	500	200
G34	340	620	200
G38	470	660	300
G29	1, 500	1, 300	----------
G32	6, 200	7, 200	>1, 000

The content of detectable bismuth of these materials, as determined by the atomic absorption method, appears to be lower than that determined by the colorimetric procedure, possibly because of differences in the severity of the sample attack during dissolution or small variations in the procedures. In geochemical exploration, where the relative bismuth content of the altered rocks is used as the measurable parameter, atomic absorption, colorimetric, or spectrographic data would lead to the same targets.

The repeatability of the atomic absorption method was established by making five separate determinations on five different samples. Initially each sample was ground to pass an 80-mesh sieve, mixed, and piled in an oval-shaped body on a clean piece of paper; from the same general area of each pile, 0.5-g portions were taken for analysis. The highest and lowest value obtained, as well as derived data such as the confidence limits at the 95-percent level and the relative standard deviation, are shown in table 2.

TABLE 2.—*Repeatability test of bismuth determinations on 0.5-g sample replicates taken from same part of total sample*

Sample	Bismuth (ppm)		Mean and confidence limits at 95-percent level	Relative standard deviation (percent)
	High	Low		
G50	30	21	25±5. 1	17
G28	40	36	38±2. 2	5
G4	63	53	58±5. 3	7
G37	340	190	260±77	24
G38	410	240	330±96	23

Because the extreme range in bismuth content may reflect heterogeneity of the material, three of the above samples were further tested by taking five 0.5-g replicates at random from different areas of the oval-shaped pile and analyzing them. The data on these samples are shown in table 3 and correspond to the data of table 2. Obviously the sampling technique used for the data shown in table 3 is preferred to that used for data in table 2; however, the demand for large volumes of data as required in geochemical exploration precludes any such replication, and other means of improving the repeatability are needed.

TABLE 3.—*Repeatability test of bismuth determinations on 0.5-g sample replicates taken from different parts of total sample*

Sample	Bismuth (ppm)		Mean and confidence limits at 95-percent level	Relative standard deviation (percent)
	High	Low		
G28	44	37	40±3. 3	7
G37	230	180	200±24	10
G50	36	29	33±4	10

Finer grinding of samples usually results in better precision, especially when using a method starting with relatively small samples to determine trace constituents. To test this idea 10-g portions of three different samples previously analyzed (table 1) were ground to pass 200-mesh sieves and mixed, and the usual 0.5-g sample was analyzed. The results are shown in table 4.

The improved precision is especially marked in the sample containing 200–300 ppm of bismuth, less so

TABLE 4.—*Repeatability test of bismuth determinations on 0.5-g random sample replicates from 10-g portion ground to pass 200-mesh sieve*

Sample	Bismuth (ppm)		Mean and confidence limits at 95-percent level	Relative standard deviation (percent)
	High	Low		
G50	30	23	26±3. 8	12
G38	270	250	260±12	4
G37	360	340	340±13	3

with samples that have more minute amounts of bismuth.

The above statements about the precision of the proposed method are based on a scant amount of data and are not amenable to a dogmatic interpretation. Nevertheless, the observed accuracy, based on comparison of the results obtained by three different analytical techniques, and the acceptable repeatability, which can be improved if needed by one of the two methods given, are sufficient evidence to show that the atomic absorption method can be used in place of, or in conjunction with, other prospecting methods to provide data of the sort needed for scanning purposes or for actual prospecting.

REFERENCES

Goldschmidt, V. M., 1954, Geochemistry: London, Oxford Univ. Press, 730 p.

Myers, A. T., Havens, R. G., and Dunton, P. J., 1961, A spectrochemical method for the semiquantitative analysis of rocks, minerals, and ores: U.S. Geol. Survey Bull. 1084–I, p. 207–229.

Sandell, E. B., 1959, Colorimetric determination of traces of metals, 3d ed.: New York, Interscience Publishers, 1054 p.

Ward, F. N., and Crowe, H. E., 1956, Colorimetric determination of traces of bismuth in rocks: U.S. Geol. Survey Bull. 1036–I, p. 173–179.

A DETERMINATION OF THE DAILY MEAN DISCHARGE OF WAIAKEA POND SPRINGS, HILO, HAWAII

By GEORGE T. HIRASHIMA, Honolulu, Hawaii

Work done in cooperation with the Hawaii State Division of Water and Land Development

Abstract.—The average discharge of Waiakea Pond on June 27–28, 1965, was computed to be 111 mgd and represents the total discharge of numerous springs feeding the pond. The rate of outflow from the pond equalled the average discharge when the pond stage had risen about 0.01 foot from each of the two low-tide stages. At the lower high tide, the outflow rate equalled the average discharge when the pond stage was at its peak. The weighted average chloride concentration of the outflow, 609 ppm, was much higher than can be accounted for by mixing of 110 million gallons of spring water containing 7 ppm of chloride and 3.6 million gallons of tidal inflow water whose maximum chloride concentration was 4,500 ppm.

The discharge of Waiakea springs, through Waiakea Pond into Hilo Bay, Hawaii (fig. 1), is a part of one of more than 25 major spring-discharge areas along the shore of the island of Hawaii that are visible on infrared images (Fischer and others, 1966). Waiakea springs consist of numerous flows surrounding and submerged in the Waiakea Pond area. Water from the springs that collects in Waiakea Pond discharges through an 18-foot-wide, 100-foot-long canal into Wailoa River and thence to Hilo Bay. Because the pond, 25.6 acres in area, is estuarine and subject to tidal inflow, its discharge includes varying amounts of sea water. This study was made to obtain an estimate of the daily average discharge of Waiakea springs and to determine the times during the tide-induced cycle of pond stages at which the outflow rate equalled the average discharge.

In June 1930, J. F. Kunesh (unpub. data) made 27 "hourly" measurements of the flow from Waiakea Pond and computed the average discharge to be 146 million gallons per day. He stated " . . . the average discharge takes place at a time when the tidal gage height has dropped 0.1 foot lower than the higher-high or risen 0.1 foot higher than the lower-low—a matter of about one-half hour after these stages are reached."

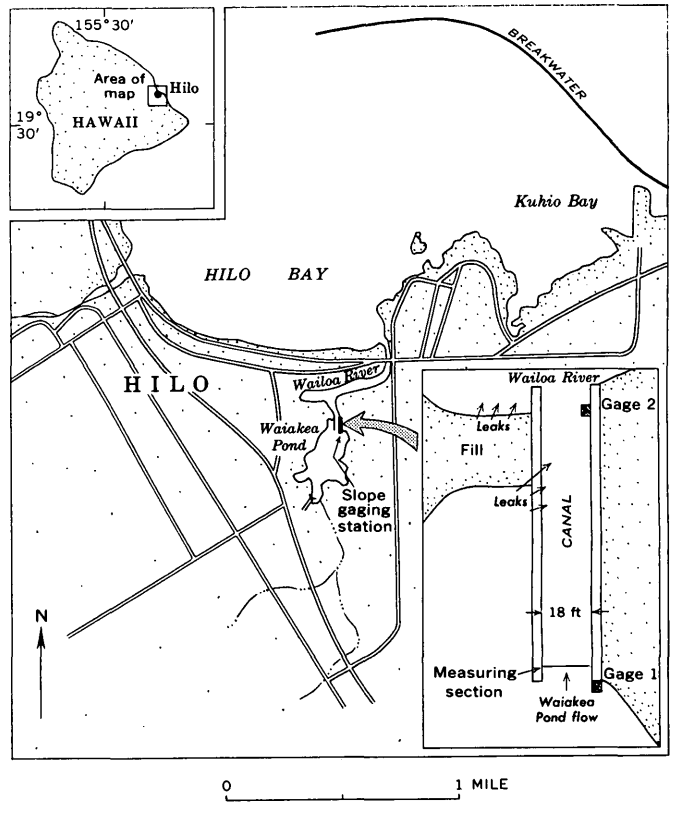

FIGURE 1.—Map showing location of Waiakea Pond in Hilo, Hawaii. Inset shows locations of recording gages and measuring section.

Kunesh made his measurements of the flow below the downstream end of the canal and used a gage near his measuring section to obtain stages. Canal gates prevented tidal inflow to the pond in 1930 when the measurements were made.

METHOD

In June 1965, no gates were in the canal. Measurements of the flow were made 5 feet downstream from the canal entrance, and stages were measured on a gage in Waiakea Pond (gage 1, fig. 1). Twenty-eight current-meter measurements were made during the tidal cycle from the high tide of June 27 to the high tide of June 28. All measurements were made with the meter suspended on a rod, and the center of the meter was kept at 0.6 of the depth for velocity readings. Near the center of the canal, when the flow was fairly steady, little difference was found between the velocity at the 0.6 depth and the average of the velocities at the 0.2 and 0.8 depths. During periods of rapidly falling or rising stages, time-saving techniques (half counts—20 to 30 seconds instead of the usual 40 to 60—of current-meter revolutions and measurements every 2 feet instead of every foot) were used to complete each measurement before a large change in discharge occurred.

RESULTS

The discharge measurements are given in table 1. Figure 2, plotted from these data, shows the variations in discharge caused by the tide-induced changes of Waiakea Pond stages.

From the highest through the lowest pond stages, and for part of the rise from the extreme low stage, there was outflow from the pond to Wailoa River (measurements 1 to 22, table 1). During the time when measurements 23 to 27 were made, tide level in the Wailoa River estuary was higher than the pond level (fig. 3) and sea water flowed through the canal into the pond.

The flow of water upstream into the pond was intermittent because of oscillations (seiches) of the water in Hilo Bay. These oscillations caused large horizontal movements of water in the bay which added to or neutralized the effect of the rising tide and resulted in alternate periods of tidal inflow and no flow. During one cycle of 16 minutes, there was no flow for 4 minutes. The direction in which the water moved was determined by observing the motion of suspended limu (seaweed).

Measurement 25 was made while the tidal inflow rate was still increasing; therefore, another measurement (26) was made when the tidal inflow rate was steady. When measurement 27 was made most of the flow was upstream into the pond but there was slight downstream movement of water at the surface; therefore, the actual inflow is slightly smaller than that indicated by the measurement.

The discharge computed from the measured discharge (106 mgd) and the discharge that bypassed the measuring section was 111 mgd. The measured discharge of 106 mgd was determined by adjusting the net-outflow volume of 110.5 million gallons (table 1) over the tidal cycle to a 24-hour period. The net-outflow volume was found by subtracting the tidal inflow of 3.6 million gallons from the outflow of 114.1 million gallons. The tidal inflow was computed by assuming that all periods of tidal inflow were interrupted by periods of no flow for one-quarter of the time.

The discharge that bypassed the measuring section was estimated from storage-change computations. In the time between measurements 21 and 28, the pond stage rose 2.83 feet (table 1). That rise indicated that 23.6 million gallons (72.45 acre feet) of water went into storage. In contrast, a change in storage of 22.4

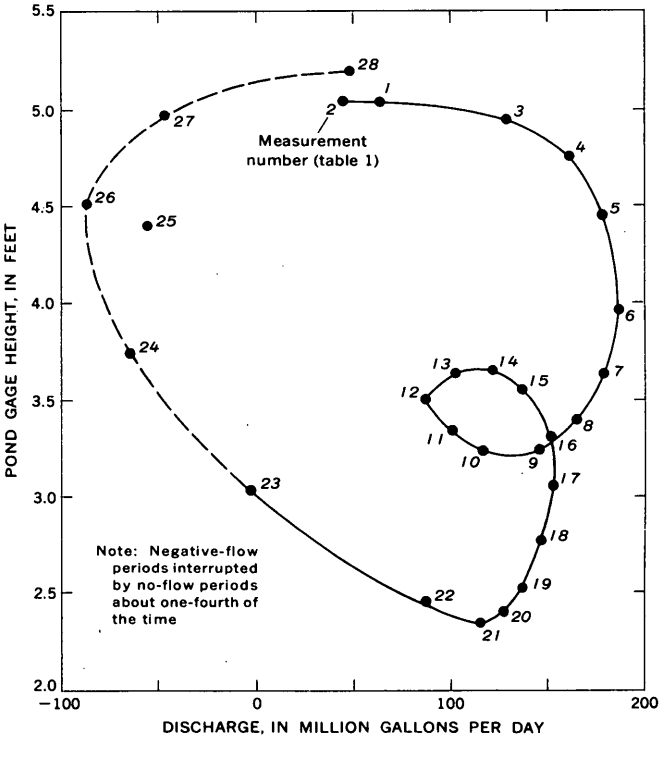

FIGURE 2.—Curve showing variation of outflow and inflow with stage of Waiakea Pond through a tidal cycle, June 27–28, 1965. Values to the right of the zero ordinate show outflow; those to the left show inflow. The dashed section of the curve indicates the period in which short-period oscillations interrupted flow.

TABLE 1.—*Measurements of discharge from Waiakea Pond through one tidal cycle, June 27–28, 1965*

No.	Time			Pond mean gage height (feet)	Discharge (mgd)	Average discharge (mgd)	Hours between mean times	Calculated discharge [1] (million gallons)	Hourly change in gage height (feet)
	Begin	End	Mean						
June 27, 1965									
1	1415	1435	1425	5.04	63.1				
						54.6	24/60	+0.91	----------
2	1440	1458	1449	5.05	46.0				
						87.5	43/60	+2.61	−0.10
3	1523	1541	1532	4.98	129				
						146	58/60	+5.88	−.23
4	1620	1640	1630	4.76	162				
						169	58/60	+6.81	−.39
5	1720	1737	1728	4.38	176				
						180	61/60	+7.62	−.40
6	1820	1838	1829	3.98	185				
						179	61/60	+7.58	−.35
7	1920	1940	1930	3.62	173				
						170	60/60	+7.08	−.26
8	2020	2040	2030	3.36	167				
						155	59/60	+6.35	−.12
9	2120	2138	2129	3.24	143				
						130	66/60	+5.96	0
10	2225	2245	2235	3.24	117				
						108	55/60	+4.12	+.12
11	2320	2340	2330	3.35	99.5				
						93.0	60/60	+3.88	+.17
June 28, 1965									
12	0020	0040	0030	3.52	86.6				
						95.8	60/60	+3.99	+.10
13	0120	0140	0130	3.62	105				
						114	60/60	+4.75	+.01
14	0220	0240	0230	3.63	122				
						129	60/60	+5.37	−.11
15	0320	0340	0330	3.52	136				
						143	62/60	+6.16	−.23
16	0420	0445	0432	3.28	150				
						152	56/60	+5.91	−.27
17	0515	1540	0528	3.03	154				
						148	64/60	+6.58	−.25
18	0620	0645	0632	2.76	143				
						140	57/60	+5.54	−.23
19	0720	0738	0729	2.54	138				
						134	60/60	+5.58	−.14
20	0820	0838	0829	2.40	129				
						122	60/60	+5.08	−.05
21	0920	0938	0929	2.35	115				
						101	59/60	+4.14	+.15
22	1020	1036	1028	2.50	87.9				
						43.1	63/60	+1.89	+.51
23	1120	1142	1131	3.04	−1.69				
24	1220	1231	1226	3.72	−63.9	----------			

25	1318	1327	1322	4.42	−54.9		3 1/3	−3.6	----------

26	1330	1335	1332	4.53	−84.7				

27	1420	1428	1424	4.98	−45.0				
						----------	1/3	+.32	----------
28	1500	1520	1510	5.18	46.8				

[1] Calculated discharge is equal to $\frac{1}{24}$ × average discharge × hours between mean times. It totals 110.5 million gallons for this tidal cycle.

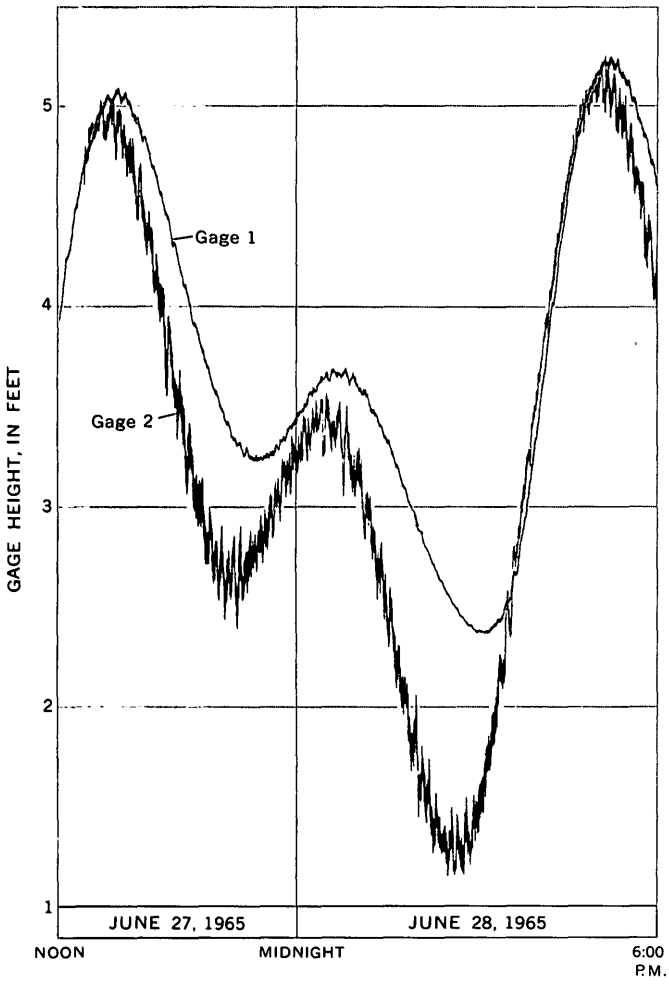

FIGURE 3.—Hydrographs showing Waiakea Pond water levels (gage 1) and tidal water levels (gage 2) through a tidal cycle, June 27–28, 1965.

million gallons was computed from the measured spring discharge (25.10 million gallons) and the outflow (6.35) and inflow (3.6) volumes between measurements 21 and 28. The difference of 1.2 million gallons in storage volume computed by the two methods is due mostly to unmeasured leakage through the fill and through the left wall of the canal (fig. 1). That leakage, computed from the difference in volume, was 5.1 mgd.

In the foregoing analysis, it was assumed that the leakage through the fill and the left wall of the canal was negligible during the period of rising tide because the difference in water level in the pond (gage 1) and in Wailoa River (gage 2) was small.

The pond gage-height changes between successive measurements adjusted to show hourly changes are shown in the last column of table 1. Maximum discharges occurred when the stage was dropping fastest. The minimum discharges occurred when the stage was rising fastest. The average discharge occurred when the stage had risen about 0.01 foot above the lowest stages reached during each of the two low tides. At the higher of the two low-tide stages, the average discharge occurred about three-quarters of an hour after the low point in stage was reached. At the lower of the two lows, the average discharge occurred about a quarter of an hour after the low point was reached.

At the lower of the two high-tide stages, the average discharge occurred when the stage was at its peak (fig. 4). At the higher high tide, the time of the occur-

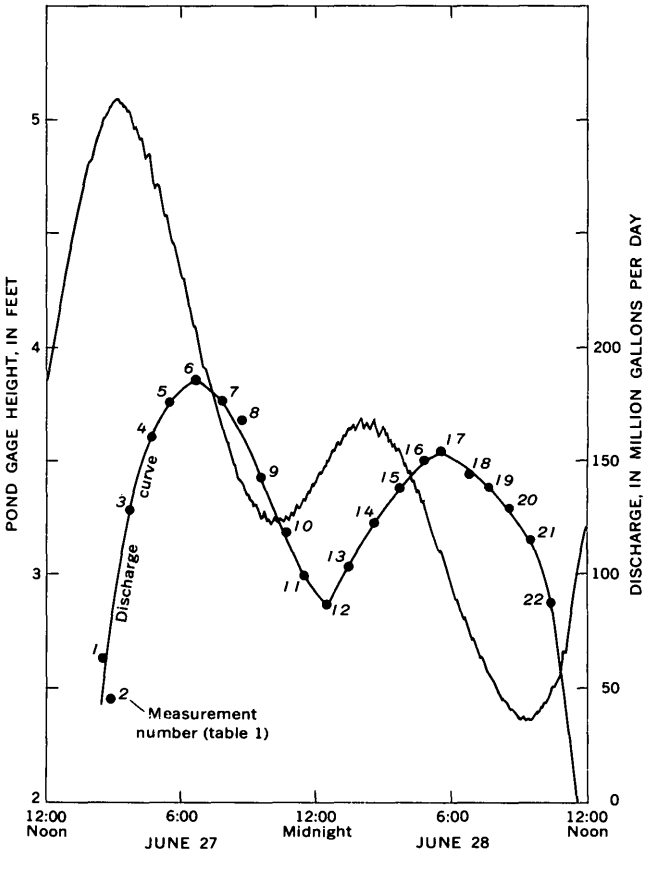

FIGURE 4.—Hydrographs showing water levels in Waiakea Pond (jagged curve) and discharge from the pond (smooth curve) during the period June 27–28, 1965.

TABLE 2.—*Chloride concentration in discharge from Waiakea Pond, June 27–28, 1965*

[All samples taken at water surface 5 ft downstream from recording gage]

Time	Chloride (ppm)	Remarks
		June 27, 1965
1430	878	Sample taken during positive flow (outflow from pond).
1450	756	Do.
1530	586	Do.
1628	756	Do.
1725	464	Do.
1820	537	Do.
1920	464	Do.
2020	610	Do.
2120	439	Do.
2220	659	Do.
2320	683	Do.
		June 28, 1965
0020	683	Sample taken during positive flow (outflow from pond).
0130	415	Do.
0220	464	Do.
0320	415	Do.
0520	488	Do.
0620	415	Do.
0720	488	Do.
0820	1, 342	Do.
0920	1, 440	Do.
1020	708	Do.
1120	659	Sample taken during positive flow (outflow from pond). Flow changed direction after sample was taken.
1220	952	Sample taken during tidal inflow (flow upstream into pond).
1320	2, 733	Do.
1420	4, 514	Do.
1500	512	Sample taken during positive flow (outflow from pond).

rence of the average discharge is a little uncertain because of the oscillation of the water level.

CHLORIDE CONTENT OF WAIAKEA POND WATER

Water samples for chloride determination were taken at the measuring section at hourly intervals throughout the tidal cycle (table 2). From the discharges (table 1) and chloride concentrations (table 2) the weighted average chloride concentration of the positive outflow was computed to be 609 parts per million. This concentration is about four times higher than can be accounted for by the mixing of 110 million gallons of spring water containing 7 ppm of chloride (sample taken from spring at upstream end of pond) and 3.6 million gallons of tidal inflow water whose maximum concentration was 4,500 ppm. The high-chloride concentration observed was probably due to:

1. Inflow into the pond of some ground water having a chloride concentration much higher than 7 ppm.
2. A carryover from previous tidal inflows which permitted a residue of sea water to accumulate in the pond.

REFERENCE

Fischer, W. A., Davis, D. A., and Sousa, T. M., 1966, Freshwater springs of Hawaii from infrared images: U.S. Geol. Survey Hydrol. Inv. Atlas 218.

HIGH-RESOLUTION SUBBOTTOM SEISMIC PROFILES OF THE DELAWARE ESTUARY AND BAY MOUTH

By D. W. MOODY and E. D. VAN REENAN,[1]
Philadelphia, Pa., Bedford, Mass.

Work done in cooperation with the U.S. Army Corps of Engineers

Abstract.—A high-resolution boomer system for continuous seismic profiling was used by the U.S. Army Corps of Engineers and the U.S. Geological Survey in a cooperative study of Delaware estuary sediments. The boomer, an electromagnetically driven low-frequency sound source, made it possible to penetrate as much as 42 m of sediment in water ranging from 2 to 35 m in depth. A resolution of less than 0.3 m produced extremely detailed profiles of subbottom structures.

The U.S. Geological Survey in cooperation with the U.S. Army Corps of Engineers made a subbottom survey of the Delaware estuary and the Delaware Bay mouth area in November 1965. Continuous longitudinal profiles were made along the centerline of the navigation channel from Philadelphia, Pa., to Woodland Beach, Del.; channel cross sections were made at 1-kilometer intervals (fig. 1). Additional profiles were made at the bay entrance between Cape Henlopen and Cape May. Three-point sextant fixes on shore signals during the survey provided horizontal control.

The primary objective of the subbottom survey was to test the high-resolution boomer system as a technique for studying shallow-water marine and estuarine sediments. The testing showed that the technique is an effective means of determining the thickness of sediments overlying bedrock in areas of proposed navigation-channel enlargement, and of studying the geometry and primary sedimentary structures of shoals. It might also be useful in locating areas where a wider and deeper channel might truncate shallow aquifers and possibly increase the movement of brackish and salt water into local ground-water supplies.

[1] EG & G International, Inc., Bedford, Mass.

INSTRUMENTATION

The high-resolution boomer system used in the Delaware estuary study is a modification of H. E. Edgerton's boomer profiling system (Van Reenan, 1964). The system consists of capacitor banks, an electromechanical transducer, a hydrophone array receiver, and a seismic recorder of the rotating helix type (fig. 2). During the survey, the hydrophone array and

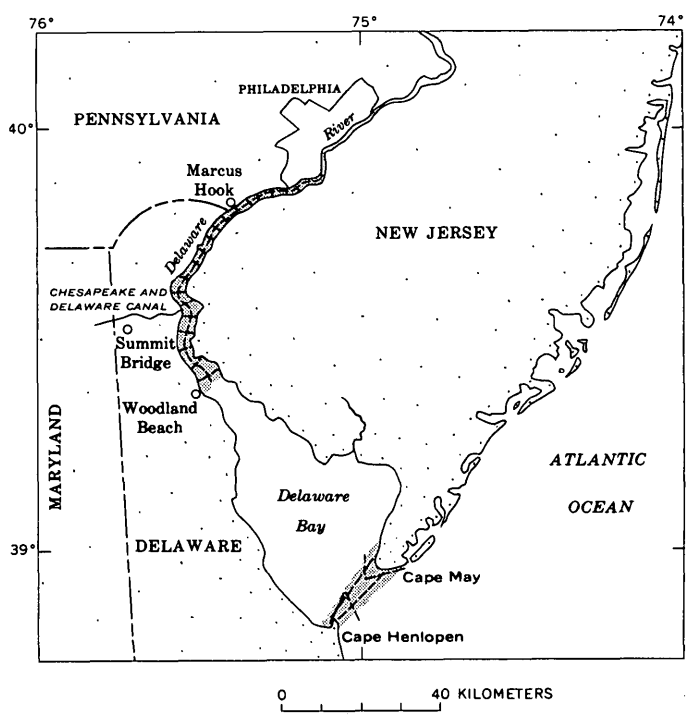

FIGURE 1.—Index map of Delaware Bay and estuary, showing areas (shaded) of subbottom surveys.

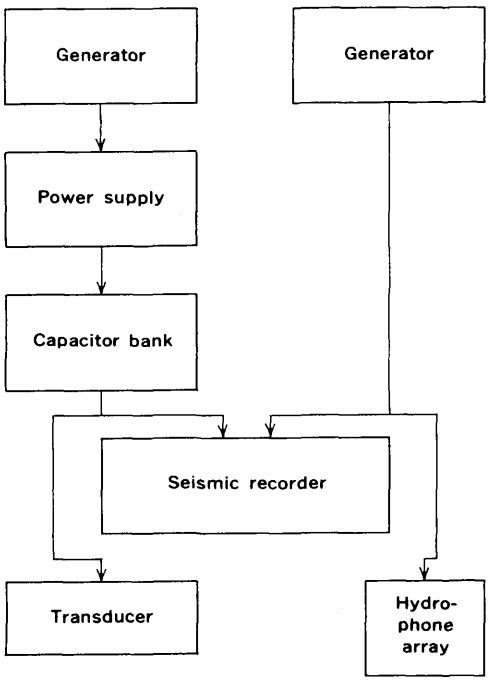

FIGURE 2.—Components of the high-resolution boomer system.

the transducer, which is mounted on a catamaran float, are towed about 5 meters behind the survey boat. These two components are kept separated by the boat's wake. The system was operated at capacitor energy levels of 200 joules.

The key component of the high-resolution boomer system is the transducer. A 3,700-volt current pulse discharges 2½ times per second through the flat-wound coil of the transducer and creates a magnetic field which violently repels a spring-loaded aluminum plate mounted against the coil. The transducer is designed to produce a monopolar sonic impulse having no secondary cavitations. The principal advantage of this system is its single line, high-resolution capability. The monopolar impulse also permits the generation of a broad low-frequency spectrum which gives good subbottom penetration but still retains a high degree of resolution. The frequency spectrum is nearly flat from less than 100 to more than 3,000 cycles per second. The acoustic pulse, thus emitted, is clear, discrete, and free from the undesired noise and record interference normally introduced by transducer cavitation. Hence, details of the near-surface sediments are shown on the records unobscured by noise. The fine-line reflectors which appear on some of the records represent individual sediment layers which reflect the high-frequency part of the output pulse.

The output frequency of the transducer cannot be precisely controlled, but it can be shifted from a high range to a lower range by varying the energy discharged into the transducer. Increasing the energy raises the peak acoustic output and lowers the frequency range, thus producing greater penetration.

RESULTS

Figure 3 (top) shows a longitudinal profile of the navigation channel in the vicinity of Marcus Hook, Pa. Two-way traveltime in seconds and apparent depths in meters are shown on this and each of the following figures. Figure 3 (bottom) is an interpretation of the boomer chart. Heavy lines indicate strong reflectors, and dashed lines indicate weak reflectors.

In the Marcus Hook area, metamorphic rocks of the Piedmont province crop out on the Pennsylvania side of the estuary. The profile (fig. 3) shows that if the channel is deepened, excavation of bedrock will be necessary. Similar adjacent profiles show that widening of the navigation channel also would require bedrock excavation. The bedrock depths, verified by a few borings, can be used to draw structure-contour maps of the bedrock surface or isopach maps of the overburden. Information such as this is of great value to the engineer planning the construction or enlargement of a navigation channel.

A longitudinal profile of the Chesapeake and Delaware Canal shows particularly well the primary sedimentary structures in sand waves, about 1–3 m high, formed by tidal currents (fig. 4). When the profile was made, tidal currents were moving eastward toward the Delaware River at about 100 centimeters per second (2 knots). Foreset beds in the sand waves dip 3°–12° in the direction of flow. These bed forms move over the channel bottom, which appears as a distinct reflector beneath them. The profiles bear a striking resemblance to ripple laminations formed in laboratory flume experiments (McKee, 1965).

Three to 4 km northeast of Cape Henlopen at the entrance to Delaware Bay, four profiles located a buried channel. Figure 5 shows that the bottom of the buried channel is 26 m below the present bay bottom (56 m below sea level). Although there are no borings to provide material for carbon-14 dating, the buried channel was probably eroded by the ancestral Delaware River during the last retreat of the sea about 18,000 years ago. Much of the entrance to Delaware Bay was found to be underlain by a complex pattern of buried channels ranging from 6 to 56 m below sea level. A more intensive survey of this type would enable the detailed mapping of these channels.

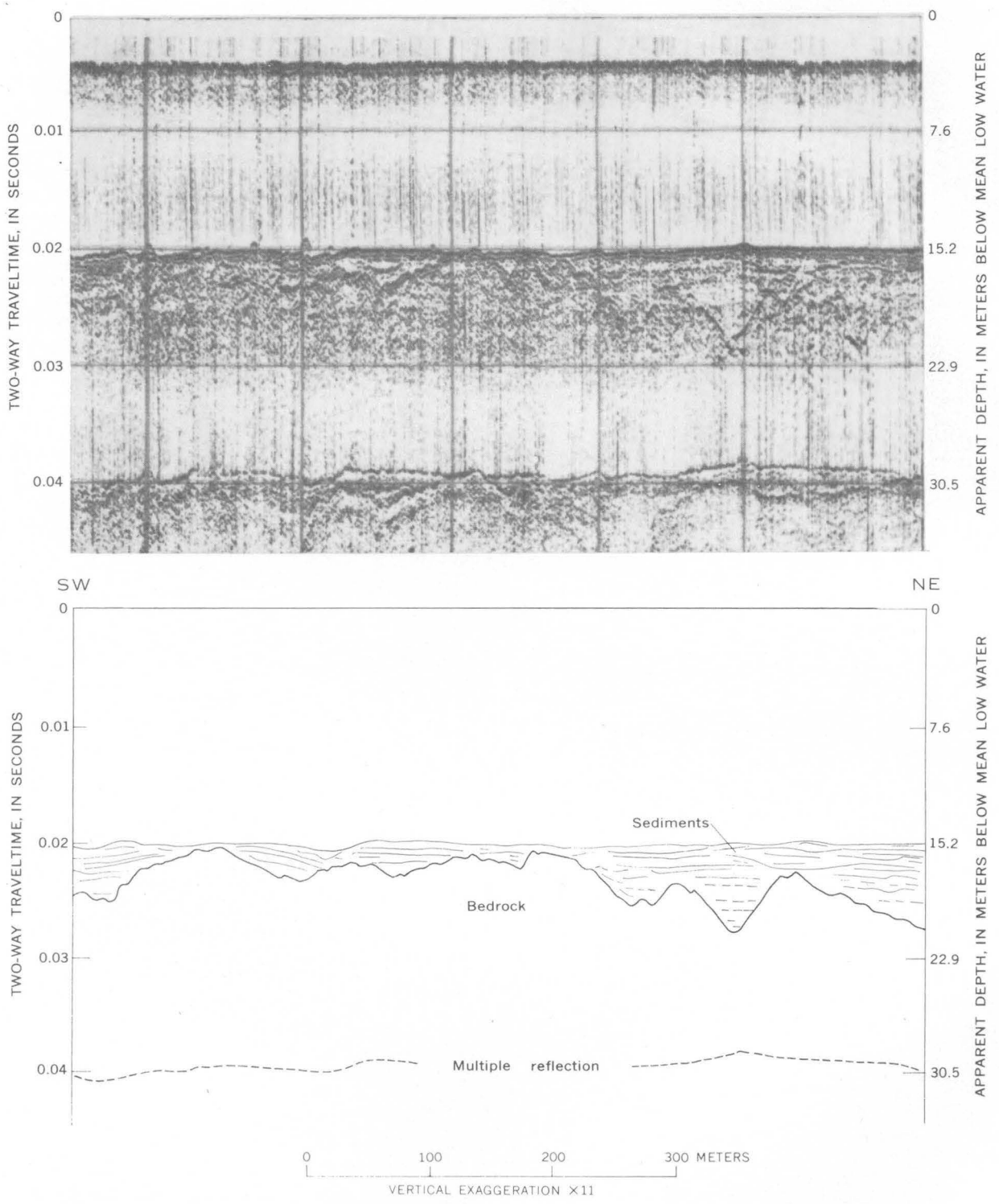

FIGURE 3.—Longitudinal profile of Delaware estuary navigation channel near Marcus Hook, Pa. Top, boomer record; bottom, interpretation of record.

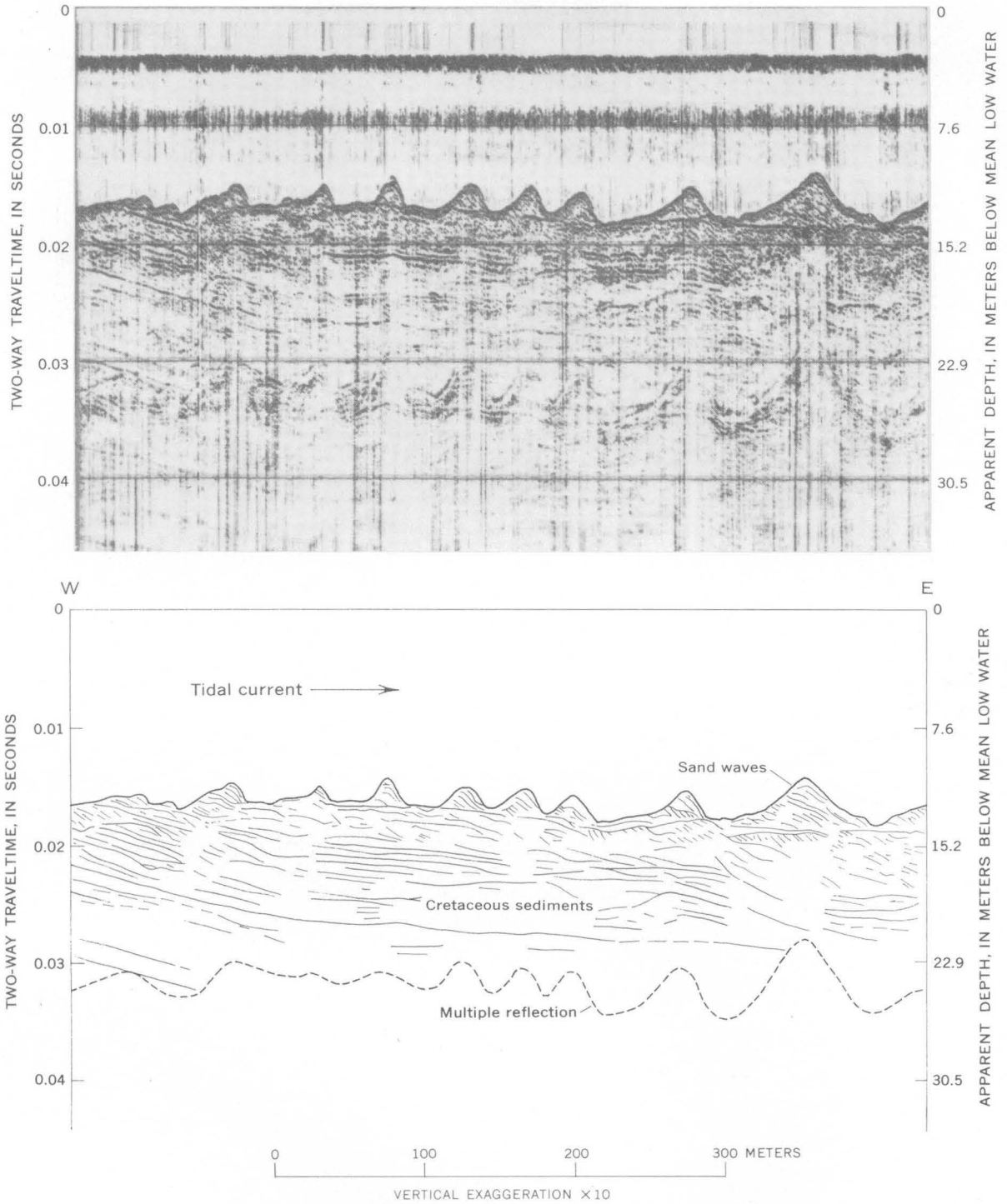

FIGURE 4.—Longitudinal profile of the Chesapeake and Delaware Canal near Summit Bridge, Del. Top, boomer record; bottom, interpretation of record.

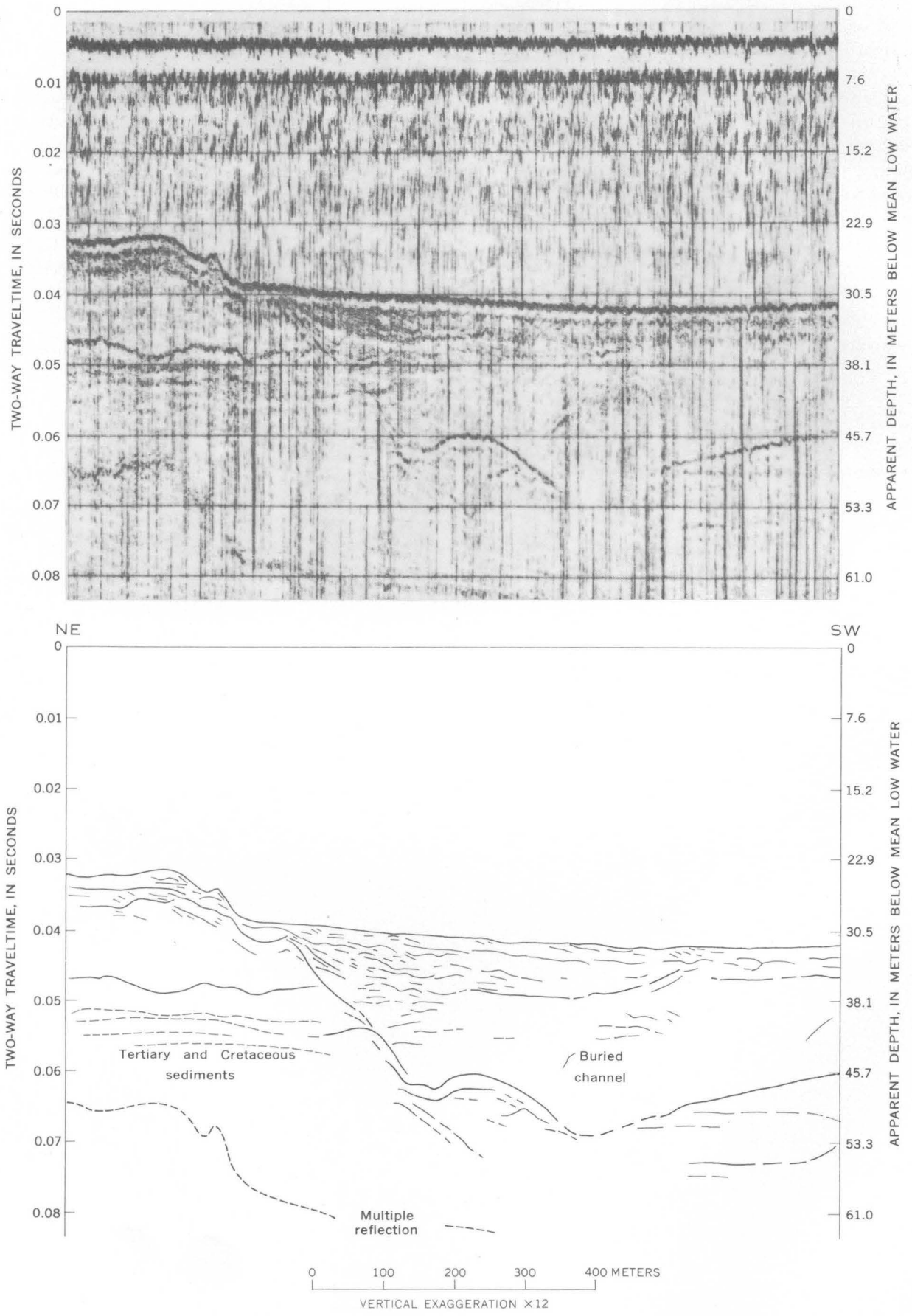

FIGURE 5.—Cross section at entrance to Delaware Bay 3–4 km northeast of Cape Henlopen, Del. Top, boomer record; bottom, interpretation of record. (Presence of Tertiary and Cretaceous sediments interpolated from Gill, 1962, and Rasmussen and others, 1960.)

Not all parts of the estuary that were surveyed produced records of as high a quality as those illustrated in this report. In some areas, particularly those bordering the shoreline, poor quality records were associated with organic fine-grained sediments collected as part of a bottom-sediment sampling program. Poor penetration and strong multiple bottom reflections may be attributed to entrapped gas bubbles formed by decomposing organic matter. Where such material had been removed by dredging or where the bottom material was coarse grained, penetration was good. Nearly all the Delaware Bay profiles were of satisfactory quality, but only about 40 percent of the records obtained from the Delaware estuary were usable.

CONCLUSIONS

The high-resolution boomer system has great potential for the investigation of shallow-water sediments. In the Delaware estuary the system made it possible to penetrate as much as 42 m of sediment. Because the boomer has an electromechanical noise source, it can be used in both fresh and salt water. The resolution capability of less than 0.3 m enables the collection of extremely detailed profiles and provides much information on the geometry and structure of sedimentary deposits. Such profiles, made in conjunction with a program of test borings and core collection, enable large areas of lakes, reservoirs, rivers and estuaries to be readily studied in connection with a variety of hydrologic, geologic, and engineering problems.

REFERENCES

Gill, H. E., 1962, Ground-water resources of Cape May County, N.J.—Salt-water invasion of principal aquifers: New Jersey Dept. Conserv. and Econ. Devel., Div. Water Policy and Supply Spec. Rept. 18, 171 p.

McKee, E. D., 1965, Experiments on ripple lamination, *in* Middleton, G. V., ed., Primary sedimentary structures and their hydrodynamic interpretation: Soc. Econ. Paleontologists and Mineralogists Spec. Pub. 12, p. 66–83.

Rasmussen, W. C., Wilkens, R. A. and Beall, R. M., and others, 1960, Water resources of Sussex County, Delaware, with a section on salt-water encroachment at Lewes: Delaware Geol. Survey Bull. 8, 228 p.

Van Reenan, E. D., 1964, Subsurface exploration by sonar seismic systems, *in* Symposium on soil exploration: Am. Soc. Testing Materials Spec. Tech. Pub. 351.

PREDICTION OF SALT-WATER INTRUSION IN THE DUWAMISH RIVER ESTUARY, KING COUNTY, WASHINGTON

By J. D. STONER, Tacoma, Wash.

Work done in cooperation with the Municipality of Metropolitan Seattle

Abstract.—Accurate predictions of salt-water intrusion 7.8 miles upstream from the mouth of the Duwamish River can be made for the 3-foot surface layer, using the relationship between tide height and fresh-water discharge. Intrusion occurs at the site regardless of the high-tide height, when discharge is less than 625 cfs, whereas a discharge of more than 1,000 cfs is sufficient to prevent intrusion at any tide stage. Between 625 and 1,000 cfs, intrusion is dependent upon both discharge and high-tide height.

In 1963 the U.S. Geological Survey, in cooperation with the Municipality of Metropolitan Seattle, initiated a comprehensive study of the effect of sewage effluent on water quality in the Duwamish River and its estuary. The presence of saline water materially affects biologic characteristics, dissolved oxygen, biochemical oxygen demand, and other similar factors. Therefore, if the extent of salt-water intrusion can be predicted, studies intended to evaluate these parameters can then be planned to give more meaningful data.

The reach of river and estuary under study extends upstream for 13.1 miles to the Renton Junction bridge (fig. 1). Within this length, at mean sea level, the channel has a water-surface area of 1.0 square mile and a volume of 400 million cubic feet. Channel depths below mean sea level in this study area range from less than 3 feet to 56 feet, and average 31 feet. The mean tide range at the mouth is 7.6 feet. Vertical-salinity profiles indicate that the estuary is of the salt-wedge type as classified by Pritchard (1955). The landward boundary of the wedge migrates upstream and downstream, dependent upon tide stage and fresh-water discharge. There is an upstream limit above which the water at all depths is always fresh, and a seaward limit below which the water at all depths is always saline.

Because the intrusion is dependent upon tidal stage and fresh-water discharge, these variables were studied to develop a relationship that could be used to predict intrusion. For this study, conductivity was chosen as the salinity indicator.

DATA COLLECTION AND DISCUSSION

At one site within the fresh–saline transitional area, an automatic water-quality monitor has been installed. At this site—the East Marginal Way Bridge, 7.8 miles from the mouth—conductivity is continuously measured. The intake of the conductivity sensing device is 3 feet below the water surface. Therefore, in this study, prediction of intrusion is limited to that which occurs within 3 feet of the surface.

A conductivity of 200 micromhos per centimeter at 20°C was chosen as the minimum value above which saline intrusion is considered to occur at East Marginal Way. The conductivity 5.3 miles farther upstream at the Renton Junction river-stage recorder site is consistently near 100 micromhos, and no inflow between these sites is of sufficient quantity and solute content to increase the conductivity at East Marginal Way from 100 micromhos to 200 micromhos or more.

The discharge figures used in the following comparisons were computed from the gage-height record of the U.S. Geological Survey river-stage recorder, at Renton Junction, 5.3 miles upstream from the East Marginal Way Bridge. Mean daily discharges were used. Tidal information was obtained from the U.S. Coast and Geodetic Survey tide tables (1963, 1964).

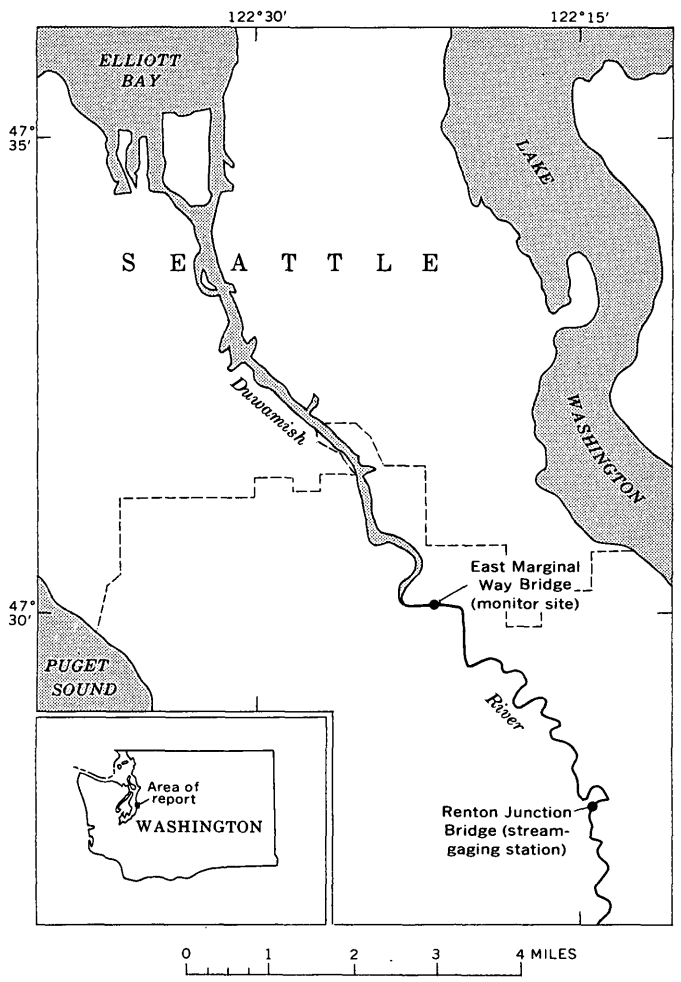

FIGURE 1.—Index map of Duwamish River and vicinity, showing location of water-quality monitor and stream-gaging station.

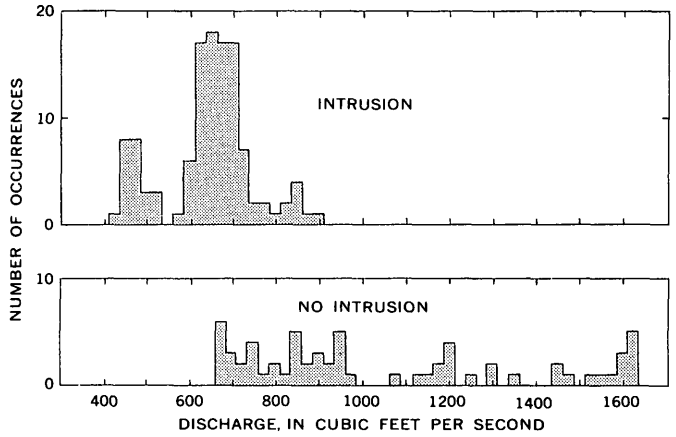

FIGURE 2.—Occurrence of salt-water intrusion at East Marginal Way Bridge for different fresh-water discharges, August–November 1964.

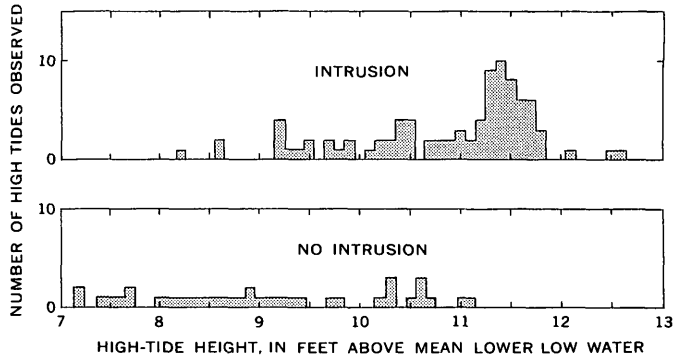

FIGURE 3.—Occurrence of salt-water intrusion at East Marginal Way Bridge for different high-tide heights, August–November 1964. Discharge range is 625 to 1,000 cfs.

Figure 2 shows the number of high tides during which intrusion did or did not occur at East Marginal Way for different fresh-water discharges. The data show three distinct discharge intervals. At values less than 675 cubic feet per second, the fresh-water discharge is too small to prevent intrusion; whereas at discharges greater than 900 cfs, the fresh-water flow is sufficient to prevent intrusion at all tide stages. Between 675 and 900 cfs, intrusion may or may not occur. For the purpose of normal day-to-day prediction, the 675- and 900-cfs limiting values are arbitrarily extended to 625 and 1,000 cfs to provide for a smaller margin of error. As more data become available, the discharge boundaries can be set more precisely.

A plot showing the presence or absence of salt-water intrusion at different high-tide heights is given in figure 3 for the discharge range from 625 to 1,000 cfs. The figure shows the effect of high-tide heights on intrusion in that range. The reference datum for both figures 3 and 4 is mean lower low water, which is the datum commonly used along this part of the west coast by the U.S. Coast and Geodetic Survey. Below 9.0 feet, the tide is usually not high enough to cause intrusion. Between 9.0 and 11.0 feet, the effect of tide height and discharge is not clear in this figure, but above 11.0 feet, intrusion is almost certain in the 625- to 1,000-cfs range. The general trend from little chance of intrusion from 9.0-foot tides to a near certainty of intrusion at the higher tides during the 625- to 1,000-cfs discharge range is fairly clear. The trend in figure 3 suggests that the occurrence of intrusion in that discharge range is dependent upon how discharge and high-tide height combine. The curve in figure 4 shows the effect of combinations of discharge and high-tide height in the 625- to 1,000-cfs range. For any combination of discharge and high-tide height above or to the left of the curve, intrusion occurs; and for any combination below or to the right, intrusion does not occur.

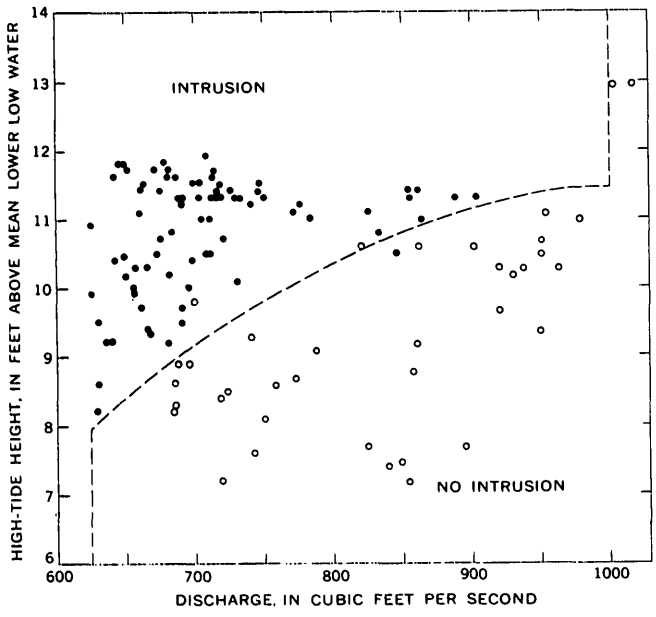

FIGURE 4.—Occurrence of salt-water intrusion at East Marginal Way Bridge for combinations of high-tide heights and fresh-water discharge, August–November 1964. Solid circle indicates intrusion; open circle indicates lack of intrusion.

Data for the period August through November 1964 were used to develop this relationship. This particular period was chosen because of the availability of continuous conductivity information. Fortunately, the fresh-water discharge varied from the minimum to well in excess of 1,000 cfs during the same period.

Of the high tides from August through November 1964, salt-water intrusion occurred consistently when the discharge was less than 625 cfs, but never when the flow was above 1,000 cfs. For the intermediate range, 625 to 1,000 cfs, the relationship illustrated in figure 4 is valid for 97 percent of the tides recorded.

As a check on the accuracy of the curve in figure 4, intrusion data based on the continuous record of conductivity from August to December 1965 were compared with the corresponding discharge and tide heights. All the tides occurring when fresh-water discharge was below 625 cfs and above 1,000 cfs during that period were in agreement with the relationship in figure 4. During the same period, 95 tides occurred when the discharge range was between 625 and 1,000 cfs; 97 percent of these tides were in agreement with the relationship in figure 4.

SALT-WATER INTRUSION PREDICTION

An approximation of the distribution of salt-water intrusion throughout the year can be made by using discharge records, as shown in table 1.

TABLE 1.—*Approximate distribution of salt-water intrusion in percent of time per year, for gaging station at Renton Junction*

[Derived from discharge records, water years 1961–65]

Discharge	Distribution		
	Mean	Maximum	Minimum
<625 cfs (insufficient to prevent intrusion)	27	35	13
>1,000 cfs (sufficient to prevent intrusion)	55	73	39
625–1,000 cfs (intrusion dependent upon tide height as well as discharge)	18	33	6

In this paper, the prediction of intrusion was limited to a single point in the stream. Using this technique at several stations along the river, one can determine the upstream intrusion distance for the different fresh-water discharges and high-tide heights. The limit of precision desired would be a function of the distance between longitudinal stations.

The prediction method described here has worked successfully in the Duwamish estuary. The tide heights used are available at least a year in advance. Knowledge of river discharge at some future time is, of course, impossible; however, in most situations, discharge can be estimated at least 1 to 2 days in advance with reasonable accuracy. With this information, sampling schedules can be established from 1 to 5 days in advance.

The Duwamish estuary, as previously noted, is of the salt-wedge type. It remains to be seen whether the prediction method will work equally well in partially mixed and vertically homogeneous estuaries.

REFERENCES

Pritchard, D. W., 1955, Estuarine circulation patterns: Am. Soc. Civil Engr. Proc., v. 81, separate 717, 11 p.

U.S. Coast and Geodetic Survey, 1963 and 1964, Tide tables, high and low water predictions, west coast North and South America, 1964 and 1965: Washington, D.C., U.S. Govt. Printing Office.

CHANGE IN QUANTITY OF DISSOLVED SOLIDS TRANSPORTED BY SHARON CREEK NEAR PALO ALTO, CALIFORNIA, AFTER SUBURBAN DEVELOPMENT

By JOHN R. CRIPPEN, Menlo Park, Calif.

Abstract.—Data collected in a small basin in the coastal region of central California before and after suburban development within the basin indicate that the total load of dissolved solids carried from the basin by streamflow increased tenfold after development. There was a slight increase in imported solutes because of the importation of irrigation water, but this was not great enough to explain the increased outflow load.

The 245-acre basin of Sharon Creek near Palo Alto, Calif., was studied from 1958 to 1965 to observe the effects of suburban development on the hydrologic regime. The basin was virtually in a natural condition through September 1961. Construction and landscaping were in progress from October 1961 through the summer of 1962, and land-use characteristics did not change from September 1962 through 1965. After development an irrigated golf course occupied 35 percent of the basin; houses and offices, about 11 percent; and streets, roads, and other paved areas, about 4 percent. The remaining 50 percent remained in its natural state of grassland with scattered brush and trees. A separate sanitary sewage system removed domestic wastes from the basin, and storm sewers within the basin conveyed runoff directly to Sharon Creek. Imported water was released into the basin for irrigation and for the maintenance of swimming pools and a pond in the golf course that served as a balancing reservoir and as a decorative feature. The imported water was of very good quality, containing about 30 parts per million of dissolved solids (California Department of Public Health, 1962, p. 41)

Records of discharge from the Sharon Creek basin and from a neighboring 302-acre basin were collected from October 1958 through September 1965. The adjacent basin, Los Trancos Creek tributary, remained in a natural state throughout the period; land use was very similar to that in the Sharon Creek basin before its development. Field and laboratory analyses were made on 45 water samples from Sharon Creek and on 38 from Los Trancos Creek tributary. Specific conductance was determined in Sharon Creek during periods of flow before development and biweekly when flow became perennial, after development. These data provide a basis for estimates of the annual loads of dissolved solids removed from the two basins by streamflow. The estimates are shown in table 1.

The estimates of annual loads of dissolved solids transported from the Sharon Creek basin before development and from the Los Trancos Creek tributary basin during the entire period, in tons per acre, have been plotted against an index of effective precipitation in figure 1. The relation shown between the two can be expressed as

$$L = 0.00208\ P_S - 0.00756,$$

where L is the annual load in tons per acre and P_S is the index, or storm precipitation, during each year. The equation cannot be considered indicative of relations in other areas or for years when annual storm precipitation greatly exceeds the observed upper and lower limits of about 16 and 3.6 inches. Storm precipitation in the study basins is probably within these limits during more than 80 percent of years. Most years having less than 10 inches of total precipitation have less than 3.6 inches of storm precipitation and therefore experience no runoff in this region, although the time distribution of occurrence of precipitation varies and occasionally even a very dry year produces small amounts of streamflow. Yearly total and storm precipitation at Sharon Creek are shown in table 1.

U.S. GEOL. SURVEY PROF. PAPER 575-D, PAGES D256-D258

TABLE 1.—*Annual input and outflow of dissolved solids, Sharon Creek and Los Trancos Creek tributary, 1959–65*

Water year (Oct. 1–Sept. 30)	Precipitation at Sharon Creek (inches)		Estimated quantity of dissolved solids (tons)					
			Sharon Creek				Los Trancos Creek tributary	
			Total outflow		Input to basin		Total outflow	Input from precipitation
	Total	Storm	Natural conditions [1]	Developed conditions	From precipitation	From imported water		
1959	12.4	8.4	2.0	----------	3.4	----------	3.8	4.4
1960	11.7	8.3	2.9	----------	3.2	----------	3.6	3.7
1961	10.3	4.1	.02	----------	2.9	----------	.12	3.5
1962	15.8	13.0	4.8	28	4.4	7.1	3.9	4.7
1963	21.3	15.9	6.3	55	5.9	7.2	6.5	7.0
1964	11.1	4.9	.7	33	3.1	7.3	1.1	3.8
1965	18.4	15.1	5.8	56	5.1	7.5	9.3	5.5

[1] 1962–65 estimated from figure 1.

Yearly inputs from precipitation in the Sharon Creek and Los Trancos Creek tributary basins are almost identical. Precipitation during the study period totaled only about 85 percent of the 1911–65 mean at Palo Alto, 4 miles from Sharon Creek.

The relation between L and P_s has been used to estimate the load of dissolved solids that would have been carried from the Sharon Creek basin by streamflow if conditions had remained natural in the period 1962–65, and these estimates are also listed in table 1. The estimates are only approximate, but the magnitude of the difference between natural and developed conditions is probably well indicated.

Development within the basin was followed by a marked change in the flow regime of Sharon Creek. Runoff from impervious surfaces and from the irrigated golf course increased greatly and occurred during periods when, under natural conditions, there would have been little or no flow. The combined effects of increased flow and increased concentration of dissolved solids resulted in a much greater load of solutes being carried from the basin under developed conditions than under natural conditions. Thus, under natural conditions in the 3 years 1963–65 there would have been about 13 tons of dissolved solids transported from the basin; the actual quantity, however, totaled about 144 tons—more than 10 times that estimated for natural conditions.

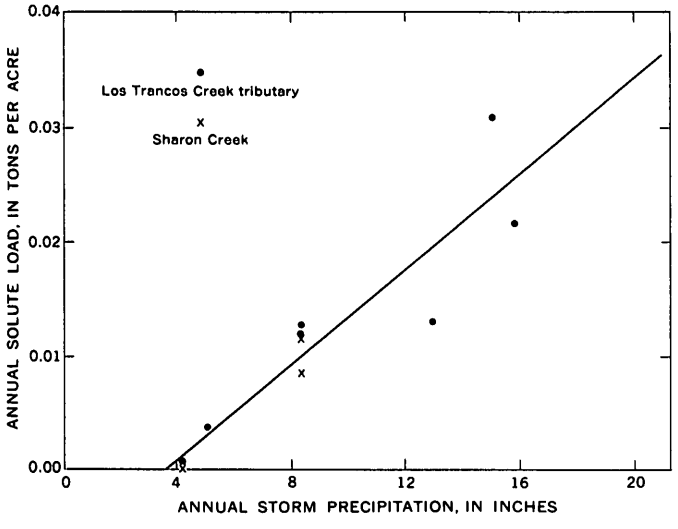

FIGURE 1.—Relation between annual outflow of dissolved solids and annual storm precipitation, Sharon Creek (1959–61) and Los Trancos Creek tributary (1959–65).

The large variation in load between the years 1960, 1961, and 1964—years having a variation of less than 1.5 inches in annual precipitation—reflects the fact that precipitation amounts during those years were very close to the threshold below which no runoff is likely. Runoff of Los Trancos Creek tributary for the 3 years was 10.8, 0.08, and 6.8 acre-feet, respectively.

Table 1 also shows the estimated amounts of dissolved solids introduced into the basins by precipitation and into the Sharon Creek basin by imported water. The solutes brought by precipitation were estimated on the basis of data reported by Whitehead and Feth (1964), and the contribution of imported water was computed from reliable estimates of the volume of imported water and from analyses previously cited. The amount of dissolved solids brought by precipitation was estimated as high as possible (10 ppm) from the data of Whitehead and Feth, because no allowance has been made for the input from dry fallout. A 7-year summation of the estimates under natural conditions shows an excess of input of solutes over outflow. This excess should not be construed as typical of the long term; the flushing action was probably greater during normal or wet periods than it was during the relatively dry study years.

The flow from paved channels, pavements, and roofs that accounts for the increased runoff ordinarily accompanying urbanization is likely to have a lower concentration of dissolved solids than the natural runoff. The cause of the higher concentration observed in Sharon Creek after 1962 under developed conditions (table 1) is not certain, but two possibilities have been suggested:

(1) The natural soil distribution was altered extensively during development, especially where cuts and fills were necessary to establish the desired golf-course topography, and thus much material which had not been thoroughly leached in the past was exposed. Runoff from this material would tend to be higher in dissolved solids than would the runoff from an undisturbed area;

(2) Irrigation water is supplied to lawns and to the golf course at a rate as nearly as possible equal to the consumptive need. Dissolved solids may be retained in the irrigated area and later be leached away by any excess of water. It is also possible that the year-round active growth in the irrigated areas may produce carbon dioxide that would increase the solvent power of soil moisture.

REFERENCES

California Department of Public Health, 1962, California domestic water supplies: Bur. Sanitary Eng., 76 p.

Whitehead, H. C., and Feth, J. H., 1964, Chemical composition of rain, dry fallout, and bulk precipitation at Menlo Park, Calif., 1957–1959: Jour. Geophys. Research, v. 69, p. 3319–3333.

A PRELIMINARY STUDY OF THE EFFECT OF URBANIZATION ON FLOODS IN JACKSON, MISSISSIPPI

By K. V. WILSON, Jackson, Miss.

Work done in cooperation with the city of Jackson, Miss.

Abstract.—Comparison of flood-frequency curves for three streams near Jackson, Miss., based on annual maximum floods for the period 1953–66, and for another stream for a shorter period, indicates thtat the mean annual flood for a totally urbanized basin is about 4½ times that of a similar rural stream. It further indicates that the 50-year flood for such an urbanized basin is about 3 times that of a rural stream.

As part of a cooperative program of the U.S. Geological Survey and the City of Jackson, Miss., flood records from Jackson streams have been collected since 1953. This paper presents a preliminary analysis of peak discharges determined from the flood data and should help fulfill an urgent need for flood-frequency data on small urbanized areas in Mississippi.

A previous report (Wilson and Trotter, 1961) presents curves from which the magnitude and frequency of floods in most rural drainage areas in Mississippi can be estimated by using size, shape, and location of basin as independent variables. This report discusses drainage basins above gaged points on urban-area streams (fig. 1) and compares the drainage with that of rural areas. The urban-area streams are Eubanks, Town, Lynch, and Three-Mile Creeks.

FLOOD-FREQUENCY ANALYSIS

Individual flood-frequency curves (based on annual peak flows) for Eubanks, Town, and Lynch Creeks (1953–66), and for Three-Mile Creek (1962–66) were used to develop the composite frequency curve shown on figure 2. This composite curve is the mean of the curves for the 4 streams. As shown by figure 2, the 50-year flood is only about twice the magnitude of the mean annual flood, a phenomenon that differs considerably from that for larger rural areas where 50-year floods are about three times the mean annual flood. The difference is attributed to storm sewers, gutters, and manmade ditches which function well during low-order floods but which are overtaxed during extreme floods.

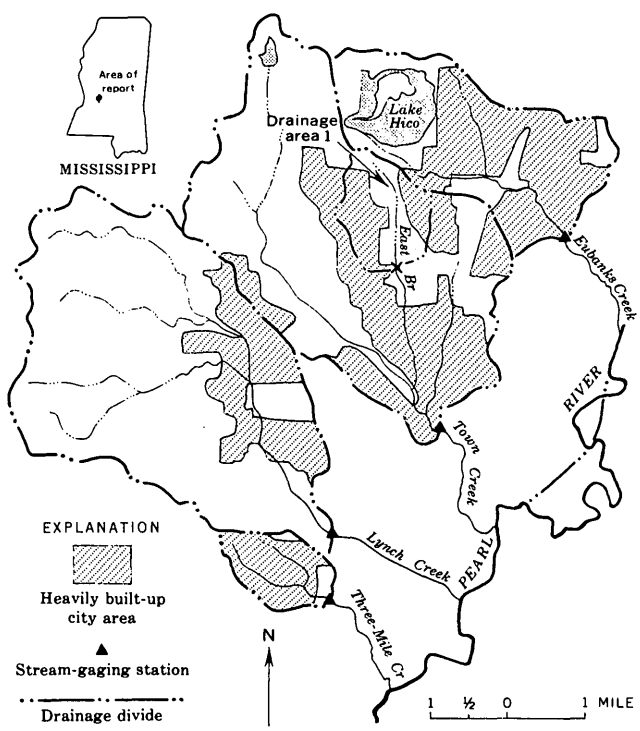

FIGURE 1.—Map showing drainage basins of gaging stations in Jackson, Miss. X, location of proposed Carnation Street crossing.

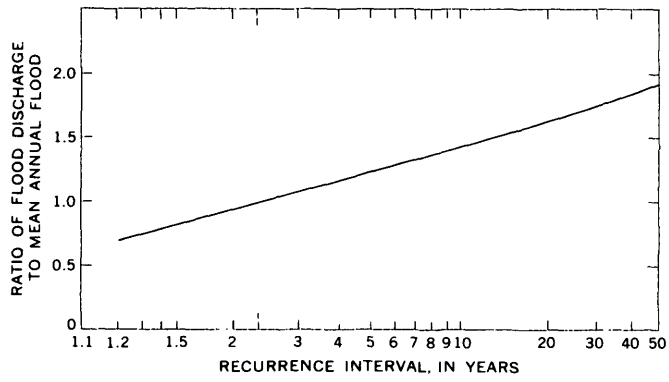

FIGURE 2.—Composite flood-frequency curve for streams in Jackson, Miss.

The values of the mean annual floods for each of the four gaged sites, determined from their individual flood-frequency curves, were found to be from 2 to 3½ times the values of the means obtained from curves for rural streams discussed in the previous report (Wilson and Trotter, 1961). A plot of these ratios versus the percentage of the basin area with storm sewers and improved channels is shown on figure 3. The curve drawn through these points and extended indicates that the mean annual flood for a basin with 100 percent of its area containing storm sewers and improved channels is about 4½ times that of a rural stream.

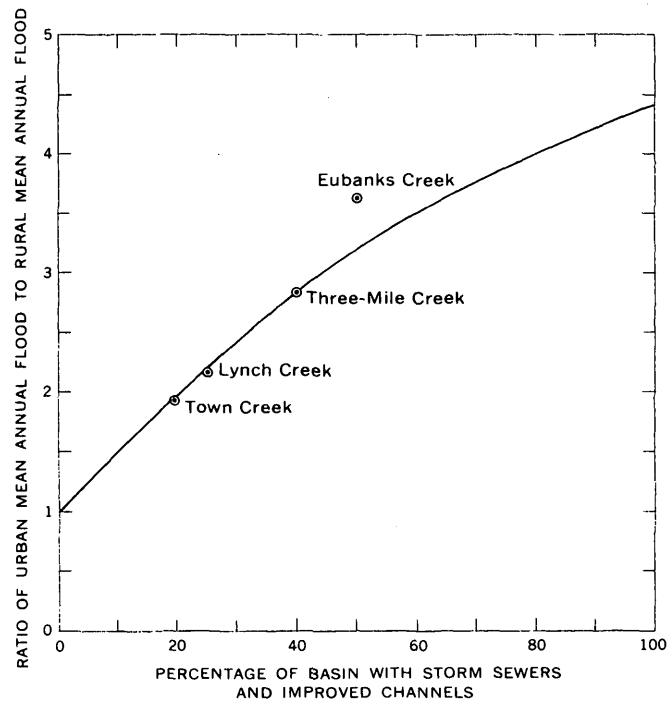

FIGURE 3.—Effect of urbanization on mean annual floods in Jackson, Miss.

Curves relating the mean annual flood to drainage area are presented on figure 4. These curves were defined for various degrees of development by using the curve in figure 3 of this paper and the curve for the mean annual flood on natural streams in hydrologic area 2 of the report by Wilson and Trotter (1961). The values of the mean annual floods determined from the individual frequency curves for the four gaged sites are plotted on figure 4.

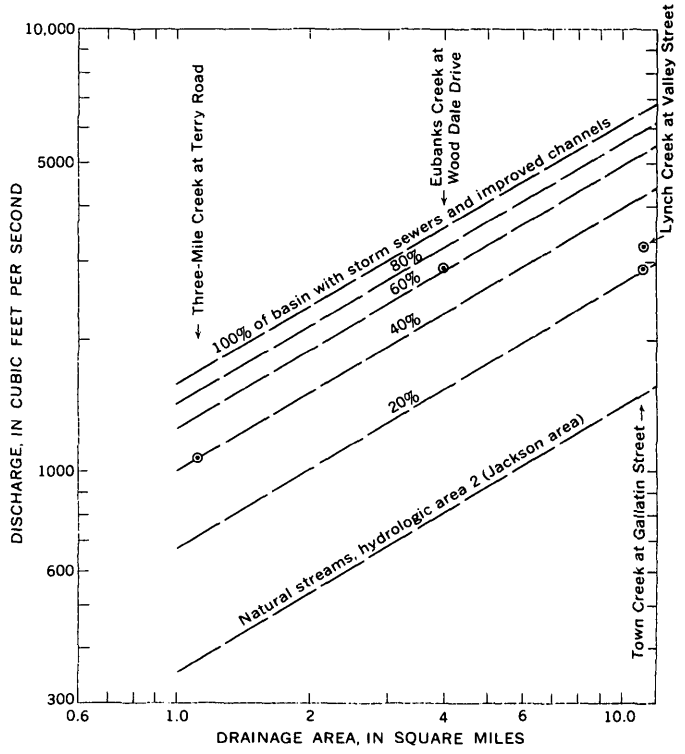

FIGURE 4.—Mean annual flood curves for streams in Jackson, Miss. The upper five curves are for the indicated percentages of basin with storm sewers and improved channels. The lowest curve is for hydrologic area 2 of Wilson and Trotter (1961).

APPLICATION OF CURVES

The curves presented on figures 2 and 4 can be used to estimate the magnitude and frequency of floods of small streams in Jackson. For the purpose of illustration, let us assume that a user is interested in the 50-year peak discharge for the following:

Site—East Branch of Town Creek at proposed Carnation Street crossing.

Drainage area—1.16 square miles (drainage area 1 on fig. 1).

Land use—70 percent residential, 10 percent industrial, 20 percent rural pasture, 20 percent of basin

presently has storm sewers and improved channels, but this figure will be raised to 50 percent within the next few years.

The discharge can be determined as follows:

1. Using figure 4 and assuming that 50 percent of the basin is developed with storm sewers and improved channels, the mean annual flood for 1.16 square miles is about 1,200 cubic feet per second.
2. From figure 2, the 50-year flood is 1.92 times the mean annual flood; therefore, the 50-year flood for East Branch of Town Creek at the proposed Carnation Street crossing site is $1{,}200 \times 1.92 = 2{,}300$ cubic feet per second.

REFERENCE

Wilson, K. V., and Trotter, I. L., Jr., 1961, Floods in Mississippi, magnitude and frequency: Mississippi State Highway Dept. Jackson, 326 p.

EFFECTS OF RELEASED RESERVOIR WATER ON THE QUALITY OF THE LEHIGH RIVER, PENNSYLVANIA

By E. F. McCARREN and W. B. KEIGHTON, Philadelphia, Pa.

Abstract.— The release of 11 billion gallons of water from the Francis E. Walter Reservoir between June 20 and 27, 1966, changed the quality of water in the Lehigh River. In the reservoir the temperature and the dissolved-oxygen concentration of the impounded water decreased with depth. Releases made from the bottom of the reservoir increased the flow and color of the river water, lowered its temperature and specific conductance, and slightly lowered its pH. Although the water released from the reservoir had a low concentration of dissolved oxygen, the turbulence and diffusion of water in the river quickly helped to reoxygenate water to near saturation for 40 river miles below the reservoir. At the termination of the releases, river water returned to base-runoff quality.

In preparation for the hurricane season, the Delaware River Basin Commission in June 1966 requested that water be released from the Francis E. Walter Reservoir on the Lehigh River in order to have more space in the reservoir for holding excessive runoff that often accompanies severe seasonal storms. Accordingly, the U.S. Army Corps of Engineers released approximately 11 billion gallons of impounded water between June 20 and 27 at the rate of approximately 3,000 cubic feet per second, or 1.3 million gallons per minute. The purpose of the study described in this paper was to determine the effects of this release on the quality of Lehigh River water.

THE FRANCIS E. WALTER RESERVOIR

The dam site of the Francis E. Walter Reservoir is on the Lehigh River a short distance below the mouth of Bear Creek in Luzerne County, Pa. (fig. 1). The Lehigh River is the second largest tributary in the Delaware River drainage system. The reservoir was completed in 1961 and was built primarily for flood control. When approved modifications to its construc-

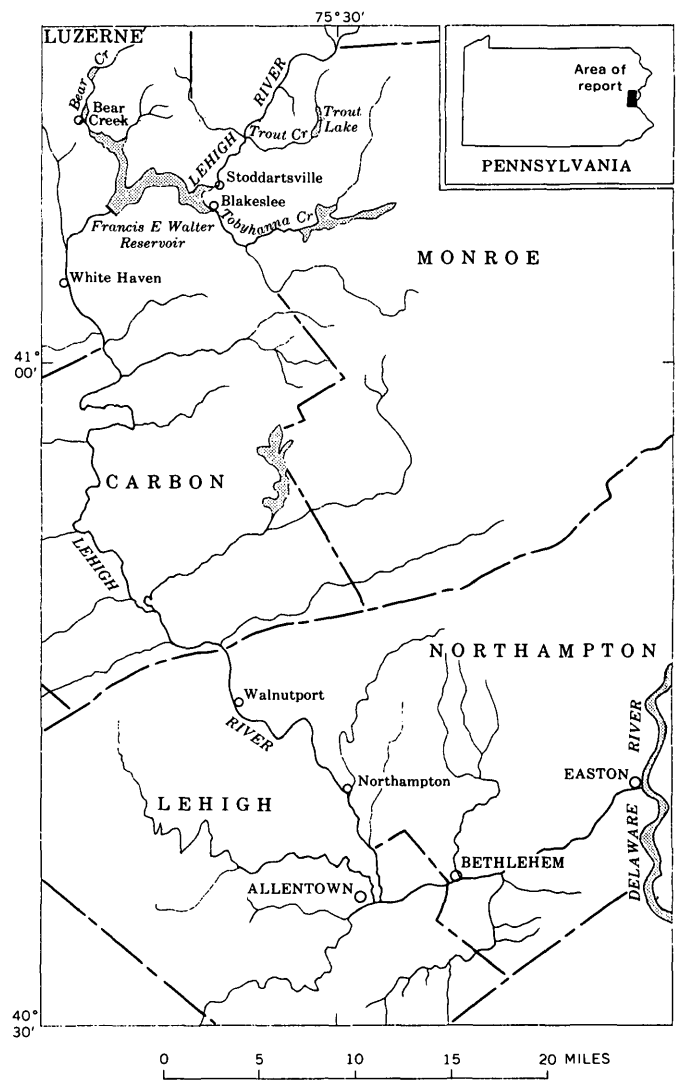

FIGURE 1.—Lehigh River drainage basin.

U.S. GEOL. SURVEY PROF. PAPER 575-D, PAGES D262-D266

tion are completed, it will also be used for long-term storage, recreation, and water supply.

The two largest streams flowing into the reservoir are Bear Creek and Tobyhanna Creek. These and other streams feeding the reservoir contain unpolluted water that is a habitat for trout and other game fish; some of the inflow is from swamps, is slightly acid, and is colored (as much as 40 units). The reservoir water has a low solute concentration and is of a calcium bicarbonate type (table 1).

On June 16, 1966, prior to the scheduled regulated releases to the Lehigh River, water in the Francis E. Walter Reservoir was about 140 feet deep near the intake. The temperature of the water decreased from 67.5°F in the 10 feet near the surface to 56.3°F at the 100-foot depth, below which it was not measured. On June 29, after the drawdown, water in the reservoir was about 55 feet deep, and the temperature decreased from 78.5°F at the surface to 74°F 10 feet down, remained at 74–75°F for the next 15 feet, and then decreased to 67°F at the 55-foot depth (fig. 2). The higher temperatures of the water on June 29 as compared to June 20 were probably related to the increase in average air temperatures from June 21 to 26.

Before the release on June 16, the dissolved-oxygen concentration at the surface of the impounded water was 7.0 parts per million (75 percent of saturation) and at a depth of 50 feet it was 6.5 ppm (63 percent of saturation). On June 29, after the drawdown, the surface concentration was 6.8 ppm (82 percent of saturation) and at 50 feet below the surface oxygen was 3.7 ppm (42 percent of saturation).

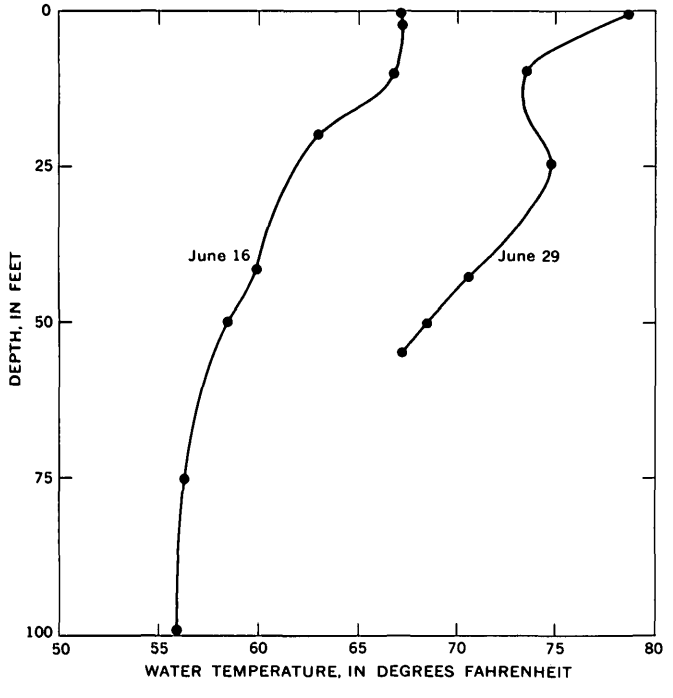

FIGURE 2.—Water-temperature variations with depth, Francis E. Walter Reservoir, June 16 and 29, 1966.

EFFECTS OF RELEASED RESERVOIR WATER

Specific conductance

From June 8 to 20 the specific conductance of Lehigh River water at Easton ranged from 187 to 244 micromhos (table 2). After the releases of June 20 the specific conductance of river water at Easton decreased from 232 micromhos at 0800 to 158 micromhos at 1400 on June 21. Specific conductance had further decreased to 97 micromhos by 0900 on June 22. A decrease in the specific conductance was noted also at Walnutport, 40 river miles downstream from the reservoir. The decline here on June 21 was from 75 micromhos to less that 50 micromhos. No comparable decrease was observed in the Delaware River at Trenton, N.J.

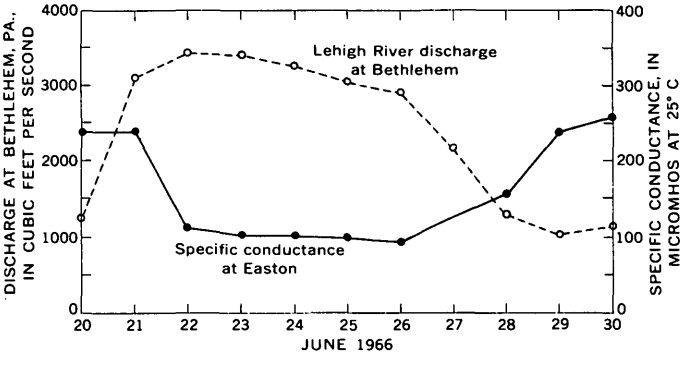

FIGURE 3.—Dilution effects of water released from the Francis E. Walter Reservoir, Lehigh River at Easton, June 20–27, 1966. (Plot is based on daily maximum specific conductances, table 2).

At Easton the specific conductance of river water remained near 100 micromhos until releases from the reservoir stopped on June 27 (fig. 3). During the release, the concentration of dissolved solids at Easton was about half that of the week preceding the release, the pH of river water decreased from 7.1 to 6.3, and the color of river water increased from 10 units on June 19 to about 30 units on June 23. Three days after the release (June 30) the chemical character of river water and the concentration of dissolved solids at Easton reverted to what they were prior to the release.

Water temperature

The temperature of water released from the reservoir was measured daily at 0800, 1200, and 1600 on June 20–27 (fig. 4). Because water was released from the bottom of the reservoir, the temperature at the outlet was initially low but increased as the warmer water of sur-

TABLE 1.—*Chemical quality of streams in the Lehigh River basin, Pennsylvania, June 16–27, 1966*

[Chemical analyses in parts per million, except where otherwise indicated]

Date and time of collection, June 1966	Mean discharge (cfs) [1]	Temperature (° F)	Silica (SiO_2)	Aluminum (Al)	Iron (Fe)	Manganese (Mn)	Calcium (Ca)	Magnesium (Mg)	Sodium (Na)	Potassium (K)	Bicarbonate (HCO_3)	Sulfate (SO_4)	Chloride (Cl)	Fluoride (F)	Nitrate (NO_3)	Dissolved solids (residue on evaporation at 180° C)	Hardness as CaCO: Calcium and Magnesium	Hardness as CaCO: Noncarbonate	Total acidity as H_2SO_4	Specific conductance (micromhos at 25° C)	pH	Color units	Dissolved oxygen
Francis E. Walter Reservoir																							
16	------	67	----	----	----	----	----	----	7.4	----	8	9.6	8.0	----	0.3	----	12	----	----	38	6.4	----	----
Bear Creek near Bear Creek, Pa.																							
16	------	63	----	----	----	----	----	----	5.5	----	5	7.4	7.0	----	0.5	----	10	----	----	38	6.3	20	----
Tobyhanna Creek near Blakeslee																							
16	------	62	----	----	----	----	----	----	2.1	----	8	7.4	1.0	----	1.2	----	12	----	----	36	6.7	40	----
29	------	79	----	----	----	----	----	----	.5	----	7	6.8	1.5	----	.6	----	14	----	----	35	6.5	25	----
Lehigh River at Stoddartsville																							
16	------	60	----	----	----	----	----	----	3.0	----	10	8.8	2.0	----	0.4	----	14	----	----	41	6.7	30	----
Lehigh River at White Haven																							
16	------	60	----	----	----	----	----	----	4.6	----	8	9.0	5.0	----	0.3	----	13	----	----	40	6.5	30	9.8
21, 1045	------	63	----	----	----	----	----	----	4.6	----	8	9.4	2.0	----	.4	----	10	----	----	40	6.3	35	9.2
21, 1230	------	63	----	----	----	----	----	----	2.3	----	7	9.6	1.5	----	.5	----	13	----	----	40	6.4	20	9.5
Lehigh River at Walnutport																							
17	------	64	----	----	----	----	----	----	9.4	----	12	32	5.0	----	1.4	----	31	----	----	119	6.7	15	8.9
21	------	67	----	----	----	----	----	----	3.4	----	11	16	10	----	.7	----	20	----	----	67	6.5	----	8.8
29	------	79	----	----	----	----	----	----	7.8	----	15	41	4.5	----	1.7	----	46	----	----	142	6.6	----	8.1
30	------	76	----	----	----	----	----	----	8.7	----	12	40	5.0	----	1.9	----	41	----	----	138	6.6	----	7.3
Lehigh River at Easton																							
14	------	73	----	----	----	----	----	----	8.7	----	40	37	11	----	7.4	----	74	41	----	224	6.9	10	----
15	------	73	----	----	----	----	----	----	14	----	42	41	12	----	9.6	----	70	36	----	222	6.9	7	----
16	------	73	----	----	----	----	----	----	11	----	39	39	7.0	----	9.5	----	66	34	----	214	7.0	15	----
17	1,290	75	----	----	----	----	----	----	12	----	42	40	12	----	9.0	----	74	40	----	228	7.1	13	5.7
18	1,190	74	----	----	----	----	----	----	15	----	43	43	15	----	9.6	----	76	41	----	232	6.9	13	----
19	1,290	75	----	----	----	----	----	----	11	----	41	39	11	----	9.1	----	74	41	----	218	7.1	10	----
20, 0800	1,290	74	----	----	----	----	----	----	17	----	40	39	16	----	8.6	----	66	33	----	210	7.0	17	----
1400	------	76	----	----	----	----	----	----	11	----	40	40	8.0	----	8.6	----	70	37	----	216	7.0	15	----
1900	------	75	----	----	----	----	----	----	12	----	40	39	11	----	9.2	----	70	37	----	209	7.0	12	----
21, 0800	3,150	73	----	----	----	----	----	----	7.6	----	38	41	12	----	10	----	82	51	----	232	6.9	10	----
1400	------	77	----	----	----	----	----	----	8.7	----	28	37	7.5	----	5.9	----	58	35	----	158	6.6	8	----
1900	------	77	----	----	----	----	----	----	8.3	----	29	36	7.0	----	5.7	----	58	34	----	161	6.6	8	----
22, 0900	3,440	73	----	----	----	----	----	----	4.4	----	16	19	4.0	----	3.8	----	32	19	----	97	6.5	18	----
1400	------	----	----	----	----	----	----	----	6.2	----	17	22	4.5	----	3.8	----	33	19	----	94	6.8	23	----
1900	------	----	----	----	----	----	----	----	.9	----	18	20	5.0	----	3.8	----	40	29	----	----	6.6	23	----
23, 0800	3,380	74	----	----	----	----	----	----	7.4	----	16	19	8.0	----	4.2	----	32	19	----	86	6.3	30	----
1400	------	75	----	----	----	----	----	----	----	----	14	20	----	----	3.2	----	32	21	----	92	6.5	30	----
1900	------	----	----	----	----	----	----	----	4.8	----	18	19	4.0	----	3.6	----	33	18	----	97	6.8	23	----
24, 0900	3,240	74	----	----	----	----	----	----	6.0	----	18	19	4.5	----	4.2	----	32	17	----	97	6.5	25	----
25	3,200	77	----	----	----	----	----	----	4.6	----	16	19	5.0	----	4.0	----	33	20	----	96	6.9	17	----
26	2,980	----	----	----	----	----	----	----	6.2	----	16	20	5.5	----	4.4	----	32	19	----	97	6.6	17	----
27	2,260	----	----	----	----	----	----	----	4.4	----	18	19	4.0	----	4.9	----	35	20	----	97	6.6	20	----
28	1,360	77	----	----	----	----	----	----	----	----	16	23	----	----	6.5	----	44	31	----	127	6.7	30	----
29	1,040	79	----	----	----	----	----	----	8.7	----	28	27	12	----	6.5	----	54	31	----	152	7.8	30	----
30	1,200	81	----	----	----	----	----	----	----	----	46	33	----	----	11	----	75	38	----	208	6.8	30	5.1

[1] Daily discharges, Lehigh River at Bethlehem, about 10 miles from Easton.

TABLE 2.—*Water-quality data, Lehigh River at Easton, Pa., June 1–30, 1966*

Date, June 1966	Temperature (°F)		Dissolved oxygen (ppm)		Dissolved oxygen (percent saturation)		Specific conductance (micromhos at 25° C)	
	Max.	Min.	Max.	Min.	Max.	Min.	Max.	Min.
1	65	60	9.4	8.7	99	87	140	120
2	64	59	9.3	8.8	93	87	145	130
3	68	61	9.2	8.6	94	92	153	130
4	70	64	8.8	7.9	94	83	170	140
5	72	68	8.3	7.4	94	81	167	150
6	75	71	8.2	6.9	96	79	157	147
7	76	74	7.6	5.7	89	66	185	157
8	77	73	6.9	5.1	82	59	207	187
9	79	76	8.1	5.7	99	68	220	200
10	78	76	8.0	5.6	96	67	220	210
11	78	74	9.3	6.3	112	73	217	210
12	78	73	9.9	6.6	119	76	215	200
13	78	73	8.9	6.6	106	76	207	200
14	80	74	7.7	4.7	90	57	223	200
15	79	76	6.1	3.5	73	41	232	216
16	80	75	5.0	3.6	60	42	232	222
17	78	74	6.4	3.6	75	43	240	228
18	76	73	6.2	4.3	73	49	244	234
19	76	74	6.6	4.2	78	49	244	231
20	78	73	6.9	4.5	83	52	230	212
21	77	73	6.5	4.2	77	49	232	110
22	73	69	7.3	6.3	84	72	110	89
23	73	69	7.2	6.6	83	75	100	90
24	74	71	6.8	6.3	79	72	100	92
25	76	72	6.7	6.0	79	69	100	91
26	76	74	6.5	5.9	77	69	98	88
27	79	74	6.2	5.5	75	64	128	100
28	82	78	5.5	4.2	69	51	152	126
29	85	80	4.5	3.2	58	40	238	152
30	86	81	4.7	2.6	62	33	253	228

face areas in the reservoir dropped toward the intake. During the release, air temperatures also increased and this probably increased the temperatures in the river between the reservoir and Easton.

Water temperature was measured continuously with a recording thermometer at the Walnutport gage from June 18 to 30. There was a diurnal water-temperature variation of 2°–8.9°F, and the water was warmer at Walnutport than that released from the reservoir. Stream water became still warmer along its course downstream to Easton.

Dissolved oxygen

At White Haven, approximately 5 miles downstream from the dam, the Lehigh River contained 9.8 ppm of dissolved oxygen on June 16. Although this concentration decreased from 9.8 ppm on June 16 to 7.9 ppm on June 29, the river at White Haven was approximately 100 percent saturated. The change in concentration was due to increasing temperature. Furthermore, the near saturation at White Haven was not surprising because the river has a high reaeration capacity. It is, in general, a winding and mostly shallow river, having a rockstrewn bed that causes turbulence and diffusion of its waters.

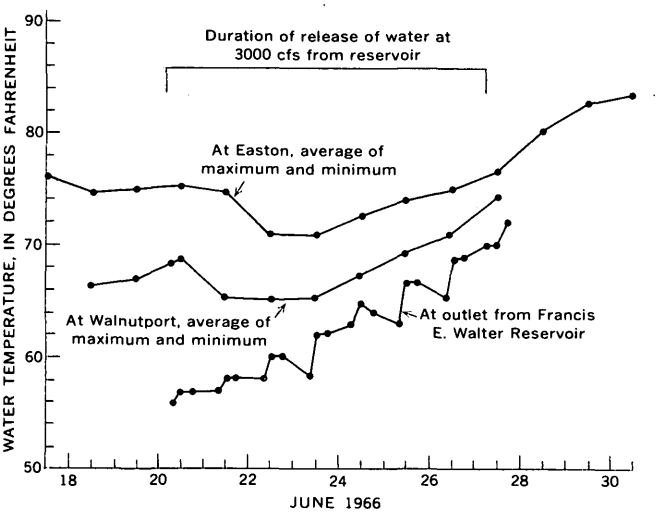

FIGURE 4.—Temperature of Lehigh River water, June 17–30, 1966.

At Walnutport the dissolved-oxygen concentration was measured on June 17, 21, 24, 29, and 30. On each day the water was close to 100 percent saturated; this was also true of a dissolved-oxygen determination of river water at Northampton sampled at 1300 on June 21. Between Northampton and Easton, however, some oxygen-consuming pollutants evidently enter the river, because the water at Easton was below saturation from June 14 to 30 (daily maximum and minimum dissolved-oxygen concentration shown in table 2). Moreover, there is no indication that the released water decreased the dissolved-oxygen concentration at Easton.

SUMMARY

Water released to the Lehigh River from the bottom of the Francis E. Walter Reservoir contained approximately 30 ppm of dissolved solids, had a pH of approximately 6.4, and was about 50 percent saturated with dissolved oxygen. This low-concentration water diluted the water of the Lehigh River. At Easton the concentration of dissolved solids in the river water was reduced nearly 50 percent on the second day of releases; 3 days after the conclusion of the releases, the concentration at Easton returned to the prerelease level. During the release period the pH of the Lehigh River water at Easton decreased slightly from 7.1 to 6.3 and the color increased from 10 units on June 19 to a high of 30 units on June 23.

The temperature of the water released from the reservoir was 57°F on June 21. After 3 days the temperature of the released water had increased to 62°F

and by the 6th day was 69°F. The warmer water of the upper strata replaced the cooler bottom water as it left the reservoir. The effects of the release of cool water from the reservoir were noted at Walnutport within 1 day and at Easton within 2 days after the release began. The temperature of the stream water was also affected by the air temperature.

The deficiency of dissolved oxygen in the lower strata of water in the reservoir might be expected to produce an oxygen deficiency in the Lehigh River water. However, as the water enters the river and diffuses over its rocky bed, turbulence brings it into contact with the air and it rapidly becomes saturated with oxygen. In the lower reach of the river (Northampton to Easton) the percent saturation is decreased by oxygen-consuming pollutants entering the stream.

TRANSVERSE MIXING IN A SAND-BED CHANNEL

By HUGO B. FISCHER, Menlo Park, Calif.

Abstract.—Rhodamine dye tracer was used to measure the transverse mixing coefficient in a large open channel. The flow was in a channel 2 feet deep and approximately 60 feet wide over a bed of sand dunes approximately 1 foot high. In one experiment the dye was injected on the channel centerline, and in another it was injected near the side. Both experiments yielded the same transverse mixing coefficient, E_z=0.11 sq ft/sec. Normalized by the depth and shear velocity, the dimensionless coefficient was E_z/dU^*=0.24, which is in excellent agreement with previous studies at laboratory scale.

Turbulent mixing, or diffusion, is the transfer of fluid particles between stream tubes which occurs in turbulent flow as a result of velocity fluctuations. The coefficient that relates the amount of material transferred to the gradient of concentration in the direction of transfer is referred to as the turbulent diffusion coefficient, or mixing coefficient. For uniform flow in an infinitely wide, open channel, the coefficient for vertical transfer of momentum can be obtained theoretically from the vertical distribution of velocity; for example, by using the logarithmic velocity distribution with a von Karman constant of 0.40, the average vertical mixing coefficient may be calculated to be $E_y = 0.067dU^*$, where d is the (constant) depth of flow and U^* is the shear velocity. The mixing coefficients for mass and momentum are generally assumed to be the same. In the transverse (z), or lateral direction, however, there is no theoretical means of predicting either mixing coefficient, and recourse must be taken to experiment.

Knowledge of the transverse mixing coefficient is important for two reasons. First, if a pollutant is introduced at the side of a stream, the rate at which mixing occurs across the stream is controlled by the transverse mixing coefficient. Second, and probably more important, the rate of transverse mixing is a controlling factor on the rate of longitudinal dispersion, which determines how fast a pollutant introduced into a stream is spread out along the length of the stream and how quickly the peak concentration is reduced. The connection between the transverse mixing coefficient and the coefficient of longitudinal dispersion has been demonstrated by Fischer (1966), who found that in many streams the longitudinal dispersion coefficient is inversely proportional to the transverse mixing coefficient. Fischer's method for predicting a longitudinal dispersion coefficient in a natural stream requires some estimate of the transverse mixing coefficient.

Only meager experimental results are available concerning transverse mixing in open-channel flow. Elder (1959) dropped dye to form spots on the surface of flow 1 centimeter deep on a laboratory water table and obtained a transverse mixing coefficient $E_z = 0.23dU^*$. Sayre and Chamberlain (1964), by dropping polyethylene particles onto the surface of a flow in a flume with a sand bed, found $E_z = 0.24dU^*$. Orlob (1959), in a flume with expanded-mesh bottom, obtained somewhat smaller coefficients, whereas Glover (1964), in studies of the Columbia River, obtained one which was larger. Glover's experiment was influenced by a density difference between the tracer and receiving water, which may have increased the apparent rate of diffusion. A more complete discussion of previous studies has been given by Fischer (1966) and Sayre and Chang (1966).

The objective of this study was to obtain experimentally the transverse mixing coefficient in a flow larger than laboratory scale. A reach of the Atrisco Feeder Canal near Bernalillo, about 15 miles north of Albuquerque, N. M., at a point where the channel is approximately 2 feet deep and 60 feet wide, was selected for the study. Two experiments were made. In the first, a dye tracer was injected continuously at the centerline of the channel, and in the second, the

U.S. GEOL. SURVEY PROF. PAPER 575-D, PAGES D267-D272

269-274 O—67——18

dye was injected next to the bank. Tracer samples were taken downstream from the injection point to observe the spread. An experimental mixing coefficient for each experiment was then calculated from the variances of observed concentration distributions.

This project was carried out by the Albuquerque Field Research Unit of the U.S. Geological Survey. The writer thanks all who participated in the study.

DESCRIPTION OF THE CHANNEL

The reach selected for the study had straight alinement for a distance of approximately 12,000 feet (fig. 1). The width varied slightly, due to irregularities in the position of the banks, from a minimum of 51 feet to a maximum of 65 feet. Channel-bed profiles were obtained by using a boat-mounted sonic sounder capable of measuring depth of flow within ±0.05 foot. The bed was made up of dunes, which were approximately 10 feet long and 0.8 to 1 foot high and were extremely uniform in size and distribution throughout the reach. Hydraulic conditions at the time of the two experiments are summarized in table 1.

TABLE 1.—*Hydraulic conditions and experimental results of transverse-mixing measurements in shallow flows as determined by dye injections in the Atrisco Feeder Canal, near Bernalillo, N. Mex.*

	Centerline injection June 21, 1966	*Side injection June 23, 1966*
Mean depth (d)[1]---(ft)	2. 24	2. 19
Mean width (w)---(ft)	58	56
Mean velocity (U)---(fps)[2]	2. 08	2. 17
Discharge (Q)---(cfs)[3]	269	263
Slope (s)	0. 00059	0. 00058
Shear velocity (U^*)---(fps)	0. 206	0. 201
Friction factor (f)	. 078	. 069
Number of cross sections sampled	5	8
Transverse mixing coefficient (E_z) (sq ft/sec)	0. 11	0. 11
Dimensionless transverse mixing coefficient (E_z/dU^*)	0. 24	0. 25

Notes: Bed material—mean size, 235 microns; geometric standard deviation, 1.25. Suspended material—mean size, 112 microns; geometric standard deviation, 1.40. Geometric standard deviation is defined by the Task Committee on the Preparation of Sedimentation Manual (1963, p. 98).

[1] Mean depth is used for natural channels to correspond to constant depth for infinitely wide two-dimensional flow.
[2] Feet per second.
[3] Cubic feet per second.

The point selected for dye injection was approximately 1,500 feet downstream from the end of a gentle curve, and 1,200 feet downstream from a wooden bridge with one center pier. Considering the roughness of the bed, these distances seemed adequate to dissipate any effects of either the curve or the bridge pier.

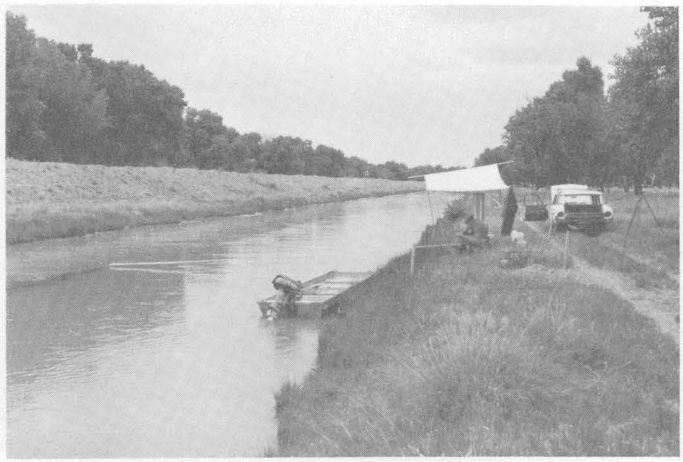

FIGURE 1.—View of Atrisco Feeder Canal, near Bernalillo, N. Mex., showing channel conditions at a discharge of 269 cubic feet per second, June 21, 1966. Centerline injection of dye is shown on the left (at end of white pipe).

EXPERIMENTAL METHOD

The tracer, Rhodamine WT dye diluted to a concentration of approximately 1 percent by weight, was injected into the channel through a tube from a constant-head vessel. Figure 1 shows the injection setup. Injection was maintained at a constant rate of approximately 5 milliliters per second, which was checked every 15 minutes. Thirty minutes were allowed after beginning of injection to establish a steady-state concentration distribution within the reach downstream from the injection point. Sampling was then begun at the farthest downstream station and progressed upstream to the point of injection.

At each station all the samples were obtained simultaneously. Samples were collected in 24-milliliter screwcap vials, which were slipped into rubber O-rings spaced at 2-foot intervals along a nylon cord. The cord was stretched tightly across the channel, and at a given instant all the bottles were submerged together. The bottles filled in approximately 5 seconds, after which the line was raised above the water, reeled in at one end, and the sample bottles removed. The procedure was then repeated at the next upstream station.

Concentration of dye in each sample bottle was read on a G. K. Turner fluorometer. The fluorometer scales were calibrated with samples of known dye concentrations which were prepared while the run was in progress. The known concentration standards were prepared using canal water containing exactly the same sediment load as the unknown samples. Samples and standards were always handled identically. Both were stored together in covered boxes until the sus-

pended sediment had settled to the bottom of the sample bottles. Before reading, all bottles were brought to the same temperature in a water bath. Standards were then read immediately prior to reading of the samples, so that any factors affecting the concentration (such as decay or adsorption on sediments) would be identical in both. The standards prepared contained 0.5, 1.0, 1.5, 2.0, 3.0, 4.0, 6.0, 8.0, 10, 15, 20, 30, 40, 60, 80, 100, 150, and 200 parts per billion of dye. Separate sets of standards were prepared for each run to ensure the same decay time and sediment concentration in both samples and standards.

EXPERIMENTAL RESULTS

The concentration distributions measured in the two experiments are shown in figures 2 and 3. Figure 2 shows concentrations downstream from a source on the channel centerline. As can be seen in figure 2, the peak and mean concentrations do not remain exactly on the centerline. Two hundred feet down from the injection point the main part of the dye cloud has shifted approximately 10 feet to the left (looking downstream) of centerline. At the 400-foot station the peak has returned to the centerline, but at the 600-foot station it again shifts to the left. The pattern is repeated at the 800-foot and 1,000-foot stations. This behavior appears to have been caused by a gentle internal meander between the banks of the stream. However, the meander was not so pronounced as to produce scour holes or increased velocities on either side of the stream, and was therefore not believed to have much effect on the lateral spread of the cloud.

Figure 3 shows the results of an injection 1 foot from the left bank. Because the experiment was conducted 2 days after the centerline injection, the meander pattern had shifted along the stream. However, the effects can still be seen; for instance, the pattern at 1,000 feet downstream appears to have been convected towards the right bank, but at 1,200 feet the pattern has once again turned toward the left. Such a pattern causes considerable scatter in results calculated at each individual section, but probably does not have a strong effect on the overall trend.

Mixing coefficients can be obtained from the data shown in figures 2 and 3 by calculating variances of each distribution and applying the formula:

$$E_z = \tfrac{1}{2} U \frac{d}{dx} \sigma_z^2 \qquad (1)$$

in which U is the mean flow velocity of the channel, x is the distance downstream, E_z is the transverse mixing coefficient, and σ_z^2 is the variance of the concentration distribution. This equation, as outlined by Sayre and Chang (1966), is based on the assumptions of a gradient-type mixing in both the longitudinal and transverse directions, and a uniform downstream vel-

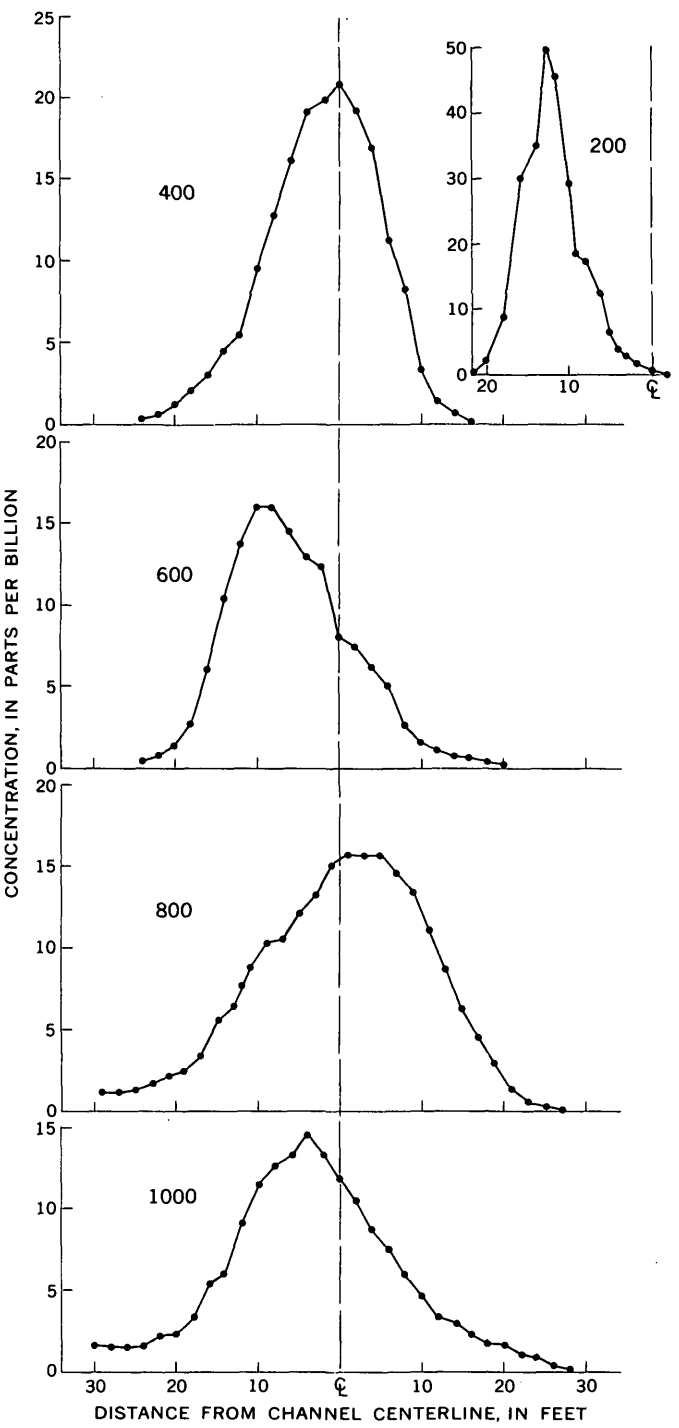

FIGURE 2.—Transverse distribution of dye at five cross sections downstream from centerline injection point, Atrisco Feeder Canal, June 21, 1966. Numbers above curves are distance downstream from injection point, in feet.

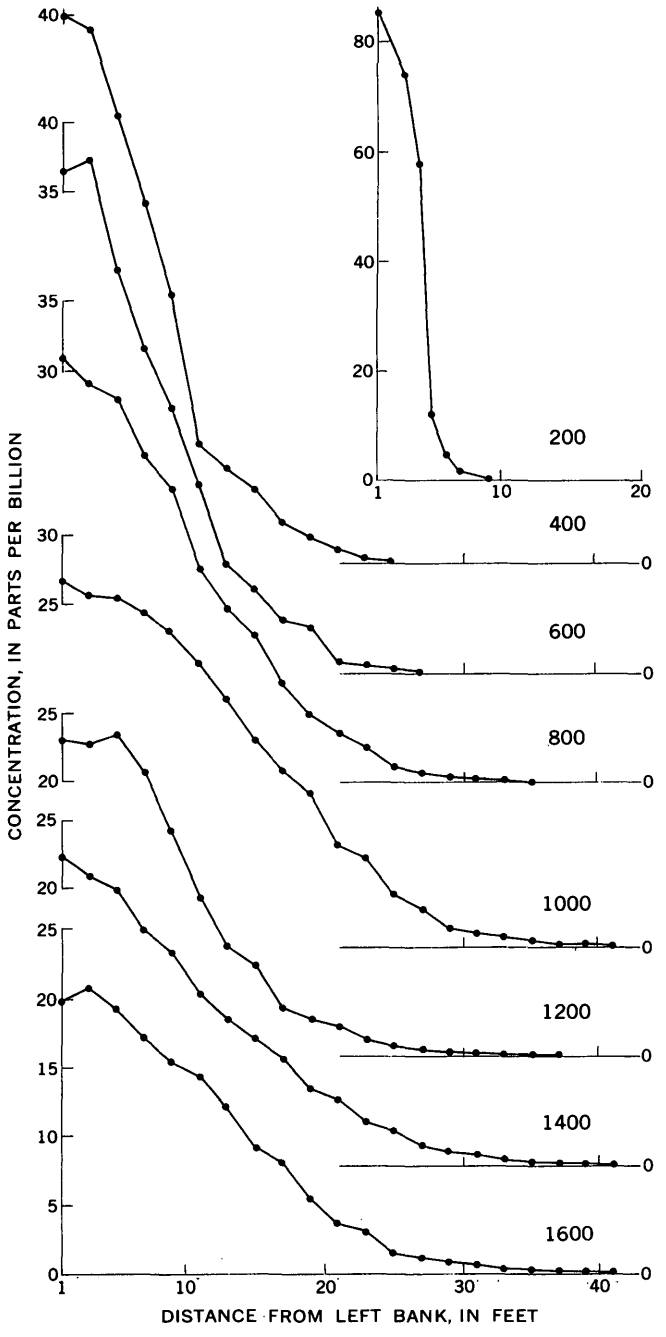

FIGURE 3.—Transverse distribution of dye at eight cross sections downstream from injection point, Atrisco Feeder Canal, 1 foot from left bank, June 23, 1966. Numbers above curves are distance downstream from injection point, in feet.

ocity at each point on the channel cross section. Gradient-type mixing in the longitudinal direction is produced by interaction between vertical differences in velocity (the velocity profile) and vertical turbulent mixing. Thus, if the mean velocity for a vertical slice at each transverse station is constant, equation 1 will apply. Although in the study channel, velocity at transverse stations was not exactly uniform, the deviations were small and were probably temporary results of shifting dune patterns rather than being the result of a fixed and steady convective pattern. Consequently, equation 1 is expected to apply within a good approximation. Figure 4 shows the configuration of the channel and the mean velocity at a cross section at the station 400 feet downstream from the injection point. The figure is typical of cross sections for the other stations. Depth and velocity were measured at 4-foot intervals in each cross section during each experiment, and mean velocity for each vertical was taken to be the velocity at the 0.6 depth.

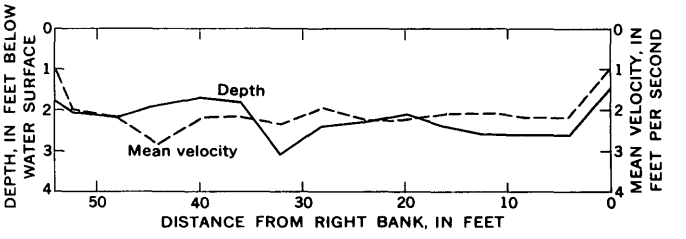

FIGURE 4.—Cross section showing depth and mean velocity distribution 400 feet downstream from injection point, Atrisco Feeder Canal, June 23, 1966.

Variances of the distributions were calculated by the formula:

$$\sigma_z^2 = \frac{\sum_i c_i u_i d_i z_i^2 \Delta z_i}{\sum_i c_i u_i d_i \Delta z_i} - \left[\frac{\sum_i c_i u_i d_i z_i \Delta z_i}{\sum_i c_i u_i d_i \Delta z_i}\right]^2, \qquad (2)$$

in which c_i is the concentration at the point i, u_i the velocity, d_i the depth, z_i the transverse distance from an arbitrary reference point, and Δz_i the width of the transverse segment. For the centerline injections, equation 2 gives the true variance about the calculated mean. However, for the bank injection experiment, it was necessary to assume an image distribution of concentration about the point 1 foot from the left bank (the point of injection), so that the assumed mean of the total real-plus-image distribution was required to be at the 1-foot point. For this calculation, z_i was the distance from the 1-foot point, and the second term on the right of equation 2 was dropped. The point of injection, rather than the point on the bank itself, was chosen so that equation 1 would apply

without change. In equation 2, measured concentration values were discharge weighted so that the variance was actually calculated from the mass of tracer passing each transverse station.

The variances calculated in each case were adjusted according to the width of the channel at each cross section. This was required to account for converging and diverging stream lines which occur as the width increases or decreases. The correction formula is:

$$\sigma_a^2=\sigma_c^2\left(\frac{W_m}{W}\right)^2, \quad (3)$$

in which σ_a^2 is the adjusted variance, σ_c^2 the calculated variance, W_m the mean channel width, and W the channel width at the section.

Figure 5 shows the adjusted variances for each measuring section. There is considerable scatter of results, particularly those obtained from the side channel injection at the further downstream stations. However, the straight line drawn on the graph is a reasonable approximation of all the data and is satisfactory for calculating a mixing coefficient. The oscillating nature of the variance between 1,000 and 1,600 feet for the side injection can probably be explained by the meander pattern in the stream, which alternately convects the major part of the diffusing tracer away from the bank and again back towards it.

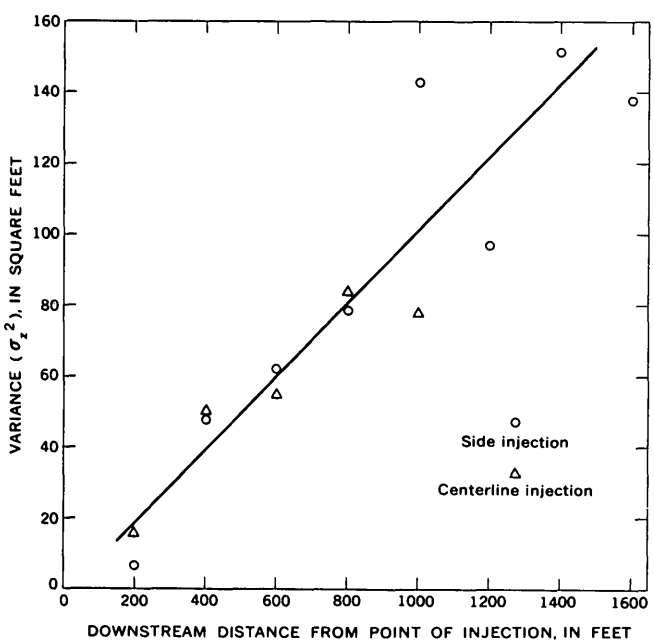

FIGURE 5.—Variance of transverse concentration distribution versus distance downstream from point of injection.

The mixing coefficient for each experiment was obtained from the line shown on figure 5, which is a good approximation of both sets of data. For both experiments the mean velocity of the flow was approximately the same, so that equation 1 yields the same result for each, $E_z = 0.11$ sq ft per second. This results in a dimensionless coefficient $E_z/dU^* = 0.24$ for the centerline injection, and $E_z/dU^* = 0.25$ for the side injection experiment. Both results are in excellent agreement with previous findings in laboratory flumes at smaller scales.

The results of both the present and previous experiments indicate that mixing in the transverse, or lateral, direction may be characterized by a coefficient approximately three times that for vertical mixing. A theoretical explanation for this cannot be attempted, because there exists no theoretical description of turbulent mixing on which an explanation might be based. Physically, however, the result is reasonable because of the restricted nature of the vertical motion as compared with that of the transverse motion. A fluid particle which is set in motion in the vertical direction is more likely to come up against a boundary and be required to cease its motion than is a particle set in motion in the horizontal direction. In other words, the scale of turbulence, or "eddy size", is partially dependent on the proximity of normal boundaries, and is more restricted in the vertical. Thus, although the turbulent motion is originally excited by the presence of boundary shear, the large-scale sustained movements which produce the maximum mixing are more effective in the transverse direction.

CONCLUSIONS

This study has been concerned solely with providing experimental data on the rate of transverse mixing in open-channel flow, at a scale larger than previous experiments. It has been found that in a wide uniform sand-bed channel the transverse mixing coefficient is approximately

$$E_z=0.24dU^*. \quad (4)$$

This result confirms previous laboratory experiments and extends the range of experimentally derived knowledge from laboratory flumes to field channels.

REFERENCES

Elder, J. W., 1959, The dispersion of marked fluid in turbulent shear flow: Jour. Fluid Mechanics, v. 5, no. 4, p. 544–560.

Fischer, H. B., 1966, Longitudinal dispersion in laboratory and natural streams: California Inst. Technology, unpub. Ph.D. thesis, Pasadena, Calif., 250 p.

Glover, R. E., 1964, Dispersion of dissolved or suspended materials in flowing streams: U.S. Geol. Survey Prof. Paper 433–B, 32 p.

Orlob, G. T., 1959, Eddy diffusion in homogeneous turbulence: Am. Soc. Civil Engineers Proc., Hydraulics Div. Jour., v. 89, no. HY9, p. 75–101.

Sayre, W. W., and Chamberlain, A. R., 1964, Exploratory laboratory study of lateral turbulent diffusion at the surface of an alluvial channel: U.S. Geol. Survey Circ. 484, 18 p.

Sayre, W. W., and Chang, F. M., 1966, A laboratory investigation of open-channel dispersion processes for dissolved, suspended and floating dispersants: U.S. Geol. Survey open-file rept., 210 p.

Task Committee on Preparation of Sedimentation Manual, Committee on Sedimentation, Hydraulics Division, ASCE, 1963, Sediment transportation mechanics, chap. B., Properties of sediments: Am. Soc. Civil Engineers Proc., Hydraulics Div. Jour., v. 88, no. HY4, July 1962, pt. 1. p. 77–107.

COMPUTATION OF TRANSIENT FLOWS IN RIVERS AND ESTUARIES BY THE MULTIPLE-REACH METHOD OF CHARACTERISTICS

By CHINTU LAI, Washington, D.C.

Abstract.—In order to compute transient flows in long reaches of rivers or estuaries having variable cross sections and other variable factors, a computer program previously developed to solve flows in a simple uniform reach by the method of characteristics has been extended. A long reach is divided into m subreaches, each of which may be considered to have uniform geometry as well as other constant factors. The basic method of characteristics is applied to each subreach, and additional boundary conditions are imposed at each junction between subreaches. The graphical display of digital computer output from sample computations indicates that the method developed is suitable for analyzing complex transient flows in long waterways.

This is a companion paper to an earlier article by Lai (1967). In order to treat the more complex river geometry of a much longer reach, the computer program for solving transient flows by the method of characteristics (Lai, 1965) has been extended to handle transient flows in a long reach of a waterway having variable cross section, variable flow-resistance coefficient, variable channel-bottom slope, variable lateral inflows, and other parameters.

In a previous report (Lai, 1965), the set of partial differential equations that represents one-dimensional transient open-channel flows of homogeneous density in an element of water was derived as

$$\bar{H}u_x+uZ_x+Z_t+uS_0-\frac{q}{B}=0, \tag{1}$$

and

$$uu_x+u_t+gZ_x+\frac{gk}{R^{4/3}}u|u|+\frac{qu}{A}=0. \tag{2}$$

The first equation is the equation of continuity, and the second one is the equation of motion. In these equations, the elevation of water surface, Z, and the flow velocity, u, are used as two dependent variables, and the horizontal distance measured along the longitudinal axis, x, and the time, t, are used as two independent variables. A variable coefficient, $\bar{H}$, represents the average depth of water in the cross section, the cross-sectional area, the top width, and the hydraulic radius are given by A, B, and R, and g, q, and S_0 represent gravitational acceleration, lateral inflow per unit length, and the slope of channel bottom, respectively. The parameter k depends on the value of flow-resistance coefficient, η (similar to Manning's n), and is expressed as $k=\left(\frac{\eta}{1.49}\right)^2$ if the English system of units is used.

Through the same mathematical procedures that were shown in detail in the previous report (Lai, 1965), the following simple characteristic equations, each of which contains only total derivatives, can be obtained:

$$\left.\begin{aligned} &dt-\frac{dx}{u\pm c}=0 \qquad (3)\\ &\frac{\pm c}{g}\,du+dZ+F_{\pm}dt=0 \qquad (4)\end{aligned}\right\}\ \text{along } C_{\pm}\text{ line,}$$

where

$$F_{\pm}=uS_0\pm\frac{ck}{R^{4/3}}u|u|-\frac{q}{B}\left(1\mp\frac{u}{c}\right), \tag{5}$$

C_+ and C_- are the two characteristic curves, and c is the celerity of gravity wave, $\sqrt{g\bar{H}}$.

For a computer solution, equations 3 and 4 are transformed into corresponding finite difference equations:

$$(t_P-t_L)-\left(\frac{1}{u+c}\right)_L(x_P-x_L)=0, \tag{6}$$

$$\frac{c_L}{g}(u_P-u_L)+(Z_P-Z_L)+(F_+)_L(t_P-t_L)=0, \tag{7}$$

$$(t_P-t_R)-\left(\frac{1}{u-c}\right)_R(x_P-x_R)=0, \tag{8}$$

and

$$-\frac{c_R}{g}(u_P-u_R)+(Z_P-Z_R)+(F_-)_R(t_P-t_R)=0, \tag{9}$$

U.S. GEOL. SURVEY PROF. PAPER 575-D, PAGES D273-D280

in which the subscript indicates the point in figure 1 to which each quantity is referred. Here, a specified time interval, Δt, is used in the t-direction.

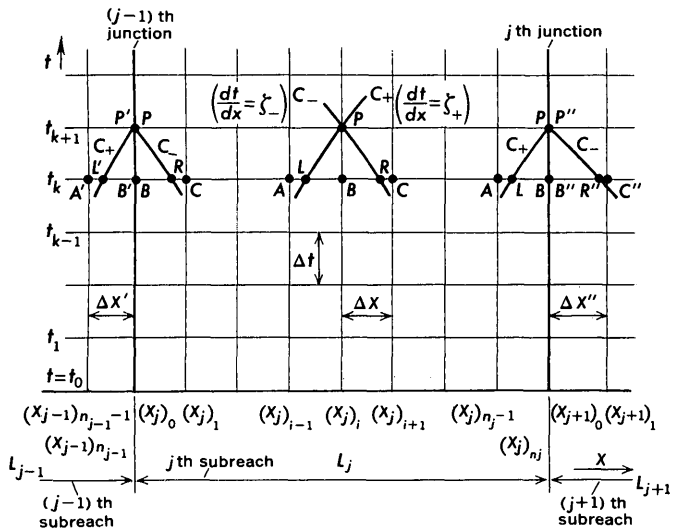

FIGURE 1.—A rectangular net and characteristic curves for a computer solution to flow equations.

If an assumption is made such that $(u+c)_L \approx (u+c)_B$, $(u-c)_R \approx (u-c)_B$, $(\zeta_+)_L \approx (\zeta_+)_B \approx \frac{\overline{PB}}{\overline{LB}}$ and $(\zeta_-)_R \approx (\zeta_-)_B \approx \frac{\overline{PB}}{\overline{BR}}$, in which $\zeta_\pm$ is the slope of the characteristic line $\left(\zeta_\pm = \frac{dt}{dx} = \frac{1}{u \pm c}\right)$, then u_L, u_R, Z_L, and Z_R values may be expressed in terms of corresponding values at points A, B, and C, say, by linear interpolation. Equations 7 and 9 can be combined to yield

$$Z_P = \frac{c_B}{2g}(u_L - u_R) + \frac{1}{2}(Z_L + Z_R) - \frac{1}{2}[(F_+)_B + (F_-)_B]\Delta t, \quad (10)$$

and

$$u_P = \frac{1}{2}(u_L + u_R) + \frac{g}{2c_B}(Z_L - Z_R) - \frac{g}{2c_B}[(F_+)_B - (F_-)_B]\Delta t. \quad (11)$$

From equations 10 and 11, the unknowns Z_P and u_P on the $t=t_{k+1}$ line can be found explicitly from known values at $t=t_k$ line. If the initial values of u and Z are given at $t=t_0$ line, all the values of u and Z on the successive t line may be found from the previously computed values and from two boundary values given by appropriate boundary conditions. It is known (Stoker, 1957, p. 291–308, 451–505) that the mesh ratio of Δt and Δx is controlled by

$$\frac{\Delta t}{\Delta x} \leq \frac{1}{|u \pm c|}. \quad (12)$$

When the channel geometry and other factors are varying in a long reach of a river, a solution by the method of characteristics can still be attained by dividing the entire reach into several subreaches so that each subreach may be treated as a simple reach having fairly uniform channel geometry and other parameters satisfying the assumptions made in the derivation of the partial differential equations. Additional boundary conditions are required, however, at each junction between subreaches in order to achieve the solution for unsteady flow occurring throughout the entire reach.

For example, consider a long channel with m subreaches. The equations for evaluating Z and u values at the $t=t_{k+1}$ line for the j^{th} subreach then, from equations 10 and 11, have the form

$$(Z_j)_{i,k+1} = \frac{(c_j)_{i,k}}{2g}[(u_{jL})_{i,k} - (u_{jR})_{i,k}] + \frac{1}{2}[(Z_{jL})_{i,k} + (Z_{jR})_{i,k}] - \frac{1}{2}[(F_{j+})_{i,k} + (F_{j-})_{i,k}]\Delta t, \quad (13)$$

and

$$(u_j)_{i,k+1} = \frac{1}{2}[(u_{jL})_{i,k} + (u_{jR})_{i,k}] + \frac{g}{2(c_j)_{i,k}}[(Z_{jL})_{i,k} - (Z_{jR})_{i,k}] - \frac{g}{2(c_j)_{i,k}}[(F_{j+})_{i,k} - (F_{j-})_{i,k}]\Delta t, \quad (14)$$

in which $(Z_j)_{i,k+1}$ means the Z value at the i^{th} point of the j^{th} subreach at a time, $t=t_{k+1}$, and so forth.

In flow computations for a long reach using m subreaches, the channel geometry parameters such as S_0, η, and k, and other parameters such as q may be considered as uniform with respect to x within each subreach, but they may vary from one subreach to another. From equations 13 and 14 all values of u and Z, except those at both ends of each subreach, can be found explicitly on the advanced time line $t=t_{k+1}$. Thus, it is apparent that some additional boundary conditions are needed at these junctions to include all points in the entire reach so that the computation can be carried out as long as desired.

According to the restriction on the size of Δt expressed by relationship 12, it is advantageous to select the number of segments in each subreach, $n_1, n_2, \ldots, n_j, \ldots$, such that

$$\frac{L_1/n_1}{\max|u_1 \pm c_1|} \approx \frac{L_2/n_2}{\max|u_2 \pm c_2|} \approx \cdots \approx \frac{L_j/n_j}{\max|u_j \pm c_j|} \approx \cdots \quad (15)$$

in order that the same time increment Δt may be used in the specified time interval procedures for all subreaches and the boundary conditions may be solved

simultaneously (Streeter and Lai, 1963). Here, L_1, L_2, . . ., denote the length of each subreach (see figs. 1 and 2).

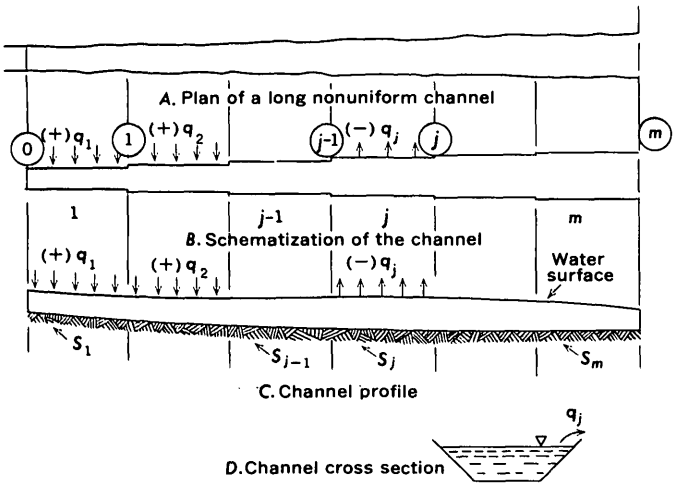

FIGURE 2.—Schematization of a long nonuniform channel (not to scale).

BOUNDARY CONDITIONS

Four boundary equations may be derived from equations 7 and 9 for a single reach. At $x=x_0$ (the left boundary)

$$u_P=u_R+\frac{g}{c_B}(Z_P-Z_R)+\frac{g}{c_B}(F_-)_B\Delta t, \tag{16}$$

and

$$Z_P=Z_R+\frac{c_B}{g}(u_P-u_R)-(F_-)_B\Delta t. \tag{17}$$

At $x=x_n$ (the right boundary)

$$u_P=u_L-\frac{g}{c_B}(Z_P-Z_L)-\frac{g}{c_B}(F_+)_B\Delta t, \tag{18}$$

and

$$Z_P=Z_L-\frac{c_B}{g}(u_P-u_L)-(F_+)_B\Delta t. \tag{19}$$

Which equations should be used depends on which type of boundary-value data is obtainable.

Because each subreach has four boundary values, a very long reach of river composed of m subreaches will have $4m$ boundary values. There will be two boundary values at each end of the entire reach, and four each at $(m-1)$ junctions. If either Z or u is given at the left end, the other value can be obtained from either equation 16 or 17. Similarly, if either Z or u is given at the right end, the other value is readily obtainable from either equation 18 or 19.

For any junction, for example the j^{th} junction, there are four unknowns, $(Z_j)_{n_j,k+1}$, $(Z_{j+1})_{0,k+1}$, $(u_j)_{n_j,k+1}$, $(u_{j+1})_{0,k+1}$, which can be solved from four boundary conditions:

$$(Z_j)_{n_j,k+1}=(Z_{j+1})_{0,k+1}, \tag{20}$$

$$(u_jA_j)_{n_j,k+1}=(u_{j+1}A_{j+1})_{0,k+1}, \tag{21}$$

$$(u_j)_{n_j,k+1}=(u_{jL})_{n_j,k}-\frac{g}{(c_j)_{n_j,k}}[(Z_j)_{n_j,k+1}-(Z_{jL})_{n_j,k}]$$
$$-\frac{g}{(c_j)_{n_j,k}}(F_{j+})_{n_j,k}\Delta t, \tag{22}$$

and

$$(u_{j+1})_{0,k+1}=(u_{(j+1)R})_{0,k}+\frac{g}{(c_{j+1})_{0,k}}[(Z_{j+1})_{0,k+1}$$
$$-(Z_{(j+1)R})_{0,k}]+\frac{g}{(c_{j+1})_{0,k}}(F_{(j+1)-})_{0,k}\Delta t. \tag{23}$$

The minor losses which occur at the junction are assumed negligible.

To solve these equations, a value of Z at the junction for $t=t_{k+1}$ is estimated, for example, by quadratic extrapolation from the previous elevations. Substituting the assumed Z value for $(Z_j)_{n_j,k+1}$ in equation 22 and for $(Z_{j+1})_{0,k+1}$ in equation 23, $(u_j)_{n_j,k+1}$ and $(u_{j+1})_{0,k+1}$ may be computed. Using the same Z value and the given channel cross section data, $(A_j)_{n_j,k+1}$ and $(A_{j+1})_{0,k+1}$ can also be evaluated. Then $(u_jA_j)_{n_j,k+1}$ and $(u_{j+1}A_{j+1})_{0,k+1}$ are computed and the difference of the two is tested. If the difference is greater than a maximum tolerable error, ϵ, a new Z value, appropriately corrected, is assumed and the computation is repeated until the difference becomes less than ϵ.

COMPUTATION PROCEDURE

The steps for the computer solution of transient flow in a long channel by the multiple-reach method of characteristics can be described briefly. First, the name of river or waterway and the required output option are read into the digital computer program. Then the channel geometry data (area versus depth and width versus depth relationships) are read in, beginning from the first subreach and successively following in the $+x$ direction until the last subreach of the channel is reached. Next, data describing the initial values and other parameters are read in. The digital computer then performs some initial computations, evaluates constants, and initializes various variables and indices.

Two boundary values—one from each end of the total reach—are obtained either by putting in field-recorded data or by calculating boundary equations. The other two boundary values are computed by using two of the equations 16 through 19 as described before. All the u and Z values on the $t=t_1$ line except those on junctions are then computed by using equations 13

and 14. The remaining Z and u values, which lie on junctions, can be computed set by set from the first junction to the $(m - 1)$th junction.

If all the dependent variables u and Z are determined on the $t = t_1$ line, discharge at any specified points on this line can also be evaluated by u times A. After all computations along the $t = t_1$ line are completed, the computer program causes the values of the variables u and Z on the $t = t_0$ line to be replaced by the corresponding newly determined values of u and Z from the $t = t_1$ line. The computer is now ready to advance the computation to the next new time line. By using the same procedures, the computation can be repeated as long as desired with respect to time.

EXAMPLES

Both prototype and hypothetical transient flow data have been used to evaluate the multiple-reach method of characteristics for determining transient flows in rivers and estuaries. The results are encouraging. The two examples presented below show the results obtained from the digital computer program.

Connecticut River

Figure 3 shows a plotting of the measured and the computed transient flows in the Connecticut River near Middletown, Conn. The overall reach used for this computation is 6.1 miles long, lying between Middletown and Canel Pier. The flow in this reach is affected by ocean tides. The reach was divided into five subreaches, each with a different channel geometry, reach length, flow-resistance coefficient, and bottom slope. The water stages at the ends of the overall reach were provided as input boundary values to the computer, and the computed discharges at the upstream end (at Arrigoni Bridge, Middletown) were compared with the measured discharges at the same place. The agreement is generally satisfactory.

A hypothetical channel

The second example presents the computation of transient flow in a long hypothetical channel, the downstream end of which is open to an ocean. The tidal variation at the mouth of the channel may be found from a tidal table. However, in this example the tidal variations were assumed to be sinusoidal, having an amplitude of 4 feet and a period of 12.4 hours. In order to perform a computer simulation of transient flow in this long reach, several hypothetical conditions were assumed as discussed in the following few paragraphs.

At a point 28.4 miles upstream from the mouth there was an automatic digital water-stage recorder that furnished continuous stage data. This gaging station was within the range of tidal effect; in other words, tidal waves could propagate upstream beyond this point. At the time the tidal computation was started, this gage was recording a sinusoidal variation of stage with amplitude of 3.5 feet and a period of 12.4 hours, but with a phase lag of 0.3 π compared with the tidal curve at the mouth.

The channel had a trapezoidal cross section with dimensions that varied along its length. The channel slope, S_o, also varied throughout the reach, being very flat near the mouth and gradually becoming steeper as one moved farther upstream.

For the purposes of tidal computation using the computer, the overall channel was divided into six subreaches of equal length. All channel data were assumed uniform within each subreach, but variable from one subreach to another, thus introducing some discontinuities at each junction (see fig. 2).

A few additional hypothetical conditions were assumed as follows: There were some demands for water in the vicinity of the fourth subreach and 0.2 cubic feet per second per linear foot of water was being drawn throughout this subreach when the computation was begun. At the same time there was rainfall in the uplands causing 0.2 cfs per linear foot and 0.1 cfs per linear foot of inflow in the first and second subreaches, respectively. Two tidal cycles after the computation began, the lateral inflow at the first subreach had stopped, and after three tidal cycles, the lateral inflow at the second subreach had also stopped. At the beginning of the fifth tidal cycle, the rate of water withdrawal was increased to 0.3 cfs per linear foot.

Utilizing the information given above as initial-value data and the subsequent boundary-value data, the transient flow in this hypothetical channel was computed by an IBM 7094/1410 computer for five tidal cycles beginning February 28, 1964, at 7:15 p.m. Stage and discharge curves at different points along the channel were plotted directly by the line-printer attached to the computer for the five tidal cycles. However, owing to space limitations, only part of the computer output is shown in figures 4 and 5. The various discharge curves (fig. 5) are a good example of the results possible using the computer system. Although the stage curves (fig. 4) are quite similar, the discharge curves are considerably different from each other; they are very close to a sinusoidal curve at the mouth of the channel and become more and more distorted as the distance upstream increases. The amplitude of the curves also diminishes as one moves upstream. All these phenomena are to be expected in natural waterways.

FLOW OF HOMOGENEOUS DENSITY IN TIDAL REACHES,
CALCULATION FOR MULTIPLE REACHES BY THE METHOD OF CHARACTERISTICS

CONNECTICUT RIVER BETWEEN MIDDLETOWN AND CANEL PIER

OCTOBER 1965 DISCHARGES AT STATION 1- 1

DISCHARGE IN 1000CFS

DAY	HR	MEAS.DIS.	COMP.DIS.
			0
14	18		
		22840	22840
		20814	18553
		20785	18323
		21046	21529
		22206	20752
		20877	20083
	20	21204	20782
		21315	20677
		21292	20798
		21064	20405
		21414	20799
		21252	20776
		20742	20465
		20883	20048
	22	20350	20095
		20094	19877
		19929	19887
		19598	19116
		19214	18646
		18414	18082
		17552	17432
		16365	16403
15	24	15280	15227
		13307	13508
		11473	11734
		9156	9226
		6643	8114
		4684	5998
		3637	4452
		1888	4072
	2	791	2651
		-16	1367
		-44	1461
		26	1973
		450	1172
		783	1124
		2273	3792
		3641	5693
	4	6079	6591
		8355	8372
		10400	12622
		11851	13726
		13016	13536
		14108	14811
		14782	15173
		15933	16422
	6	16510	16720
		16733	16580
		17104	17296
		17586	17841
		17700	17953
		18093	17488
		18177	18090
		18200	18027
	8	18207	17688
		18115	17906
		18327	17861
		18394	17933
		18100	17693
		17898	17680
		17671	17477
		17479	16910
	10	17000	16828
		16548	15814
		15901	15464
		15137	15122
		14400	13452
		12658	12372
		11648	11360
		9708	9563
	12	7281	5763
		5964	2402
		4891	636
		-1500	-2087
		-3491	-4107
		-5300	-5643
		-6800	-7429
		-8197	-8188
	14	-9091	-7967
		-9700	-9523
		-9894	-9329
		-10100	-8783
		-10175	-9207
		-9886	-9157
		-8753	-7948
		-7500	-6053
	16	-5982	-4988
		-5065	-3346
		-1000	1647
		2490	6016
		6558	8631
		10293	12233
		13000	15740
		14516	17147
	18	16327	17675
		17200	18423
		18000	18944
		18555	18362
		18758	19258
		18898	19873
		19036	19135

FIGURE 3.—Computed and measured discharges, Connecticut River near Middletown, Conn. Asterisks indicate measured discharge at 15-minute intervals; zeros indicate computed discharge.

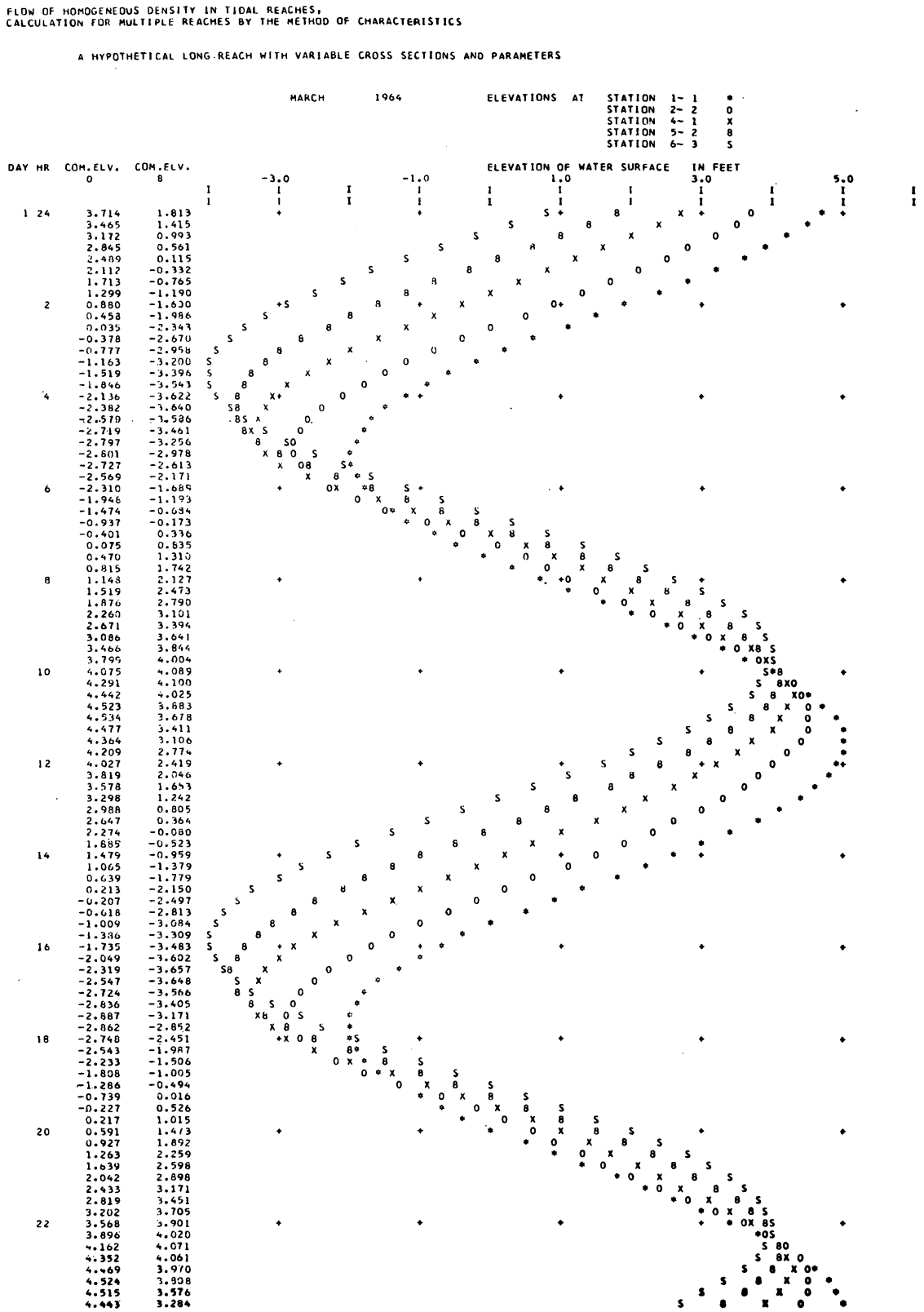

FIGURE 4.—Curves showing computed stage versus time at points along a long nonuniform channel.

FLOW OF HOMOGENEOUS DENSITY IN TIDAL REACHES,
CALCULATION FOR MULTIPLE REACHES BY THE METHOD OF CHARACTERISTICS

A HYPOTHETICAL LONG REACH WITH VARIABLE CROSS SECTIONS AND PARAMETERS

MARCH 1964 DISCHARGES AT STATION 1- 1 *
STATION 2- 2 0
STATION 4- 1 X
STATION 5- 2 8
STATION 6- 3 S

DAY	HR	COM.DIS. 0	COM.DIS. 8
1	24	36631	51411
		40287	56762
		42152	60977
		43179	63740
		43323	64982
		43076	65643
		42675	65448
		41863	64570
	2	40821	63427
		39720	61745
		38341	59816
		37015	57383
		35824	54601
		34519	51496
		33242	48320
		32127	44481
	4	30958	40239
		29968	35751
		29068	30628
		28184	24722
		27289	18353
		26066	11071
		24809	2642
		23038	-5434
	6	20475	-14754
		16909	-21719
		12051	-27727
		6492	-32220
		1141	-35895
		-4764	-38895
		-10942	-41029
		-16835	-43183
	8	-20967	-45614
		-23122	-48398
		-24161	-50749
		-24629	-52304
		-24535	-52151
		-23830	-51144
		-23510	-48173
		-22646	-43448
	10	-21634	-37459
		-19687	-30313
		-16898	-21887
		-13148	-12968
		-7837	-2557
		-875	8525
		7904	19730
		17746	30274
	12	26662	39404
		33854	47301
		38362	53535
		41372	58035
		42947	61651
		43631	63576
		43675	64826
		43395	64954
	14	42723	64550
		41811	63518
		40794	62113
		39560	60262
		38190	58005
		36994	55541
		35602	52574
		34266	49453
	16	33245	45904
		31988	41867
		30915	37556
		29993	32712
		29087	27350
		28086	21113
		26985	14244
		25773	6462
	18	24204	-2660
		22212	-11594
		19164	-19375
		14756	-25931
		9464	-31184
		4080	-35165
		-1295	-38230
		-7295	-40679
	20	-13249	-42860
		-18274	-45187
		-21752	-47642
		-23529	-50337
		-23988	-52467
		-23748	-54221
		-23356	-53505
		-23089	-51819
	22	-22200	-48537
		-21129	-43387
		-20015	-36757
		-17750	-29094
		-14541	-20516
		-10443	-10813
		-4759	-98
		-3110	11274

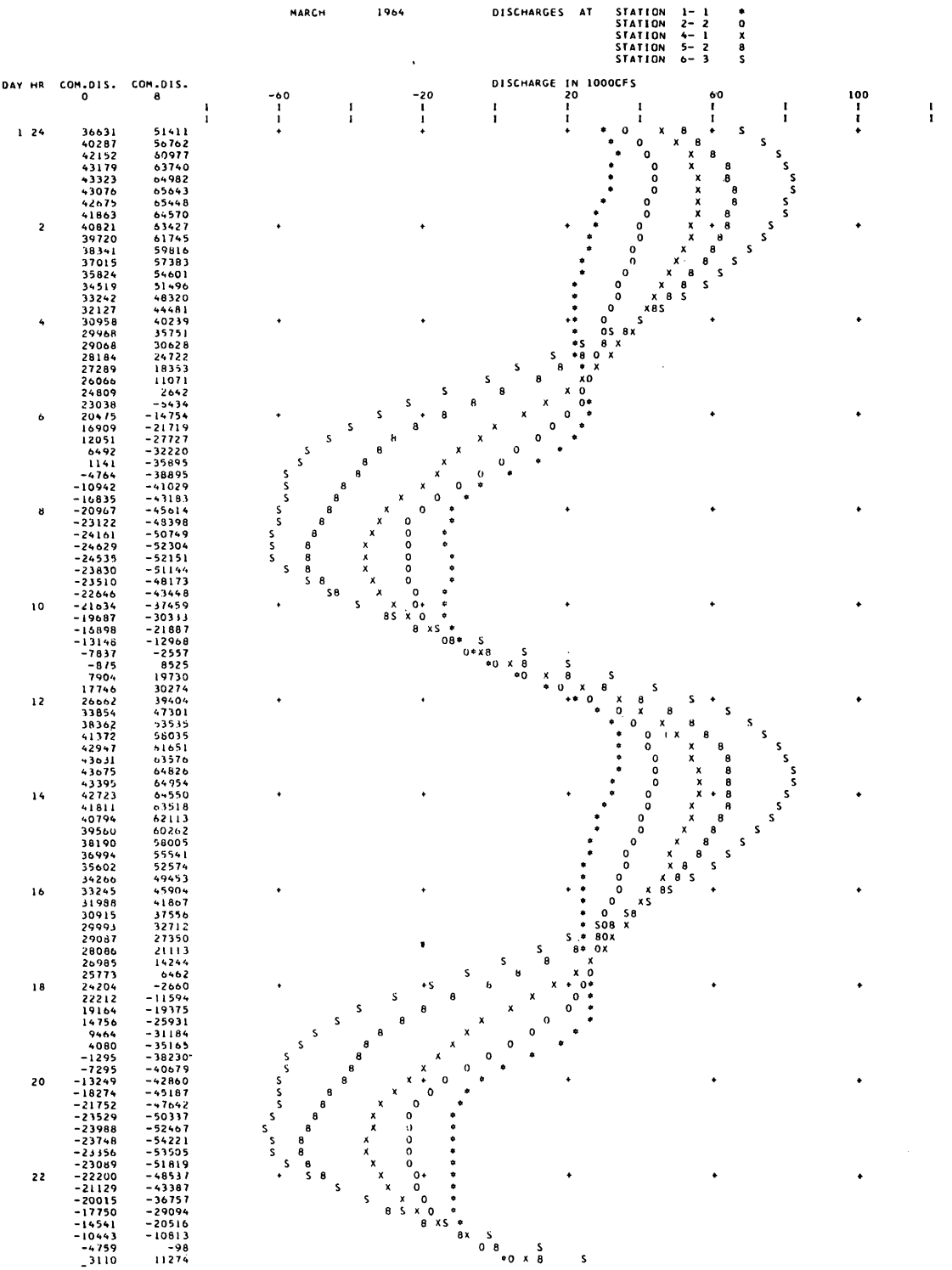

FIGURE 5.—Curves showing computed discharge versus time at points along a long nonuniform channel.

CONCLUSIONS

The technique and computer programs developed to evaluate transient flows in simple reaches of rivers and estuaries by the method of characteristics can be extended to treat flows in a very long waterway with variable cross sections and other variable factors. The long channel may be divided into many subreaches, each of which can be treated as a simple uniform reach. Suitable and sufficient boundary conditions may be applied at each junction and the transient flows throughout the entire reach can be definitely determined. The application of the technique to an actual river, the Connecticut River, shows good agreement with the field-measured discharges. The simulation of the transient flows in a long hypothetical channel by this technique produced rather interesting and informative results. Each of the plotted curves from the computer output for various points along the channel closely resembled some field-observed curves. Thus the method described in this study affords an adequate and economical means of evaluating transient flows simultaneously at many points throughout a long and complex waterway.

REFERENCES

Lai, Chintu, 1965, Flows of homogeneous density in tidal reaches, solution by the method of characteristics: U.S. Geol. Survey open-file rept., 58 p.

———1967, Computation of transient flows in rivers and estuaries by the multiple-reach implicit method, *in* Geological Survey Research 1967: U.S. Geol. Survey Prof. Paper 575–B, p. B228–B232.

Stoker, J. J., 1957, Water waves: New York-London, Interscience Publishers, 567 p.

Streeter, V. L., and Lai, Chintu, 1963, Water-hammer analysis including fluid friction: Am. Soc. Civil Engineers Trans., Paper 3502, v. 128, pt. I, p. 1491–1552.

MEAN ANNUAL PRECIPITATION-RUNOFF RELATIONS IN NORTH COASTAL CALIFORNIA

By S. E. RANTZ, Menlo Park, Calif.

Work done in cooperation with the California Department of Water Resources

Abstract.—Mean annual runoff is linearly related to mean annual precipitation and potential evapotranspiration in the humid basins of north coastal California. Mean annual water loss is virtually independent of mean annual precipitation because the great bulk of the annual precipitation and runoff occur in the winter months when evapotranspiration demands are light.

The purpose of this study was to derive a relation between mean annual runoff and mean annual precipitation in California coastal basins north of San Francisco Bay. The report area (fig. 1) includes about 17,000 square miles of terrain that is mostly wooded and mountainous. The area includes parts of two physiographic sections, as delineated by Fenneman (1931)—that part of the Klamath Mountains that lies in California, and the northwestern part of the California Coast Ranges. The geology and topography of these two parts, here designated as subregions, significantly affect the climate, drainage conditions, soils, and natural vegetation; and the hydrologic regimes of the two subregions are distinctly different. Although there is some variation in the topography, geology, and vegetation within each subregion, each subregion is treated here as being hydrologically homogeneous. The principal streams are the Russian, Eel, Mad, Klamath, and Smith Rivers; all drain large interior basins. Most of the other streams in the region drain only the coastal slopes of the Coast Ranges.

Two earlier reports (Rantz, 1964; Rantz and Thompson, 1966) presented values of mean annual precipitation and runoff for 99 basins in the study area. The basinwide values of precipitation had been obtained from isohyetal maps, and the values of runoff (natural flow) had been obtained either from long-term streamflow records or from short-term records whose time base was extended by correlation with long-term records. In the 1964 report, which covered the northern part of the area, the period 1900–59 was used as a time base; in the 1966 report, covering the southern part of the area, the period 1931–63 was used as a base. However, examination of long-term (80-year) precipitation records in the study area shows that records for either of the two base periods are representative of those for the long term, and therefore the values of mean annual runoff and precipitation given in the two cited reports were used without adjustment as the base data for this study.

ANNUAL PRECIPITATION

Precipitation in the region is distinctly seasonal very little occurring from June through September. Roughly three-fourths of the total annual precipitation occurs during the five months November through March. The bulk of the precipitation occurs during general storms of several days duration and relatively moderate intensity. Snow occurs in moderate amounts at altitudes above 2,000 feet, but only at altitudes above 4,000 feet does snow remain on the ground for appreciably long periods of time.

Mean annual precipitation is influenced by distance from the ocean, altitude, shape and steepness of mountain slopes, and direction of slopes in relation to the moisture-bearing winds. As a rule, precipitation increases from south to north and is much heavier on southern and western mountain slopes than on northern and eastern slopes. Table 1, which summarizes the base data used in this study, shows the wide range of

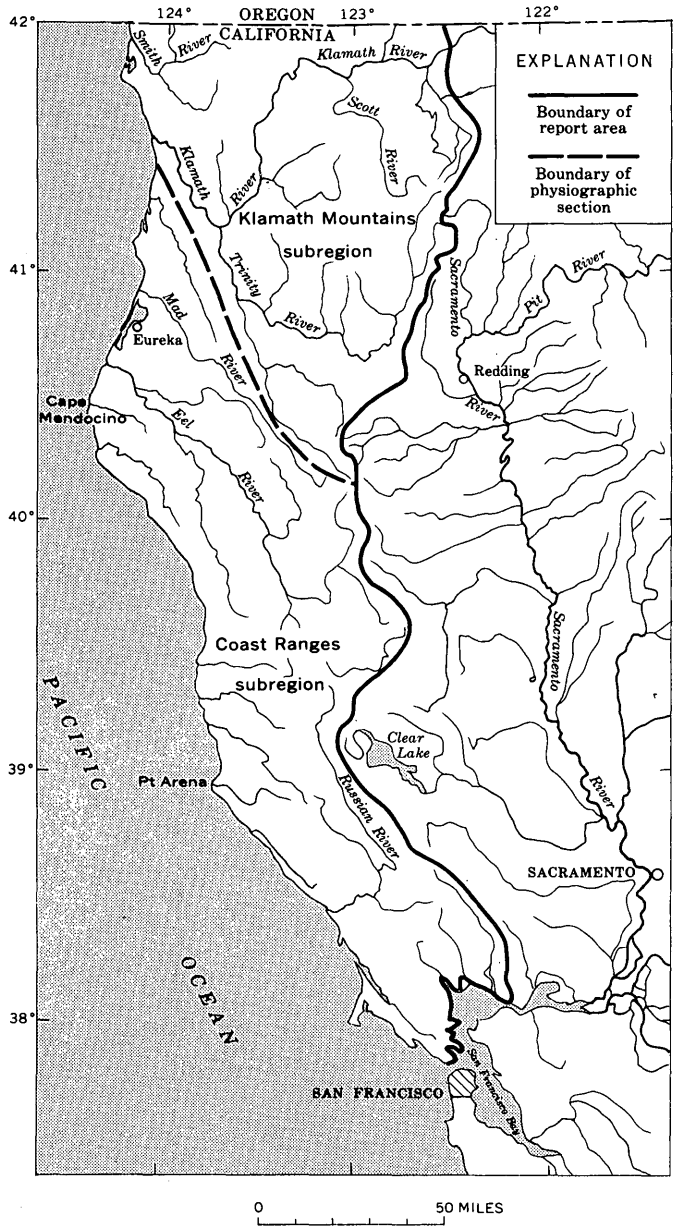

FIGURE 1.—Outline map of the Klamath Mountains subregion and the Coast Ranges subregion in north coastal California, showing areas where mean annual precipitation and runoff data were obtained.

mean annual basinwide precipitation in the region—30 inches to 116 inches.

ANNUAL RUNOFF

The runoff pattern in the study area is influenced not only by the distribution of precipitation, but also by the geology and topography. In the Coast Ranges subregion the mountains are relatively low, and there is therefore little snowmelt runoff. Because of the shallowness of the soil and low permeability of the soil and surficial rock, base flow is poorly sustained. Consequently, the bulk of the runoff in the subregion occurs during and shortly after the rains of late fall and winter. In the Klamath Mountains subregion a large part of the area is above 5,000 feet in altitude. Much of the winter precipitation is therefore stored as snow, and a large amount of snowmelt runoff occurs in late spring, in addition to the storm runoff in winter. The soil and surficial rock are more permeable here than in the Coast Ranges subregion, and base flow is therefore better sustained.

Mean annual runoff in the study area totals about 31 million acre-feet, which is the equivalent of about 34 inches of water over the entire area. Table 1 shows that mean annual runoff ranges from 7 to 90 inches.

DERIVATION OF MEAN ANNUAL PRECIPITATION-RUNOFF RELATIONS

In deriving a relation of mean annual runoff to mean annual precipitation, the following line of reasoning was used. By definition,

$$R=P-L, \tag{1}$$

where

R=mean annual runoff, in inches,
P=mean annual precipitation, in inches, and
L=mean annual water loss, in inches.

Furthermore, it was hypothesized that in a humid region, such as north coastal California, where the annual precipitation is generally equal to, or greater than, the annual potential evapotranspiration, the annual water loss will be virtually independent of the annual precipitation and will depend almost entirely on the annual potential evapotranspiration. This would be particularly true of the Coast Ranges subregion, where about 75 percent of the precipitation and about 80 percent of the runoff occur during the period of November through March, when the evapotranspiration demand is light. In the Klamath Mountains subregion where snowmelt maintains the runoff at a significant level until midsummer, it was expected that annual precipitation would be a small, but significant, factor in the water loss. In other words, we would expect the equation for average annual water loss to be

$$L=K+aP+b(PET), \tag{2}$$

where PET is the average annual potential evapotranspiration, in inches, and K, a, and b are constants. In addition, we would expect the value of a, the precipitation coefficient, to be small for the Klamath Mountains subregion, and probably zero for the Coast Ranges subregion.

TABLE 1.—*Summary of basic hydrologic data for the drainage basins of the Coast Ranges subregion and the Klamath Mountains subregion in north coastal California*

[Data compiled from Rantz, 1964; Rantz and Thompson, 1966]

Subregion	Number of basins in subregion	Range in size of basins (sq mi)	Mean annual basinwide values (inches)							
			Precipitation (*P*)		Runoff (*R*)		Water loss (*L*)		Potential evapotranspiration (*PET*)	
			Average of all basins	Range	Average of all basins	Range	Average of all basins	Range	Average of all basins	Range
Coast Ranges	75	6–427	55. 3	30–92	30. 4	7–68	24. 9	18–36	40. 4	31–48
Klamath Mountains	24	30–1, 000	65. 9	32–116	41. 5	12–90	24. 4	18–30	36. 3	28–46

When we substitute equation 2 in equation 1, we obtain

$$R=P-[K+aP+b(PET)],$$

or

$$R=(1-a)P-b(PET)-K. \quad (3)$$

To apply equation 3 it is necessary to have an index of average annual potential evapotranspiration. A commonly used index of that type is the average annual evaporation from the surface of water bodies, such as lakes and reservoirs. A generalized map of average annual lake evaporation in the United States is available (Kohler and others, 1959, pl. 2), and from that map average annual basinwide values of lake evaporation, or potential evapotranspiration, were computed. Table 1 shows that these values ranged from 28 to 48 inches. The values of R, P, and PET were used in a least-squares determination of the constants in equation 3. Separate determinations were made for the Coast Ranges subregion (75 basins) and for the Klamath Mountains subregion (24 basins), because of the differing hydrologic characteristics of the two regions. Because equation 3 is linear, basinwide average values of the variables could be used in the determination of the runoff equations, regardless of the fact that these variables often had a wide range of values within the larger individual basins.

The regression equations obtained for computing runoff were as follows:

Coast Ranges,

$$R=1.00P-0.40(PET)-9.1, \quad (4)$$

Klamath Mountains,

$$R=0.93P-0.32(PET)-8.1. \quad (5)$$

These equations confirm that a in equation 3 is zero for the Coast Ranges subregion and small (0.07) for the Klamath Mountains subregion. For the Coast Ranges regression equation, the correlation coefficient is 0.964 and the standard error is 3.9 inches; for the Klamath Mountains regression equation, the correlation coefficient is 0.994 and the standard error is 2.6 inches.

DISCUSSION OF RESULTS

For some of the basins that have relatively light runoff, the percentage differences between computed and actual runoff were large. This was due primarily to inherent inaccuracies in the generalized maps of mean annual precipitation and potential evapotranspiration that were used to obtain basinwide values of those two parameters of runoff. Another probable reason for discordant results was the assumption of hydrologic homogeneity within the subregions. The variability of other factors that are pertinent in the hydrologic equation, such as degree of forestation and surficial rock type, could have been considered, but most of these factors are difficult to measure and evaluate. In view of these difficulties and the uncertainties connected with the basic data, refinement of equations 4 and 5 by the inclusion of additional variables was not warranted.

Equations 4 and 5 will be useful for estimating the runoff from ungaged areas in north coastal California, or for constructing isopleths of mean annual runoff on a map of that region.

REFERENCES

Fenneman, N. M., 1931, Physiography of western United States: New York, McGraw-Hill Book Co., 534 p.

Kohler, M. A., Nordenson, T. J., and Baker, D. R., 1959, Evaporation maps for the United States: U.S. Weather Bureau Tech. Paper 37, 13 p.

Rantz, S. E., 1964, Surface water hydrology of coastal basins of northern California: U.S. Geol. Survey Water-Supply Paper 1758, 77 p.

Rantz, S. E., and Thompson, T. H., 1966, Surface-water hydrology of California coastal basins between San Francisco Bay and Eel River: U.S. Geol. Survey open-file rept., 134 p.

269-274 O—67——19

NEW SYSTEM FOR VIEWING MAPPING PHOTOGRAPHS

By J. WILLIAM KNAUF, Washington, D.C.

Abstract.—The U.S. Geological Survey has developed an image-separation system for viewing either black-and-white or color stereoscopic models on projection-type stereoplotters that does not require the use of filters. Known as the StereoImage Alternator (SIA), the system consists of rotating cylindrical shutters in both the projection field and the viewing field, synchronized so that each eye can see only the image from the corresponding (left or right) projector. Although the concept of alternating images for stereoscopic viewing is not new, the system by which they are obtained is both unique and practical.

A new system of viewing aerial photographs in three dimensions for delineation of map detail has been developed by the U.S. Geological Survey. Known as the StereoImage Alternator (SIA), the system permits the operator of a double-projection stereoplotting instrument to view the projected stereopairs of aerial photographs through rotating cylindrical shutters. The formerly required red and blue filters, which greatly reduced the amount of light reaching the operator's eyes, have been eliminated.

The shutters of the SIA flash alternate images of the left and right photographs onto a screen and then into the corresponding eyes of the observer to give him a stereoview of the terrain.

The advantages of SIA over anaglyphic (color-filter) image-separation systems are: (1) SIA requires no color filters or spectacles; hence, more than twice the amount of light reaches the viewing screen. (2) Resolution of the stereomodel is greatly improved, and the two images on the tracing-table platen are matched in sharpness of definition. (3) Complete image separation is effected—the observer sees no disturbing subimage intended for the other eye. (4) The SIA system is suitable for use with color photographs; more color photographs probably will be used in map compilation in the years ahead.

THE STEREOIMAGE ALTERNATOR

Operating principles

The StereoImage Alternator is illustrated diagramatically in figure 1. A rotating cylindrical shutter, having equal-area solid and open segments, is situated in front of each projection lens so that the beam from each projector is alternately stopped and released. The two shutters are out of phase; one shut-

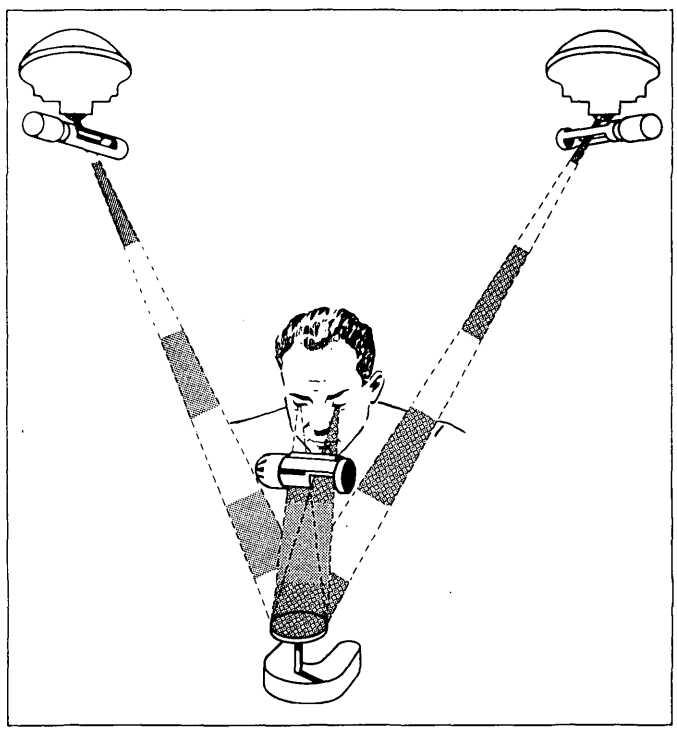

FIGURE 1.—Principles of StereoImage Alternator. Alternate images of the left and right photographs are flashed by synchronized shutters onto the screen and then into the corresponding eyes of the observer. A rate of about 60 flashes per second produces a steady stereoimage.

U.S. GEOL. SURVEY PROF. PAPER 575-D, PAGES D284-D288

ter is closed when the other is open, and vice versa. Correspondingly, the viewing shutters open and close to present the proper images to the right and left eyes of the observer. As is well known from motion-picture theory, if the flash rate of successive images to the separate eyes is rapid enough, there is no impression of flicker. Instead, a steady image is seen. Although the critical flash rate for a steady image varies with the individual observer, a rate of 60 flashes per second will produce a steady image for all.

Synchronization

The central problem in designing a mechanical system of alternating projection is synchronization; that is, the relationship between the projected flashes and the images received by each eye must be exact and constant. Modern technology has provided the answer to this problem by the availability of miniature stepping motors.

The stepping motors consist of a permanent-magnet rotor and a wired-field stator divided into four segments so that each sequential pulse from the control circuitry imparts a rotation of 90° to the motor shaft. The size-11 and size-8 motors used in the SIA can respond to pulse rates of 200 and 300 pulses per second, which means that they can operate synchronously at speeds as high as 3,000 and 4,500 revolutions per minute respectively.

The motors are physically very small, $1\frac{1}{16}$ inches in diameter by $1\frac{1}{8}$ inches long for the size-11 motor, and $\frac{3}{4}$ by $\frac{7}{8}$ inch for the size-8 motor. Both have rotor shafts $\frac{3}{8}$ inch long. The shutters are attached directly to the rotor shafts and must be lightweight and dynamically balanced. Because the operating temperature of the motors is rather high, around 200°F, safety guards are required. Life expectancy of the motors at the speeds of operation of the SIA is predicted in thousands of hours, and the bearings, which are the only wearing components, can be replaced by the manufacturer as necessary.

Adaption to plotters

The general principles of SIA are illustrated in figure 1, but the details of adapting it to specific plotters vary with the physical characteristics of each plotter; usually several configurations are possible, depending on the ingenuity of the designer as well as on considerations of practicality and convenience. The examples presented here are by no means exhaustive, and further possibilities are being tested to arrive at the most useful and convenient configurations.

With Kelsh-type plotters, several placements of the projection shutters are possible—in front of the projection lens, between the lamp and the projection lens, and around the lamp. Theoretically, the first two placements are preferable because they provide 100-percent separation of images, whereas the third will lead to overlapping images and a disturbing subimage. However, the subimage is small in comparison with those produced by anaglyphic filters, about 5 percent instead of 10–30 percent. Figure 2 shows a complete SIA installed on a Kelsh K-100 plotter. Figure 3 shows three types of the shutters used.

With ER-55 (Balplex) plotters (fig. 4) the only feasible placement for the projection shutter, without modifying the projector, is below the projection lens. However, the lenses of this plotter project the entire model at one time, over the full field of the photographs, whereas the area of interest is centered on the tracing table. A shutter capable of stopping and releasing the entire projected beam would be too large and heavy. The problem of adapting the SIA to the ER-55 plotter is solved by incorporating swing suspensions which allow the two small projection shutters, with their longitudinal axes alined in the y direction (front-back), to move a limited distance in the x direction (left-right). This sort of x motion is easily controlled by metal roller tapes attached to the tracing table, and the shuttered parts of the projected beams are kept centered on the tracing table. The tapes are hinged and flexible when moved in the y direction but adequately rigid when moved in the x direction.

Viewing-shutter assembly

As shown in figure 2, the assembly containing the pair of viewing shutters is attached to the tracing table. Here again the design is only one of several possibilities. Others could include spectacle frames, harnesses, and headgear containing cylinder, disk, or belt shutters. The present design, however, has served adequately for all the installations thus far. It does not require the operator to wear anything extra and avoids the problem of interference with eyeglasses that the operator may already wear. Moreover, the viewing field is kept centered on the tracing-table platen.

A single rotating cylindrical component contains the rectangular slots and solid segments which provide the shutters for both eyes. Thus only one motor is needed for the viewer. The eye slots are made rectangular rather than circular to eliminate the need for an eye-base adjustment. An outer protective shell houses the

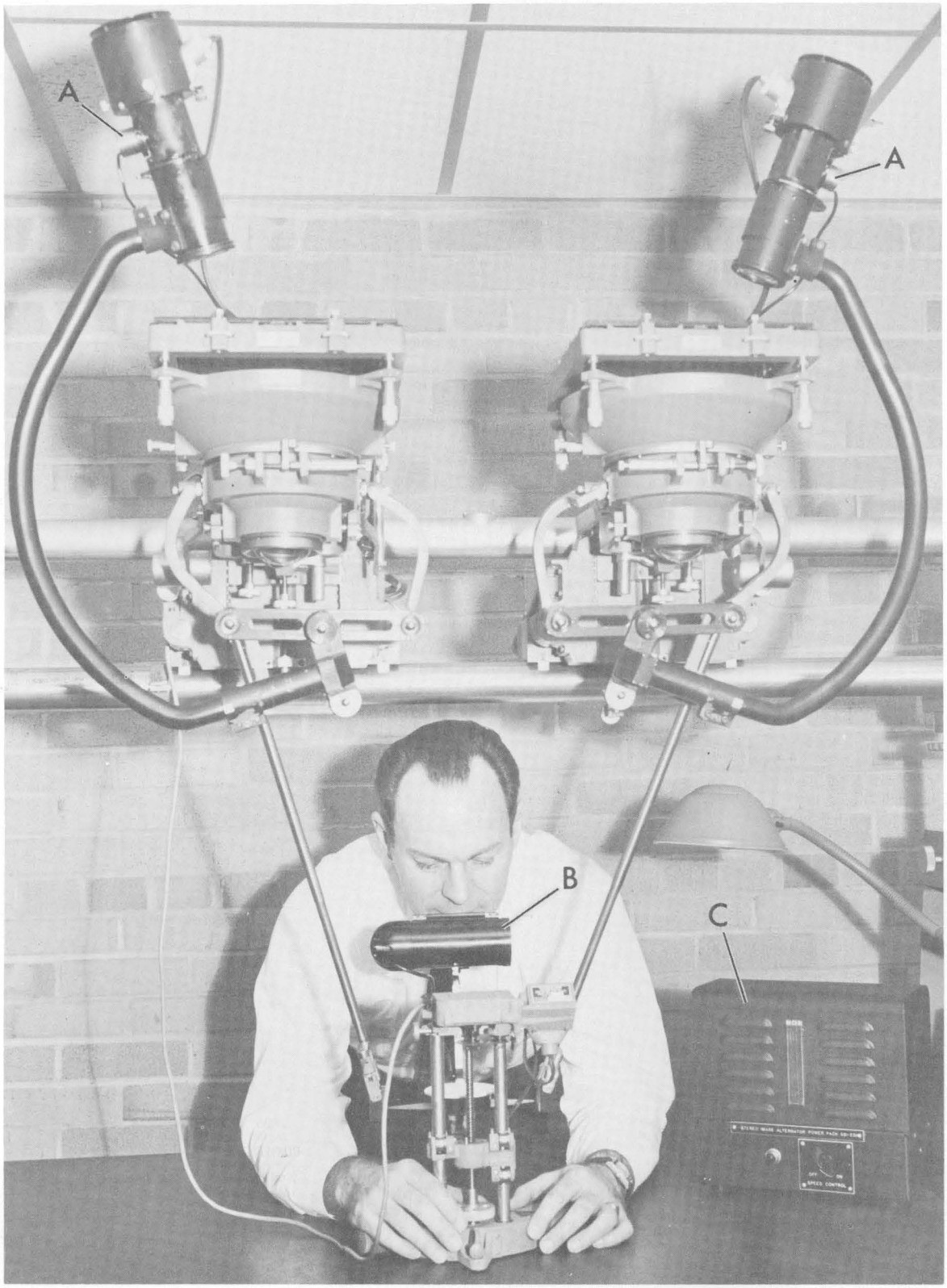

FIGURE 2.—Kelsh K–100 plotter equipped with the SIA. *A*, projection shutter motors. *B*, viewing shutter assembly. *C*, control-logic unit.

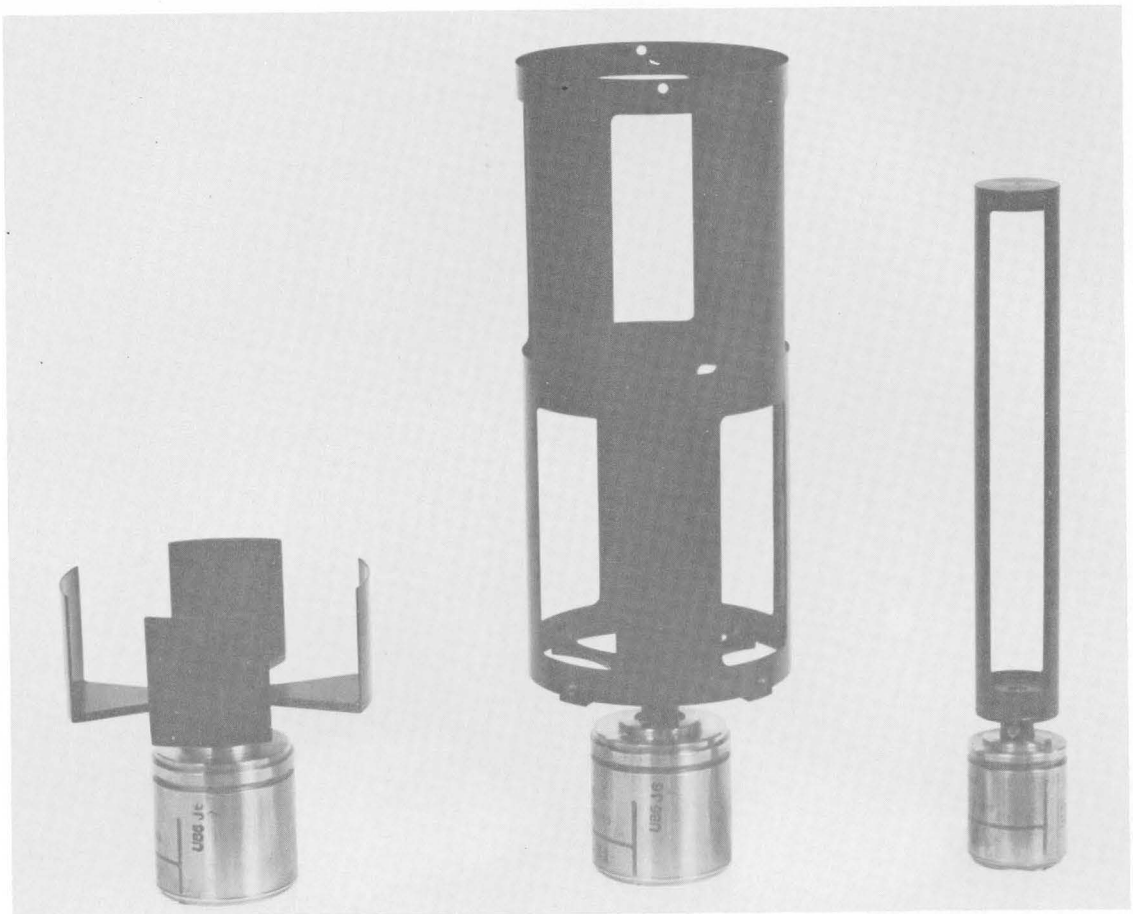

FIGURE 3.—Three types of SIA shutters. Left to right, Kelsh projection shutter, viewing shutter, and ER–55 projection shutter.

rotating component and the motor. The motor and attached shutter can be rotated within the housing to adjust for optimum orientation for either normal or pseudoscopic viewing.

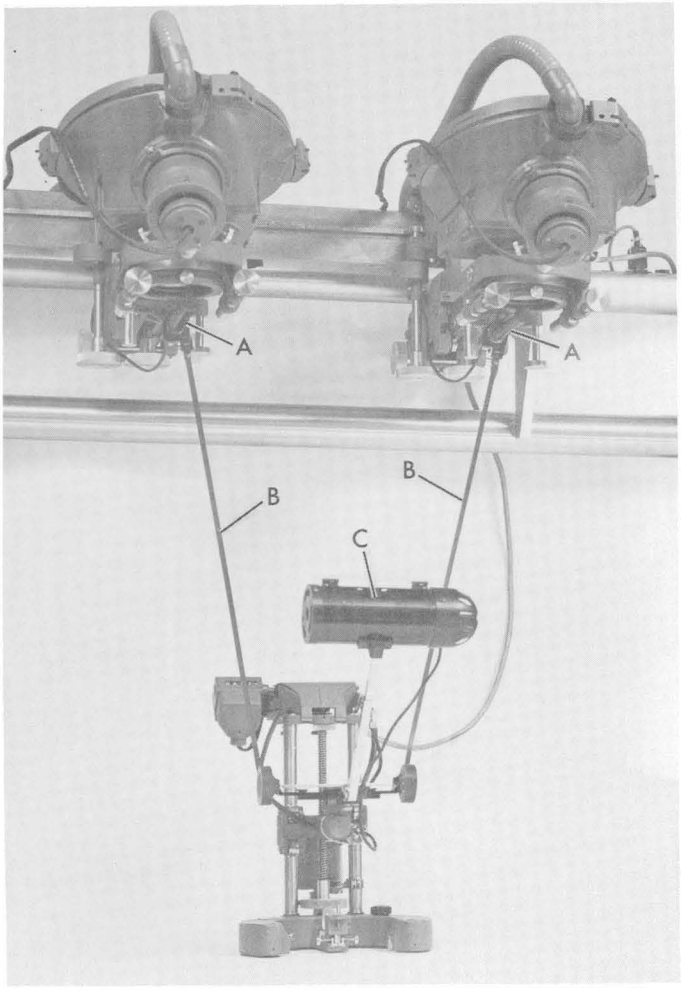

FIGURE 4.—SIA adapted to ER–55 plotter. *A*, projection shutters. *B*, roller tapes controlling x motion of projection shutters. *C*, viewing shutter assembly.

The shutter assembly is attached to the tracing table by a hinge block which contains a square telescoping tube that permits adjustment of the viewing distance from the platen. A friction hinge permits the operator to adjust the viewing angle as necessary. The assembly can also be rotated around the tracing table for observations from the rear of the plotting table.

System adjustment

As already noted, the viewing shutters are instantaneously adjustable by rotating the motor housing. Similar rotational adjustments are provided for the projection shutters. With the system in synchronous operation, it is only necessary to rotate the motor housing of each projection shutter (with the other projector turned off) until no light is visible through the shutter intended for the other eye—that is, until complete cutoff is obtained. The motors can be stalled without damage and will realine themselves in the sequential operation when released. Once adjusted and placed in operation, the system seldom needs readjustment.

OPERATIONAL EVALUATIONS

Production units of the SIA have been in daily use since November 1965, and no appreciable time has been lost because of malfunction of the system. All operators who have tried SIA report that the brightness and sharpness of the models are excellent and that they are able to compile with more assurance from difficult models.

The Geological Survey, which now has some 400 conventional stereoplotters in use in the national topographic mapping program, plans to install SIA's on many of these instruments as a standard accessory. When SIA units are attached to these plotters, they will provide, without penalty of greatly increased cost or complexity, many of the visual advantages inherent in European optical-train plotters.

AUTOMATIC PLOTTER FOR MAP BASE PREPARATION

By ROY MULLEN, Washington, D.C.

Abstract.—The Autoplot, an automatic coordinate plotting system, has been developed by the U.S. Geological Survey for preparing base sheets used in map compilation. It consists of (1) a standard coordinatograph modified by the addition of stepping motors to drive the coordinate arms; (2) a plotting head redesigned to perform point plotting, line scribing, and labeling; (3) a control-logic unit for generating commands for the stepping motors; and (4) a magnetic-tape reader for supplying data to the logic unit. Computer programs process the basic data, and coded commands are recorded on magnetic tape for plotting map projections and grids, basic control points, stereomodel pass points, and identification labels. The Autoplot system features high precision and compatibility with existing instrumentation. Automatic plotting time for a complete map base is usually less than 1 hour compared with the 8–12 hours required for manual plotting.

In recent years many advancements have been made in instrumentation and techniques for surveying and mapping, particularly in the processes which lend themselves to automation and (or) digitization. The preparation of base sheets on which topographic maps are compiled is one such process which held great opportunities for improvement in both speed and accuracy by automation.

The Topographic Division of the U.S. Geological Survey each year compiles about 1,800 standard quadrangle maps; the framework and control for all these maps have been plotted with manually operated coordinatographs. The advent of analytical and semianalytical aerotriangulation techniques greatly increased the need for automation in map base preparation. The output of these new aerotriangulation techniques is produced in the form of x and y coordinates of pass points—as many as 200 on some map bases—which are used for positioning stereomodels in the map-compilation phase. The new requirement to plot this number of pass points, along with the usual projections, grids, and geodetic control points, placed an unusually heavy workload on the coordinate plotter operators.

Several commercial firms have designed and produced automatic coordinate plotters which are useful in many graphic production operations, including some of the steps in map production. However, there was a need for an additional automatic plotter, designed specifically for the Geological Survey mapping operations. Hence, the Autoplot was developed with the basic design requirements of high precision, relatively low cost, and compatibility with existing instrumentation of the Geological Survey

The system components shown in figure 1 consist of a standard coordinatograph with a compound plotting head, drive motors for the x and y axes, and a magnetic-tape-controlled logic unit for generating commands for the drive motors. The Autoplot system operates as an incremental plotter; that is, each position is expressed as a delta x and delta y with respect to the x and y coordinates of the preceding position. The drive motors move the plotting head at a rate of 0.7 inch per second.

The Autoplot system was built around a standard Haag-Streit 48 × 48 inch coordinatograph, a precision instrument with rack-and-pinion drive and a basic plotting accuracy of ±0.0015 inch. Any other rack-and-pinion drive coordinatograph with equivalent accuracy would have served equally well. The only modifications required to adapt this coordinatograph to the Autoplot system were (1) the installation of motors for driving the pinions and thus positioning the carriage and rail arms, (2) redesign of the plotting head to provide additional capability, and (3) the addition of register studs on the plotting surface.

Stepping motors are used for driving the coordinate arms. To meet the basic accuracy requirements, a gearbox with a 10-to-1 reduction ratio was designed to adapt the drive motors to the instrument. The stepping motors are driven by pulses generated in the indexer

U.S. GEOL. SURVEY PROF. PAPER 575-D, PAGES D289-D291

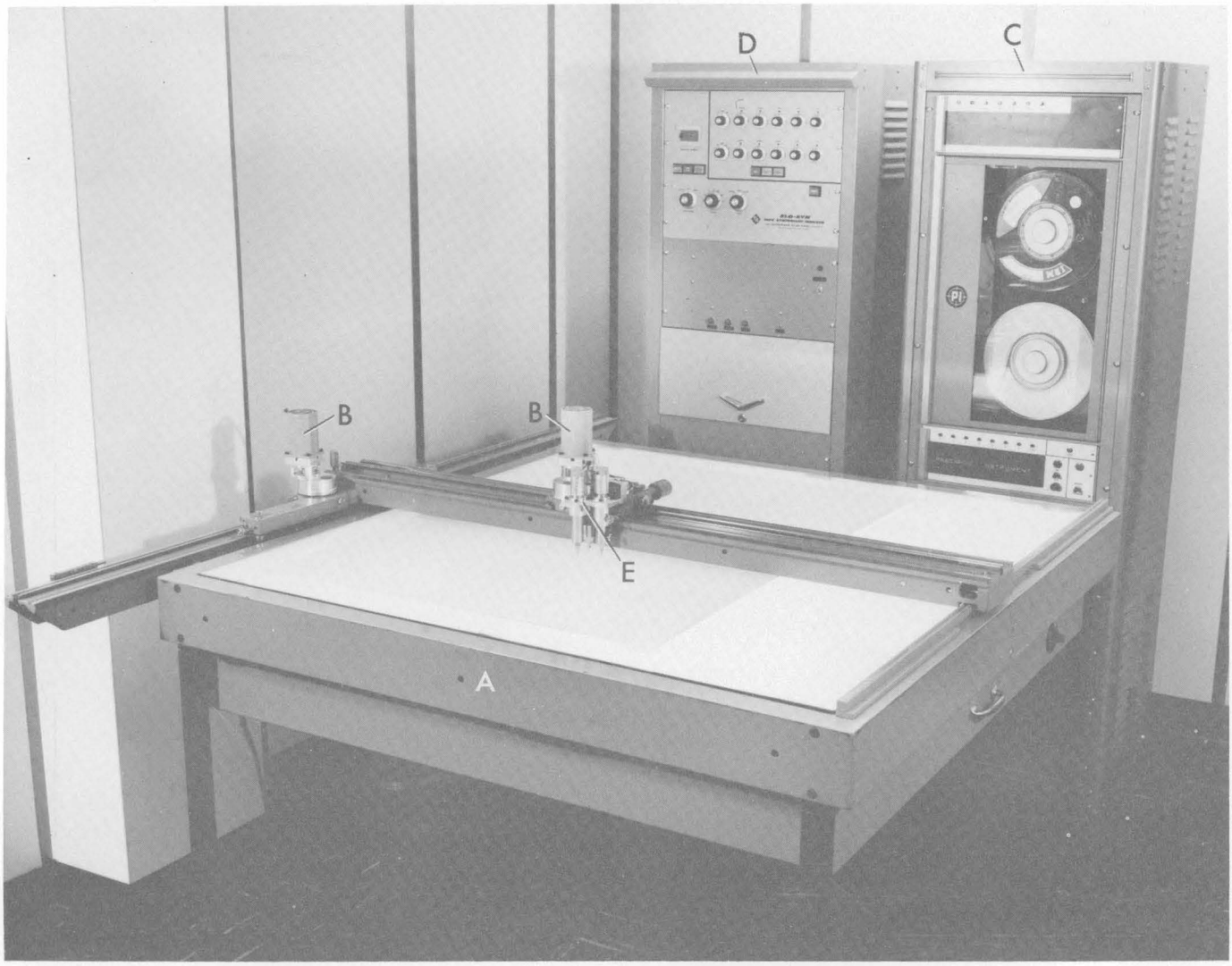

FIGURE 1.—The Autoplot. *A*, standard coordinatograph. *B*, drive motors. *C*, magnetic-tape reader. *D*, control-logic unit. *E*, plotting head assembly.

so that each discrete pulse rotates the motor shaft 1.8°, or 1/200 of a revolution. Therefore, through the gearbox, the motor advances the coordinate carriage along its rail in increments of 1/2000, or 0.0005, of an inch. Thus the plotting head can be positioned with a high order of accuracy by the automatic control logic.

The basic plotting head was redesigned to incorporate three separate operations—point plotting, line scribing, and labeling (fig. 2). The three individual heads are not turret mounted but are fixed with respect to each other and are brought into proper register by incremental step commands. The point-plotting head contains a sharp stylus for fine point marking. The scribing head is designed to accept interchangeable points so that the weight of the scribed lines may be varied to conform to fixed standards. The labeling head contains an inking point for printing alphameric characters.

The prototype Autoplot system contained a paper-tape-controlled indexer to read instructions to the control logic. In a later development stage the paper-tape unit was replaced with an incremental magnetic-tape reader which makes the Autoplot system conform more closely to the development objectives. The input data are recorded on seven-channel magnetic tape in standard IBM format at a density of 200 bits per inch. Coding in the seven-track array is binary coded decimal, non-return-to-zero. Four tracks contain the numeric bits, 1, 2, 4, and 8; two tracks, A and B, contain the zone bits; and track C contains the vertical parity bit. The tape reader will accept data from an asynchronous source at rates as high as 300 parallel characters per second. Manual commands can be inserted by means of rotary switches located on the front panel of the control-logic unit.

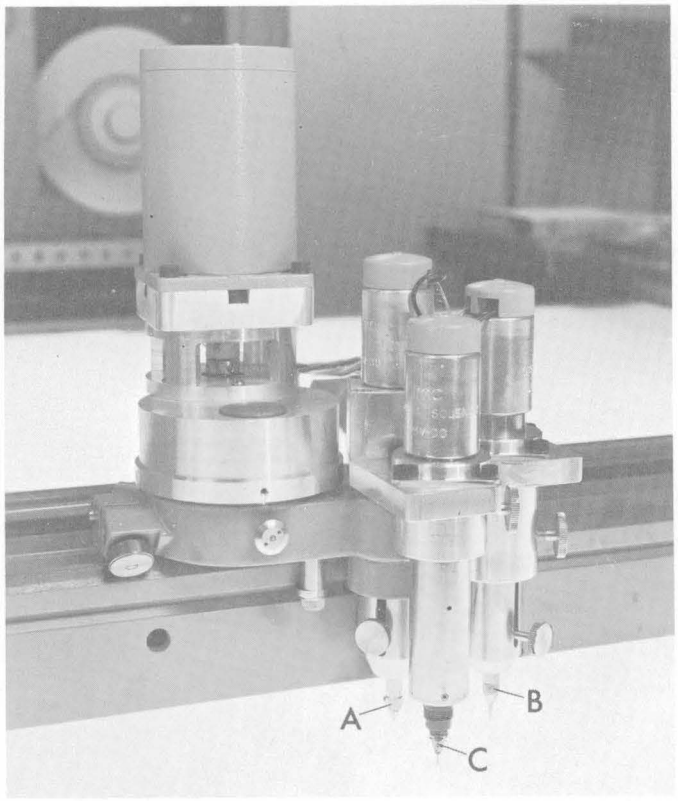

FIGURE 2.—Plotting head assembly. *A*, point-plotting head. *B*, scribing head. *C*, labeling head.

The heart of the Autoplot system is the supporting software. The magnetic-tape input for the system is generated from basic data processed on an IBM 7094 or System/360 computer. The basic data include all the pass-point and geodetic-control coordinates for a quadrangle and other pertinent information, such as scale, kind of projection, limit of overedge plotting, and quadrangle name. The master program, written in FORTRAN IV, generates on the magnetic-tape all instructions needed for (1) scribing the map projections, grids, and symbols, (2) plotting the pass points and geodetic control points, and (3) printing the alphameric characters required for identifying the quadrangle and the various plotted points.

Subroutines provide for interconversion between geographic coordinates and plane coordinates so that the various map projections and grid systems may be handled, including the Lambert conformal, transverse Mercator, Albers equal area, and polyconic projections and the Universal Transverse Mercator and State grid systems. A separate subroutine generates instructions for printing the alphameric characters required to identify pertinent map details.

One other item of information that is expected to be useful is a printout of transformation parameters which will allow a single point to be added by manually inserting a computed delta x and delta y with respect to a starting point.

The most important benefit derived from the use of the Autoplot is a significant saving in time. Manual plotting and scribing of a standard U.S. Geological Survey map base with horizontal pass-point positions require 8–12 hours of tedious work by the coordinatograph operator. This same operator can now thread the magnetic tape, set the appropriate switches and then attend to other duties while the Autoplot system produces a map base in less than an hour. Another benefit is increased accuracy which results from the elimination of the human error in observing the plotter dials.

Other applications for this automatic plotting system are being investigated. Techniques are being developed for extracting digital data from stereomodels and from existing map manuscripts. These digitized map data can be used for generating incremental instruction for automatic plotting of selected lines and symbols. The advent of ultra-high-speed computers has presented unlimited opportunities to apply digitization and automation to cartographic equipment and techniques.

SUBJECT INDEX

[For major headings such as "Economic geology," "Geophysics," "Paleontology," see under State names or refer to table of contents]

AUTHOR INDEX

U.S. GOVERNMENT PRINTING OFFICE : 1967 O - 269-274